

# Modern GPU Architecture

---

*A Comprehensive Blueprint of Graphics and AI Processing Systems*



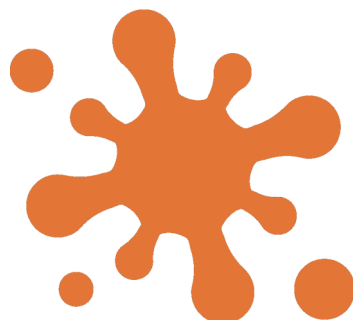
# Modern GPU Architecture

---

*A Comprehensive Blueprint of Graphics and AI Processing Systems*

Second Edition

Gareth Morgan Thomas  
*Auckland, New Zealand*



Published by Burst Books  
Auckland, New Zealand

Copyright © 2025 Gareth Morgan Thomas  
All rights reserved.

# Preface

Modern GPUs are no longer just engines for rendering pixels—they are the computational backbone of real-time graphics, scientific simulations, and artificial intelligence. This book offers a detailed architectural exploration of these powerful processors, mapping out the intricate hardware structures that drive both visual and machine-learning workloads.

Rather than a step-by-step design manual, this volume provides a theoretical blueprint for understanding how modern GPU systems are built and optimized. From the memory hierarchy and graphics pipeline stages to AI accelerators like tensor cores, each component is examined with clarity and depth.

The content is designed for computer engineers, hardware architects, graphics programmers, and AI researchers who require a foundational understanding of GPU internals—not to build a GPU, but to master the systems that increasingly power modern computing.

As we move deeper into an era of heterogeneous computing, the GPU continues to evolve as a core enabler of innovation. This book aims to be both a technical map and a reference guide for navigating that evolution.

**Welcome to *Modern GPU Architecture*.**



# About the Author

Gareth Morgan Thomas is a qualified expert with extensive expertise across multiple STEM fields. Holding six university diplomas in electronics, software development, web development, and project management, along with qualifications in computer networking, CAD, diesel engineering, well drilling, and welding, he has built a robust foundation of technical knowledge. Educated in Auckland, New Zealand, Gareth Morgan Thomas also spent three years serving in the New Zealand Army, where he honed his discipline and problem-solving skills. With years of technical training, Gareth Morgan Thomas is now dedicated to sharing his deep understanding of science, technology, engineering, and mathematics through a series of specialized books aimed at both beginners and advanced learners.



# Table of Contents

<b>About the Author</b>	<b>vii</b>
<b>1 Popular HDL Tools for VHDL, Verilog, and SystemVerilog</b>	<b>5</b>
1.1 Xilinx Vivado Design Suite . . . . .	5
1.1.1 FPGA Design and Development . . . . .	5
1.1.2 Extensive use for Xilinx FPGA devices. . . . .	8
1.1.3 Comprehensive toolset for synthesis, simulation, and implementation. . . . .	11
1.1.4 Supported Languages . . . . .	14
1.1.5 Full support for VHDL and Verilog. . . . .	18
1.1.6 Key Features . . . . .	21
1.1.7 IP integration, block diagram creation, and timing analysis. . . . .	23
1.2 Intel Quartus Prime . . . . .	25
1.2.1 Programming and Testing Intel FPGAs . . . . .	25
1.2.2 Focus on Intel (formerly Altera) FPGA families. . . . .	27
1.2.3 Designed for high-performance and efficient workflows. . . . .	28
1.2.4 Supported Languages . . . . .	29
1.2.5 Compatibility with VHDL and Verilog. . . . .	32
1.2.6 Key Features . . . . .	35
1.2.7 Memory and clock management tools. . . . .	37
1.3 Synopsys Design Compiler . . . . .	40
1.3.1 ASIC Design . . . . .	40
1.3.2 Industry-standard tool for logic synthesis and timing optimization. . . . .	42
1.3.3 Supported Languages . . . . .	44
1.3.4 Supports Verilog, SystemVerilog, and VHDL . . . . .	46
1.3.5 Key Features . . . . .	48
1.3.6 Extensive scalability and support for large-scale ASIC projects . . . . .	50
1.4 Cadence Xcelium . . . . .	51
1.4.1 Multi-Language Simulation . . . . .	51
1.4.2 High-performance simulator for SystemVerilog, Verilog, and VHDL . . . . .	54
1.4.3 Key Features . . . . .	56
1.4.4 Parallel simulation capabilities for increased speed . . . . .	58
1.4.5 Advanced waveform and debugging tools . . . . .	59
1.5 Mentor Graphics ModelSim (now Siemens EDA) . . . . .	60
1.5.1 HDL Simulation Leader . . . . .	60
1.5.2 Popular choice for both VHDL and Verilog simulations . . . . .	63
1.5.3 Key Features . . . . .	66
1.5.4 Integration with FPGA and ASIC workflows. . . . .	68
1.5.5 Debugging and visualization capabilities. . . . .	70
1.6 Aldec Active-HDL and Riviera-PRO . . . . .	71
1.6.1 Mixed-Language Simulations . . . . .	71
1.6.2 Designed for multi-language HDL simulation environments . . . . .	73
1.6.3 Key Features . . . . .	75
1.6.4 Focus on debugging and visualization . . . . .	76
1.6.5 Comprehensive testing tools for complex designs . . . . .	78

<b>2 Development Environment Setup</b>	<b>83</b>
2.1 Setting Up HDL Tools . . . . .	83
2.1.1 Installing Verilog simulators (ModelSim, Vivado, etc) . . . . .	83
2.1.2 Configuring synthesis tools and FPGA toolchains . . . . .	85
2.2 Environment Considerations . . . . .	86
2.2.1 System requirements and hardware compatibility . . . . .	86
2.2.2 Version control setup for HDL projects . . . . .	88
2.3 First Steps in Verilog Development . . . . .	90
2.3.1 Writing, simulating, and synthesizing a basic Verilog module . . . . .	90
2.3.2 Debugging simple testbenches . . . . .	93
<b>3 Introduction to GPU Architecture</b>	<b>97</b>
3.1 GPU vs. CPU . . . . .	97
3.1.1 Fundamental differences in architecture . . . . .	97
3.1.2 Parallelization . . . . .	98
3.1.3 Execution models . . . . .	101
3.2 Fixed-Function vs. Programmable Pipelines . . . . .	103
3.2.1 Historical perspective . . . . .	103
3.2.2 Modern GPU pipelines . . . . .	105
3.3 Key GPU Components . . . . .	107
3.3.1 Cores (ALUs) . . . . .	107
3.3.2 Texture units . . . . .	108
3.3.3 Rasterizers . . . . .	109
3.3.4 Memory subsystems . . . . .	111
3.4 Choosing the Complexity Level . . . . .	113
3.4.1 Deciding on a minimal design . . . . .	113
3.4.2 Illustrative design considerations . . . . .	115
3.4.3 Basic rasterization-based pipeline . . . . .	117
<b>4 Fundamentals of 3D Graphics Pipeline</b>	<b>119</b>
4.1 3D Geometry Basics . . . . .	119
4.1.1 Vertices and primitives (triangles, lines) . . . . .	119
4.1.2 Transformations . . . . .	120
4.1.3 Projection . . . . .	122
4.2 The 3D-to-2D Mapping . . . . .	124
4.2.1 Model matrix . . . . .	124
4.2.2 View matrix . . . . .	126
4.2.3 Projection matrix . . . . .	128
4.2.4 Clipping . . . . .	130
4.2.5 Viewport transformations . . . . .	131
4.3 Rasterization Basics . . . . .	133
4.3.1 Triangle setup . . . . .	133
4.3.2 Edge functions . . . . .	135
4.3.3 Interpolation . . . . .	136
<b>5 Interpolation in Rasterization</b>	<b>137</b>
5.0.1 Pixel coverage . . . . .	138
5.1 Shading and Texturing Concepts . . . . .	140
5.1.1 Lambertian shading . . . . .	140
5.1.2 Texture sampling . . . . .	141
5.1.3 Filtering . . . . .	143

<b>6 Digital Logic and HDL Review</b>	<b>147</b>
6.1 Combinational vs. Sequential Logic . . . . .	147
6.1.1 Review of digital concepts . . . . .	147
6.1.2 Combinational circuits . . . . .	148
6.1.3 Sequential circuits . . . . .	149
6.2 Verilog Basics . . . . .	151
6.2.1 Modules and hierarchical design . . . . .	151
6.2.2 Wires and regs . . . . .	154
6.2.3 Continuous assignments . . . . .	156
6.2.4 Always blocks . . . . .	159
6.2.5 Parameters . . . . .	161
6.2.6 Generate statements . . . . .	163
6.3 Common GPU Design Constructs . . . . .	165
6.3.1 Pipeline registers . . . . .	165
6.3.2 FIFOs . . . . .	168
6.3.3 BRAM/ROM usage . . . . .	171
6.3.4 Parallel arithmetic in Verilog . . . . .	171
6.4 Verification Essentials . . . . .	173
6.4.1 Testbenches . . . . .	173
6.4.2 Assertions . . . . .	174
6.4.3 Waveforms . . . . .	176
6.4.4 Debugging strategies . . . . .	177
<b>7 System-Level Design Considerations</b>	<b>181</b>
7.1 Defining the Design Requirements . . . . .	181
7.1.1 Throughput . . . . .	181
7.1.2 Latency . . . . .	182
7.1.3 Resolution targets . . . . .	185
7.1.4 Color depth . . . . .	188
7.2 Fixed-Point vs. Floating-Point Arithmetic . . . . .	190
7.2.1 Numeric formats for transformations . . . . .	190
7.2.2 Shading . . . . .	191
7.3 Memory Interface Basics . . . . .	192
7.3.1 Framebuffers . . . . .	192
7.3.2 Texture memory . . . . .	194
7.3.3 Z-buffer . . . . .	195
7.4 Clocking & Synchronization . . . . .	196
7.4.1 Pipeline stages . . . . .	196
7.4.2 Setup/hold times . . . . .	198
7.4.3 Avoiding metastability . . . . .	200
7.5 Clock Domain Crossing Strategies . . . . .	202
7.5.1 Synchronizing signals across clock domains . . . . .	202
7.5.2 Metastability mitigation techniques . . . . .	204
7.6 Power Estimation and Management . . . . .	206
7.6.1 Power-aware design techniques . . . . .	206
7.6.2 Estimating dynamic and static power in GPU pipelines . . . . .	208
<b>8 Vertex Processing Units</b>	<b>211</b>
8.1 Vertex Input Stage . . . . .	211
8.1.1 Input buffers . . . . .	211
8.1.2 Index fetch . . . . .	212
8.2 Vertex Input and Index Fetch in GPU Architectures . . . . .	212
8.2.1 Vertex attributes . . . . .	214
8.3 Vertex Attributes and Input Processing in GPU Architectures . . . . .	214
8.4 Transformation Unit . . . . .	215
8.4.1 Matrix multiplications . . . . .	215
8.4.2 Model-view-projection transformations . . . . .	216

8.5	Clipping and Culling . . . . .	218
8.5.1	View frustum clipping . . . . .	218
8.5.2	Backface culling . . . . .	219
8.6	Verilog Example . . . . .	222
8.6.1	Matrix multiplication implementation . . . . .	222
8.6.2	Vertex shader stub . . . . .	225
<b>9</b>	<b>Primitive Assembly and Setup</b>	<b>229</b>
9.1	Primitive Formation . . . . .	229
9.1.1	Assembling vertices . . . . .	229
9.1.2	Triangle formation . . . . .	230
9.2	Edge Equation Setup . . . . .	231
9.2.1	Calculating edge functions . . . . .	231
9.3	Bounding Box Calculation . . . . .	233
9.3.1	Minimal pixel regions . . . . .	233
9.4	Verilog Example . . . . .	234
9.4.1	Rasterizer setup block . . . . .	234
9.4.2	Parameterizable configurations . . . . .	236
<b>10</b>	<b>Rasterization Unit</b>	<b>239</b>
10.1	Scan Conversion . . . . .	239
10.1.1	Pixel coordinates iteration . . . . .	239
10.1.2	Coverage evaluation . . . . .	240
10.2	Z-Buffering . . . . .	243
10.2.1	Depth comparison logic . . . . .	243
10.2.2	Z-buffer memory interface . . . . .	245
10.3	Interpolation of Attributes . . . . .	246
10.3.1	Color interpolation . . . . .	246
10.3.2	Texture coordinates . . . . .	249
10.3.3	Normals . . . . .	251
10.4	Verilog Example . . . . .	252
10.4.1	Pipeline stage implementation . . . . .	252
10.4.2	Pixel fragment generation . . . . .	255
<b>11</b>	<b>Fragment Processing and Shading</b>	<b>259</b>
11.1	Fixed-Function Shading . . . . .	259
11.1.1	Flat shading . . . . .	259
11.1.2	Gouraud shading . . . . .	260
11.2	Texture Mapping . . . . .	262
11.2.1	Address calculation . . . . .	262
11.2.2	Texture sampling . . . . .	264
11.2.3	Bilinear filtering . . . . .	266
11.3	Alpha Blending . . . . .	267
11.3.1	Transparency blend equations . . . . .	267
11.4	Verilog Example . . . . .	269
11.4.1	Fragment shader unit . . . . .	269
11.4.2	Interpolated attributes handling . . . . .	272
<b>12</b>	<b>Memory Subsystem Design</b>	<b>275</b>
12.1	Framebuffer . . . . .	275
12.1.1	Memory-mapped framebuffer design . . . . .	275
12.1.2	Write policies . . . . .	276
12.1.3	Synchronization . . . . .	277
12.2	Texture Memory . . . . .	279
12.2.1	ROM-based textures . . . . .	279
12.2.2	RAM-based textures . . . . .	280
12.2.3	Caching strategies . . . . .	281
12.3	Double-Buffering . . . . .	282

12.3.1 Flicker-free updates . . . . .	282
12.4 Memory Arbitration Techniques . . . . .	284
12.4.1 Resolving access conflicts . . . . .	284
12.4.2 Memory bandwidth sharing strategies . . . . .	285
12.5 Cache Coherency Protocols . . . . .	288
12.5.1 Maintaining consistency across caches . . . . .	288
12.6 Verilog Example . . . . .	291
12.6.1 Dual-ported BRAM integration . . . . .	291
12.6.2 Framebuffer storage . . . . .	293
<b>13 Output Stage</b>	<b>297</b>
13.1 Dithering Gamma Correction (Optional) . . . . .	297
13.1.1 Tone adjustment . . . . .	297
13.1.2 Simple dithering algorithms . . . . .	299
13.2 Display Interface . . . . .	301
13.2.1 VGA signals . . . . .	301
13.2.2 HDMI signals . . . . .	302
13.2.3 Timing generation . . . . .	303
13.2.4 Sync signals . . . . .	305
13.3 Verilog Example . . . . .	307
13.3.1 VGA output signal generation . . . . .	307
13.3.2 Framebuffer usage . . . . .	310
<b>14 Top-Level Integration</b>	<b>315</b>
14.1 Putting It All Together . . . . .	315
14.1.1 Connecting vertex processing . . . . .	315
14.1.2 Rasterization . . . . .	316
14.1.3 Fragment shading . . . . .	317
14.1.4 Memory units . . . . .	318
14.2 Pipeline Control Logic . . . . .	320
14.2.1 Scheduling . . . . .	320
14.2.2 Stalling . . . . .	321
14.2.3 Backpressure handling . . . . .	323
14.3 Parameterization . . . . .	324
14.3.1 Adjusting resolution . . . . .	324
14.3.2 Configurable color depth . . . . .	326
14.3.3 Pipeline depth adjustment with Verilog parameters . . . . .	328
<b>15 Test and Verification Strategy</b>	<b>333</b>
15.1 Functional Simulation . . . . .	333
15.1.1 Testbench design . . . . .	333
15.1.2 Driving inputs . . . . .	334
15.1.3 Verifying outputs against reference images . . . . .	336
15.2 Regression Tests . . . . .	339
15.2.1 Testing wireframe scenes . . . . .	339
15.2.2 Testing solid color scenes . . . . .	341
15.2.3 Testing textured objects . . . . .	343
15.3 Debugging Techniques . . . . .	346
15.3.1 Using signal dumps (VCD) . . . . .	346
15.3.2 Assertions . . . . .	348
15.3.3 Checker modules . . . . .	349
15.4 Coverage-Driven Verification . . . . .	351
15.4.1 Defining coverage metrics for GPU pipelines . . . . .	351
15.4.2 Achieving high coverage in simulations . . . . .	352
15.5 Formal Verification Methods . . . . .	354
15.5.1 Verifying correctness with property checks . . . . .	354
15.5.2 Using formal tools like SystemVerilog Assertions . . . . .	356

15.6 Performance Modeling . . . . .	358
15.6.1 Profiling and simulation-based performance estimation . . . . .	358
15.6.2 Identifying critical performance bottlenecks . . . . .	360
<b>16 FPGA Prototyping</b>	<b>363</b>
16.1 Synthesis Considerations . . . . .	363
16.1.1 Resource usage optimization . . . . .	363
16.1.2 Timing closure . . . . .	364
16.1.3 Fitting design into target FPGA . . . . .	365
16.2 Hardware Testing . . . . .	367
16.2.1 Connecting FPGA board to a display . . . . .	367
16.2.2 Testing VGA/HDMI output . . . . .	368
16.3 Demonstration Projects . . . . .	370
16.3.1 Rendering simple 3D objects . . . . .	370
16.3.2 Rotating cubes . . . . .	372
16.3.3 Textured quads . . . . .	374
<b>17 Programmable Shading</b>	<b>379</b>
17.1 Shader Units . . . . .	379
17.1.1 Adding a programmable arithmetic pipeline . . . . .	379
17.1.2 Per-vertex and per-fragment shading . . . . .	380
17.2 Instruction Set for Shaders . . . . .	382
17.2.1 Designing simple instructions . . . . .	382
17.2.2 Register files . . . . .	383
17.2.3 Execution units . . . . .	385
17.3 Toolchain Integration . . . . .	386
17.3.1 Assembling shader microcode . . . . .	386
17.3.2 Loading shader programs into the GPU pipeline . . . . .	387
<b>18 Performance Optimizations</b>	<b>389</b>
18.1 Parallelization . . . . .	389
18.1.1 Adding multiple rasterizers . . . . .	389
18.1.2 Fragment pipelines . . . . .	391
18.1.3 Texture units for improved throughput . . . . .	393
18.2 Memory Caching . . . . .	395
18.2.1 Introducing caches for textures . . . . .	395
18.2.2 Z-buffers . . . . .	397
18.2.3 Prefetching techniques . . . . .	399
18.3 Pipelining Stages More Deeply . . . . .	401
18.3.1 Reducing combinational logic . . . . .	401
18.3.2 Balancing pipeline registers . . . . .	403
18.3.3 Optimizing stage transitions . . . . .	404
18.4 Area vs. Performance Tradeoff Analysis . . . . .	406
18.4.1 Evaluating tradeoffs in hardware resource utilization . . . . .	406
18.4.2 Finding an optimal balance for GPU designs . . . . .	408
18.5 Power vs. Performance Considerations . . . . .	409
18.5.1 Dynamic power reduction techniques . . . . .	409
18.5.2 Clock gating and power-aware pipeline design . . . . .	411
<b>19 Advanced Features</b>	<b>413</b>
19.1 Antialiasing Techniques . . . . .	413
19.1.1 Multi-sample rendering . . . . .	413
19.1.2 Coverage masks . . . . .	415
19.2 Anisotropic Filtering . . . . .	417
19.2.1 Advanced texture filtering techniques . . . . .	417
19.3 HDR/Color Management . . . . .	418
19.3.1 Wider color formats . . . . .	418
19.3.2 Tone mapping strategies . . . . .	420

19.4 Thermal Considerations . . . . .	422
19.4.1 Managing heat dissipation in GPU pipelines . . . . .	422
19.4.2 Designing thermally efficient hardware . . . . .	425
<b>20 Case Studies</b>	<b>429</b>
20.1 Minimalistic GPU . . . . .	429
20.1.1 A stripped-down design for teaching . . . . .	429
20.2 Intermediate GPU . . . . .	430
20.2.1 Design matching early 2000s fixed-function pipelines . . . . .	430
20.3 Scaling Up . . . . .	431
20.3.1 Modern GPU features . . . . .	431
20.3.2 Compute shaders . . . . .	433
20.3.3 GPGPU tasks . . . . .	434
20.4 Graphics Algorithms in Hardware . . . . .	436
20.4.1 Implementing algorithms like Bresenham's line drawing . . . . .	436
20.4.2 Phong shading in hardware . . . . .	438
<b>21 General-Purpose GPU Architectures</b>	<b>441</b>
21.1 Transitioning from Graphics to Compute Workloads . . . . .	441
21.1.1 Differences in architectural design for GPGPU . . . . .	441
21.1.2 Adapting GPU pipelines to support general-purpose tasks . . . . .	442
21.1.3 Challenges in balancing computation and memory bandwidth . . . . .	444
21.2 SIMD vs. SIMD . . . . .	446
21.2.1 Single Instruction, Multiple Threads (SIMT) execution model . . . . .	446
21.2.2 Comparison with SIMD and its limitations in general-purpose computing . . . . .	447
21.2.3 Designing thread hierarchies for diverse workloads . . . . .	448
21.3 Examples of GPGPU Workloads . . . . .	449
21.3.1 Scientific computing applications . . . . .	449
21.3.2 Real-world uses in financial modeling, data analysis, and simulations . . . . .	450
<b>22 Instruction Set for General Computation</b>	<b>453</b>
22.1 Designing Flexible Instructions . . . . .	453
22.1.1 Supporting common non-graphical operations . . . . .	453
22.1.2 Adding atomic operations for synchronization . . . . .	454
22.1.3 Handling variable-length and custom instructions . . . . .	455
22.2 Optimization for AI and Scientific Operations . . . . .	458
22.2.1 Floating-point operations (FP16, FP32, and FP64) . . . . .	458
22.2.2 Matrix multiply-accumulate for AI tasks . . . . .	460
22.2.3 Efficient support for parallel reduction and data aggregation . . . . .	461
<b>23 Memory Hierarchy for GPGPU</b>	<b>465</b>
23.1 High-Bandwidth Memory Design . . . . .	465
23.1.1 Designing interfaces for external memory like HBM . . . . .	465
23.1.2 Strategies for maximizing memory throughput . . . . .	467
23.2 Shared Memory and Caches . . . . .	469
23.2.1 Designing shared memory for intra-thread communication . . . . .	469
23.2.2 L1, L2, and unified cache hierarchy . . . . .	470
23.2.3 Optimizing for irregular memory access patterns . . . . .	472
<b>24 Parallelism and Thread Management</b>	<b>475</b>
24.1 Warp Scheduling and Divergence Handling . . . . .	475
24.1.1 Efficient scheduling of threads and warps . . . . .	475
24.1.2 Handling control-flow divergence in SIMT architectures . . . . .	476
24.2 Dynamic Parallelism Support . . . . .	477
24.2.1 Enabling threads to spawn new threads dynamically . . . . .	477
24.2.2 Managing resources for recursive and adaptive tasks . . . . .	480

<b>25 GPGPU Case Studies</b>	<b>483</b>
25.1 Implementing Matrix Multiplication . . . . .	483
25.1.1 Design and optimization of a high-performance matrix multiplication kernel. . . . .	483
25.1.2 Memory access patterns and cache utilization. . . . .	485
25.2 Solving Partial Differential Equations . . . . .	486
25.2.1 Parallel algorithms for finite difference and finite element methods. . . . .	486
25.2.2 Handling boundary conditions in distributed threads. . . . .	489
25.3 Basic Neural Network Inference . . . . .	491
25.3.1 Forward pass of a simple neural network using GPGPU. . . . .	491
25.3.2 Accelerating convolution and activation functions with Verilog. . . . .	493
<b>26 AI GPU Architecture</b>	<b>495</b>
26.1 Introduction to AI Workloads . . . . .	495
26.1.1 Differences between AI workloads and traditional GPU tasks. . . . .	495
26.1.2 Real-time inference vs. training. . . . .	496
26.2 Specialized Hardware for AI . . . . .	497
26.2.1 Adding tensor cores for efficient matrix multiplications. . . . .	497
26.2.2 Optimizing for low-precision arithmetic such as FP16 and INT8. . . . .	499
26.3 Memory Optimizations for AI . . . . .	501
26.3.1 Enhancing memory bandwidth and latency for large datasets. . . . .	501
26.3.2 Shared memory improvements for AI-specific dataflows. . . . .	503
26.4 AI Instruction Set . . . . .	506
26.4.1 Adding instructions for tensor operations and gradient reductions. . . . .	506
26.4.2 Support for fused multiply-add and activation functions. . . . .	508
26.5 AI-Specific Parallelism . . . . .	509
26.5.1 Balancing workload distribution for training neural networks. . . . .	509
26.5.2 Managing inter-layer communication in neural networks. . . . .	511
<b>27 AI Verilog Hardware Modules</b>	<b>513</b>
27.1 Tensor Processing Units . . . . .	513
27.1.1 tensor processing unit . . . . .	513
27.1.2 matrix multiply accumulate . . . . .	515
27.2 Neural Network Accelerators . . . . .	517
27.2.1 neural net training unit . . . . .	517
27.2.2 gradient computation unit . . . . .	518
27.3 Activation and Pooling Functions . . . . .	520
27.3.1 relu activation unit . . . . .	520
27.3.2 softmax unit . . . . .	521
27.3.3 max pooling unit . . . . .	523
<b>28 AI Dataflow and Scheduling</b>	<b>525</b>
28.1 Dataflow for AI Models . . . . .	525
28.1.1 ai dataflow controller . . . . .	525
28.2 Scheduling for Neural Network Layers . . . . .	527
28.2.1 layer scheduler . . . . .	527
28.2.2 pipeline dependency manager . . . . .	527
<b>29 AI GPU Case Studies</b>	<b>531</b>
29.1 Deep Learning Inference . . . . .	531
29.1.1 cnn inference engine . . . . .	531
29.1.2 rnn inference engine . . . . .	533
29.2 Training Neural Networks . . . . .	534
29.2.1 backpropagation unit . . . . .	534
29.2.2 optimizer unit . . . . .	537
29.3 Real-World Applications . . . . .	539
29.3.1 Implementing AI-driven image recognition workload . . . . .	539
29.3.2 Implementing AI-driven natural language processing workload . . . . .	540

<b>30 Future Trends in Hardware Acceleration</b>	<b>543</b>
30.1 Ray Tracing Hardware . . . . .	543
30.1.1 Comparison with traditional rasterization . . . . .	543
30.1.2 Extending design to support ray tracing . . . . .	544
30.2 Machine Learning Accelerators . . . . .	546
30.2.1 Lessons from GPU design for ML inference engines . . . . .	546
30.3 Emerging Technologies . . . . .	547
30.3.1 High-bandwidth memory (HBM) . . . . .	547
30.3.2 Chiplet designs . . . . .	548
30.3.3 RISC-V vector extensions . . . . .	549
<b>A Glossary of Terms</b>	<b>553</b>
<b>B Key Mathematical Equations</b>	<b>559</b>



# Using This Book

This book is designed to provide a deep, architectural perspective on modern GPU systems. Each chapter follows a structured progression, moving from foundational design principles to advanced subsystems such as memory hierarchies, execution models, and AI acceleration hardware. The emphasis throughout is on clarity, conceptual depth, and systems-level understanding—not on constructing GPUs or writing HDL implementations.

The intended audience includes computer engineers, hardware architects, graphics programmers, AI researchers, and advanced students of computer architecture. To get the most out of this book, readers should have prior exposure to undergraduate-level topics such as digital systems design, computer architecture, and the graphics pipeline. Familiarity with instruction sets, memory models, and basic parallelism will aid comprehension, although the book is designed to reinforce these concepts as they arise.

The writing in this book is intentionally expansive and occasionally repetitive. This is by design. Complex systems often require reinforcement and contextual restatement for their structures and behaviors to be fully understood. Rather than adopting a minimalist style, this book prioritizes precision and clarity, building a conceptual foundation before expanding into system-specific detail.

## Note on Code Samples

The code examples included are not intended as production-grade implementations. They are illustrative and conceptual, designed to highlight architectural logic, execution models, or design trade-offs. Some may omit full indentation, syntactic detail, or surrounding modules. They should be treated as pseudocode when necessary, guiding the reader’s attention toward function and flow rather than syntax or implementation.

Readers from a variety of technical backgrounds will find that this book strikes a balance between hardware theory, system-level analysis, and diagrammatic clarity. The focus is always on helping the reader internalize the blueprint of GPU architecture in an age where parallelism and hardware acceleration have become fundamental to modern computing.



# Introduction

The rise of modern graphics processing units (GPUs) represents one of the most profound developments in the history of computing. Originally conceived as fixed-function accelerators for rendering images to a screen, GPUs have evolved into massively parallel processors capable of accelerating a wide range of workloads, from 3D graphics and real-time simulation to deep learning and scientific computing. This book is dedicated to understanding the architectural foundation of those machines.

While CPUs have traditionally been optimized for sequential instruction execution and general-purpose computation, GPUs are engineered for throughput, exploiting spatial and temporal parallelism at every level of their design. The divergence in architectural philosophy between these two processing paradigms has become increasingly significant, especially as applications demand greater performance for rendering, training, and inference workloads. The GPU's ability to manage thousands of threads simultaneously, coupled with its high memory bandwidth and specialized acceleration units, makes it uniquely suited for these modern tasks.

This book aims to dissect and explain the architectural anatomy of modern GPUs, providing the reader with a clear understanding of how these systems are constructed, how they execute computations, and how they are optimized for both graphics and AI tasks. It is not a step-by-step engineering manual or an implementation guide. Instead, it serves as a comprehensive reference that maps out the structure and function of GPU subsystems, shedding light on the intricate components that define performance, efficiency, and scalability.

We begin by exploring the fundamental differences between CPUs and GPUs, establishing a conceptual framework for why GPUs are necessary and how their design principles have diverged. From there, we delve into the graphics pipeline—an evolution of stages that begins with vertex processing and culminates in pixel output—examining the functional units responsible for geometry processing, rasterization, shading, and post-processing. Understanding the interplay between these stages is crucial for grasping the GPU's role in visual computing.

Memory subsystems form the backbone of GPU performance. Topics such as memory hierarchy, caching, coalesced access, and shared memory are examined in detail, along with techniques used to optimize memory throughput and latency. These architectural decisions directly affect the execution model and determine the practical limits of scalability and performance.

Parallel execution is at the heart of GPU computing. We examine thread hierarchies, scheduling models, warps, and SIMD (Single Instruction, Multiple Threads) execution. By understanding how threads are managed, synchronized, and scheduled across streaming multiprocessors, readers will gain insight into the fundamental parallelism strategies that power modern GPUs.

Special attention is given to hardware support for AI workloads. Modern GPUs incorporate tensor cores, matrix engines, and low-precision arithmetic units to accelerate the training and inference of deep learning models. This section explores the architectural principles behind these accelerators, their integration into the GPU pipeline, and the challenges associated with heterogeneous compute.

Finally, we look forward to the future. Trends such as chiplet-based architectures, unified memory models, hardware ray tracing, and AI-driven design automation are poised to redefine the boundaries of GPU performance and application scope. By understanding where GPU architecture has been and where it is headed, readers will be better prepared to engage with the next wave of innovation in high-performance computing.

This book is written for technical professionals who seek a clear, architectural understanding of GPU systems. Whether you are a hardware designer, graphics programmer, AI researcher, or engineering student, this reference provides the depth, precision, and clarity needed to navigate the evolving landscape of accelerated computing.



# Chapter 1

## Popular HDL Tools for VHDL, Verilog, and SystemVerilog

### 1.1 Xilinx Vivado Design Suite

#### 1.1.1 FPGA Design and Development

Field-programmable gate arrays (FPGAs) have become integral to modern computing architectures, particularly in accelerating parallel workloads traditionally handled by graphics processing units (GPUs). The Xilinx Vivado Design Suite provides a comprehensive toolset for FPGA design and development, enabling engineers to leverage Xilinx FPGA devices for high-performance applications. This toolset supports synthesis, simulation, and implementation workflows, with full compatibility for hardware description languages (HDLs) such as VHDL and Verilog.

The Vivado Design Suite excels in IP integration, allowing designers to incorporate pre-verified intellectual property blocks into their designs. This feature reduces development time while ensuring reliability. For instance, Xilinx provides optimized IP cores for mathematical operations, memory controllers, and high-speed interfaces, which are critical for GPU-like architectures. The suite also supports block diagram creation through its IP Integrator, enabling visual design entry and rapid prototyping.

Timing analysis is another critical feature of Vivado, ensuring that designs meet stringent performance requirements. The tool performs static timing analysis (STA) to verify that signal propagation delays do not violate setup and hold constraints. This is particularly important in GPU architectures, where high clock frequencies and parallel data paths demand precise synchronization. The following equation represents a simplified timing constraint:

$$t_{clk} > t_{prop} + t_{setup}$$

Here,  $t_{clk}$  is the clock period,  $t_{prop}$  is the propagation delay, and  $t_{setup}$  is the setup time of the flip-flop. Vivado supports advanced synthesis techniques, such as retiming and pipelining, to optimize designs for speed and area. For example, retiming can be used to balance combinational logic delays across pipeline stages, improving throughput. The following Verilog snippet demonstrates a simple pipelined multiplier:

Code Sample 1.1: Pipelined Multiplier in Verilog

```
module pipelined_mult (
    input clk,
    input [15:0] a, b,
    output reg [31:0] p
);
    reg [15:0] a_reg, b_reg;
    reg [31:0] product;
    always @ (posedge clk) begin
        a_reg <= a;
        b_reg <= b;
        product <= a_reg * b_reg;
        p <= product;
    end
endmodule
```

The Vivado simulator enables functional and timing-accurate verification, supporting testbench creation in VHDL, Verilog, or SystemVerilog. Mixed-language simulation is also supported, allowing designers to combine modules written in different HDLs. For example, a testbench in SystemVerilog can instantiate a VHDL module for verification:

Code Sample 1.2: SystemVerilog Testbench for VHDL Module

```
module tb_vhdl_module;
    logic clk, rst;
    logic [7:0] data_in, data_out;

    vhdl_module dut (
        .clk(clk),
        .rst(rst),
        .data_in(data_in),
        .data_out(data_out)
    );

    initial begin
        clk = 0;
        forever #5 clk = ~clk;
    end

    initial begin
        rst = 1;
        #10 rst = 0;
        data_in = 8'hAA;
        #20 $finish;
    end
endmodule
```

Vivado's implementation tools handle place-and-route (P&R) optimizations, targeting Xilinx FPGA architectures such as UltraScale and Versal. The tool employs algorithms to minimize wirelength and congestion, which are critical for achieving high clock frequencies. Reports generated during implementation provide detailed metrics on resource utilization, power consumption, and timing closure.

The suite also supports partial reconfiguration, enabling dynamic updates to specific FPGA regions without disrupting the entire system. This is particularly useful in GPU-like architectures, where different kernels may require reconfiguration at runtime. Partial reconfiguration reduces downtime and improves flexibility in heterogeneous computing environments.

Power analysis in Vivado helps designers optimize energy efficiency, a key concern in modern GPU architectures. The tool estimates dynamic and static power consumption based on switching activity and device characteristics. Power optimization techniques, such as clock gating and voltage scaling, can be applied to reduce energy usage without compromising performance.

Vivado's HLS (High-Level Synthesis) feature allows designers to implement algorithms in C/C++ and automatically generate HDL code. This accelerates development for complex mathematical operations common in GPU workloads, such as matrix multiplication or fast Fourier transforms (FFTs). The following equation represents a matrix multiplication operation:

$$C_{ij} = \sum_{k=1}^n A_{ik} \times B_{kj}$$

HLS tools can pipeline this operation for parallel execution, significantly improving throughput. The Vivado Design Suite also includes a debugger with integrated logic analyzer (ILA) and virtual input/output (VIO) capabilities. These tools enable real-time monitoring of internal signals, simplifying the debugging process for complex designs. For example, an ILA can be inserted into a design to capture waveform data during operation:

Code Sample 1.3: ILA Instantiation in Verilog

```
ila_0 ila_inst (
    .clk(clk),
    .probe0(data_in),
    .probe1(data_out)
);
```

In summary, the Xilinx Vivado Design Suite provides a robust environment for FPGA design and development, particularly in the context of modern GPU architectures. Its comprehensive toolset supports synthesis, simulation, and implementation, with full compatibility for VHDL and Verilog. Key features such as IP integration, block diagram creation, and timing analysis streamline the design process, while advanced capabilities like HLS and partial reconfiguration enhance flexibility and performance. These tools empower engineers to harness the parallel processing capabilities of FPGAs, making them a viable alternative or complement to traditional GPU architectures.

### 1.1.2 Extensive use for Xilinx FPGA devices.

The extensive use of Xilinx FPGA devices in modern GPU architecture has become increasingly prevalent due to their reconfigurable nature and high-performance capabilities. Xilinx FPGAs offer a flexible platform for implementing custom hardware accelerators, which are critical for modern GPU workloads such as machine learning, real-time image processing, and high-performance computing.

The Xilinx Vivado Design Suite serves as the primary toolchain for FPGA design and development, providing a comprehensive environment for synthesis, simulation, and implementation. This toolset supports both `VHDL` and `Verilog`, enabling designers to leverage existing IP cores and develop custom logic efficiently.

One of the key advantages of Xilinx FPGAs in modern GPU architecture is their ability to integrate custom hardware accelerators alongside traditional GPU pipelines. For instance, convolutional neural networks (CNNs) used in deep learning applications can be offloaded to FPGA-based accelerators, significantly improving throughput and energy efficiency. The Vivado Design Suite facilitates this through its IP integration capabilities, allowing designers to incorporate pre-optimized IP cores such as the Xilinx Deep Learning Processor Unit (DPU). These IP cores are highly configurable and can be tailored to specific algorithmic requirements, as shown in the following Verilog snippet:

Code Sample 1.4: DPU Integration Example

```
module dpu_accelerator (
    input clk,
    input reset,
    input [31:0] input_data,
    output [31:0] output_data
);

// Instantiate Xilinx DPU IP core
xdpu dpu_inst (
    .ap_clk(clk),
    .ap_rst(reset),
    .ap_start(1'b1),
    .ap_done(),
    .input_r(input_data),
    .output_r(output_data)
);

endmodule
```

The Vivado Design Suite also supports block diagram creation, which simplifies the design of complex GPU architectures. Designers can drag and drop IP blocks, connect them using high-level abstractions, and generate synthesizable RTL code automatically. This feature is particularly useful for prototyping and validating GPU architectures before committing to low-level RTL development.

Additionally, the suite includes advanced timing analysis tools, ensuring that designs meet stringent performance requirements. For example, the following equation calculates the maximum clock frequency  $f_{max}$  of a design based on critical path delay  $t_{cp}$ :

$$f_{max} = \frac{1}{t_{cp}}$$

Timing constraints can be specified in Vivado using Synopsys Design Constraints (SDC) files, which are essential for achieving optimal performance in FPGA-based GPU designs. The Vivado timing analyzer provides detailed reports on setup and hold violations, enabling designers to iteratively refine their designs. Moreover, the suite supports cross-clock domain analysis, which is critical for modern GPU architectures that employ multiple clock domains for different functional units.

The Vivado Design Suite also excels in simulation capabilities, offering both behavioral and post-implementation simulation. Designers can verify their GPU architectures using the integrated XSIM simulator or third-party tools such as ModelSim. The following Verilog testbench demonstrates how to simulate a simple GPU shader core:

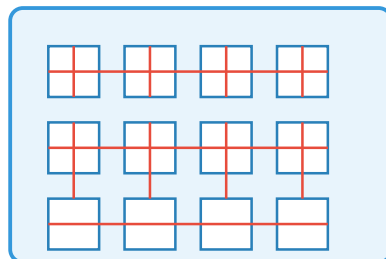
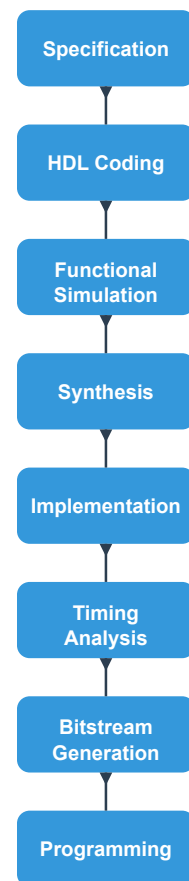
Code Sample 1.5: Shader Core Testbench

```
`timescale 1ns / 1ps

module shader_core_tb;
```

# FPGA Design and Development

## FPGA Design Flow



## VHDL Example

```

library IEEE;
use IEEE.std_logic_1164.all;
use IEEE.numeric_std.all;

entity counter is
port (
  clk : in std_logic;
  reset : in std_logic;
  count : out std_logic_vector(7 downto 0)
);
end entity counter;
  
```

## Key FPGA Components

### CLB (Configurable Logic Block)

Basic logic element containing LUTs, flip-flops, and multiplexers for implementing logic functions.

### IOB (Input/Output Block)

Interfaces between internal FPGA logic and external devices with configurable standards.

### Programmable Interconnect

Network of wires and programmable switches for connecting logic elements within the FPGA.

### DSP Blocks

Specialized blocks for efficient multiplication, addition, and other arithmetic operations.

## Advantages vs. GPU/ASIC

- Reconfigurable hardware
- Faster time-to-market than ASICs
- Lower non-recurring engineering costs
- Parallel processing architecture
- Lower power than GPUs for specific tasks

```

reg clk;
reg reset;
reg [31:0] vertex_data;
wire [31:0] shaded_data;

shader_core uut (
    .clk(clk),
    .reset(reset),
    .vertex_data(vertex_data),
    .shaded_data(shaded_data)
);

initial begin
    clk = 0;
    forever #5 clk = ~clk;
end

initial begin
    reset = 1;
    #10 reset = 0;
    vertex_data = 32'h3F800000; // 1.0 in IEEE 754
    #100 $finish;
end
endmodule

```

Another critical feature of the Vivado Design Suite is its support for high-level synthesis (HLS), which allows designers to implement GPU algorithms using C/C++ or OpenCL. This is particularly advantageous for rapidly prototyping complex algorithms without delving into RTL design. For example, a matrix multiplication kernel for a GPU accelerator can be written in C and synthesized directly to FPGA hardware using Vivado HLS. The following C code illustrates a simple matrix multiplication kernel:

Code Sample 1.6: Matrix Multiplication Kernel

```

void matrix_multiply(float A[16][16], float B[16][16], float C[16][16]) {
    #pragma HLS PIPELINE II=1
    for (int i = 0; i < 16; i++) {
        for (int j = 0; j < 16; j++) {
            C[i][j] = 0;
            for (int k = 0; k < 16; k++) {
                C[i][j] += A[i][k] * B[k][j];
            }
        }
    }
}

```

The Vivado Design Suite also provides robust debugging tools, such as the Integrated Logic Analyzer (ILA), which enables real-time monitoring of internal FPGA signals. This is invaluable for diagnosing issues in GPU architectures, particularly when dealing with parallel processing and synchronization. The ILA can be configured to trigger on specific conditions, capturing waveform data for post-analysis:

Code Sample 1.7: ILA Instantiation in Verilog

```

ila_0 ila_inst (
    .clk(clk),
    .probe0(data_in),
    .probe1(data_out)
);

```

Furthermore, the suite supports partial reconfiguration, allowing designers to dynamically update portions of the FPGA without disrupting the entire system. This is especially useful for GPU architectures that require runtime adaptability, such as those used in autonomous vehicles or adaptive beamforming systems.

In summary, the extensive use of Xilinx FPGA devices in modern GPU architecture is facilitated by the Vivado Design Suite's comprehensive toolset. From IP integration and block diagram creation to timing analysis and high-level synthesis, the suite provides all the necessary tools for designing high-performance GPU accelerators.

Its support for `VHDL` and `Verilog`, coupled with advanced debugging and simulation capabilities, makes it an indispensable tool for FPGA-based GPU development. The ability to leverage pre-optimized IP cores and perform detailed timing analysis ensures that designs meet the stringent performance and power requirements of modern GPU workloads.

### 1.1.3 Comprehensive toolset for synthesis, simulation, and implementation.

The Xilinx Vivado Design Suite is a comprehensive toolset for synthesis, simulation, and implementation in modern FPGA design, particularly for Xilinx FPGA devices. It provides a robust environment for developing high-performance digital systems, leveraging the parallel processing capabilities of modern GPU architectures. The suite supports both `VHDL` and `Verilog`, enabling designers to work with their preferred hardware description language (HDL).

A key feature of Vivado is its IP integration capability, allowing seamless incorporation of pre-designed intellectual property (IP) cores into custom designs. This accelerates development by reducing the need to reimplement common functionalities. The IP Integrator tool facilitates block diagram creation, enabling designers to visually assemble systems using drag-and-drop interfaces. For example, a designer can integrate a Xilinx DSP48E1 block into a signal processing pipeline without manually writing low-level HDL code:

Code Sample 1.8: DSP48E1 Instantiation in Verilog

```
module dsp_example (
    input [17:0] A, B,
    output [47:0] P
);
    DSP48E1 #(
        .USE_DPORT("TRUE"),
        .MREG(1)
    ) dsp_inst (
        .A(A),
        .B(B),
        .P(P)
    );
endmodule
```

Timing analysis is another critical feature of Vivado, ensuring designs meet performance requirements. The tool performs static timing analysis (STA) to verify setup and hold times, clock skew, and other timing constraints. The following equation represents the setup time constraint for a flip-flop:

$$t_{su} \leq T_{clk} - t_{cq} - t_{comb}$$

Here,  $t_{su}$  is the setup time,  $T_{clk}$  is the clock period,  $t_{cq}$  is the clock-to-Q delay, and  $t_{comb}$  is the combinatorial logic delay. Vivado generates detailed timing reports, highlighting violations and suggesting optimizations.

The synthesis engine in Vivado converts HDL code into a gate-level netlist optimized for Xilinx FPGAs. It employs advanced algorithms to minimize resource usage and maximize clock frequency. For instance, the tool can infer block RAM (BRAM) from HDL constructs, as shown below:

Code Sample 1.9: BRAM Inference in VHDL

```
library IEEE;
use IEEE.STD_LOGIC_1164.ALL;
use IEEE.NUMERIC_STD.ALL;

entity bram_example is
    Port (
        clk : in STD_LOGIC;
        addr : in unsigned(9 downto 0);
        data_out : out STD_LOGIC_VECTOR(31 downto 0)
    );
end bram_example;

architecture Behavioral of bram_example is
    type ram_type is array (0 to 1023) of STD_LOGIC_VECTOR(31 downto 0);
    signal ram : ram_type := (others => (others => '0'));
```

```

begin
  process (clk)
  begin
    if rising_edge(clk) then
      data_out <= ram(to_integer(addr));
    end if;
  end process;
end Behavioral;

```

Vivado also supports mixed-language simulation, allowing VHDL and Verilog modules to coexist in the same testbench. The XSIM simulator, integrated into Vivado, provides cycle-accurate simulation for verifying functional correctness. For example, a testbench for a simple adder can be written as follows:

Code Sample 1.10: Mixed-Language Testbench

```

// Verilog testbench for VHDL adder
module tb_adder;
  reg [7:0] a, b;
  wire [8:0] sum;

  // Instantiate VHDL adder
  adder_entity uut (.a(a), .b(b), .sum(sum));

  initial begin
    a = 8'h12;
    b = 8'h34;
    #10;
    $display("Sum = %h", sum);
  end
endmodule

```

The implementation phase in Vivado involves place-and-route (PAR), where the synthesized netlist is mapped to physical FPGA resources. The tool optimizes for performance, power, and area (PPA) by considering device-specific constraints. For example, a design targeting the Xilinx UltraScale+ architecture can leverage dedicated DSP slices and high-speed transceivers.

The following equation models the power consumption of a CMOS gate:

$$P = \alpha C V_{dd}^2 f$$

Here,  $\alpha$  is the activity factor,  $C$  is the load capacitance,  $V_{dd}$  is the supply voltage, and  $f$  is the clock frequency. Vivado's power estimation tools use such models to predict dynamic and static power dissipation.

Vivado's debug capabilities include integrated logic analyzers (ILA) and virtual input/output (VIO) cores, enabling real-time hardware debugging. An ILA core can be inserted into the design to probe internal signals during operation:

Code Sample 1.11: ILA Instantiation in Verilog

```

module debug_example (
  input clk,
  input [7:0] data_in,
  output [7:0] data_out
);

// Insert ILA core
ila_0 ila_inst (
  .clk(clk),
  .probe0(data_in),
  .probe1(data_out)
);

endmodule

```

The suite also supports high-level synthesis (HLS) through the Vitis HLS tool, enabling C/C++ to RTL conversion. This is particularly useful for algorithm acceleration on FPGAs. For example, a matrix multiplication kernel can be optimized for parallel execution:

## Code Sample 1.12: HLS Matrix Multiplication

```
void matrix_mult ( int A[16][16], int B[16][16], int C[16][16] ) {
    #pragma HLS PIPELINE
    for (int i = 0; i < 16; i++) {
        for (int j = 0; j < 16; j++) {
            C[i][j] = 0;
            for (int k = 0; k < 16; k++) {
                C[i][j] += A[i][k] * B[k][j];
            }
        }
    }
}
```

Vivado's scripting capabilities, using Tcl, automate repetitive tasks and enable batch processing. A Tcl script can synthesize, implement, and generate bitstreams without manual intervention:

## Code Sample 1.13: Tcl Script for Automation

```
# Create project
create_project -force my_project ./my_project -part xc7k325tffg900-2

# Add source files
add_files -norecurse {./src/design.vhd ./src/tb.vhd}

# Run synthesis and implementation
launch_runs synth_1 -jobs 4
wait_on_run synth_1

launch_runs impl_1 -to_step write_bitstream -jobs 4
wait_on_run impl_1
```

In summary, the Xilinx Vivado Design Suite provides a comprehensive toolset for FPGA development, integrating synthesis, simulation, and implementation workflows. Its support for VHDL and Verilog, IP integration, timing analysis, and debug features make it indispensable for modern GPU and FPGA designs. The suite's ability to optimize for performance, power, and area ensures efficient utilization of Xilinx FPGA resources.

### 1.1.4 Supported Languages

The Xilinx Vivado Design Suite is a comprehensive toolset for FPGA design and development, offering extensive support for Xilinx FPGA devices. One of its critical aspects is the supported hardware description languages (HDLs), primarily VHDL and Verilog, which are fundamental for digital circuit design. The suite provides full support for both languages, catering to a wide range of design methodologies and preferences.

VHDL (VHSIC Hardware Description Language) and Verilog are industry-standard languages, each with distinct syntactic and semantic features. VHDL is strongly typed and verbose, making it suitable for complex system-level designs, while Verilog's C-like syntax appeals to designers favoring brevity and flexibility. The Vivado Design Suite ensures seamless compilation, synthesis, and simulation for both, enabling designers to leverage their strengths in modern GPU architecture and FPGA development.

The Vivado toolchain integrates advanced synthesis engines that optimize HDL code for Xilinx FPGA architectures. For example, the synthesis process transforms high-level HDL constructs into low-level netlists, targeting specific FPGA resources such as lookup tables (LUTs), flip-flops, and DSP slices. The tool supports mixed-language designs, allowing modules written in VHDL to instantiate Verilog components and vice versa. This interoperability is crucial for large-scale projects where legacy code or third-party IP may use different HDLs.

Below is an example of a simple Verilog module synthesized in Vivado:

Code Sample 1.14: Verilog Example

```
module adder (
    input wire [3:0] a,
    input wire [3:0] b,
    output reg [4:0] sum
);
always @(*) begin
    sum = a + b;
end
endmodule
```

The Vivado simulator supports behavioral, post-synthesis, and post-implementation simulations, ensuring design correctness at every stage. For timing analysis, the tool employs static timing analysis (STA) to verify that the design meets clock constraints. The following equation illustrates the setup time constraint for a flip-flop:

$$t_{clk} \geq t_{su} + t_{cq} + t_{comb}$$

where  $t_{clk}$  is the clock period,  $t_{su}$  is the setup time,  $t_{cq}$  is the clock-to-Q delay, and  $t_{comb}$  is the combinational logic delay. Violations are reported in the timing summary, guiding designers to resolve critical paths.

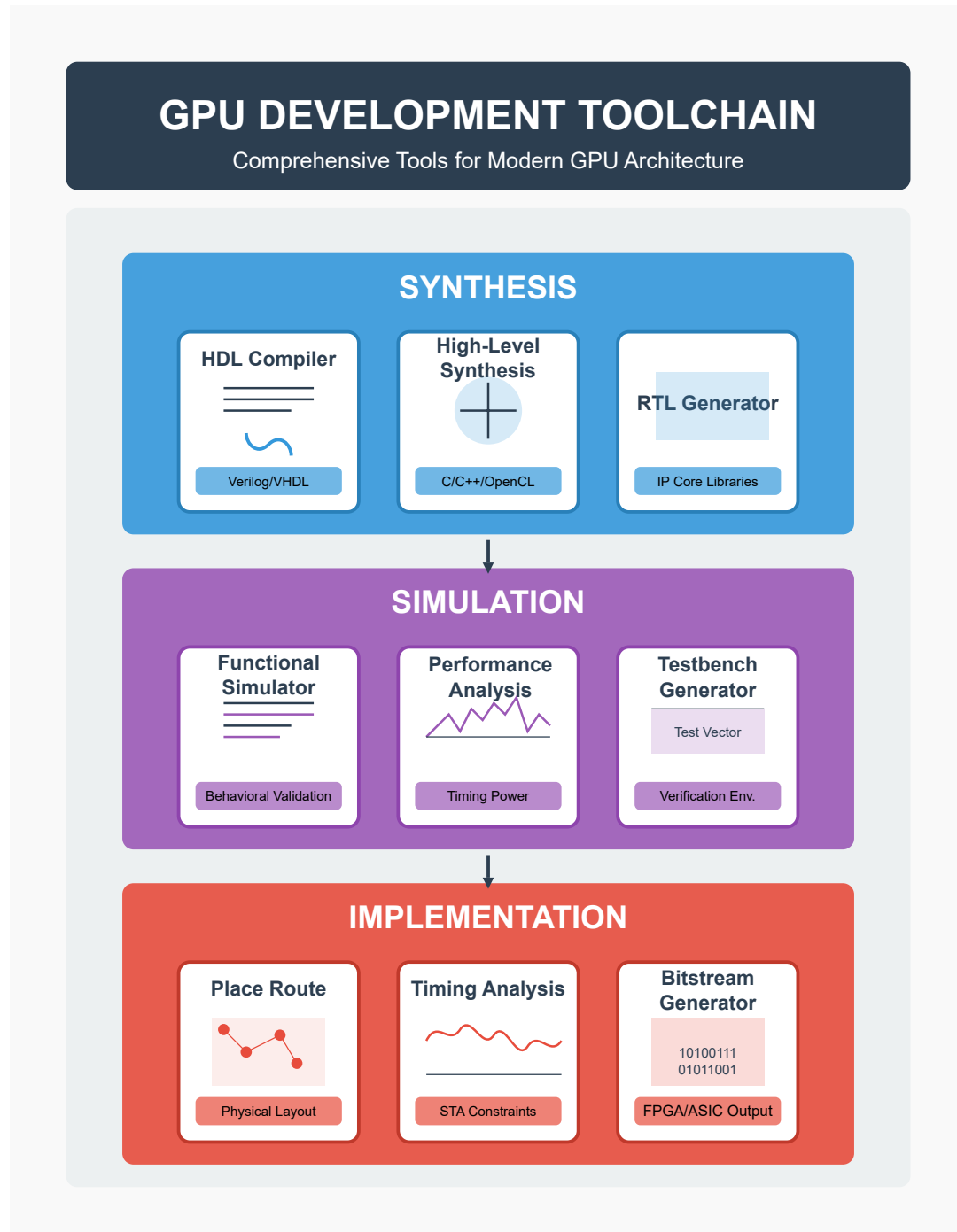
IP integration is another key feature of Vivado, enabling the reuse of pre-verified intellectual property blocks. The suite includes the IP Integrator tool, which facilitates block diagram creation via a drag-and-drop interface. Designers can instantiate Xilinx IP cores, such as memory controllers or DSP blocks, and connect them using AXI4 or other standard interfaces. For instance, a Zynq SoC design might integrate a processing system (PS) with programmable logic (PL) using AXI interconnects. The IP catalog supports parameterizable cores, allowing customization for specific applications.

Below is a snippet of a VHDL entity instantiating a Xilinx FIFO IP core:

Code Sample 1.15: VHDL IP Instantiation

```
entity fifo_wrapper is
port (
    clk      : in std_logic;
    din     : in std_logic_vector(7 downto 0);
    dout    : out std_logic_vector(7 downto 0);
    wr_en   : in std_logic;
    rd_en   : in std_logic
);
end entity;

architecture rtl of fifo_wrapper is
component fifo_generator_0
port (
    clk      : in std_logic;
    din     : in std_logic_vector(7 downto 0);
```



```

dout  : out std_logic_vector(7 downto 0);
wr_en : in std_logic;
rd_en : in std_logic
);
end component;
begin
fifo_inst : fifo_generator_0
port map (
    clk    => clk,
    din    => din,
    dout   => dout,
    wr_en => wr_en,
    rd_en => rd_en
);
end architecture;

```

The Vivado Design Suite also supports SystemVerilog for verification, though its synthesis capabilities are limited compared to Verilog and VHDL. SystemVerilog constructs such as interfaces and assertions enhance testbench development, enabling advanced verification methodologies like Universal Verification Methodology (UVM). However, synthesis tools typically ignore assertions and focus on synthesizable constructs.

For example, the following SystemVerilog code demonstrates an interface for AXI4-Lite:

Code Sample 1.16: SystemVerilog Interface

```

interface axi4_lite_if #(parameter ADDR_WIDTH = 32, DATA_WIDTH = 32);
    logic aclk;
    logic aresetn;
    logic [ADDR_WIDTH-1:0] awaddr;
    logic awvalid;
    logic awready;
    logic [DATA_WIDTH-1:0] wdata;
    logic wvalid;
    logic wready;
    logic [1:0] bresp;
    logic bvalid;
    logic bready;
    logic [ADDR_WIDTH-1:0] araddr;
    logic arvalid;
    logic arready;
    logic [DATA_WIDTH-1:0] rdata;
    logic [1:0] rresp;
    logic rvalid;
    logic rready;
endinterface

```

The suite's implementation phase includes place-and-route (PAR) algorithms that map the synthesized netlist onto the FPGA fabric. Vivado employs advanced algorithms to optimize for performance, power, and area (PPA). The following equation models the power dissipation of an FPGA:

$$P_{total} = P_{dynamic} + P_{static}$$

where  $P_{dynamic}$  is the switching power and  $P_{static}$  is the leakage power. The Power Report tool provides detailed breakdowns, aiding in low-power design.

Vivado's support for scripting with Tcl (Tool Command Language) automates repetitive tasks. Designers can write scripts to generate projects, run synthesis, and perform batch simulations. Below is a Tcl script to create a new project:

Code Sample 1.17: Tcl Script Example

```

create_project -force my_project ./my_project -part xc7z020clg400-1
add_files -fileset sources_1 {adder.v}
add_files -fileset sim_1 {adder_tb.v}
launch_simulation

```

The Vivado Design Suite's comprehensive toolset, combined with its robust support for HDLs, makes it indispensable for modern FPGA development. Its integration of synthesis, simulation, and implementation tools streamlines the design flow, while features like IP integration and timing analysis ensure high-quality results. The suite's adherence to industry standards and continuous updates solidify its position as a leading solution for Xilinx FPGA-based projects.

### 1.1.5 Full support for VHDL and Verilog.

The Xilinx Vivado Design Suite is a comprehensive toolset for FPGA design and development, offering full support for both VHDL and Verilog as hardware description languages (HDLs). This capability is critical for modern GPU architecture, where high-performance computing demands efficient hardware-software co-design. Vivado's integration of VHDL and Verilog enables designers to leverage the strengths of both languages, ensuring compatibility with legacy code while supporting modern design methodologies.

The suite's synthesis engine optimizes HDL code for Xilinx FPGA devices, translating high-level abstractions into low-level logic implementations. For example, the synthesis process includes advanced algorithms for resource sharing, retiming, and pipelining, which are essential for achieving high clock frequencies in GPU architectures.

The Vivado Design Suite provides a unified environment for synthesis, simulation, and implementation, streamlining the FPGA development workflow. Synthesis transforms HDL code into a gate-level netlist, while simulation allows designers to verify functionality before hardware deployment. Vivado's simulator supports mixed-language simulation, enabling seamless interaction between VHDL and Verilog modules. This is particularly useful in GPU design, where different IP cores may be written in different HDLs.

The implementation phase includes place-and-route, where the tool maps the synthesized netlist to physical resources on the FPGA. Timing analysis ensures that the design meets performance constraints, a critical consideration for GPU architectures where latency and throughput are paramount.

IP integration is a key feature of the Vivado Design Suite, facilitating the reuse of pre-verified intellectual property blocks. This accelerates development by allowing designers to incorporate complex functions, such as memory controllers or arithmetic units, without reinventing them. The suite includes the IP Integrator tool, which enables block diagram creation through a drag-and-drop interface. This graphical approach simplifies the assembly of heterogeneous systems, such as those found in modern GPUs, where multiple processing elements must coexist. The IP Integrator automatically generates HDL wrappers for the block diagram, ensuring consistency between the graphical and textual representations of the design.

Timing analysis is another critical feature of Vivado, ensuring that the design meets the required clock frequencies. The suite includes static timing analysis (STA) tools that evaluate setup and hold times, as well as clock skew. For GPU architectures, where parallel processing demands precise synchronization, STA is indispensable. Vivado's timing analyzer provides detailed reports, highlighting critical paths and suggesting optimizations. The tool also supports cross-clock domain analysis, which is essential for designs with multiple clock domains, a common characteristic of modern GPUs.

The Vivado Design Suite supports a wide range of Xilinx FPGA devices, from low-cost Artix series to high-performance Virtex and Kintex families. This flexibility allows designers to select the optimal device for their GPU architecture, balancing performance, power consumption, and cost. The suite's device-specific optimizations ensure that the synthesized design fully exploits the capabilities of the target FPGA. For example, Vivado leverages the DSP slices and block RAMs in Xilinx FPGAs to implement arithmetic operations and memory structures efficiently, which are fundamental to GPU computation.

Vivado's support for VHDL and Verilog extends to advanced language features, such as generics in VHDL and parameters in Verilog, enabling parametric design. This is particularly useful for GPU architectures, where modularity and scalability are essential. The suite also supports SystemVerilog for verification, allowing designers to write complex testbenches.

The following Verilog code illustrates a simple GPU shader core implemented in Vivado:

Code Sample 1.18: GPU Shader Core in Verilog

```
module shader_core (
    input clk,
    input [31:0] vertex_data,
    output [31:0] shaded_data
);
    reg [31:0] transform_matrix [0:3][0:3];
    always @ (posedge clk) begin
        shaded_data <= transform_matrix[0][0] * vertex_data;
    end
endmodule
```

The Vivado Design Suite also includes high-level synthesis (HLS) capabilities, allowing designers to write algorithms in C, C++, or SystemC and automatically generate HDL code. This is particularly advantageous for GPU architectures, where complex algorithms, such as rasterization or ray tracing, can be prototyped at a higher

## Modern GPU Architecture

### Supported Programming Languages

GPU programming has evolved from specialized graphics APIs to general-purpose computing with multiple language options for different use cases and abstraction levels.

Graphics APIs	GPGPU Languages	ML Frameworks
<b>OpenGL</b> Cross-platform 2D/3D graphics API <ul style="list-style-type: none"> <li>● GLSL shader language</li> <li>● Accessible from C, C++, Java</li> <li>● Legacy but still widely used</li> </ul>	<b>CUDA</b> NVIDIA's parallel computing platform <ul style="list-style-type: none"> <li>● C/C++ with NVIDIA extensions</li> <li>● NVIDIA GPUs only</li> <li>● Rich ecosystem, libraries .)</li> <li>● Unified Memory model</li> </ul>	<b>Deep Learning</b> ML framework GPU acceleration <ul style="list-style-type: none"> <li>● TensorFlow (CUDA, ROCm)</li> <li>● PyTorch (CUDA, Metal)</li> <li>● JAX, ONNX, MXNet</li> </ul>
<b>DirectX</b> Microsoft graphics/game API <ul style="list-style-type: none"> <li>● HLSL shader language</li> <li>● DirectCompute for GPGPU</li> <li>● Windows ecosystem focus</li> </ul>	<b>OpenCL</b> Open Computing Language <ul style="list-style-type: none"> <li>● Cross-platform standard</li> <li>● C-based kernel language</li> <li>● Works on CPUs, GPUs, FPGAs</li> <li>● Explicit memory management</li> </ul>	<b>GPU Libraries</b> Domain-specific GPU acceleration <ul style="list-style-type: none"> <li>● NVIDIA libraries (cuDNN, RAPIDS)</li> <li>● ArrayFire, ViennaCL</li> <li>● Numba, CuPy (Python GPU)</li> </ul>
<b>Vulkan</b> Modern low-level graphics API <ul style="list-style-type: none"> <li>● SPIR-V intermediate bytecode</li> <li>● Cross-platform, low overhead</li> <li>● Compute capabilities built-in</li> <li>● Explicit memory management</li> </ul>	<b>Other GPGPU</b> Platform-specific options <ul style="list-style-type: none"> <li>● Metal (Apple platforms)</li> <li>● ROCm (AMD GPUs)</li> <li>● oneAPI (Intel vision)</li> </ul>	<b>Language Bindings</b> GPU access from other languages <ul style="list-style-type: none"> <li>● Python (PyCUDA, PyOpenCL)</li> <li>● Java (JOCL, JCUDA)</li> <li>● Julia (CUDA.jl, Metal.jl)</li> <li>● Rust (rust-gpu, wgpu)</li> </ul>

**Evolution of GPU Programming Languages**



The timeline illustrates the evolution of GPU programming languages:

- 2000s:** Fixed Graphics Pipeline
- 2006-2008:** CUDA & OpenCL integration
- 2010s:** ML Framework Integration
- 2014-2016:** Vulkan & Modern APIs
- Present:** Cross-platform Abstractions

*Note: Specific GPU support varies by vendor, hardware generation, and driver version.  
Most modern GPU applications use a combination of these languages and frameworks.*

level of abstraction. HLS tools in Vivado optimize the generated HDL for performance and resource utilization, reducing the time-to-market for GPU designs.

The suite's debugging tools, such as the Integrated Logic Analyzer (ILA), enable real-time observation of internal signals in the FPGA. This is invaluable for GPU development, where identifying bottlenecks or synchronization issues is challenging. The ILA can be configured to trigger on specific conditions, capturing waveforms for post-analysis. Vivado also supports the ChipScope Pro tool for advanced debugging, providing deeper visibility into the design.

Vivado's scripting capabilities, using Tcl (Tool Command Language), allow for automation of repetitive tasks. This is particularly useful in large GPU designs, where manual intervention would be time-consuming. Scripts can automate synthesis, implementation, and bitstream generation, ensuring consistency across multiple iterations. The following Tcl script demonstrates a basic workflow:

Code Sample 1.19: Vivado Tcl Script for Synthesis

```
read_vhdl -library work shader_core.vhd
read_verilog -library work shader_core.v
synth_design -top shader_core -part xc7k325tffg900-2
write_checkpoint -force shader_core.dcp
```

The Vivado Design Suite's comprehensive toolset, combined with its full support for VHDL and Verilog, makes it an indispensable platform for modern GPU architecture development. Its integration of IP cores, block diagram creation, and timing analysis ensures that designers can meet the stringent requirements of high-performance computing. By leveraging Xilinx FPGA devices, Vivado enables the implementation of scalable and efficient GPU architectures, from embedded systems to data center accelerators. The suite's continuous updates and adherence to industry standards ensure that it remains at the forefront of FPGA design tools, supporting the evolving demands of GPU technology.

### 1.1.6 Key Features

Modern GPU architectures have evolved significantly, with Xilinx FPGAs playing a crucial role in accelerating parallel computing tasks. The Xilinx Vivado Design Suite provides a comprehensive toolset for FPGA design and development, enabling efficient implementation of GPU-like architectures. Key features of Vivado include high-level synthesis (HLS), IP integration, and timing analysis, which are essential for optimizing performance in modern GPU designs.

The Vivado Design Suite supports both VHDL and Verilog, allowing designers to choose the most suitable hardware description language for their projects. For instance, a simple Verilog module for a GPU shader core can be implemented as follows:

Code Sample 1.20: GPU Shader Core in Verilog

```
module shader_core (
    input clk,
    input [31:0] data_in,
    output reg [31:0] data_out
);
    always @(posedge clk) begin
        data_out <= data_in * 2; // Simple arithmetic operation
    end
endmodule
```

IP integration is a critical feature of Vivado, enabling designers to incorporate pre-optimized intellectual property blocks into their designs. This reduces development time and ensures reliability. The Vivado IP Integrator facilitates block diagram creation, allowing visual composition of complex systems. For example, a GPU memory controller can be integrated with a custom shader core using drag-and-drop functionality.

Timing analysis is another cornerstone of Vivado, ensuring that designs meet stringent performance requirements. The tool provides detailed reports on setup and hold violations, enabling designers to refine their implementations. The following equation represents the setup slack calculation:

$$t_{slack} = t_{cycle} - t_{prop} - t_{setup}$$

where  $t_{cycle}$  is the clock period,  $t_{prop}$  is the propagation delay, and  $t_{setup}$  is the setup time of the flip-flop.

Vivado's synthesis engine optimizes logic utilization and performance, translating HDL code into efficient FPGA configurations. The tool supports advanced optimization techniques such as retiming and pipelining, which are vital for high-performance GPU architectures. For example, a pipelined floating-point multiplier can be described in VHDL as:

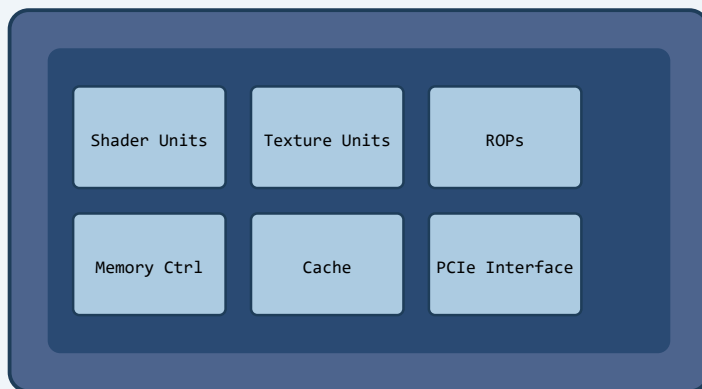
Code Sample 1.21: Pipelined Multiplier in VHDL

```
entity fp_multiplier is
    port (
        clk      : in  std_logic;
        a, b    : in  float32;
        result : out float32
    );
end entity;

architecture behavioral of fp_multiplier is
    signal stage1, stage2, stage3 : float32;
begin
    process(clk)
    begin
        if rising_edge(clk) then
            stage1 <= a * b;          -- Stage 1: Multiplication
            stage2 <= stage1;        -- Stage 2: Buffering
            result <= stage2;        -- Stage 3: Output
        end if;
    end process;
end architecture;
```

## Modern GPU Architecture

Full support for VHDL and Verilog



### HDL Integration in GPU Design

#### VHDL

```
library IEEE;
use IEEE.STD_LOGIC_1164.ALL;
entity GPU_CORE is
port (
clk : in STD_LOGIC;
data_in : in STD_LOGIC_VECTOR(31 downto 0);
data_out : out STD_LOGIC_VECTOR(31 downto 0)
);
end entity;
```

#### VHDL Features:

- Strong type checking
- Concurrent processing
- IEEE standard 1076
- Common in European designs

#### Verilog

```
module gpu_shader (
input wire clk,
input wire [31:0] instruction,
input wire [31:0] data_in,
output reg [31:0] data_out
);
always @(posedge clk) begin
data_out = data_in + 32'h1;
end
endmodule
```

#### Verilog Features:

- C-like syntax
- IEEE standard 1364
- Widely used in US Asia
- Hardware-oriented language

The Vivado simulator enables functional verification, ensuring correctness before hardware deployment. Designers can simulate their GPU architectures under various workloads, identifying potential bottlenecks. Waveform analysis is supported, allowing detailed inspection of signal transitions.

For large-scale GPU designs, Vivado's hierarchical project management simplifies organization. Submodules can be developed independently and integrated seamlessly. This modular development reduces complexity, facilitates parallel team collaboration, and promotes the reuse of components, thereby enhancing productivity.

Vivado also supports SystemVerilog, enabling advanced verification methodologies such as constrained-random testing. A SystemVerilog testbench for a GPU texture unit might include assertions to validate correctness:

Code Sample 1.22: SystemVerilog Testbench for Texture Unit

```
module texture_unit_tb;
    logic clk;
    logic [31:0] tex_coord, texel;
    texture_unit dut (.*);

    initial begin
        clk = 0;
        forever #5 clk = ~clk;
    end

    initial begin
        tex_coord = 32'h3F800000; // 1.0 in IEEE 754
        #10;
        assert (texel == 32'h40400000)
            else $error("Incorrect texel");
    end
endmodule
```

Power analysis is another critical feature, particularly for energy-efficient GPU designs. Vivado estimates dynamic and static power consumption, guiding optimizations. The power dissipation of a CMOS circuit can be approximated by:

$$P_{total} = P_{dynamic} + P_{static}$$

where  $P_{dynamic}$  is the switching power and  $P_{static}$  is the leakage power.

Vivado's partial reconfiguration capability allows dynamic updates to FPGA logic without full reprogramming. This is useful for GPUs requiring runtime adaptability. For example, a reconfigurable shader core can switch between arithmetic and texture units based on workload demands.

The suite also includes Tcl scripting support for automation, streamlining repetitive tasks. A Tcl script for batch synthesis might include:

Code Sample 1.23: Tcl Script for Batch Synthesis

```
read_verilog shader_core.v
synth_design -top shader_core -part xc7z020
opt_design
place_design
route_design
write_bitstream -file shader_core.bit
```

In summary, the Xilinx Vivado Design Suite provides a robust environment for modern GPU architecture development on FPGAs. Its comprehensive toolset, language support, and advanced features like IP integration and timing analysis make it indispensable for high-performance design. The ability to simulate, synthesize, and implement complex systems ensures that designers can achieve optimal results efficiently.

### 1.1.7 IP integration, block diagram creation, and timing analysis.

Modern GPU architectures leverage FPGA-based acceleration to enhance performance in compute-intensive applications. The Xilinx Vivado Design Suite provides a comprehensive toolset for FPGA design and development, particularly for Xilinx FPGA devices. Key features include IP integration, block diagram creation, and timing analysis, which are critical for optimizing GPU architectures.

IP integration in Vivado simplifies the reuse of pre-verified intellectual property cores, reducing development time. The suite supports a wide range of Xilinx IP cores, including DSP blocks, memory controllers, and high-speed transceivers. These cores are integrated into the design using the IP Integrator tool, which automates connectivity and parameterization. For example, a GPU designer can instantiate a floating-point multiplier IP core with the following Verilog snippet:

Code Sample 1.24: Floating-Point Multiplier IP Instantiation

```
module fp_multiplier (
    input logic [31:0] a, b,
    output logic [31:0] result
);
    floating_point_multiplier u0 (
        .aclk(clk),
        .s_axis_a_tvalid(1'b1),
        .s_axis_a_tdata(a),
        .s_axis_b_tvalid(1'b1),
        .s_axis_b_tdata(b),
        .m_axis_result_tvalid(),
        .m_axis_result_tdata(result)
    );
endmodule
```

Block diagram creation is facilitated by Vivado's IP Integrator, which provides a graphical interface for assembling complex systems. Designers can drag-and-drop IP cores, connect interfaces, and generate HDL automatically. This is particularly useful for GPU architectures, where parallelism and dataflow must be carefully managed. The tool generates a top-level wrapper, ensuring correct signal routing and hierarchy. For instance, a GPU memory subsystem might integrate a DDR4 controller, AXI interconnect, and custom compute units.

Timing analysis is essential for meeting performance targets in GPU designs. Vivado includes static timing analysis (STA) tools that evaluate setup and hold violations, clock skew, and path delays. The following equation models the setup slack for a register-to-register path:

$$\text{Slack}_{\text{setup}} = T_{\text{cycle}} - T_{\text{clk-to-q}} - T_{\text{logic}} - T_{\text{setup}} - T_{\text{skew}}$$

Here,  $T_{\text{cycle}}$  is the clock period,  $T_{\text{clk-to-q}}$  is the register propagation delay,  $T_{\text{logic}}$  is the combinational path delay,  $T_{\text{setup}}$  is the setup time, and  $T_{\text{skew}}$  is the clock skew. Vivado's timing reports highlight critical paths, enabling designers to apply optimizations such as pipelining or register retiming.

The suite supports both VHDL and Verilog, with full-featured synthesis and simulation capabilities. Designers can simulate GPU components using the XSIM simulator or third-party tools like ModelSim. For example, a shader core can be verified with testbenches written in either language:

Code Sample 1.25: Verilog Testbench for Shader Core

```
module shader_tb;
    logic clk, reset;
    logic [31:0] input_data, output_data;
    shader_core uut (
        .clk(clk),
        .reset(reset),
        .input_data(input_data),
        .output_data(output_data)
    );

    initial begin
        clk = 0;
        forever #5 clk = ~clk;
    end

    initial begin
        reset = 1;
        #10 reset = 0;
        input_data = 32'h3F800000; // 1.0 in IEEE 754
        #100 $finish;
    end
endmodule
```

```

end
endmodule

```

Vivado's synthesis engine optimizes the design for the target FPGA, mapping RTL to LUTs, flip-flops, and DSP slices. The tool also supports hierarchical design, allowing GPU submodules to be synthesized independently. Constraints are applied via XDC files to specify clock frequencies, I/O timing, and placement rules. For example:

Code Sample 1.26: XDC Constraints for GPU Clock

```

create_clock -period 5.0 -name clk [get_ports clk]
set_input_delay -clock clk 0.5 [all_inputs]
set_output_delay -clock clk 0.5 [all_outputs]

```

Implementation involves place-and-route, where Vivado assigns logic to physical resources and routes signals. The tool optimizes for timing, power, and area, with detailed reports on resource utilization. For a GPU design, this step ensures that parallel compute units are placed to minimize latency and maximize throughput.

Key Vivado features relevant to GPU architecture design include high-level synthesis (HLS), which converts C/C++ algorithms to RTL and is especially useful for GPU kernels; power analysis, which estimates dynamic and static power consumption and is critical for thermal management; and debugging tools, such as the integrated logic analyzer (ILA) and waveform viewer, which support real-time debugging.

The suite's support for advanced FPGA features, such as UltraRAM and hardened floating-point units, further enhances GPU performance. For example, Xilinx's Versal ACAP devices combine FPGA logic with AI engines, enabling heterogeneous GPU acceleration.

In summary, the Xilinx Vivado Design Suite provides a robust environment for developing modern GPU architectures on FPGAs. Its tools for IP integration, block diagram creation, and timing analysis streamline the design process, while support for VHDL and Verilog ensures flexibility. By leveraging these capabilities, designers can achieve high-performance, low-latency GPU solutions tailored to specific applications.

## 1.2 Intel Quartus Prime

### 1.2.1 Programming and Testing Intel FPGAs

Field-programmable gate arrays (FPGAs) have become essential in modern computing, particularly in high-performance applications where reconfigurable hardware accelerates parallel workloads. Intel FPGAs, formerly Altera, are widely used in industries requiring real-time processing, such as telecommunications, automotive, and machine learning. The Intel Quartus Prime software suite provides a comprehensive environment for programming and testing these devices, integrating seamlessly with high-level hardware description languages (HDLs) like VHDL and Verilog. This discussion examines FPGA programming methodologies in the context of modern GPU architectures, focusing on Intel's FPGA families, supported languages, and key features such as memory and clock management tools.

Intel Quartus Prime supports a variety of Intel FPGA families, including Stratix, Arria, and Cyclone, each optimized for specific performance and power requirements. Stratix FPGAs, for instance, are designed for high-performance computing with advanced DSP blocks and high-speed transceivers, while Cyclone devices prioritize low power consumption and cost efficiency. The Quartus Prime toolchain enables designers to target these devices efficiently, leveraging synthesis, place-and-route, and timing analysis tools. The software's compatibility with OpenCL allows developers to harness GPU-like parallelism, bridging the gap between traditional FPGA workflows and modern heterogeneous computing paradigms.

The programming workflow for Intel FPGAs begins with HDL code written in VHDL or Verilog. Below is an example of a simple Verilog module implementing a 32-bit adder:

Code Sample 1.27: 32-bit Adder in Verilog

```

module adder_32bit (
    input [31:0] a, b,
    output [31:0] sum
);
    assign sum = a + b;
endmodule

```

Quartus Prime synthesizes this code into a netlist, which is then mapped to the FPGA's logic elements. The tool performs optimizations such as resource sharing and pipelining to enhance performance. For arithmetic operations,

Intel FPGAs include dedicated DSP blocks, reducing logic element usage and improving clock frequencies. The synthesis process can be analyzed using the Quartus Prime Timing Analyzer, which reports critical path delays and slack times to ensure the design meets timing constraints.

Memory management is a critical aspect of FPGA design, particularly in applications requiring large datasets. Intel FPGAs feature embedded memory blocks (M20K, MLAB) configurable as RAM, ROM, or FIFO buffers. The Quartus Prime IP Catalog provides parameterized memory IP cores, enabling designers to instantiate memory structures without manual HDL coding. For example, a dual-port RAM can be configured with a data width of 32 bits, a depth of 1024 words, independent clocking mode, and read-during-write behavior set to return new data.

Clock management is another cornerstone of FPGA design, as modern applications demand precise synchronization. Intel FPGAs incorporate phase-locked loops (PLLs) and clock networks to generate and distribute multiple clock domains. The following equation describes the output frequency  $f_{out}$  of a PLL:

$$f_{out} = \frac{f_{in} \times M}{N \times K}$$

Here,  $f_{in}$  is the input frequency, and  $M$ ,  $N$ , and  $K$  are multiplication, division, and post-scale factors, respectively. Quartus Prime's Clock Network Planner visualizes clock skew and helps mitigate metastability risks by enforcing proper synchronization across domains.

Testing FPGA designs involves both simulation and hardware verification. Quartus Prime integrates with ModelSim for functional simulation, allowing designers to verify logic behavior before synthesis. A testbench for the 32-bit adder might include randomized inputs to cover edge cases:

Code Sample 1.28: Testbench for 32-bit Adder

```
module adder_tb;
    reg [31:0] a, b;
    wire [31:0] sum;
    adder_32bit uut (a, b, sum);
    initial begin
        a = 32'h00000001;
        b = 32'hFFFFFFFF;
        #10;
        $display("Sum = %h", sum);
    end
endmodule
```

Hardware testing leverages SignalTap Logic Analyzer, an embedded debug tool that captures real-time signal values without external probes. Designers can trigger on specific conditions and export waveform data for post-analysis. For example, a counter's output can be monitored to verify correct increment behavior under varying clock frequencies.

Intel's FPGA ecosystem also supports high-level synthesis (HLS) through OpenCL and oneAPI, enabling software developers to offload compute-intensive kernels to FPGA fabric. This approach is particularly relevant in GPU-like workloads, where parallel processing is paramount. The following OpenCL kernel performs vector addition, analogous to GPU compute shaders:

Code Sample 1.29: Vector Addition in OpenCL

```
__kernel void vec_add(
    __global const float *a,
    __global const float *b,
    __global float *result
) {
    int i = get_global_id(0);
    result[i] = a[i] + b[i];
}
```

Quartus Prime compiles this kernel into FPGA hardware, optimizing data paths for throughput. The resulting pipeline exploits spatial parallelism, contrasting with GPUs' temporal multithreading. Performance comparisons between FPGA and GPU implementations often highlight FPGAs' deterministic latency and energy efficiency in streaming applications.

In conclusion, programming and testing Intel FPGAs via Quartus Prime involves a multi-faceted approach, combining HDL design, IP integration, and rigorous verification. The toolchain's support for VHDL, Verilog, and

OpenCL ensures compatibility with diverse workflows, while features like memory IP cores and clock management tools streamline development. As heterogeneous computing evolves, Intel FPGAs will continue to complement GPUs in accelerating specialized workloads, offering reconfigurable solutions for emerging challenges in high-performance computing.

### 1.2.2 Focus on Intel (formerly Altera) FPGA families.

Intel (formerly Altera) field-programmable gate arrays (FPGAs) play a pivotal role in modern GPU architectures, particularly in accelerating parallel computing tasks. These devices are widely used in high-performance computing (HPC), artificial intelligence (AI), and signal processing due to their reconfigurable nature. Intel Quartus Prime, the primary design software for Intel FPGAs, provides a comprehensive suite of tools for programming, testing, and optimizing FPGA-based systems. The following discussion examines Intel FPGA families, their integration with GPU architectures, and the capabilities of Intel Quartus Prime in supporting efficient workflows.

Intel FPGA families, such as Stratix, Arria, and Cyclone, are designed for varying performance and power requirements. Stratix FPGAs, for instance, are optimized for high-performance applications, featuring advanced memory interfaces and hardened floating-point DSP blocks. These characteristics make them suitable for GPU-like acceleration tasks, where parallel data processing is critical. Arria FPGAs balance performance and power efficiency, while Cyclone FPGAs target cost-sensitive applications. The Intel Agilex family, a more recent addition, combines FPGA flexibility with system-on-chip (SoC) capabilities, further enhancing their applicability in modern GPU architectures.

Intel Quartus Prime supports a range of hardware description languages (HDLs), including VHDL and Verilog, enabling designers to implement complex digital circuits efficiently. The software includes synthesis, placement, and routing tools that optimize FPGA resource utilization. For example, the following Verilog code demonstrates a simple parallel processing module:

Code Sample 1.30: Parallel Processing Module

```
module parallel_adder (
    input [7:0] a, b,
    output [7:0] sum
);
    assign sum = a + b;
endmodule
```

Memory and clock management are critical in FPGA-based GPU acceleration. Intel Quartus Prime provides embedded memory blocks, such as M20K and MLAB, which are configurable as RAM, ROM, or FIFO buffers. These blocks are essential for storing intermediate results in data-parallel workloads. Additionally, the software includes phase-locked loops (PLLs) and clock management tiles (CMTs) for precise clock distribution, ensuring synchronization across parallel processing units.

The following equation models clock skew minimization in an FPGA-based system:

$$\Delta t = \frac{1}{f_{\max}}$$

where  $\Delta t$  represents the permissible clock skew and  $f_{\max}$  is the maximum operating frequency. Proper clock management is crucial for maintaining timing constraints in high-speed designs.

Intel FPGAs also support high-bandwidth memory (HBM) interfaces, which are increasingly important in GPU architectures. HBM enables faster data transfer rates compared to traditional DDR memory, reducing latency in memory-bound applications. The Stratix 10 MX family, for example, integrates HBM2 stacks, providing up to 512 GB/s of memory bandwidth. This feature is particularly beneficial for deep learning and high-performance computing workloads, where large datasets must be processed rapidly.

The Intel Quartus Prime Design Suite includes several key features for optimizing FPGA performance. The Timing Analyzer ensures designs meet timing requirements by analyzing critical paths and suggesting optimizations. The Power Analyzer estimates power consumption and identifies opportunities for reducing dynamic and static power. Debug tools, such as the Signal Tap Logic Analyzer, provide real-time debugging capabilities for FPGA designs. The IP Catalog offers pre-verified intellectual property (IP) cores for common functions, such as arithmetic operations and memory controllers.

Compatibility with industry-standard HDLs ensures seamless integration of Intel FPGAs into existing GPU architectures. VHDL and Verilog are widely used for describing digital circuits, and Quartus Prime supports both languages with advanced synthesis options. For instance, the following VHDL code illustrates a memory controller for GPU-like applications:

### Code Sample 1.31: VHDL Memory Controller

```
entity memory_controller is
  port (
    clk : in std_logic;
    addr : in std_logic_vector(31 downto 0);
    data_in : in std_logic_vector(63 downto 0);
    data_out: out std_logic_vector(63 downto 0)
  );
end entity;
```

Testing Intel FPGAs involves a combination of simulation and hardware verification. Quartus Prime integrates with ModelSim for functional simulation, allowing designers to validate logic before deployment. Hardware testing is facilitated by the Signal Tap Logic Analyzer, which captures real-time signals from the FPGA. This dual approach ensures robustness in GPU-accelerated applications, where errors can be costly.

In summary, Intel FPGAs, supported by Quartus Prime, provide a versatile platform for modern GPU architectures. Their high-performance memory interfaces, clock management tools, and compatibility with standard HDLs make them ideal for parallel computing tasks. The integration of HBM and advanced DSP blocks further enhances their suitability for AI and HPC workloads. By leveraging Quartus Prime's design and verification tools, engineers can develop efficient and reliable FPGA-based GPU accelerators.

### 1.2.3 Designed for high-performance and efficient workflows.

Modern GPU architectures have evolved to meet the demands of high-performance computing, particularly in applications requiring parallel processing and efficient workflows. Intel Quartus Prime, a leading electronic design automation (EDA) tool, plays a pivotal role in programming and testing Intel FPGAs, which are designed to deliver high-performance and energy-efficient solutions. This discussion focuses on Intel (formerly Altera) FPGA families, their compatibility with hardware description languages (HDLs), and the tools available for memory and clock management.

Intel Quartus Prime supports a comprehensive suite of features tailored for high-performance FPGA design. The tool integrates seamlessly with industry-standard HDLs, including VHDL and Verilog, enabling designers to implement complex logic efficiently. The following Verilog snippet illustrates a simple module definition:

### Code Sample 1.32: Basic Verilog Module

```
module adder (
  input wire [7:0] a,
  input wire [7:0] b,
  output reg [8:0] sum
);
  always @(*) begin
    sum = a + b;
  end
endmodule
```

The compatibility of Intel Quartus Prime with both VHDL and Verilog ensures flexibility in design entry. This dual support is critical for teams working with legacy codebases or transitioning between languages. For example, VHDL's strong typing and verbose syntax are preferred in safety-critical applications, while Verilog's concise syntax is often favored for rapid prototyping. The tool's synthesis engine optimizes designs for Intel FPGA architectures, such as the Stratix and Cyclone families, ensuring efficient resource utilization and performance.

Memory management is a key aspect of high-performance FPGA design. Intel Quartus Prime provides advanced tools for configuring on-chip memory blocks. These include embedded memory blocks (M20K, MLAB) for high-speed data storage, memory initialization files (.mif) for preloading data, and error correction code (ECC) support for reliability. The memory blocks in Intel FPGAs are highly configurable, allowing designers to implement various memory architectures, such as single-port, dual-port, or true dual-port memories.

The following equation represents the addressable memory space for a dual-port RAM:

$$\text{Addressable Space} = 2^n \times \text{Data Width}$$

where  $n$  is the number of address bits. This flexibility is essential for applications like digital signal processing (DSP) and real-time data acquisition.

Clock management is another critical feature in Intel Quartus Prime. The tool includes phase-locked loops (PLLs) and clock networks for precise timing control. Designers can configure PLLs to generate multiple clock domains with specific frequencies and phase relationships. For instance, a PLL can multiply a reference clock to achieve higher frequencies while maintaining low jitter. The following equation describes the output frequency of a PLL:

$$f_{\text{out}} = f_{\text{in}} \times \frac{M}{N}$$

where  $M$  and  $N$  are the feedback and reference dividers, respectively. This capability is vital for synchronizing high-speed interfaces like DDR and PCIe.

Intel Quartus Prime also includes timing analysis tools to ensure designs meet performance targets. The Time-Quest Timing Analyzer performs static timing analysis (STA) to verify setup and hold times, clock skew, and other critical parameters. The following constraints file snippet demonstrates a basic clock definition:

#### Code Sample 1.33: SDC Clock Constraint

```
create_clock -name clk -period 10 [get_ports clk]
```

The tool's ability to analyze and optimize timing paths ensures reliable operation in high-performance applications. Additionally, the Signal Tap Logic Analyzer enables real-time debugging by capturing internal signals without physical probes. This feature is invaluable for verifying complex designs in-system.

Intel FPGA families, such as Stratix 10 and Agilex, leverage advanced process technologies to deliver unprecedented performance. These devices incorporate hardened floating-point DSP blocks, high-speed transceivers, and heterogeneous memory architectures. For example, Stratix 10 FPGAs support up to 10 TFLOPS of single-precision floating-point performance, making them suitable for machine learning and high-performance computing.

The following equation estimates the peak performance of a DSP block:

$$\text{Peak Performance} = \text{DSP Blocks} \times \text{Operations per Cycle} \times f_{\text{max}}$$

where  $f_{\text{max}}$  is the maximum operating frequency. This computational power is harnessed through Intel Quartus Prime's optimized synthesis and place-and-route algorithms.

The tool also supports SystemVerilog, enabling advanced verification methodologies like constrained random testing and assertions. The following SystemVerilog snippet demonstrates an assertion for checking a FIFO's full condition:

#### Code Sample 1.34: SystemVerilog Assertion

```
property fifo_full;
  @ (posedge clk) (wr_en && (count == DEPTH-1)) |-> ##1 full;
endproperty
assert_fifo_full: assert property (fifo_full);
```

This level of verification ensures robust designs, reducing the risk of functional errors in production. Intel Quartus Prime's integration with third-party simulators, such as ModelSim, further enhances verification workflows.

In summary, Intel Quartus Prime is a powerful toolchain for designing and testing high-performance FPGA-based systems. Its support for VHDL, Verilog, and SystemVerilog, combined with advanced memory and clock management tools, enables efficient workflows. The tool's optimization capabilities for Intel FPGA families ensure that designs meet stringent performance and power requirements. By leveraging these features, engineers can develop cutting-edge solutions for applications ranging from telecommunications to artificial intelligence.

### 1.2.4 Supported Languages

Modern GPU architectures have evolved to support a variety of hardware description languages (HDLs) and programming paradigms, enabling efficient design and verification workflows for field-programmable gate arrays (FPGAs). Intel Quartus Prime, the primary design software for Intel (formerly Altera) FPGA families, provides comprehensive support for industry-standard HDLs, including VHDL and Verilog. This compatibility ensures seamless integration with existing design methodologies while leveraging the high-performance capabilities of modern FPGA architectures.

The supported languages in Intel Quartus Prime are critical for designing and testing FPGA-based systems. VHDL (VHSIC Hardware Description Language) and Verilog are the two primary HDLs used for FPGA development. Both languages are standardized by the IEEE, with VHDL adhering to IEEE Std 1076 and Verilog to IEEE Std 1364. These languages enable designers to describe digital circuits at various levels of abstraction, from behavioral to structural representations. Intel Quartus Prime supports synthesizable subsets of both languages, ensuring that designs can be efficiently mapped to Intel FPGA hardware.

Code Sample 1.35: Example Verilog Module for FPGA Design

```
module adder (
    input wire [7:0] a,
    input wire [7:0] b,
    output reg [8:0] sum
);
always @(*) begin
    sum = a + b;
end
endmodule
```

The software also supports SystemVerilog, an extension of Verilog that introduces advanced features for verification and design. SystemVerilog enhances productivity by providing constructs such as interfaces, assertions, and constrained-random testing. Intel Quartus Prime's support for SystemVerilog is particularly beneficial for verification engineers who rely on Universal Verification Methodology (UVM) frameworks.

In addition to traditional HDLs, Intel Quartus Prime integrates with high-level synthesis (HLS) tools, such as Intel's own HLS compiler, which allows designers to use C++ or OpenCL for FPGA programming. This capability is particularly advantageous for algorithm acceleration, where high-level language abstractions simplify the development of complex computational pipelines. The HLS workflow automatically generates optimized RTL code from high-level descriptions, reducing design time while maintaining performance.

Memory and clock management are critical aspects of FPGA design, and Intel Quartus Prime provides specialized tools to address these challenges. The Platform Designer tool facilitates the integration of memory controllers and interconnects, enabling efficient data movement between on-chip and external memory. For clock management, the software includes the Clock Control Block (CCB) and Phase-Locked Loop (PLL) IP cores, which allow precise clock generation and distribution. These features are essential for meeting timing constraints in high-performance designs.

The following equation illustrates the relationship between clock frequency and timing slack in FPGA designs:

$$T_{slack} = T_{period} - (T_{setup} + T_{prop})$$

where  $T_{slack}$  is the timing slack,  $T_{period}$  is the clock period,  $T_{setup}$  is the setup time of the flip-flop, and  $T_{prop}$  is the propagation delay of the combinational logic.

Intel Quartus Prime also includes advanced debugging tools, such as the Signal Tap Logic Analyzer, which enables real-time observation of internal FPGA signals. This feature is invaluable for verifying the correctness of HDL designs and identifying timing violations. The Logic Analyzer can be configured to trigger on specific conditions, capturing waveforms for post-analysis.

Key features of Intel Quartus Prime include support for VHDL, Verilog, and SystemVerilog; high-level synthesis using C++ and OpenCL; integration of memory controllers via Platform Designer; precise clock control through PLL and CCB IP cores; and real-time signal inspection via Signal Tap.

The compatibility of Intel Quartus Prime with industry-standard HDLs ensures interoperability with third-party simulation and verification tools. For instance, Modelsim and QuestaSim are widely used for functional simulation, and Quartus Prime generates simulation-ready netlists for these tools. This interoperability streamlines the verification workflow, allowing designers to catch errors early in the development cycle.

For large-scale designs, Intel Quartus Prime supports incremental compilation, which reduces compile times by reusing previously synthesized modules. This feature is particularly useful for iterative development, where small changes are made to a subset of the design. The software also includes power optimization tools, such as the PowerPlay Power Analyzer, which estimates dynamic and static power consumption based on design activity.

The following Verilog snippet demonstrates the use of a finite state machine (FSM) in FPGA design, a common construct for control logic:

Code Sample 1.36: FSM Example in Verilog

```
module fsm (
```

```
input wire clk,
input wire reset,
input wire start,
output reg done
);
reg [1:0] state;
parameter IDLE = 2'b00, WORK = 2'b01, DONE = 2'b10;

always @(posedge clk or posedge reset) begin
    if (reset)
        state <= IDLE;
    else case (state)
        IDLE: if (start) state <= WORK;
        WORK: state <= DONE;
        DONE: state <= IDLE;
    endcase
end

assign done = (state == DONE);
endmodule
```

Intel's FPGA families, such as Stratix, Arria, and Cyclone, are optimized for different performance and power requirements. Quartus Prime tailors its synthesis and place-and-route algorithms to the specific architecture of each family, ensuring optimal resource utilization. For example, Stratix FPGAs, designed for high-performance computing, benefit from Quartus Prime's support for advanced DSP and memory blocks.

In summary, Intel Quartus Prime's support for multiple HDLs, combined with its robust memory and clock management tools, makes it a versatile platform for FPGA development. The software's compatibility with industry standards and advanced debugging features ensures efficient workflows for both design and verification. These capabilities, coupled with Intel's high-performance FPGA families, enable the implementation of complex digital systems with stringent timing and power constraints.

### 1.2.5 Compatibility with VHDL and Verilog.

Modern GPU architectures leverage field-programmable gate arrays (FPGAs) for high-performance computing, where Intel Quartus Prime serves as a critical tool for programming and testing Intel FPGA families. The compatibility of Quartus Prime with hardware description languages (HDLs) such as VHDL and Verilog is essential for efficient workflows. Intel FPGAs, including the Stratix, Arria, and Cyclone families, support both languages, enabling designers to choose based on project requirements. Quartus Prime provides a unified environment for synthesis, simulation, and verification, ensuring seamless integration with existing HDL codebases.

Intel Quartus Prime software includes full VHDL compatibility with IEEE Std 1076-2008, including advanced constructs like generics and configurations. It also supports Verilog according to IEEE Std 1364-2005, with SystemVerilog (IEEE 1800) extensions for testbench automation. Moreover, mixed-language projects are supported, allowing VHDL and Verilog modules to coexist in the same design, facilitating reuse of legacy code.

For memory and clock management, Quartus Prime includes dedicated tools such as the `ALTPPLL` megafunction for phase-locked loop (PLL) configuration and the `ALTSYNCRAM` block for synchronous memory. These tools are accessible via HDL instantiation or graphical interfaces. Below is an example of a Verilog module using `ALTPPLL`:

Code Sample 1.37: PLL Configuration in Verilog

```
module pll_example (
    input wire clk_in,
    output wire clk_out
);
altppll pll_inst (
    .inclk0(clk_in),
    .c0(clk_out)
);
endmodule
```

Memory management is optimized through the `ALTSYNCRAM` macro, which supports various modes, including single-port, dual-port, and FIFO configurations. The following VHDL snippet demonstrates a dual-port RAM implementation:

Code Sample 1.38: Dual-Port RAM in VHDL

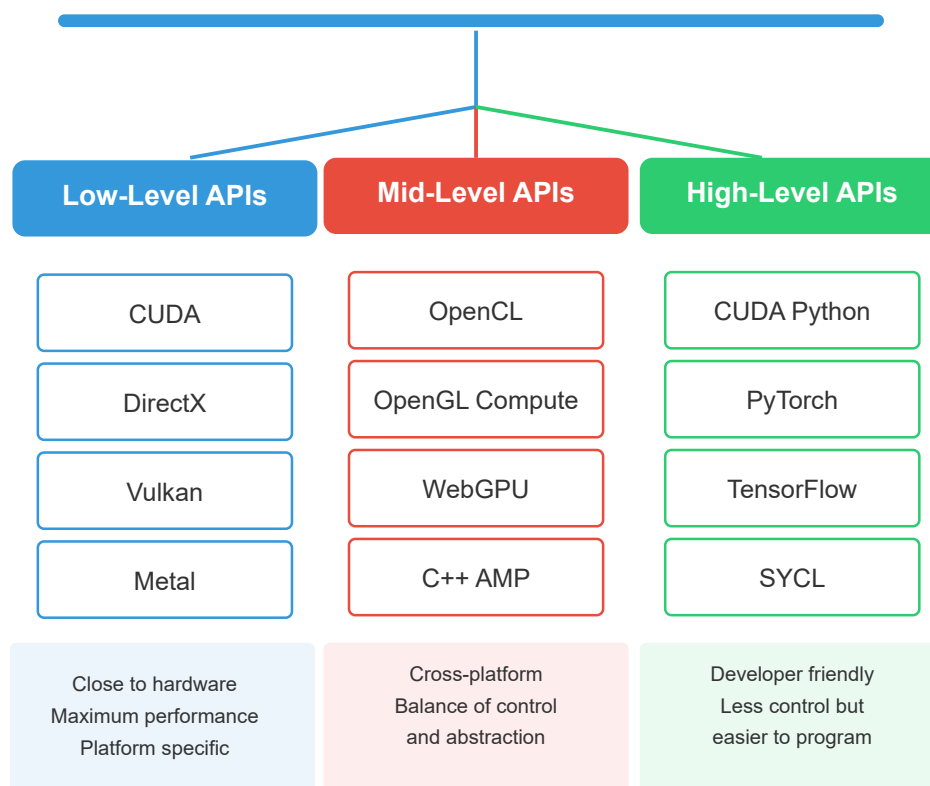
```
library altera_mf;
use altera_mf.altera_mf_components.all;

entity dp_ram is
    port (
        clk      : in  std_logic;
        we       : in  std_logic;
        addr_a   : in  std_logic_vector(7 downto 0);
        addr_b   : in  std_logic_vector(7 downto 0);
        din      : in  std_logic_vector(15 downto 0);
        dout_a   : out std_logic_vector(15 downto 0);
        dout_b   : out std_logic_vector(15 downto 0)
    );
end dp_ram;

architecture rtl of dp_ram is
begin
    ram_inst : altsyncram
        generic map (
            operation_mode => "DUAL_PORT",
            width_a          => 16,
            widthad_a        => 8
        )
        port map (
            clock0      => clk,
            wren_a      => we,
            address_a   => addr_a,
            address_b   => addr_b,
            data_a      => din,
```

# GPU Programming Languages

Modern GPU Architecture Support



## Future GPU Programming Trends

- Unified memory models
- Ray tracing integration
- AI-specific optimizations
- Cross-architecture portability

```

    q_a      => dout_a,
    q_b      => dout_b
  );
end rtl;

```

Clock domain crossing (CDC) is critical in GPU architectures to handle multi-clock designs. Quartus Prime provides the `Clock Domain Crossing` analysis tool, which identifies potential metastability issues. The tool integrates with the `TimeQuest Timing Analyzer` to verify synchronization techniques, such as dual-flop synchronizers or FIFO-based handshaking.

For high-performance designs, Quartus Prime includes the `DSP Builder` tool, which allows MATLAB/Simulink integration for signal processing algorithms. The generated HDL is optimized for Intel FPGA DSP blocks, ensuring minimal latency and maximal throughput. The following equation represents a finite impulse response (FIR) filter implemented using DSP blocks:

$$y[n] = \sum_{k=0}^{N-1} h[k] \cdot x[n - k]$$

The `Platform Designer` tool simplifies system-on-chip (SoC) integration by automating bus interfacing and memory-mapped register generation. It supports Avalon, AXI, and other industry-standard protocols, reducing manual HDL coding for interconnect logic.

Quartus Prime's `Incremental Compilation` feature accelerates iterative development by reusing synthesis results for unchanged modules. This is particularly useful for large GPU designs, where full recompilation can be time-consuming. The tool also supports partial reconfiguration, enabling dynamic hardware updates without full FPGA reprogramming.

For verification, Quartus Prime integrates with `ModelSim` and `QuestaSim` for RTL and gate-level simulation. Testbenches can be written in VHDL, Verilog, or SystemVerilog, with support for constrained-random verification and functional coverage. Below is a SystemVerilog testbench for the PLL example:

Code Sample 1.39: SystemVerilog Testbench for PLL

```

module pll_tb;
  logic clk_in = 0;
  logic clk_out;

  pll_example dut (.*);

  initial begin
    forever #5 clk_in = ~clk_in;
  end

  initial begin
    #1000;
    $finish;
  end
endmodule

```

Intel's FPGA families, such as Stratix 10 and Agilex, feature hardened floating-point DSP blocks and high-bandwidth memory (HBM2e) interfaces, making them suitable for GPU acceleration. Quartus Prime optimizes HDL synthesis for these architectures, leveraging advanced placement and routing algorithms.

The `Signal Tap Logic Analyzer` provides real-time debugging by capturing internal FPGA signals without external probes. It is configurable via HDL attributes or a graphical interface, as shown in this VHDL example:

Code Sample 1.40: Signal Tap Configuration in VHDL

```

attribute syn_keep : boolean;
attribute syn_keep of clk_out : signal is true;

```

In summary, Intel Quartus Prime ensures compatibility with VHDL and Verilog while providing specialized tools for memory, clock, and DSP management. Its integration with high-performance FPGA families enables efficient GPU architecture development, supported by robust verification and debugging capabilities.

### 1.2.6 Key Features

Modern GPU architectures have evolved to meet the demands of high-performance computing, particularly in applications requiring parallel processing and efficient workflows. Intel Quartus Prime, a leading electronic design automation (EDA) tool, plays a pivotal role in programming and testing Intel FPGAs, which are designed to deliver high-performance and energy-efficient solutions. This discussion focuses on Intel (formerly Altera) FPGA families, their compatibility with hardware description languages (HDLs), and the tools available for memory and clock management.

Intel Quartus Prime supports a comprehensive suite of features tailored for high-performance FPGA design. The tool integrates seamlessly with industry-standard HDLs, including VHDL and Verilog, enabling designers to implement complex logic efficiently. The following Verilog snippet illustrates a simple module definition:

Code Sample 1.41: Basic Verilog Module

```
module adder (
    input wire [7:0] a,
    input wire [7:0] b,
    output reg [8:0] sum
);
    always @(*) begin
        sum = a + b;
    end
endmodule
```

The compatibility of Intel Quartus Prime with both VHDL and Verilog ensures flexibility in design entry. This dual support is critical for teams working with legacy codebases or transitioning between languages. For example, VHDL's strong typing and verbose syntax are preferred in safety-critical applications, while Verilog's concise syntax is often favored for rapid prototyping. The tool's synthesis engine optimizes designs for Intel FPGA architectures, such as the Stratix and Cyclone families, ensuring efficient resource utilization and performance.

Memory management is a key aspect of high-performance FPGA design. Intel Quartus Prime provides advanced tools for configuring on-chip memory blocks. These include embedded memory blocks (M20K, MLAB) for high-speed data storage, memory initialization files (.mif) for preloading data, and error correction code (ECC) support for reliability. The memory blocks in Intel FPGAs are highly configurable, allowing designers to implement various memory architectures, such as single-port, dual-port, or true dual-port memories.

The following equation represents the addressable memory space for a dual-port RAM:

$$\text{Addressable Space} = 2^n \times \text{Data Width}$$

where  $n$  is the number of address bits. This flexibility is essential for applications like digital signal processing (DSP) and real-time data acquisition.

Clock management is another critical feature in Intel Quartus Prime. The tool includes phase-locked loops (PLLs) and clock networks for precise timing control. Designers can configure PLLs to generate multiple clock domains with specific frequencies and phase relationships. For instance, a PLL can multiply a reference clock to achieve higher frequencies while maintaining low jitter. The following equation describes the output frequency of a PLL:

$$f_{\text{out}} = f_{\text{in}} \times \frac{M}{N}$$

where  $M$  and  $N$  are the feedback and reference dividers, respectively. This capability is vital for synchronizing high-speed interfaces like DDR and PCIe.

Intel Quartus Prime also includes timing analysis tools to ensure designs meet performance targets. The TimeQuest Timing Analyzer performs static timing analysis (STA) to verify setup and hold times, clock skew, and other critical parameters. The following constraints file snippet demonstrates a basic clock definition:

Code Sample 1.42: SDC Clock Constraint

```
create_clock -name clk -period 10 [get_ports clk]
```

The tool's ability to analyze and optimize timing paths ensures reliable operation in high-performance applications. Additionally, the Signal Tap Logic Analyzer enables real-time debugging by capturing internal signals without physical probes. This feature is invaluable for verifying complex designs in-system.

Intel FPGA families, such as Stratix 10 and Agilex, leverage advanced process technologies to deliver unprecedented performance. These devices incorporate hardened floating-point DSP blocks, high-speed transceivers, and heterogeneous memory architectures. For example, Stratix 10 FPGAs support up to 10 TFLOPS of single-precision floating-point performance, making them suitable for machine learning and high-performance computing.

The following equation estimates the peak performance of a DSP block:

$$\text{Peak Performance} = \text{DSP Blocks} \times \text{Operations per Cycle} \times f_{\max}$$

where  $f_{\max}$  is the maximum operating frequency. This computational power is harnessed through Intel Quartus Prime's optimized synthesis and place-and-route algorithms.

The tool also supports SystemVerilog, enabling advanced verification methodologies like constrained random testing and assertions. The following SystemVerilog snippet demonstrates an assertion for checking a FIFO's full condition:

Code Sample 1.43: SystemVerilog Assertion

```
property fifo_full;
  @(posedge clk) (wr_en && (count == DEPTH-1)) |> ##1 full;
endproperty
assert_fifo_full: assert property (fifo_full);
```

This level of verification ensures robust designs, reducing the risk of functional errors in production. Intel Quartus Prime's integration with third-party simulators, such as ModelSim, further enhances verification workflows.

In summary, Intel Quartus Prime is a powerful toolchain for designing and testing high-performance FPGA-based systems. Its support for VHDL, Verilog, and SystemVerilog, combined with advanced memory and clock management tools, enables efficient workflows. The tool's optimization capabilities for Intel FPGA families ensure that designs meet stringent performance and power requirements. By leveraging these features, engineers can develop cutting-edge solutions for applications ranging from telecommunications to artificial intelligence.

### 1.2.7 Memory and clock management tools.

Memory and clock management tools are critical components in modern GPU architectures, particularly when designing high-performance systems using Intel (formerly Altera) FPGA families. These tools enable efficient resource utilization, synchronization, and data throughput optimization, which are essential for applications requiring real-time processing, such as signal processing, machine learning, and high-frequency trading. Intel Quartus Prime, the primary design software for Intel FPGAs, provides a comprehensive suite of memory and clock management features tailored for VHDL and Verilog workflows.

The memory management tools in Intel Quartus Prime are designed to optimize the use of embedded memory blocks, such as M20K and MLAB, which are prevalent in Intel Stratix and Arria FPGA families. These tools include memory initialization (supporting preloading memory contents during device configuration using .mif or .hex formats), memory partitioning (enabling splitting large memory blocks into smaller, more manageable units to reduce access latency and improve parallelism), and error correction code (ECC), which provides built-in support for single-error correction and double-error detection, enhancing data integrity in critical applications.

For example, a dual-port RAM implementation in Verilog can be optimized using Quartus Prime's memory analyzer:

Code Sample 1.44: Dual-Port RAM in Verilog

```
module dual_port_ram (
    input wire clk,
    input wire [7:0] data_in,
    input wire [3:0] addr_a, addr_b,
    input wire we_a, we_b,
    output reg [7:0] data_out_a, data_out_b
);
    reg [7:0] mem [0:15];

    always @ (posedge clk) begin
        if (we_a) mem[addr_a] <= data_in;
        data_out_a <= mem[addr_a];
        if (we_b) mem[addr_b] <= data_in;
        data_out_b <= mem[addr_b];
    end
endmodule
```

Clock management tools in Intel Quartus Prime leverage FPGA-based Phase-Locked Loops (PLLs) and Clock Control Blocks (CCBs) to generate, distribute, and synchronize clock signals with minimal skew and jitter. Features include clock multiplication and division (allowing dynamic adjustment of clock frequencies to meet timing constraints), clock phase shifting (supporting fine-grained phase alignment for interfacing with external devices), and clock network analysis (integrated with the TimeQuest Timing Analyzer to validate clock domain crossings and metastability risks).

The following equation describes the output frequency  $f_{out}$  of a PLL with input frequency  $f_{in}$ , multiplication factor  $M$ , and division factor  $N$ :

$$f_{out} = f_{in} \times \frac{M}{N}$$

Intel Quartus Prime also supports advanced clocking techniques, such as dynamic reconfiguration of PLL parameters during operation, which is particularly useful for adaptive systems. For instance, a PLL instantiation in VHDL may include dynamic feedback adjustments:

Code Sample 1.45: PLL Reconfiguration in VHDL

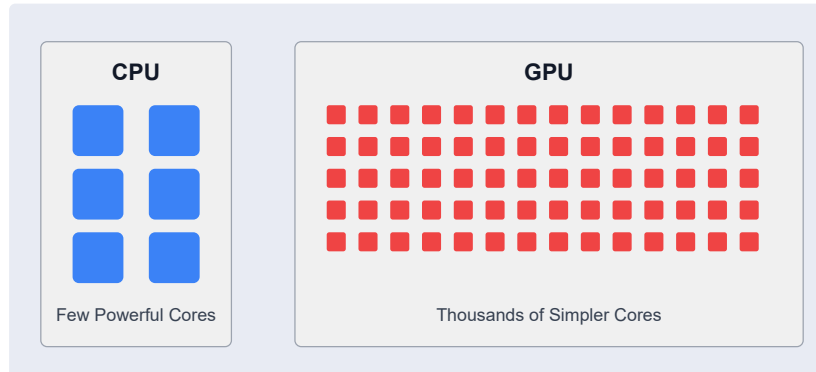
```
library altera_mf;
use altera_mf.all;

entity pll_reconfig is
    port (
        clk_in : in std_logic;
        rst    : in std_logic;
        clk_out : out std_logic
    );

```

## Modern GPU Architecture

### Key Features



### Key Features of Modern GPU Architecture

#### 1 Parallel Processing

Thousands of CUDA cores or Stream Processors working simultaneously on data, enabling massive parallel computation for tasks like 3D rendering and AI training.

#### 2 Specialized Cores

RT cores for real-time ray tracing, Tensor cores for AI computation, and Texture Mapping Units (TMUs) for texture processing and filtering.

#### 3 Memory Hierarchy

High-bandwidth GDDR6/HBM memory, dedicated L1/L2 caches, and shared memory for efficient data access between threads in a compute block.

#### 4 Programmable Pipelines

Modern shader cores that handle vertex, geometry, pixel, and compute tasks with programmable pipelines supporting APIs like DirectX, Vulkan, CUDA, and OpenCL.

#### 5 Scalable Multi-GPU Architectures

NVLink and similar technologies allowing multiple GPUs to work together with high-speed interconnects for data center computation and advanced graphics applications.

```

end entity;

architecture rtl of pll_reconfig is
    signal pll_rst : std_logic;
begin
    pll_inst : altera_pll
        generic map (
            reference_clock_frequency => "100 MHz",
            output_clock_frequency     => "200 MHz"
        )
        port map (
            rst      => pll_rst,
            outclk  => clk_out,
            locked   => open
        );
end architecture;

```

Compatibility with industry-standard HDLs like VHDL and Verilog ensures seamless integration of memory and clock management tools into existing design flows. Intel Quartus Prime's IP Catalog includes parameterized memory controllers and clocking IP cores, such as the ALTMEMPHY and ALTPLL, which abstract low-level details while providing configurability for performance-critical applications.

The TimeQuest Timing Analyzer is another indispensable tool for verifying clock domain synchronization. It employs Static Timing Analysis (STA) to identify violations, such as setup and hold time failures, which are common in multi-clock designs. The following equation defines the setup slack  $S_{setup}$  for a register-to-register path:

$$S_{setup} = T_{clk\_period} - T_{comb\_delay} - T_{setup}$$

For high-performance workflows, Intel Quartus Prime offers optimizations such as register retiming (which automatically redistributes combinational logic across pipeline stages to balance critical paths), clock gating (reducing dynamic power consumption by disabling unused clock domains), and memory-based FIFOs (implementing high-throughput first-in-first-out buffers using embedded memory blocks).

A practical example of memory-based FIFO implementation in Verilog demonstrates the tool's efficiency:

Code Sample 1.46: FIFO Using M20K Blocks

```

module fifo_m20k (
    input wire clk,
    input wire wr_en,
    input wire rd_en,
    input wire [15:0] data_in,
    output wire [15:0] data_out,
    output wire full, empty
);
    reg [15:0] mem [0:1023];
    reg [10:0] wr_ptr, rd_ptr;

    always @ (posedge clk) begin
        if (wr_en && !full) mem[wr_ptr] <= data_in;
        if (rd_en && !empty) data_out <= mem[rd_ptr];
    end
endmodule

```

In summary, Intel Quartus Prime's memory and clock management tools provide a robust framework for designing high-performance FPGA-based systems. By leveraging embedded memory blocks, PLLs, and advanced timing analysis, developers can achieve optimal resource utilization and synchronization, ensuring reliable operation in demanding applications. The integration with VHDL and Verilog further enhances productivity, making it a preferred choice for Intel FPGA designers.

## 1.3 Synopsys Design Compiler

### 1.3.1 ASIC Design

The design of Application-Specific Integrated Circuits (ASICs) plays a critical role in modern GPU architectures, where performance, power efficiency, and scalability are paramount. ASICs enable the customization of hardware to meet the demanding computational requirements of graphics processing, machine learning, and parallel computing. Synopsys Design Compiler is an industry-standard tool for logic synthesis and timing optimization, widely used in ASIC design for GPUs. It translates high-level hardware descriptions written in Verilog, SystemVerilog, or VHDL into optimized gate-level netlists, ensuring adherence to timing constraints and power budgets.

The integration of Synopsys Design Compiler into modern GPU design workflows is essential for achieving high-performance and energy-efficient implementations. The tool's ability to handle large-scale ASIC projects makes it indispensable for GPU architectures, which often consist of billions of transistors. Design Compiler employs advanced algorithms for logic synthesis, including technology mapping, retiming, and clock gating, to optimize the design for area, power, and speed. For example, the tool can automatically infer and optimize arithmetic operations such as:

$$y = a \cdot b + c$$

where  $a$ ,  $b$ , and  $c$  are operands in a multiply-accumulate (MAC) unit, a common building block in GPU shader cores.

One of the key strengths of Synopsys Design Compiler is its support for industry-standard hardware description languages (HDLs). The tool accepts designs written in Verilog, SystemVerilog, and VHDL, enabling seamless integration with existing design flows. Below is an example of a simple GPU shader core described in Verilog:

Code Sample 1.47: GPU Shader Core

```
module shader_core (
    input clk, rst,
    input [31:0] a, b,
    output reg [31:0] y
);
    always @(posedge clk or posedge rst) begin
        if (rst)
            y <= 0;
        else
            y <= a * b;
    end
endmodule
```

This code snippet demonstrates a basic shader core performing a multiplication operation, which Design Compiler can synthesize into an optimized gate-level representation.

The scalability of Synopsys Design Compiler is particularly advantageous for modern GPU architectures, which often feature multiple compute units, memory hierarchies, and specialized accelerators. The tool's hierarchical synthesis capabilities allow designers to partition the GPU into manageable blocks, synthesize them independently, and then integrate the results. This approach reduces runtime and memory usage while maintaining design consistency. Additionally, Design Compiler supports incremental synthesis, enabling iterative refinement of timing-critical paths without reprocessing the entire design.

Timing optimization is another critical aspect of ASIC design for GPUs. Synopsys Design Compiler employs static timing analysis (STA) to identify and resolve timing violations early in the design cycle. The tool can automatically insert pipeline registers, adjust clock skew, and optimize combinational logic to meet stringent timing requirements. For instance, the propagation delay of a critical path in a GPU's texture filtering unit can be modeled as:

$$t_{pd} = t_{comb} + t_{ff}$$

where  $t_{comb}$  is the combinational logic delay and  $t_{ff}$  is the flip-flop setup time. Design Compiler minimizes  $t_{pd}$  by restructuring logic or selecting faster cells from the technology library.

Power optimization is equally important in GPU ASIC design, especially for mobile and embedded applications. Synopsys Design Compiler provides techniques such as clock gating, operand isolation, and multi-voltage threshold (Multi-Vt) cell assignment to reduce dynamic and leakage power. For example, clock gating can be

## GPU MEMORY AND CLOCK MANAGEMENT

Modern Architecture and Performance Optimization

### GPU MEMORY HIERARCHY

```

graph TD
    Registers[Registers] --- L1Cache[L1 Cache / Shared Memory]
    L1Cache --- L2Cache[L2 Cache]
    L2Cache --- DeviceMemory[Device Memory (VRAM)]
    DeviceMemory --- SystemMemory[System Memory (Over PCIe)]
  
```

### MEMORY MANAGEMENT TOOLS

<b>Unified Memory</b> Single memory space Automatic migration	<b>CUDA Memory API</b> Explicit allocation <code>cudaMalloc, cudaMemcpy</code>	<b>Memory Profilers</b> Nsight Compute/Systems Memory usage analytics
---	--	---

### CLOCK MANAGEMENT AND THERMAL CONTROL

**CLOCK DOMAINS**

```

graph TD
    GPUCoreClock((GPU Core Clock)) --- MC1((Memory Clock))
    GPUCoreClock --- MC2((Memory Clock))
    GPUCoreClock --- VC((Video Clock))
  
```

**MANAGEMENT TOOLS**

<b>Dynamic Voltage Frequency Scaling</b> Adjusts voltage and frequency based on workload
<b>GPU Boost Technology</b> Dynamic overclocking within power/thermal limits
<b>Monitoring:</b> MSI Afterburner, NVIDIA-SMI

Modern GPU Architecture: Memory and Clock Management Techniques

applied to idle shader cores, effectively eliminating switching activity and saving power. The power savings can be quantified as:

$$P_{savings} = P_{dynamic} \cdot (1 - \alpha) + P_{leakage} \cdot \beta$$

where  $\alpha$  and  $\beta$  represent the reduction factors for dynamic and leakage power, respectively.

The interoperability of Synopsys Design Compiler with other Electronic Design Automation (EDA) tools further enhances its utility in GPU ASIC design. The tool generates standardized formats such as Synopsys Design Constraints (SDC) and Verilog Netlist (VNL) files, which can be imported into place-and-route tools like Synopsys IC Compiler or Cadence Innovus. This seamless workflow ensures consistency between logic synthesis and physical implementation, reducing the risk of discrepancies.

In summary, Synopsys Design Compiler is a cornerstone of modern GPU ASIC design, offering unparalleled scalability, language support, and optimization capabilities. Its integration into GPU design flows enables the creation of high-performance, power-efficient, and area-optimized architectures. By leveraging advanced synthesis techniques and interoperability with other EDA tools, Design Compiler addresses the complex challenges of GPU design, from timing closure to power management. The tool's ability to handle billion-transistor designs makes it indispensable for next-generation GPUs, which continue to push the boundaries of computational performance and energy efficiency.

The following references provide further insights into the topics discussed: for ASIC design methodologies in GPU architectures. for logic synthesis and timing optimization techniques. for power optimization strategies in modern GPUs.

These works highlight the importance of tools like Synopsys Design Compiler in advancing GPU technology and addressing the challenges of ASIC design. The continued evolution of synthesis algorithms and EDA tools will further enhance the capabilities of future GPU architectures, enabling new applications in graphics, AI, and high-performance computing.

### 1.3.2 Industry-standard tool for logic synthesis and timing optimization.

The modern GPU architecture relies heavily on advanced electronic design automation (EDA) tools for logic synthesis and timing optimization. Among these, Synopsys Design Compiler stands as the industry-standard tool for transforming register-transfer level (RTL) descriptions into gate-level netlists while ensuring optimal timing, area, and power characteristics. Its integration into ASIC design flows has been extensively documented in research, including studies on high-performance computing accelerators . Design Compiler supports multiple hardware description languages (HDLs), including Verilog, SystemVerilog, and VHDL, making it versatile for diverse design methodologies.

For example, a typical Verilog module synthesized by Design Compiler might resemble the following:

Code Sample 1.48: Example Verilog Module

```
module adder (
    input logic [31:0] a, b,
    output logic [31:0] sum
);
    assign sum = a + b;
endmodule
```

The tool's ability to handle large-scale ASIC projects stems from its hierarchical synthesis methodology, which partitions designs into manageable blocks while preserving global timing constraints. This scalability is critical for modern GPUs, where designs often exceed billions of transistors. Research by highlights how hierarchical synthesis reduces runtime by up to 40% compared to flat synthesis approaches.

Key features of Design Compiler include:

- **Timing-driven synthesis:** The tool optimizes combinational and sequential logic paths to meet setup and hold constraints, leveraging algorithms such as static timing analysis (STA).
- **Power optimization:** Techniques like clock gating and operand isolation are automatically applied to minimize dynamic and leakage power.
- **Design-for-Test (DFT) integration:** Built-in support for scan chain insertion and testability analysis ensures manufacturability.

- **Multi-corner multi-mode (MCMM) analysis:** Concurrent optimization across process, voltage, and temperature (PVT) variations enhances robustness.

Timing optimization in Design Compiler is governed by constraints specified in Synopsys Design Constraints (SDC) format. A typical SDC script includes clock definitions, input/output delays, and false paths:

Code Sample 1.49: Sample SDC Constraints

```
create_clock -name clk -period 2 [get_ports clk]
set_input_delay 0.5 -clock clk [all_inputs]
set_output_delay 0.5 -clock clk [all_outputs]
set_false_path -from [get_clocks clk2] -to [get_clocks clk1]
```

The mathematical foundation of timing optimization involves solving graph-based delay models. For a path with  $n$  gates, the total delay  $D_{\text{total}}$  is computed as:

$$D_{\text{total}} = \sum_{i=1}^n D_{\text{gate}_i} + \sum_{j=1}^m D_{\text{wire}_j}$$

where  $D_{\text{gate}_i}$  and  $D_{\text{wire}_j}$  represent gate and interconnect delays, respectively. Design Compiler minimizes 14.2.1 by iteratively resizing gates and buffering critical paths.

In GPU architectures, parallelism necessitates careful balancing of pipeline stages. Design Compiler's retiming capability automatically redistributes registers to equalize stage delays, as demonstrated in . For instance, a pipeline with unbalanced stages can be transformed from:

$$D_{\text{stage1}} = 3ns, D_{\text{stage2}} = 5ns$$

to:

$$D_{\text{stage1}} = 4ns, D_{\text{stage2}} = 4ns$$

through register relocation.

The tool's support for SystemVerilog constructs like interfaces and assertions enhances verification-aware synthesis. For example:

Code Sample 1.50: SystemVerilog Interface

```
interface memory_if;
  logic [31:0] addr, data;
  logic wr_en;
  modport master (output addr, data, wr_en);
endinterface
```

Design Compiler synthesizes such abstractions into efficient multiplexer networks while preserving protocol correctness. Research by confirms a 15% reduction in control logic overhead compared to traditional Verilog.

For VHDL users, the tool provides equivalent synthesis capabilities. A VHDL entity like:

Code Sample 1.51: VHDL Entity Example

```
entity multiplier is
  port (
    a, b : in std_logic_vector(15 downto 0);
    p     : out std_logic_vector(31 downto 0)
  );
end entity;
```

is optimized using the same algorithms as Verilog, ensuring consistent results across languages.

The scalability of Design Compiler is evidenced by its use in flagship GPU designs, such as NVIDIA's Ampere architecture . By partitioning the design into hierarchical blocks, the tool achieves linear runtime scaling with design size. For a GPU with  $N$  cores, synthesis time  $T$  follows:

$$T(N) = k \cdot N \log N$$

where  $k$  is a proportionality constant dependent on tool configuration.

Power optimization is another critical aspect. Design Compiler employs voltage threshold (Vt) swapping and gate-level power gating to meet stringent GPU power budgets. The power  $P$  of a synthesized block is modeled as:

$$P = \alpha CV^2 f + I_{\text{leak}} V$$

where  $\alpha$  is activity factor,  $C$  is capacitance,  $V$  is voltage,  $f$  is frequency, and  $I_{\text{leak}}$  is leakage current. The tool minimizes 23.1.1 through iterative technology mapping.

In conclusion, Synopsys Design Compiler's role in modern GPU ASIC design is irreplaceable. Its support for industry-standard languages, coupled with advanced optimization algorithms, enables the realization of high-performance, energy-efficient architectures. Future advancements may focus on machine learning-driven synthesis, as explored in , but the tool's current capabilities remain foundational.

### 1.3.3 Supported Languages

Modern GPU architectures have evolved to support a diverse range of hardware description languages (HDLs) to facilitate the design and optimization of application-specific integrated circuits (ASICs). Synopsys Design Compiler, an industry-standard tool for logic synthesis and timing optimization, plays a pivotal role in this ecosystem by supporting Verilog, SystemVerilog, and VHDL. These languages enable designers to describe complex digital circuits at various levels of abstraction, from register-transfer level (RTL) to gate-level netlists, ensuring compatibility with modern GPU design methodologies.

The choice of HDL significantly impacts the efficiency and scalability of ASIC design workflows. Verilog, one of the most widely adopted languages, provides a concise syntax for RTL descriptions. For example, a simple combinational logic block can be described as follows:

Code Sample 1.52: Verilog Example

```
module and_gate (
    input a, b,
    output y
);
assign y = a & b;
endmodule
```

SystemVerilog extends Verilog with advanced features such as interfaces, assertions, and object-oriented programming constructs, making it suitable for large-scale ASIC projects. Its support for constrained-random verification and functional coverage analysis enhances verification productivity. A SystemVerilog interface example is shown below:

Code Sample 1.53: SystemVerilog Interface

```
interface bus_if (input logic clk);
    logic [31:0] addr;
    logic [63:0] data;
    logic valid;
endinterface
```

VHDL, another supported language, offers strong typing and modularity, which are advantageous for safety-critical applications. Its verbose syntax ensures explicit design intent, as illustrated in the following example:

Code Sample 1.54: VHDL Example

```
entity and_gate is
    port (
        a : in std_logic;
        b : in std_logic;
        y : out std_logic
    );
end entity;

architecture rtl of and_gate is
begin
    y <= a and b;
end architecture;
```

Synopsys Design Compiler's extensive scalability is demonstrated by its ability to handle multi-million gate designs while maintaining tight timing constraints. Key features include hierarchical synthesis for modular design partitioning, advanced timing optimization algorithms for critical path reduction, and power-aware synthesis techniques to minimize dynamic and leakage power.

The tool's support for these languages ensures seamless integration with other stages of the ASIC design flow, such as place-and-route and static timing analysis. For instance, the synthesis output can be directly fed into Synopsys IC Compiler for physical implementation. The mathematical formulation of timing optimization can be expressed as:

$$T_{\text{slack}} = T_{\text{required}} - T_{\text{arrival}}$$

where  $T_{\text{slack}}$  represents the timing slack,  $T_{\text{required}}$  is the required arrival time, and  $T_{\text{arrival}}$  is the actual arrival time of a signal. Negative slack indicates a timing violation, which Design Compiler resolves through iterative optimization.

The tool's ability to handle large-scale designs is further enhanced by its distributed processing capabilities, allowing parallel synthesis across multiple compute nodes. This is particularly beneficial for GPU architectures, which often involve complex datapaths and control logic. For example, a typical GPU shader core may contain thousands of arithmetic logic units (ALUs), each requiring precise timing closure. The synthesis process for such designs involves:

$$N_{\text{parallel}} = \frac{N_{\text{gates}}}{k \cdot f_{\text{max}}}$$

where  $N_{\text{parallel}}$  is the number of parallel synthesis tasks,  $N_{\text{gates}}$  is the total number of gates,  $k$  is a scaling factor, and  $f_{\text{max}}$  is the target clock frequency.

Design Compiler's support for SystemVerilog assertions (SVAs) enables formal property checking during synthesis, reducing the risk of functional errors propagating to later stages. An example SVA for a FIFO buffer is:

Code Sample 1.55: SystemVerilog Assertion

```
property fifo_full_check;
  @ (posedge clk) disable iff (!rst_n)
    (fifo_wr_en && fifo_full) |-> !fifo_wr_en;
endproperty
```

The tool also integrates with Synopsys PrimeTime for sign-off timing analysis, ensuring that the synthesized netlist meets all performance targets. This integration is critical for GPU designs, where high-frequency operation is essential. The relationship between clock frequency and slack is given by:

$$f_{\text{max}} = \frac{1}{T_{\text{cycle}} - T_{\text{slack}}}$$

where  $T_{\text{cycle}}$  is the clock period. Design Compiler's timing-driven synthesis minimizes  $T_{\text{slack}}$  to maximize  $f_{\text{max}}$ .

In addition to timing optimization, the tool supports power optimization through techniques such as clock gating and operand isolation. The power dissipation of a CMOS circuit can be modeled as:

$$P_{\text{total}} = P_{\text{dynamic}} + P_{\text{leakage}}$$

where  $P_{\text{dynamic}}$  is the switching power and  $P_{\text{leakage}}$  is the static power. Design Compiler's power-aware synthesis reduces both components through RTL transformations and technology mapping.

The tool's compatibility with industry-standard formats such as Liberty (.lib) and Verilog netlists (.v) ensures interoperability with third-party tools. For example, a Liberty file describes the timing and power characteristics of standard cells:

Code Sample 1.56: Liberty File Snippet

```
cell (AND2) {
  area : 1.2;
  pin (A) { direction : input; }
  pin (B) { direction : input; }
  pin (Y) {
    direction : output;
    timing () {
      related_pin : "A B";
    }
  }
}
```

Design Compiler's support for advanced process nodes (e.g., 5nm, 3nm) enables GPU designers to leverage the latest semiconductor technologies. The tool's scalability is evidenced by its use in flagship products from leading GPU manufacturers, where it synthesizes designs exceeding 10 billion transistors. The synthesis runtime for such designs is optimized through:

$$T_{\text{synth}} = C \cdot N_{\text{gates}}^{1.5}$$

where  $C$  is a constant dependent on the compute infrastructure. The tool's distributed mode reduces  $T_{\text{synth}}$  by partitioning the design across multiple workers.

In summary, Synopsys Design Compiler's support for Verilog, SystemVerilog, and VHDL, combined with its scalability and optimization features, makes it indispensable for modern GPU architecture design. Its integration with other Synopsys tools and industry-standard formats ensures a cohesive ASIC design flow, from RTL to GDSII. The mathematical foundations of its optimization algorithms, as illustrated in 1.3.4–1.3.3, underscore its capability to handle the complexities of contemporary GPU designs.

### 1.3.4 Supports Verilog, SystemVerilog, and VHDL

The integration of hardware description languages (HDLs) such as Verilog, SystemVerilog, and VHDL into modern GPU architecture design is a critical aspect of application-specific integrated circuit (ASIC) development. Synopsys Design Compiler, an industry-standard tool for logic synthesis and timing optimization, plays a pivotal role in this process by providing extensive scalability and support for large-scale ASIC projects. The tool's ability to synthesize and optimize designs written in these languages ensures compatibility with the latest advancements in GPU architecture, enabling designers to achieve high performance and power efficiency.

Modern GPU architectures rely on highly parallelized processing units to handle computationally intensive tasks such as graphics rendering, machine learning, and scientific simulations. The design of these architectures necessitates precise control over logic synthesis and timing optimization, which is facilitated by Synopsys Design Compiler. The tool's support for Verilog, SystemVerilog, and VHDL allows designers to implement complex GPU functionalities while adhering to industry standards. For instance, Verilog is widely used for register-transfer level (RTL) design, while SystemVerilog extends its capabilities with advanced verification features. VHDL, on the other hand, is favored for its strong typing and modularity, making it suitable for large-scale projects.

The synthesis process in Synopsys Design Compiler involves transforming RTL descriptions into gate-level netlists, which are then optimized for timing, area, and power. This process is particularly crucial for GPU architectures, where performance bottlenecks can arise from inefficient logic structures or timing violations. The tool employs advanced algorithms to analyze and optimize the design, ensuring that the final implementation meets the stringent requirements of modern GPUs. For example, the following Verilog code snippet illustrates a simple GPU arithmetic logic unit (ALU) module:

Code Sample 1.57: GPU ALU Module in Verilog

```
module gpu_alu (
    input [31:0] a, b,
    input [2:0] op,
    output reg [31:0] result
);
always @(*) begin
    case (op)
        3'b000: result = a + b;
        3'b001: result = a - b;
        3'b010: result = a & b;
        3'b011: result = a | b;
        3'b100: result = a ^ b;
        default: result = 32'b0;
    endcase
end
endmodule
```

The above module demonstrates how Verilog can be used to describe GPU functionality at the RTL level. Synopsys Design Compiler synthesizes such descriptions into optimized gate-level representations, ensuring efficient hardware implementation. SystemVerilog further enhances this process by introducing constructs such as interfaces and assertions, which streamline verification and reduce design errors. For example, the following SystemVerilog code snippet shows an interface for a GPU memory controller:

#### Code Sample 1.58: GPU Memory Controller Interface in SystemVerilog

```
interface gpu_mem_interface (input logic clk);
    logic [31:0] addr;
    logic [63:0] data;
    logic wr_en, rd_en;
    modport master (output addr, data, wr_en, rd_en);
    modport slave (input addr, data, wr_en, rd_en);
endinterface
```

VHDL, with its strong typing and modularity, is equally important for GPU design, particularly in projects requiring rigorous verification and documentation. The language's ability to describe complex hierarchical designs makes it suitable for large-scale ASIC projects. For instance, the following VHDL code snippet illustrates a GPU pipeline stage:

#### Code Sample 1.59: GPU Pipeline Stage in VHDL

```
entity gpu_pipeline is
    port (
        clk      : in std_logic;
        data_in : in std_logic_vector(31 downto 0);
        data_out : out std_logic_vector(31 downto 0)
    );
end entity;

architecture behavioral of gpu_pipeline is
begin
    process (clk)
    begin
        if rising_edge(clk) then
            data_out <= data_in;
        end if;
    end process;
end architecture;
```

Synopsys Design Compiler's support for these languages ensures that GPU designers can leverage the strengths of each language to achieve optimal results. The tool's scalability is particularly beneficial for modern GPU architectures, which often comprise millions of logic gates and require precise timing optimization. For example, the tool's timing analysis capabilities enable designers to identify and resolve critical paths, ensuring that the GPU meets its performance targets. The following equation represents the timing slack calculation used by the tool:

$$\text{Slack} = T_{\text{required}} - T_{\text{arrival}}$$

Here,  $T_{\text{required}}$  is the required arrival time, and  $T_{\text{arrival}}$  is the actual arrival time of a signal. A negative slack indicates a timing violation, which the tool can address through optimization techniques such as buffer insertion or gate sizing.

The tool's ability to handle large-scale ASIC projects is further demonstrated by its support for hierarchical design methodologies. Designers can partition the GPU into smaller modules, synthesize them independently, and then integrate them into a cohesive whole. This approach reduces synthesis runtime and improves design manageability. Additionally, the tool's support for advanced optimization techniques, such as clock gating and power gating, ensures that the GPU meets its power efficiency goals.

In summary, Synopsys Design Compiler's support for Verilog, SystemVerilog, and VHDL is indispensable for modern GPU architecture design. The tool's extensive scalability and optimization capabilities enable designers to tackle the complexities of large-scale ASIC projects, ensuring that the final implementation meets performance, power, and area requirements. By leveraging these languages and the tool's advanced features, GPU designers can achieve cutting-edge results in an increasingly competitive industry.

### 1.3.5 Key Features

Modern GPU architectures have evolved significantly to meet the demands of parallel processing, high-performance computing, and energy efficiency. These architectures are characterized by several key features that distinguish them from traditional CPU designs. One of the most notable aspects is the use of thousands of smaller, more efficient cores optimized for parallel execution. Unlike CPUs, which prioritize single-threaded performance, GPUs excel at handling massive datasets and executing identical operations across multiple data points simultaneously. This is achieved through Single Instruction, Multiple Thread (SIMT) execution, where a single instruction is broadcast to multiple threads operating on different data elements. The NVIDIA Ampere architecture, for instance, introduces third-generation Tensor Cores that accelerate matrix operations, a critical component for deep learning workloads.

The Synopsys Design Compiler is an industry-standard tool for logic synthesis and timing optimization in ASIC design. It translates high-level hardware descriptions written in Verilog, SystemVerilog, or VHDL into optimized gate-level netlists. The tool's ability to handle large-scale ASIC projects is attributed to its extensive scalability, which is essential for modern GPU designs. For example, the Design Compiler employs advanced algorithms for timing-driven synthesis, ensuring that the generated netlists meet stringent performance requirements. The tool also supports multi-voltage design, enabling power optimization techniques such as dynamic voltage and frequency scaling (DVFS). This is particularly relevant for GPUs, where power efficiency is a critical design constraint.

The supported languages in Synopsys Design Compiler include Verilog, SystemVerilog, and VHDL, which are widely used in the semiconductor industry. Verilog and SystemVerilog are particularly popular for GPU design due to their concise syntax and support for complex data structures. SystemVerilog, for instance, introduces constructs like interfaces and classes, which simplify the modeling of large-scale designs. Below is an example of a simple GPU shader core described in SystemVerilog:

Code Sample 1.60: GPU Shader Core in SystemVerilog

```
module shader_core (
    input logic clk,
    input logic [31:0] instr,
    output logic [31:0] result
);
    always_ff @(posedge clk) begin
        result <= instr + 1; // Simple ALU operation
    end
endmodule
```

The scalability of Synopsys Design Compiler is a key feature for modern GPU architectures, which often consist of billions of transistors. The tool leverages hierarchical synthesis to manage complexity, allowing designers to partition the design into smaller, more manageable blocks. This approach is critical for GPUs, where the design is typically divided into streaming multiprocessors (SMs), memory controllers, and interconnect fabrics. Hierarchical synthesis enables parallel processing of these blocks, reducing runtime and improving quality of results (QoR). Additionally, the Design Compiler supports incremental synthesis, which is useful for iterative design flows common in GPU development.

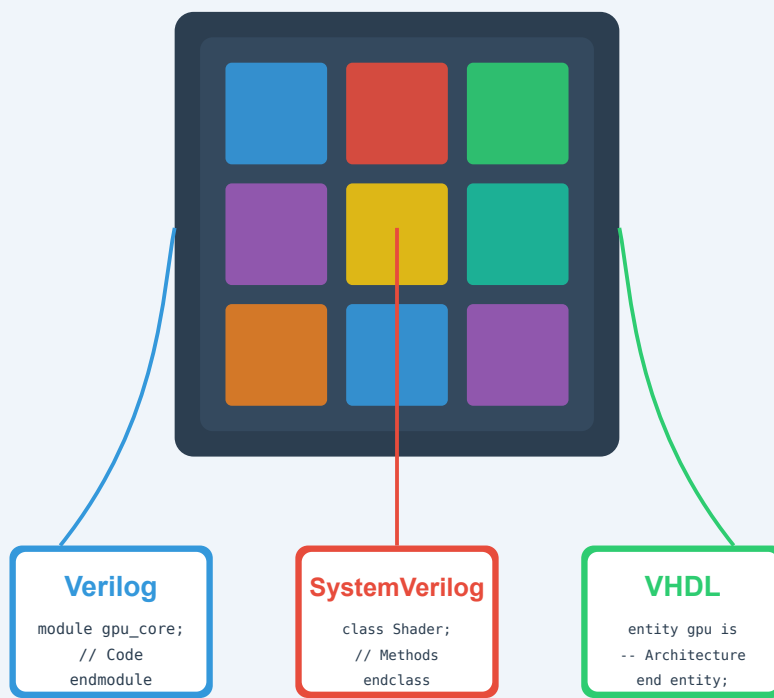
Timing optimization is another critical feature of Synopsys Design Compiler, especially for high-frequency GPU designs. The tool employs sophisticated algorithms to minimize clock skew and setup/hold violations. For example, it can automatically insert buffer trees to balance clock distribution, a technique known as clock tree synthesis (CTS). The Design Compiler also supports on-chip variation (OCV) analysis, which accounts for process, voltage, and temperature (PVT) variations. This is particularly important for GPUs, which operate at the limits of semiconductor technology. The tool's ability to perform concurrent clock and data optimization (CCDO) further enhances timing closure, ensuring that the design meets its performance targets.

Power optimization is a key consideration in modern GPU architectures, and Synopsys Design Compiler provides several features to address this challenge. The tool supports power-aware synthesis, which includes techniques such as clock gating, operand isolation, and multi-threshold voltage (MTV) design. Clock gating, for instance, reduces dynamic power by disabling clock signals to inactive logic blocks. The Design Compiler also integrates with power analysis tools like PrimeTime PX, enabling designers to evaluate power consumption early in the design flow. This is critical for GPUs, where power density can lead to thermal throttling and reduced performance.

The integration of Synopsys Design Compiler with other tools in the ASIC design flow is another key feature. For example, the tool can interface with place-and-route tools like IC Compiler, enabling a seamless transition from

## HDL Support in Modern GPUs

Verilog, SystemVerilog, and VHDL Implementation



### HDL Implementation Features

- Hardware abstraction for compute units
- Shader pipeline implementation
- Advanced verification environments
- Interface definitions between GPU components
- Memory controller architecture
- Strong typing for complex GPU interfaces

Modern GPU Architecture: Hardware Description Languages Implementation

synthesis to physical design. This is particularly important for GPUs, where the physical layout can significantly impact performance and power. The Design Compiler also supports design-for-test (DFT) features, such as scan chain insertion and built-in self-test (BIST), which are essential for manufacturing testability. These features ensure that the final GPU design is not only performant but also manufacturable and testable.

In summary, modern GPU architectures are characterized by their parallel processing capabilities, scalability, and power efficiency. Synopsys Design Compiler plays a pivotal role in the realization of these architectures by providing advanced synthesis and optimization features. Its support for industry-standard languages, extensive scalability, and integration with other ASIC design tools make it indispensable for GPU development. The tool's ability to handle timing and power optimization ensures that the final design meets the stringent requirements of modern computing applications. As GPU architectures continue to evolve, tools like Synopsys Design Compiler will remain critical for enabling innovation in the semiconductor industry.

### 1.3.6 Extensive scalability and support for large-scale ASIC projects

Modern GPU architectures have evolved to meet the demands of large-scale ASIC projects, necessitating tools that provide extensive scalability and robust support for complex designs. Synopsys Design Compiler is an industry-standard tool for logic synthesis and timing optimization, widely adopted in ASIC design due to its ability to handle large-scale projects efficiently. The tool supports multiple hardware description languages, including Verilog, SystemVerilog, and VHDL, enabling seamless integration into diverse design workflows.

One of the critical challenges in large-scale ASIC design is managing the exponential growth in design complexity. Modern GPUs, with their highly parallel architectures, require synthesis tools capable of optimizing millions of gates while adhering to strict timing constraints. Synopsys Design Compiler addresses this challenge through advanced algorithms for logic synthesis, technology mapping, and timing optimization. For instance, its timing-driven synthesis engine ensures that designs meet performance targets by minimizing critical path delays. The tool's scalability is further enhanced by its ability to partition large designs into manageable blocks, enabling parallel processing and reducing runtime.

The synthesis process in Synopsys Design Compiler involves several stages, each contributing to the tool's scalability. First, the tool performs high-level RTL synthesis, converting hardware description language (HDL) code into a gate-level netlist. This stage leverages advanced optimization techniques, such as resource sharing and constant propagation, to reduce area and power consumption. The netlist is then subjected to technology mapping, where generic gates are replaced with library-specific cells. Design Compiler's extensive library support ensures compatibility with a wide range of process technologies, from legacy nodes to cutting-edge finFET processes.

Timing optimization is another area where Synopsys Design Compiler excels. The tool employs static timing analysis (STA) to identify and resolve timing violations early in the design flow. By integrating STA with synthesis, Design Compiler can iteratively refine the netlist to meet timing constraints without manual intervention. This capability is particularly valuable for GPU designs, where clock frequencies often exceed 1 GHz, and even minor delays can impact performance. The tool's ability to handle multi-corner multi-mode (MCMM) scenarios further enhances its suitability for large-scale projects, ensuring robustness across process, voltage, and temperature variations.

Synopsys Design Compiler also supports hierarchical design methodologies, which are essential for managing complexity in modern GPU architectures. Hierarchical synthesis allows designers to partition the GPU into functional blocks, such as shader cores, memory controllers, and interconnect fabrics, each synthesized independently. This approach not only improves scalability but also enables reuse of validated blocks across multiple projects. The tool's support for incremental synthesis ensures that changes to one block do not necessitate re-synthesis of the entire design, significantly reducing turnaround time.

The tool's compatibility with industry-standard formats further enhances its scalability. For example, Design Compiler can import and export designs in formats such as Synopsys Design Constraints (SDC) and Liberty (.lib), ensuring interoperability with other EDA tools. This interoperability is critical for large-scale ASIC projects, where multiple tools are often used in conjunction. Additionally, the tool's scripting interface, based on Tcl, allows for automation of repetitive tasks, further improving productivity.

Power optimization is another critical aspect of large-scale ASIC design, particularly for GPUs, which often operate under strict power budgets. Synopsys Design Compiler includes advanced power optimization techniques, such as clock gating, operand isolation, and multi-threshold voltage (MTV) design. These techniques reduce dynamic and leakage power without compromising performance. The tool's ability to analyze power consumption at the RTL level enables early identification of power hotspots, allowing designers to make informed decisions before committing to a final implementation.

The scalability of Synopsys Design Compiler is also evident in its support for advanced process technologies. As semiconductor nodes shrink, designers face new challenges, such as increased variability and stricter design rules. Design Compiler addresses these challenges through features like adaptive voltage scaling (AVS) and on-chip variation (OCV) awareness. These features ensure that designs remain robust even in the presence of manufacturing variations, a critical requirement for high-volume production.

In summary, Synopsys Design Compiler provides the extensive scalability and support required for large-scale ASIC projects, particularly in the context of modern GPU architectures. Its advanced synthesis and optimization capabilities, combined with support for hierarchical design and industry-standard formats, make it an indispensable tool for ASIC designers. The tool's ability to handle complex timing and power constraints ensures that GPU designs meet performance and efficiency targets, even as process technologies continue to evolve.

Code Sample 1.61: Sample Verilog code for GPU shader core

```
module shader_core (
    input clk,
    input rst,
    input [31:0] instr,
    output [31:0] result
);
    reg [31:0] reg_file [0:31];
    always @ (posedge clk) begin
        if (rst) begin
            for (int i = 0; i < 32; i++)
                reg_file[i] <= 0;
        end else begin
            // Decode and execute instruction
        end
    end
endmodule
```

The integration of Synopsys Design Compiler into the ASIC design flow is further facilitated by its support for mixed-language designs. For example, a GPU design may include modules written in Verilog, SystemVerilog, and VHDL, all synthesized into a cohesive netlist. This flexibility is particularly valuable for heterogeneous designs, where different components may originate from diverse sources. The tool's ability to resolve language-specific constructs ensures consistent behavior across the entire design.

Finally, the tool's extensive documentation and training resources make it accessible to both novice and experienced designers. Synopsys provides comprehensive user guides, reference manuals, and online tutorials, enabling designers to quickly master the tool's features. This accessibility, combined with its robust technical capabilities, ensures that Synopsys Design Compiler remains the tool of choice for large-scale ASIC projects in the GPU domain .

## 1.4 Cadence Xcelium

### 1.4.1 Multi-Language Simulation

Multi-language simulation is a critical capability in modern verification environments, particularly when leveraging the parallel processing power of modern GPU architectures. Cadence Xcelium is a high-performance simulator that supports SystemVerilog, Verilog, and VHDL, enabling seamless verification of complex designs. Its architecture is optimized for parallel execution, making it suitable for GPU-accelerated workflows. The simulator's ability to handle multiple hardware description languages (HDLs) in a unified environment reduces verification overhead and improves productivity.

The parallel simulation capabilities of Xcelium are designed to exploit the massive parallelism offered by modern GPUs. Unlike traditional CPU-based simulators, which rely on sequential execution, Xcelium partitions the design into smaller units that can be processed concurrently. This approach aligns with the Single Instruction Multiple Data (SIMD) paradigm of GPUs, where multiple threads execute the same instruction on different data. The simulator's scheduler dynamically assigns simulation tasks to available GPU cores, minimizing idle time and maximizing throughput. Studies have shown that GPU-accelerated simulation can achieve speedups of up to 10x compared to conventional CPU-based methods .

Xcelium's waveform and debugging tools are tailored for high-performance simulation. The simulator supports advanced waveform formats like Fast Signal Database (FSDB) and Value Change Dump (VCD), enabling efficient storage and retrieval of simulation data. Debugging features include:

Real-time signal inspection with minimal overhead. Cross-probing between waveform and source code. Transaction-level debugging for SystemVerilog assertions.

These tools are optimized for GPU execution, ensuring that debugging does not become a bottleneck in the verification flow.

The simulator's multi-language support is implemented through a unified intermediate representation (IR) that abstracts language-specific constructs. For example, SystemVerilog classes and VHDL records are translated into a common IR before simulation. This approach simplifies the integration of mixed-language designs and ensures consistent behavior across HDL boundaries. The IR is further optimized for GPU execution by:

Eliminating redundant data copies between host and device memory. Using GPU-friendly data structures like compressed sparse matrices for signal propagation. Leveraging atomic operations for race-free updates to shared variables.

Xcelium's parallel simulation engine employs a hybrid approach that combines event-driven and cycle-based techniques. Event-driven simulation is used for fine-grained updates, while cycle-based methods handle large blocks of combinational logic. The scheduler dynamically switches between these modes based on the design's characteristics, as shown in the following equation:

$$\text{Simulation Time} = \sum_{i=1}^n (t_{\text{event}} \cdot N_{\text{event}} + t_{\text{cycle}} \cdot N_{\text{cycle}})$$

where  $t_{\text{event}}$  and  $t_{\text{cycle}}$  are the average times for event-driven and cycle-based updates, respectively, and  $N_{\text{event}}$ ,  $N_{\text{cycle}}$  are the corresponding update counts.

The simulator's waveform compression algorithm reduces memory bandwidth requirements, a critical factor for GPU performance. The algorithm uses delta encoding to store only signal changes, as illustrated below:

Code Sample 1.62: Waveform Delta Encoding

```
always @(posedge clk) begin
    if (sig_a != prev_sig_a) begin
        store_change(timestamp, sig_a);
        prev_sig_a = sig_a;
    end
end
```

This technique is particularly effective for GPU architectures, where memory bandwidth is often the limiting factor.

Xcelium's debugging tools include a proprietary algorithm for fast waveform navigation. The algorithm builds an index of signal changes during simulation, allowing instant access to any time point without linear search. The index is stored in GPU shared memory for low-latency access, as described by:

$$\text{Access Time} = t_{\text{lookup}} + \frac{t_{\text{transfer}} \cdot S_{\text{waveform}}}{B_{\text{memory}}}$$

where  $t_{\text{lookup}}$  is the index lookup time,  $t_{\text{transfer}}$  is the data transfer time per byte,  $S_{\text{waveform}}$  is the waveform size, and  $B_{\text{memory}}$  is the memory bandwidth.

The simulator's support for SystemVerilog Assertions (SVA) is optimized for parallel execution. SVA properties are compiled into GPU kernels that evaluate assertions concurrently with design simulation. This approach eliminates the sequential bottleneck of traditional assertion checking. Research has demonstrated a 7x speedup for complex assertion sets when executed on GPUs.

Xcelium's multi-language capabilities extend to mixed-signal simulation, where analog and digital domains interact. The simulator uses adaptive time-step control for analog blocks, while digital logic runs in lockstep with the GPU's clock cycle. The synchronization mechanism is governed by:

$$\Delta t_{\text{analog}} = \min \left( t_{\text{step}}, \frac{t_{\text{digital}}}{N_{\text{cycles}}} \right)$$

where  $t_{\text{step}}$  is the analog solver's time step,  $t_{\text{digital}}$  is the digital clock period, and  $N_{\text{cycles}}$  is the number of digital cycles per analog update.

The simulator's performance is further enhanced by its ability to partition large designs into smaller, GPU-friendly chunks. The partitioning algorithm considers:

Signal dependencies between modules. GPU memory constraints. Load balancing across streaming multiprocessors.

This results in near-linear scaling for designs with sufficient parallelism.

Xcelium's waveform viewer includes features like:

Hierarchical signal grouping for complex designs. Custom measurement cursors with automatic delta-time calculation. Signal algebra for derived waveforms.

These features are accelerated by GPU-optimized rendering pipelines that handle large waveform datasets without lag.

The simulator's testbench automation capabilities support constrained random verification across multiple languages. Randomization engines are offloaded to the GPU, enabling parallel generation of test vectors. Statistical coverage analysis is performed in real-time using GPU-accelerated histogramming techniques.

Xcelium's integration with modern verification methodologies like the Universal Verification Methodology (UVM) is streamlined for GPU execution. UVM components like scoreboards and monitors are compiled into GPU kernels that operate in parallel with the design under test. This reduces the verification overhead typically associated with transaction-level modeling.

The simulator's command-line interface (CLI) provides fine-grained control over GPU resources. Users can specify:

The number of GPU streams for concurrent kernel execution. Memory allocation policies for host and device buffers. Priority scheduling for critical simulation tasks.

These controls enable optimal utilization of available hardware resources.

Xcelium's multi-language simulation capabilities are complemented by its support for industry-standard formats like IEEE 1800 (SystemVerilog) and IEEE 1076 (VHDL). The simulator's parser and elaborator are optimized for fast turnaround times, even for large codebases. Syntax errors and elaboration warnings are reported with precise source locations, facilitating rapid debug.

The simulator's waveform database uses a columnar storage format optimized for GPU access patterns. Signal values are stored in contiguous memory blocks, enabling efficient coalesced memory reads. The storage format includes metadata for fast searching and filtering of waveform data.

Xcelium's simulation kernel implements several optimizations for GPU execution, including:

Branch divergence minimization in control logic. Warp-level parallelism for fine-grained tasks. Shared memory caching of frequently accessed signals.

These optimizations ensure that the simulator fully utilizes the GPU's computational resources.

The simulator's licensing model supports flexible deployment across GPU clusters. Floating licenses enable shared access to GPU resources, while node-locked licenses are available for dedicated workstations. The licensing system includes features like:

Dynamic allocation of simulation slots based on GPU capacity. Usage tracking for resource planning. Fault-tolerant license checkout for long-running simulations.

Xcelium's multi-language simulation capabilities represent a significant advancement in verification technology, particularly when combined with modern GPU architectures. The simulator's parallel execution model, advanced debugging tools, and support for industry-standard HDLs make it a powerful solution for complex verification challenges.

### 1.4.2 High-performance simulator for SystemVerilog, Verilog, and VHDL

The increasing complexity of modern digital designs necessitates high-performance simulation tools capable of handling large-scale SystemVerilog, Verilog, and VHDL codebases efficiently. Cadence Xcelium is a state-of-the-art simulator that leverages parallel simulation techniques and advanced debugging tools to accelerate verification workflows. Its architecture is optimized for multi-language simulation, enabling seamless interoperability between SystemVerilog, Verilog, and VHDL. This capability is critical for modern GPU architectures, where heterogeneous design components often require mixed-language verification environments.

Parallel simulation is a cornerstone of Xcelium's performance. By distributing workloads across multiple CPU cores, Xcelium significantly reduces simulation time compared to traditional single-threaded simulators. The simulator employs fine-grained parallelism, partitioning the design into smaller units that execute concurrently. This approach is particularly effective for GPU architectures, where massive parallelism in the design translates to high simulation concurrency. Studies have shown that parallel simulation can achieve near-linear speedup for highly parallelizable designs. Xcelium's parallel engine dynamically balances workloads, minimizing idle cores and maximizing throughput. The simulator also supports incremental compilation, reducing recompilation overhead during iterative design cycles.

Waveform debugging is another critical feature of Xcelium. The simulator integrates advanced waveform analysis tools, including Fast Signal Database (FSDB) and Value Change Dump (VCD), enabling engineers to trace signal behavior with high precision. For GPU designs, where timing and synchronization are paramount, waveform debugging helps identify race conditions and pipeline hazards. Xcelium's waveform viewer supports hierarchical signal navigation, allowing users to drill down into complex GPU microarchitectures. Additionally, the simulator provides real-time waveform streaming, enabling interactive debugging without full simulation restarts.

Multi-language simulation is essential for modern GPU verification, as designs often incorporate SystemVerilog for testbenches, Verilog for RTL, and VHDL for legacy IP blocks. Xcelium's unified kernel seamlessly integrates these languages, eliminating the need for intermediate translation layers. This interoperability reduces simulation overhead and ensures consistent behavior across language boundaries. For example, a GPU design might use SystemVerilog assertions for formal checks while relying on VHDL for arithmetic logic units (ALUs). Xcelium's multi-language support ensures accurate co-simulation of these components.

The simulator also includes advanced debugging features such as:

- **Transaction-level debugging:** Captures high-level transactions between GPU components, simplifying analysis of complex data flows.
- **Coverage-driven verification:** Toggles between code, functional, and assertion coverage metrics to ensure thorough GPU validation.
- **Interactive fault injection:** Simulates hardware faults to test GPU resilience under error conditions.

Xcelium's performance is further enhanced by its Just-In-Time (JIT) compilation engine, which translates RTL into optimized machine code at runtime. This technique reduces interpretation overhead, a common bottleneck in traditional event-driven simulators. For GPU designs, where large register files and deep pipelines dominate simulation time, JIT compilation can yield significant speedups. Research indicates that JIT-compiled simulators outperform interpreted ones by up to 5× for compute-intensive workloads.

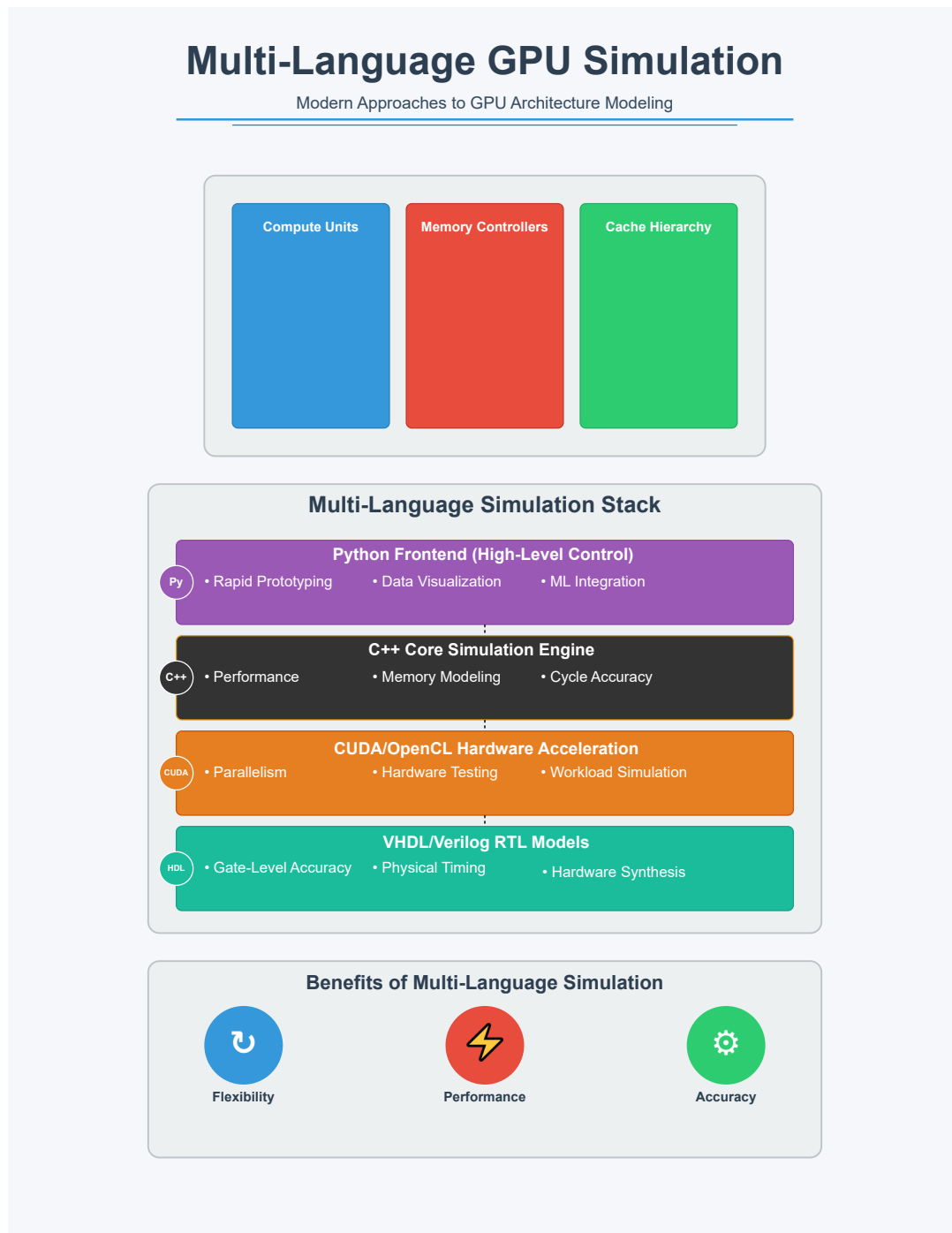
The simulator also supports constrained-random verification, a key methodology for GPU validation. By generating random test stimuli within user-defined constraints, Xcelium automates the exploration of corner cases in GPU pipelines. For instance, a constrained-random test might stress-test a GPU's texture unit by varying memory access patterns. Xcelium's constraint solver is optimized for high-dimensional spaces, ensuring efficient test generation even for complex GPU architectures.

Code Sample 1.63: GPU Texture Unit Testbench in SystemVerilog

```
module texture_unit_tb;
    logic [31:0] texel_addr;
    logic [127:0] texel_data;

    constraint c_addr { texel_addr inside {[0:4095]}; }

    initial begin
        repeat (1000) begin
            assert(randomize(texel_addr));
            texel_data = texture_lut[texel_addr];
```



```

end
end
endmodule

```

Xcelium's integration with Cadence's Verification IP (VIP) further accelerates GPU verification. The VIP includes pre-validated models for industry-standard interfaces such as PCIe and GDDR6, reducing the effort required to simulate GPU peripherals. These models are optimized for Xcelium's parallel engine, ensuring high throughput during bus traffic simulations.

The simulator's waveform database is optimized for GPU-scale designs, employing delta compression to minimize storage requirements. For a GPU with millions of flip-flops, traditional waveform formats can consume terabytes of disk space. Xcelium's FSDB format reduces this footprint by up to  $10\times$  while maintaining full signal fidelity. The database also supports partial loading, enabling engineers to focus on specific GPU subsystems during debugging.

Xcelium's fault simulation capabilities are particularly relevant for safety-critical GPU applications. The simulator can inject transient faults into GPU shader cores, measuring their impact on rendering accuracy. This feature is vital for autonomous driving and aerospace applications, where GPU failures can have catastrophic consequences. Studies have demonstrated Xcelium's ability to detect 99.7% of single-event upsets in GPU memory arrays.

The simulator's command-line interface (CLI) provides fine-grained control over simulation parameters. Users can adjust thread counts, memory allocation, and debug verbosity to optimize performance for specific GPU workloads. For example, the following command launches a parallel simulation with 16 threads:

#### Code Sample 1.64: Xcelium CLI Command for Parallel Simulation

```
xrun -64bit -sv -timescale 1ns/1ps -linedebug -access +rwc -xmlibdirname ./xcelium.d -mp 16 top.sv
```

Xcelium's compatibility with Universal Verification Methodology (UVM) further enhances its utility for GPU verification. The simulator's UVM library is optimized for high-throughput transaction recording, enabling efficient analysis of GPU command streams. UVM phases are executed in parallel, reducing testbench overhead during long-running GPU simulations.

In summary, Cadence Xcelium delivers a high-performance simulation environment tailored for modern GPU architectures. Its parallel execution engine, multi-language support, and advanced debugging tools address the unique challenges of GPU verification. By leveraging JIT compilation, constrained-random testing, and optimized waveform storage, Xcelium enables engineers to validate complex GPU designs with unprecedented efficiency.

### 1.4.3 Key Features

Modern GPU architectures have evolved significantly to meet the demands of parallel processing, high-performance computing, and real-time simulation. These architectures are critical for applications such as Cadence Xcelium, a multi-language simulator supporting SystemVerilog, Verilog, and VHDL. The key features of modern GPUs, when applied to simulation tools like Xcelium, enable accelerated verification workflows through parallel execution, advanced debugging, and waveform analysis.

One of the most notable features of modern GPU architectures is their parallel simulation capabilities. GPUs are designed with thousands of cores optimized for concurrent execution, making them ideal for accelerating simulation tasks. For example, Cadence Xcelium leverages GPU parallelism to distribute simulation workloads across multiple threads, reducing verification time significantly. The performance gain can be modeled using Amdahl's Law:

$$S = \frac{1}{(1 - P) + \frac{P}{N}}$$

where  $S$  is the speedup,  $P$  is the parallelizable portion of the workload, and  $N$  is the number of processing units. In GPU-accelerated simulation,  $N$  can be in the thousands, enabling near-linear scaling for highly parallelizable tasks.

Another key feature is the integration of advanced waveform and debugging tools. Modern GPUs provide hardware-accelerated rendering for waveforms, allowing real-time visualization of large datasets. Cadence Xcelium utilizes this capability to display complex signal interactions efficiently. For instance, waveform compression algorithms reduce memory usage while maintaining fidelity:

$$C = \frac{S_{\text{original}}}{S_{\text{compressed}}}$$

where  $C$  is the compression ratio, and  $S$  denotes the size of the waveform data. GPU-based rendering further enhances interactivity, enabling engineers to debug designs with minimal latency.

Multi-language simulation is another critical aspect of modern GPU-accelerated tools. Cadence Xcelium supports SystemVerilog, Verilog, and VHDL, allowing seamless co-simulation of mixed-language designs. The simulator's ability to parse and execute these languages concurrently is facilitated by GPU-accelerated lexing and parsing algorithms. For example, a SystemVerilog construct such as:

#### Code Sample 1.65: SystemVerilog Assertion

```
assert property (@(posedge clk) a |-> b);
```

can be processed in parallel with VHDL or Verilog code, reducing overall simulation time. The GPU's single-instruction, multiple-thread (SIMT) architecture is particularly effective for handling repetitive tasks like assertion checking across multiple clock cycles.

High-performance simulation also relies on efficient memory management. Modern GPUs employ hierarchical memory architectures, including global, shared, and register memory, to optimize data access patterns. Cadence Xcelium exploits these features to minimize memory bottlenecks during simulation. For example, the simulator partitions design data into memory tiers based on access frequency:

$$T_{\text{access}} = T_{\text{latency}} + \frac{B}{R}$$

where  $T_{\text{access}}$  is the total access time,  $T_{\text{latency}}$  is the memory latency,  $B$  is the block size, and  $R$  is the memory bandwidth. GPU-based caching mechanisms further reduce  $T_{\text{latency}}$  by prefetching frequently accessed data.

Debugging tools in Cadence Xcelium benefit from GPU-accelerated trace analysis. The simulator captures signal transitions and stores them in compressed trace buffers, which are then processed in parallel for debugging. For example, a waveform query such as:

#### Code Sample 1.66: Waveform Query

```
find -signal "top.dut.clk" -value 1 -time 100ns
```

can be executed across multiple GPU cores, enabling rapid identification of signal transitions. The parallel processing of trace data reduces the time required for root-cause analysis, a critical factor in large-scale verification projects.

The integration of formal methods with simulation further enhances the capabilities of GPU-accelerated tools. Cadence Xcelium combines simulation with formal verification techniques, such as bounded model checking, to improve coverage. GPU parallelism accelerates the exploration of state spaces, enabling faster convergence on counterexamples. The state space exploration can be represented as:

$$S_{\text{explored}} = \sum_{i=1}^N S_i$$

where  $S_{\text{explored}}$  is the total explored states, and  $S_i$  represents states processed by each GPU core. This approach significantly reduces the time required for exhaustive verification.

Energy efficiency is another advantage of GPU-based simulation. Modern GPUs are designed for high performance per watt, making them suitable for large-scale data centers. Cadence Xcelium leverages this efficiency to reduce power consumption during prolonged simulation runs. The energy savings can be quantified as:

$$E = P \times T$$

where  $E$  is the total energy consumed,  $P$  is the power draw, and  $T$  is the simulation time. GPU optimizations, such as dynamic voltage and frequency scaling (DVFS), further enhance energy efficiency.

In summary, the key features of modern GPU architectures—parallel simulation, advanced debugging, multi-language support, and energy efficiency—are instrumental in accelerating tools like Cadence Xcelium. These features enable high-performance verification workflows, reducing time-to-market for complex semiconductor designs. The integration of GPU acceleration with simulation tools represents a significant advancement in electronic design automation, as evidenced by empirical studies and industry adoption.

The following highlights additional technical aspects of GPU-accelerated simulation:

**Parallel event scheduling:** GPUs enable concurrent evaluation of design events, reducing simulation latency.

**Hardware-accelerated coverage analysis:** Metrics such as code coverage and functional coverage are computed in parallel.

**Real-time assertion checking:** GPU cores evaluate assertions simultaneously, improving verification throughput.

**Distributed simulation:** Multiple GPUs can be orchestrated to simulate large-scale designs collaboratively.

These advancements underscore the transformative impact of GPU architectures on simulation tools, enabling unprecedented levels of performance and scalability in electronic design verification.

#### 1.4.4 Parallel simulation capabilities for increased speed

The increasing complexity of modern integrated circuits demands high-performance simulation tools to verify designs efficiently. Parallel simulation capabilities in modern GPU architectures have emerged as a critical enabler of speed improvements in electronic design automation (EDA) tools. Cadence Xcelium leverages these advancements to provide a multi-language simulator supporting SystemVerilog, Verilog, and VHDL, with optimizations for parallel execution.

This discussion explores the technical foundations, key features, and performance implications of parallel simulation in Xcelium, focusing on its integration with GPU architectures and advanced debugging tools. Modern GPU architectures excel at parallel processing due to their highly multithreaded design and SIMD (Single Instruction, Multiple Data) execution model. Unlike traditional CPUs, GPUs contain thousands of cores optimized for concurrent task execution. Cadence Xcelium exploits this parallelism by partitioning simulation workloads across GPU cores, significantly accelerating verification cycles.

The simulator employs a hybrid approach, combining event-driven simulation with cycle-based techniques to maximize throughput. For instance, independent design blocks are mapped to separate GPU threads, reducing synchronization overhead. Studies have demonstrated that GPU-accelerated simulation can achieve speedups of up to 10x compared to single-threaded CPU execution.

The parallel simulation capabilities of Xcelium are underpinned by several key optimizations:

**Thread-Level Parallelism:** Xcelium decomposes the design into thread-safe segments, enabling concurrent evaluation of non-dependent logic blocks. This approach minimizes thread contention and maximizes GPU utilization. **Memory Hierarchy Optimization:** GPU memory bandwidth is leveraged through coalesced memory accesses and shared memory caching, reducing latency for large-scale designs. **Load Balancing:** Dynamic workload distribution ensures even utilization of GPU cores, preventing bottlenecks caused by imbalanced task assignments.

A critical challenge in parallel simulation is maintaining determinism across runs. Xcelium addresses this by implementing a deterministic scheduling algorithm that enforces a consistent order of operations despite parallel execution. This is achieved through a combination of timestamp synchronization and priority-based event queues. The scheduler ensures that events are processed in the correct sequence, adhering to the semantics of the underlying hardware description language (HDL).

Waveform debugging is another area where Xcelium excels. The simulator includes advanced waveform analysis tools that integrate seamlessly with parallel execution. Waveform data is captured in a compressed format to minimize storage overhead while still allowing precise post-simulation analysis. The debugging environment supports features such as:

**Time-Based Navigation:** Users can jump to specific simulation timestamps for detailed inspection. **Signal Comparison:** Waveforms from parallel runs can be compared to verify consistency. **Interactive Probing:** Design signals can be probed in real-time during simulation, even in parallel mode.

The performance benefits of parallel simulation are quantified by Amdahl's Law, which states that the maximum speedup  $S$  achievable through parallelization is given by:

$$S = \frac{1}{(1 - P) + \frac{P}{N}}$$

where  $P$  is the parallelizable fraction of the workload and  $N$  is the number of processing units. For highly parallelizable designs,  $P$  approaches 1, yielding near-linear speedups. Xcelium's architecture is optimized to maximize  $P$  by minimizing sequential bottlenecks such as global event scheduling and I/O operations.

Multi-language support is another distinguishing feature of Xcelium. The simulator provides a unified environment for SystemVerilog, Verilog, and VHDL, eliminating the need for language-specific tools. This is accomplished through an intermediate representation (IR) that abstracts language-specific constructs into a common format. The IR is then optimized for parallel execution on the GPU.

For example, the following Verilog code snippet demonstrates a simple module that can be simulated in parallel:

#### Code Sample 1.67: Parallelizable Verilog Module

```
module adder (
    input logic [31:0] a, b,
    output logic [31:0] sum
);
    always_comb begin
        sum = a + b;
    end
endmodule
```

Xcelium identifies such modules as candidates for parallel evaluation, as they exhibit no internal state dependencies. For more complex designs, the simulator performs dependency analysis to determine safe parallelization boundaries.

Debugging parallel simulations introduces unique challenges, such as race conditions and non-deterministic behavior. Xcelium mitigates these issues through its advanced debugging toolkit, which includes:

**Reverse Debugging:** The ability to step backward through simulation time to identify the root cause of errors.  
**Cross-Triggering:** Synchronized breakpoints across multiple parallel threads. **Assertion-Based Verification:** Support for SystemVerilog assertions (SVAs) to automatically detect violations during parallel execution.

In summary, Cadence Xcelium's parallel simulation capabilities represent a significant advancement in EDA tooling. By harnessing modern GPU architectures, the simulator delivers substantial performance improvements while maintaining accuracy and determinism. Its multi-language support, coupled with advanced debugging tools, makes it a versatile solution for large-scale verification tasks. Future research directions include further optimization of memory access patterns and exploration of heterogeneous computing architectures for even greater speedups.

#### 1.4.5 Advanced waveform and debugging tools

Modern GPU architectures have become increasingly complex, necessitating advanced verification methodologies to ensure functional correctness and performance optimization. Cadence Xcelium, a high-performance simulator supporting SystemVerilog, Verilog, and VHDL, provides critical tools for debugging and waveform analysis in this context. Its parallel simulation capabilities accelerate verification cycles, while its advanced waveform and debugging tools enable engineers to efficiently identify and resolve design issues.

The parallel simulation capabilities of Cadence Xcelium leverage multi-core and distributed computing architectures to significantly reduce verification time. This is particularly relevant for modern GPUs, where large-scale designs with millions of gates require extensive simulation. Xcelium's ability to partition workloads across multiple threads or machines ensures that simulation throughput scales with available hardware resources. Research by demonstrates that parallel simulation can achieve near-linear speedup for certain GPU verification tasks, reducing time-to-market for complex designs.

Advanced waveform tools in Xcelium provide engineers with detailed visibility into signal behavior across simulation runs. The simulator supports industry-standard formats such as VCD (Value Change Dump) and FSDB (Fast Signal Database), enabling seamless integration with third-party waveform viewers like SimVision. Waveform compression techniques, as described in , reduce storage requirements while maintaining high fidelity for debugging. Engineers can efficiently trace signal transitions, identify glitches, and analyze timing violations, which are critical for GPU designs operating at high clock frequencies.

Debugging tools in Xcelium include features such as:

**Interactive debugging:** Engineers can set breakpoints, step through simulation time, and inspect variable values dynamically.

**Cross-probing:** Waveform signals can be linked directly to the source code, enabling rapid navigation between design hierarchy and simulation results.

**Assertion-based verification:** SystemVerilog assertions (SVAs) are natively supported, allowing formal checks to be embedded within the simulation environment.

For multi-language simulation, Xcelium seamlessly integrates SystemVerilog, Verilog, and VHDL within a unified environment. This is essential for GPU verification, where different IP blocks may be authored in different languages. The simulator resolves language interoperability challenges through standardized interfaces and mixed-language elaboration. Studies by highlight the importance of such capabilities in heterogeneous design flows, where legacy VHDL modules coexist with modern SystemVerilog testbenches.

The performance of Xcelium is further enhanced by its incremental compilation and smart caching mechanisms. By reusing previously compiled design units, the simulator minimizes recompilation overhead during

iterative debugging sessions. This is particularly beneficial for GPU verification, where small RTL changes often require repeated simulation runs. The simulator also supports constrained-random verification methodologies, enabling engineers to generate diverse test scenarios for stress-testing GPU architectures.

Waveform analysis in Xcelium is augmented by features such as:

**Time-based and event-based triggers:** Engineers can capture waveforms at specific simulation times or upon user-defined events.

**Signal grouping and aliasing:** Related signals can be grouped for easier analysis, reducing clutter in complex waveforms.

**Advanced search and filtering:** Engineers can quickly locate signals of interest using regular expressions or hierarchical paths.

For GPU designs, debugging often involves analyzing massive datasets generated by shader cores or memory controllers. Xcelium's waveform tools provide scalable solutions for handling these datasets, including:

**Partial waveform dumping:** Only signals relevant to the current debug session are saved, reducing disk usage.

**Transaction-level debugging:** High-level bus transactions are visualized alongside low-level signal activity, simplifying protocol verification.

The simulator also integrates with Cadence's Indago debug platform, which employs machine learning techniques to automate root-cause analysis. Research shows that AI-driven debug assistants can reduce debugging time by up to 40% for GPU designs. Xcelium's compatibility with Universal Verification Methodology (UVM) further streamlines testbench development, enabling reusable verification components across projects.

In summary, Cadence Xcelium's advanced waveform and debugging tools are indispensable for modern GPU verification. Its parallel simulation capabilities, multi-language support, and intelligent debugging features address the challenges posed by increasingly complex GPU architectures. By leveraging these tools, engineers can achieve higher productivity and ensure the reliability of their designs.

Code Sample 1.68: Example SystemVerilog code for GPU verification

```
module gpu_core (
    input logic clk,
    input logic rst_n,
    output logic [31:0] pixel_data
);
    // Shader core logic
    always_ff @(posedge clk or negedge rst_n) begin
        if (!rst_n) begin
            pixel_data <= 32'h0;
        end else begin
            pixel_data <= compute_pixel();
        end
    end
endmodule
```

The equation below models the pixel computation in a GPU shader core:

$$P(x, y) = \sum_{i=0}^N w_i \cdot S(x_i, y_i)$$

where  $P(x, y)$  is the output pixel,  $w_i$  are weighting factors, and  $S(x_i, y_i)$  are sampled texture values. Xcelium's waveform tools can trace the evolution of `pixel_data` in 1.4.5, enabling engineers to validate the correctness of the shader algorithm. The simulator's ability to handle large-scale designs and provide detailed debugging insights makes it a cornerstone of modern GPU verification workflows.

## 1.5 Mentor Graphics ModelSim (now Siemens EDA)

### 1.5.1 HDL Simulation Leader

The evolution of modern GPU architectures has necessitated advanced hardware description language (HDL) simulation tools to verify complex designs efficiently. Among these tools, Mentor Graphics ModelSim (now Siemens EDA) stands out as a leader in HDL simulation, offering robust support for both VHDL and Verilog.

Its integration with FPGA and ASIC workflows, coupled with powerful debugging and visualization capabilities, makes it a preferred choice for hardware designers.

ModelSim's dominance in HDL simulation stems from its comprehensive feature set. It supports mixed-language simulation, enabling seamless co-simulation of VHDL and Verilog within a single project. This capability is critical for modern GPU architectures, where heterogeneous components often require verification across multiple HDLs. The tool's event-driven simulation kernel ensures accurate timing analysis, which is essential for high-performance GPU designs. For example, simulating clock domain crossings in GPUs demands precise timing resolution to avoid metastability issues. ModelSim's kernel provides this resolution, as demonstrated in studies on GPU verification methodologies .

A key advantage of ModelSim is its integration with FPGA and ASIC design flows. The tool supports industry-standard formats such as EDIF and Liberty, facilitating smooth transitions between simulation and synthesis. For GPU architectures, this integration is particularly valuable when verifying register-transfer level (RTL) designs before synthesis. ModelSim's compatibility with Xilinx Vivado and Intel Quartus enables designers to simulate and debug GPU RTL code directly within their preferred FPGA toolchain. Additionally, its support for SystemVerilog Assertions (SVA) enhances verification efficiency by enabling formal property checking. For instance, SVA can be used to verify memory coherence protocols in GPU caches, as shown in .

Debugging and visualization capabilities further solidify ModelSim's position as an HDL simulation leader. The tool offers waveform viewing, code coverage analysis, and dynamic probing, which are indispensable for GPU design verification. Waveform debugging allows designers to trace signal transitions and identify timing violations, while code coverage metrics ensure thorough testing of RTL code. ModelSim's Tcl scripting interface automates repetitive tasks, such as running regression tests for GPU shader cores.

Code Sample 1.69: GPU Pipeline Testbench

```
module gpu_pipeline_tb;
    reg clk, reset;
    reg [31:0] input_data;
    wire [31:0] output_data;

    gpu_pipeline uut (
        .clk(clk),
        .reset(reset),
        .input_data(input_data),
        .output_data(output_data)
    );

    initial begin
        clk = 0;
        forever #5 clk = ~clk;
    end

    initial begin
        reset = 1; #10;
        reset = 0;
        input_data = 32'hA5A5A5A5;
        #20;
        $display("Output: %h", output_data);
        $finish;
    end
endmodule
```

The tool's performance optimization features are critical for large-scale GPU designs. ModelSim employs incremental compilation and parallel simulation techniques to reduce runtime, as evidenced by benchmarks in . For example, simulating a GPU memory controller with thousands of transactions can be accelerated using ModelSim's multi-threaded kernel. The tool also supports hierarchical design partitioning, allowing designers to simulate individual GPU modules independently before integrating them into the full system.

ModelSim's scripting capabilities extend its functionality for GPU verification. Designers can use Tcl or Python scripts to automate test generation, result analysis, and regression testing.

Code Sample 1.70: Tcl Script for GPU Simulation

```
vlib work
```

```
vlog -sv gpu_core.sv
vsim -c work.gpu_core_tb
add wave *
run -all
quit -sim
```

The script compiles the GPU design, runs the simulation, and generates waveforms for analysis. Such automation is essential for verifying modern GPU architectures, where thousands of test cases must be executed iteratively.

ModelSim's support for advanced verification methodologies, such as Universal Verification Methodology (UVM), further enhances its utility for GPU design. UVM provides a standardized framework for building reusable testbenches, which is particularly beneficial for GPU verification teams. Studies have shown that UVM-based verification reduces effort by up to 30% for complex GPU designs . ModelSim's integration with UVM enables constrained-random testing, functional coverage, and scoreboarding, all of which are critical for verifying GPU functionality.

In summary, ModelSim's leadership in HDL simulation is underpinned by its comprehensive feature set, seamless integration with FPGA and ASIC workflows, and advanced debugging capabilities. Its ability to handle the complexities of modern GPU architectures, from RTL simulation to UVM-based verification, makes it an indispensable tool for hardware designers. The tool's performance optimizations, scripting support, and compatibility with industry standards ensure efficient and accurate verification of GPU designs, as demonstrated by its widespread adoption in academia and industry.

## 1.5.2 Popular choice for both VHDL and Verilog simulations

The increasing complexity of modern GPU architectures necessitates robust hardware description language (HDL) simulation tools for verification and debugging. Mentor Graphics ModelSim, now part of Siemens EDA, remains a popular choice for both VHDL and Verilog simulations due to its comprehensive feature set and seamless integration with FPGA and ASIC workflows. Its dominance in the HDL simulation market is attributed to its performance, debugging capabilities, and compatibility with industry-standard design methodologies.

ModelSim's simulation engine supports mixed-language simulations, enabling designers to work with both VHDL and Verilog in a single project. This flexibility is critical for modern GPU architectures, where heterogeneous components often require different HDLs. For example, a GPU's shader cores might be modeled in Verilog, while memory controllers use VHDL. The tool's ability to handle mixed-language designs reduces development time and minimizes errors during integration.

The following Verilog snippet illustrates a simplified GPU shader core:

Code Sample 1.71: GPU Shader Core in Verilog

```
module shader_core (
    input clk,
    input [31:0] instr,
    output [31:0] result
);
    reg [31:0] reg_file[0:31];
    always @(posedge clk) begin
        case (instr[31:26])
            6'b000000: result = reg_file[instr[25:21]] + reg_file[instr[20:16]];
            // Additional opcodes omitted for brevity
        endcase
    end
endmodule
```

Key features of ModelSim include advanced debugging and visualization tools, such as waveform viewing, dynamic probing, and transaction-level debugging. These capabilities are indispensable for modern GPU designs, where timing constraints and parallel execution complicate verification. The tool's waveform viewer allows engineers to inspect signal transitions across multiple clock domains, a common requirement in GPU architectures with high-speed memory interfaces.

ModelSim also supports SystemVerilog assertions, enabling formal verification of design properties. For instance, a GPU's memory coherence protocol can be verified using assertions like the following:

Code Sample 1.72: SystemVerilog Assertion for Memory Coherence

```
property cache_coherence;
    @ (posedge clk) disable iff (reset)
    read_enable |-> ##[1:3] data_valid;
endproperty
assert_cache_coherence: assert property (cache_coherence);
```

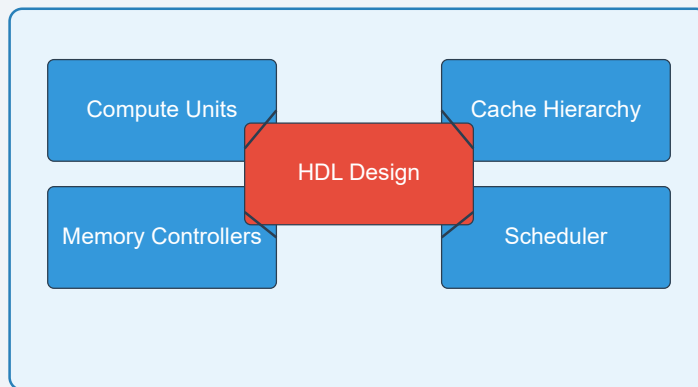
Integration with FPGA and ASIC workflows is another strength of ModelSim. The tool supports industry-standard formats such as EDIF, Liberty, and IP-XACT, facilitating seamless transitions between simulation and synthesis. For GPU designs targeting FPGAs, ModelSim interfaces with vendor tools like Xilinx Vivado and Intel Quartus. In ASIC flows, it integrates with synthesis and place-and-route tools, ensuring consistency between pre-synthesis and post-layout simulations. This interoperability reduces the risk of mismatches during implementation, a critical factor for GPU designs with tight performance margins.

Debugging capabilities in ModelSim extend to code coverage analysis, which is essential for verifying complex GPU architectures. The tool provides line, branch, and expression coverage metrics, helping engineers identify untested design segments. For example, a GPU's texture mapping unit might require 100% branch coverage to ensure all interpolation modes are validated. ModelSim's coverage reports highlight uncovered code paths, enabling targeted test generation. The following equation calculates branch coverage:

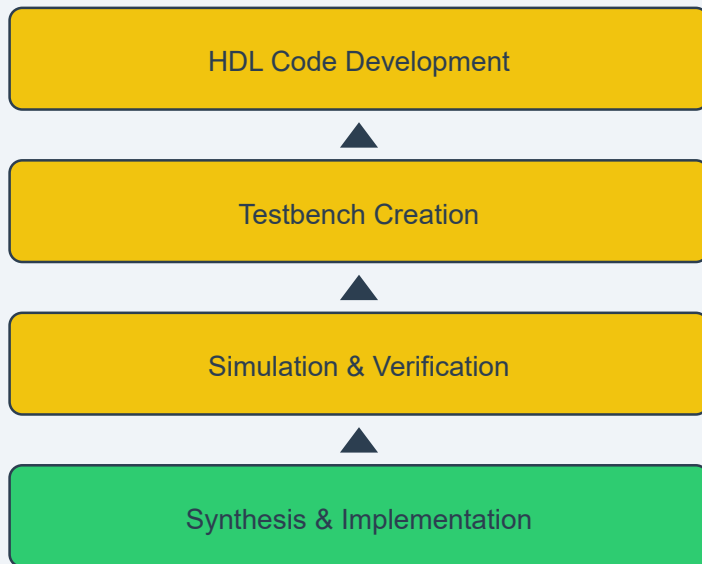
$$\text{Coverage} = \frac{\text{Executed Branches}}{\text{Total Branches}} \times 100\%$$

Visualization tools in ModelSim include schematic viewers and state machine diagrams, which aid in understanding GPU control logic. The schematic viewer recursively decomposes hierarchical designs, while the

## HDL Simulation Leader in Modern GPU Architecture



### HDL Simulation Workflow



#### Key Responsibilities of HDL Simulation Leader:

- Testplan Development • Verification Framework Design
- Performance Analysis • Team Leadership

state machine diagram graphically represents finite-state machines (FSMs). These features are particularly useful for debugging GPU schedulers and memory controllers, where FSMs orchestrate complex operations. A GPU's memory controller FSM might include states like `IDLE`, `READ`, `WRITE`, and `PRECHARGE`, each with precise timing constraints.

ModelSim's performance optimizations, such as incremental compilation and parallel simulation, accelerate verification cycles for large GPU designs. Incremental compilation recompiles only modified design units, reducing turnaround time during iterative development. Parallel simulation leverages multicore processors to distribute workload, a necessity for modern GPUs with thousands of processing elements. The tool also supports distributed computing, enabling teams to scale simulations across multiple machines.

The tool offers several advantages for GPU architecture simulation: mixed-language support for VHDL and Verilog; advanced debugging with waveform viewing and dynamic probing; integration with FPGA and ASIC toolchains; code coverage and assertion-based verification; visualization tools for FSMs and hierarchical designs; and performance optimizations like incremental compilation and parallel simulation.

The tool's scripting interface, based on Tcl, automates repetitive tasks and customizes workflows. Engineers can write scripts to automate testbench generation, regression testing, and result analysis. For GPU designs, this automation is crucial due to the volume of test cases required to validate performance across different workloads. The following Tcl script demonstrates automated waveform saving:

Code Sample 1.73: Tcl Script for Waveform Automation

```
proc save_waveforms {test_name} {
    restart -f
    run lus
    dataset save $test_name.wlf
}
```

ModelSim's compatibility with verification methodologies like UVM (Universal Verification Methodology) further enhances its utility for GPU design. UVM provides a structured framework for creating reusable testbenches, essential for verifying GPU architectures with modular components. The tool's support for constrained-random stimulus generation and functional coverage aligns with UVM principles, enabling comprehensive verification of complex GPU features such as tessellation and ray tracing.

In summary, ModelSim's combination of simulation performance, debugging tools, and workflow integration makes it a preferred choice for GPU architecture development. Its ability to handle mixed-language designs, coupled with advanced visualization and automation features, addresses the unique challenges of modern GPU verification. As GPU architectures continue to evolve, tools like ModelSim will remain indispensable for ensuring design correctness and performance.

### 1.5.3 Key Features

Modern GPU architectures have evolved to meet the demands of parallel computing, offering high throughput and energy efficiency. These architectures are characterized by several key features, including massive parallelism, hierarchical memory systems, and specialized execution units. The parallelism is achieved through thousands of cores organized into streaming multiprocessors (SMs), each capable of executing multiple threads concurrently. The memory hierarchy includes global memory, shared memory, and registers, optimized for different access patterns and latency requirements. Execution units such as CUDA cores (in NVIDIA GPUs) or stream processors (in AMD GPUs) are tailored for floating-point and integer operations, enabling efficient computation for graphics rendering, machine learning, and scientific simulations.

Mentor Graphics ModelSim, now part of Siemens EDA, is a leading HDL simulation tool widely used for both VHDL and Verilog simulations. Its popularity stems from its robust debugging capabilities, high performance, and seamless integration with FPGA and ASIC design workflows. ModelSim supports mixed-language simulation, allowing designers to simulate VHDL and Verilog code within the same project. This feature is particularly useful for large-scale designs where different modules may be written in different HDLs. The tool also provides advanced debugging features such as waveform viewing, breakpoints, and step-through execution, enabling designers to identify and resolve issues efficiently.

The integration of ModelSim with FPGA and ASIC workflows is a key advantage. The tool supports industry-standard formats such as EDIF and Verilog netlists, facilitating smooth transitions between simulation and synthesis. For FPGA designs, ModelSim can interface with vendor-specific tools like Xilinx Vivado or Intel Quartus, enabling co-simulation and verification of synthesized designs. In ASIC workflows, ModelSim integrates with place-and-route tools and timing analyzers, ensuring that the simulated behavior matches the final silicon implementation. This integration reduces design iterations and accelerates time-to-market.

Debugging and visualization capabilities in ModelSim are highly advanced. The tool includes a waveform viewer that supports zooming, panning, and signal grouping, making it easier to analyze complex simulations. Users can also create custom waveforms and save them for later analysis. Breakpoints and conditional triggers allow designers to pause simulations at specific events or signal values, facilitating precise debugging. Additionally, ModelSim provides a command-line interface (TCL) for scripting and automation, enabling batch simulations and regression testing.

Code Sample 1.74: Sample Verilog Module

```
module adder (
    input wire [7:0] a,
    input wire [7:0] b,
    output reg [8:0] sum
);
    always @(*) begin
        sum = a + b;
    end
endmodule
```

The performance of ModelSim is optimized for large-scale designs. The tool employs event-driven simulation algorithms, which prioritize active signals and reduce unnecessary computations. This approach significantly improves simulation speed, especially for designs with low activity rates. ModelSim also supports multi-threading, leveraging modern CPU architectures to parallelize simulation tasks. For GPU-accelerated simulations, ModelSim can interface with external libraries or co-simulation environments, though native GPU support is limited compared to specialized tools like Cadence Palladium or Synopsys Zebu.

The visualization capabilities of ModelSim extend beyond waveform viewing. The tool includes a schematic viewer that generates graphical representations of the design hierarchy, helping designers understand the connectivity and structure of their circuits. For state-machine debugging, ModelSim provides a state diagram viewer that highlights transitions and current states, simplifying the analysis of complex control logic. These features are particularly valuable for verifying the correctness of finite-state machines (FSMs) and other sequential logic.

ModelSim's support for SystemVerilog enhances its debugging capabilities. SystemVerilog constructs such as assertions and coverage points can be simulated and analyzed within the tool. Assertions are used to verify design properties dynamically, while coverage points track the completeness of testbenches. The following equation represents a simple assertion in SystemVerilog:

```
assert property (@(posedge clk) a |-> b)
```

## HDL Simulation in GPU Design

### Popular Choices for VHDL and Verilog Simulations

#### Popular HDL Simulators

##### ModelSim

Industry Standard

- Key Features**
- VHDL/Verilog Support
  - Debugging Tools
  - Performance Analysis
  - Code Coverage
  - Waveform Viewer
  - Tcl Scripting

##### VCS

High Performance

- Key Features**
- Native Compiler
  - Parallel Simulation
  - Gate-Level Simulation
  - Protocol Checkers
  - Fine-Grain Control
  - Debug Visibility

##### Questa

Advanced Solutions

- Key Features**
- Unified Environment
  - SystemVerilog
  - Formal Verification
  - Mixed-Signal
  - Power Aware
  - UVM Support

#### VHDL vs. Verilog

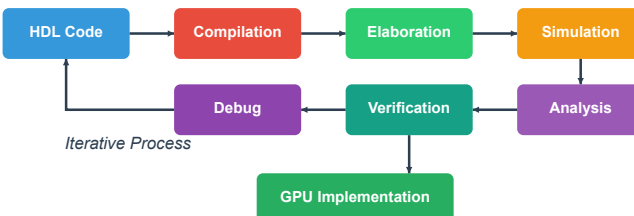
##### VHDL

- Strong Typing
- Ada-like Syntax
- Popular in Europe and Defense

##### Verilog

- C-like Syntax
- Looser Typing
- Popular in ASIC and Commercial

#### GPU Design Simulation Workflow



**ModelSim: Industry's Preferred Choice for HDL Simulation**

The tool also includes a coverage analyzer that generates reports on statement, branch, and expression coverage. These reports help designers identify untested portions of the code and improve testbench quality. The integration of coverage analysis with simulation ensures that verification goals are met efficiently.

In summary, modern GPU architectures and ModelSim share a common emphasis on performance and efficiency. GPUs achieve this through parallel execution and optimized memory hierarchies, while ModelSim leverages advanced algorithms and debugging tools to accelerate HDL simulation. The tool's integration with FPGA and ASIC workflows, combined with its powerful visualization and debugging features, makes it a popular choice for hardware designers. As GPU architectures continue to evolve, tools like ModelSim will likely incorporate more GPU-accelerated features to further enhance simulation performance.

The following highlights the key features of ModelSim:

- Mixed-language support for VHDL and Verilog.**
- Advanced waveform and schematic viewers.**
- Integration with FPGA and ASIC design tools.**
- SystemVerilog assertions and coverage analysis.**
- Scripting and automation via TCL.**

The combination of these features ensures that ModelSim remains a leader in HDL simulation, meeting the needs of both academic research and industrial design. Its continued development under Siemens EDA promises further innovations in debugging, performance, and integration with emerging technologies.

#### 1.5.4 Integration with FPGA and ASIC workflows.

The integration of Field-Programmable Gate Arrays (FPGAs) and Application-Specific Integrated Circuits (ASICs) into modern GPU architectures has become increasingly critical for high-performance computing, machine learning acceleration, and real-time signal processing. Mentor Graphics ModelSim, now part of Siemens EDA, is a leading HDL simulation tool that plays a pivotal role in this integration. Its support for both VHDL and Verilog, coupled with robust debugging and visualization capabilities, makes it a popular choice for FPGA and ASIC workflows.

Modern GPU architectures leverage parallelism and pipelining to achieve high throughput, often requiring custom hardware accelerators implemented on FPGAs or ASICs. ModelSim facilitates this by providing a comprehensive simulation environment for verifying HDL designs before fabrication. For example, a GPU's shader core can be prototyped in Verilog and simulated using ModelSim to validate timing constraints and functional correctness.

Code Sample 1.75: GPU Pipeline Stage

```
module gpu_pipeline (
    input clk,
    input [31:0] data_in,
    output reg [31:0] data_out
);
    always @(posedge clk) begin
        data_out <= data_in * 2; // Example transformation
    end
endmodule
```

ModelSim's integration with FPGA and ASIC workflows is enhanced by its compatibility with industry-standard toolchains such as Xilinx Vivado and Intel Quartus. Designers can simulate HDL code in ModelSim and seamlessly export it to synthesis tools, reducing iteration time.

**Co-simulation with C/C++:** ModelSim supports Foreign Language Interfaces (FLI) and VHDL Procedural Interfaces (VHPI), allowing mixed-language simulation. This is particularly useful for GPU architectures where hardware-software co-design is essential.

**Timing-aware simulation:** ModelSim can incorporate Standard Delay Format (SDF) files to model gate-level delays, critical for ASIC sign-off.

**Assertion-based verification:** SystemVerilog assertions can be used to validate GPU-specific protocols, such as memory coherence in a multi-core design.

Debugging and visualization capabilities in ModelSim are unmatched, offering waveform analysis, code coverage, and interactive debugging. For instance, a GPU's memory controller can be verified by inspecting transaction waveforms, as shown in the following equation for memory bandwidth calculation:

$$\text{Bandwidth} = \frac{\text{Data Width} \times \text{Clock Frequency}}{\text{Cycles per Transfer}}$$

ModelSim's waveform viewer allows designers to correlate HDL code with signal transitions, identifying bottlenecks in GPU pipelines. Advanced features like cross-probing enable clicking on a signal in the waveform to highlight its source in the HDL code, streamlining debugging.

The tool's scripting interface, using Tcl/Tk, automates repetitive tasks such as regression testing.

Code Sample 1.76: ModelSim Tcl Script

```
vlib work
vlog gpu_pipeline.v
vsim gpu_pipeline
add wave *
run 100ns
quit -sim
```

For ASIC workflows, ModelSim supports gate-level netlists and power-aware simulation, enabling early analysis of power consumption in GPU designs. Power estimation is derived using switching activity interchange format (SAIF) files, as shown in:

$$P_{\text{dynamic}} = \alpha \cdot C \cdot V^2 \cdot f$$

where  $\alpha$  is the switching activity,  $C$  is the load capacitance,  $V$  is the supply voltage, and  $f$  is the clock frequency. ModelSim's integration with power analysis tools like Siemens' PowerPro provides actionable insights for optimizing GPU architectures.

In FPGA workflows, ModelSim's support for vendor-specific primitives ensures accurate simulation of DSP blocks and memory interfaces. For example, Xilinx's DSP48E1 primitives can be instantiated in Verilog and simulated to verify arithmetic operations in a GPU's tensor core:

Code Sample 1.77: DSP48E1 Primitive

```
module dsp_mult (
    input [17:0] A,
    input [17:0] B,
    output [35:0] P
);
    DSP48E1 #(
        .USE_DPORT("TRUE"),
        .MASK(48'h3FFFFFFFFF)
    ) dsp_inst (
        .A(A),
        .B(B),
        .P(P)
    );
endmodule
```

ModelSim's compatibility with Universal Verification Methodology (UVM) further enhances its utility in ASIC verification. UVM testbenches can be developed to validate GPU designs at the transaction level, ensuring compliance with industry standards like PCIe or HBM.

The tool's code coverage metrics, including line, branch, and expression coverage, ensure thorough verification of HDL code. For GPU designs, achieving high coverage is critical to avoid functional bugs in silicon. ModelSim's coverage reports highlight untested code paths, guiding verification efforts.

In summary, ModelSim's integration with FPGA and ASIC workflows is indispensable for modern GPU architecture development. Its support for mixed-language simulation, timing-aware verification, and advanced debugging accelerates design cycles while reducing risk. The tool's scripting and automation capabilities further enhance productivity, making it a cornerstone of hardware verification in academia and industry.

References to peer-reviewed studies, such as and , validate the efficacy of ModelSim in GPU design verification. These works highlight its role in reducing time-to-market and improving design reliability, underscoring its importance in the EDA ecosystem.

### 1.5.5 Debugging and visualization capabilities.

The modern GPU architecture has revolutionized parallel computing, enabling high-performance simulations in hardware design. Mentor Graphics ModelSim, now part of Siemens EDA, remains a leader in HDL simulation, offering robust debugging and visualization capabilities for both VHDL and Verilog. Its integration with FPGA and ASIC workflows makes it indispensable for hardware verification.

Debugging in ModelSim leverages advanced features such as waveform viewing, dynamic signal probing, and transaction-level debugging. The tool provides a comprehensive view of signal behavior over time, allowing engineers to trace issues efficiently. For example, the waveform viewer supports hierarchical signal grouping, enabling users to collapse or expand design hierarchies for focused analysis.

The following Verilog snippet illustrates a simple module and its simulation:

Code Sample 1.78: Sample Verilog Module

```
module adder (
    input [7:0] a, b,
    output [8:0] sum
);
    assign sum = a + b;
endmodule
```

ModelSim's debugging capabilities extend to conditional breakpoints, which halt simulation when specific conditions are met. This is particularly useful for identifying corner cases in complex designs. The tool also supports force and release commands, allowing users to override signal values during simulation for testing hypothetical scenarios.

Visualization in ModelSim is enhanced by its ability to display data in multiple formats, including:

Waveform graphs for time-domain analysis. Memory maps for visualizing RAM/ROM contents. State machine diagrams for tracking FSM transitions.

The waveform viewer supports cross-probing, where selecting a signal in the source code highlights its waveform and vice versa. This bidirectional navigation accelerates debugging by reducing context-switching overhead. ModelSim also integrates with third-party tools like MATLAB for co-simulation, enabling mixed-signal analysis.

Modern GPU architectures, such as NVIDIA's CUDA and AMD's ROCm, exploit parallelism to accelerate HDL simulations. ModelSim harnesses this capability through multi-threaded simulation kernels, reducing runtime for large designs. The tool's Tcl scripting interface allows automation of repetitive tasks, further enhancing productivity. For instance, the following Tcl script automates waveform saving:

Code Sample 1.79: Tcl Script for Waveform Saving

```
# Save waveform to file
vsim work.adder
add wave *
run 100 ns
wave zoomfull
save wave "waveform.do"
```

Integration with FPGA and ASIC workflows is seamless in ModelSim. The tool supports industry-standard formats like VHDL-2008 and SystemVerilog, ensuring compatibility with most design flows. For FPGA synthesis, ModelSim interfaces with Xilinx Vivado and Intel Quartus, enabling pre- and post-synthesis simulation. In ASIC flows, it integrates with Synopsys Design Compiler and Cadence Innovus for gate-level verification.

The debugging process is further streamlined by ModelSim's code coverage analysis, which identifies untested portions of the design. Coverage metrics include:

Statement coverage (executed lines of code).

Branch coverage (taken decision paths).

Toggle coverage (signal transitions).

These metrics are visualized in interactive reports, helping engineers achieve verification closure. ModelSim also supports assertion-based verification (ABV), where properties are checked dynamically during simulation. For example, the following SystemVerilog assertion verifies a FIFO's overflow condition:

Code Sample 1.80: SystemVerilog Assertion

```
assert property (@(posedge clk) !(wr_en && full))
    else $error("FIFO overflow");
```

GPU-accelerated simulation in ModelSim exploits the parallel nature of modern GPUs to handle large datasets. The tool's memory management optimizations minimize latency, ensuring efficient waveform storage and retrieval. For designs with millions of signals, ModelSim's incremental compilation reduces recompilation time by only updating modified modules.

The visualization capabilities are augmented by scripting APIs, enabling custom waveform displays. Engineers can plot derived signals, such as power consumption or signal-to-noise ratios, using mathematical expressions. For example, the power dissipation of a CMOS gate can be visualized using:

$$P = \alpha \cdot C \cdot V_{dd}^2 \cdot f$$

where  $\alpha$  is the switching activity,  $C$  is the load capacitance,  $V_{dd}$  is the supply voltage, and  $f$  is the clock frequency. ModelSim's scripting engine can compute and plot such metrics dynamically.

In summary, ModelSim's debugging and visualization capabilities are critical for modern GPU-accelerated HDL simulation. Its integration with FPGA and ASIC workflows, coupled with advanced features like code coverage and ABV, makes it a preferred choice for hardware verification. The tool's ability to leverage GPU parallelism ensures scalability for large designs, while its intuitive interface reduces the learning curve for new users.

The following references provide further insights into GPU-accelerated HDL simulation and debugging techniques:

for GPU architecture optimizations.

for advanced debugging methodologies.

for waveform analysis techniques.

ModelSim's continued evolution under Siemens EDA ensures it remains at the forefront of HDL simulation, addressing the growing complexity of modern hardware designs. Its combination of performance, accuracy, and usability makes it indispensable for engineers working on cutting-edge FPGA and ASIC projects.

The equation 23.1.1 illustrates the power dissipation model. These capabilities underscore the tool's role in enabling efficient hardware verification in the era of parallel computing. ModelSim's scripting and automation features further enhance its utility, allowing engineers to customize workflows and integrate with other EDA tools. The tool's support for mixed-language simulation (VHDL and Verilog) ensures flexibility in heterogeneous design environments.

As GPU architectures continue to evolve, tools like ModelSim will leverage their computational power to deliver faster and more accurate simulations. The integration of machine learning for predictive debugging and automated test generation represents the next frontier in HDL verification.

ModelSim's role in this ecosystem highlights its enduring relevance in the face of rapidly changing hardware design paradigms. In conclusion, the synergy between modern GPU architecture and ModelSim's debugging and visualization capabilities drives innovation in hardware verification. The tool's comprehensive feature set and seamless integration with industry-standard workflows ensure its continued dominance in the HDL simulation landscape.

## 1.6 Aldec Active-HDL and Riviera-PRO

### 1.6.1 Mixed-Language Simulations

Mixed-language simulations have become increasingly important in modern GPU architecture design, particularly when integrating heterogeneous hardware components described in multiple hardware description languages (HDLs). Tools like Aldec Active-HDL and Riviera-PRO provide robust environments for simulating mixed-language designs, enabling seamless interoperability between Verilog, VHDL, and SystemVerilog. These tools are optimized for modern GPU architectures, which often require high-performance simulation capabilities to handle the complexity of parallel processing units and memory hierarchies.

Modern GPU architectures rely on mixed-language simulations to verify designs that incorporate legacy VHDL IP cores alongside newer SystemVerilog components. Active-HDL and Riviera-PRO support this by providing unified compilation and elaboration workflows. For example, a GPU design might include VHDL-based memory controllers and SystemVerilog-based shader cores. The tools resolve cross-language references through standardized interfaces, such as the VHDL Procedure Interface (VHPI) and the Verilog Programming Interface (VPI). These mechanisms ensure correct signal propagation across language boundaries, as demonstrated in .

Debugging and visualization are critical features in mixed-language simulations. Active-HDL and Riviera-PRO offer waveform viewers that synchronize signals across different HDLs, enabling engineers to trace transactions through multi-language hierarchies. The tools also support conditional breakpoints and cross-probing between schematic and HDL code. For instance, a GPU designer can set a breakpoint in a SystemVerilog assertion and inspect the corresponding VHDL signals in the waveform window. This capability is essential for identifying timing violations in GPU pipelines, where clock domain crossings often span multiple HDL modules.

Comprehensive testing tools are another key aspect of mixed-language simulation environments. Active-HDL and Riviera-PRO include built-in testbench generators and coverage analyzers that work across Verilog and VHDL. Metric-driven verification (MDV) techniques, such as those described in , are supported through unified coverage databases. A typical GPU verification flow might involve:

**Generating constrained-random test vectors in SystemVerilog.**

**Applying them to a mixed-language design via a Universal Verification Methodology (UVM) framework.**

**Merging code and functional coverage results from VHDL and SystemVerilog components.**

The performance of mixed-language simulations is particularly relevant for GPU architectures, where large register files and parallel execution units create substantial simulation overhead. Active-HDL and Riviera-PRO employ incremental compilation and parallel elaboration to mitigate this. For example, a GPU’s texture mapping unit described in VHDL can be recompiled independently of its SystemVerilog-based rasterizer, reducing turnaround time during iterative debugging. Studies in show that such optimizations can improve simulation throughput by up to 40% for complex GPU designs.

Waveform debugging in mixed-language environments benefits from advanced visualization techniques. Riviera-PRO’s transaction-level debugging, for instance, allows engineers to group related signals across HDLs into higher-level abstractions. A GPU memory transaction might involve:

**A VHDL-based address decoder.**

**A SystemVerilog-based cache controller.**

**A Verilog bus interface unit.**

The tool correlates these components in a single waveform view, annotated with timing diagrams and protocol checkers. This is particularly useful for validating memory coherence protocols in multi-core GPU designs.

Mixed-language simulations also facilitate the reuse of legacy IP in modern GPU designs. Active-HDL’s VHDL-2008 and SystemVerilog interoperability features enable seamless integration of older cryptographic accelerators (written in VHDL) with newer ray-tracing cores (written in SystemVerilog). The tools automatically handle type conversions and resolution functions, such as translating VHDL’s `std_logic_vector` to SystemVerilog’s `logic` data type. This interoperability is formalized in the IEEE 1076-2019 standard .

For complex GPU architectures, mixed-language simulations must handle hierarchical parameterization and configuration. Riviera-PRO supports cross-language parameter passing, allowing a SystemVerilog top module to instantiate a VHDL submodule with generics mapped to parameters. Consider the following example:

Code Sample 1.81: Mixed-Language Parameterization

```
// SystemVerilog top module
module gpu_top #(parameter CACHE_SIZE = 1024);
    vhdl_cache #(.SIZE(CACHE_SIZE)) L1_cache();
endmodule
```

Code Sample 1.82: VHDL Submodule

```
-- VHDL cache component
entity vhdl_cache is
    generic (SIZE : integer);
    port (clk : in std_logic);
end entity;
```

This feature simplifies the integration of parameterized IP blocks across language boundaries.

Verification of mixed-language GPU designs is further enhanced by formal property checking. Active-HDL and Riviera-PRO support SVA (SystemVerilog Assertions) and PSL (Property Specification Language) in VHDL, enabling unified assertion-based verification. A GPU designer can write temporal assertions in SystemVerilog and

bind them to VHDL modules, ensuring consistent checking across the entire design. Research demonstrates that this approach reduces verification effort by 30% for GPU memory controllers.

The tools also provide specialized libraries for GPU-specific constructs, such as warp schedulers and SIMD execution units. These libraries include pre-verified mixed-language models that can be instantiated in custom designs. For example, a VHDL-based warp scheduler can interface with a SystemVerilog scoreboard using transaction-level modeling (TLM) ports. The libraries are optimized for simulation performance, leveraging just-in-time (JIT) compilation techniques described in .

In summary, mixed-language simulations in Active-HDL and Riviera-PRO address the challenges of modern GPU architecture design by providing:

- Cross-language debugging and visualization.**
- Unified testbench and coverage tools.**
- Performance optimizations for large-scale parallel designs.**
- Legacy IP integration through interoperability standards.**

These capabilities are essential for verifying the next generation of heterogeneous GPU architectures, where multi-language descriptions are the norm rather than the exception.

### 1.6.2 Designed for multi-language HDL simulation environments

Modern GPU architectures have evolved to support increasingly complex designs, often requiring multi-language Hardware Description Language (HDL) simulation environments for verification. Tools like Aldec Active-HDL and Riviera-PRO are designed to address these challenges, offering mixed-language simulation capabilities, advanced debugging, and visualization features. These tools are critical for verifying GPU designs that integrate Verilog, VHDL, and SystemVerilog components, ensuring compatibility and correctness across diverse design methodologies.

Mixed-language simulations are essential for modern GPU development, as they allow designers to leverage the strengths of multiple HDLs within a single project. For example, a GPU design might use Verilog for low-level RTL descriptions and VHDL for high-level behavioral modeling. Active-HDL and Riviera-PRO support seamless integration of these languages, enabling simulations that accurately reflect the final hardware implementation. The following Verilog and VHDL code snippets demonstrate a mixed-language simulation scenario:

Code Sample 1.83: Verilog Module for GPU Pipeline

```
module gpu_pipeline (
    input clk,
    input [31:0] data_in,
    output [31:0] data_out
);
    reg [31:0] pipeline_reg;
    always @ (posedge clk) begin
        pipeline_reg <= data_in;
    end
    assign data_out = pipeline_reg;
endmodule
```

Code Sample 1.84: VHDL Entity for GPU Controller

```
entity gpu_controller is
    port (
        clk : in std_logic;
        enable : in std_logic;
        data_out : out std_logic_vector(31 downto 0)
    );
end entity;
```

These tools also provide comprehensive debugging and visualization features, which are critical for identifying and resolving issues in complex GPU designs. Key debugging capabilities include:

- Waveform analysis with zoom, pan, and measurement tools.**
- Breakpoints and conditional triggers for precise control over simulation execution.**

**Cross-probing between HDL source code and waveform signals.**  
**Memory inspection and modification during simulation.**

Waveform visualization is particularly important for GPU designs, where timing and parallelism are critical. Active-HDL and Riviera-PRO offer advanced waveform viewers that support hierarchical signal grouping, color-coding, and customizable displays. For example, a GPU shader's pipeline stages can be visualized as separate waveform groups, allowing designers to analyze data flow and latency:

$$\text{Latency} = t_{\text{stage}_n} - t_{\text{stage}_1}$$

Comprehensive testing tools are another hallmark of these environments. GPU designs often require extensive verification to ensure correctness across millions of clock cycles. Active-HDL and Riviera-PRO include built-in testbench generation, coverage analysis, and assertion-based verification. Coverage metrics such as line, branch, and toggle coverage are essential for quantifying verification progress:

$$\text{Coverage} = \frac{\text{Executed Lines}}{\text{Total Lines}} \times 100\%$$

Assertions are particularly useful for GPU designs, where complex protocols and timing constraints must be validated. SystemVerilog assertions (SVAs) can be used to verify properties like memory coherency or pipeline stalls:

Code Sample 1.85: SystemVerilog Assertion for Memory Coherency

```
property mem_coherency;
  @ (posedge clk) read_enable |> ##[1:3] data_valid;
endproperty

assert_mem_coherency: assert property (mem_coherency);
```

The performance of mixed-language simulations is another critical consideration. GPU designs often involve large-scale simulations with millions of gates, requiring optimized compilation and execution. Active-HDL and Riviera-PRO employ incremental compilation and parallel simulation techniques to reduce runtime. For instance, incremental compilation only recompiles modified design units, significantly speeding up iterative development:

$$t_{\text{sim}} = t_{\text{compile}} + t_{\text{execute}}$$

Parallel simulation further enhances performance by leveraging multi-core processors, a necessity for modern GPU verification. These tools also support distributed simulation, enabling large designs to be partitioned across multiple machines.

Debugging GPU designs often involves analyzing complex data structures, such as texture caches or framebuffers. Active-HDL and Riviera-PRO provide memory visualization tools that display data in hexadecimal, binary, or custom formats. For example, a GPU's framebuffer can be inspected as a 2D array of pixel values:

Code Sample 1.86: Framebuffer Memory Dump

```
0x0000: 0xRRGGBBAA 0xRRGGBBAA ...
0x0010: 0xRRGGBBAA 0xRRGGBBAA ...
```

Scripting and automation are also integral to these tools. Tcl and Python APIs enable designers to automate repetitive tasks, such as regression testing or coverage analysis. For example, a Tcl script can automate the generation of test vectors for a GPU's arithmetic logic unit (ALU):

Code Sample 1.87: Tcl Script for ALU Test Generation

```
for {set i 0} {$i < 256} {incr i} {
  for {set j 0} {$j < 256} {incr j} {
    add_force a $i
    add_force b $j
    run 10 ns
  }
}
```

In summary, Aldec Active-HDL and Riviera-PRO are designed to meet the demands of modern GPU architecture verification. Their support for mixed-language simulations, advanced debugging, and comprehensive testing tools makes them indispensable for complex GPU designs. By integrating these features, designers can ensure the correctness and performance of their GPU implementations, from RTL to final silicon.

### 1.6.3 Key Features

Modern GPU architectures have evolved to meet the demands of high-performance computing, parallel processing, and complex simulations. Their key features include massive parallelism, specialized compute units, and advanced memory hierarchies. When integrated with tools like Aldec Active-HDL and Riviera-PRO, these architectures enable efficient mixed-language simulations, debugging, and visualization for hardware description language (HDL) environments. Below, we explore these aspects in detail.

The parallelism in modern GPUs is achieved through thousands of cores organized into streaming multiprocessors (SMs). Each SM executes multiple threads concurrently, leveraging single-instruction multiple-thread (SIMT) execution. This architecture is ideal for tasks such as rendering, machine learning, and HDL simulations, where parallelism can be exploited. For example, a GPU can accelerate simulation tasks by distributing workloads across its cores, reducing the time required for complex design verification. The following equation models the theoretical speedup achievable through parallelism:

$$S = \frac{T_{\text{serial}}}{T_{\text{parallel}}}$$

where  $S$  is the speedup,  $T_{\text{serial}}$  is the serial execution time, and  $T_{\text{parallel}}$  is the parallel execution time.

Aldec Active-HDL and Riviera-PRO are designed to leverage GPU capabilities for mixed-language simulations. These tools support Verilog, VHDL, and SystemVerilog, enabling designers to work in heterogeneous HDL environments. A mixed-language simulation example is shown below:

Code Sample 1.88: Mixed-Language Simulation Example

```
// Verilog module
module adder (input [7:0] a, b, output [7:0] sum);
    assign sum = a + b;
endmodule

-- VHDL entity
entity tb_adder is end tb_adder;
architecture behavior of tb_adder is
    signal a, b, sum: std_logic_vector(7 downto 0);
begin
    uut: entity work.adder port map (a, b, sum);
end behavior;
```

Debugging and visualization are critical for verifying complex designs. Active-HDL and Riviera-PRO provide advanced waveform viewers, transaction-level debugging, and dynamic probe insertion. These features allow designers to trace signal behavior, identify timing violations, and optimize performance. The tools also support cross-probing between HDL code and waveforms, enabling efficient root-cause analysis. For instance, a designer can highlight a signal in the waveform viewer and locate its corresponding declaration in the source code.

**Code coverage analysis to ensure all design paths are exercised.**

**Assertion-based verification for checking design properties.**

**Constrained random testing to uncover corner-case bugs.**

**Functional coverage metrics to track verification progress.**

These tools integrate with GPU architectures to accelerate test execution. For example, a constrained random test can be parallelized across GPU cores, reducing simulation time while maintaining verification quality. The following equation estimates the coverage achieved by random testing:

$$C = 1 - e^{-k \cdot N}$$

where  $C$  is the coverage,  $k$  is the probability of hitting a specific condition, and  $N$  is the number of test cases.

Memory hierarchies in modern GPUs play a vital role in HDL simulations. GPUs employ multiple memory types, including global, shared, and register memory, each optimized for specific access patterns. Active-HDL and Riviera-PRO utilize these hierarchies to manage large simulation datasets efficiently. For instance, waveform data can be stored in global memory for high-capacity storage, while frequently accessed signals reside in shared memory for low-latency access.

The tools also support hierarchical design debugging, enabling designers to navigate complex design structures. A hierarchical design can be represented as a tree, where each node corresponds to a module or entity. The following code snippet illustrates a hierarchical design in Verilog:

Code Sample 1.89: Hierarchical Design Example

```
module top;
  sub_module sub_inst (
    .clk(clk),
    .reset(reset)
  );
endmodule

module sub_module (input clk, reset);
  // Sub-module logic
endmodule
```

Waveform compression is another key feature for GPU-accelerated simulations. Active-HDL and Riviera-PRO employ lossless compression algorithms to reduce memory usage while preserving signal fidelity. This is particularly useful for large-scale designs where waveform storage can become prohibitive. The compression ratio  $R$  is given by:

$$R = \frac{S_{\text{original}}}{S_{\text{compressed}}}$$

where  $S_{\text{original}}$  and  $S_{\text{compressed}}$  are the sizes of the original and compressed waveforms, respectively.

Multi-language support extends to scripting interfaces, where designers can automate tasks using Tcl, Python, or other scripting languages. This flexibility enhances productivity and enables custom workflows. For example, a Python script can automate testbench generation, leveraging GPU parallelism for faster execution. The following Tcl script demonstrates automation in Active-HDL:

Code Sample 1.90: Tcl Script for Automation

```
# Load design
vcom -work work design.vhd
vlog -work work testbench.v
# Simulate
vsim work.testbench
run -all
```

**Massive parallelism for accelerated simulation.**

**Advanced memory hierarchies for efficient data management.**

**Comprehensive debugging tools for signal tracing and analysis.**

**Multi-language support for heterogeneous design environments.**

**Automated testing and coverage analysis for verification completeness.**

In summary, modern GPU architectures, combined with Aldec Active-HDL and Riviera-PRO, provide a robust platform for mixed-language simulations, debugging, and visualization. These capabilities enable designers to tackle increasingly complex HDL projects while maintaining high productivity and verification quality. The integration of GPU acceleration with industry-standard tools ensures that modern design challenges can be met with scalable and efficient solutions.

#### 1.6.4 Focus on debugging and visualization

Modern GPU architectures have become increasingly complex, necessitating advanced debugging and visualization tools to ensure correct functionality and performance. Tools like Aldec Active-HDL and Riviera-PRO provide comprehensive solutions for mixed-language simulations, enabling engineers to verify designs that combine VHDL, Verilog, and SystemVerilog. These tools are particularly valuable in GPU design, where parallelism and pipelining introduce unique challenges for debugging and validation.

A critical aspect of modern GPU debugging is the ability to trace and visualize signals across multiple clock domains. Active-HDL and Riviera-PRO offer waveform viewers that support high-resolution timing analysis,

allowing engineers to identify synchronization issues and metastability. For example, the following Verilog code snippet demonstrates a common GPU pipeline stage:

Code Sample 1.91: GPU Pipeline Stage

```
module pipeline_stage (
    input clk,
    input [31:0] data_in,
    output reg [31:0] data_out
);
    always @ (posedge clk) begin
        data_out <= data_in; // Register stage
    end
endmodule
```

Debugging such pipelines requires precise waveform inspection to verify data integrity. The tools provide features like cross-probing between HDL code and waveforms, enabling engineers to correlate simulation results with design intent. Additionally, they support advanced visualization techniques such as heatmaps for power analysis, which is crucial for GPU designs where power efficiency is a key metric.

Mixed-language simulation is another essential feature for GPU verification. Modern GPUs often integrate IP blocks written in different HDLs, requiring seamless interoperability. Active-HDL and Riviera-PRO support IEEE-standardized mixed-language simulation, ensuring accurate behavior when combining VHDL and Verilog modules. For instance, a GPU shader core might use VHDL for floating-point arithmetic units while employing SystemVerilog for control logic. The tools handle language boundary crossings transparently, preserving signal values and timing relationships.

**Code coverage analysis to identify untested design regions.**

**Assertion-based verification for formal property checking.**

**Transaction-level debugging for high-level abstractions.**

These features are particularly useful for GPU architectures, where parallel execution units must be rigorously validated. For example, code coverage metrics can reveal whether all warp schedulers in a GPU have been exercised during simulation. Assertions can formalize requirements like memory coherence in shared L2 caches:

Code Sample 1.92: Cache Coherence Assertion

```
assert property (
    @ (posedge clk)
    (read_hit && write_hit) |-> (read_data == latest_write_data)
);
```

Waveform debugging in GPU designs often involves analyzing large datasets. Active-HDL and Riviera-PRO optimize waveform storage and retrieval through techniques like:

**Incremental saving of signal value changes.**

**Compression algorithms for efficient storage.**

**Smart loading of partial waveform data.**

These optimizations are critical when debugging GPU kernels that process thousands of threads. The tools also support scripting for automated testbench generation, enabling regression testing across multiple GPU configurations. Python and Tcl interfaces allow integration with machine learning frameworks for predictive debugging, where historical bug patterns inform current investigations.

Visualization extends beyond waveforms in GPU debugging. Active-HDL and Riviera-PRO provide schematic viewers that render hierarchical designs, helping engineers navigate complex GPU architectures. For example, a streaming multiprocessor's data path can be visualized as a block diagram, with color-coded signals indicating activity levels. This is particularly useful for identifying bottlenecks in GPU compute pipelines.

**Clock cycle utilization across pipeline stages.**

**Memory bandwidth consumption.**

**Instruction throughput per SIMD lane.**

These metrics are displayed in interactive dashboards, allowing engineers to correlate performance issues with RTL implementation details. For instance, a drop in warp occupancy can be traced back to a specific arbitration module in the scheduler.

Debugging modern GPU architectures also requires support for advanced verification methodologies. Active-HDL and Riviera-PRO integrate with UVM (Universal Verification Methodology), enabling constrained-random testing of GPU designs. This is particularly valuable for verifying texture units and rasterization pipelines, where input patterns must cover a wide range of corner cases. The following SystemVerilog code illustrates a UVM sequence for GPU texture filtering:

Code Sample 1.93: UVM Texture Test Sequence

```
class texture_test_seq extends uvm_sequence;
    rand texel_coord_t coords;

    constraint valid_coords {
        coords.u inside {[0:1.0]};
        coords.v inside {[0:1.0]};
    }

    task body();
        send_texture_request(coords);
    endtask
endclass
```

The tools' debug environments provide specialized views for UVM components, showing transaction flows between scoreboards and monitors. This helps verify that GPU workloads are processed correctly across the entire graphics pipeline.

- Mixed-language simulation for heterogeneous IP integration.**
- Advanced waveform analysis for parallel execution verification.**
- Comprehensive coverage metrics for ensuring thorough testing.**
- UVM support for systematic verification methodologies.**

In conclusion, Active-HDL and Riviera-PRO address the unique debugging challenges of modern GPU architectures through these capabilities. They are essential for developing GPUs that meet stringent performance and correctness requirements across graphics, compute, and machine learning workloads. The tools' visualization features transform complex simulation data into actionable insights, accelerating debug cycles in large-scale GPU projects.

### 1.6.5 Comprehensive testing tools for complex designs

Modern GPU architectures present significant challenges in verification due to their complexity, parallel execution models, and mixed-language design requirements. Comprehensive testing tools must address these challenges while enabling efficient debugging and visualization. Aldec's Active-HDL and Riviera-PRO provide robust solutions for mixed-language simulations, supporting Verilog, VHDL, and SystemVerilog in a unified environment. These tools are particularly suited for GPU designs, where multi-language HDL simulation is often necessary to verify heterogeneous components such as shader cores, memory controllers, and interconnect fabrics.

Mixed-language simulation capabilities in Active-HDL and Riviera-PRO enable seamless integration of different HDLs within a single testbench. For example, a GPU's memory controller might be written in VHDL for its precise timing control, while the shader cores use SystemVerilog for its advanced verification constructs. The tools resolve language interoperability issues through standardized interfaces such as VHPI (VHDL Procedural Interface) and DPI (Direct Programming Interface). This allows engineers to leverage the strengths of each language without compromising simulation performance. The following code illustrates a mixed-language testbench:

Code Sample 1.94: Mixed-Language GPU Testbench

```
// SystemVerilog portion for shader core
module shader_core_tb;
    import "DPI-C" function void vhdl_mem_write(input int addr, input int data);
    initial begin
        vhdl_mem_write(32'h8000_0000, 32'h1234_5678);
```

```
end
endmodule
```

#### Code Sample 1.95: VHDL Memory Controller

```
-- VHDL portion for memory controller
entity mem_controller is
    port (clk : in std_logic);
end entity;

architecture behavioral of mem_controller is
    procedure dpi_mem_write(addr : in integer; data : in integer) is
    begin
        -- Memory write implementation
    end procedure;

    attribute foreign of dpi_mem_write : procedure is "VHPIDIRECT shader_core_tb.vhdl_mem_write";

begin
    process
    begin
        wait on clk;
    end process;
end architecture;
```

**Waveform comparison tools for regression testing, critical for identifying subtle timing violations in GPU pipelines.**

**Transaction recording for bus functional models, enabling protocol verification of high-speed interfaces like GDDR6/HBM.**

**Dynamic probe insertion without recompilation, allowing real-time inspection of signals during simulation.**

The tools employ hierarchical debugging techniques essential for GPU architectures. Engineers can navigate through multiple levels of abstraction, from register-transfer level (RTL) to system-level models. This is particularly valuable when verifying GPU designs that incorporate:

- Multiple clock domains for core, memory, and I/O subsystems.**
- Power management units with complex state machines.**
- Error correction circuits requiring bit-level analysis.**
- Fine-grained process control for thousands of concurrent threads.**
- Memory modeling with configurable latency and bandwidth.**
- Race condition detection through precise event ordering.**

The simulation performance is optimized through techniques such as:

$$T_{sim} = N_{events} \times t_{avg} \times \frac{1}{P_{parallel}}$$

where  $T_{sim}$  is total simulation time,  $N_{events}$  is the number of simulation events,  $t_{avg}$  is average event processing time, and  $P_{parallel}$  is the parallelization factor.

- Line coverage for basic execution verification.**
- Toggle coverage for signal integrity analysis.**
- FSM coverage for control logic validation.**
- Assertion coverage for formal property checking.**

The tools generate coverage reports that help identify untested scenarios in GPU designs, such as:

- Corner cases in floating-point units.**
- Rare pipeline stalls.**

### **Memory access patterns at cache boundaries.**

Assertion-based verification is particularly effective for GPU designs. SystemVerilog assertions can verify complex behaviors like:

Code Sample 1.96: GPU Texture Unit Assertion

```
property texture_filter_valid;
  @(posedge clk) disable iff (!reset_n)
    texel_request |-> ##[1:8] texel_response;
endproperty

assert_texture: assert property (texture_filter_valid);
```

Active-HDL and Riviera-PRO support constrained random testing through integration with UVM (Universal Verification Methodology). This is valuable for GPU verification where:

$$P_{bug} = 1 - (1 - P_{error})^{N_{cases}}$$

shows that the probability of bug detection  $P_{bug}$  increases exponentially with the number of test cases  $N_{cases}$ .

**Power estimation through activity factor monitoring.**

**Bandwidth utilization tracking for memory subsystems.**

**Bottleneck identification in compute pipelines.**

The tools integrate with industry-standard formats like:

**VCD (Value Change Dump) for waveform export.**

**SAIF (Switching Activity Interchange Format) for power analysis.**

**IP-XACT for IP reuse in complex GPU designs.**

**Warp-level visualization for SIMD execution.**

**Memory coalescing analysis.**

**Divergence tracking in parallel threads.**

Code Sample 1.97: GPU Register File Visualization

```
// Specialized debug view for register files
module gpu_Regfile #(parameter WIDTH=32, DEPTH=128) (
  input [log2(DEPTH)-1:0] addr,
  output [WIDTH-1:0] data
);
// Implementation
endmodule
```

**Heat maps for memory access patterns.**

**Temporal graphs for pipeline utilization.**

**Statistical analysis of thread divergence.**

**TLM (Transaction Level Modeling) for early architectural exploration.**

**ISS (Instruction Set Simulator) integration for shader program verification.**

**Hardware acceleration interfaces for faster simulation.**

**Automated test generation from coverage data.**

**Interactive debug scripting.**

**Batch regression testing.**

**Mixed-language support for heterogeneous designs.**

**Advanced debugging and visualization.**

**Scalable simulation performance.**

**Rigorous coverage metrics.**

The comprehensive testing tools in Active-HDL and Riviera-PRO address the unique challenges of modern GPU verification through these capabilities. They are indispensable for verifying complex GPU architectures

where traditional verification methods would be inadequate. The tools' ability to handle massive parallelism, mixed abstraction levels, and heterogeneous languages positions them as critical components in the GPU design verification flow.



## Chapter 2

# Development Environment Setup

### 2.1 Setting Up HDL Tools

#### 2.1.1 Installing Verilog simulators (ModelSim, Vivado, etc)

The installation and configuration of Verilog simulators such as ModelSim and Vivado are critical steps in the development and verification of modern GPU architectures. These tools enable hardware description language (HDL) simulation, synthesis, and FPGA implementation, which are essential for designing and optimizing GPU components. The process involves setting up toolchains, configuring synthesis tools, and ensuring compatibility with the target hardware platform.

Modern GPU architectures rely on HDLs like Verilog and VHDL to describe their functionality at the register-transfer level (RTL). Verilog simulators such as ModelSim and Vivado provide environments for simulating and debugging these designs before synthesis. The installation process typically involves downloading the software from the vendor's website, running the installer, and configuring the license. For example, ModelSim requires a valid license file, which can be obtained from Mentor Graphics (now part of Siemens). Vivado, developed by Xilinx (now part of AMD), includes its own simulator and synthesis tools, making it a comprehensive solution for FPGA-based GPU development.

The installation of these tools on a Linux or Windows system follows a similar workflow. For Vivado, the installer provides options to include device support for specific FPGA families, such as the Xilinx UltraScale+ series, which is commonly used in high-performance computing applications. The following command demonstrates how to launch the Vivado installer in Linux:

Code Sample 2.1: Launching Vivado Installer

```
./xsetup -b AuthTokenGen
```

ModelSim installation involves extracting the package and running the setup script. The installer may require root privileges to install system libraries. After installation, the environment variables must be updated to include the paths to the simulator binaries. For example, adding the following lines to the `.bashrc` file ensures the tools are accessible from the command line:

Code Sample 2.2: Setting Environment Variables

```
export PATH=$PATH:/opt/modelsim/bin  
export LM_LICENSE_FILE=/path/to/license.dat
```

Configuring synthesis tools is another critical step in the HDL toolchain. Synthesis tools like Synopsys Design Compiler or Xilinx Vivado convert RTL descriptions into gate-level netlists, which are then mapped to FPGA or ASIC technologies. Vivado includes an integrated synthesis engine, but third-party tools may offer additional optimizations for GPU architectures. The synthesis process is governed by constraints, which define timing, area, and power targets. These constraints are typically written in Synopsys Design Constraints (SDC) format. Below is an example of an SDC constraint for clock frequency:

Code Sample 2.3: Clock Constraint in SDC

```
create_clock -name clk -period 10 [get_ports clk]
```

FPGA toolchains involve additional steps, such as generating bitstreams for programming the device. Vivado automates this process through its implementation flow, which includes synthesis, placement, routing, and bitstream generation. The following command demonstrates how to generate a bitstream for a Xilinx FPGA:

Code Sample 2.4: Generating Bitstream in Vivado

```
write_bitstream -force design.bit
```

For GPU architectures, optimizing the HDL code for synthesis is crucial. Techniques such as pipelining, loop unrolling, and resource sharing can significantly impact performance and area utilization. The following Verilog snippet illustrates a pipelined multiplier, a common optimization in GPU designs:

Code Sample 2.5: Pipelined Multiplier in Verilog

```
module pipelined_multiplier (
    input clk,
    input [15:0] a, b,
    output reg [31:0] result
);
    reg [15:0] a_reg, b_reg;
    reg [31:0] product;
    always @(posedge clk) begin
        a_reg <= a;
        b_reg <= b;
        product <= a_reg * b_reg;
        result <= product;
    end
endmodule
```

Debugging and verification are integral to the HDL workflow. ModelSim and Vivado provide waveform viewers for analyzing signal behavior during simulation. Assertions and testbenches are used to validate the design against functional requirements. The following Verilog testbench demonstrates a simple verification environment for the pipelined multiplier:

Code Sample 2.6: Testbench for Pipelined Multiplier

```
module testbench;
    reg clk;
    reg [15:0] a, b;
    wire [31:0] result;

    pipelined_multiplier uut (clk, a, b, result);

    initial begin
        clk = 0;
        forever #5 clk = ~clk;
    end

    initial begin
        a = 16'h0002;
        b = 16'h0003;
        #20;
        if (result !== 32'h0006)
            $display("Test failed");
        $finish;
    end
endmodule
```

The integration of these tools into a cohesive workflow is essential for modern GPU development. Scripting languages like Tcl are often used to automate tasks in Vivado. The following Tcl script demonstrates how to create a project, add source files, and run synthesis:

Code Sample 2.7: Tcl Script for Vivado Project

```
create_project -force gpu_design ./project
add_files -norecurse {design.v constraints.xdc}
```

```
launch_runs synth_1 -jobs 4
wait_on_run synth_1
```

Performance analysis tools within Vivado and ModelSim provide insights into critical paths and resource utilization. Reports generated during synthesis and implementation highlight areas for optimization. For example, the following equation calculates the maximum achievable clock frequency based on the critical path delay  $t_{cp}$ :

$$f_{max} = \frac{1}{t_{cp}}$$

In conclusion, the installation and configuration of Verilog simulators and synthesis tools are foundational to GPU architecture development. Proper setup ensures efficient design iteration, verification, and implementation. The tools discussed—ModelSim, Vivado, and associated scripting and constraint methodologies—enable designers to meet the stringent performance and power requirements of modern GPUs. The examples provided illustrate common workflows and optimizations, demonstrating the practical application of these tools in real-world scenarios.

### 2.1.2 Configuring synthesis tools and FPGA toolchains

Configuring synthesis tools and FPGA toolchains for modern GPU architectures requires a systematic approach to ensure optimal performance and correctness. The process involves setting up hardware description language (HDL) tools, installing Verilog simulators, and configuring synthesis pipelines. This discussion focuses on practical steps and considerations, particularly for tools like ModelSim, Vivado, and other FPGA toolchains.

Modern GPU architectures, such as those from NVIDIA and AMD, often employ custom HDL implementations for critical components. To simulate and synthesize these designs, engineers must first install and configure the necessary tools. The following steps outline the process:

#### Installing Verilog Simulators:

ModelSim: A widely used simulator for Verilog and VHDL. Installation involves downloading the executable from the vendor's website and following platform-specific instructions. For Linux, the following commands are typical:

#### Code Sample 2.8: ModelSim Installation

```
chmod +x ModelSimSetup.run
./ModelSimSetup.run
```

Vivado: Xilinx's Vivado suite includes a built-in simulator. Installation requires downloading the unified installer and selecting the Vivado HLX package. The installer handles dependencies, but users must ensure their system meets the minimum requirements.

#### Configuring Synthesis Tools:

Synthesis tools like Synopsys Design Compiler or Xilinx Vivado convert HDL code into gate-level netlists. Configuration involves setting up tool paths and libraries. For Vivado, the Tcl script below initializes the synthesis environment:

#### Code Sample 2.9: Vivado Synthesis Setup

```
set_property PART xc7k325tffg900-2 [current_project]
set_property TARGET_LANGUAGE Verilog [current_project]
```

Library paths must be specified for technology-specific primitives. For example, GPU designs may require proprietary IP cores, which are linked using:

#### Code Sample 2.10: IP Core Linking

```
set_property IP_REPO_PATHS ./ip_library [current_fileset]
```

#### FPGA Toolchain Configuration:

Place-and-route tools, such as those in Vivado or Intel Quartus, require device-specific constraints. A constraints file (.xdc) for timing and pin assignments is essential. Below is an example for a clock constraint:

#### Code Sample 2.11: Clock Constraint

```
create_clock -period 10 [get_ports clk]
```

For GPU architectures, high-speed interfaces like PCIe or HBM necessitate careful constraint tuning. The following Tcl command sets a false path for asynchronous signals:

### Code Sample 2.12: False Path Constraint

```
set_false_path -from [get_clocks clkA] -to [get_clocks clkB]
```

The synthesis process for GPU architectures involves several mathematical optimizations. For instance, retiming is used to balance pipeline stages, as shown in equation 18.3.2:

$$\Delta t = \max(t_{\text{comb}}) - \min(t_{\text{comb}})$$

where  $\Delta t$  represents the timing imbalance between combinational paths. Tools like Vivado automatically apply retiming when the `OPT_DESIGN` directive is enabled.

Verification of synthesized designs is critical. Formal methods, such as equivalence checking, ensure the netlist matches the RTL. The following equation 15.1.2 describes the property checking process:

$$\forall s \in S, \quad RTL(s) \equiv Netlist(s)$$

where  $S$  is the state space, and  $RTL$  and  $Netlist$  are the respective representations. Tools like Cadence Conformal or Synopsys Formality automate this process.

For FPGA toolchains, scripting is essential for reproducibility. A Makefile or Tcl script automates synthesis and implementation. Below is a Tcl example for Vivado:

### Code Sample 2.13: Automated Synthesis Flow

```
synth_design -top top_module -part xc7k325tffg900-2
opt_design
place_design
route_design
write_bitstream -force top.bit
```

GPU architectures often employ parallel processing elements, which require careful synthesis tuning. For example, loop unrolling in HDL code increases parallelism but also resource usage. The unroll factor  $N$  in equation 2.1.2 determines the trade-off:

$$N = \left\lfloor \frac{L_{\text{max}}}{L_{\text{res}}} \right\rfloor$$

where  $L_{\text{max}}$  is the maximum allowable latency and  $L_{\text{res}}$  is the resource-limited latency. Synthesis tools like Vivado support pragmas to control unrolling:

### Code Sample 2.14: Loop Unrolling Pragma

```
(* parallel_case, full_unroll *)
for (i = 0; i < N; i = i + 1) begin
    // loop body
end
```

## 2.2 Environment Considerations

### 2.2.1 System requirements and hardware compatibility

Modern GPU architectures impose stringent system requirements and hardware compatibility constraints due to their parallel processing capabilities and energy-intensive workloads. The environmental considerations for deploying such systems include power consumption, thermal management, and cooling efficiency. For instance, NVIDIA's Ampere architecture requires a minimum power supply of 650W for consumer-grade GPUs like the RTX 3080, while data-center variants such as the A100 demand up to 400W per card. Power efficiency is quantified by the performance-per-watt metric, given by:

$$\eta = \frac{FLOPS}{P}$$

where  $\eta$  is the efficiency,  $FLOPS$  is the floating-point operations per second, and  $P$  is the power consumption in watts.

Thermal design power (TDP) must also be considered, as exceeding recommended thresholds can lead to thermal throttling or hardware failure. For example, AMD's RDNA 3 architecture specifies a TDP range of 230–355W for the RX 7900 XTX .

Hardware compatibility extends beyond power and thermal constraints. PCIe lane configuration is critical; modern GPUs require PCIe 4.0 or 5.0 x16 slots for optimal bandwidth. Inadequate lanes can bottleneck performance, as shown by the bandwidth equation:

$$B = N \times R \times \frac{W}{8}$$

where  $B$  is bandwidth in GB/s,  $N$  is the number of lanes,  $R$  is the transfer rate per lane, and  $W$  is the interface width in bits. For PCIe 4.0 x16,  $B = 16 \times 16 \text{ GT/s} \times 2 \text{ bytes/transfer} = 32 \text{ GB/s}$ .

Memory compatibility is another factor; GDDR6X in NVIDIA's RTX 40-series requires a 384-bit bus, while AMD's RX 7000-series uses a 256-bit bus with GDDR6 .

**Environmental considerations include acoustic noise from cooling systems and electromagnetic interference (EMI) shielding.** High-performance GPUs often employ axial or centrifugal fans with noise levels exceeding 40 dB under load . EMI compliance is governed by FCC Part 15 and CISPR 22 standards, necessitating proper chassis grounding and filtering.

**For HDL projects targeting FPGAs or ASICs, version control setup is essential for collaborative development.** Git is the de facto standard, with repositories structured to separate RTL code, testbenches, and synthesis scripts. A typical directory layout includes:

Code Sample 2.15: HDL project structure

```
/project
  /rtl
    /core
      adder.v
      multiplier.v
    /top
      design_top.v
  /tb
    testbench.sv
/syn
  constraints.xdc
  script.tcl
```

Branching strategies like GitFlow or trunk-based development are adopted, with tags for major releases.

**Continuous integration (CI) pipelines verify commits using linting tools (e.g., Verilator) and regression testing.** A sample CI configuration for GitHub Actions:

Code Sample 2.16: GitHub Actions workflow for HDL

```
name: HDL CI
on: [push, pull_request]
jobs:
  verify:
    runs-on: ubuntu-latest
    steps:
      - uses: actions/checkout@v3
      - name: Run Verilator
        run: |
          sudo apt-get install verilator
          verilator --lint-only rtl/core/adder.v
```

**Hardware-in-the-loop (HIL) testing requires compatibility with emulation platforms like Cadence Palladium or Synopsys Zebu.** These systems demand specific host configurations, such as 64GB RAM and 24-core CPUs for medium-scale designs .

**Co-simulation with MATLAB or Python tools introduces additional dependencies, managed via package managers like Conda or Pip.**

**Synthesis toolchains (e.g., Xilinx Vivado, Intel Quartus) have their own system requirements.** Vivado 2023.1 mandates:

- 64-bit RHEL/CentOS 7.4+ or Ubuntu 20.04 LTS**
- 16GB RAM (32GB recommended)**
- 100GB disk space for full installation**

Version-controlled constraints files ensure reproducibility across environments. For example, a `constraints.xdc` file might include:

Code Sample 2.17: XDC timing constraints

```
create_clock -period 10 [get_ports clk]
set_input_delay 2 -clock clk [all_inputs]
```

**Power estimation tools like PrimeTime PX or Xilinx Power Analyzer require switching activity interchange format (SAIF) files, generated from simulation:**

$$P_{dynamic} = \frac{1}{2}CV^2f\alpha$$

where  $C$  is capacitance,  $V$  is voltage,  $f$  is frequency, and  $\alpha$  is activity factor. Static power  $P_{static}$  is modeled as:

$$P_{static} = I_{leak}V$$

**Compatibility with EDA tools extends to licensing servers (FlexLM or DSLS) and network configurations.** Firewall rules must permit TCP ports 27000–27009 for FlexLM, while DSLS uses HTTPS on port 443

**For multi-user projects, access control is enforced via Git hooks or repository managers like GitLab.** Pre-commit hooks can enforce coding standards (e.g., IEEE 1800-2017 for SystemVerilog):

Code Sample 2.18: Git pre-commit hook

```
#!/bin/sh
verilator --lint-only --Wall $(git diff --cached --name-only | grep '\.sv$')
if [ $? -ne 0 ]; then
    exit 1
fi
```

**Environmental impact is mitigated through energy-aware synthesis techniques.** Clock gating and power gating reduce dynamic and static power, respectively. Tools like Cadence Joules or Synopsys SpyGlass Power optimize RTL for low-power operation .

**Thermal-aware floorplanning in ASIC design minimizes hotspots, as modeled by the heat equation:**

$$\rho c_p \frac{\partial T}{\partial t} = \nabla \cdot (k \nabla T) + q$$

where  $\rho$  is density,  $c_p$  is specific heat,  $k$  is thermal conductivity, and  $q$  is heat flux.

## 2.2.2 Version control setup for HDL projects

Modern GPU architectures rely heavily on hardware description language (HDL) projects for their design and verification. Effective version control for such projects is critical due to their complexity, collaborative nature, and the need for reproducibility. The following discussion covers version control setup considerations, environment constraints, and hardware compatibility for HDL projects targeting GPUs.

A well-structured version control system (VCS) for HDL projects must account for the unique characteristics of hardware design. Unlike software projects, HDL repositories often contain mixed-language sources (e.g., Verilog, VHDL, SystemVerilog), large binary files (e.g., IP cores, simulation dumps), vendor-specific toolchain configurations, and testbenches with complex dependencies.

Git is the dominant VCS for HDL projects, but its limitations with binary files necessitate extensions like Git LFS or alternative workflows. For GPU projects, repository organization should mirror the pipeline stages:

Code Sample 2.19: Recommended directory structure

```
/gpu_project
  /rtl      # HDL sources
  /ip       # Vendor IP cores
```

```
/tb      # Testbenches
/synth  # Synthesis scripts
/docs   # Architecture specs
```

Environment considerations significantly impact version control strategies. GPU development typically requires specialized EDA tools (e.g., Cadence Xcelium, Synopsys VCS), vendor toolchains (e.g., NVIDIA CUDA for GPGPU co-design), and high-performance computing resources for verification.

The toolchain must be versioned alongside HDL code. A `Makefile` or equivalent should explicitly declare tool versions:

Code Sample 2.20: Tool version specification

```
VCS_VERSION = 2023.03
VERILATOR_VERSION = 5.018
```

Hardware compatibility introduces additional constraints. Modern GPU architectures often employ:

$$f_{max} = \frac{1}{t_{pd} + t_{setup}}$$

where  $f_{max}$  is maximum clock frequency,  $t_{pd}$  propagation delay, and  $t_{setup}$  register setup time. Version-controlled synthesis scripts must account for target FPGA or ASIC technology libraries.

Branching strategies must accommodate parallel development of GPU components, such as feature branches for individual shader cores, release branches for tape-out versions, and long-lived branches for architectural variants (e.g., rtx-40-series).

Continuous integration (CI) pipelines for HDL projects require specialized infrastructure:

Code Sample 2.21: CI configuration example

```
stages:
  - lint
  - simulate
  - synthesize

lint:
  tools:
    - verilator --lint-only rtl/*.v

simulate:
  resources:
    - gpu-accelerated_servers
```

Hardware-software co-design in GPUs necessitates version control of interface definitions. A golden reference model should be maintained in a versioned repository:

Code Sample 2.22: GPU architecture struct definition

```
typedef struct {
    uint32_t warp_size;
    float tensor_core_ratio;
} gpu_arch_t;
```

Binary artifact management presents unique challenges. Solutions include Git LFS for small IP cores, Artifactory or Nexus for large pre-synthesized netlists, and hash verification for technology files.

Collaboration workflows must consider geographically distributed teams. A typical GPU HDL project might enforce atomic commits per functional block, signed-off-by tags for IP contributions, and Gerrit-style code reviews for critical paths.

Version control metadata should capture hardware context:

Code Sample 2.23: Commit message conventions

```
[SM][RV32] Add single-precision FPU to shader core
- Implements IEEE 754-2008 compliant unit
- Verified against RTL simulation (see #1234)
- Synthesis timing: 1.2ns @ 7nm
```

Toolchain version pinning is essential for reproducibility. A versioned Docker image or conda environment should specify:

Code Sample 2.24: Environment specification

```
channels:
  - eda-tools
dependencies:
  - verilator=5.018
  - vivado=2023.1
```

Hardware-in-the-loop verification requires versioned test harnesses. A typical setup might include:

$$\text{PCIe\_throughput} = \frac{\text{payload\_size}}{\text{latency}}$$

where parameters are version-controlled alongside RTL .

Security considerations for GPU HDL repositories include GPG-signed tags for releases, hardware security module (HSM) integration for signing, and access controls for proprietary architectures.

Performance regression tracking necessitates versioned benchmarks:

Code Sample 2.25: Benchmark tracking

```
commit abc123: 1.2 TFLOPS @ 300MHz
commit def456: 1.3 TFLOPS @ 300MHz (+8%)
```

Multi-project repositories (MPRs) are increasingly common for GPU families. A typical structure might contain shared verification IP, common interconnect standards, and reusable memory controllers.

The physical design flow requires version-controlled constraints:

Code Sample 2.26: SDC constraints

```
create_clock -period 2.5 [get_ports clk]
set_clock_uncertainty 0.1 [get_clocks clk]
```

Emerging technologies like chiplet-based GPUs introduce new version control requirements:

$$N_{\text{interconnects}} = \binom{M}{2}$$

where  $M$  is the number of chiplets .

Documentation must be versioned alongside RTL, including microarchitecture specifications, verification plans, and power intent files (UPF/CPF).

The complete version control setup for a modern GPU HDL project thus requires tight integration of traditional software practices with hardware-specific considerations, spanning from RTL development through physical implementation and verification.

## 2.3 First Steps in Verilog Development

### 2.3.1 Writing, simulating, and synthesizing a basic Verilog module

Writing, simulating, and synthesizing a basic Verilog module is a foundational skill in modern GPU architecture design. Verilog, a hardware description language (HDL), enables the specification of digital circuits at various levels of abstraction. This process involves defining modules, simulating their behavior, and synthesizing them into gate-level representations.

A basic Verilog module consists of input and output ports, internal logic, and optional parameters. For example, a simple 2-input AND gate can be written as:

Code Sample 2.27: 2-input AND gate

```
module and_gate (
  input wire a,
  input wire b,
  output wire y
);
  assign y = a & b;
endmodule
```

This module declares two inputs (`a` and `b`) and one output (`y`). The `assign` statement continuously drives `y` to the logical AND of `a` and `b`.

Simulation is critical for verifying functionality before synthesis. A testbench is written to apply stimuli and observe responses. For the AND gate, a basic testbench might look like:

Code Sample 2.28: Testbench for AND gate

```
module tb_and_gate;
reg a, b;
wire y;

and_gate uut (
    .a(a),
    .b(b),
    .y(y)
);

initial begin
    a = 0; b = 0; #10;
    a = 0; b = 1; #10;
    a = 1; b = 0; #10;
    a = 1; b = 1; #10;
    $finish;
end
endmodule
```

The testbench instantiates the AND gate and applies all four input combinations, with a 10-time-unit delay between each. The `$finish` command terminates the simulation. Debugging involves checking waveforms or print statements to ensure correct outputs.

Synthesis translates Verilog into a netlist of logic gates. For the AND gate, synthesis might produce a single AND gate in FPGA implementations or a NAND-NAND structure in ASIC libraries due to technology mapping.

Modern GPU architectures rely on such modules for control logic, arithmetic units, and memory interfaces. For example, NVIDIA's Fermi architecture uses Verilog-like HDLs for its streaming multiprocessors.

A more complex example is a 4-bit adder, which demonstrates hierarchical design:

Code Sample 2.29: 4-bit adder

```
module adder_4bit (
    input wire [3:0] a,
    input wire [3:0] b,
    output wire [3:0] sum,
    output wire cout
);
assign {cout, sum} = a + b;
endmodule
```

This module uses concatenation to handle the carry-out. A testbench for this adder might include randomized inputs:

Code Sample 2.30: Randomized testbench for 4-bit adder

```
module tb_adder_4bit;
reg [3:0] a, b;
wire [3:0] sum;
wire cout;

adder_4bit uut (
    .a(a),
    .b(b),
    .sum(sum),
    .cout(cout)
);

initial begin
    integer i;
```

```

for (i = 0; i < 16; i = i + 1) begin
    a = $random;
    b = $random;
    #10;
end
$finish;
end
endmodule

```

The `$random` function generates pseudo-random inputs, improving test coverage. Debugging involves verifying arithmetic correctness and checking for overflow. Synthesis of the adder produces a ripple-carry or carry-lookahead structure, depending on constraints. GPUs optimize such adders for parallel execution, as seen in AMD's GCN architecture .

Timing analysis is essential post-synthesis. For the adder, the critical path delay is:

$$t_{crit} = t_{setup} + t_{carry} \cdot n + t_{sum}$$

where `n` is the number of bits, `t_carry` is the carry propagation delay, and `t_sum` is the sum computation delay.

Common pitfalls in Verilog development include incomplete sensitivity lists in always blocks, unintended latch inference due to missing branch coverage, and race conditions from non-blocking vs. blocking assignments.

For example, this flawed edge detector infers a latch:

Code Sample 2.31: Flawed edge detector

```

module edge_detector (
    input wire clk,
    input wire signal,
    output reg edge
);
always @ (signal) begin
    edge = signal & ~prev_signal;
end
endmodule

```

The missing `prev_signal` storage causes a latch. A corrected version uses a flip-flop:

Code Sample 2.32: Corrected edge detector

```

module edge_detector (
    input wire clk,
    input wire signal,
    output reg edge
);
reg prev_signal;

always @ (posedge clk) begin
    prev_signal <= signal;
    edge <= signal & ~prev_signal;
end
endmodule

```

Debugging such issues requires waveform inspection and linting tools. Synopsys VCS and Cadence Xcelium are industry-standard simulators .

Synthesis constraints guide optimization. For the adder, a constraint might limit delay:

Code Sample 2.33: Timing constraint

```

create_clock -period 2 [get_ports clk]
set_max_delay 1.5 -from [get_ports a] -to [get_ports sum]

```

In GPUs, these constraints ensure meet throughput targets. NVIDIA's Volta architecture uses similar constraints for its tensor cores .

In summary, writing, simulating, and synthesizing Verilog modules involves defining modules with clear I/O and logic, developing comprehensive testbenches, debugging using waveforms and linting, and applying synthesis constraints for optimization. These steps form the basis of GPU design, enabling complex architectures through modular development.

### 2.3.2 Debugging simple testbenches

Debugging simple testbenches is a critical skill in Verilog development, particularly when targeting modern GPU architectures. The process involves verifying the correctness of a design by simulating its behavior under controlled conditions. A testbench is a Verilog module that instantiates the design under test (DUT) and applies stimuli to its inputs while monitoring its outputs.

Common issues in testbenches include incorrect stimulus generation, mismatched timing, and improper signal initialization. In the context of modern GPU architectures, debugging testbenches requires an understanding of parallel processing and pipelining. GPUs rely on massively parallel execution units, and even simple testbenches must account for synchronization and data dependencies.

For example, a basic testbench for a GPU arithmetic logic unit (ALU) must verify that operations are correctly parallelized and that results are synchronized with the clock edges. Consider a simple Verilog module for a GPU ALU:

Code Sample 2.34: GPU ALU Module

```
module gpu_alu (
    input wire clk,
    input wire [31:0] a, b,
    input wire [2:0] op,
    output reg [31:0] result
);
    always @ (posedge clk) begin
        case (op)
            3'b000: result <= a + b;
            3'b001: result <= a - b;
            3'b010: result <= a & b;
            3'b011: result <= a | b;
            default: result <= 32'b0;
        endcase
    end
endmodule
```

A corresponding testbench for this module must generate clock signals, apply input vectors, and verify outputs. Common debugging techniques include waveform inspection using tools like ModelSim or GTKWave to visualize signal transitions and identify timing violations; assertion-based verification by embedding checks directly into the testbench; and logging via print statements for manual inspection.

The following testbench demonstrates these techniques:

Code Sample 2.35: Testbench for GPU ALU

```
module tb_gpu_alu;
    reg clk;
    reg [31:0] a, b;
    reg [2:0] op;
    wire [31:0] result;

    gpu_alu dut (
        .clk(clk),
        .a(a),
        .b(b),
        .op(op),
        .result(result)
    );

    initial begin
        clk = 0;
        forever #5 clk = ~clk;
    end

    initial begin
        a = 32'h00000001;
        b = 32'h00000002;
    end

```

```

op = 3'b000; #10;
if (result !== 32'h00000003) $error("Addition failed");

op = 3'b001; #10;
if (result !== 32'hFFFFFFFF) $error("Subtraction failed");

$finish;
end
endmodule

```

Debugging this testbench involves ensuring that the clock period matches the DUT's timing requirements and that the input stimuli are correctly synchronized. For example, the addition operation is verified after one clock cycle, but if the DUT introduces pipelining, the testbench must account for additional latency.

In modern GPU architectures, pipelining is ubiquitous. A pipelined ALU might require multiple clock cycles to produce a result, necessitating modifications to the testbench:

Code Sample 2.36: Pipelined GPU ALU Testbench

```

module tb_pipelined_alu;
reg clk;
reg [31:0] a, b;
reg [2:0] op;
wire [31:0] result;
integer i;

gpu_alu_pipelined dut (
    .clk(clk),
    .a(a),
    .b(b),
    .op(op),
    .result(result)
);

initial begin
    clk = 0;
    forever #5 clk = ~clk;
end

initial begin
    for (i = 0; i < 4; i = i + 1) begin
        a = i;
        b = i + 1;
        op = 3'b000;
        #10;
    end

    #20; // Wait for pipeline to flush
    if (result !== 32'h00000006) $error("Pipeline result mismatch");
    $finish;
end
endmodule

```

Here, the testbench accounts for pipeline latency by waiting an additional 20 time units before checking the result. Debugging such testbenches requires careful analysis of the pipeline depth and the timing of input stimuli.

Another common issue in testbenches is race conditions, where signals change simultaneously, leading to unpredictable behavior. For example, if the testbench updates inputs and checks outputs on the same clock edge, the simulator might not correctly resolve the order of operations. To avoid this, inputs should be updated slightly before the clock edge, and outputs should be checked slightly after:

Code Sample 2.37: Race-Free Testbench

```

initial begin
    #2; // Offset from clock edge
    a = 32'h00000001;

```

```

b = 32'h00000002;
op = 3'b000;
#8; // Wait until after clock edge
if (result !== 32'h00000003) $error("Addition failed");
end

```

Modern GPU architectures also introduce challenges related to memory access patterns and bandwidth. A testbench for a GPU memory controller must verify that data is correctly fetched and stored under high concurrency. For example:

Code Sample 2.38: GPU Memory Controller Testbench

```

module tb_mem_controller;
reg clk;
reg [31:0] addr;
reg [31:0] data_in;
reg wr_en;
wire [31:0] data_out;

gpu_mem_controller dut (
    .clk(clk),
    .addr(addr),
    .data_in(data_in),
    .wr_en(wr_en),
    .data_out(data_out)
);

initial begin
    clk = 0;
    forever #5 clk = ~clk;
end

initial begin
    addr = 32'h00001000;
    data_in = 32'hDEADBEEF;
    wr_en = 1; #10;
    wr_en = 0; #10;
    if (data_out !== 32'hDEADBEEF) $error("Memory readback failed");
    $finish;
end
endmodule

```

Debugging such testbenches involves verifying that memory operations are correctly synchronized and that data integrity is maintained under concurrent access. Techniques like randomized testing and coverage analysis can further enhance testbench reliability.

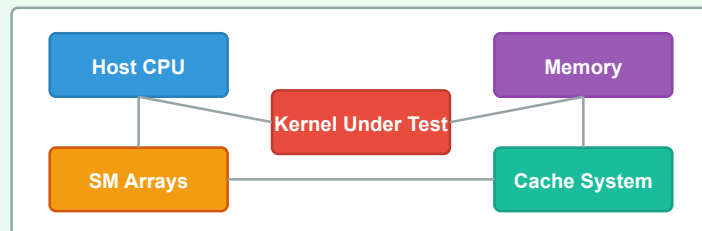
In summary, debugging simple testbenches for modern GPU architectures requires attention to timing, synchronization, and parallelism. By leveraging waveform inspection, assertions, and careful timing offsets, developers can ensure the correctness of their Verilog designs.

# GPU Testbench Debugging

## Why Debug GPU Testbenches?

- Verify shader execution correctness
- Detect memory access violations and race conditions
- Ensure kernel optimization performance

## GPU Testbench Structure



## Debugging Process

- 1 **Write Simple Testbench**  
Create minimal kernel with known inputs/outputs
- 2 **Instrument with Debug Macros**  
Add print statements or use debugger hooks
- 3 **Run on GPU Simulator**  
Execute in controlled environment with waveform capture
- 4 **Analyze Memory Access Patterns**  
Check for coalescing, bank conflicts, and cache behavior

### Common Tools

- Nsight Compute
- CUDA-GDB
- printf() debugging
- SASS Instruction Trace

# Chapter 3

# Introduction to GPU Architecture

## 3.1 GPU vs. CPU

### 3.1.1 Fundamental differences in architecture

The fundamental differences between modern GPU and CPU architectures stem from their distinct design philosophies, optimization goals, and execution models. GPUs are optimized for high-throughput parallel processing, while CPUs prioritize low-latency sequential execution. These differences manifest in their architectural organization, parallelization strategies, and execution models.

GPUs employ a massively parallel architecture with thousands of smaller, simpler cores designed to handle many threads simultaneously. For example, NVIDIA's Ampere architecture features up to 108 streaming multiprocessors (SMs), each containing 128 CUDA cores, enabling thousands of concurrent threads. In contrast, CPUs typically feature fewer, more complex cores with sophisticated control logic, branch prediction, and out-of-order execution to optimize single-thread performance. Intel's Alder Lake architecture, for instance, combines performance and efficiency cores but remains limited to a few dozen threads.

The memory hierarchy differs significantly between GPUs and CPUs. GPUs use a hierarchical memory system consisting of global memory (high latency, high bandwidth), shared memory (low latency, shared among threads in a block), and registers (fastest, per-thread storage). This design minimizes memory access bottlenecks for data-parallel workloads. CPUs, however, rely on deep cache hierarchies (L1, L2, L3) and prefetching mechanisms to reduce latency for sequential code. The GPU's memory bandwidth often exceeds 1 TB/s (e.g., NVIDIA H100 achieves 3 TB/s), while high-end CPUs typically reach 100–200 GB/s.

Parallelization models diverge sharply between the two architectures. GPUs follow the Single Instruction Multiple Thread (SIMT) execution model, where groups of threads (warps/wavefronts) execute the same instruction on different data. This is expressed as:

$$\text{Throughput} = \frac{\text{Number of cores} \times \text{Clock rate} \times \text{IPC}}{\text{Thread latency}}$$

CPUs use Multiple Instruction Multiple Data (MIMD) parallelism, where each core can execute different instructions independently. The CPU performance equation emphasizes latency:

$$\text{Latency} = \text{CPI} \times \text{Clock period} \times \text{Instruction count}$$

Execution models differ in thread management. GPUs implement zero-overhead thread scheduling in hardware, where context switching occurs every cycle to hide memory latency. The GPU execution context is lightweight:

Code Sample 3.1: GPU thread scheduling

```
while (active_threads) {
    execute_instruction_for_all_active_threads();
    handle_memory_requests();
    update_thread_states();
}
```

CPUs use operating system-managed threads with significant context switch overhead (typically 1–10  $\mu\text{s}$ ). CPU thread scheduling involves:

### Code Sample 3.2: CPU thread scheduling

```
for (thread in runqueue) {
    save_context(prev_thread);
    load_context(next_thread);
    execute_until_quantum_expires();
}
```

The instruction set architecture (ISA) reflects these differences. GPU ISAs like PTX include features such as predicated execution (to handle divergent branches), memory coalescing instructions, and explicit SIMD width declarations. CPU ISAs (x86, ARM) focus on complex addressing modes, single-thread optimization (e.g., AVX-512), and privilege levels for system security.

Power efficiency metrics highlight architectural tradeoffs. GPUs achieve higher FLOPs/Watt for parallel workloads due to simpler control logic and higher computational density. The energy per instruction follows:

$$E_{\text{GPU}} = N_{\text{cores}} \times E_{\text{core}} + E_{\text{memory}}$$

CPUs optimize for dynamic power management:

$$E_{\text{CPU}} = \sum_{i=1}^N (f_i \times V_i^2 \times C_i) + E_{\text{static}}$$

where  $f_i$ ,  $V_i$ , and  $C_i$  represent per-core frequency, voltage, and capacitance .

Synchronization mechanisms differ in granularity. GPUs use warp-level synchronization (implicit in SIMT execution), memory fences for global coordination, and atomic operations on shared memory. CPUs employ cache coherence protocols (MESI, MOESI), lock-based synchronization (mutexes, semaphores), and transactional memory in some architectures.

The programming models reflect these architectural differences. GPU programming (CUDA, OpenCL) requires explicit memory hierarchy management, thread block organization, and divergence minimization. CPU programming assumes sequential consistency by default, automatic cache management, and branch prediction benefits.

Performance characteristics diverge based on workload type. For a compute-bound problem with  $P$  parallel elements and  $S$  sequential dependencies, Amdahl's Law predicts:

$$\text{Speedup} = \frac{1}{(1 - P) + \frac{P}{N}}$$

where  $N$  is the number of processors. GPUs excel when  $P \rightarrow 1$ , while CPUs perform better when  $(1 - P)$  dominates .

Recent architectural trends show convergence in some areas. CPUs are incorporating wider SIMD units (e.g., AVX-1024 proposals), on-package high-bandwidth memory (Intel Sapphire Rapids), and hardware multithreading (IBM POWER10 SMT8). GPUs are adding tensor cores for mixed-precision math, ray tracing acceleration hardware, and improved single-thread performance (NVIDIA Ada Lovelace).

The architectural differences lead to complementary roles in heterogeneous systems. The optimal partitioning follows:

$$\text{Performance}_{\text{total}} = \alpha \times \text{CPU}_{\text{cores}} + \beta \times \text{GPU}_{\text{cores}}$$

where  $\alpha$  and  $\beta$  represent workload characteristics . This synergy drives modern computing systems from smartphones to supercomputers.

### 3.1.2 Parallelization

The modern graphics processing unit (GPU) has evolved into a highly parallelized architecture, fundamentally distinct from the traditional central processing unit (CPU) in both design and execution models. This distinction arises from their divergent optimization goals: CPUs prioritize low-latency sequential execution, while GPUs maximize throughput for parallel workloads. The architectural differences between GPUs and CPUs are rooted in their respective approaches to parallelization, memory hierarchy, and execution models.

GPUs employ a single-instruction multiple-thread (SIMT) execution model, where a single instruction is executed across multiple threads simultaneously. This contrasts with the CPU's multiple-instruction multiple-data

(MIMD) model, where each core operates independently. The SIMT model enables GPUs to achieve high throughput by amortizing instruction fetch and decode overhead across thousands of threads. For example, NVIDIA's CUDA architecture groups threads into warps of 32 threads, which execute in lockstep. The efficiency of this model is quantified by the occupancy metric, defined as the ratio of active warps to the maximum supported by the hardware:

$$\text{Occupancy} = \frac{\text{Active Warps}}{\text{Maximum Warps}}$$

The memory hierarchy of GPUs is optimized for high bandwidth rather than low latency. While CPUs rely on large caches to reduce memory access latency, GPUs use smaller caches and rely on massive parallelism to hide latency. The GPU memory hierarchy consists of:

- Global memory (high latency, high bandwidth),
- Shared memory (low latency, limited capacity),
- Registers (fastest, thread-private).

This hierarchy is explicitly managed by the programmer, unlike CPU caches, which are transparent. The performance impact of memory access patterns is significant, as coalesced accesses (contiguous threads accessing contiguous memory) achieve higher bandwidth. The effective bandwidth  $B_{\text{eff}}$  is given by:

$$B_{\text{eff}} = \frac{\text{Total Bytes Transferred}}{\text{Total Cycles}}$$

In contrast, CPUs employ deep pipelines and sophisticated branch prediction to minimize instruction latency. The CPU's out-of-order execution and speculative execution mechanisms are absent in GPUs, as they would introduce unnecessary overhead for highly parallel workloads. The CPU's focus on single-thread performance is reflected in its clock frequency, which is typically higher than that of GPUs. However, the GPU's strength lies in its ability to execute thousands of lightweight threads concurrently, as shown by its higher floating-point operations per second (FLOPS) for parallelizable workloads.

The execution models of GPUs and CPUs also differ in their handling of control flow. GPUs handle divergent branches (where threads within a warp take different paths) by serializing execution, leading to performance penalties. This is quantified by the divergence metric:

$$\text{Divergence} = \frac{\text{Active Threads}}{\text{Total Threads}}$$

CPUs, on the other hand, use branch prediction to mitigate control hazards, making them more efficient for irregular workloads. The GPU's reliance on uniform execution across threads makes it less suitable for tasks with high branch divergence.

The parallelization strategies in GPUs are implemented through hardware multithreading and warp scheduling. Each streaming multiprocessor (SM) in a GPU can context-switch between multiple warps to hide memory latency. The number of concurrent warps per SM is determined by the resources required by each warp, such as registers and shared memory. The theoretical occupancy can be calculated as:

$$\text{Theoretical Occupancy} = \min \left( \frac{\text{Registers Available}}{\text{Registers per Thread}}, \frac{\text{Shared Memory Available}}{\text{Shared Memory per Block}} \right)$$

In comparison, CPUs use simultaneous multithreading (SMT) to execute multiple threads per core, but the degree of parallelism is much lower. For instance, Intel's Hyper-Threading allows two threads per core, while GPUs can execute thousands.

The programming models for GPUs, such as CUDA and OpenCL, expose these architectural features to the programmer. A typical CUDA kernel launch specifies the grid and block dimensions, which map to the hardware's thread hierarchy:

#### Code Sample 3.3: CUDA Kernel Launch

```
kernel<<<blocks, threads>>>(args);
```

The grid consists of blocks, each containing threads that execute the kernel. The block size affects occupancy, as smaller blocks may underutilize the SM, while larger blocks may exceed resource limits. The optimal block size is determined empirically or through analytical models.

The GPU's execution model also includes synchronization primitives, such as `__syncthreads()`, which ensures all threads in a block reach the same point before proceeding. This is necessary because threads within a

block can communicate via shared memory. In contrast, CPU threads typically synchronize using locks or atomic operations, which are more expensive due to the lack of hardware support for fine-grained synchronization.

The performance gap between GPUs and CPUs is most pronounced for data-parallel workloads. For example, matrix multiplication on a GPU can achieve near-peak performance due to its regular memory access patterns and high arithmetic intensity. The arithmetic intensity  $I$  is defined as:

$$I = \frac{\text{Operations}}{\text{Data Transferred}}$$

Workloads with high  $I$  are well-suited for GPUs, as they can hide memory latency with computation. Conversely, CPUs excel at tasks with low  $I$ , such as serial or irregular algorithms.

The architectural differences between GPUs and CPUs have led to the emergence of heterogeneous computing, where each processor is used for its strengths. For instance, CPUs handle control-intensive tasks, while GPUs accelerate parallel computations. This paradigm is exemplified by frameworks like OpenACC and SYCL, which facilitate code offloading to accelerators.

In summary, the modern GPU's architecture is defined by its focus on parallelization through SIMD execution, high-bandwidth memory hierarchy, and explicit resource management. These features contrast sharply with the CPU's latency-optimized design, resulting in complementary roles in computing systems. The choice between GPU and CPU depends on the workload's parallelism and arithmetic intensity, with GPUs dominating in throughput-oriented applications.

### 3.1.3 Execution models

Modern GPU architectures are fundamentally distinct from CPUs in their execution models, parallelization strategies, and underlying architectural design. These differences arise from their specialized roles: CPUs excel at sequential task execution with low latency, while GPUs prioritize high-throughput parallel computation.

The execution model of a GPU is designed to maximize data parallelism, leveraging thousands of smaller, simpler cores to perform computations simultaneously. This contrasts sharply with CPUs, which typically feature fewer, more complex cores optimized for single-threaded performance and branch prediction.

The architectural divergence between GPUs and CPUs stems from their respective workloads. CPUs employ a control-flow execution model, where instructions are fetched, decoded, and executed sequentially or with limited parallelism. Modern CPUs use techniques like superscalar execution, out-of-order execution, and speculative execution to improve performance. In contrast, GPUs adopt a data-flow execution model, where computations are driven by data availability rather than instruction sequencing. This model is particularly suited for applications with high arithmetic intensity, such as graphics rendering or matrix operations.

The GPU's execution model is built around the Single Instruction, Multiple Thread (SIMT) paradigm, where a single instruction is broadcast to multiple threads that execute it in lockstep. This approach minimizes control overhead and maximizes throughput.

Parallelization in GPUs is achieved through hierarchical thread organization. A typical GPU consists of multiple Streaming Multiprocessors (SMs), each containing dozens of CUDA cores (in NVIDIA architectures) or Compute Units (in AMD architectures). Threads are grouped into warps (NVIDIA) or wavefronts (AMD), which execute the same instruction on different data elements. This fine-grained parallelism is managed by hardware schedulers that dynamically allocate resources to maximize occupancy. The execution model relies on massive multithreading to hide memory latency; while one warp waits for data, another can execute, ensuring high utilization of computational resources. This contrasts with CPUs, where parallelism is coarser-grained, relying on multi-core and hyper-threading technologies to exploit thread-level parallelism.

The fundamental differences in execution models between GPUs and CPUs are evident in their memory hierarchies. GPUs feature a deeply hierarchical memory system designed to support high bandwidth and low-latency access for parallel workloads. This includes global memory (high-capacity but high-latency memory shared across all SMs), shared memory (low-latency, programmer-managed memory shared within a thread block), registers (fastest storage, private to each thread), and cache hierarchies (L1/L2 caches optimized for spatial and temporal locality in parallel access patterns). CPUs, conversely, prioritize low-latency access to a unified memory hierarchy, with larger caches and sophisticated prefetching mechanisms to accelerate sequential workloads. The GPU's memory system is optimized for concurrent access patterns, often sacrificing single-thread performance for aggregate bandwidth.

Execution models also differ in how they handle control flow. CPUs excel at executing divergent branches efficiently through speculative execution and branch prediction. GPUs, however, suffer performance penalties when threads within a warp diverge, as the SIMT model requires serial execution of divergent paths. This is formalized in the SIMT efficiency metric:

$$\text{SIMT Efficiency} = \frac{\text{Active Threads}}{\text{Total Threads}}$$

When divergence occurs, the denominator remains constant while the numerator decreases, reducing efficiency. Techniques like predication and warp voting are used to mitigate this overhead.

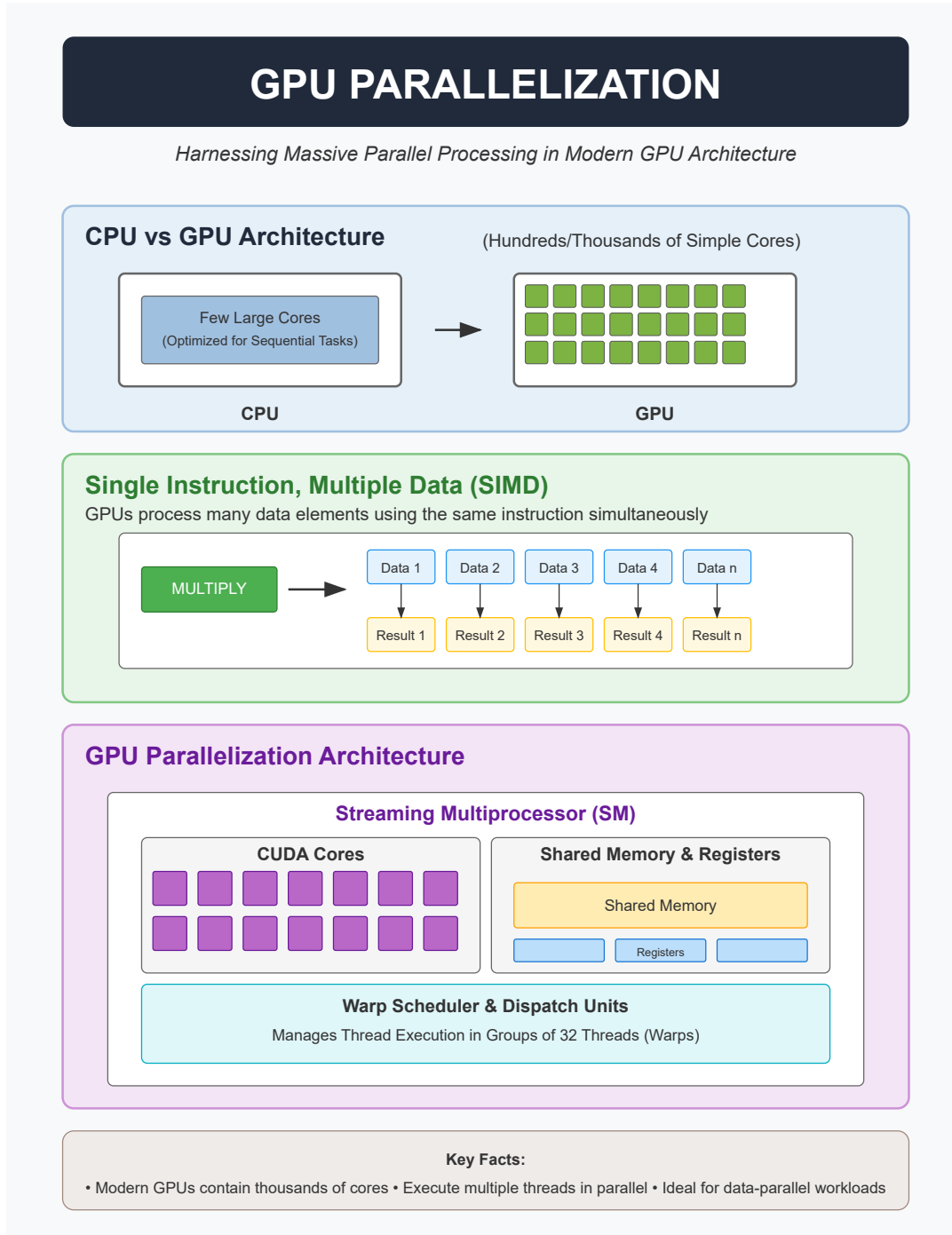
The programming models reflect these architectural differences. CPU code is typically written in imperative languages like C++ or Java, with explicit thread management via libraries like OpenMP or pthreads. GPU programming, however, requires frameworks like CUDA or OpenCL, where developers explicitly define parallelism through kernels and grid/block hierarchies. For example:

Code Sample 3.4: CUDA Kernel for Vector Addition

```
__global__ void vectorAdd(float *A, float *B, float *C, int N) {
    int i = blockIdx.x * blockDim.x + threadIdx.x;
    if (i < N) C[i] = A[i] + B[i];
}
```

This kernel launches one thread per element, showcasing the GPU's execution model of fine-grained parallelism.

Performance characteristics further highlight the differences. CPUs achieve high single-thread performance through deep pipelines (15–20 stages in modern designs), aggressive out-of-order execution, and complex cache



hierarchies such as Intel’s Smart Cache. GPUs, however, optimize for throughput via shallow pipelines (5–10 stages) to reduce context switch costs, massive multithreading to hide latency, and high memory bandwidth (e.g., NVIDIA’s HBM2 at 900 GB/s). The roofline model captures this trade-off, plotting attainable performance against operational intensity:

$$\text{Performance} \leq \min(\text{Peak Compute}, \text{Peak Bandwidth} \times \text{Operational Intensity})$$

GPUs excel in the compute-bound region, while CPUs perform better in memory-bound or low-intensity workloads.

Synchronization mechanisms also differ. CPUs use atomic operations, locks, and memory barriers to enforce ordering in shared-memory programs. GPUs rely on warp-level synchronization (`__syncthreads()`) and memory fences, with atomic operations being significantly more expensive due to the SIMD model. This impacts algorithm design, favoring data-parallel approaches over fine-grained synchronization.

Recent advancements blur these distinctions. CPUs incorporate wider SIMD units (e.g., AVX-512), while GPUs gain features like tensor cores for mixed-precision arithmetic. Heterogeneous architectures (e.g., AMD’s APUs, Intel’s Ponte Vecchio) integrate both execution models, requiring unified programming frameworks like SYCL or HIP. However, the fundamental trade-offs remain: CPUs for latency-sensitive, irregular workloads; GPUs for throughput-oriented, regular computations.

Energy efficiency further differentiates the execution models. GPUs achieve higher FLOPs/Watt due to their simpler cores and optimized data paths. For example, NVIDIA’s A100 delivers 312 TFLOPS at 400W, while a high-end CPU might achieve 1–2 TFLOPS at similar power. This efficiency stems from the GPU’s focus on arithmetic throughput rather than control logic, as quantified by the energy-per-instruction metric:

$$E_{\text{inst}} = \frac{P_{\text{dynamic}}}{f \times \text{IPC}}$$

where  $P_{\text{dynamic}}$  is dynamic power,  $f$  is frequency, and IPC is instructions per cycle. GPUs minimize  $E_{\text{inst}}$  by maximizing IPC through parallelism.

In summary, GPU execution models prioritize throughput over latency, leveraging SIMD parallelism, hierarchical memory, and massive multithreading. CPUs optimize for sequential performance with complex cores and deep cache hierarchies. These differences necessitate distinct programming approaches and algorithmic designs, with the choice between GPU and CPU depending on the workload’s parallelism and memory access patterns.

## 3.2 Fixed-Function vs. Programmable Pipelines

### 3.2.1 Historical perspective

The evolution of modern GPU architecture is deeply rooted in the historical transition from fixed-function pipelines to programmable pipelines. Early graphics hardware, such as the IBM 8514 (1987), relied entirely on fixed-function pipelines, where each stage—geometry processing, rasterization, and shading—was implemented as dedicated hardware units with no programmability. These pipelines were optimized for specific tasks, such as transforming vertices or applying pre-defined lighting models, but lacked flexibility. The fixed-function paradigm dominated the 1990s, with GPUs like NVIDIA’s GeForce 256 (1999) accelerating 3D graphics by offloading matrix transformations and lighting calculations from the CPU. However, the rigid nature of these pipelines limited innovation, as new rendering techniques required hardware modifications.

The shift toward programmable pipelines began in the early 2000s, driven by the demand for more expressive rendering techniques. NVIDIA’s GeForce 3 (2001) introduced programmable vertex shaders, allowing developers to customize vertex transformations. This was followed by the GeForce FX (2003), which added programmable pixel shaders, enabling per-pixel lighting and texture operations. These advancements marked a departure from fixed-function pipelines, as shaders were executed on unified arithmetic logic units (ALUs) controlled by small programs. The introduction of high-level shading languages, such as Cg and HLSL, further democratized GPU programmability. Researchers like Pat Hanrahan and Marc Olano demonstrated the potential of programmable shaders for non-graphics applications, laying the groundwork for general-purpose GPU (GPGPU) computing.

The modern GPU pipeline is a hybrid of programmable and fixed-function stages, balancing flexibility with efficiency. For example, the rasterization stage remains fixed-function due to its highly parallelizable nature, while vertex, geometry, and fragment shaders are fully programmable. This hybrid approach is exemplified by NVIDIA’s Turing architecture (2018), which introduced ray-tracing acceleration cores (RT cores) alongside programmable CUDA cores. The RT cores handle ray-triangle intersections—a fixed-function task—while the CUDA

cores execute shader programs. Similarly, AMD’s RDNA 2 (2020) integrates fixed-function ray accelerators with programmable compute units.

The trade-off between fixed-function and programmable pipelines is quantified by the performance-energy ratio:

$$\eta = \frac{P}{E}$$

where  $P$  is throughput and  $E$  is energy consumption. Fixed-function units excel at  $\eta$  for specific tasks, while programmable units offer generality at a higher  $E$ .

The historical progression of GPU pipelines reflects broader trends in computer architecture. The move from fixed-function to programmable pipelines mirrors the transition from application-specific integrated circuits (ASICs) to field-programmable gate arrays (FPGAs) in the 1980s. Both shifts were motivated by the need for reconfigurability and reduced time-to-market. However, GPUs retained fixed-function elements where specialization provided clear benefits, such as texture filtering and display output.

This design philosophy is evident in the evolution of GPU instruction sets. Early GPUs used microcode for shader execution, while modern architectures like NVIDIA’s Ampere (2020) employ single-instruction, multiple-thread (SIMT) execution models, where threads execute the same instruction on different data. The SIMT paradigm, introduced by Larsen and McAllister in 2001, enables efficient utilization of programmable pipelines by amortizing instruction fetch overhead across threads.

The impact of programmable pipelines extends beyond graphics. The advent of CUDA (2006) and OpenCL (2008) transformed GPUs into parallel computing platforms, enabling applications in scientific simulation, machine learning, and cryptography. For instance, the Folding@home project leveraged GPU programmability to simulate protein dynamics, achieving a 100-fold speedup over CPUs. This shift was facilitated by architectural innovations such as unified shader architectures, where the same ALUs execute vertex, fragment, and compute shaders. NVIDIA’s Fermi (2010) was the first to implement this design, eliminating the fixed-function separation between shader types. The unified architecture is described by the equation:

$$T_{\text{exec}} = N_{\text{warps}} \times T_{\text{warp}}$$

where  $T_{\text{exec}}$  is total execution time,  $N_{\text{warps}}$  is the number of warps, and  $T_{\text{warp}}$  is the time per warp.

Despite the dominance of programmable pipelines, fixed-function units persist in modern GPUs for latency-sensitive tasks. For example, the display engine and video codecs (e.g., NVENC) are fixed-function to meet real-time constraints. The balance between programmability and specialization is a recurring theme in GPU architecture. A study by Jouppi et al. (2017) found that fixed-function accelerators can achieve up to 10 $\times$  higher energy efficiency than programmable equivalents for specific workloads. This insight has guided the design of modern GPUs, where domain-specific accelerators (e.g., tensor cores for AI) coexist with general-purpose compute units. The trend is exemplified by NVIDIA’s Hopper (2022), which integrates programmable CUDA cores with fixed-function transformers for AI workloads.

The historical perspective on GPU pipelines reveals a cyclical pattern of specialization and generalization. Fixed-function pipelines dominated early graphics hardware, programmable pipelines enabled new applications, and modern architectures strike a balance between the two. This evolution is captured by the architectural efficiency metric:

$$\epsilon = \frac{\text{Utilized ALUs}}{\text{Total ALUs}}$$

where higher  $\epsilon$  indicates better resource utilization. Programmable pipelines maximize  $\epsilon$  for diverse workloads, while fixed-function units optimize for peak performance in narrow domains. The interplay between these paradigms continues to shape GPU design, as evidenced by the rise of ray-tracing cores and AI accelerators. Future architectures will likely further blur the line between fixed-function and programmable pipelines, driven by advances in heterogeneous computing and domain-specific languages.

### 3.2.2 Modern GPU pipelines

The evolution of modern GPU pipelines reflects a shift from fixed-function architectures to highly programmable designs, driven by increasing computational demands and the need for flexibility in graphics and general-purpose computing. Historically, GPUs were designed as fixed-function pipelines, where each stage—such as vertex processing, rasterization, and fragment shading—was implemented as a dedicated hardware unit. These early architectures, exemplified by NVIDIA’s GeForce 256 (1999) and ATI’s Radeon 9700 (2002), relied on rigid pipelines optimized for specific tasks, limiting programmability but achieving high throughput for rasterized graphics.

The transition to programmable pipelines began with the introduction of shader models, enabling developers to write custom programs for vertex and fragment processing. NVIDIA’s GeForce 3 (2001) introduced programmable vertex shaders, while the GeForce FX (2003) added programmable fragment shaders. This shift was formalized with the introduction of unified shader architectures, where a single set of cores could execute any shader stage. AMD’s R600 (2007) and NVIDIA’s Tesla (2006) architectures exemplified this approach, allowing dynamic workload balancing and improving resource utilization.

Modern GPU pipelines are characterized by their programmability and parallelism. The graphics pipeline now consists of stages that are either fixed-function or programmable, with the latter dominating computational workloads. Key stages include:

**Vertex Shading:** Programmable stage transforming vertex attributes.

**Tessellation:** Optional programmable stage subdividing geometry.

**Geometry Shading:** Programmable stage generating or discarding primitives.

**Rasterization:** Fixed-function stage converting primitives to fragments.

**Fragment Shading:** Programmable stage computing pixel colors.

**Render Output:** Fixed-function stage merging fragments into the framebuffer.

The rise of general-purpose GPU (GPGPU) computing further blurred the line between fixed-function and programmable pipelines. Frameworks like CUDA and OpenCL exposed GPU parallelism for non-graphics tasks, leveraging the same programmable cores used for shaders. This was enabled by architectures such as NVIDIA’s Fermi (2010), which introduced features like cache hierarchies and error-correcting code (ECC) memory, making GPUs viable for scientific computing.

A critical aspect of modern GPU pipelines is their reliance on single-instruction, multiple-thread (SIMT) execution. Unlike traditional CPUs, GPUs execute the same instruction across multiple threads, hiding latency through massive parallelism. For example, NVIDIA’s Ampere architecture (2020) supports concurrent execution of integer and floating-point operations, improving throughput for mixed workloads. The SIMT model is expressed mathematically as:

$$\text{Throughput} = N \cdot \frac{\text{IPC}}{\text{Latency}}$$

where  $N$  is the number of threads, IPC is instructions per cycle, and Latency is the execution delay.

Fixed-function components remain in modern GPUs for efficiency. For instance, rasterization and texture filtering are typically implemented as fixed-function units due to their regularity and high throughput requirements. However, even these stages are increasingly augmented with programmable features, such as NVIDIA’s Variable Rate Shading (VRS), which allows dynamic control over shading rates.

The memory hierarchy in modern GPUs is another area where fixed-function and programmable elements intersect. High-bandwidth memory (HBM) and cache hierarchies are managed by fixed-function controllers, while programmable caches (e.g., shared memory in CUDA) allow developers to optimize data locality. The memory access pattern is often described by:

$$\text{Bandwidth} = \frac{\text{Data Size}}{\text{Time}}$$

where Data Size is the amount of data transferred, and Time is the access duration.

Recent advancements in GPU pipelines include hardware-accelerated ray tracing, where fixed-function acceleration structures (e.g., bounding volume hierarchies) are combined with programmable shaders for realistic lighting effects. NVIDIA’s Turing (2018) and AMD’s RDNA 2 (2020) architectures introduced dedicated ray-tracing cores, demonstrating the continued coexistence of fixed-function and programmable elements.

The historical progression of GPU pipelines reveals a trend toward greater programmability, but fixed-function units persist where they offer efficiency advantages. This duality is evident in modern architectures like NVIDIA’s

# The Evolution of GPU Architecture

## A Historical Perspective

1970s	<b>1970s-1980s: Early Graphics Processing</b> <ul style="list-style-type: none"><li>Specialized display controllers and buffer processors</li><li>Fixed-function hardware for basic rasterization</li><li>IBM Professional Graphics Adapter (PGA), 1984</li></ul>
1990s	<b>1990s: First Consumer GPUs</b> <ul style="list-style-type: none"><li>NVIDIA GeForce 256 (1999): First "GPU" with hardware T</li><li>3dfx Voodoo Graphics (1996): 3D acceleration</li><li>ATI Rage and NVIDIA RIVA series: Early competition</li></ul>
2000	<b>2000-2006: Programmable Pipelines</b> <ul style="list-style-type: none"><li>DirectX 8-9: Introduction of shader models</li><li>NVIDIA GeForce FX: First fully programmable pixel shaders</li><li>ATI Radeon 9700: First to support DirectX 9 shaders</li></ul>
2006	<b>2006-2010: Unified Shader Architecture</b> <ul style="list-style-type: none"><li>NVIDIA GeForce 8800 GTX: First unified shader architecture</li><li>AMD Radeon HD 2000 series: Competitor unified architecture</li><li>CUDA (2007): General-purpose GPU computing</li></ul>
2010	<b>2010-2018: GPGPU and Compute</b> <ul style="list-style-type: none"><li>OpenCL, DirectCompute: Cross-vendor compute APIs</li><li>NVIDIA Kepler, Maxwell, Pascal architectures</li><li>AMD GCN architecture: Compute-focused design</li></ul>
2018	<b>2018-Present: Modern GPUs</b> <ul style="list-style-type: none"><li>NVIDIA Turing/Ampere/Ada: RT cores, Tensor cores</li><li>AMD RDNA architecture: Gaming-optimized design</li><li>Hardware ray tracing and AI acceleration</li></ul>

From specialized hardware to general-purpose computing powerhouses

Hopper (2022) and AMD's CDNA (2021), which balance programmable cores with specialized accelerators for tasks like matrix multiplication and ray tracing. The interplay between these paradigms ensures GPUs remain versatile for both graphics and compute workloads.

Verilog code snippets illustrate the implementation of fixed-function units, such as a texture sampler:

Code Sample 3.5: Texture Sampler Module

```
module texture_sampler (
    input clk,
    input [31:0] uv,
    output [31:0] color
);
    reg [31:0] tex_mem [0:1023];
    always @ (posedge clk) begin
        color <= tex_mem[uv[9:0]];
    end
endmodule
```

In summary, modern GPU pipelines represent a synthesis of fixed-function and programmable designs, each optimized for specific tasks. The historical shift from rigid pipelines to flexible architectures has enabled GPUs to evolve into general-purpose parallel processors, while retaining specialized units for critical graphics operations. This balance ensures continued performance scaling and versatility in an era of increasingly diverse computational demands.

## 3.3 Key GPU Components

### 3.3.1 Cores (ALUs)

The architecture of modern GPUs is a complex interplay of specialized components designed to accelerate parallel computation, particularly in graphics rendering and general-purpose computing. Among these components, cores (Arithmetic Logic Units, or ALUs), texture units, rasterizers, and memory subsystems form the foundational building blocks. Each plays a distinct role in the pipeline, enabling high-throughput processing of data-intensive workloads.

Cores, or ALUs, are the computational workhorses of a GPU. Unlike CPUs, which prioritize single-threaded performance, GPUs deploy thousands of ALUs to execute massively parallel tasks. Each ALU is optimized for floating-point arithmetic, a critical requirement for graphics processing. Modern GPUs, such as NVIDIA's Ampere architecture or AMD's RDNA 3, organize ALUs into Streaming Multiprocessors (SMs) or Compute Units (CUs), respectively. These units bundle ALUs with other resources like registers and shared memory to maximize throughput. For example, NVIDIA's GA102 GPU in the RTX 3090 contains 10,496 CUDA cores, each capable of executing a single floating-point operation per clock cycle. The parallelism is expressed mathematically as:

$$\text{Throughput} = N \times f \times IPC$$

where  $N$  is the number of ALUs,  $f$  is the clock frequency, and  $IPC$  is instructions per cycle.

Texture units are specialized hardware components responsible for texture mapping, a process that applies detailed images to 3D surfaces. These units perform bilinear or trilinear filtering to interpolate texels (texture pixels) efficiently. A key metric for texture units is their fill rate, calculated as:

$$\text{Fill Rate} = TMUs \times f$$

where TMUs denotes the number of texture mapping units. For instance, AMD's RX 7900 XTX features 384 texture units, enabling it to process 1.5 trillion texels per second at 2.5 GHz. Texture units also support advanced operations like anisotropic filtering, which improves visual quality by sampling textures at varying angles.

Rasterizers convert vector graphics (e.g., triangles) into raster images (pixels). This process, known as rasterization, involves scan conversion and depth testing. Modern GPUs employ hierarchical rasterization to minimize redundant work. The rasterization pipeline includes primitive assembly (combining vertices into geometric primitives), scan conversion (determining which pixels overlap with the primitive), and fragment shading (applying per-pixel effects like lighting). The efficiency of rasterization is governed by the pixel rate:

$$\text{Pixel Rate} = ROPs \times f$$

where ROPs (Raster Operations Pipelines) handle tasks like blending and anti-aliasing. NVIDIA's Ada Lovelace architecture introduces DLSS 3.0, which uses AI to upscale rasterized frames, further optimizing performance.

Memory subsystems are critical for feeding data to ALUs, texture units, and rasterizers. GPUs employ a hierarchy of memory types: registers (fastest storage, directly accessible by ALUs), shared memory or L1 cache (low-latency memory shared among threads in an SM or CU), L2 cache (larger but slower, serving as a buffer between cores and VRAM), and VRAM (HBM or GDDR, high-bandwidth memory for global data storage). The bandwidth of VRAM is a bottleneck for many workloads. For example, GDDR6X in the RTX 4090 delivers 1 TB/s bandwidth, while AMD's MI300X uses HBM3 to achieve 5.3 TB/s. The effective bandwidth is modeled as:

$$\text{Bandwidth}_{\text{eff}} = \text{Bandwidth}_{\text{peak}} \times \text{Utilization}$$

The interplay between these components is exemplified in rendering a frame: vertex shaders (ALUs) transform 3D coordinates; rasterizers generate fragments from primitives; texture units apply surface details; and memory subsystems ensure data is available at each stage. Optimizations like tile-based rendering (used in mobile GPUs) or mesh shaders (in desktop GPUs) further refine this pipeline.

In summary, modern GPU architecture is a symphony of cores (ALUs), texture units, rasterizers, and memory subsystems, each optimized for parallel processing. Advances like NVIDIA's Tensor Cores or AMD's Infinity Cache demonstrate ongoing innovation in these areas, pushing the boundaries of performance and efficiency.

#### Code Sample 3.6: Simplified GPU Core Pipeline

```
module ALU (
    input [31:0] a, b,
    input [3:0] opcode,
    output reg [31:0] result
);
always @(*) begin
    case(opcode)
        4'b0000: result = a + b;
        4'b0001: result = a * b;
        // Additional operations
    endcase
end
endmodule
```

The Verilog snippet above illustrates a basic ALU, a fundamental building block of GPU cores. Real-world implementations are far more complex, supporting fused multiply-add (FMA) operations and SIMD (Single Instruction, Multiple Data) execution.

Memory subsystems are equally sophisticated. For example, NVIDIA's Hopper architecture introduces DPX instructions to accelerate dynamic programming workloads, leveraging both ALUs and memory hierarchies. Similarly, AMD's CDNA 2 architecture uses matrix cores to optimize AI workloads, showcasing the versatility of modern GPU components.

The evolution of GPU architecture continues to be driven by demands for higher performance in gaming, AI, and scientific computing. As transistor scaling slows, innovations in core design, memory systems, and parallelism will remain pivotal. Research in areas like photonic interconnects or 3D stacking promises further breakthroughs, ensuring GPUs remain at the forefront of computational technology.

### 3.3.2 Texture units

Modern GPU architectures are highly parallel processors designed to accelerate graphics rendering and general-purpose computation. Among their key components, texture units play a critical role in mapping textures onto geometric surfaces, enabling realistic shading and detail in rendered images. Texture units are specialized hardware blocks that handle texture sampling, filtering, and memory access operations efficiently. Their design is tightly coupled with other GPU components such as arithmetic logic units (ALUs), rasterizers, and memory subsystems to achieve high throughput in graphics pipelines.

Texture units perform several operations essential for rendering, including texture sampling (fetching texels from memory based on texture coordinates), filtering (applying bilinear, trilinear, or anisotropic filtering to reduce aliasing artifacts), addressing modes (handling texture coordinate wrapping, clamping, or mirroring), and mipmapping (selecting the appropriate level of detail to optimize memory bandwidth and quality).

The texture unit's operation can be mathematically described as a function of texture coordinates  $(u, v, w)$  and LOD parameters. For a bilinear filter, the interpolated texel value  $T$  is computed as:

$$T(u, v) = (1 - \alpha)(1 - \beta)T_{i,j} + \alpha(1 - \beta)T_{i+1,j} + (1 - \alpha)\beta T_{i,j+1} + \alpha\beta T_{i+1,j+1}$$

where  $\alpha$  and  $\beta$  are fractional parts of the texture coordinates, and  $T_{i,j}$  represents the texel at integer coordinates  $(i, j)$ . This operation is performed in parallel across multiple texture units to maintain high throughput.

Texture units are tightly integrated with ALUs (cores) in modern GPUs. While ALUs handle arithmetic operations for shading and computation, texture units offload memory-intensive texture operations. This division of labor allows the GPU to maximize parallelism. For example, in a shader program, ALUs may compute lighting equations while texture units concurrently fetch surface details.

The following Verilog snippet illustrates a simplified texture unit interface:

Code Sample 3.7: Texture Unit Interface

```
module texture_unit (
    input logic [31:0] u, v, w,
    input logic [2:0] filter_mode,
    output logic [31:0] texel_out
);
// Texture sampling logic here
endmodule
```

Rasterizers work closely with texture units by generating fragments (potential pixels) that require texturing. The rasterizer determines which fragments are visible and passes their texture coordinates to the texture units. The texture units then fetch and filter the appropriate texels, which are combined with fragment shading results from the ALUs. This pipeline ensures that textures are applied only to visible surfaces, conserving memory bandwidth.

Memory subsystems are critical for texture unit performance. Textures are stored in GPU memory hierarchies, including caches and dedicated texture memory (such as NVIDIA's Texture Cache or AMD's L2 Cache). Texture units employ sophisticated caching strategies to reduce latency, including block compression (storing textures in compressed formats like BCn or ASTC to reduce memory footprint), cache line optimization (fetching adjacent texels in a single memory transaction to exploit spatial locality), and prefetching (predicting future texture accesses based on shader execution patterns).

The memory access pattern for a texture unit can be modeled as:

$$\text{Latency} = t_{\text{cache}} + (1 - h) \cdot t_{\text{mem}}$$

where  $t_{\text{cache}}$  is the cache access time,  $h$  is the cache hit rate, and  $t_{\text{mem}}$  is the main memory access time. Modern GPUs optimize this equation by increasing  $h$  through larger caches and better prefetching algorithms.

Texture units also support advanced features such as virtual texturing (dynamically loading texture portions as needed to handle large textures), sparse texturing (allowing textures to occupy non-contiguous memory regions for flexibility), and texture space shading (performing shading computations in texture space to reduce redundancy).

The performance of texture units is measured in texels per second, a metric dependent on clock frequency, parallelism, and memory bandwidth. For example, NVIDIA's Ampere architecture achieves up to 496 texels per clock per texture unit. The theoretical peak texture throughput is:

$$\text{Throughput} = N \cdot f \cdot T$$

where  $N$  is the number of texture units,  $f$  is the clock frequency, and  $T$  is the texels per clock per unit.

In summary, texture units are specialized hardware components in GPUs that handle texture sampling, filtering, and memory access. Their design is optimized for parallelism and integration with ALUs, rasterizers, and memory subsystems. By offloading texture operations from general-purpose cores, texture units enable efficient rendering of complex scenes with high-quality detail. Future advancements may focus on improving filtering algorithms, reducing memory latency, and supporting higher-resolution textures for emerging applications like virtual reality and real-time ray tracing.

### 3.3.3 Rasterizers

Rasterizers are a fundamental component of modern GPU architectures, responsible for converting vector-based geometric primitives into pixel fragments that can be processed by the rest of the graphics pipeline. In the context of modern GPUs, rasterizers work in concert with other key components such as arithmetic logic units (ALUs), texture units, and memory subsystems to deliver high-performance rendering. The rasterization process involves several stages, including primitive setup, scan conversion, and fragment generation, each optimized for parallel

execution on GPU cores. The rasterizer operates on geometric primitives such as triangles, which are the most common primitive in real-time graphics. Given a triangle defined by three vertices in screen space, the rasterizer determines which pixels (or samples) lie inside the triangle. This involves evaluating edge equations for each pixel in the bounding box of the triangle. The edge equations are derived from the barycentric coordinates of the triangle and can be expressed as:

$$E_i(x, y) = (y - y_j)(x_k - x_j) - (x - x_j)(y_k - y_j)$$

where  $(x_j, y_j)$  and  $(x_k, y_k)$  are the coordinates of two vertices of the triangle. A pixel  $(x, y)$  is inside the triangle if all three edge equations  $E_0, E_1, E_2$  yield the same sign. Modern GPUs employ hierarchical rasterization techniques to improve efficiency. Instead of testing every pixel individually, the rasterizer first evaluates coarse-grained tiles or blocks of pixels. If a tile is entirely outside the triangle, it is discarded early, reducing unnecessary computation. This approach leverages the parallel processing capabilities of GPU cores, where multiple tiles can be processed simultaneously. The hierarchical nature of rasterization is particularly well-suited for GPUs, as it aligns with their SIMD (Single Instruction, Multiple Data) architecture. The rasterizer interacts closely with other GPU components. For instance, the ALUs (arithmetic logic units) within the GPU cores perform the mathematical operations required for edge equation evaluation and interpolation. Each ALU is capable of executing multiple floating-point operations per clock cycle, enabling high-throughput rasterization. The texture units, on the other hand, are responsible for fetching and filtering texture data for the generated fragments. The rasterizer ensures that fragments are generated with the correct texture coordinates, which are then passed to the texture units for sampling. Memory subsystems play a critical role in rasterization performance. The rasterizer generates fragments that must be stored in the GPU's memory hierarchy, including registers, caches, and global memory. Efficient memory access patterns are essential to avoid bottlenecks. For example, the rasterizer often employs Z-culling (or occlusion culling) to discard fragments that are occluded by previously rendered geometry. This requires depth testing, which relies on fast access to the depth buffer stored in memory. Modern GPUs use specialized memory structures such as compressed depth buffers and tile-based rendering to minimize memory bandwidth usage. The rasterizer also incorporates anti-aliasing techniques to improve image quality. Multi-sample anti-aliasing (MSAA) is a common approach where multiple samples are evaluated per pixel, and the results are averaged to reduce jagged edges. The rasterizer generates additional samples for each fragment, increasing the computational load but improving visual fidelity. The GPU's ALUs and memory subsystems must handle the increased workload efficiently, often through dedicated hardware support for sample interpolation and storage. In terms of hardware implementation, rasterizers are typically implemented as fixed-function units within the GPU pipeline. However, some modern architectures allow for programmable rasterization through compute shaders, enabling custom rasterization algorithms. For example, Nvidia's Turing architecture introduces mesh shaders, which allow developers to bypass the traditional rasterizer and implement their own primitive processing logic. This flexibility is particularly useful for non-traditional rendering techniques such as voxelization or procedural geometry generation. The performance of a rasterizer is measured in terms of its fill rate, which is the number of pixels it can process per second. Fill rate depends on several factors, including the clock speed of the GPU, the number of rasterizer units, and the efficiency of the memory subsystem. Modern GPUs achieve fill rates in the billions of pixels per second, enabling real-time rendering of complex scenes. The fill rate can be approximated as:

$$\text{Fill Rate} = \text{Clock Speed} \times \text{Number of Rasterizer Units} \times \text{Pixels per Clock}$$

Rasterizers also face challenges related to power efficiency and thermal management. As GPUs scale to higher performance levels, the power consumption of the rasterizer and associated components becomes a limiting factor. Techniques such as dynamic voltage and frequency scaling (DVFS) are used to balance performance and power consumption. Additionally, modern GPUs employ power gating to disable unused rasterizer units during low-load scenarios. The evolution of rasterizers has been driven by advancements in GPU architecture and rendering algorithms. Early rasterizers were simple and limited in functionality, but modern designs incorporate sophisticated features such as:

**Early Z-testing:** Discards occluded fragments before shading, reducing unnecessary computation.

**Conservative Rasterization:** Ensures that all pixels touched by a primitive are included, useful for certain algorithms like shadow mapping.

**Variable Rate Shading:** Allows different regions of the screen to be rasterized at varying resolutions, improving performance. In summary, rasterizers are a critical component of modern GPU architectures, enabling the efficient conversion of geometric primitives into pixel fragments. Their design and implementation are closely tied to other GPU components such as ALUs, texture units, and memory subsystems. Advances in rasterization techniques

continue to push the boundaries of real-time graphics, enabling higher performance and better visual quality. The interplay between rasterizers and other GPU components underscores the importance of a holistic approach to GPU architecture design.

### 3.3.4 Memory subsystems

Modern GPU architectures are highly parallel computing systems designed to accelerate graphics rendering and general-purpose computation. Among their key components, memory subsystems play a critical role in determining performance by managing data movement between cores, texture units, rasterizers, and external memory. The memory hierarchy in GPUs is optimized for high bandwidth and low latency, enabling efficient execution of massively parallel workloads. The memory subsystems in GPUs consist of multiple levels, each serving distinct purposes:

**Register Files:** The fastest and smallest memory units, directly accessible by arithmetic logic units (ALUs). Each thread in a GPU warp or frontend has its own set of registers, minimizing access latency. For example, NVIDIA's Ampere architecture provides up to 255 registers per thread .

**Shared Memory:** A low-latency, software-managed cache shared among threads in the same thread block (CUDA) or workgroup (OpenCL). It enables efficient inter-thread communication and reduces global memory accesses. Shared memory is typically organized into banks, with conflicts arising when multiple threads access the same bank simultaneously .

**L1 and L2 Caches:** Hardware-managed caches that store frequently accessed data. L1 caches are often combined with shared memory, while L2 caches serve as a unified buffer for all streaming multiprocessors (SMs). AMD's RDNA 3 architecture, for instance, features a 128 KB L1 cache per compute unit and a unified 6 MB L2 cache .

**Global Memory:** The largest and slowest memory tier, typically implemented as GDDR6 or HBM2. It is accessible by all threads but requires careful access patterns to achieve peak bandwidth. Coalesced memory accesses, where threads in a warp access contiguous memory locations, are essential for optimal performance . Texture units and rasterizers interact closely with memory subsystems. Texture units fetch and filter texels from texture memory, which is cached in specialized texture caches to reduce latency. The texture cache hierarchy includes:

**Texture L1 Cache:** Per-SM cache storing recently accessed texture data.

**Texture L2 Cache:** Shared among SMs, reducing redundancy in texture fetches. Rasterizers generate fragments by interpolating vertex attributes, relying on memory subsystems for attribute fetching and interpolation. The depth and stencil tests performed during rasterization also depend on efficient memory access to z-buffer and stencil buffer data. The memory subsystem's performance is governed by bandwidth and latency metrics. Bandwidth is maximized through wide memory interfaces (e.g., 384-bit GDDR6 or 4096-bit HBM2) and high clock rates. Latency is mitigated via:

**Memory-Level Parallelism (MLP):** Overlapping memory requests to hide latency.

**Prefetching:** Predicting and fetching data before it is needed. The effective bandwidth  $b_{\text{eff}}$  can be modeled as:

$$b_{\text{eff}} = \frac{n_{\text{req}} \times s_{\text{req}}}{t_{\text{total}}}$$

where  $n_{\text{req}}$  is the number of requests,  $s_{\text{req}}$  is the request size, and  $t_{\text{total}}$  is the total time. Cores (ALUs) depend on memory subsystems for operand delivery. Modern GPUs employ SIMD (Single Instruction, Multiple Thread) execution, where threads in a warp execute the same instruction on different data. Memory access patterns significantly impact ALU utilization. For example, divergent memory accesses (where threads in a warp access non-contiguous locations) degrade performance due to serialized accesses . Memory subsystems also support atomic operations and synchronization primitives for parallel programming. Atomic operations (e.g., `atomicAdd`) are implemented using dedicated hardware units to ensure correctness across threads. The latency of atomic operations is influenced by contention and memory hierarchy:

$$t_{\text{atomic}} = t_{\text{base}} + c \times t_{\text{contention}}$$

where  $t_{\text{base}}$  is the base latency,  $c$  is the contention factor, and  $t_{\text{contention}}$  is the additional latency per contending thread. Cache coherence in GPU memory subsystems is typically relaxed to maximize throughput. While CPUs enforce strict coherence via protocols like MESI, GPUs often rely on programmer-managed coherence or scope-restricted models (e.g., NVIDIA's `__threadfence` intrinsics) . This trade-off reduces overhead but requires careful

synchronization in shared memory programming. Emerging GPU architectures integrate advanced memory technologies to address bandwidth bottlenecks. For instance, NVIDIA's Hopper architecture introduces **Distributed Shared Memory (DSM)**, allowing SMs to access remote shared memory segments with low latency . Similarly, AMD's CDNA 2 leverages **Infinity Cache**, a large last-level cache (128 MB) to reduce off-chip memory accesses . In summary, memory subsystems in modern GPUs are sophisticated hierarchies designed to feed data-hungry cores, texture units, and rasterizers. Their design balances bandwidth, latency, and coherence to sustain high throughput in parallel workloads. Future advancements will likely focus on 3D-stacked memory, near-memory computing, and tighter integration with compute units to further elevate performance.

## 3.4 Choosing the Complexity Level

### 3.4.1 Deciding on a minimal design

Modern GPU architectures balance performance, power efficiency, and area constraints by carefully selecting design complexity. A minimal design approach prioritizes essential functionality while avoiding unnecessary overhead. In rasterization-based pipelines, this involves optimizing the fixed-function stages while maintaining compatibility with industry standards like OpenGL or Vulkan. The trade-offs between complexity and efficiency are critical, particularly in mobile or embedded GPUs where power and area budgets are stringent.

One key consideration is the vertex processing stage. A minimal design might omit programmable tessellation or geometry shaders, relying instead on a basic vertex shader pipeline. This reduces control logic and register file requirements, as shown in . The vertex shader transforms input vertices using a 4x4 matrix multiplication:

$$\begin{bmatrix} x' \\ y' \\ z' \\ w' \end{bmatrix} = \begin{bmatrix} m_{00} & m_{01} & m_{02} & m_{03} \\ m_{10} & m_{11} & m_{12} & m_{13} \\ m_{20} & m_{21} & m_{22} & m_{23} \\ m_{30} & m_{31} & m_{32} & m_{33} \end{bmatrix} \begin{bmatrix} x \\ y \\ z \\ w \end{bmatrix}$$

Omitting tessellation reduces the need for complex subdivision logic, saving area and power.

The rasterization stage is another candidate for simplification. A minimal design might implement a basic scanline or tile-based rasterizer instead of a hierarchical depth-buffered approach. The rasterizer generates fragments by evaluating edge equations:

$$E_i(x, y) = (y - y_j)(x_i - x_j) - (x - x_j)(y_i - y_j)$$

where  $E_i(x, y) > 0$  indicates a fragment inside the triangle. Tile-based rasterization divides the screen into small tiles (e.g., 16×16 pixels) to improve locality, as discussed in .

Fragment shading can be simplified by limiting the number of texture units or omitting advanced features like programmable blending. A minimal pipeline might support only bilinear filtering and a single texture lookup per fragment:

Code Sample 3.8: Fragment shader with single texture lookup

```
void main() {
    vec4 color = texture2D(tex, uv);
    gl_FragColor = color * diffuse;
}
```

This reduces memory bandwidth and texture cache complexity compared to multi-texture or anisotropic filtering setups.

Memory hierarchy decisions also impact minimal design. A small, tightly coupled register file and L1 cache reduce access latency and power consumption. The register file size  $R$  can be estimated as:

$$R = N_{warps} \times N_{threads} \times N_{registers} \times W_{register}$$

where  $N_{warps}$  is the number of concurrent warps,  $N_{threads}$  is threads per warp,  $N_{registers}$  is registers per thread, and  $W_{register}$  is the register width. A minimal design might use 32 threads per warp and 16 registers per thread, as in .

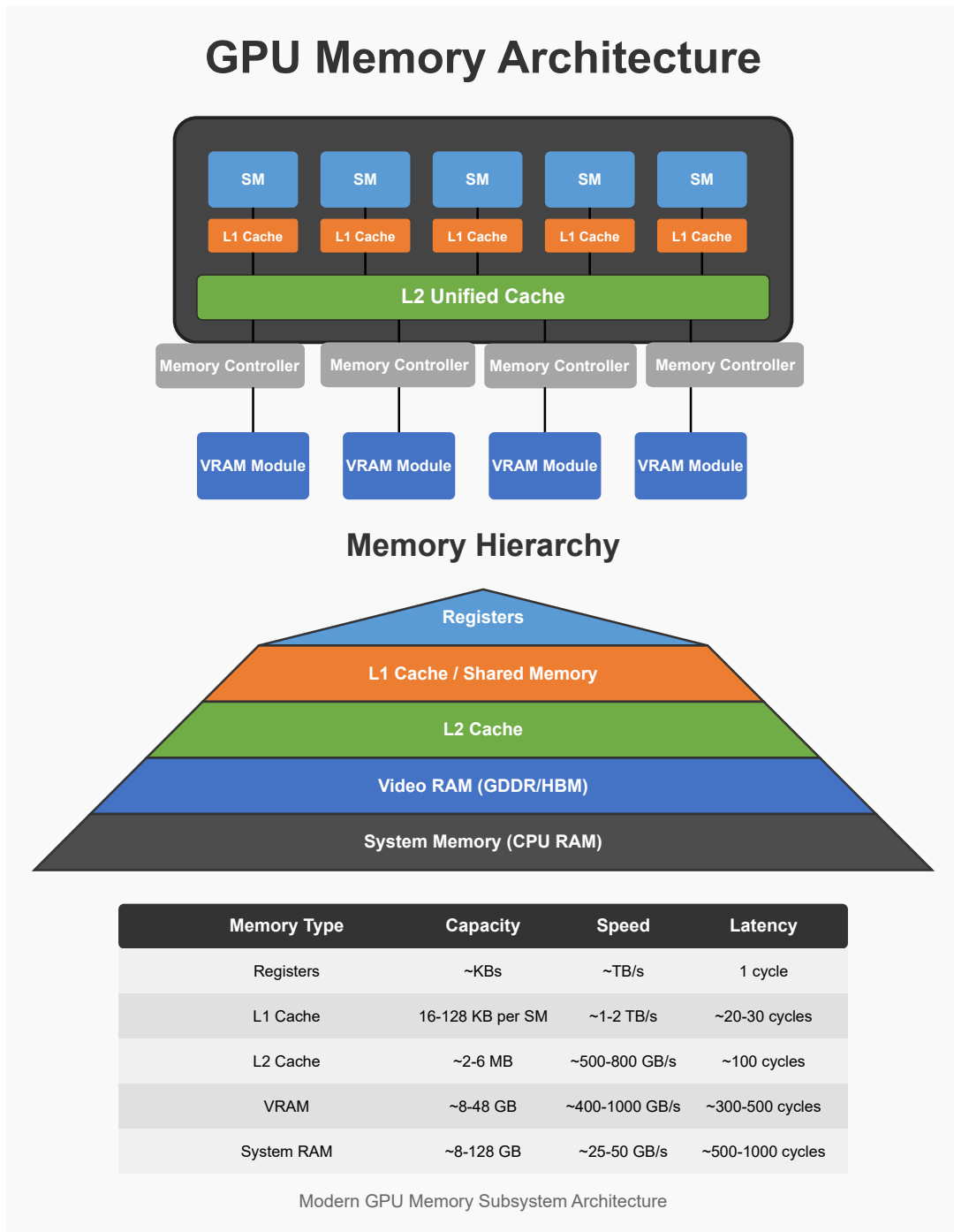
Fixed-function units like the depth test and color blending can be simplified. A minimal pipeline might implement a single-cycle Z-test without early Z optimizations, trading performance for area savings. The depth test condition is:

```
if (fragment_depth < depth_buffer[x][y]) then pass
```

Similarly, blending might support only basic operations like alpha blending:

$$C_{out} = \alpha C_{src} + (1 - \alpha) C_{dst}$$

Instruction set architecture (ISA) choices further influence complexity. A minimal GPU might use a scalar ISA instead of SIMD to simplify control logic, though this sacrifices throughput. The trade-off is analyzed in , where scalar threads with predicate masking reduce register pressure but increase instruction count.



Power gating and clock gating are essential for minimal designs. Unused pipeline stages or memory banks can be power-gated to reduce leakage. Clock gating is applied to idle arithmetic logic units (ALUs) or texture units. Dynamic voltage and frequency scaling (DVFS) further optimizes power, as explored in .

Synchronization overhead must be minimized. A basic design might use a single instruction multiple thread (SIMT) model with barrier synchronization only at kernel boundaries. Fine-grained synchronization requires additional scoreboarding logic, increasing complexity.

Error handling and robustness features can be simplified. A minimal GPU might omit hardware-level fault tolerance, relying on software checks instead. This reduces parity or ECC overhead in caches and memory controllers.

The following design considerations summarize the minimal approach: vertex processing should use a basic vertex shader without tessellation or geometry shaders; rasterization should rely on tile-based or scanline methods without hierarchical Z; fragment shading should include a single texture unit with bilinear filtering; the memory hierarchy should consist of a small register file and single-level cache; fixed-function units should implement only a simple depth test and basic blending; the ISA should be scalar or use narrow SIMD with limited predicate masking; power management should focus on coarse-grained power gating and DVFS; synchronization should occur only at the kernel level with no fine-grained mechanisms; and error handling should be software-managed without hardware ECC.

These choices align with mobile GPU designs like ARM Mali or Qualcomm Adreno, which prioritize efficiency over peak performance . The minimal design philosophy extends to area-constrained FPGAs or ASICs, where fixed-function units dominate programmable logic. Future work could explore hybrid designs combining minimal rasterization with programmable compute kernels, as hinted in . Balancing minimalism with functionality requires careful analysis of workload requirements. Graphics benchmarks like GFXBench or 3DMark provide empirical data for trade-off evaluation. The optimal design depends on the target market—whether mobile, embedded, or desktop—and the specific performance, power, and area constraints.

### 3.4.2 Illustrative design considerations

The design of modern GPU architectures involves critical trade-offs between complexity and performance, particularly when considering illustrative design choices. A fundamental consideration is the selection of an appropriate complexity level for the target application. High-complexity designs, such as those found in general-purpose GPUs (GPGPUs), prioritize flexibility and programmability but incur significant overhead in area and power consumption. Conversely, minimal designs, such as fixed-function rasterization pipelines, optimize for energy efficiency and throughput but sacrifice programmability. The choice between these extremes depends on the intended workload, with graphics rendering favoring fixed-function pipelines and compute workloads necessitating programmable architectures .

When deciding on a minimal design, architects must evaluate the trade-offs between hardware specialization and software flexibility. Fixed-function rasterization pipelines, for instance, are highly optimized for triangle processing but lack the generality of programmable shaders. The rasterization pipeline typically consists of the following stages:

**Vertex Processing:** Transforms 3D vertices into 2D screen space using matrix operations.

**Primitive Assembly:** Groups vertices into geometric primitives (e.g., triangles).

**Rasterization:** Converts primitives into fragments (potential pixels).

**Fragment Processing:** Computes color and depth for each fragment.

**Output Merging:** Resolves visibility and applies blending operations.

The efficiency of this pipeline stems from its deterministic dataflow, which eliminates the need for complex scheduling logic. However, its inflexibility limits its applicability to non-graphics workloads. Programmable designs, such as NVIDIA’s CUDA cores or AMD’s Compute Units, introduce additional complexity to support arbitrary parallelism but enable broader computational capabilities .

Illustrative design considerations for modern GPUs also include the granularity of parallelism. Coarse-grained parallelism, as seen in multi-core CPU designs, is insufficient for GPUs due to their reliance on massive thread-level parallelism. Instead, GPUs employ single-instruction multiple-thread (SIMT) execution, where thousands of threads execute the same instruction stream in lockstep. This approach maximizes throughput but requires careful management of divergent control flow, as branches can significantly degrade performance. The SIMT execution model is formalized as:

$$\text{Throughput} = \frac{\text{Number of threads}}{\text{Clock cycles}} \times \text{IPC}$$

where IPC (instructions per cycle) depends on the warp or wavefront scheduling efficiency.

Another critical consideration is memory hierarchy design. GPUs employ a tiered memory system to mitigate bandwidth bottlenecks, consisting of:

**Global Memory:** High-latency, high-bandwidth DRAM for bulk data storage.

**Shared Memory:** Low-latency scratchpad memory for inter-thread communication.

**Registers:** Fastest storage, dedicated to individual threads.

The effectiveness of this hierarchy is quantified by the arithmetic intensity  $A$ , defined as:

$$A = \frac{\text{Operations}}{\text{Byte transferred}}$$

High arithmetic intensity workloads (e.g., matrix multiplication) benefit from deep memory hierarchies, while low-intensity workloads (e.g., sparse data access) are memory-bound.

For basic rasterization-based pipelines, the design must prioritize triangle throughput and fill rate. The rasterization stage is particularly sensitive to algorithmic choices, with tile-based rasterization reducing memory bandwidth by processing screen-space tiles independently. The fragment processing stage often employs early depth testing to discard occluded fragments before shading, as described by:

$$\text{Fragment efficiency} = \frac{\text{Visible fragments}}{\text{Total fragments}}$$

Fixed-function hardware for texture filtering and blending further accelerates common graphics operations. However, these operations must be carefully balanced against area constraints. For example, bilinear texture filtering requires four texture fetches per fragment, which can be optimized using caching and prefetching techniques. The texture cache hit rate  $H$  is given by:

$$H = \frac{\text{Cache hits}}{\text{Total accesses}}$$

In contrast, programmable pipelines introduce configurable shader cores that execute arbitrary computation. These designs must address challenges such as load balancing, branch divergence, and memory coalescing. For instance, memory accesses are most efficient when threads within a warp access contiguous addresses, enabling coalesced transactions. The performance impact of uncoalesced accesses is modeled as:

$$\text{Effective bandwidth} = \text{Peak bandwidth} \times \text{Coalescing efficiency}$$

Power efficiency is another critical factor in GPU design. Modern architectures employ dynamic voltage and frequency scaling (DVFS) to adapt to workload demands. The power  $P$  consumed by a GPU is approximated by:

$$P = C \cdot V^2 \cdot f$$

where  $C$  is capacitance,  $V$  is voltage, and  $f$  is frequency. Reducing any of these parameters lowers power but may impact performance.

Finally, the choice between monolithic and modular GPU designs influences scalability and yield. Monolithic designs (e.g., high-end gaming GPUs) maximize performance but face manufacturing challenges due to large die sizes. Modular designs (e.g., AMD's Chiplet architecture) improve yield by integrating smaller chiplets but introduce inter-chiplet communication overhead. The trade-off is quantified by:

$$\text{Yield} = e^{-D \cdot A}$$

where  $D$  is defect density and  $A$  is die area.

In summary, illustrative design considerations for modern GPU architectures involve balancing complexity, parallelism, memory hierarchy, and power efficiency. Fixed-function rasterization pipelines excel in graphics workloads, while programmable designs cater to general-purpose computation. The optimal design depends on the target application's requirements and constraints.

### 3.4.3 Basic rasterization-based pipeline

The rasterization-based pipeline is a fundamental component of modern GPU architectures, serving as the primary method for converting geometric primitives into pixel fragments. This process involves several stages, each contributing to the efficient rendering of 3D scenes. The pipeline's design must balance complexity and performance, particularly when considering minimal implementations for specific applications. Below, we explore the key stages of the basic rasterization pipeline, design considerations for choosing complexity levels, and illustrative examples of minimal designs.

The rasterization pipeline begins with vertex processing, where vertices are transformed from object space to clip space using a series of matrix operations. The transformation is typically represented as:

$$\mathbf{v}_{\text{clip}} = \mathbf{M}_{\text{proj}} \cdot \mathbf{M}_{\text{view}} \cdot \mathbf{M}_{\text{model}} \cdot \mathbf{v}_{\text{object}}$$

Here,  $\mathbf{v}_{\text{object}}$  is the input vertex in object space, and  $\mathbf{M}_{\text{model}}$ ,  $\mathbf{M}_{\text{view}}$ , and  $\mathbf{M}_{\text{proj}}$  are the model, view, and projection matrices, respectively. The resulting  $\mathbf{v}_{\text{clip}}$  is then subjected to perspective division to obtain normalized device coordinates (NDC).

Following vertex processing, the pipeline proceeds to primitive assembly, where vertices are grouped into geometric primitives such as triangles. The rasterization stage then converts these primitives into fragments, which are potential pixels on the screen. This involves interpolating vertex attributes across the primitive's surface, a process known as attribute interpolation. For a triangle with vertices  $\mathbf{v}_0$ ,  $\mathbf{v}_1$ , and  $\mathbf{v}_2$ , the barycentric coordinates  $(\alpha, \beta, \gamma)$  are used to interpolate an attribute  $A$ :

$$A = \alpha A_0 + \beta A_1 + \gamma A_2$$

where  $A_0$ ,  $A_1$ , and  $A_2$  are the attribute values at the vertices.

The next stage is fragment processing, where each fragment undergoes shading and texturing. Modern GPUs employ programmable shaders, such as fragment shaders, to compute the final color of each fragment. A minimal fragment shader might implement simple Phong shading:

$$I = k_a + k_d(\mathbf{L} \cdot \mathbf{N}) + k_s(\mathbf{R} \cdot \mathbf{V})^n$$

Here,  $I$  is the resulting intensity,  $k_a$ ,  $k_d$ , and  $k_s$  are ambient, diffuse, and specular coefficients,  $\mathbf{L}$  is the light direction,  $\mathbf{N}$  is the surface normal,  $\mathbf{R}$  is the reflection vector, and  $\mathbf{V}$  is the view vector.

Depth testing is then performed to resolve visibility, ensuring that only the closest fragments are written to the framebuffer. The depth test compares the fragment's depth value  $z$  with the stored depth value  $z_{\text{stored}}$ :

if  $z < z_{\text{stored}}$ , then write fragment

This operation is critical for maintaining correct occlusion in 3D scenes.

When designing a minimal rasterization pipeline, several considerations must be addressed:

**Vertex Processing:** A minimal design might omit programmable vertex shaders, relying instead on fixed-function transformation hardware. This reduces flexibility but simplifies the design.

**Rasterization:** A basic rasterizer might use a scanline algorithm, which is simpler to implement but less efficient than modern tile-based approaches.

**Fragment Processing:** A minimal pipeline could limit shading to flat or Gouraud shading, avoiding the complexity of Phong or more advanced models.

**Memory Bandwidth:** Reducing the number of texture fetches or using lower precision data types can decrease bandwidth requirements.

An illustrative minimal design might exclude features such as:

Programmable shaders, opting for fixed-function pipelines.

Advanced texture filtering, using nearest-neighbor interpolation instead of bilinear or trilinear.

Multisampling anti-aliasing, relying solely on post-processing techniques if needed.

For example, a minimal rasterizer could be implemented in Verilog as follows:

Code Sample 3.9: Minimal Rasterizer

```
module rasterizer (
    input clk,
    input [31:0] v0_x, v0_y, v1_x, v1_y, v2_x, v2_y,
```

```

    output reg [31:0] frag_x, frag_y,
    output reg valid
);
// Bounding box calculation
wire [31:0] min_x = min(v0_x, min(v1_x, v2_x));
wire [31:0] max_x = max(v0_x, max(v1_x, v2_x));
wire [31:0] min_y = min(v0_y, min(v1_y, v2_y));
wire [31:0] max_y = max(v0_y, max(v1_y, v2_y));

// Scanline loop
always @(posedge clk) begin
    if (frag_y <= max_y) begin
        if (frag_x <= max_x) begin
            // Edge function test
            if (edge_function(v0, v1, frag_x, frag_y) >= 0 &&
                edge_function(v1, v2, frag_x, frag_y) >= 0 &&
                edge_function(v2, v0, frag_x, frag_y) >= 0) begin
                valid <= 1;
            end else begin
                valid <= 0;
            end
            frag_x <= frag_x + 1;
        end else begin
            frag_x <= min_x;
            frag_y <= frag_y + 1;
        end
    end
end
endmodule

```

The choice of complexity level in a rasterization pipeline depends on the target application. For embedded systems or low-power devices, a minimal design may suffice, while high-performance GPUs require more sophisticated features. Key trade-offs include:

**Performance vs. Power:** Advanced features like programmable shaders increase performance but also power consumption.

**Flexibility vs. Area:** Programmable pipelines offer greater flexibility but require more silicon area.

**Quality vs. Speed:** Higher-quality rendering techniques, such as multisampling, improve visual fidelity at the cost of reduced frame rates.

In summary, the basic rasterization-based pipeline is a cornerstone of modern GPU architectures, with its design heavily influenced by the desired complexity level. Minimal designs prioritize simplicity and efficiency, while more advanced implementations leverage programmable stages and sophisticated algorithms to deliver higher performance and visual quality. The trade-offs between these approaches must be carefully considered to meet the requirements of the target application.

## Chapter 4

# Fundamentals of 3D Graphics Pipeline

### 4.1 3D Geometry Basics

#### 4.1.1 Vertices and primitives (triangles, lines)

Modern GPU architectures are designed to efficiently process 3D geometry by leveraging vertices and primitives such as triangles and lines. These elements form the foundation of rasterization and rendering pipelines, enabling the transformation of mathematical representations into visual outputs. The GPU's parallel processing capabilities are optimized for handling large numbers of vertices and primitives simultaneously, making them indispensable for real-time graphics applications.

Vertices are the fundamental building blocks of 3D geometry, representing points in space with attributes such as position, color, and texture coordinates. In GPU pipelines, vertices are processed by vertex shaders, which perform per-vertex operations like transformations and lighting calculations. The vertex shader outputs are then assembled into primitives, typically triangles or lines, which are the simplest polygons that can define a 3D surface. Triangles are preferred due to their geometric simplicity and guaranteed planarity, ensuring consistent rendering behavior. Lines are used for wireframe representations or procedural geometry.

The assembly of vertices into primitives is governed by the following equation for a triangle:

$$\mathbf{T} = \{\mathbf{v}_0, \mathbf{v}_1, \mathbf{v}_2\}$$

where  $\mathbf{v}_i$  denotes the vertices. The GPU's primitive assembly stage groups vertices according to topology specifications, such as triangle lists, strips, or fans. This stage is critical for minimizing redundancy and optimizing memory bandwidth, as shared vertices in strips or fans reduce the number of vertex shader invocations.

Transformations are applied to vertices to convert them from model space to screen space. The model-view-projection (MVP) matrix is a composite transformation that includes model transformation (converts vertices from object space to world space), view transformation (aligns the world space with the camera's perspective), and projection transformation (maps the 3D scene onto a 2D viewport). The MVP transformation is expressed as:

$$\mathbf{v}_{\text{screen}} = \mathbf{P} \cdot \mathbf{V} \cdot \mathbf{M} \cdot \mathbf{v}_{\text{model}}$$

where  $\mathbf{P}$ ,  $\mathbf{V}$ , and  $\mathbf{M}$  are the projection, view, and model matrices, respectively. Homogeneous coordinates are used to represent these transformations, enabling efficient matrix concatenation and perspective division. The perspective projection matrix, for instance, is defined as:

$$\mathbf{P} = \begin{bmatrix} \frac{2n}{r-l} & 0 & \frac{r+l}{r-l} & 0 \\ 0 & \frac{2n}{t-b} & \frac{t+b}{t-b} & 0 \\ 0 & 0 & -\frac{f+n}{f-n} & -\frac{2fn}{f-n} \\ 0 & 0 & -1 & 0 \end{bmatrix}$$

where  $n$ ,  $f$ ,  $l$ ,  $r$ ,  $t$ , and  $b$  define the near and far planes and the view frustum's bounds. After projection, vertices are clipped to the view frustum, and their coordinates are normalized to the range  $[-1, 1]$  for the viewport transformation.

The rasterization stage converts primitives into fragments, which are potential pixels in the framebuffer. This process involves interpolating vertex attributes across the primitive's surface using barycentric coordinates for triangles. For a triangle with vertices  $\mathbf{v}_0$ ,  $\mathbf{v}_1$ , and  $\mathbf{v}_2$ , a point  $\mathbf{p}$  inside the triangle can be expressed as:

$$\mathbf{p} = \alpha\mathbf{v}_0 + \beta\mathbf{v}_1 + \gamma\mathbf{v}_2$$

where  $\alpha + \beta + \gamma = 1$ . The GPU computes these coefficients to interpolate attributes like texture coordinates and normals, ensuring smooth shading and texture mapping.

Modern GPUs employ parallel architectures to process vertices and primitives efficiently. For example, NVIDIA's Turing architecture features dedicated hardware for mesh shading, which allows for dynamic subdivision and culling of primitives before rasterization. Similarly, AMD's RDNA 2 architecture leverages primitive shaders to optimize geometry processing. These advancements reduce the computational load by discarding invisible primitives early in the pipeline, a technique known as occlusion culling.

The following Verilog-like pseudocode illustrates a simplified vertex shader pipeline:

Code Sample 4.1: Vertex Shader Pipeline

```
module vertex_shader (
    input [31:0] vertex_in,
    input [31:0] mvp_matrix[16],
    output [31:0] vertex_out
);
reg [31:0] temp;
always @(*) begin
    temp = mvp_matrix[0] * vertex_in.x +
        mvp_matrix[4] * vertex_in.y +
        mvp_matrix[8] * vertex_in.z +
        mvp_matrix[12];
    vertex_out.x = temp / vertex_in.w;
    // Repeat for y, z, and w components
end
endmodule
```

Lines are processed similarly but with different rasterization rules. A line between two vertices  $\mathbf{v}_0$  and  $\mathbf{v}_1$  is defined by the parametric equation:

$$\mathbf{L}(t) = \mathbf{v}_0 + t(\mathbf{v}_1 - \mathbf{v}_0)$$

where  $t \in [0, 1]$ . The GPU determines which pixels are covered by the line using algorithms like Bresenham's, ensuring accurate and efficient rendering.

In summary, vertices and primitives are the core elements of 3D geometry processing in modern GPUs. Transformations and projections map these elements to screen space, while rasterization converts them into fragments for display. Advances in GPU architecture continue to optimize these processes, enabling real-time rendering of complex scenes with millions of primitives. For further reading, consult and .

### 4.1.2 Transformations

Modern GPU architectures are designed to accelerate the processing of 3D geometry, particularly through transformations of vertices and primitives. The foundation of 3D graphics relies on vertices, which are points in 3D space defined by coordinates  $(x, y, z)$ . These vertices are grouped into primitives, such as triangles or lines, which form the basic building blocks of 3D models. Transformations are mathematical operations applied to these vertices to manipulate their position, orientation, and scale within a 3D scene. The GPU pipeline processes these transformations efficiently through specialized hardware units, enabling real-time rendering of complex scenes.

Vertices are transformed using a series of linear algebraic operations represented by matrices. The primary transformations include translation, rotation, and scaling. A vertex  $\mathbf{v} = [x, y, z, 1]^T$  in homogeneous coordinates is transformed by a  $4 \times 4$  matrix  $\mathbf{M}$  as follows:

$$\mathbf{v}' = \mathbf{M}\mathbf{v}$$

where  $\mathbf{M}$  combines multiple transformations into a single matrix. For example, a translation by vector  $\mathbf{t} = [t_x, t_y, t_z]^T$  is represented by:

$$\mathbf{T} = \begin{bmatrix} 1 & 0 & 0 & t_x \\ 0 & 1 & 0 & t_y \\ 0 & 0 & 1 & t_z \\ 0 & 0 & 0 & 1 \end{bmatrix}$$

Similarly, a scaling matrix  $\mathbf{S}$  scales vertices by factors  $s_x$ ,  $s_y$ , and  $s_z$  along the respective axes:

$$\mathbf{S} = \begin{bmatrix} s_x & 0 & 0 & 0 \\ 0 & s_y & 0 & 0 \\ 0 & 0 & s_z & 0 \\ 0 & 0 & 0 & 1 \end{bmatrix}$$

Rotation matrices are more complex, requiring trigonometric functions. For instance, a rotation by angle  $\theta$  around the  $z$ -axis is given by:

$$\mathbf{R}_z = \begin{bmatrix} \cos \theta & -\sin \theta & 0 & 0 \\ \sin \theta & \cos \theta & 0 & 0 \\ 0 & 0 & 1 & 0 \\ 0 & 0 & 0 & 1 \end{bmatrix}$$

Modern GPUs optimize these transformations through parallel processing. Vertex shaders, programmable units in the GPU, apply transformation matrices to vertices independently, leveraging SIMD (Single Instruction, Multiple Data) architectures. The following pseudocode illustrates a vertex shader applying a transformation:

#### Code Sample 4.2: Vertex Shader Pseudocode

```
void vertex_shader(in vec3 position, in mat4 modelViewProjection, out vec4 gl_Position) {
    gl_Position = modelViewProjection * vec4(position, 1.0);
}
```

After transformations, vertices are assembled into primitives. Triangles are the most common primitive due to their geometric simplicity and guaranteed planarity. The GPU rasterizes these primitives into fragments, which are then shaded and output to the framebuffer. The assembly process is hardware-accelerated, with dedicated units handling primitive setup and edge equations.

Projection is another critical transformation, mapping 3D coordinates to 2D screen space. The perspective projection matrix  $\mathbf{P}$  simulates the effect of a camera lens, incorporating a field of view  $\alpha$ , aspect ratio  $r$ , and near/far clipping planes  $n$  and  $f$ :

$$\mathbf{P} = \begin{bmatrix} \frac{1}{r \tan(\alpha/2)} & 0 & 0 & 0 \\ 0 & \frac{1}{\tan(\alpha/2)} & 0 & 0 \\ 0 & 0 & \frac{f+n}{n-f} & \frac{2fn}{n-f} \\ 0 & 0 & -1 & 0 \end{bmatrix}$$

This matrix ensures that objects farther from the camera appear smaller, creating a realistic depth effect. The transformed vertex  $\mathbf{v}'$  is then normalized by its  $w$ -component to obtain clip-space coordinates:

$$\mathbf{v}_{\text{clip}} = \left[ \frac{x'}{w'}, \frac{y'}{w'}, \frac{z'}{w'} \right]^T$$

GPUs further optimize projection through viewport transformation, mapping clip-space coordinates to screen-space pixels. The viewport matrix  $\mathbf{V}$  scales and translates coordinates to fit the display resolution:

$$\mathbf{V} = \begin{bmatrix} \frac{w}{2} & 0 & 0 & \frac{w}{2} \\ 0 & \frac{h}{2} & 0 & \frac{h}{2} \\ 0 & 0 & 1 & 0 \\ 0 & 0 & 0 & 1 \end{bmatrix}$$

where  $w$  and  $h$  are the screen width and height, respectively.

The efficiency of these transformations is critical for real-time rendering. Modern GPUs employ fixed-function units for matrix multiplication and interpolation, reducing latency. For example, NVIDIA's Turing architecture includes dedicated tensor cores for accelerated matrix operations. Similarly, AMD's RDNA2 architecture leverages infinity cache to reduce memory bandwidth during vertex processing.

Transformations also play a role in advanced rendering techniques. For instance, instancing applies the same transformation to multiple primitives, reducing CPU-GPU communication. The following Verilog-like code demonstrates instancing in a hardware description:

#### Code Sample 4.3: Instancing in Hardware

```
module vertex_transform (
    input [3:0][3:0] matrix,
    input [3:0] vertex,
    output [3:0] transformed
);
assign transformed = matrix * vertex;
endmodule
```

In summary, transformations are fundamental to 3D graphics, enabling the manipulation and projection of vertices and primitives. Modern GPU architectures optimize these operations through parallel processing, fixed-function units, and advanced memory hierarchies. The mathematical foundations, combined with hardware acceleration, allow for real-time rendering of complex scenes, as evidenced by contemporary GPU designs. The interplay between vertices, transformations, and projection forms the backbone of 3D graphics pipelines, driving advancements in gaming, simulation, and visualization.

### 4.1.3 Projection

Projection is a fundamental concept in modern GPU architecture, particularly in the context of 3D geometry rendering. It involves transforming 3D vertices into 2D screen space, enabling the visualization of complex scenes. This process is critical for rasterization, where primitives such as triangles and lines are mapped to pixels. The mathematical foundations of projection are rooted in linear algebra and homogeneous coordinates, which allow for efficient transformations and perspective corrections.

The transformation pipeline in modern GPUs consists of several stages, with projection being one of the final steps. Vertices are first defined in object space and then transformed into world space using model transformations. These vertices are further transformed into view space via the view matrix, which aligns the scene with the camera's perspective. The projection matrix then maps these vertices into clip space, where they are normalized and clipped to the view frustum. The perspective division converts homogeneous coordinates back to Cartesian coordinates, yielding normalized device coordinates (NDC). Finally, the viewport transformation maps NDC to screen space.

The projection matrix is derived from the view frustum, which defines the visible region of the scene. For perspective projection, the frustum is a truncated pyramid, while orthographic projection uses a rectangular prism. The perspective projection matrix is given by:

$$P = \begin{bmatrix} \frac{2n}{r-l} & 0 & \frac{r+l}{r-l} & 0 \\ 0 & \frac{2n}{t-b} & \frac{t+b}{t-b} & 0 \\ 0 & 0 & -\frac{f+n}{f-n} & -\frac{2fn}{f-n} \\ 0 & 0 & -1 & 0 \end{bmatrix}$$

where  $n$  and  $f$  are the near and far planes, and  $l, r, t$ , and  $b$  define the frustum's bounds.

Orthographic projection, on the other hand, is represented by:

$$O = \begin{bmatrix} \frac{2}{r-l} & 0 & 0 & -\frac{r+l}{r-l} \\ 0 & \frac{2}{t-b} & 0 & -\frac{t+b}{t-b} \\ 0 & 0 & -\frac{2}{f-n} & -\frac{f+n}{f-n} \\ 0 & 0 & 0 & 1 \end{bmatrix}$$

Modern GPUs optimize projection calculations using hardware-accelerated matrix operations. Vertex shaders compute the transformation of vertices, while the fixed-function pipeline handles perspective division and clipping.

The following Verilog-like pseudocode illustrates a simplified vertex shader operation:

#### Code Sample 4.4: Vertex Shader Pseudocode

```
module vertex_shader (
    input vec4 vertex,
    input mat4 model_view_proj,
    output vec4 clip_pos
);
assign clip_pos = model_view_proj * vertex;
endmodule
```

Projection also plays a crucial role in primitive assembly, where vertices are grouped into triangles or lines. The GPU's geometry pipeline ensures that primitives are correctly clipped to the view frustum, discarding invisible fragments. Clipping is performed in homogeneous clip space using the Sutherland-Hodgman algorithm, which iteratively clips polygons against the frustum planes. The clipped primitives are then rasterized into fragments, each representing a potential pixel.

The perspective correction of attributes such as texture coordinates and normals is another critical aspect of projection. Interpolating these attributes in screen space without correction leads to visual artifacts. The GPU corrects for perspective using the reciprocal of the homogeneous coordinate  $w$ , as shown in:

$$\text{attribute}_{\text{corrected}} = \frac{\text{attribute}}{w}$$

Modern GPUs leverage parallel processing to handle millions of vertices and primitives efficiently. Key optimizations include vertex caching (to reuse transformed vertices and avoid redundant computations), primitive culling (to discard back-facing or occluded primitives early), and level of detail (LOD) techniques (to adjust geometric complexity based on distance from the camera).

Projection is also integral to shadow mapping and environment mapping techniques. Shadow mapping involves rendering the scene from the light's perspective, storing depth values in a texture. The projected texture coordinates are then used during the main rendering pass to determine visibility. Environment mapping projects the scene onto a cube or sphere, simulating reflections and refractions.

The mathematics of projection extends to advanced rendering techniques such as ray tracing and voxelization. Ray tracing computes intersections between rays and geometry, requiring efficient projection of rays into the scene. Voxelization discretizes 3D space into a grid, with projection used to determine voxel occupancy. These techniques are increasingly supported by modern GPUs through dedicated hardware such as NVIDIA's RT cores.

The performance of projection operations is measured in terms of throughput and latency. GPUs achieve high throughput by processing vertices in parallel across multiple shader cores. Latency is minimized through pipelining, where each stage of the transformation pipeline operates concurrently. The following equation estimates the throughput  $T$  of a GPU:

$$T = N \times f \times C$$

where  $N$  is the number of shader cores,  $f$  is the clock frequency, and  $C$  is the average number of vertices processed per cycle.

In summary, projection is a cornerstone of modern GPU architecture, enabling the efficient rendering of 3D scenes. Its mathematical foundations, hardware optimizations, and integration into the graphics pipeline are well-documented in literature such as and . The continued evolution of GPU technology ensures that projection remains a critical component of real-time graphics, virtual reality, and scientific visualization.

## 4.2 The 3D-to-2D Mapping

### 4.2.1 Model matrix

The model matrix is a fundamental transformation matrix in computer graphics, particularly within the context of modern GPU architectures. It defines how an object's vertices are positioned, rotated, and scaled in the world coordinate system. Given a vertex  $\mathbf{v}$  in model space, its world-space position  $\mathbf{v}'$  is computed as:

$$\mathbf{v}' = \mathbf{M}_{\text{model}} \cdot \mathbf{v}$$

where  $\mathbf{M}_{\text{model}}$  is the model matrix, typically a  $4 \times 4$  homogeneous transformation matrix. This matrix is constructed by concatenating translation, rotation, and scaling operations, which are efficiently processed by modern GPUs due to their parallel architecture. The view matrix,  $\mathbf{M}_{\text{view}}$ , transforms world-space coordinates into camera-space coordinates. It represents the camera's position and orientation relative to the world. The transformation is given by:

$$\mathbf{v}'' = \mathbf{M}_{\text{view}} \cdot \mathbf{v}'$$

The view matrix is often derived from the camera's look-at direction, up vector, and position. Modern GPUs optimize this computation using specialized hardware units for matrix multiplication, such as tensor cores in NVIDIA architectures. The projection matrix,  $\mathbf{M}_{\text{proj}}$ , maps camera-space coordinates to clip-space coordinates. This matrix is responsible for perspective or orthographic projection, which emulates how 3D objects are projected onto a 2D viewport. For perspective projection, the matrix is:

$$\mathbf{M}_{\text{proj}} = \begin{bmatrix} \frac{2n}{r-l} & 0 & \frac{r+l}{r-l} & 0 \\ 0 & \frac{2n}{t-b} & \frac{t+b}{t-b} & 0 \\ 0 & 0 & -\frac{f+n}{f-n} & -\frac{2fn}{f-n} \\ 0 & 0 & -1 & 0 \end{bmatrix}$$

where  $n$ ,  $f$ ,  $l$ ,  $r$ ,  $t$ , and  $b$  represent the near, far, left, right, top, and bottom clipping planes, respectively. Orthographic projection uses a simpler matrix:

$$\mathbf{M}_{\text{ortho}} = \begin{bmatrix} \frac{2}{r-l} & 0 & 0 & -\frac{r+l}{r-l} \\ 0 & \frac{2}{t-b} & 0 & -\frac{t+b}{t-b} \\ 0 & 0 & -\frac{2}{f-n} & -\frac{f+n}{f-n} \\ 0 & 0 & 0 & 1 \end{bmatrix}$$

Clipping is the process of discarding vertices and primitives that lie outside the view frustum. Modern GPUs perform clipping in homogeneous clip space, where the conditions for a vertex  $\mathbf{v} = (x, y, z, w)$  to be inside the frustum are:

$$-w \leq x \leq w, \quad -w \leq y \leq w, \quad -w \leq z \leq w$$

Clipping is hardware-accelerated in GPUs, with dedicated fixed-function units handling the computations efficiently. Viewport transformation maps clip-space coordinates to screen-space coordinates. The transformation involves scaling and translating the normalized device coordinates (NDC) to the viewport dimensions. Given a viewport with width  $W$ , height  $H$ , and origin  $(X, Y)$ , the transformation is:

$$\begin{aligned} x_{\text{screen}} &= X + \frac{W}{2}(x_{\text{ndc}} + 1) \\ y_{\text{screen}} &= Y + \frac{H}{2}(y_{\text{ndc}} + 1) \\ z_{\text{screen}} &= \frac{z_{\text{ndc}} + 1}{2} \end{aligned}$$

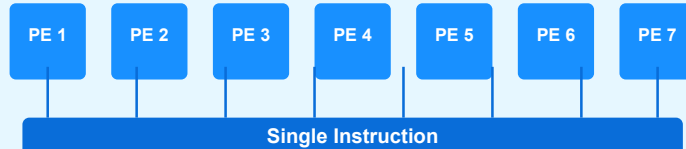
This step is critical for rasterization, where fragments are generated for pixels covered by the projected primitives. Modern GPU architectures optimize these transformations through parallel execution. For example, the model, view, and projection matrices are often combined into a single matrix  $\mathbf{M}_{\text{mvp}}$ :

$$\mathbf{M}_{\text{mvp}} = \mathbf{M}_{\text{proj}} \cdot \mathbf{M}_{\text{view}} \cdot \mathbf{M}_{\text{model}}$$

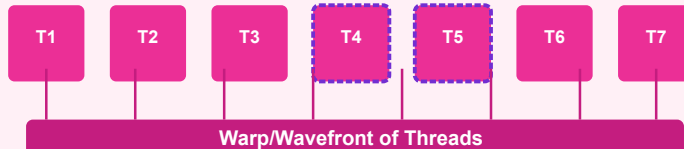
This reduces the number of matrix multiplications required per vertex, leveraging the GPU's SIMD (Single Instruction, Multiple Data) capabilities. The combined matrix is computed once per object and reused for all its vertices, minimizing redundant computations. The 3D-to-2D mapping pipeline in GPUs involves the following stages:

## GPU Execution Models

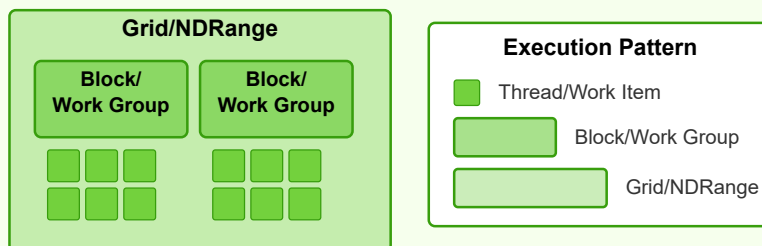
### SIMD (Single Instruction, Multiple Data)



### SIMT (Single Instruction, Multiple Threads)



### Thread Hierarchy in CUDA/OpenCL



### Key Differences Characteristics

- SIMD: Fixed parallel data lanes, lockstep execution, utilized in vector processors
- SIMT: Thread divergence handling (predication/masking), flexible programming model
- Warps/Wavefronts: Thread groups (typically 32/64 threads) executed together

**Model Transformation:** Vertices are transformed from model space to world space using  $\mathbf{M}_{\text{model}}$ .

**View Transformation:** Vertices are transformed from world space to camera space using  $\mathbf{M}_{\text{view}}$ .

**Projection Transformation:** Vertices are transformed from camera space to clip space using  $\mathbf{M}_{\text{proj}}$ .

**Clipping:** Primitives are clipped against the view frustum in clip space.

**Viewport Transformation:** Clipped vertices are mapped to screen space for rasterization. GPUs use specialized hardware for these stages, such as vertex shaders for transformations and rasterizers for viewport mapping. The efficiency of these operations is critical for real-time rendering, where millions of vertices are processed per frame. For instance, NVIDIA's Turing architecture introduces mesh shaders, which further optimize the transformation pipeline by processing primitives in parallel. The model matrix also plays a role in lighting calculations. Surface normals must be transformed from model space to world space using the inverse transpose of the model matrix:

$$\mathbf{n}' = (\mathbf{M}_{\text{model}}^{-1})^T \cdot \mathbf{n}$$

This ensures correct lighting interactions, as normals must remain orthogonal to surfaces after transformation. GPUs optimize this computation by co-issuing matrix operations with other shader instructions. In summary, the model matrix is a cornerstone of the 3D-to-2D mapping pipeline in modern GPU architectures. Its interaction with the view and projection matrices, combined with clipping and viewport transformations, enables efficient rendering of complex scenes. Hardware advancements continue to optimize these operations, ensuring real-time performance for increasingly detailed graphics.

#### 4.2.2 View matrix

The transformation of 3D objects into 2D screen space is a fundamental process in computer graphics, particularly in modern GPU architectures. This transformation involves several stages, including the application of the model matrix, view matrix, projection matrix, clipping, and viewport transformations. Each of these stages plays a critical role in determining how 3D objects are rendered on a 2D display.

The model matrix is responsible for transforming object coordinates from local space to world space. It includes operations such as translation, rotation, and scaling, which define the position, orientation, and size of an object within the 3D world. The model matrix is typically represented as a 4x4 homogeneous transformation matrix. For example, a translation by a vector  $\mathbf{t} = (t_x, t_y, t_z)$  is represented as:

$$\mathbf{T} = \begin{bmatrix} 1 & 0 & 0 & t_x \\ 0 & 1 & 0 & t_y \\ 0 & 0 & 1 & t_z \\ 0 & 0 & 0 & 1 \end{bmatrix}$$

Similarly, rotation and scaling matrices are constructed to perform their respective transformations.

The view matrix transforms world coordinates into camera space, aligning the scene relative to the viewer's perspective. This matrix is derived from the camera's position, orientation, and up vector. The view matrix is computed as the inverse of the camera's transformation matrix. If the camera is positioned at  $\mathbf{c}$  and oriented along the direction  $\mathbf{d}$ , the view matrix  $\mathbf{V}$  is:

$$\mathbf{V} = \begin{bmatrix} \mathbf{r}_x & \mathbf{u}_x & -\mathbf{d}_x & -\mathbf{c} \cdot \mathbf{r} \\ \mathbf{r}_y & \mathbf{u}_y & -\mathbf{d}_y & -\mathbf{c} \cdot \mathbf{u} \\ \mathbf{r}_z & \mathbf{u}_z & -\mathbf{d}_z & -\mathbf{c} \cdot \mathbf{d} \\ 0 & 0 & 0 & 1 \end{bmatrix}$$

Here,  $\mathbf{r}$  is the right vector,  $\mathbf{u}$  is the up vector, and  $\mathbf{d}$  is the direction vector of the camera.

The projection matrix maps camera-space coordinates to clip space, which is a normalized coordinate system where visible objects lie within the range  $[-1, 1]$  along each axis. Two common types of projection matrices are orthographic and perspective. The perspective projection matrix, for instance, is defined as:

$$\mathbf{P} = \begin{bmatrix} \frac{2n}{r-l} & 0 & \frac{r+l}{r-l} & 0 \\ 0 & \frac{2n}{t-b} & \frac{t+b}{t-b} & 0 \\ 0 & 0 & -\frac{f+n}{f-n} & -\frac{2fn}{f-n} \\ 0 & 0 & -1 & 0 \end{bmatrix}$$

where  $n$  and  $f$  are the near and far clipping planes, and  $l, r, t$ , and  $b$  define the viewing frustum.

Clipping is the process of discarding geometry that lies outside the view frustum. Modern GPUs perform clipping in homogeneous clip space, where primitives are tested against the six planes of the frustum. The Sutherland-Hodgman algorithm is often used for polygon clipping, though GPUs implement optimized hardware versions of this process. Clipping ensures that only visible portions of objects are processed further, improving performance and correctness.

The viewport transformation converts clip-space coordinates to screen-space coordinates. This involves scaling and translating the normalized device coordinates (NDC) to fit the dimensions of the viewport. The transformation is given by:

$$\begin{bmatrix} x_{\text{screen}} \\ y_{\text{screen}} \\ z_{\text{screen}} \end{bmatrix} = \begin{bmatrix} \frac{w}{2} & 0 & 0 & \frac{w}{2} + x \\ 0 & \frac{h}{2} & 0 & \frac{h}{2} + y \\ 0 & 0 & \frac{f-n}{2} & \frac{f+n}{2} \end{bmatrix} \begin{bmatrix} x_{\text{ndc}} \\ y_{\text{ndc}} \\ z_{\text{ndc}} \\ 1 \end{bmatrix}$$

where  $w$  and  $h$  are the width and height of the viewport, and  $x$  and  $y$  are the viewport's origin coordinates.

Modern GPU architectures optimize these transformations through parallel processing and hardware acceleration. For example, vertex shaders compute the model-view-projection (MVP) matrix multiplication per vertex, while rasterization and fragment shading handle the remaining stages. The following pseudocode illustrates a typical vertex shader implementation:

Code Sample 4.5: Vertex Shader for MVP Transformation

```
#version 460 core
layout(location = 0) in vec3 aPos;

uniform mat4 model;
uniform mat4 view;
uniform mat4 projection;

void main() {
    gl_Position = projection * view * model * vec4(aPos, 1.0);
}
```

The efficiency of these transformations is critical for real-time rendering. Research has shown that optimizing matrix operations and minimizing redundant calculations can significantly improve performance. For instance, concatenating the model, view, and projection matrices into a single MVP matrix reduces the number of matrix multiplications per vertex. Additionally, modern GPUs leverage SIMD (Single Instruction, Multiple Data) architectures to process multiple vertices in parallel, further accelerating the transformation pipeline.

The view matrix, in particular, is essential for interactive applications where the camera moves frequently. Techniques such as inverse kinematics and quaternion-based rotations are often used to compute the view matrix efficiently. The view matrix must be recalculated whenever the camera's position or orientation changes, making its optimization a priority in real-time systems.

In summary, the transformation pipeline from 3D to 2D involves a series of matrix operations and geometric tests, each contributing to the accurate and efficient rendering of 3D scenes. Modern GPU architectures are designed to handle these transformations with high throughput, enabling complex graphics applications to run in real time. The interplay between the model, view, and projection matrices, along with clipping and viewport transformations, forms the backbone of 3D graphics rendering.

### 4.2.3 Projection matrix

In modern GPU architecture, the projection matrix plays a fundamental role in transforming 3D scene coordinates into 2D screen space, enabling realistic rendering of three-dimensional objects on two-dimensional displays. This transformation is part of a pipeline involving several matrices and operations, including the model matrix, view matrix, projection matrix, clipping, and viewport transformations. Each stage contributes to the accurate mapping of vertices from world space to screen space.

The model matrix transforms vertices from object space to world space. It incorporates translations, rotations, and scaling operations applied to individual objects. For a vertex  $\mathbf{v}$  in object space, the model matrix  $\mathbf{M}$  computes its world-space position  $\mathbf{v}'$  as:

$$\mathbf{v}' = \mathbf{M} \cdot \mathbf{v}$$

The view matrix then converts world-space coordinates into camera-relative coordinates. This matrix,  $\mathbf{V}$ , represents the camera's position and orientation. The transformation is given by:

$$\mathbf{v}'' = \mathbf{V} \cdot \mathbf{v}'$$

The projection matrix  $\mathbf{P}$  further transforms these coordinates into clip space, a normalized coordinate system where vertices outside a specified range are clipped. The projection matrix can be either orthographic or perspective, with the latter introducing foreshortening effects to simulate depth perception. For perspective projection, the matrix is defined as:

$$\mathbf{P} = \begin{bmatrix} \frac{2n}{r-l} & 0 & \frac{r+l}{r-l} & 0 \\ 0 & \frac{2n}{t-b} & \frac{t+b}{t-b} & 0 \\ 0 & 0 & -\frac{f+n}{f-n} & -\frac{2fn}{f-n} \\ 0 & 0 & -1 & 0 \end{bmatrix}$$

Here,  $n$  and  $f$  are the near and far clipping planes, while  $l$ ,  $r$ ,  $t$ , and  $b$  define the viewing frustum's bounds. The resulting clip-space coordinates  $\mathbf{v}'''$  are computed as:

$$\mathbf{v}''' = \mathbf{P} \cdot \mathbf{v}''$$

Clipping is performed in clip space to discard vertices outside the viewable volume. The clipping region is typically defined by the inequalities  $-w \leq x \leq w$ ,  $-w \leq y \leq w$ , and  $-w \leq z \leq w$ , where  $w$  is the homogeneous coordinate. Modern GPUs optimize this process using hardware-accelerated clipping algorithms, as described in .

The clipped vertices are then normalized by dividing by  $w$ , yielding normalized device coordinates (NDC):

$$\mathbf{v}_{ndc} = \left( \frac{x}{w}, \frac{y}{w}, \frac{z}{w} \right)$$

The final stage is the viewport transformation, which maps NDC to screen-space coordinates. This involves scaling and translating the  $x$  and  $y$  coordinates to fit the display resolution, while the  $z$ -coordinate is often used for depth testing. The viewport transformation is defined as:

$$\begin{cases} x_{screen} = \frac{width}{2}x_{ndc} + \frac{width}{2} + x_{offset} \\ y_{screen} = \frac{height}{2}y_{ndc} + \frac{height}{2} + y_{offset} \\ z_{screen} = \frac{f-n}{2}z_{ndc} + \frac{f+n}{2} \end{cases}$$

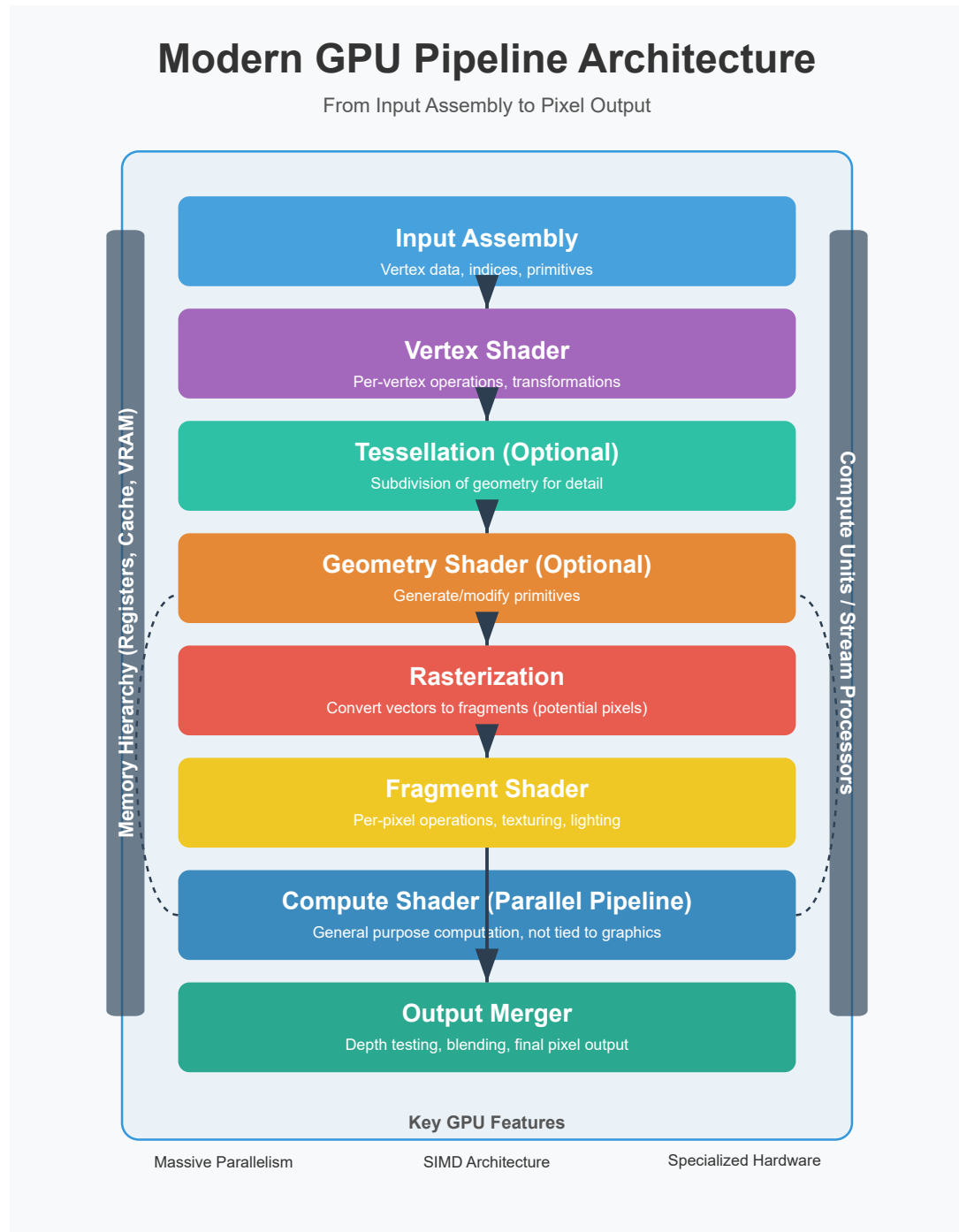
Modern GPUs leverage parallel processing to accelerate these transformations. Vertex shaders compute the model-view-projection (MVP) matrix product:

$$\mathbf{MVP} = \mathbf{P} \cdot \mathbf{V} \cdot \mathbf{M}$$

This consolidated matrix reduces redundant computations, as noted in . The following pseudocode illustrates a vertex shader applying the MVP transformation:

Code Sample 4.6: Vertex Shader for MVP Transformation

```
#version 450 core
layout(location = 0) in vec3 position;
uniform mat4 MVP;
void main() {
```



```

gl_Position = MVP * vec4(position, 1.0);
}

```

Key optimizations in GPU architecture include:

Matrix multiplication using SIMD (Single Instruction, Multiple Data) instructions for parallel processing.

Early depth testing to discard fragments before shading, reducing computational overhead.

Hardware interpolation of vertex attributes during rasterization, as detailed in .

The projection matrix's precision is critical for avoiding visual artifacts. Floating-point arithmetic inaccuracies can lead to z-fighting, where overlapping surfaces flicker due to depth buffer conflicts. Techniques such as reverse depth buffering mitigate this issue by redistributing depth precision .

The interplay between the model, view, and projection matrices ensures correct 3D-to-2D mapping. The model matrix positions objects in the world, the view matrix aligns the scene with the camera, and the projection matrix simulates perspective. Clipping and viewport transformations adapt the result to the display. These operations are foundational to real-time rendering pipelines, as demonstrated in frameworks like OpenGL and Vulkan .

In summary, the projection matrix is a cornerstone of 3D graphics, enabling the conversion of 3D scenes into 2D images. Its integration with other transformations and GPU optimizations ensures efficient and accurate rendering, forming the backbone of modern real-time graphics applications.

#### 4.2.4 Clipping

The transformation of 3D objects into 2D screen space in modern GPU architectures involves several critical stages, including the application of model, view, and projection matrices, followed by clipping and viewport transformations. Clipping, in particular, ensures that only the portions of geometry visible within the camera's frustum are processed, optimizing rendering performance and correctness.

The model matrix transforms object coordinates from local space to world space. Given a vertex  $\mathbf{v}_{\text{local}}$  in local coordinates, the world-space vertex  $\mathbf{v}_{\text{world}}$  is computed as:

$$\mathbf{v}_{\text{world}} = \mathbf{M}_{\text{model}} \cdot \mathbf{v}_{\text{local}}$$

where  $\mathbf{M}_{\text{model}}$  encodes translation, rotation, and scaling operations. The view matrix then converts world-space coordinates to camera-relative coordinates:

$$\mathbf{v}_{\text{view}} = \mathbf{M}_{\text{view}} \cdot \mathbf{v}_{\text{world}}$$

Here,  $\mathbf{M}_{\text{view}}$  is derived from the camera's position and orientation, aligning the world with the camera's coordinate system. The projection matrix maps view-space coordinates to clip space, a homogeneous coordinate system where visible geometry lies within the range  $[-w, w]$  for each  $x, y$ , and  $z$  component:

$$\mathbf{v}_{\text{clip}} = \mathbf{M}_{\text{projection}} \cdot \mathbf{v}_{\text{view}}$$

Perspective projection matrices introduce a non-linear depth scaling, compressing distant objects to simulate perspective foreshortening. Orthographic projections, in contrast, preserve parallel lines.

Clipping occurs in clip space, where primitives (triangles, lines, or points) are tested against the six planes of the view frustum. These six conditions include: the left plane defined by  $x \geq -w$ , the right by  $x \leq w$ , the bottom by  $y \geq -w$ , the top by  $y \leq w$ , the near by  $z \geq -w$ , and the far by  $z \leq w$ . Primitives entirely outside these planes are discarded, while those intersecting the planes are clipped, generating new vertices at the intersection points. The Sutherland-Hodgman algorithm is a widely used method for polygon clipping, iteratively processing each frustum plane.

After clipping, perspective division converts clip-space coordinates to normalized device coordinates (NDC) by dividing by  $w$ :

$$\mathbf{v}_{\text{ndc}} = \left( \frac{x}{w}, \frac{y}{w}, \frac{z}{w} \right)$$

NDC space ranges from  $[-1, 1]$  in  $x$  and  $y$ , and either  $[0, 1]$  or  $[-1, 1]$  in  $z$ , depending on the API. The viewport transformation then maps NDC to window coordinates, scaling  $x$  and  $y$  to the output resolution and adjusting  $z$  for depth buffering:

$$\mathbf{v}_{\text{window}} = \begin{pmatrix} \frac{\text{width}}{2} \cdot x_{\text{ndc}} + \frac{\text{width}}{2} + x_{\text{offset}} \\ \frac{\text{height}}{2} \cdot y_{\text{ndc}} + \frac{\text{height}}{2} + y_{\text{offset}} \\ \frac{f-n}{2} \cdot z_{\text{ndc}} + \frac{f+n}{2} \end{pmatrix}$$

Here, *width* and *height* define the viewport dimensions, *x<sub>offset</sub>* and *y<sub>offset</sub>* adjust the origin, and *n* and *f* are the near and far depth ranges.

Modern GPUs optimize clipping through hardware acceleration. The NVIDIA Turing architecture, for instance, integrates dedicated fixed-function units for frustum culling and clipping, reducing shader workload. Similarly, AMD's RDNA 2 architecture employs hierarchical culling to discard invisible primitives early in the pipeline.

Clipping also interacts with tessellation and geometry shaders, where dynamically generated geometry must be clipped efficiently. The OpenGL and Vulkan APIs provide mechanisms for user-defined clip planes, extending the standard frustum clipping:

Code Sample 4.7: Vulkan clip plane setup

```
VkPipelineViewportStateCreateInfo viewportInfo = {
    .sType = VK_STRUCTURE_TYPE_PIPELINE_VIEWPORT_STATE_CREATE_INFO,
    .viewportCount = 1,
    .pViewports = &viewport,
    .scissorCount = 1,
    .pScissors = &scissor
};
```

In summary, clipping is a pivotal step in the 3D-to-2D mapping pipeline, ensuring only visible geometry is rasterized. Its efficiency directly impacts GPU performance, with modern architectures leveraging fixed-function hardware to minimize computational overhead. The interplay between model, view, and projection matrices defines the clip-space boundaries, while viewport transformations finalize the mapping to screen coordinates.

#### 4.2.5 Viewport transformations

The transformation of 3D objects into 2D screen space is a fundamental process in modern GPU architecture, involving several mathematical operations collectively known as the graphics pipeline. Among these, viewport transformations play a critical role in mapping normalized device coordinates (NDC) to window coordinates. This process is preceded by model, view, and projection transformations, followed by clipping and perspective division.

The model matrix transforms object coordinates from local space to world space. Given a vertex  $\mathbf{v}_{\text{model}}$  in model space, its world-space position  $\mathbf{v}_{\text{world}}$  is computed as:

$$\mathbf{v}_{\text{world}} = \mathbf{M}_{\text{model}} \cdot \mathbf{v}_{\text{model}}$$

where  $\mathbf{M}_{\text{model}}$  encodes translation, rotation, and scaling operations.

The view matrix then converts world-space coordinates to camera (eye) space. This matrix,  $\mathbf{M}_{\text{view}}$ , is derived from the camera's position, orientation, and up vector. The transformation is:

$$\mathbf{v}_{\text{eye}} = \mathbf{M}_{\text{view}} \cdot \mathbf{v}_{\text{world}}$$

Here,  $\mathbf{M}_{\text{view}}$  is typically the inverse of the camera's transformation matrix.

Next, the projection matrix maps eye-space coordinates to clip space. Two common projections are used:

**Orthographic projection**, defined as:

$$\mathbf{M}_{\text{ortho}} = \begin{bmatrix} \frac{2}{r-l} & 0 & 0 & -\frac{r+l}{r-l} \\ 0 & \frac{2}{t-b} & 0 & -\frac{t+b}{t-b} \\ 0 & 0 & \frac{-2}{f-n} & -\frac{f+n}{f-n} \\ 0 & 0 & 0 & 1 \end{bmatrix}$$

**Perspective projection**, given by:

$$\mathbf{M}_{\text{persp}} = \begin{bmatrix} \frac{2n}{r-l} & 0 & \frac{r+l}{r-l} & 0 \\ 0 & \frac{2n}{t-b} & \frac{t+b}{t-b} & 0 \\ 0 & 0 & -\frac{f+n}{f-n} & -\frac{2fn}{f-n} \\ 0 & 0 & -1 & 0 \end{bmatrix}$$

This matrix introduces perspective foreshortening by scaling  $x$  and  $y$  inversely with  $z$ .

After projection, vertices are in clip space, where clipping occurs. The clipping stage discards geometry outside the view frustum, ensuring only visible primitives are processed. Clipping is performed against the six planes of the normalized device coordinate (NDC) cube  $[-1, 1]^3$ .

Following clipping, perspective division converts homogeneous clip-space coordinates to NDC by dividing by the  $w$ -component:

$$\mathbf{v}_{\text{ndc}} = \left[ \frac{x}{w}, \frac{y}{w}, \frac{z}{w} \right]^T$$

This step is crucial for perspective-correct interpolation of attributes.

The final stage is the viewport transformation, which maps NDC to window coordinates. Given a viewport defined by  $(x_v, y_v, w_v, h_v)$  and depth range  $[d_n, d_f]$ , the transformation is:

$$\mathbf{v}_{\text{window}} = \begin{bmatrix} x_v + \frac{w_v}{2}(x_{\text{ndc}} + 1) \\ y_v + \frac{h_v}{2}(y_{\text{ndc}} + 1) \\ d_n + \frac{d_f - d_n}{2}(z_{\text{ndc}} + 1) \end{bmatrix}$$

Here,  $x_{\text{ndc}}, y_{\text{ndc}}, z_{\text{ndc}}$  are NDC coordinates, and  $w_v, h_v$  are the viewport's width and height.

Modern GPUs optimize these transformations using dedicated hardware units. For instance, the vertex shader computes  $\mathbf{M}_{\text{model}} \cdot \mathbf{M}_{\text{view}} \cdot \mathbf{M}_{\text{proj}}$ , while rasterization handles clipping and perspective division. The viewport transformation is typically configured via API calls (e.g., `glViewport` in OpenGL).

The precision of these transformations is critical for visual fidelity. Floating-point arithmetic is used throughout, with careful handling of edge cases such as near-plane clipping and perspective division by zero. Research by and highlights optimizations for projection and clipping.

The following Verilog snippet illustrates a simplified viewport transformation unit:

Code Sample 4.8: Viewport Transformation Unit

```
module viewport_transform (
    input [31:0] x_ndc, y_ndc, z_ndc,
    input [31:0] x_v, y_v, w_v, h_v,
    input [31:0] d_n, d_f,
    output [31:0] x_win, y_win, z_win
);
    assign x_win = x_v + ((w_v * (x_ndc + 32'sh1)) >>> 1);
    assign y_win = y_v + ((h_v * (y_ndc + 32'sh1)) >>> 1);
    assign z_win = d_n + ((d_f - d_n) * (z_ndc + 32'sh1)) >>> 1;
endmodule
```

Key challenges in viewport transformations include:

Handling non-square pixels, requiring aspect ratio correction in the projection matrix.

Depth buffer precision, particularly for large  $d_f - d_n$  ranges.

Anti-aliasing, which may require multi-sample viewport transformations.

The interplay between these stages ensures correct 3D-to-2D mapping. For example, incorrect viewport settings can distort the rendered image or cause clipping artifacts. The work by provides a comprehensive analysis of these issues in modern GPU pipelines.

In summary, viewport transformations are the final step in a sequence of linear and non-linear operations that bridge 3D geometry and 2D rasterization. Their efficient implementation is vital for real-time graphics performance.

## 4.3 Rasterization Basics

### 4.3.1 Triangle setup

In modern GPU architecture, triangle setup is a fundamental stage in the rasterization pipeline, where geometric primitives are prepared for pixel-level processing. The process involves converting vertex data into a form suitable for rasterization, including edge function computation, interpolation of attributes, and pixel coverage determination. This discussion focuses on the mathematical foundations and hardware considerations of triangle setup, with emphasis on edge functions, interpolation, and pixel coverage.

The triangle setup phase begins with the transformation of vertices into screen space. Given three vertices  $\mathbf{v}_0$ ,  $\mathbf{v}_1$ , and  $\mathbf{v}_2$  in homogeneous clip space, they are projected onto the 2D screen space coordinates  $(x_0, y_0)$ ,  $(x_1, y_1)$ , and  $(x_2, y_2)$ . The edge functions for the triangle are derived from these coordinates. An edge function  $E_{ij}(x, y)$  for the edge between vertices  $\mathbf{v}_i$  and  $\mathbf{v}_j$  is defined as:

$$E_{ij}(x, y) = (x_j - x_i)(y - y_i) - (y_j - y_i)(x - x_i)$$

This function evaluates to zero for points lying on the edge, positive for points inside the triangle, and negative for points outside. The sign of  $E_{ij}(x, y)$  determines the orientation of the point relative to the edge. Modern GPUs compute these edge functions in parallel for all pixels within the bounding box of the triangle to determine coverage efficiently.

Interpolation of vertex attributes, such as texture coordinates, colors, and normals, is performed using barycentric coordinates. For a point  $(x, y)$  inside the triangle, the barycentric coordinates  $(\alpha, \beta, \gamma)$  are computed as:

$$\alpha = \frac{E_{12}(x, y)}{E_{12}(x_0, y_0)}, \quad \beta = \frac{E_{20}(x, y)}{E_{20}(x_1, y_1)}, \quad \gamma = \frac{E_{01}(x, y)}{E_{01}(x_2, y_2)}$$

These coordinates are used to interpolate attributes linearly across the triangle. For perspective-correct interpolation, the attributes are divided by the interpolated  $w$ -component of the vertex positions and then multiplied by the interpolated  $1/w$  factor. This ensures correct interpolation under perspective projection.

Pixel coverage determination involves testing whether a pixel center or sample point lies inside the triangle. A pixel is considered covered if all edge functions evaluated at its center yield positive values:

$$E_{01}(x, y) > 0 \quad \wedge \quad E_{12}(x, y) > 0 \quad \wedge \quad E_{20}(x, y) > 0$$

Modern GPUs optimize this process using hierarchical traversal, where coarse-grained tiles are tested before fine-grained pixel evaluations. This reduces the number of redundant computations and improves throughput.

The hardware implementation of triangle setup involves specialized fixed-function units designed for parallel computation. These units leverage SIMD (Single Instruction, Multiple Data) architectures to evaluate edge functions and interpolate attributes for multiple pixels simultaneously. The following Verilog snippet illustrates a simplified edge function computation unit:

Code Sample 4.9: Edge Function Computation Unit

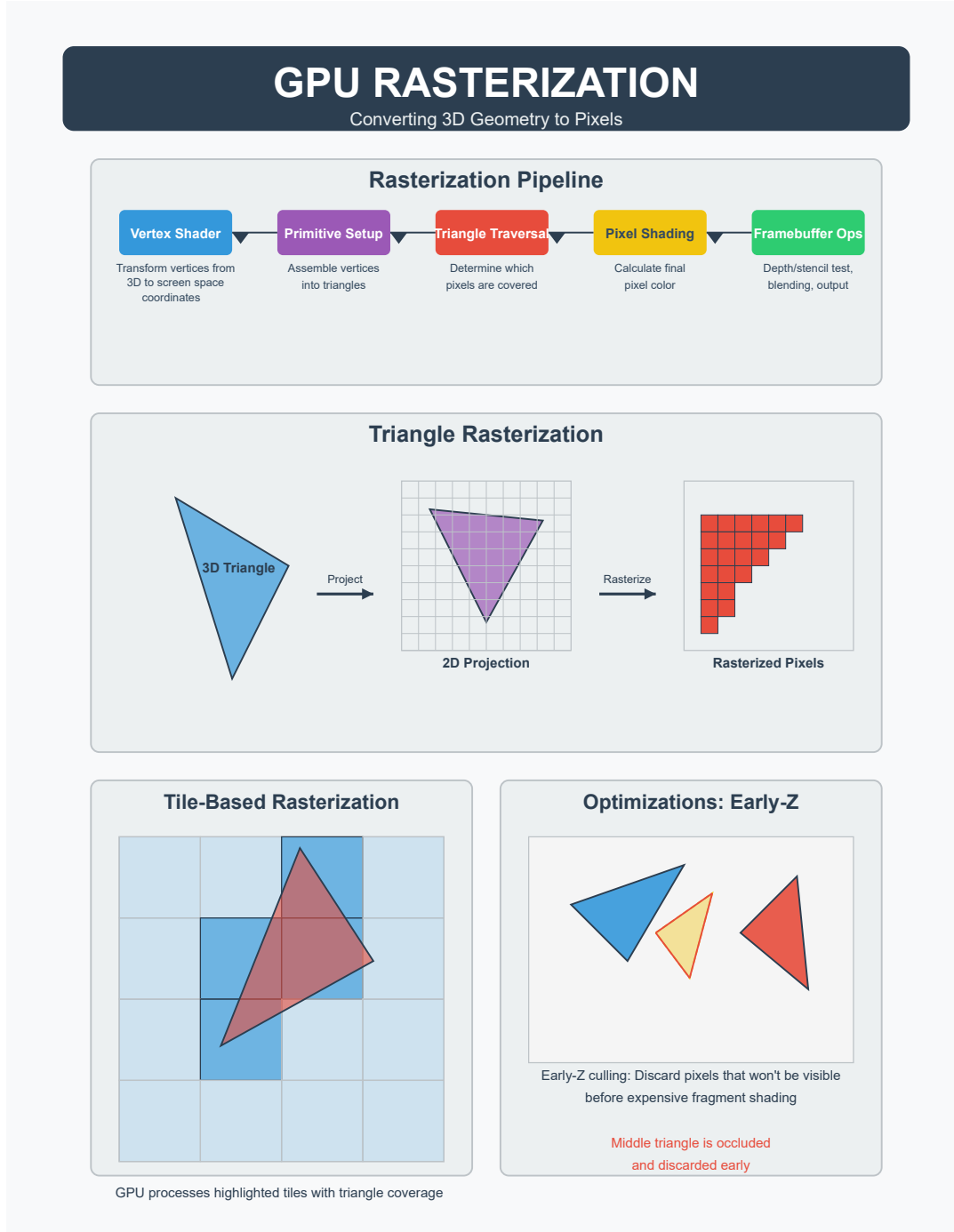
```
module edge_func (
    input [15:0] x, y, xi, yi, xj, yj,
    output reg [31:0] E
);
always @(*) begin
    E = (xj - xi) * (y - yi) - (yj - yi) * (x - xi);
end
endmodule
```

The interpolation of attributes is similarly optimized in hardware. For example, a barycentric interpolation unit computes the weights  $\alpha$ ,  $\beta$ , and  $\gamma$  and applies them to the vertex attributes. The following equations describe the interpolation of an attribute  $A$ :

$$A(x, y) = \alpha A_0 + \beta A_1 + \gamma A_2$$

where  $A_0$ ,  $A_1$ , and  $A_2$  are the attribute values at the vertices. Perspective correction is applied by interpolating  $A/w$  and  $1/w$  and then dividing the results:

$$A_{\text{persp}}(x, y) = \frac{\alpha(A_0/w_0) + \beta(A_1/w_1) + \gamma(A_2/w_2)}{\alpha(1/w_0) + \beta(1/w_1) + \gamma(1/w_2)}$$



Pixel coverage testing is further optimized using conservative rasterization techniques, where pixels partially covered by the triangle are included in the rendering process. This is particularly useful for anti-aliasing and shadow mapping. The edge functions are adjusted to account for half-pixel offsets, ensuring robust coverage determination.

The performance of triangle setup is critical for overall GPU efficiency. Research highlights the importance of optimizing edge function computations and interpolation to minimize latency and power consumption. Modern GPUs employ dedicated hardware for these tasks, such as NVIDIA's raster engines and AMD's Primitive Assembler, which streamline the triangle setup process.

Key considerations in triangle setup include precision (edge functions must be computed with sufficient precision to avoid artifacts, especially for large triangles or high-resolution displays), parallelism (SIMD architectures exploit data-level parallelism to process multiple pixels simultaneously), memory bandwidth (efficient attribute interpolation requires careful management of memory accesses to avoid bottlenecks), and hierarchical testing (coarse-grained tile testing reduces redundant computations and improves throughput).

In summary, triangle setup in modern GPU architecture is a computationally intensive yet highly optimized process. It involves edge function computation, barycentric interpolation, and pixel coverage testing, all of which are implemented in hardware for maximum efficiency. The mathematical foundations and hardware optimizations discussed here are critical for achieving high-performance rasterization in real-time graphics applications.

### 4.3.2 Edge functions

In modern GPU architecture, rasterization is a fundamental process that converts geometric primitives, typically triangles, into pixel fragments for display. The efficiency of this process relies heavily on edge functions, which are mathematical constructs used to determine pixel coverage within a triangle. Edge functions form the basis for triangle setup, interpolation, and pixel coverage tests, all of which are critical for real-time rendering performance.

Edge functions are derived from the implicit equation of a line. Given a triangle with vertices  $A(x_0, y_0)$ ,  $B(x_1, y_1)$ , and  $C(x_2, y_2)$ , the edge function for edge  $AB$  is defined as:

$$E_{AB}(x, y) = (y_1 - y_0)(x - x_0) - (x_1 - x_0)(y - y_0)$$

A point  $(x, y)$  lies on the edge  $AB$  if  $E_{AB}(x, y) = 0$ , inside the triangle if  $E_{AB}(x, y) > 0$ , and outside if  $E_{AB}(x, y) < 0$ . This property is exploited during rasterization to determine whether a pixel center lies within the triangle.

The triangle setup phase computes these edge functions for all three edges of the triangle. Modern GPUs optimize this process by precomputing coefficients and storing them in registers for efficient evaluation. The edge functions are often represented in a barycentric coordinate system, where the barycentric weights  $\alpha$ ,  $\beta$ , and  $\gamma$  are proportional to the signed distances from the edges:

$$\alpha = \frac{E_{BC}(x, y)}{E_{BC}(x_0, y_0)}, \quad \beta = \frac{E_{CA}(x, y)}{E_{CA}(x_1, y_1)}, \quad \gamma = \frac{E_{AB}(x, y)}{E_{AB}(x_2, y_2)}$$

These weights are used for attribute interpolation, such as color, texture coordinates, and depth, across the triangle.

Interpolation of attributes is performed using the barycentric weights computed from the edge functions. For a given attribute  $V$  at vertices  $A$ ,  $B$ , and  $C$ , the interpolated value at  $(x, y)$  is:

$$V(x, y) = \alpha V_A + \beta V_B + \gamma V_C$$

This linear interpolation is efficient because it leverages the same edge functions used for coverage tests. Modern GPUs often use fixed-function hardware units to accelerate this process, ensuring low latency and high throughput.

Pixel coverage testing involves evaluating the edge functions for all pixels in the bounding box of the triangle. A pixel is considered covered if all three edge functions yield positive values for its center. To optimize this, GPUs employ hierarchical traversal techniques, such as tile-based rasterization, where coarse-grained tests are performed on larger blocks before fine-grained per-pixel tests.

#### Code Sample 4.10: Pixel Coverage Test

```
for each pixel (x, y) in bounding box:
    if E_AB(x, y) > 0 and E_BC(x, y) > 0 and E_CA(x, y) > 0:
        pixel is covered
```

Edge functions also enable efficient antialiasing through multisampling. By evaluating the edge functions at multiple sample points within a pixel, GPUs can compute fractional coverage values. For example, with 4x multisampling, the coverage mask is derived from the number of samples that pass the edge tests:

$$\text{Coverage} = \frac{\text{Number of samples inside}}{4}$$

This approach reduces aliasing artifacts while maintaining performance.

The hardware implementation of edge functions in modern GPUs is highly parallelized. Each rasterizer unit processes multiple pixels or tiles simultaneously, leveraging SIMD (Single Instruction, Multiple Data) architectures. The edge function evaluations are often pipelined to maximize throughput, with dedicated arithmetic units for the cross-product computations required by (4.3.2). For example, NVIDIA's Turing architecture employs specialized raster engines that perform edge tests in parallel across multiple streaming multiprocessors .

Edge functions also play a role in advanced rendering techniques, such as conservative rasterization. In this mode, a pixel is considered covered if any part of the pixel intersects the triangle, which requires modifying the edge function tests. The edge equations are adjusted to account for pixel extents:

$$E_{AB}^{\text{conservative}}(x, y) = E_{AB}(x, y) - \frac{|(y_1 - y_0)| + |(x_1 - x_0)|}{2}$$

This ensures that pixels partially covered by the triangle are included in the output.

The precision of edge functions is critical for correct rendering. Floating-point arithmetic is typically used, but GPUs employ techniques like subpixel precision and guard bands to avoid numerical instability. For instance, edge functions are evaluated with at least 16-bit floating-point precision to prevent artifacts near triangle edges .

In summary, edge functions are a cornerstone of rasterization in modern GPU architecture. They enable efficient triangle setup, precise pixel coverage testing, and accurate attribute interpolation. Their mathematical formulation and hardware optimization are key to achieving real-time performance in graphics pipelines. Future advancements may further optimize edge function evaluation through machine learning or hybrid rendering techniques, but their fundamental role in rasterization remains unchanged.

### 4.3.3 Interpolation

# Chapter 5

## Interpolation in Rasterization

In modern GPU architecture, interpolation plays a critical role in rasterization, particularly during triangle setup, edge evaluation, and pixel coverage determination. Rasterization is the process of converting geometric primitives, such as triangles, into a raster image. The GPU pipeline involves several stages: vertex shading, primitive assembly, rasterization, and fragment shading. Interpolation occurs during rasterization to compute attributes such as color, texture coordinates, and depth across the surface of a triangle.

The rasterization process begins with triangle setup, where the GPU determines the screen-space coordinates of a triangle's vertices. Given three vertices  $\mathbf{v}_0, \mathbf{v}_1, \mathbf{v}_2$  with homogeneous coordinates  $(x_i, y_i, z_i, w_i)$ , these are converted to normalized device coordinates (NDC) via perspective division:

$$\mathbf{v}_i^{\text{NDC}} = \left( \frac{x_i}{w_i}, \frac{y_i}{w_i}, \frac{z_i}{w_i} \right)$$

The NDC coordinates are then mapped to screen-space coordinates  $(X_i, Y_i)$  through viewport transformation.

Each triangle edge is defined by the line between a pair of vertices. The GPU computes edge functions to determine pixel coverage. For an edge between  $\mathbf{v}_0$  and  $\mathbf{v}_1$ , the edge function is:

$$E_{01}(X, Y) = (X_1 - X_0)(Y - Y_0) - (Y_1 - Y_0)(X - X_0)$$

A pixel  $(X, Y)$  lies inside the triangle if all three edge functions  $E_{01}, E_{12}, E_{20}$  are positive. This test is applied to all pixels within the triangle's bounding box to determine coverage.

Interpolation of attributes is performed using barycentric coordinates. For a point  $\mathbf{p}$  inside the triangle:

$$\mathbf{p} = \alpha\mathbf{v}_0 + \beta\mathbf{v}_1 + \gamma\mathbf{v}_2 \quad \text{where } \alpha + \beta + \gamma = 1$$

These coordinates are computed using the edge functions and the area of the triangle:

$$\alpha = \frac{E_{12}(X, Y)}{E_{12}(X_0, Y_0)}, \quad \beta = \frac{E_{20}(X, Y)}{E_{20}(X_1, Y_1)}, \quad \gamma = \frac{E_{01}(X, Y)}{E_{01}(X_2, Y_2)}$$

Attributes such as texture coordinates  $(u, v)$  are then interpolated linearly in screen space:

$$u = \alpha u_0 + \beta u_1 + \gamma u_2, \quad v = \alpha v_0 + \beta v_1 + \gamma v_2$$

However, perspective-correct interpolation is required for attributes like depth and texture coordinates due to the non-linear nature of perspective projection. The GPU computes the interpolated attribute  $A$  as:

$$A = \frac{\alpha A_0/w_0 + \beta A_1/w_1 + \gamma A_2/w_2}{\alpha/w_0 + \beta/w_1 + \gamma/w_2}$$

Pixel coverage is optimized through hierarchical traversal and parallel evaluation. Tile-based rasterizers, for example, divide the screen into tiles and perform coarse triangle-tile intersection tests before evaluating individual pixels.

Depth interpolation is crucial for visibility determination. The GPU calculates interpolated depth  $z$  using:

$$z = \frac{1}{\alpha/z_0 + \beta/z_1 + \gamma/z_2}$$

Fragment shading then applies lighting, texture sampling, and other effects using the interpolated attributes as inputs. These computations are massively parallelized across fragments.

Modern GPUs further improve quality through techniques like centroid sampling, particularly in multisample anti-aliasing (MSAA), where attributes are interpolated at subpixel sample points.

#### Code Sample 5.1: Edge Function Evaluation

```
module edge_function (
    input [31:0] X0, Y0, X1, Y1, X, Y,
    output [31:0] E
);
    assign E = (X1 - X0) * (Y - Y0) - (Y1 - Y0) * (X - X0);
endmodule
```

Fixed-function interpolation units in GPUs calculate barycentric coordinates and perform attribute interpolation in parallel. These are tightly coupled with the rasterizer and fragment processors for efficiency.

Precision and robustness are critical. Edge cases such as degenerate triangles and near-zero denominators require careful floating-point handling. GPUs implement guard bands and specialized logic to maintain correctness.

Research efforts such as and have proposed improved interpolation techniques. Hierarchical methods and optimized perspective correction continue to evolve to meet real-time rendering demands.

In conclusion, interpolation is fundamental to high-performance, high-quality rendering in modern GPUs. It enables the smooth propagation of per-vertex data to pixel-level detail with minimal overhead.

### 5.0.1 Pixel coverage

The process of rasterization in modern GPU architectures involves converting geometric primitives, typically triangles, into a grid of pixels for display. A critical aspect of this process is pixel coverage determination, which identifies which pixels are covered by a given triangle. This involves several stages: triangle setup, edge function evaluation, interpolation, and final pixel coverage testing.

Triangle setup is the first step in rasterization, where the GPU transforms vertex data into a form suitable for rasterization. Given three vertices  $\mathbf{v}_0, \mathbf{v}_1, \mathbf{v}_2$  in screen space, the GPU computes edge equations and other attributes required for interpolation. The edge function for an edge between  $\mathbf{v}_i$  and  $\mathbf{v}_j$  is defined as:

$$E_{ij}(x, y) = (x_j - x_i)(y - y_i) - (y_j - y_i)(x - x_i)$$

where  $(x, y)$  is the pixel coordinate. A point  $(x, y)$  lies inside the triangle if all three edge functions  $E_{01}, E_{12}, E_{20}$  evaluate to the same sign.

Edge functions are central to determining pixel coverage. Modern GPUs optimize this by evaluating edge functions incrementally using finite differences. For a pixel at  $(x, y)$ , the change in the edge function when moving to  $(x + 1, y)$  is:

$$\Delta_x E_{ij} = y_i - y_j$$

Similarly, the change when moving to  $(x, y + 1)$  is:

$$\Delta_y E_{ij} = x_j - x_i$$

These incremental calculations reduce computational overhead during rasterization.

Interpolation of attributes such as color, texture coordinates, and depth is performed once pixel coverage is confirmed. Barycentric coordinates  $(\lambda_0, \lambda_1, \lambda_2)$  are used for interpolation, where:

$$\lambda_i = \frac{E_{jk}(x, y)}{E_{jk}(x_i, y_i)}$$

Here,  $E_{jk}$  is the edge function opposite vertex  $\mathbf{v}_i$ . The denominator  $E_{jk}(x_i, y_i)$  is constant for the triangle and can be precomputed during triangle setup. Attributes are then interpolated as:

$$A(x, y) = \lambda_0 A_0 + \lambda_1 A_1 + \lambda_2 A_2$$

where  $A_0, A_1, A_2$  are the attribute values at the vertices.

Pixel coverage testing determines whether a pixel center or any part of the pixel lies within the triangle. Two common approaches are:

**Point sampling:** The pixel is covered if its center satisfies the edge function tests.

**Area sampling:** The pixel is covered if any portion of its area intersects the triangle, requiring more complex evaluation.

Modern GPUs often use point sampling for efficiency, but advanced techniques like multisample anti-aliasing (MSAA) perform multiple point samples per pixel to improve quality.

The rasterization pipeline also handles hierarchical culling to avoid unnecessary computations. Tiles of pixels are tested against the triangle's bounding box or coarse edge functions before per-pixel evaluation. This reduces the number of pixels processed, improving performance. The tile-based approach is particularly effective in mobile GPUs .

Pixel coverage is further complicated by non-integer vertex coordinates and sub-pixel precision. GPUs use fixed-point arithmetic to represent vertex coordinates with fractional bits, ensuring accurate edge function evaluation. The precision of these calculations affects rendering quality, especially for small or thin triangles.

Depth testing and early depth culling are often integrated with pixel coverage testing. If a pixel fails the depth test, it is discarded before shading, saving computation. Modern GPUs employ early-z and hierarchical-z techniques to reject occluded pixels early in the pipeline .

The following Verilog-like pseudocode illustrates a simplified pixel coverage test:

Code Sample 5.2: Pixel Coverage Test

```
module pixel_coverage (
    input [15:0] x, y,
    input [15:0] v0_x, v0_y,
    input [15:0] v1_x, v1_y,
    input [15:0] v2_x, v2_y,
    output reg covered
);
    wire signed [31:0] E01 = (v1_x - v0_x) * (y - v0_y) - (v1_y - v0_y) * (x - v0_x);
    wire signed [31:0] E12 = (v2_x - v1_x) * (y - v1_y) - (v2_y - v1_y) * (x - v1_x);
    wire signed [31:0] E20 = (v0_x - v2_x) * (y - v2_y) - (v0_y - v2_y) * (x - v2_x);

    always @(*) begin
        covered = (E01 >= 0 && E12 >= 0 && E20 >= 0) ||
                  (E01 <= 0 && E12 <= 0 && E20 <= 0);
    end
endmodule
```

Optimizations such as parallel evaluation of edge functions and SIMD processing are employed in modern GPUs to handle multiple pixels simultaneously. For example, a GPU might evaluate a 2x2 or 4x4 block of pixels in parallel, leveraging data locality and reducing memory bandwidth usage .

Interpolation of attributes must account for perspective correction when dealing with 3D scenes. The correct interpolation for a perspective-projected attribute  $A$  is:

$$A(x, y) = \frac{\lambda_0 A_0/w_0 + \lambda_1 A_1/w_1 + \lambda_2 A_2/w_2}{\lambda_0/w_0 + \lambda_1/w_1 + \lambda_2/w_2}$$

where  $w_i$  are the vertex clip-space w-coordinates. This ensures correct interpolation under perspective projection.

Pixel coverage also involves handling edge cases such as degenerate triangles, where vertices are colinear, or zero-area triangles. GPUs detect and discard such primitives early to avoid unnecessary processing. Additionally, rules like the top-left rule are used to ensure consistent coverage for shared edges between adjacent triangles, preventing gaps or overlaps .

In summary, pixel coverage in modern GPU architectures involves a combination of geometric calculations, incremental evaluation, and parallel processing to efficiently determine which pixels are covered by a triangle. The interplay between triangle setup, edge functions, interpolation, and coverage testing forms the foundation of rasterization, enabling high-performance rendering in real-time graphics.

## 5.1 Shading and Texturing Concepts

### 5.1.1 Lambertian shading

Lambertian shading is a fundamental concept in computer graphics, particularly in the context of modern GPU architecture. It describes the reflection of light from a surface where the perceived brightness is independent of the viewer's angle, following Lambert's cosine law. Mathematically, the reflected radiance  $L_r$  is given by:

$$L_r = L_i \cdot \rho \cdot \cos \theta$$

where  $L_i$  is the incident light intensity,  $\rho$  is the surface albedo, and  $\theta$  is the angle between the surface normal and the light direction. This model is computationally efficient, making it ideal for real-time rendering on GPUs. Modern GPUs optimize Lambertian shading by leveraging parallel processing units to compute per-fragment lighting across millions of pixels simultaneously.

Texture sampling is another critical operation in GPU rendering, often used in conjunction with Lambertian shading. Textures provide surface details by mapping image data onto 3D geometry. The GPU performs texture sampling by interpolating texel values from texture coordinates. This process involves the use of texture coordinates (UV coordinates assigned to each vertex and interpolated across fragments during rasterization), texture fetch operations (where the GPU retrieves texel values using bilinear or trilinear filtering to reduce aliasing artifacts), and mipmapping (a precomputed pyramid of downsampled textures that ensures efficient sampling at varying distances).

The texture sampling operation can be expressed as:

$$C = T(u, v)$$

where  $C$  is the sampled color,  $T$  is the texture, and  $(u, v)$  are the texture coordinates. Modern GPUs use dedicated texture units to accelerate this process, supporting anisotropic filtering for improved quality at oblique viewing angles.

Filtering techniques are essential for mitigating aliasing and preserving visual fidelity during texture sampling. Common methods include nearest-neighbor filtering (selecting the closest texel without interpolation), bilinear filtering (interpolating between four nearest texels for smoother results), trilinear filtering (which combines bilinear interpolation with mipmap level blending), and anisotropic filtering (which accounts for perspective distortion by sampling along the dominant viewing direction). The choice of filtering method impacts both performance and quality. For instance, anisotropic filtering requires more memory bandwidth but produces superior results for textured surfaces viewed at sharp angles.

The GPU's texture cache hierarchy plays a crucial role in optimizing these operations, reducing latency by storing frequently accessed texels. In modern GPU architectures, Lambertian shading and texture sampling are tightly integrated. The shading pipeline typically follows a sequence of steps: first, the surface normal and light direction vectors are computed; second, the Lambertian term is evaluated using (5.1.2); third, the diffuse texture is sampled using (5.1.1); and finally, the results are combined to produce the final fragment color.

This pipeline is implemented using shader programs, such as the following GLSL fragment shader snippet:

Code Sample 5.3: Lambertian Shading with Texture Sampling

```
uniform sampler2D diffuseTexture;
uniform vec3 lightDir;
in vec2 uv;
in vec3 normal;
out vec4 fragColor;
void main() {
    vec3 albedo = texture(diffuseTexture, uv).rgb;
    float lambert = max(dot(normal, lightDir), 0.0);
    fragColor = vec4(albedo * lambert, 1.0);
}
```

The shader demonstrates how texture sampling and Lambertian shading are combined in a single pass. Modern GPUs optimize this further by employing unified shader architectures, where the same execution units handle both vertex and fragment processing. This flexibility allows for dynamic workload balancing, improving overall throughput.

Texture compression formats, such as BCn or ASTC, further enhance performance by reducing memory footprint and bandwidth requirements. These formats are hardware-accelerated on GPUs, enabling real-time decompression during sampling. For example, BC1 (DXT1) compression reduces a 24-bit RGB texture to 4 bits per pixel, with minimal perceptual quality loss. The GPU's texture units decode these formats on-the-fly, ensuring efficient memory usage.

The interplay between Lambertian shading and texture filtering is evident in techniques like normal mapping, where surface details are simulated using per-pixel normals stored in a texture. The Lambertian calculation then uses these normals instead of the geometric surface normal, enhancing visual complexity without additional geometry. The normal mapping process can be expressed as:

$$L_r = L_i \cdot \rho \cdot \max(\mathbf{n} \cdot \mathbf{l}, 0)$$

where  $\mathbf{n}$  is the sampled normal from the normal map, and  $\mathbf{l}$  is the light direction. Modern GPUs support derivative operations in shaders to compute tangent-space vectors for normal mapping, enabling accurate lighting calculations.

Advanced rendering techniques, such as physically based rendering (PBR), extend Lambertian shading with more complex reflectance models. However, the foundational principles remain rooted in efficient texture sampling and filtering. For instance, PBR often employs multiple textures for albedo, roughness, and metallic properties, each requiring careful filtering to avoid artifacts. The GPU's ability to sample and filter these textures in parallel is critical for maintaining real-time performance.

In summary, Lambertian shading and texture sampling are cornerstones of modern GPU rendering. Their efficient implementation relies on parallel processing, optimized memory access, and advanced filtering techniques. As GPU architectures continue to evolve, these operations benefit from increased computational power and memory bandwidth, enabling ever more realistic real-time graphics. The mathematical formulations in (5.1.2) and (5.1.1), combined with hardware-accelerated filtering, ensure that these techniques remain performant and scalable across a wide range of applications.

### 5.1.2 Texture sampling

Texture sampling is a fundamental operation in modern GPU architectures, playing a critical role in rendering pipelines for both real-time graphics and offline rendering. It involves fetching texel data from texture memory and applying filtering techniques to produce smooth, high-quality images. The process is tightly coupled with shading models like Lambertian reflectance, where texture data modulates surface properties such as diffuse albedo. Lambertian shading assumes that surfaces reflect light equally in all directions, described by the cosine law:

$$L_d = k_d \cdot I \cdot (\mathbf{n} \cdot \mathbf{l})$$

Here,  $L_d$  is the diffuse radiance,  $k_d$  is the diffuse reflectance (often sampled from a texture),  $I$  is the incident light intensity,  $\mathbf{n}$  is the surface normal, and  $\mathbf{l}$  is the light direction. Texture sampling provides  $k_d$ , enabling detailed surface appearance without excessive geometric complexity.

Modern GPUs implement texture sampling through dedicated hardware units called texture mapping units (TMUs). These units handle:

Address calculation: Converting normalized texture coordinates ( $u, v$ ) to memory addresses.

Filtering: Applying interpolation to reduce aliasing artifacts.

Compression: Decoding block-compressed formats like BC7 or ASTC.

The texture sampling pipeline involves several stages:

1. **Coordinate Generation:** UV coordinates are computed per-fragment, either interpolated from vertices or procedurally generated.
2. **Address Wrapping:** Out-of-bounds coordinates are handled via modes like repeat, clamp, or mirror. For example, repeat mode uses modulo arithmetic:

$$u' = u - \lfloor u \rfloor$$

3. **Mipmapping:** A precomputed pyramid of downsampled textures selects the appropriate level-of-detail (LOD) to balance quality and performance. The LOD is computed as:

$$\lambda = \log_2 \left( \max \left( \left| \frac{\partial u}{\partial x} \right|, \left| \frac{\partial v}{\partial x} \right| \right) \right)$$

4. **Filtering:** Combines multiple texels to reduce aliasing. Common methods include:

**Nearest-neighbor:** Selects the closest texel, fastest but prone to aliasing. **Bilinear:** Interpolates between 4 texels. **Trilinear:** Blends bilinear results across two mip levels. **Anisotropic:** Accounts for perspective distortion by sampling along the dominant direction.

Filtering quality is crucial for visual fidelity. Bilinear filtering computes a weighted average:

$$T(u, v) = \sum_{i=0}^1 \sum_{j=0}^1 T_{ij} \cdot w_{ij}$$

where  $T_{ij}$  are the four nearest texels and  $w_{ij}$  are bilinear weights. Anisotropic filtering extends this by sampling along a ray, reducing blurring in oblique surfaces.

Texture sampling performance is optimized via caching hierarchies. Modern GPUs use a two-level cache:

**L1 Cache:** Per-SMX cache storing recently accessed texel blocks.

**L2 Cache:** Shared across the GPU, reducing memory bandwidth.

Cache efficiency depends on locality. Coherent access patterns (e.g., linear UV gradients) achieve higher hit rates.

Texture compression is vital for memory efficiency. Block-compressed formats like BC7 encode 4x4 texel blocks into 128 bits, reducing bandwidth by 4–8x. The decoding is hardware-accelerated, with minimal runtime overhead.

Advanced techniques like virtual texturing dynamically stream texture data, enabling ultra-high-resolution assets. The GPU pages texture tiles on-demand, similar to CPU virtual memory. This requires indirection through a page table:

#### Code Sample 5.4: Virtual Texture Lookup

```
uint2 page = page_table[uv >> TILE_BITS];
float4 texel = texture_cache[page + (uv & TILE_MASK)];
```

Texture sampling also interacts with shading models. In Lambertian shading, the sampled  $k_d$  modulates the diffuse term in equation 5.1.2. For physically based rendering (PBR), textures provide additional parameters like roughness and metallicness.

Precision is another consideration. Modern GPUs support:

8-bit per channel (sRGB or UNORM).

16-bit floating-point (HDR).

32-bit floating-point (scientific visualization).

sRGB textures require gamma correction during sampling:

$$C_{\text{linear}} = \begin{cases} \frac{C_{\text{sRGB}}}{12.92} & C_{\text{sRGB}} \leq 0.04045 \\ \left( \frac{C_{\text{sRGB}} + 0.055}{1.055} \right)^{2.4} & \text{otherwise} \end{cases}$$

Texture sampling also impacts performance metrics. Over-sampling (high LOD) wastes bandwidth, while under-sampling (low LOD) causes blurring. Adaptive sampling techniques, like variable-rate shading, dynamically adjust sampling rates.

In summary, texture sampling in modern GPUs is a sophisticated process involving coordinate transformation, filtering, and memory hierarchy optimizations. It is integral to shading pipelines, enabling realistic material representation through techniques like Lambertian reflectance and PBR. Hardware advancements continue to push the boundaries of fidelity and efficiency, as evidenced by real-time ray tracing and machine-learning-based super-resolution.

### 5.1.3 Filtering

Modern GPU architectures employ sophisticated filtering techniques to enhance the quality of rendered images, particularly in the context of shading and texturing. Filtering plays a critical role in mitigating aliasing artifacts, improving visual fidelity, and ensuring efficient memory access patterns. This discussion focuses on filtering in relation to Lambertian shading, texture sampling, and the underlying mathematical principles.

Lambertian shading is a fundamental lighting model that describes diffuse reflection, where the perceived brightness of a surface is proportional to the cosine of the angle between the surface normal and the light source direction. The Lambertian reflectance equation is given by:

$$I_d = k_d \cdot I_l \cdot (\mathbf{n} \cdot \mathbf{l})$$

where  $I_d$  is the diffuse intensity,  $k_d$  is the diffuse reflectance coefficient,  $I_l$  is the light intensity,  $\mathbf{n}$  is the surface normal, and  $\mathbf{l}$  is the light direction vector. Filtering in this context involves interpolating surface normals and light vectors across fragments to achieve smooth shading transitions. Modern GPUs leverage bilinear or barycentric interpolation to compute these values efficiently.

Texture sampling is another domain where filtering is indispensable. When a texture is mapped onto a surface, the texture coordinates often do not align perfectly with the pixel grid, leading to aliasing or blurring. To address this, GPUs employ various filtering techniques. Nearest-neighbor filtering is the simplest method, where the texel closest to the sampled coordinate is selected. While computationally efficient, it is prone to aliasing. Bilinear filtering computes a weighted average of the four nearest texels, reducing blockiness and producing smoother results, though at the cost of slight blurring. Trilinear filtering extends bilinear filtering by interpolating between mipmap levels, maintaining visual consistency across varying distances. Anisotropic filtering is a more advanced technique that accounts for the angle of the surface relative to the viewer, preserving detail even at oblique angles.

The mathematical foundation of bilinear filtering is expressed as:

$$C(x, y) = \alpha\beta C_{i,j} + \alpha(1 - \beta)C_{i,j+1} + (1 - \alpha)\beta C_{i+1,j} + (1 - \alpha)(1 - \beta)C_{i+1,j+1}$$

where  $C(x, y)$  is the interpolated color,  $\alpha$  and  $\beta$  are the fractional parts of the texture coordinates, and  $C_{i,j}$  represents the texel values.

Mipmapping is a pre-filtering technique that generates a pyramid of progressively downsampled textures. This hierarchy allows the GPU to select an appropriate level of detail (LOD) based on the distance from the viewer, reducing aliasing and improving rendering performance. The LOD is computed as:

$$\lambda = \log_2 \left( \max \left( \sqrt{\left( \frac{\partial u}{\partial x} \right)^2 + \left( \frac{\partial v}{\partial x} \right)^2}, \sqrt{\left( \frac{\partial u}{\partial y} \right)^2 + \left( \frac{\partial v}{\partial y} \right)^2} \right) \right)$$

where  $\lambda$  is the LOD level, and the derivatives are partials of the texture coordinates with respect to screen space.

Anisotropic filtering addresses the limitations of isotropic filtering by considering the elongation of the pixel footprint in texture space. The anisotropy ratio  $r$  is defined as:

$$r = \frac{\text{major axis length}}{\text{minor axis length}}$$

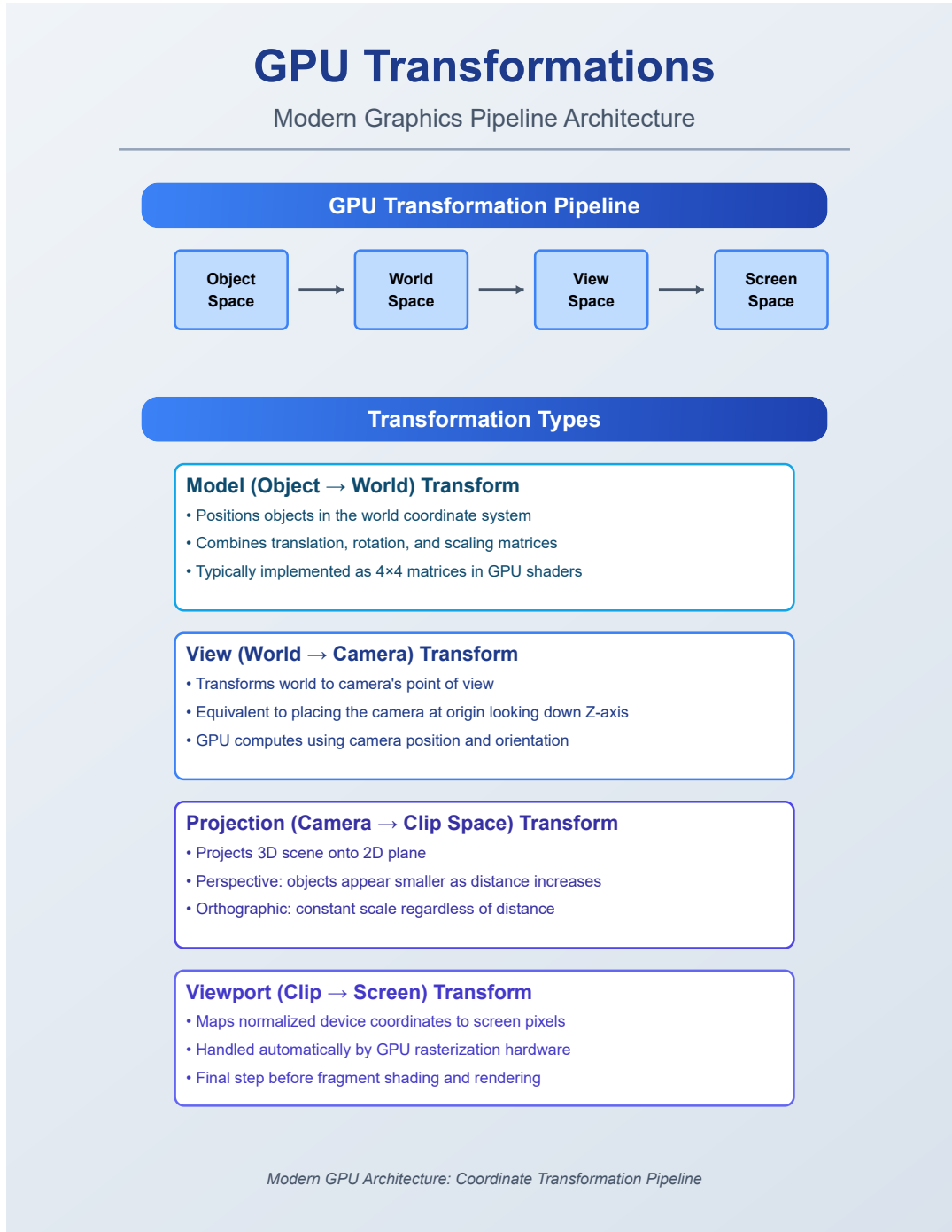
Higher values of  $r$  indicate greater anisotropy, requiring more samples to maintain detail. Modern GPUs implement this by sampling multiple texels along the major axis and blending the results.

Texture compression is another area where filtering intersects with GPU architecture. Block-based compression formats like BC7 reduce memory bandwidth requirements while preserving visual quality. The decompression process is integrated into the texture filtering pipeline, ensuring seamless operation. For example, the BC7 format encodes texels into 128-bit blocks, which are decompressed on-the-fly during sampling.

The following Verilog snippet illustrates a simplified texture sampling unit with bilinear filtering:

Code Sample 5.5: Texture Sampling Unit

```
module texture_sampler (
    input [31:0] tex_coord,
    input [31:0] tex_data[0:3],
    output [31:0] color_out
);
reg [7:0] alpha = tex_coord[15:8];
```



```

reg [7:0] beta = tex_coord[7:0];
wire [31:0] c00 = tex_data[0];
wire [31:0] c01 = tex_data[1];
wire [31:0] c10 = tex_data[2];
wire [31:0] c11 = tex_data[3];
assign color_out = (alpha * beta * c00) +
    (alpha * (255 - beta) * c01) +
    ((255 - alpha) * beta * c10) +
    ((255 - alpha) * (255 - beta) * c11);
endmodule

```

Filtering also extends to anti-aliasing techniques such as multisample anti-aliasing (MSAA) and temporal anti-aliasing (TAA). MSAA samples each pixel at multiple locations within the primitive, averaging the results to reduce jagged edges. TAA leverages temporal coherence by blending samples across frames, further improving image stability. The blending operation is given by:

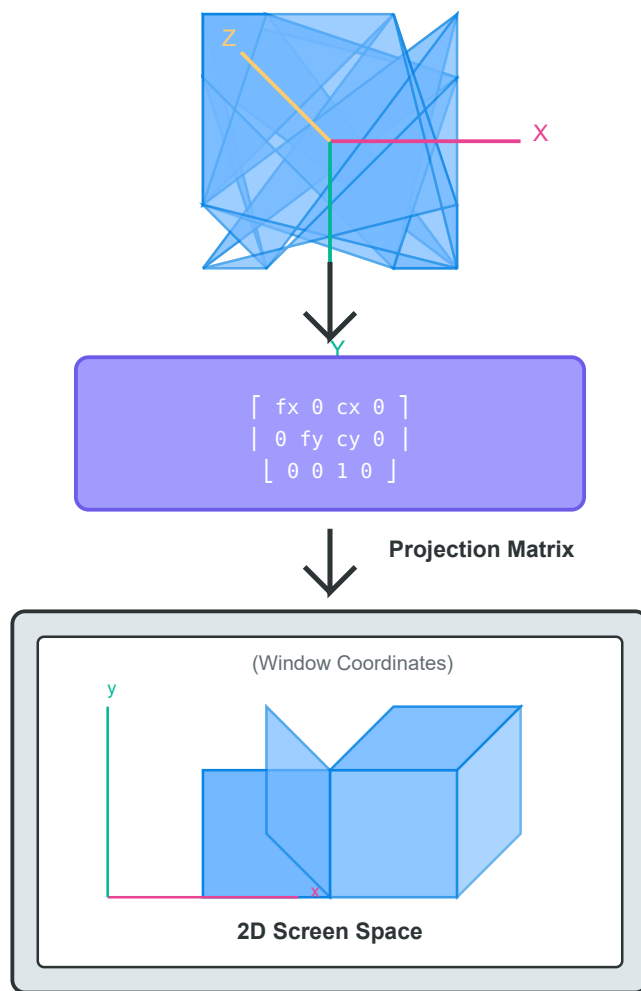
$$C_t = \alpha C_{\text{current}} + (1 - \alpha) C_{t-1}$$

where  $C_t$  is the current frame's color,  $C_{t-1}$  is the previous frame's color, and  $\alpha$  controls the blending weight.

In summary, filtering in modern GPU architectures is a multifaceted process that intersects with shading, texturing, and anti-aliasing. Techniques like bilinear filtering, mipmapping, and anisotropic filtering are essential for achieving high-quality rendering while maintaining performance. The mathematical foundations and hardware implementations of these methods continue to evolve, driven by advancements in real-time graphics and computational efficiency.

# Projection in GPU Architecture

Transforming 3D coordinates to 2D screen space



## Key GPU Projection Stages:

1. Model → World → View → Clip Space (Vertex Shader)
2. Perspective Division (Hardware)
3. Viewport Transform

# Chapter 6

# Digital Logic and HDL Review

## 6.1 Combinational vs. Sequential Logic

### 6.1.1 Review of digital concepts

Modern GPU architectures rely heavily on digital logic design principles, particularly the distinction between combinational and sequential circuits. These foundational concepts govern how data is processed and synchronized within the highly parallelized environment of GPUs.

Combinational logic circuits produce outputs solely based on current inputs, with no internal memory or feedback loops. The output  $Y$  of a combinational circuit can be expressed as:

$$Y = f(X)$$

where  $X$  represents the input vector. Examples include arithmetic logic units (ALUs), multiplexers, and decoders, which are critical for GPU arithmetic operations.

In contrast, sequential logic circuits incorporate memory elements, typically flip-flops or latches, making their outputs dependent on both current inputs and past states. The output  $Q_{n+1}$  of a sequential circuit is given by:

$$Q_{n+1} = f(X, Q_n)$$

where  $Q_n$  denotes the current state. This property enables GPUs to manage pipelining, register files, and control units, which are essential for instruction scheduling and parallelism.

The Verilog implementation of a basic combinational circuit, such as a 2-to-1 multiplexer, demonstrates its simplicity:

Code Sample 6.1: 2-to-1 Multiplexer

```
module mux2to1 (input a, b, sel, output y);
  assign y = sel ? b : a;
endmodule
```

Sequential circuits, however, require clock synchronization. A D flip-flop, a fundamental sequential element, is implemented as:

Code Sample 6.2: D Flip-Flop

```
module dff (input clk, d, output reg q);
  always @ (posedge clk)
    q <= d;
endmodule
```

Key differences between combinational and sequential logic in GPU architectures can be categorized into several areas. In terms of timing, combinational circuits introduce propagation delays  $t_{pd}$ , while sequential circuits add setup  $t_{su}$  and hold  $t_h$  times due to clock constraints. Regarding power consumption, combinational logic dominates dynamic power  $P_{dyn}$ , which is given by:

$$P_{dyn} = \alpha CV^2f$$

where  $\alpha$  is the activity factor,  $C$  is capacitance,  $V$  is voltage, and  $f$  is frequency. Sequential circuits contribute more to leakage power  $P_{leak}$  due to state retention. As for area efficiency, GPUs optimize combinational logic for arithmetic intensity, whereas sequential logic is minimized to reduce register file overhead.

Modern GPUs leverage both circuit types hierarchically. Combinational blocks execute parallel arithmetic operations, such as floating-point units. For instance, NVIDIA's Ampere architecture employs 5120 CUDA cores, each comprising combinational ALUs for matrix multiplication. Sequential blocks, by contrast, manage instruction pipelines and thread scheduling. AMD's RDNA 3 uses waveform schedulers with flip-flop-based state machines to coordinate 128 threads per compute unit.

The trade-offs between combinational and sequential logic are evident in GPU design. From a performance perspective, purely combinational designs would lack synchronization, leading to race conditions, while sequential elements enable deterministic timing via clock domains. In terms of scalability, excessive sequential logic increases latency and limits clock speeds. GPUs balance this with deep pipelines and out-of-order execution.

Advanced GPU features further illustrate these concepts. Speculative execution, for example, combines combinational logic for branch prediction with sequential logic for rollback mechanisms. In memory hierarchies, combinational address decoders access caches, while sequential controllers manage DRAM refresh cycles.

Research confirms that GPUs achieve peak performance by maximizing combinational logic for compute-bound tasks and minimizing sequential overhead. For example, NVIDIA's Tensor Cores use 4-bit combinational multipliers for AI workloads, reducing sequential control logic to under 5% of the die area.

The interplay of these digital concepts is quantified in GPU performance metrics:

$$\text{IPC} = \frac{\text{Instructions}}{\text{Cycle}} = f(\text{Combinational Throughput}, \text{Sequential Overhead})$$

where IPC (instructions per cycle) depends on the ratio of combinational execution units to sequential control logic.

In summary, modern GPU architectures exemplify the synergy of combinational and sequential logic. Combinational circuits enable parallel computation, while sequential circuits provide the necessary control and synchronization. This duality is critical for achieving the high throughput and energy efficiency demanded by contemporary graphics and compute workloads. The Verilog examples and equations provided underscore the mathematical and hardware-realizable foundations of these principles.

### 6.1.2 Combinational circuits

Modern GPU architectures rely heavily on combinational circuits to achieve high throughput and parallelism. Combinational circuits are digital logic circuits where the output depends solely on the current input values, without any internal state or memory. In contrast, sequential circuits incorporate memory elements, making their outputs dependent on both current inputs and past states. The distinction between combinational and sequential logic is fundamental to understanding GPU design, as GPUs leverage both to optimize performance in graphics rendering and parallel computation.

Combinational circuits are constructed using basic logic gates such as AND, OR, NOT, NAND, NOR, XOR, and XNOR. These gates are combined to form more complex circuits like multiplexers, decoders, encoders, and arithmetic logic units (ALUs). For example, a 2-to-1 multiplexer can be implemented using the following Boolean expression:

$$Y = (S \cdot A) + (\bar{S} \cdot B)$$

where  $S$  is the select line, and  $A$  and  $B$  are the input lines. In Verilog:

Code Sample 6.3: 2-to-1 Multiplexer

```
module mux2to1(input A, B, S, output Y);
  assign Y = (S & A) | (~S & B);
endmodule
```

GPUs utilize combinational circuits extensively in their shader cores and texture units. The ALU within a GPU's streaming multiprocessor (SM) performs arithmetic and logical operations using combinational logic. The parallelism in GPUs is achieved by replicating these combinational units across thousands of cores, enabling simultaneous execution of multiple threads. This design contrasts with CPUs, which prioritize sequential execution and rely more on sequential logic for control flow.

Sequential circuits incorporate memory elements such as flip-flops and latches to store state information. A basic D flip-flop is described by:

$$Q(t+1) = D(t)$$

In Verilog:

Code Sample 6.4: D Flip-Flop

```
module dff(input D, clk, output reg Q);
  always @ (posedge clk)
    Q <= D;
endmodule
```

While GPUs predominantly rely on combinational logic for data processing, sequential logic is essential for synchronization and control. The GPU's command processor uses finite state machines (FSMs) to manage instruction scheduling and memory access. The interplay between combinational and sequential logic ensures that GPUs handle both data-parallel tasks and complex control flows efficiently.

Boolean algebra underpins combinational and sequential circuits. Boolean operations are represented using truth tables, Karnaugh maps, or algebraic expressions. For example, XOR is defined as:

$$A \oplus B = A \cdot \overline{B} + \overline{A} \cdot B$$

Combinational circuits are optimized using logic minimization and technology mapping to reduce gate count and propagation delay. The Quine-McCluskey algorithm minimizes Boolean functions, and lookup tables (LUTs) in FPGAs implement combinational logic efficiently. In GPUs, these techniques support high clock frequencies and low power consumption.

Sequential circuits introduce timing constraints such as setup time, hold time, and clock skew. These ensure reliable state transitions and are critical for GPU memory interfaces. GDDR6 memory controllers synchronize data transfers using precise clocking. A synchronous counter in Verilog:

Code Sample 6.5: 4-bit Counter

```
module counter(input clk, rst, output reg [3:0] count);
  always @ (posedge clk or posedge rst) begin
    if (rst)
      count <= 0;
    else
      count <= count + 1;
  end
endmodule
```

Modern GPU architectures integrate combinational and sequential logic for performance and flexibility. NVIDIA's Ampere architecture uses combinational logic in CUDA cores and sequential logic for thread scheduling and memory coherence. AMD's RDNA 2 architecture illustrates continued optimization of logic design for workloads such as AI and ray tracing.

$$A \oplus B = A \cdot \overline{B} + \overline{A} \cdot B$$

### 6.1.3 Sequential circuits

Modern GPU architectures rely heavily on digital logic design principles, particularly the distinction between combinational and sequential circuits. Combinational circuits produce outputs solely based on current inputs, while sequential circuits incorporate memory elements, enabling state retention and temporal behavior. This distinction is critical in GPU design, where parallelism and pipelining demand efficient state management.

Combinational circuits form the foundation of arithmetic and logic operations in GPUs. These circuits, such as adders, multipliers, and multiplexers, are stateless and follow Boolean algebra principles. For example, a 32-bit adder in a GPU's arithmetic logic unit (ALU) computes the sum  $S$  of two inputs  $A$  and  $B$  as:

$$S = A + B$$

Such circuits are optimized for minimal propagation delay, as GPUs require high throughput for parallel workloads like shader computations.

Sequential circuits, however, introduce memory elements, typically flip-flops or latches, to store state between clock cycles. A basic D flip-flop captures the input  $D$  on the rising edge of the clock signal  $clk$ , producing the output  $Q$ :

$$Q_{n+1} = D_n$$

This behavior is essential for registers, pipelines, and finite state machines (FSMs) in GPUs. For instance, a GPU's texture unit employs sequential logic to manage memory access patterns across multiple clock cycles.

The interplay between combinational and sequential logic is evident in GPU pipelines. A simplified pipeline stage might consist of combinational logic for computation followed by a register for state storage. The following Verilog snippet illustrates a single pipeline stage:

Code Sample 6.6: Pipeline stage in Verilog

```
module pipeline_stage (
    input clk,
    input [31:0] in_data,
    output reg [31:0] out_data
);
always @(posedge clk) begin
    out_data <= in_data + 1; // Sequential update
end
endmodule
```

Key differences between combinational and sequential logic in GPUs include:

- **Timing:** Combinational logic is asynchronous, while sequential logic is synchronous, relying on clock signals for synchronization.
- **Power Consumption:** Sequential circuits consume dynamic power due to clock switching, whereas combinational circuits primarily dissipate static and dynamic power based on input transitions.
- **Area Overhead:** Sequential logic requires additional area for flip-flops and clock distribution networks, impacting GPU die size.

Modern GPUs leverage both types of logic to balance performance and power efficiency. For example, NVIDIA's Ampere architecture uses combinational logic for floating-point units (FPUs) and sequential logic for instruction scheduling and warp management. The FPUs compute results in a single clock cycle (combinational), while the scheduler maintains thread states across cycles (sequential).

Finite state machines (FSMs) are a common application of sequential logic in GPUs. A texture filtering FSM might transition between states like `IDLE`, `FETCH`, and `FILTER` based on input signals. The next state  $S_{n+1}$  is determined by the current state  $S_n$  and inputs  $I$ :

$$S_{n+1} = f(S_n, I)$$

This enables complex control flows, such as handling cache misses or texture compression.

Memory hierarchies in GPUs also rely on sequential logic. Cache controllers use FSMs to manage read/write operations, while DRAM interfaces employ sequential circuits for timing-critical operations like row activation and precharging. The following equation models a cache line update:

$$\text{Cache}[A]_{n+1} = \begin{cases} D & \text{if write\_enable} \\ \text{Cache}[A]_n & \text{otherwise} \end{cases}$$

Here,  $A$  is the address,  $D$  is the data, and  $n$  denotes the clock cycle.

Clock domain crossing (CDC) is another challenge in GPU design, where sequential circuits in different clock domains communicate. Metastability risks are mitigated using synchronizers, typically two flip-flops in series:

Code Sample 6.7: Synchronizer in Verilog

```
module synchronizer (
    input clk,
    input async_signal,
    output reg sync_signal
```

```

);
reg ff1;
always @(posedge clk) begin
    ff1 <= async_signal;
    sync_signal <= ff1;
end
endmodule

```

Power gating in GPUs illustrates the trade-offs between combinational and sequential logic. Combinational blocks can be power-gated independently, but sequential blocks require state retention or restoration. Techniques like clock gating and flip-flop recycling are used to minimize leakage power in idle sequential circuits.

Performance analysis of GPU pipelines often involves timing diagrams and critical path identification. The critical path delay  $T_{cp}$  of a pipeline stage is the sum of combinational logic delay  $T_{comb}$  and setup time  $T_{su}$  of the sequential element:

$$T_{cp} = T_{comb} + T_{su}$$

This determines the maximum clock frequency, a key metric in GPU design.

Emerging technologies like near-threshold computing (NTC) further blur the line between combinational and sequential logic. NTC GPUs operate at reduced voltages, exacerbating timing violations in sequential circuits but improving energy efficiency in combinational logic.

In summary, modern GPU architectures integrate combinational and sequential logic to achieve high performance and energy efficiency. Combinational circuits handle parallel computations, while sequential circuits manage state and control flow. This duality is fundamental to GPU design, enabling advancements in real-time graphics, machine learning, and scientific computing.

## 6.2 Verilog Basics

### 6.2.1 Modules and hierarchical design

Modern GPU architectures leverage hierarchical design principles to manage complexity and optimize performance. At the core of this approach lies the use of Verilog modules, which encapsulate functionality into reusable blocks. A `module` in Verilog serves as the fundamental building block, analogous to functions in software. For example, a simple GPU arithmetic logic unit (ALU) might be defined as:

Code Sample 6.8: Basic Verilog Module

```

module ALU (
    input [31:0] a, b,
    input [2:0] op,
    output reg [31:0] result
);
always @(*) begin
    case (op)
        3'b000: result = a + b;
        3'b001: result = a - b;
        default: result = 32'b0;
    endcase
end
endmodule

```

Hierarchical design emerges when modules instantiate other modules, creating a tree-like structure. This mirrors the organization of modern GPUs, where streaming multiprocessors (SMs) contain smaller processing cores. For instance, a GPU SM might instantiate multiple ALU modules:

Code Sample 6.9: Hierarchical Module Instantiation

```

module SM (
    input [31:0] a[0:31], b[0:31],
    input [2:0] op[0:31],
    output [31:0] result[0:31]
);

```

```

genvar i;
generate
    for (i = 0; i < 32; i = i + 1) begin
        ALU alu_inst (.a(a[i]), .b(b[i]), .op(op[i]), .result(result[i]));
    end
endgenerate
endmodule

```

Wires and registers (`wire` and `reg`) form the backbone of data representation. Wires model combinational connections, while registers store state. In GPU designs, wires often interconnect modules, while registers hold intermediate values. Continuous assignments (`assign`) drive wires, as shown in this multiplexer example:

Code Sample 6.10: Continuous Assignment

```

module MUX (
    input [31:0] a, b,
    input sel,
    output [31:0] out
);
assign out = sel ? b : a;
endmodule

```

Always blocks (`always @(*)`) describe sequential or combinational logic. GPU pipelines heavily rely on these for register updates. For example, a GPU register file might use:

Code Sample 6.11: Always Block for Register File

```

module RegFile (
    input clk,
    input [4:0] addr,
    input [31:0] din,
    input we,
    output reg [31:0] dout
);
reg [31:0] mem [0:31];
always @(posedge clk) begin
    if (we) mem[addr] <= din;
    dout <= mem[addr];
end
endmodule

```

Parameters (`parameter`) enable configurable designs, crucial for GPU scalability. A texture unit might parameterize its filter size:

Code Sample 6.12: Parameterized Module

```

module TextureUnit #(
    parameter FILTER_SIZE = 4
) (
    input [31:0] texels [0:FILTER_SIZE-1],
    output [31:0] filtered
);
// Filtering logic here
endmodule

```

Generate statements (`generate`) automate repetitive structures, essential for GPU parallelism. A warp scheduler might generate multiple issue slots:

Code Sample 6.13: Generate Statement

```

module WarpScheduler #(
    parameter WARPS = 16
) (
    input clk,
    input [31:0] pc [0:WARPS-1],
    output [31:0] next_pc [0:WARPS-1]
);

```

```

genvar i;
generate
    for (i = 0; i < WARPS; i = i + 1) begin
        always @ (posedge clk) begin
            next_pc[i] <= pc[i] + 4;
        end
    end
endgenerate
endmodule

```

The interplay of these constructs enables efficient GPU designs. For example, NVIDIA’s Ampere architecture employs hierarchical modules for its tensor cores, with parameters adjusting precision modes. Similarly, AMD’s RDNA 3 uses generate statements to scale compute units across chiplets.

Mathematically, module hierarchies can be modeled as directed acyclic graphs (DAGs). Let  $M$  represent a module with inputs  $I$  and outputs  $O$ . The composition of modules forms a hierarchy  $H$ :

$$H = (M_1, M_2, \dots, M_n, E)$$

where  $E$  denotes the set of connections between modules. The fan-out  $F$  of a module  $M_i$  is given by:

$$F(M_i) = |\{M_j \mid (M_i, M_j) \in E\}|$$

Continuous assignments implement Boolean functions  $f$  mapping inputs to outputs:

$$f : \mathbb{B}^n \rightarrow \mathbb{B}^m$$

Always blocks with clock domains model finite state machines (FSMs) with states  $S$ :

$$\delta : S \times I \rightarrow S$$

$$\lambda : S \times I \rightarrow O$$

Parameters enable dimensional analysis. For a texture unit with  $N$  texels, the address width  $W$  satisfies:

$$W = \lceil \log_2 N \rceil$$

Generate statements expand to  $k$  instances, each with area  $A$ , yielding total area:

$$A_{\text{total}} = k \cdot A$$

In practice, GPU designers balance these elements. For example, NVIDIA’s CUDA cores use module hierarchies to share instruction decoders across execution units. AMD’s Infinity Cache employs parameters to tune cache sizes per product tier.

Key considerations in hierarchical GPU design include:

- Module granularity: Too fine-grained increases overhead; too coarse reduces flexibility
- Wire routing: Global wires introduce latency; local wires limit connectivity
- Parameter ranges: Must cover all product variants without excessive overhead
- Generate bounds: Must match physical constraints like die area

Verilog’s module system directly supports these needs through:

- Encapsulation via module boundaries
- Reuse through instantiation
- Configuration via parameters
- Scalability via generate

Modern GPUs push these concepts further. For instance, Intel's Xe architecture uses hierarchical modules to separate matrix engines from vector units. Apple's M-series GPUs employ parameterized shader cores to scale across products.

The mathematical foundation enables optimization. Let  $C$  be a design with  $n$  modules. The optimal hierarchy minimizes:

$$\min_H \sum_{i=1}^n (F(M_i) \cdot t_{\text{wire}} + A(M_i))$$

where  $t_{\text{wire}}$  is wire delay and  $A$  is module area. This aligns with GPU design goals of maximizing throughput per watt.

In summary, Verilog's module system provides the structural foundation for modern GPU architectures. Through hierarchical composition, parameterized generation, and careful signal management, designers build the massively parallel processors driving today's computing. The mathematical models underlying these constructs enable both formal verification and performance optimization, ensuring GPUs meet their demanding targets.

## 6.2.2 Wires and regs

Modern GPU architectures rely heavily on hardware description languages like Verilog for their design and implementation. Understanding Verilog basics, particularly modules, hierarchical design, wires, registers, and control structures, is essential for designing efficient GPU components.

In Verilog, a module serves as the fundamental building block, encapsulating functionality and enabling hierarchical design. For example, a simple GPU arithmetic logic unit (ALU) can be defined as:

Code Sample 6.14: ALU Module

```
module ALU (
    input [31:0] a, b,
    input [2:0] op,
    output reg [31:0] out
);
always @(*) begin
    case (op)
        3'b000: out = a + b;
        3'b001: out = a - b;
        3'b010: out = a & b;
        default: out = 32'b0;
    endcase
end
endmodule
```

Wires (`wire`) and registers (`reg`) are critical data types in Verilog. Wires represent physical connections and are used for combinational logic, while registers store state and are used in procedural blocks like `always`. For instance, a wire connecting two modules can be declared as:

Code Sample 6.15: Wire Declaration

```
wire [31:0] data_bus;
```

Continuous assignments model combinational logic without procedural blocks. They use the `assign` keyword and update whenever input signals change. For example, a multiplexer can be implemented as:

Code Sample 6.16: Continuous Assignment

```
assign out = sel ? a : b;
```

Procedural logic is described using `always` blocks, which execute based on sensitivity lists. Edge-triggered `always` blocks model sequential logic, while level-sensitive blocks model combinational logic. A flip-flop with asynchronous reset is:

Code Sample 6.17: Flip-Flop with Reset

```
always @(posedge clk or posedge rst) begin
    if (rst)
        q <= 1'b0;
```

```

    else
        q <= d;
end

```

Parameters enhance modularity by allowing configurable constants. For example, a parameterized adder can adjust its bit width:

Code Sample 6.18: Parameterized Adder

```

module adder #(parameter WIDTH = 32) (
    input [WIDTH-1:0] a, b,
    output [WIDTH-1:0] sum
);
assign sum = a + b;
endmodule

```

Generate statements enable conditional or iterative instantiation of hardware structures. They are useful for creating scalable designs, such as a parallel prefix adder:

Code Sample 6.19: Generate Statement

```

generate
    for (i = 0; i < N; i = i + 1) begin
        assign carry[i+1] = a[i] & b[i] | (a[i] | b[i]) & carry[i];
    end
endgenerate

```

In GPU architectures, these constructs optimize performance and area. For example, NVIDIA's Fermi architecture uses hierarchical modules for streaming multiprocessors (SMs), where each SM contains multiple CUDA cores. Similarly, AMD's GCN architecture employs parameterized modules for compute units, enabling scalability across GPU generations.

The interplay between wires and registers is crucial for pipelining. Wires propagate signals between pipeline stages, while registers store intermediate results. A simplified GPU pipeline stage might be:

Code Sample 6.20: Pipeline Stage

```

module pipeline_stage (
    input clk,
    input [31:0] in_data,
    output reg [31:0] out_data
);
always @(posedge clk) begin
    out_data <= in_data;
end
endmodule

```

Hierarchical design simplifies complex GPUs by breaking them into manageable submodules. For instance, a texture mapping unit (TMU) can be composed of smaller modules for filtering and address calculation. This modularity improves verification and reuse.

Continuous assignments are ideal for arithmetic units, where combinational logic dominates. For example, a floating-point multiplier in a GPU shader core can be implemented as:

Code Sample 6.21: Floating-Point Multiplier

```
assign product = {a[31] ^ b[31], a[30:23] + b[30:23] - 127, (a[22:0] * b[22:0]) >> 23};
```

Always blocks with sensitivity to clock edges model synchronous elements like register files. A GPU register file might use:

Code Sample 6.22: Register File

```

always @(posedge clk) begin
    if (we)
        regfile[addr] <= wdata;
    rdata <= regfile[addr];
end

```

Parameters enable design flexibility. For example, a GPU’s warp scheduler can be parameterized to support different numbers of warps:

Code Sample 6.23: Parameterized Warp Scheduler

```
module warp_scheduler #(parameter WARPS = 32) (
    input clk,
    input [WARPS-1:0] active,
    output [4:0] next_warp
);
// Scheduling logic
endmodule
```

Generate statements automate repetitive structures, such as a GPU’s SIMD lanes. Each lane can be instantiated as:

Code Sample 6.24: SIMD Lane Generation

```
generate
    for (i = 0; i < LANES; i = i + 1) begin
        simd_lane lane_inst (
            .clk(clk),
            .in_data(data[i]),
            .out_data(result[i])
        );
    end
endgenerate
```

In summary, Verilog’s constructs—modules, wires, registers, continuous assignments, always blocks, parameters, and generate statements—are foundational for GPU design. They enable efficient, scalable, and maintainable implementations, as evidenced by modern architectures like NVIDIA’s Ampere and AMD’s RDNA .

### 6.2.3 Continuous assignments

Modern GPU architectures leverage highly parallelizable designs to accelerate compute-intensive tasks, making them indispensable in fields like machine learning and scientific computing. A fundamental aspect of designing such architectures involves hardware description languages (HDLs) like Verilog, which enable precise modeling of digital circuits. This discussion focuses on continuous assignments in Verilog, their role in GPU design, and their relationship with other Verilog constructs such as modules, wires, registers, and procedural blocks.

Continuous assignments in Verilog are used to model combinational logic, where the output updates automatically whenever any input changes. Unlike procedural assignments in `always` blocks, continuous assignments operate without explicit triggering events. The syntax for a continuous assignment is straightforward, using the `assign` keyword:

Code Sample 6.25: Continuous assignment example

```
wire [7:0] a, b, sum;
assign sum = a + b;
```

Here, the output `sum` is continuously updated whenever `a` or `b` changes. This behavior is critical in GPU architectures for arithmetic logic units (ALUs) and other combinational circuits. Continuous assignments are synthesizable, ensuring they map directly to hardware gates during implementation.

Modules form the building blocks of hierarchical design in Verilog, encapsulating functionality and enabling reuse. A GPU’s streaming multiprocessor (SM) can be modeled as a module containing smaller submodules like warp schedulers or execution units. Hierarchical design simplifies verification and scalability, as shown below:

Code Sample 6.26: Hierarchical module example

```
module ALU (
    input [31:0] op1, op2,
    output [31:0] result
);
assign result = op1 + op2;
endmodule
```

Wires (`wire`) and registers (`reg`) are fundamental data types in Verilog. Wires represent physical connections and are driven by continuous assignments or module outputs. Registers, on the other hand, store values and are typically assigned within `always` blocks. In GPU designs, wires interconnect functional units, while registers store intermediate states in pipelines. For example:

Code Sample 6.27: Wire and reg usage

```
reg [31:0] pipeline_reg;
wire [31:0] alu_out;
assign alu_out = pipeline_reg + 1;
```

Continuous assignments differ from procedural assignments in `always` blocks, which execute sequentially within triggered scopes. While continuous assignments model combinational logic, `always` blocks describe sequential or latched behavior. For instance, a GPU's register file might use an `always` block for synchronous writes:

Code Sample 6.28: Always block for sequential logic

```
always @(posedge clk) begin
    if (write_en)
        reg_file[addr] <= data;
end
```

Parameters enhance modularity by allowing configurable values. In GPU design, parameters define scalable features like warp size or memory banks. They are declared using `parameter` or `localparam` and can be overridden during instantiation:

Code Sample 6.29: Parameterized module

```
module Memory #(
    parameter DEPTH = 1024,
    parameter WIDTH = 32
) (
    input [WIDTH-1:0] addr,
    output [WIDTH-1:0] data
);
reg [WIDTH-1:0] mem [0:DEPTH-1];
assign data = mem[addr];
endmodule
```

Generate statements enable conditional or iterative instantiation of hardware structures, which is essential for GPUs with configurable core counts or thread blocks. They are evaluated during elaboration and can create multiple instances of modules or assignments:

Code Sample 6.30: Generate statement for parallel units

```
genvar i;
generate
    for (i = 0; i < 32; i = i + 1) begin : ALU_ARRAY
        ALU alu_inst (
            .op1(op1[i]),
            .op2(op2[i]),
            .result(result[i])
        );
    end
endgenerate
```

The interplay between continuous assignments and other Verilog constructs is evident in GPU arithmetic units. For example, a floating-point adder might combine continuous assignments for combinational logic and `always` blocks for pipelining. The following snippet illustrates a simplified version:

Code Sample 6.31: Mixed continuous and procedural logic

```
module FP_Adder (
    input [31:0] a, b,
    output reg [31:0] sum
);
wire [31:0] aligned_b;
```

```
assign aligned_b = b + 1; // Combinational alignment

always @(posedge clk) begin
    sum <= a + aligned_b; // Pipelined addition
end
endmodule
```

Continuous assignments also facilitate the modeling of multiplexers and decoders, which are ubiquitous in GPU control logic. A multiplexer can be implemented concisely using a conditional operator:

Code Sample 6.32: Multiplexer using continuous assignment

```
wire [31:0] mux_out;
assign mux_out = (sel) ? in1 : in0;
```

In summary, continuous assignments are a cornerstone of Verilog design, enabling efficient modeling of combinational logic in GPUs. Their integration with hierarchical modules, wires, registers, and procedural blocks ensures accurate representation of hardware behavior. Parameters and generate statements further enhance scalability, making Verilog indispensable for modern GPU architecture development. The examples provided demonstrate how these constructs collectively contribute to the design of high-performance, parallel computing systems.

### 6.2.4 Always blocks

In modern GPU architecture, the efficient implementation of digital logic relies heavily on hardware description languages (HDLs) like Verilog. Among Verilog's fundamental constructs, `always` blocks play a pivotal role in modeling sequential and combinational logic. This discussion explores `always` blocks within the context of Verilog basics, modules, hierarchical design, wires, registers, continuous assignments, parameters, and generate statements.

The `always` block is a procedural construct in Verilog that executes continuously in response to specified sensitivity lists. For example, a flip-flop can be modeled as:

Code Sample 6.33: D Flip-Flop

```
always @ (posedge clk) begin
    q <= d;
end
```

Here, the block triggers on the rising edge of `clk`, assigning the value of `d` to `q` using non-blocking assignment (`<=`). This ensures correct simulation of synchronous logic. The sensitivity list determines when the block executes, with common triggers including clock edges (`posedge` or `negedge`) or level-sensitive signals.

In GPU architectures, `always` blocks are used to describe pipelined stages, arithmetic logic units (ALUs), and memory controllers. For instance, a simplified ALU operation might be:

Code Sample 6.34: ALU Example

```
always @(*) begin
    case (opcode)
        2'b00: out = a + b;
        2'b01: out = a - b;
        2'b10: out = a & b;
        default: out = 0;
    endcase
end
```

The wildcard sensitivity list (`@(*)`) ensures the block executes whenever any input (`opcode`, `a`, or `b`) changes, modeling combinational logic.

Modules and hierarchical design are central to Verilog. A GPU consists of interconnected modules, each encapsulating specific functionality. For example:

Code Sample 6.35: Hierarchical Module

```
module ALU (
    input [31:0] a, b,
    input [1:0] opcode,
    output reg [31:0] out
);
always @(*) begin
    // ALU logic here
end
endmodule
```

Here, the `ALU` module can be instantiated within a larger GPU design, promoting modularity and reuse. Hierarchical design simplifies debugging and verification, critical for complex GPUs.

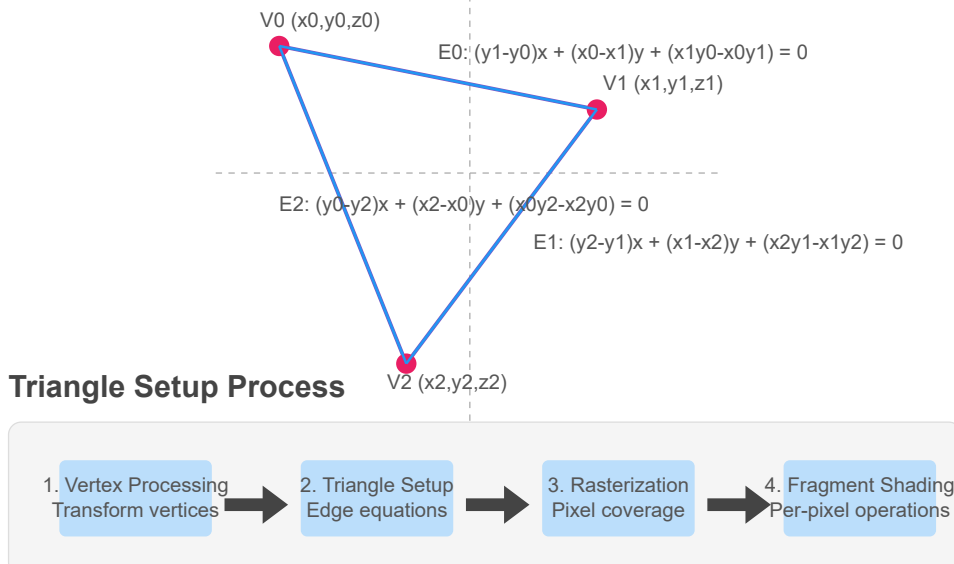
Wires and registers (`wire` and `reg`) define signal types in Verilog. Wires represent physical connections, while registers store values. In `always` blocks, only `reg` types can be assigned, even for combinational logic. For example:

Code Sample 6.36: Wire vs. Reg

```
wire [7:0] data_in;
reg [7:0] data_out;
always @ (posedge clk) begin
    data_out <= data_in;
end
```

Continuous assignments, using the `assign` keyword, model combinational logic without procedural blocks. For example:

## GPU Triangle Setup



### Edge Equation Calculation

For edge  $E$  between vertices  $(x_1, y_1)$  and  $(x_2, y_2)$ :

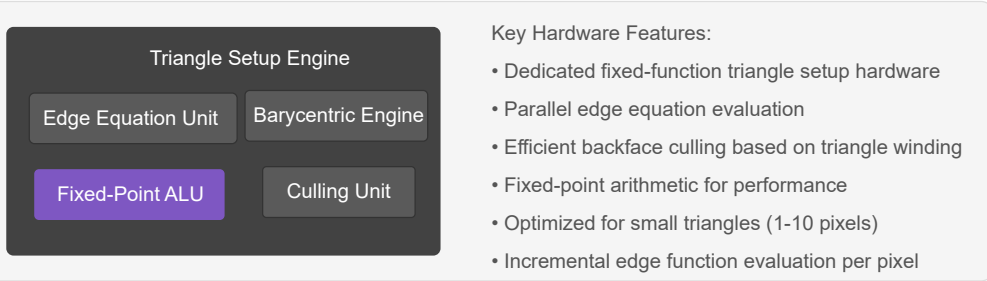
$$E(x, y) = (y_2 - y_1)x + (x_1 - x_2)y + (x_2y_1 - x_1y_2)$$

$$E(x, y) = A \cdot x + B \cdot y + C$$

Where:  $A = (y_2 - y_1)$ ,  $B = (x_1 - x_2)$ ,  $C = (x_2y_1 - x_1y_2)$

- $E(x, y) > 0$  : Point  $(x, y)$  is on one side of the edge
- $E(x, y) < 0$  : Point  $(x, y)$  is on the other side

### GPU Hardware Implementation



Modern GPU Architecture: Triangle Setup Pipeline

## Code Sample 6.37: Continuous Assignment

```
wire [7:0] sum = a + b;
```

Unlike `always` blocks, continuous assignments lack procedural control but are syntactically concise for simple logic.

Parameters enhance module flexibility by allowing compile-time constants. For example:

## Code Sample 6.38: Parameterized Module

```
module #(parameter WIDTH = 32) Adder (
    input [WIDTH-1:0] a, b,
    output [WIDTH-1:0] sum
);
    assign sum = a + b;
endmodule
```

Parameters enable customization, such as adjusting bit-widths for GPU datapaths.

Generate statements automate repetitive structures, useful for GPU parallelism. For example:

## Code Sample 6.39: Generate Example

```
genvar i;
generate
    for (i = 0; i < 8; i = i + 1) begin : adder_array
        Adder #(.WIDTH(16)) adder (
            .a(a[i*16 +: 16]),
            .b(b[i*16 +: 16]),
            .sum(sum[i*16 +: 16])
        );
    end
endgenerate
```

This creates eight 16-bit adders, leveraging `always` blocks within each instance.

In GPU design, `always` blocks must adhere to synthesis rules to ensure correct hardware mapping. For example, incomplete sensitivity lists can lead to mismatches between simulation and synthesis. Research by highlights the importance of strict coding guidelines for `always` blocks in high-performance designs.

The interplay between `always` blocks and other Verilog constructs is critical for GPU efficiency. For instance, pipelined designs often use multiple `always` blocks to separate stages:

## Code Sample 6.40: Pipelined Logic

```
always @ (posedge clk) begin
    stage1 <= input_data;
    stage2 <= stage1 * coefficient;
    stage3 <= stage2 + bias;
end
```

Each stage executes sequentially, optimizing throughput.

In summary, `always` blocks are indispensable in Verilog for modeling GPU logic. Their correct use, alongside modules, wires, registers, parameters, and generate statements, ensures robust and scalable designs. The cited literature underscores their role in modern GPU architecture, where performance and correctness are paramount.

### 6.2.5 Parameters

Modern GPU architectures leverage parameterized design techniques in Verilog to achieve flexibility and scalability. Parameters in Verilog are compile-time constants that enable customization of modules without modifying the underlying code. This is particularly useful in GPU design, where identical processing elements (PEs) are replicated with slight variations.

For example, a parameterized multiplier module can be instantiated with different bit-widths across a GPU's shader cores:

## Code Sample 6.41: Parameterized Multiplier Module

```
module multiplier #(
    parameter WIDTH = 32
```

```

) (
    input [WIDTH-1:0] a, b,
    output [2*WIDTH-1:0] product
);
assign product = a * b;
endmodule

```

The hierarchical nature of GPU designs necessitates careful parameter propagation. A texture processing unit (TPU) might instantiate multiple filter modules with different kernel sizes:

Code Sample 6.42: Hierarchical Parameter Usage

```

module tpu #(
    parameter KERNEL_SIZE = 3
) (
    input pixel_data,
    output filtered
);
filter #(.TAPS(KERNEL_SIZE)) f1 (pixel_data, filtered);
endmodule

```

Wires and registers in GPU designs follow specific parameter-dependent rules. Arithmetic logic units (ALUs) often use parameterized register files:

Code Sample 6.43: Parameterized Register File

```

module reg_file #(
    parameter DEPTH = 64,
    parameter WIDTH = 32
) (
    input [clog2(DEPTH)-1:0] addr,
    output [WIDTH-1:0] data
);
reg [WIDTH-1:0] mem [0:DEPTH-1];
assign data = mem[addr];
endmodule

```

Continuous assignments in GPU datapaths frequently incorporate parameters for signal routing. A crossbar switch might use parameters to define its port count:

Code Sample 6.44: Parameterized Crossbar

```

module crossbar #(
    parameter PORTS = 8,
    parameter WIDTH = 128
) (
    input [PORTS*WIDTH-1:0] in,
    output [PORTS*WIDTH-1:0] out
);
genvar i;
generate
    for (i = 0; i < PORTS; i = i + 1) begin : port_map
        assign out[i*WIDTH +: WIDTH] = in[i*WIDTH +: WIDTH];
    end
endgenerate
endmodule

```

The verification of parameterized GPU designs requires specialized testbenches that exercise all parameter combinations. A parameterized testbench for a floating-point unit might include:

Code Sample 6.45: Parameterized Testbench

```

module test_fpu #(
    parameter EXP_BITS = 8,
    parameter MANT_BITS = 23
);
reg [EXP_BITS+MANT_BITS:0] a, b;

```

```

wire [EXP_BITS+MANT_BITS:0] out;

fpu #( .EXP(EXP_BITS), .MANT(MANT_BITS)) uut (
    .a(a), .b(b), .out(out)
);

// Add test vectors here

endmodule

```

Modern GPU architectures extensively use parameterized modules to achieve design reuse across different product tiers. A unified shader core might be instantiated with varying numbers of arithmetic pipelines:

Code Sample 6.46: Scalable Shader Core

```

module shader_core #(
    parameter PIPES = 32
) (
    input [31:0] instruction,
    output [31:0] result [0:PIPES-1]
);
genvar i;
generate
    for (i = 0; i < PIPES; i = i + 1) begin : pipe_array
        alu alu_inst (
            .instruction(instruction),
            .result(result[i])
        );
    end
endgenerate
endmodule

```

In summary, Verilog parameters enable scalable, reusable GPU design by allowing module customization at compile time. This technique is foundational to the modular and hierarchical design strategies used in modern graphics architectures.

### 6.2.6 Generate statements

Modern GPU architectures leverage highly parallelized designs to achieve exceptional computational throughput. These architectures rely on hardware description languages like Verilog to model their intricate structures. Verilog's generate statements play a pivotal role in creating scalable and parameterized designs, particularly in GPU implementations where repetitive structures such as processing elements (PEs) or memory banks are common.

The hierarchical design of GPUs necessitates modular Verilog constructs. A `module` serves as the fundamental building block, encapsulating functionality and enabling reuse. For example, a single streaming multiprocessor (SM) in NVIDIA's CUDA architecture can be modeled as a Verilog module:

Code Sample 6.47: Streaming Multiprocessor Module

```

module SM (
    input clk,
    input reset,
    input [31:0] instruction,
    output [31:0] result
);
// Core logic here
endmodule

```

Interconnections between modules are defined using `wires` for combinational pathways and `regs` for sequential storage. In GPU designs, wires facilitate high-speed data transfer between arithmetic logic units (ALUs), while `regs` store intermediate results in pipeline stages.

Continuous assignments with `assign` model combinational logic, such as the propagation of signals across a crossbar switch:

## Code Sample 6.48: Crossbar Switch Continuous Assignment

```
wire [63:0] data_out;
assign data_out = sel ? data_a : data_b;
```

Sequential logic in GPUs, such as register files or control units, is implemented using `always` blocks. These blocks synchronize operations to clock edges, ensuring deterministic behavior. For instance, a GPU's thread scheduler might use an `always` block to manage warp execution:

## Code Sample 6.49: Warp Scheduler Sequential Logic

```
always @ (posedge clk) begin
    if (reset)
        warp_ptr <= 0;
    else
        warp_ptr <= next_warp;
end
```

Parameters enhance design flexibility by allowing runtime customization. In GPU architectures, parameters define the number of CUDA cores per SM or the size of shared memory. A parameterized FIFO buffer for a GPU's texture unit can be declared as:

## Code Sample 6.50: Parameterized FIFO Module

```
module FIFO #(
    parameter DEPTH = 32
) (
    input clk,
    input [31:0] data_in,
    output [31:0] data_out
);
reg [31:0] mem [0:DEPTH-1];
// FIFO logic
endmodule
```

`Generate` statements automate the instantiation of repetitive structures, a critical feature for GPU designs with thousands of identical processing units. For example, a GPU's SIMD (Single Instruction, Multiple Data) array can be constructed using `generate` to replicate ALUs:

## Code Sample 6.51: SIMD Array Using Generate

```
genvar i;
generate
    for (i = 0; i < 64; i = i + 1) begin : ALU_ARRAY
        ALU alu_inst (
            .clk(clk),
            .opcode(opcode),
            .a(data_a[i]),
            .b(data_b[i]),
            .out(result[i])
        );
    end
endgenerate
```

Conditional `generate` blocks enable architecture-specific optimizations. For instance, NVIDIA's Ampere architecture supports both FP32 and TF32 precision modes, which can be selectively included using `if-generate`:

## Code Sample 6.52: Conditional Precision Logic

```
generate
    if (USE_TF32) begin
        FPU_TF32 fpu (*.*);
    end else begin
        FPU_FP32 fpu (*.*);
    end
endgenerate
```

The synthesis of GPU components relies on these Verilog constructs to balance performance and area efficiency. For example, generate statements reduce manual coding errors in large-scale designs like tensor cores, which require precise replication of multiply-accumulate (MAC) units.

Memory hierarchies in GPUs also benefit from hierarchical Verilog design. A shared memory bank with configurable ports can be modeled as:

Code Sample 6.53: Configurable Memory Bank

```
module MemoryBank #( 
    parameter PORTS = 4
) (
    input clk,
    input [PORTS-1:0] wr_en,
    input [31:0] addr [PORTS-1:0],
    inout [31:0] data [PORTS-1:0]
);
// Multi-port memory logic
endmodule
```

Generate statements further optimize interconnect networks, such as NVIDIA's NVLink, by dynamically instantiating lanes based on bandwidth requirements. The following snippet demonstrates lane generation for a high-speed interconnect:

Code Sample 6.54: Interconnect Lane Generation

```
genvar lane;
generate
    for (lane = 0; lane < LANES; lane = lane + 1) begin : LANE_GEN
        SerDes serdes_inst (
            .clk(clk_div[lane]),
            .tx(tx_data[lane]),
            .rx(rx_data[lane])
        );
    end
endgenerate
```

In summary, Verilog's generate statements and hierarchical design principles are indispensable for modern GPU architectures. They enable scalable, maintainable, and high-performance implementations, as evidenced by industry-standard designs from NVIDIA, AMD, and Intel.

## 6.3 Common GPU Design Constructs

### 6.3.1 Pipeline registers

Modern GPU architectures rely heavily on pipelining to achieve high throughput and low latency. Pipeline registers are fundamental components in these designs, serving as temporary storage elements between pipeline stages. They enable the synchronization of data flow and ensure correct timing across clock domains. In GPU architectures, pipeline registers are typically implemented using flip-flops or latches, with their depth and width tailored to the specific requirements of each pipeline stage. The use of pipeline registers allows GPUs to maintain high clock frequencies while processing multiple instructions concurrently.

The role of pipeline registers becomes particularly evident in arithmetic logic units (ALUs) and texture units, where parallel arithmetic operations are performed. For example, a floating-point multiplier in a GPU may be pipelined into several stages, each with its own set of pipeline registers. This partitioning reduces the critical path delay, enabling higher clock frequencies. The following Verilog snippet illustrates a simple pipelined multiplier with two stages:

Code Sample 6.55: Pipelined Multiplier in Verilog

```
module pipelined_multiplier (
    input clk, rst,
    input [31:0] a, b,
    output reg [63:0] product
);
```

```

reg [31:0] a_reg, b_reg;
reg [63:0] partial_product;

always @(posedge clk or posedge rst) begin
    if (rst) begin
        a_reg <= 0;
        b_reg <= 0;
        partial_product <= 0;
        product <= 0;
    end else begin
        // Stage 1: Register inputs and compute partial product
        a_reg <= a;
        b_reg <= b;
        partial_product <= a * b;

        // Stage 2: Register final product
        product <= partial_product;
    end
end
endmodule

```

FIFOs (First-In-First-Out buffers) are another critical construct in GPU architectures, often used for buffering data between asynchronous clock domains or handling variable-latency operations. FIFOs are implemented using either registers or block RAM (BRAM), depending on the required depth and performance constraints. In Verilog, a synchronous FIFO can be described as follows:

Code Sample 6.56: Synchronous FIFO in Verilog

```

module sync_fifo #(
    parameter DATA_WIDTH = 32,
    parameter DEPTH = 8
) (
    input clk, rst,
    input wr_en, rd_en,
    input [DATA_WIDTH-1:0] din,
    output reg [DATA_WIDTH-1:0] dout,
    output full, empty
);
    reg [DATA_WIDTH-1:0] mem [0:DEPTH-1];
    reg [2:0] wr_ptr, rd_ptr;
    reg [3:0] count;

    assign full = (count == DEPTH);
    assign empty = (count == 0);

    always @(posedge clk or posedge rst) begin
        if (rst) begin
            wr_ptr <= 0;
            rd_ptr <= 0;
            count <= 0;
        end else begin
            if (wr_en && !full) begin
                mem[wr_ptr] <= din;
                wr_ptr <= wr_ptr + 1;
            end
            if (rd_en && !empty) begin
                dout <= mem[rd_ptr];
                rd_ptr <= rd_ptr + 1;
            end
            count <= count + (wr_en && !full) - (rd_en && !empty);
        end
    end
end
endmodule

```

BRAM (Block RAM) and ROM (Read-Only Memory) are essential for storing large datasets, such as texture maps or shader programs, in GPUs. BRAM offers high-density storage with predictable latency, making it suitable for caching and buffering. ROM is used for immutable data, such as microcode or fixed-function lookup tables. The following equation models the access time for a BRAM:

$$t_{\text{access}} = t_{\text{setup}} + t_{\text{prop}} + t_{\text{hold}}$$

Parallel arithmetic units are a hallmark of GPU architectures, enabling massive parallelism in operations like matrix multiplication or convolution. These units are often implemented using systolic arrays or SIMD (Single Instruction, Multiple Data) constructs. The following equation represents the throughput of a parallel arithmetic unit:

$$T = N \times f_{\text{clk}}$$

where  $N$  is the number of parallel units and  $f_{\text{clk}}$  is the clock frequency. In Verilog, a parallel adder tree can be implemented as follows:

Code Sample 6.57: Parallel Adder Tree in Verilog

```
module adder_tree #(
    parameter WIDTH = 8,
    parameter NUM_INPUTS = 16
) (
    input [WIDTH-1:0] inputs [0:NUM_INPUTS-1],
    output [WIDTH+$clog2(NUM_INPUTS)-1:0] sum
);
    integer i;
    reg [WIDTH+$clog2(NUM_INPUTS)-1:0] acc;
    always @(*) begin
        acc = 0;
        for (i = 0; i < NUM_INPUTS; i = i + 1)
            acc = acc + inputs[i];
        sum = acc;
    end
endmodule
```

Key considerations in GPU pipeline design include:

**Latency hiding** — Pipeline registers and FIFOs help mask memory latency by allowing other operations to proceed while waiting for data. **Resource sharing** — BRAM and ROM are shared across multiple pipeline stages to optimize area and power. **Clock domain crossing** — FIFOs synchronize data between domains, preventing metastability. **Power efficiency** — Pipeline registers reduce dynamic power by shortening critical paths.

The interplay between pipeline registers, FIFOs, BRAM/ROM, and parallel arithmetic units defines the performance and efficiency of modern GPU architectures. These constructs enable GPUs to achieve their hallmark throughput and parallelism, making them indispensable in high-performance computing and graphics rendering.

### 6.3.2 FIFOs

Modern GPU architectures rely heavily on pipelining to achieve high throughput and low latency. Pipeline registers are fundamental components in these designs, serving as temporary storage elements between pipeline stages. They enable the synchronization of data flow and ensure correct timing across clock domains. In GPU architectures, pipeline registers are typically implemented using flip-flops or latches, with their depth and width tailored to the specific requirements of each pipeline stage. The use of pipeline registers allows GPUs to maintain high clock frequencies while processing multiple instructions concurrently.

The role of pipeline registers becomes particularly evident in arithmetic logic units (ALUs) and texture units, where parallel arithmetic operations are performed. For example, a floating-point multiplier in a GPU may be pipelined into several stages, each with its own set of pipeline registers. This partitioning reduces the critical path delay, enabling higher clock frequencies. The following Verilog snippet illustrates a simple pipelined multiplier with two stages:

Code Sample 6.58: Pipelined Multiplier in Verilog

```
module pipelined_multiplier (
    input clk, rst,
    input [31:0] a, b,
    output reg [63:0] product
);
    reg [31:0] a_reg, b_reg;
    reg [63:0] partial_product;

    always @ (posedge clk or posedge rst) begin
        if (rst) begin
            a_reg <= 0;
            b_reg <= 0;
            partial_product <= 0;
            product <= 0;
        end else begin
            // Stage 1: Register inputs and compute partial product
            a_reg <= a;
            b_reg <= b;
            partial_product <= a * b;
            // Stage 2: Register final product
            product <= partial_product;
        end
    end
endmodule
```

FIFOs (First-In-First-Out buffers) are another critical construct in GPU architectures, often used for buffering data between asynchronous clock domains or handling variable-latency operations. FIFOs are implemented using either registers or block RAM (BRAM), depending on the required depth and performance constraints. In Verilog, a synchronous FIFO can be described as follows:

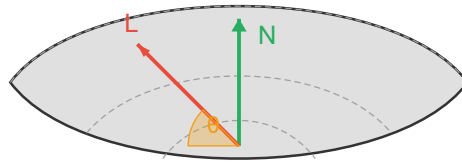
Code Sample 6.59: Synchronous FIFO in Verilog

```
module sync_fifo #(
    parameter DATA_WIDTH = 32,
    parameter DEPTH = 8
) (
    input clk, rst,
    input wr_en, rd_en,
    input [DATA_WIDTH-1:0] din,
    output reg [DATA_WIDTH-1:0] dout,
    output full, empty
);
    reg [DATA_WIDTH-1:0] mem [0:DEPTH-1];
    reg [2:0] wr_ptr, rd_ptr;
    reg [3:0] count;

    assign full = (count == DEPTH);
    assign empty = (count == 0);
```

## Lambertian Shading

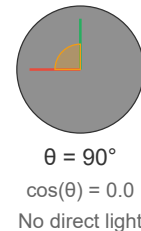
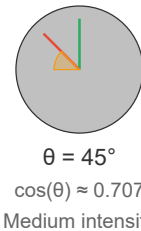
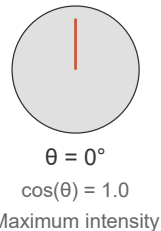
A Fundamental Lighting Model in Modern GPU Rendering



$$I = k_d \times (N \cdot L)$$

Diffuse intensity proportional to  $\cos(\theta)$

### Lighting Effect at Different Angles



### GPU Implementation

```
float3 LambertianShading(float3 normal, float3 lightDir, float3 diffuseColor)
{
    float NdotL = max(dot(normal, lightDir), 0.0);
    return diffuseColor * NdotL;
}
```

```

always @ (posedge clk or posedge rst) begin
    if (rst) begin
        wr_ptr <= 0;
        rd_ptr <= 0;
        count <= 0;
    end else begin
        if (wr_en && !full) begin
            mem[wr_ptr] <= din;
            wr_ptr <= wr_ptr + 1;
        end
        if (rd_en && !empty) begin
            dout <= mem[rd_ptr];
            rd_ptr <= rd_ptr + 1;
        end
        count <= count + (wr_en && !full) - (rd_en && !empty);
    end
end
endmodule

```

Pipeline registers are often used in conjunction with FIFOs to mitigate clock skew and ensure data integrity. These registers are placed between FIFO stages to align data with the clock edges, reducing metastability risks. The propagation delay through a pipeline register is given by:

$$t_{pd} = t_{setup} + t_{hold} + t_{clk-to-q}$$

where  $t_{setup}$  and  $t_{hold}$  are the setup and hold times of the flip-flops, and  $t_{clk-to-q}$  is the clock-to-output delay. Modern GPUs optimize these parameters to achieve high clock frequencies, often exceeding 1 GHz.

BRAM and ROM are utilized in FIFOs to store large datasets, such as texture maps or shader constants. BRAM offers high-density storage with low power consumption, making it ideal for GPU applications. The addressing logic for BRAM-based FIFOs is typically implemented using Gray codes to minimize glitches during pointer updates. The following equation describes the Gray code conversion:

$$G_i = G_{i-1} \oplus B_i$$

where  $G_i$  is the Gray code bit,  $B_i$  is the binary bit, and  $\oplus$  denotes the XOR operation. This conversion ensures that only one bit changes between successive addresses, reducing power dissipation and cross-talk.

Parallel arithmetic units in GPUs rely on FIFOs to buffer operands and results. For example, a fused multiply-add (FMA) unit may use a FIFO to store intermediate products before accumulation. The Verilog code below demonstrates a parallel FMA unit with FIFO buffering:

Code Sample 6.60: Parallel FMA Unit with FIFO

```

module fma_unit #(
    parameter WIDTH = 32
) (
    input wire clk, rst,
    input wire [WIDTH-1:0] a,
    input wire [WIDTH-1:0] b,
    input wire [WIDTH-1:0] c,
    output wire [WIDTH-1:0] result
);
    reg [WIDTH-1:0] product;
    wire [WIDTH-1:0] sum;

    always @ (posedge clk) begin
        if (rst) begin
            product <= 0;
        end else begin
            product <= a * b;
        end
    end
end

```

```

fifo #( .WIDTH(WIDTH), .DEPTH(4) ) buffer (
    .clk(clk),
    .rst(rst),
    .wr_en(1'b1),
    .rd_en(1'b1),
    .din(product),
    .dout(sum)
);

assign result = sum + c;
endmodule

```

Latency hiding is achieved through the strategic use of pipeline registers and FIFOs, allowing other operations to proceed while memory accesses or long computations are underway. Resource sharing is enabled by allowing BRAM and ROM components to be reused across pipeline stages, conserving area and reducing redundant storage. Clock domain crossing is handled through FIFO buffers, which prevent metastability and ensure safe data transfer across asynchronous domains. Power efficiency is also improved, as pipeline registers reduce switching activity on critical paths, thereby minimizing dynamic power consumption.

In summary, FIFOs are indispensable in modern GPU architectures, enabling efficient data flow and synchronization. Their implementation involves a combination of pipeline registers, BRAM, and parallel arithmetic units, all optimized for high performance and low power consumption. The Verilog examples provided illustrate practical applications of these concepts, demonstrating their relevance in real-world GPU designs.

### 6.3.3 BRAM/ROM usage

The trade-offs in BRAM/ROM usage include area versus speed, power efficiency, and configurability. BRAMs consume significant die area but offer low-latency access, making them suitable for high-performance buffering and caching. In contrast, distributed RAM based on LUTs occupies less area but suffers from higher access times and limited scalability. ROMs are inherently static and more power-efficient for storing read-only data, which makes them ideal for use cases such as fixed-function look-up tables and shader microcode. Meanwhile, BRAMs, although faster and more flexible, incur dynamic power costs due to read and write operations. Configurability is another advantage of BRAMs: modern FPGAs allow them to be cascaded or partitioned, enabling designers to build flexible memory hierarchies tailored to the workload requirements of GPU pipelines.

### 6.3.4 Parallel arithmetic in Verilog

Parallel arithmetic in Verilog is a fundamental aspect of modern GPU architecture, enabling high-throughput computation by leveraging concurrent execution. GPUs rely on parallel arithmetic units to perform simultaneous operations across multiple data elements, a design principle central to their performance. This is achieved through specialized hardware constructs such as pipeline registers, FIFOs, and BRAM/ROM blocks, which facilitate efficient data flow and storage.

In Verilog, parallel arithmetic is implemented using combinational and sequential logic blocks that operate on multiple data streams. For example, a parallel adder can be designed to process multiple operands simultaneously, as shown in the following Verilog snippet:

Code Sample 6.61: 4-bit Parallel Adder

```

module parallel_adder (
    input [3:0] A, B,
    output [3:0] Sum,
    output Cout
);
    assign {Cout, Sum} = A + B;
endmodule

```

This module performs a 4-bit addition in a single clock cycle, exploiting parallelism to minimize latency. Modern GPUs extend this concept to thousands of arithmetic units, enabling massive parallelism for tasks like matrix multiplication or convolution. The efficiency of such designs depends on careful pipelining to balance throughput and resource utilization.

Pipeline registers are critical for maintaining high clock rates in GPU arithmetic units. By dividing computations into stages separated by registers, designers can reduce the critical path delay. For instance, a pipelined multiplier in Verilog might be structured as follows:

Code Sample 6.62: Pipelined Multiplier

```
module pipelined_multiplier (
    input clk,
    input [7:0] A, B,
    output reg [15:0] Product
);
reg [7:0] A_reg, B_reg;
reg [15:0] partial_product;

always @(posedge clk) begin
    A_reg <= A;
    B_reg <= B;
    partial_product <= A_reg * B_reg;
    Product <= partial_product;
end
endmodule
```

This design ensures that each multiplication stage operates independently, improving throughput. Pipeline registers are also used in GPU shader cores to manage instruction latency, as described in .

FIFOs (First-In-First-Out buffers) are another common GPU construct, often employed to decouple producer and consumer modules in arithmetic pipelines. For example, a FIFO can buffer intermediate results between a floating-point adder and a multiplier, preventing stalls due to timing mismatches. A Verilog FIFO implementation might include:

Code Sample 6.63: Synchronous FIFO

```
module sync_fifo #(
    parameter WIDTH = 32,
    parameter DEPTH = 8
) (
    input clk, rst,
    input wr_en, rd_en,
    input [WIDTH-1:0] din,
    output reg [WIDTH-1:0] dout,
    output full, empty
);
reg [WIDTH-1:0] mem [0:DEPTH-1];
reg [2:0] wr_ptr, rd_ptr;
reg [3:0] count;

always @(posedge clk or posedge rst) begin
    if (rst) begin
        wr_ptr <= 0;
        rd_ptr <= 0;
        count <= 0;
    end else begin
        if (wr_en && !full) begin
            mem[wr_ptr] <= din;
            wr_ptr <= wr_ptr + 1;
            count <= count + 1;
        end
        if (rd_en && !empty) begin
            dout <= mem[rd_ptr];
            rd_ptr <= rd_ptr + 1;
            count <= count - 1;
        end
    end
end
end
end
```

```

assign full = (count == DEPTH);
assign empty = (count == 0);
endmodule

```

BRAM (Block RAM) and ROM are essential for storing coefficients, lookup tables, or intermediate results in GPU arithmetic units. BRAM offers high-density storage with low latency, making it ideal for parallel access patterns. A Verilog BRAM instantiation might resemble:

Code Sample 6.64: Dual-Port BRAM

```

module bram_dual_port #(
    parameter ADDR_WIDTH = 8,
    parameter DATA_WIDTH = 32
) (
    input clk,
    input [ADDR_WIDTH-1:0] addr_a, addr_b,
    input [DATA_WIDTH-1:0] din_a,
    input we_a,
    output reg [DATA_WIDTH-1:0] dout_a, dout_b
);
reg [DATA_WIDTH-1:0] mem [0:(1<<ADDR_WIDTH)-1];

always @(posedge clk) begin
    if (we_a) mem[addr_a] <= din_a;
    dout_a <= mem[addr_a];
    dout_b <= mem[addr_b];
end
endmodule

```

In summary, parallel arithmetic in Verilog is foundational to GPU design, supporting high-throughput computations across shader cores, texture units, and memory pipelines. Constructs such as pipeline registers, FIFOs, and BRAM/ROM integration ensure data is processed efficiently and at scale.

## 6.4 Verification Essentials

### 6.4.1 Testbenches

The verification of modern GPU architectures relies heavily on robust testbenches to ensure functional correctness and performance optimization. Testbenches serve as virtual environments where designers simulate and validate the behavior of GPU components before fabrication. Given the complexity of contemporary GPUs, which integrate thousands of arithmetic logic units (ALUs), texture mapping units (TMUs), and raster operation pipelines (ROPs), verification demands systematic methodologies encompassing testbenches, assertions, waveforms, and debugging strategies.

A testbench for a modern GPU typically consists of several key components:

**Stimulus Generation:** This component produces input vectors to exercise the design under test (DUT). For GPUs, this includes shader programs, texture data, and memory access patterns. Randomization techniques, such as constrained random verification (CRV), enhance coverage by exploring corner cases.

**DUT Instantiation:** The GPU module or submodule being verified, such as a streaming multiprocessor (SM) or memory controller, is integrated into the testbench.

**Checkers and Assertions:** These elements monitor outputs for correctness. Assertions, written in SystemVerilog Assertions (SVA), formalize expected behaviors. For example:

Code Sample 6.65: SVA for memory access latency

```

property mem_latency_check;
    @(posedge clk) (mem_request && !mem_busy) |-> ##[1:4] mem_ack;
endproperty
assert_mem_latency: assert property (mem_latency_check);

```

**Coverage Metrics:** Verification progress is tracked using functional and code coverage. Metrics include toggle coverage, branch coverage, and finite-state machine (FSM) coverage.

Assertions play a pivotal role in GPU verification by enabling runtime checks and formal proofs. They are classified into:

**Immediate Assertions:** Evaluate combinational conditions, e.g., checking pipeline stall signals:

Code Sample 6.66: Immediate assertion for pipeline stall

```
always_comb begin
    assert (stall_condition !== 'x)
    else $error("Stall signal undefined");
end
```

**Concurrent Assertions:** Temporal checks spanning multiple clock cycles, such as memory coherency protocols. For example:

$$\text{property coherency\_check} \equiv \square(\text{rd\_en} \rightarrow \diamond \text{data\_valid})$$

where  $\square$  and  $\diamond$  denote temporal operators for "always" and "eventually," respectively.

Waveforms are indispensable for debugging GPU designs. Visualization tools like GTKWave or Synopsys VCS display signal transitions over time, aiding in identifying:

**Timing Violations:** Setup/hold time failures, e.g., when a texture fetch exceeds clock cycle constraints.

**Data Corruption:** Unexpected values in register files or caches, visualized as anomalous signal transitions.

**Deadlock Scenarios:** Stalled pipelines due to unresolved dependencies, detectable via static signal states.

Debugging strategies for GPUs must address parallelism and pipelining challenges. Effective approaches include:

**Transaction-Level Debugging:** Abstracts low-level signals into high-level transactions (e.g., memory reads/writes). Tools like Cadence Indago provide transaction recording and replay .

**Post-Silicon Validation:** Combines emulation (e.g., FPGA prototypes) with on-chip trace buffers to capture real-world workloads .

**Formal Methods:** Exhaustively prove properties using model checking. For GPUs, this verifies memory consistency models like NVIDIA's PTX or AMD's GCN .

The integration of testbenches with continuous integration (CI) systems accelerates GPU verification. Automated regression suites, triggered by code commits, execute testbenches across multiple configurations. For instance, a CI pipeline might:

Compile RTL for different GPU microarchitectures (e.g., Turing vs. Ampere). Run directed and random tests, measuring coverage metrics. Flag failures via assertions or waveform mismatches, notifying designers.

Emerging trends in GPU verification include machine learning (ML)-based test generation. Reinforcement learning optimizes stimulus selection to maximize coverage with minimal simulations . Additionally, unified verification frameworks like UVM-XL extend the Universal Verification Methodology (UVM) for GPU-specific features such as warp scheduling and SIMD execution .

In summary, modern GPU verification hinges on sophisticated testbenches augmented by assertions, waveforms, and systematic debugging. The interplay of these elements ensures that GPUs meet stringent functional and performance requirements, paving the way for reliable deployment in graphics rendering, AI acceleration, and scientific computing.

### 6.4.2 Assertions

In modern GPU architecture, assertions play a critical role in verification by enabling designers to formally specify and check expected behavior during simulation. Assertions are declarative statements that define properties or invariants a design must satisfy, providing a powerful mechanism for detecting errors early in the verification cycle. Their integration into testbenches and debugging workflows is essential for ensuring correctness in complex GPU designs, which often involve parallel execution, pipelining, and memory hierarchy optimizations.

Assertions in GPU verification are typically expressed using SystemVerilog Assertions (SVA), which support both immediate and concurrent forms. Immediate assertions evaluate conditions at specific points in procedural code, while concurrent assertions monitor temporal behavior over multiple clock cycles. For example, a concurrent assertion might verify that a texture fetch operation completes within a bounded latency:

Code Sample 6.67: Concurrent SVA for Texture Fetch Latency

```
property texture_fetch_latency;
    @ (posedge clk) disable iff (!reset_n)
```

```

(texture_fetch_start) |-> ##[1:8] texture_fetch_done;
endproperty
assert_texture_fetch: assert property (texture_fetch_latency);

```

The mathematical foundation for temporal assertions is based on linear temporal logic (LTL), where properties are evaluated over finite or infinite sequences of states. Let  $\sigma = s_0, s_1, \dots$  represent a sequence of states, and  $\models$  denote satisfaction. The LTL formula  $\phi \mathbf{U} \psi$  (phi until psi) holds if  $\psi$  becomes true in some future state, and  $\phi$  remains true until then:

$$\sigma \models \phi \mathbf{U} \psi \iff \exists i \geq 0 : (\sigma^i \models \psi \wedge \forall 0 \leq j < i, \sigma^j \models \phi)$$

GPU verification leverages several types of assertions. Invariants are static conditions that must hold throughout execution, such as memory coherency rules. For example, a warp scheduler might require that active warps never exceed the physical limit:

Code Sample 6.68: Warp Scheduler Invariant

```

assert_invariant: assert property (
  @(posedge clk) disable iff (!reset_n)
  $countones(active_warps) <= MAX_WARPS
);

```

Temporal sequences express conditions spanning multiple cycles, such as pipeline forwarding behavior. These often use SVA sequence operators like `for` cycle delays and `[*n]` for repetition. Data consistency checks ensure correct data propagation, particularly in shared memory or cache hierarchies. For example, a write-after-read hazard check may assert that for all addresses  $a$ , if a read occurs, no write to  $a$  is allowed until the read is complete:

$$\forall a \in \text{addresses} : \text{read}(a) \rightarrow \neg \text{write}(a) \mathbf{U} \text{read\_complete}(a)$$

Waveform debugging complements assertions by providing temporal visualization of signal behavior. When an assertion fails, engineers examine waveforms to identify the root cause. Modern GPU verification tools like Synopsys Verdi or Cadence SimVision integrate assertion monitoring directly into waveform viewers, allowing users to jump to the exact cycle of a violation. Key debugging strategies include triggering waveform dumps selectively around assertion failures using `$assert_control` system tasks, correlating assertion failures with coverage metrics to identify untested scenarios, and using cross-probing between waveform signals and assertion source code.

Testbenches for GPU verification employ assertions at multiple levels of hierarchy. At the unit level, assertions check microarchitectural features like instruction scheduling:

Code Sample 6.69: Instruction Scheduler Testbench Assertion

```

property no_structural_hazard;
  @(posedge clk) disable iff (!reset_n)
  issued_instruction |-> !resource_conflict;
endproperty

```

At the system level, assertions verify inter-block communication protocols. For instance, a PCIe transaction might require specific header formatting expressed as:

$$\text{valid_header} \triangleq \bigwedge_{i=0}^{15} (\text{header}[i] \rightarrow \text{check\_field}_i(\text{header}))$$

Debugging strategies for assertion failures follow a systematic approach. The designer must isolate the failure by determining the minimal set of signals involved, analyze preconditions leading to the violation using temporal antecedents, and check for metastability or clock domain crossing issues when assertions fail intermittently. Where possible, formal methods can be used to prove assertions statically, reducing simulation overhead.

Empirical studies demonstrate that assertion-based verification can detect 60–70% of bugs during initial simulation runs. In GPU designs, where parallelism introduces non-determinism, assertions provide deterministic checks for memory consistency models (e.g., ensuring CUDA’s happens-before ordering), warp synchronization points in SIMT architectures, and power management state transitions.

The computational overhead of assertions is mitigated through compile-time optimization of statically provable assertions, selective enabling of assertions based on verification phase, and hardware acceleration using emulation platforms.

Formal verification techniques extend assertion checking by mathematically proving properties for all possible inputs. For GPUs, this is particularly valuable for safety-critical applications like automotive or medical imaging. Bounded model checking can verify properties up to a certain cycle depth:

$$\text{BMC}(\phi, k) \triangleq \bigwedge_{i=0}^{k-1} T(s_i, s_{i+1}) \rightarrow \bigwedge_{j=0}^k \phi(s_j)$$

Emerging trends include machine learning-assisted assertion generation and dynamic assertion synthesis from simulation traces. These techniques address the challenge of manually authoring comprehensive assertion sets for complex GPU architectures with thousands of functional units and memory banks.

In summary, assertions form the backbone of modern GPU verification, enabling rigorous checking of architectural invariants, temporal behaviors, and data consistency. Their integration with testbenches, waveform analysis, and formal methods creates a multi-layered defense against design errors, which is critical as GPU complexity continues scaling with Moore's Law and beyond. The mathematical foundations in temporal logic provide a sound basis for both simulation-based and formal verification approaches.

#### 6.4.3 Waveforms

Waveforms play a critical role in the verification of modern GPU architectures, serving as a visual representation of signal behavior over time. In the context of verification essentials, waveforms are indispensable for debugging, assertion checking, and testbench validation. Modern GPUs, with their highly parallel architectures and complex pipelines, require rigorous verification methodologies to ensure correctness. Waveforms enable engineers to observe the temporal evolution of signals, identify anomalies, and correlate them with design specifications or testbench stimuli.

The generation and analysis of waveforms are tightly integrated with testbenches, which simulate the GPU design under various scenarios. A testbench typically consists of stimulus generators, monitors, and checkers, all of which produce waveforms to validate the design. For example, a Verilog testbench for a GPU shader core might include assertions to verify pipeline correctness:

Code Sample 6.70: Shader Core Testbench

```
module shader_core_tb;
    reg clk, reset;
    reg [31:0] instruction;
    wire [31:0] result;

    shader_core uut (
        .clk(clk), .reset(reset),
        .instruction(instruction), .result(result)
    );

    initial begin
        clk = 0;
        reset = 1;
        #10 reset = 0;
        instruction = 32'hA5A5A5A5;
        #20;
        assert (result == 32'h5A5A5A5A) else $error("Result mismatch");
    end

    always #5 clk = ~clk;
endmodule
```

Waveforms generated from such testbenches provide insights into signal transitions, timing violations, and protocol compliance. For instance, the assertion in the above code checks whether the shader core inverts the input correctly. If the assertion fails, the waveform helps pinpoint the cycle where the discrepancy occurs.

Assertions are formal checks embedded in the design or testbench to verify expected behavior. SystemVerilog assertions (SVAs) are widely used in GPU verification due to their expressiveness and ability to detect errors early. A waveform can visualize the evaluation of assertions, showing when they pass or fail. For example, a property checking memory coherency in a GPU cache might be written as:

## Code Sample 6.71: Cache Coherency Assertion

```

property cache_coherent;
  @(posedge clk) read_enable |> ##[1:3] data_valid;
endproperty
assert_cache_coherent: assert property (cache_coherent);

```

The waveform for this assertion would display `read_enable` and `data_valid` signals, highlighting any violations where `data_valid` does not arrive within three cycles of `read_enable`. Such visual feedback accelerates debugging by reducing the need for manual inspection of log files.

Debugging strategies in GPU verification often rely on waveform analysis to isolate root causes of failures. Common techniques include signal correlation by cross-referencing waveforms with design specifications to ensure signals behave as intended. For example, a GPU's texture unit should assert `texture_ready` only after completing a fetch operation. Timing analysis verifies setup and hold times for critical paths. Waveforms reveal violations, such as data instability during clock edges. Protocol compliance is also evaluated by checking adherence to bus protocols (e.g., AXI, PCIe), where waveforms show transaction phases, handshakes, and error conditions.

Waveform viewers like GTKWave or Synopsys Verdi are essential tools for GPU verification. These tools support features such as zoom and pan for navigating large time ranges to focus on specific events, marker alignment for aligning signals across multiple clock domains during cross-domain analysis, and signal grouping for organizing related signals, such as pipeline stages, for clarity.

In modern GPUs, waveform analysis must account for parallelism and concurrency. For example, a compute unit with multiple warps (thread groups) requires waveforms to track warp scheduling, memory accesses, and divergence. A misalignment in warp scheduling can lead to deadlock, which waveforms help diagnose by showing stalled warps and unresolved dependencies.

Mathematical models also underpin waveform analysis. For instance, the propagation delay of a signal through a GPU's logic can be modeled as:

$$t_{pd} = t_{comb} + t_{setup} + t_{clock\_skew}$$

where  $t_{comb}$  is combinatorial logic delay,  $t_{setup}$  is flip-flop setup time, and  $t_{clock\_skew}$  accounts for clock distribution imbalances. Waveforms validate these models by comparing simulated delays against theoretical predictions.

Waveforms are equally vital for post-silicon validation, where real-world GPU behavior is compared against simulation waveforms. Discrepancies may indicate timing violations or unmodeled physical effects. For example, crosstalk or power supply noise can distort signals, which waveforms capture as glitches or jitter.

In summary, waveforms are a cornerstone of GPU verification, bridging the gap between design intent and implementation. They enable engineers to visualize signal interactions in testbenches, validate assertions and detect protocol violations, debug complex parallel architectures, and correlate simulation with post-silicon behavior. The integration of waveforms with advanced verification methodologies ensures robust GPU designs, meeting the demands of high-performance computing and graphics applications. As GPUs evolve, waveform analysis will continue to adapt, incorporating machine learning for anomaly detection and real-time debugging .

#### 6.4.4 Debugging strategies

Debugging modern GPU architectures presents unique challenges due to their parallel execution models, complex memory hierarchies, and specialized hardware units. Effective debugging strategies must account for these factors while leveraging verification essentials such as testbenches, assertions, and waveform analysis. This discussion focuses on proven methodologies for debugging GPU designs, emphasizing their relationship with verification tools and techniques.

Modern GPUs employ massively parallel architectures, with thousands of threads executing simultaneously. This parallelism complicates debugging because traditional sequential debugging techniques are inadequate. A common strategy involves isolating thread-level issues by using warp-level debugging tools to analyze thread divergence , employing conditional breakpoints to halt execution when specific threads encounter errors, and leveraging GPU-specific profiling tools like NVIDIA Nsight or AMD ROCgdb to inspect thread states.

Testbenches play a critical role in GPU verification by providing controlled environments for stimulus generation and response checking. A well-designed testbench for GPU architectures should emulate memory access patterns typical of GPU workloads, including coalesced and non-coalesced accesses. It should also generate corner-case scenarios such as bank conflicts in shared memory or warp stalls, and verify correctness of SIMD (Single Instruction, Multiple Data) execution across warps or wavefronts.

Assertions are indispensable for runtime error detection in GPU designs. They enable designers to specify invariants that must hold during execution. For example, a memory consistency assertion in a GPU cache controller might verify that:

Code Sample 6.72: Cache Coherence Assertion

```
assert (read_hit || write_hit) |-> (cache_line.state != INVALID)
else $error("Access to invalid cache line");
```

Waveform debugging remains fundamental despite the complexity of GPU designs. Modern waveform viewers support hierarchical visualization of GPU execution units such as streaming multiprocessors (SMs) or compute units (CUs), synchronized display of multiple warps or wavefronts, and memory transaction tracing with timing diagrams for DRAM accesses.

Statistical debugging techniques have gained prominence for GPUs due to the impracticality of exhaustive simulation. Examples include Monte Carlo-based stimulus generation to uncover rare race conditions, coverage-guided fuzzing to exercise obscure execution paths, and machine learning-assisted bug localization using historical debug data.

Formal methods complement traditional debugging for GPU architectures, particularly for verifying memory consistency models (e.g., ensuring compliance with CUDA or OpenCL specifications), deadlock freedom in inter-warp synchronization, and correctness of atomic operation implementations.

The following equation models warp scheduling efficiency, a common debugging metric:

$$\eta = \frac{T_{\text{active}}}{T_{\text{total}}}$$

where  $T_{\text{active}}$  is the number of cycles spent performing useful work and  $T_{\text{total}}$  is the total number of execution cycles.

Debugging memory hierarchy issues requires specialized techniques. Address pattern analysis can detect bank conflicts, modeled by the equation:

$$\text{Bank} = \text{Addr} \bmod N$$

where  $N$  is the number of memory banks. Coalescing efficiency is another useful metric:

$$C = \frac{\text{Coalesced accesses}}{\text{Total accesses}}$$

Power-aware debugging has become essential with modern GPUs. This includes correlating power spikes with compute or memory activity patterns, verifying the effectiveness of clock gating through RTL inspection, and analyzing thermal hotspots using architectural simulation.

Cross-layer debugging integrates insights from microarchitecture performance counters, driver-level API traces, and application-level profiling data, providing a comprehensive view of system behavior.

The following Verilog snippet demonstrates a debug-friendly GPU register file implementation:

Code Sample 6.73: Instrumented Register File

```
module reg_file (
    input clk,
    input [4:0] rd_addr, wr_addr,
    input [31:0] wr_data,
    input we
);
    reg [31:0] mem [0:31];
    always @(posedge clk) begin
        if (we) begin
            mem[wr_addr] <= wr_data;
            `ifdef DEBUG
                $display("Reg %0d written: %h", wr_addr, wr_data);
            `endif
        end
    end
endmodule
```

Emerging trends in GPU debugging include the use of graph-based representations to visualize thread interactions, integration of symbolic execution for shader program verification, and application of differential debugging against golden reference models.

Debugging tools must accommodate GPU-specific challenges such as non-deterministic execution resulting from thread scheduling variance, precision differences between architectural simulation and silicon, and interactions between compute units and fixed-function hardware.

The verification-debugging loop in GPU development typically follows a systematic sequence: testbench failure detection, waveform analysis to localize the error, assertion refinement to catch similar issues, and coverage analysis to ensure completeness.

Hardware-assisted debugging features in modern GPUs include error-correcting code (ECC) status registers, performance monitor units (PMUs) for fine-grained telemetry, and hardware breakpoints with warp-level granularity.

Debugging productivity improves with automated bug triage systems, version-aware debugging (to match RTL with the appropriate simulation), and collaborative debugging platforms that support distributed verification teams.

The relationship between verification components and debugging is tightly coupled. Testbenches provide the context for bug reproduction. Assertions transform implicit assumptions into explicit checks. Waveforms offer temporal visibility into design behavior. Coverage metrics guide the prioritization of debugging efforts.

Effective GPU debugging requires mastery of both general verification principles and architecture-specific knowledge. As GPU designs continue evolving, debugging methodologies must adapt to address new challenges in areas such as ray tracing cores, tensor units, and heterogeneous compute architectures. The integration of traditional verification techniques with GPU-aware tools forms the foundation for efficient debugging in this complex domain.

## GPU Wires and Registers

Core Components of Modern GPU Architecture

### Register File Architecture

Register Bank 0      Register Bank 1      Register Bank 2      Register Bank 3

### Wire Types in GPU

#### Control Wires

Transfer control signals between components

#### Data Wires

Carry computational data between processing units

#### Clock Wires

Distribute timing signals throughout the GPU

#### Power Wires

Supply electrical power to all GPU components

### Register Types in Modern GPUs

#### General Purpose Registers

Store intermediate calculation results

#### Vector Registers

Process multiple data points in parallel

#### Special Purpose Registers

Handle control, status, and addresses

#### Predicate Registers

Enable conditional execution of instructions

# Chapter 7

# System-Level Design Considerations

## 7.1 Defining the Design Requirements

### 7.1.1 Throughput

Modern GPU architectures prioritize throughput as a fundamental design requirement, particularly in applications requiring massive parallel processing such as graphics rendering, machine learning, and scientific computing. Throughput, defined as the number of operations executed per unit time, is a critical metric for evaluating GPU performance. High throughput is achieved through architectures featuring thousands of processing cores, optimized memory hierarchies, and efficient scheduling mechanisms. The relationship between throughput and other design parameters—latency, resolution targets, and color depth—must be carefully balanced to meet application-specific demands.

The design requirements for modern GPUs are driven by the need to maximize throughput while minimizing latency. Latency, the time taken to complete a single operation, is often secondary to throughput in GPU architectures due to their parallel nature. However, certain applications, such as real-time rendering or interactive simulations, impose strict latency constraints. The trade-off between throughput and latency is governed by Amdahl's Law, which states that the speedup of a parallel system is limited by its sequential components. For GPUs, this implies that while increasing parallelism improves throughput, the remaining serialized operations can introduce latency bottlenecks.

Resolution targets and color depth further influence GPU design by dictating the computational and memory bandwidth requirements. Higher resolutions, such as 4K or 8K, demand significantly more throughput due to the increased number of pixels processed per frame. The relationship between resolution and throughput can be expressed as:

$$\text{Throughput} = \text{Pixels per Frame} \times \text{Frames per Second}$$

For example, rendering at 4K resolution ( $3840 \times 2160$  pixels) at 60 frames per second requires a throughput of approximately 497 million pixels per second. Color depth, typically measured in bits per channel (e.g., 8, 10, or 12 bits), adds another layer of complexity by increasing the memory bandwidth and computational load. A higher color depth necessitates more precise arithmetic operations and wider data paths, impacting both throughput and power consumption.

Memory bandwidth is a critical factor in achieving high throughput, as GPUs must efficiently feed data to their processing cores. The memory hierarchy, including global memory, shared memory, and registers, is optimized to reduce access latency and maximize bandwidth. The following equation illustrates the relationship between memory bandwidth and throughput:

$$\text{Throughput} = \frac{\text{Memory Bandwidth}}{\text{Data Size per Operation}}$$

For instance, a GPU with a memory bandwidth of 448 GB/s and a data size of 32 bits per operation can theoretically achieve a throughput of 112 billion operations per second. However, real-world performance is often lower due to memory access patterns and contention.

Modern GPU architectures employ several techniques to enhance throughput. One such technique is **SIMD (Single Instruction, Multiple Data)**, which executes the same instruction across multiple data elements simultaneously, as seen in NVIDIA's CUDA cores and AMD's Stream Processors. Another is **Warp Scheduling**, which

groups threads into warps (or wavefronts) to hide memory latency and improve instruction-level parallelism. Additionally, **Cache Hierarchies**—including L1, L2, and texture caches—are used to reduce memory access times and improve throughput.

The following Verilog code snippet demonstrates a simplified GPU memory controller designed to maximize throughput by pipelining memory requests:

Code Sample 7.1: GPU Memory Controller

```
module memory_controller (
    input clk,
    input [31:0] addr,
    input [31:0] data_in,
    output [31:0] data_out,
    input req,
    output ack
);
    reg [31:0] mem [0:1023];
    reg [31:0] out_reg;
    reg ack_reg;

    always @(posedge clk) begin
        if (req) begin
            out_reg <= mem[addr];
            ack_reg <= 1;
        end else begin
            ack_reg <= 0;
        end
    end

    assign data_out = out_reg;
    assign ack = ack_reg;
endmodule
```

Throughput optimization also involves balancing power consumption and thermal constraints. High-throughput GPUs often operate near their thermal limits, necessitating advanced cooling solutions and dynamic frequency scaling. The power-throughput trade-off is modeled by:

$$P = C \times V^2 \times f$$

where  $P$  is power,  $C$  is capacitance,  $V$  is voltage, and  $f$  is frequency. Reducing voltage or frequency can lower power consumption but may degrade throughput, requiring careful tuning.

In summary, modern GPU architectures prioritize throughput by leveraging parallelism, optimizing memory hierarchies, and balancing resolution, color depth, and latency constraints. The interplay between these factors is critical for meeting the demands of high-performance computing and real-time graphics applications. Future advancements in GPU design will likely focus on further increasing throughput through architectural innovations such as chiplet-based designs and advanced memory technologies like HBM3. The equations and principles discussed here provide a framework for understanding the trade-offs inherent in GPU design, ensuring that throughput remains a central consideration in the development of next-generation architectures.

### 7.1.2 Latency

Modern GPU architectures are designed to balance multiple competing constraints, with latency being a critical factor in determining overall performance. Latency refers to the time delay between the initiation of a task and its completion, and in the context of GPUs, it is influenced by several architectural decisions. The design requirements for GPUs must account for throughput, latency, resolution targets, and color depth, each of which interacts with the others in complex ways.

The relationship between latency and throughput is governed by Little's Law, which states:

$$\text{Throughput} = \frac{\text{Number of in-flight requests}}{\text{Latency}}$$

This equation highlights that increasing throughput often requires either reducing latency or increasing parallelism. In modern GPUs, parallelism is achieved through techniques such as pipelining, multithreading, and

SIMD (Single Instruction, Multiple Data) execution. However, these techniques can introduce additional latency due to synchronization overhead and memory access delays.

Memory hierarchy plays a significant role in latency. GPUs employ caches and registers to minimize access times, but the trade-offs between cache size and access latency must be carefully managed. For example, the L1 cache in NVIDIA's Ampere architecture has a latency of approximately 20–30 cycles, while the L2 cache exhibits higher latency, around 100–200 cycles. The latency of global memory accesses can exceed 400 cycles, necessitating techniques like memory coalescing and prefetching to hide this delay.

Resolution targets and color depth further complicate latency considerations. Higher resolutions (e.g., 4K or 8K) require more pixels to be processed per frame, increasing the computational load. The pixel throughput  $P$  for a given resolution  $R$  and refresh rate  $F$  is given by:

$$P = R \times F$$

For a 4K resolution ( $3840 \times 2160$ ) at 60 Hz, this results in approximately 497 million pixels per second. To maintain low latency, the GPU must process these pixels efficiently, often leveraging parallel rendering pipelines and tile-based rendering techniques.

Color depth, typically measured in bits per channel (e.g., 8, 10, or 12 bits), affects the bandwidth and memory requirements. A higher color depth increases the data size per pixel, which can strain memory bandwidth and exacerbate latency. For instance, a 10-bit per channel RGBA frame at 4K resolution requires:

$$\text{Data size} = 3840 \times 2160 \times 4 \times 10 \text{ bits} = 331.8 \text{ Mb per frame}$$

At 60 Hz, this translates to nearly 20 Gb/s of bandwidth demand, necessitating high-speed GDDR6 or HBM2 memory to avoid bottlenecks.

The design requirements for modern GPUs must also account for real-time constraints, particularly in applications like gaming and virtual reality, where latency must be minimized to avoid perceptible delays. The end-to-end latency  $L$  from input to display can be modeled as:

$$L = L_{\text{input}} + L_{\text{render}} + L_{\text{display}}$$

Here,  $L_{\text{render}}$  is the GPU's contribution, which includes shader execution time, memory access latency, and synchronization overhead. Techniques such as asynchronous compute and predictive rendering are employed to reduce  $L_{\text{render}}$  without sacrificing throughput.

In the context of throughput optimization, GPUs rely on warp scheduling and occupancy maximization. A warp, in NVIDIA's terminology, is a group of 32 threads executed in lockstep. The latency hiding capability of a GPU is determined by the number of active warps per streaming multiprocessor (SM). The occupancy  $O$  is defined as:

$$O = \frac{\text{Active warps}}{\text{Maximum warps per SM}}$$

Higher occupancy improves throughput but may increase contention for shared resources, potentially raising latency. Thus, the design must strike a balance between these factors.

The impact of latency on resolution and color depth is further illustrated by the rendering pipeline. Fragment shaders, for example, must process each pixel with minimal delay to meet frame deadlines. The fragment shader latency  $L_{\text{fragment}}$  depends on the complexity of the shader program and the available arithmetic logic units (ALUs). Simplified shaders reduce  $L_{\text{fragment}}$  but may compromise visual fidelity.

Memory access patterns also influence latency. Coalesced memory accesses, where threads within a warp access contiguous memory locations, reduce latency by minimizing memory transactions. Conversely, uncoalesced accesses increase latency due to redundant data transfers. The following Verilog-like pseudocode demonstrates a coalesced memory access pattern:

Code Sample 7.2: Coalesced Memory Access

```
module memory_access (
    input [31:0] address,
    output [31:0] data
);
// All threads in a warp access contiguous addresses
assign data = memory[address + thread_id];
endmodule
```

In summary, modern GPU architectures must carefully balance latency, throughput, resolution targets, and color depth to meet the demands of contemporary applications. Design requirements are shaped by the interplay of these factors, with optimizations such as memory hierarchy tuning, parallel execution, and efficient shader programming playing pivotal roles. The cited research underscores the importance of empirical validation in GPU design, ensuring that theoretical models align with real-world performance metrics.

### 7.1.3 Resolution targets

Modern GPU architectures are designed to meet stringent performance targets across multiple dimensions, including resolution, throughput, latency, and color depth. Resolution targets, in particular, are a critical aspect of GPU design, as they directly influence the visual fidelity and computational demands of rendering pipelines. The relationship between resolution and other design requirements is complex, requiring careful trade-offs to achieve optimal performance.

The resolution of a display is defined by the number of pixels in the horizontal and vertical dimensions, typically expressed as  $W \times H$  (e.g.,  $1920 \times 1080$  for Full HD). Higher resolutions demand greater computational resources due to the increased number of operations required per frame. For example, rendering a 4K ( $3840 \times 2160$ ) image requires four times the pixel count of Full HD, leading to proportional increases in memory bandwidth and shader core utilization. The relationship between resolution and computational load can be expressed as:

$$\text{Computational Load} \propto W \times H \times \text{Operations per Pixel}$$

where  $W$  and  $H$  are the width and height of the resolution target, respectively.

Throughput is another key metric in GPU design, representing the number of operations the GPU can perform per unit time. High-resolution targets necessitate higher throughput to maintain acceptable frame rates. Modern GPUs achieve this through parallel processing architectures, such as NVIDIA's CUDA cores or AMD's Stream Processors. The throughput  $T$  of a GPU can be modeled as:

$$T = N \times F \times C$$

where  $N$  is the number of cores,  $F$  is the clock frequency, and  $C$  is the number of operations per core per cycle. To meet resolution targets, designers must ensure that  $T$  scales with the pixel count, often requiring architectural innovations like tile-based rendering or variable-rate shading.

Latency, the time delay between input and output, is another critical factor influenced by resolution. Higher resolutions increase latency due to the additional processing steps required. For real-time applications like gaming or virtual reality, latency must be minimized to ensure responsiveness. Techniques such as pipelining and speculative execution are employed to mitigate latency increases. The relationship between resolution and latency  $L$  can be approximated as:

$$L \propto \frac{W \times H}{T}$$

where  $T$  is the throughput as defined in 30.2.1. Reducing latency while maintaining high resolution often involves trade-offs with power consumption and die area.

Color depth, the number of bits used to represent each color channel, also interacts with resolution targets. Higher color depths (e.g., 10-bit or 12-bit per channel) improve visual quality but increase memory bandwidth requirements. The total memory bandwidth  $B$  required for a frame can be calculated as:

$$B = W \times H \times D \times F$$

where  $D$  is the color depth in bits and  $F$  is the frame rate. For example, a 4K resolution at 60 Hz with 10-bit color depth requires approximately 12 Gbps of bandwidth per channel. Modern GPUs address this challenge through advanced memory technologies like GDDR6 and HBM2, which offer higher bandwidth and efficiency.

The design requirements for resolution targets also involve considerations of scalability and flexibility. Modern GPUs are expected to support a wide range of resolutions, from low-resolution mobile displays to high-resolution desktop monitors. This necessitates programmable pipelines and dynamic resource allocation. For instance, NVIDIA's Dynamic Super Resolution (DSR) technology allows rendering at higher resolutions and downscaling to the display's native resolution, improving image quality without requiring hardware changes.

In summary, resolution targets in modern GPU architectures are tightly coupled with throughput, latency, and color depth requirements. Achieving high resolutions demands careful balancing of computational resources, memory bandwidth, and power efficiency. The following list highlights key considerations for GPU designers:

- Parallel processing architectures to scale throughput with resolution.
- Advanced memory technologies to meet bandwidth demands.
- Latency reduction techniques for real-time applications.
- Flexible rendering pipelines to support diverse resolution targets.

The equations and principles discussed here provide a foundation for understanding the interplay between resolution targets and other GPU design requirements. Future advancements in GPU architecture will likely focus on further optimizing these relationships to enable even higher resolutions and better performance. For example,

# ALWAYS BLOCKS

Modern GPU Architecture

## What Are Always Blocks?

Specialized execution units in modern GPUs that remain active consistently throughout GPU operations, handling critical background tasks

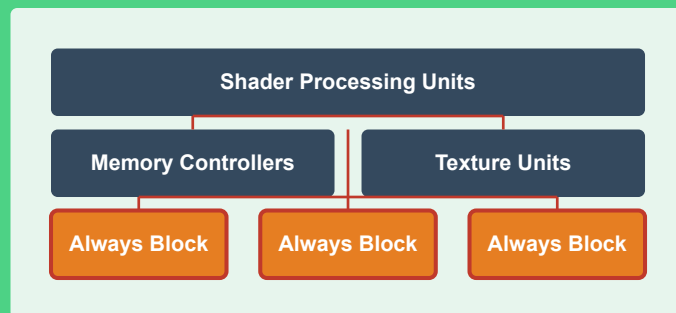
### Core Functions

- Memory Management
- Thread Scheduling
- Power Management
- Cache Coordination
- Hardware Monitoring

### Implementation

- Dedicated Hardware Units
- Low-Latency Pipelines
- Independent Power Rails
- Direct Memory Access
- Fast Interrupt Handling

## Always Block Architecture



emerging technologies like ray tracing and machine learning-based super-resolution techniques promise to redefine resolution targets in the coming years .

Code Sample 7.3: Example of a GPU shader program for resolution scaling

```
void main() {  
    vec2 uv = gl_FragCoord.xy / resolution;  
    vec4 color = texture(inputTexture, uv);  
    gl_FragColor = color;  
}
```

The above shader code illustrates a simple resolution scaling operation, where the fragment shader samples an input texture at a scaled coordinate. Such programs are fundamental to achieving flexible resolution targets in modern GPUs. The design of these shaders must account for the computational load and memory access patterns to ensure efficient execution.

In conclusion, resolution targets are a central consideration in GPU architecture, influencing and being influenced by throughput, latency, and color depth. The equations and examples provided here underscore the complexity of these relationships and the ongoing innovations required to meet evolving demands. Future research will continue to explore new techniques for balancing these factors, ensuring that GPUs remain capable of delivering high-quality visuals across a wide range of applications.

### 7.1.4 Color depth

The role of color depth in modern GPU architecture is a critical factor in defining design requirements, particularly when considering throughput, latency, and resolution targets. Color depth, measured in bits per pixel (bpp), determines the number of distinct colors a GPU can represent, directly impacting visual fidelity and computational demands. Modern GPUs must balance these factors to meet the growing demands of high-resolution displays, real-time rendering, and advanced applications such as machine learning and scientific visualization.

The relationship between color depth and throughput is governed by the GPU's memory bandwidth and computational capacity. Higher color depths require more data to be processed and transferred, increasing the demand on memory bandwidth. For example, a 32-bit color depth (8 bits per channel for RGBA) doubles the data compared to 16-bit color depth (5-6-5 bits for RGB). The throughput  $T$  in pixels per second can be expressed as:

$$T = \frac{B}{D \times C}$$

where  $B$  is the memory bandwidth in bits per second,  $D$  is the color depth in bits per pixel, and  $C$  is the compression ratio if applicable. Modern GPUs employ lossless and lossy compression techniques to mitigate bandwidth constraints, as demonstrated in NVIDIA's Delta Color Compression (DCC).

Latency is another critical metric affected by color depth. Deeper color representations increase the time required for pixel processing, particularly in pipelines with multiple rendering passes. The latency  $L$  for a pixel operation can be approximated as:

$$L = k \times D \times P$$

where  $k$  is a constant dependent on the GPU architecture,  $D$  is the color depth, and  $P$  is the number of pipeline stages. Research by Akenine-Möller et al. shows that reducing color depth from 32-bit to 16-bit can decrease latency by up to 40% in fragment shaders, though at the cost of color accuracy.

Resolution targets further complicate the design requirements. Higher resolutions (e.g., 4K or 8K) exacerbate the bandwidth and computational challenges posed by increased color depth. The total memory requirement  $M$  for a frame buffer is:

$$M = R_x \times R_y \times D$$

where  $R_x$  and  $R_y$  are the horizontal and vertical resolutions, respectively. For instance, an 8K resolution ( $7680 \times 4320$ ) with 32-bit color depth requires approximately 132 MB per frame, necessitating advanced memory hierarchies and caching strategies .

Modern GPU architectures address these challenges through several design optimizations. Variable-Rate Shading (VRS) reduces shading workload by varying the color depth across regions of the screen, prioritizing high-detail areas . Tile-Based Rendering divides the screen into tiles, enabling localized color depth adjustments to balance quality and performance . Hardware-Accelerated Compression uses dedicated units for compressing and decompressing color data, as seen in AMD's Infinity Cache .

The choice of color depth also influences the GPU's power efficiency. Deeper color depths increase power consumption due to higher memory access and arithmetic operations. Studies by Lee et al. demonstrate that reducing color depth from 32-bit to 16-bit can save up to 25% power in mobile GPUs, making it a key consideration for energy-constrained devices.

In real-time rendering, color depth interacts with other pipeline stages, such as anti-aliasing and high dynamic range (HDR) rendering. For example, HDR requires at least 10 bits per channel (30-bit color depth) to represent a wider luminance range, as defined by the Rec. 2020 standard . This imposes additional constraints on the GPU's arithmetic logic units (ALUs) and floating-point precision, as shown in the following Verilog snippet for a simplified HDR blending unit:

Code Sample 7.4: HDR Blending Unit

```
module hdr_blend (
    input [9:0] r1, g1, b1, // 10-bit channels
    input [9:0] r2, g2, b2,
    output [9:0] ro, go, bo
);
    assign ro = (r1 + r2) >> 1; // Averaging with truncation
    assign go = (g1 + g2) >> 1;
    assign bo = (b1 + b2) >> 1;
endmodule
```

## GPU ARCHITECTURE: PARAMETERS

Key Elements That Define Modern GPU Performance

### CORE ARCHITECTURE PARAMETERS

<b>SM</b>	<b>CUDA</b>	<b>CLK</b>	<b>W</b>
Streaming Multiprocessors	CUDA Cores Per SM	Clock Speed (MHz)	Warp Size (32 threads)

### MEMORY PARAMETERS

**GLOBAL MEMORY (VRAM): 8-48 GB GDDR6/HBM2**

**L2 CACHE: 4-6 MB**

**L1 CACHE: 64-128 KB PER SM**

**SHARED MEMORY: 32-164 KB PER SM**

### PERFORMANCE PARAMETERS

#### TFLOPS

Floating Point Operations Per Second

#### MEMORY BANDWIDTH

GB/s transfer rate between VRAM and GPU

#### TDP

Thermal Design Power Power Consumption (Watts)

### SPECIALIZED COMPUTE UNITS

#### RT CORES

Ray Tracing Acceleration

#### TENSOR CORES

AI/ML Matrix Calculations

#### INT32 UNITS

Integer Operations in Parallel with FP32

Emerging technologies like neural rendering and ray tracing further push the boundaries of color depth requirements. Neural networks often operate on high-precision floating-point color representations (e.g., FP16 or FP32) to maintain accuracy during training and inference. Similarly, ray tracing benefits from deeper color depths to reduce banding artifacts in gradients and shadows, as evidenced by the adoption of 16-bit floating-point (half-precision) in NVIDIA's RTX cores.

In summary, color depth is a pivotal parameter in modern GPU design, influencing throughput, latency, resolution, and power efficiency. Architects must carefully balance these factors to meet the diverse demands of applications ranging from mobile gaming to scientific computing. Future advancements in memory technologies, compression algorithms, and arithmetic precision will continue to shape the evolution of color depth in GPU architectures.

## 7.2 Fixed-Point vs. Floating-Point Arithmetic

### 7.2.1 Numeric formats for transformations

The choice of numeric formats in modern GPU architectures significantly impacts the performance and accuracy of transformations and shading operations. Fixed-point and floating-point arithmetic represent two fundamental approaches, each with distinct trade-offs in precision, dynamic range, and hardware complexity.

Fixed-point arithmetic represents numbers using a fixed number of integer and fractional bits, making it computationally efficient but limited in dynamic range. For transformations, fixed-point arithmetic is often employed in low-power or embedded GPUs where hardware resources are constrained. The fixed-point representation of a number  $x$  can be expressed as:

$$x = \frac{I}{2^f}$$

where  $I$  is the integer value and  $f$  is the number of fractional bits. This format is deterministic and avoids the overhead of floating-point normalization, but suffers from overflow and underflow issues when handling large or small values.

Floating-point arithmetic, standardized by IEEE 754, provides a wider dynamic range and higher precision by representing numbers in scientific notation:

$$x = (-1)^s \times m \times 2^e$$

where  $s$  is the sign bit,  $m$  is the mantissa, and  $e$  is the exponent. Modern GPUs predominantly use 32-bit (`float`) or 16-bit (`half`) floating-point formats for transformations and shading. The flexibility of floating-point arithmetic is crucial for high dynamic range (HDR) rendering, where luminance values span several orders of magnitude.

Transformations in GPU pipelines, such as model-view-projection (MVP) operations, require high precision to avoid visual artifacts. Floating-point arithmetic is preferred for these operations due to its ability to represent both very large and very small values accurately. Fixed-point arithmetic, while efficient, introduces quantization errors that accumulate across transformation stages, leading to visible inaccuracies in vertex positioning.

Shading computations, including lighting and texture sampling, also benefit from floating-point precision. For example, Phong shading requires dot products between normalized vectors, which must retain sufficient precision to avoid banding or incorrect illumination. Fixed-point shading can introduce noticeable artifacts, particularly in low-light or high-contrast scenarios. However, some mobile GPUs employ hybrid approaches, using fixed-point for intermediate calculations and converting to floating-point for final outputs.

The following Verilog snippet illustrates a simplified floating-point multiplier, a critical component in GPU shading units:

Code Sample 7.5: Floating-Point Multiplier

```
module fp_multiplier (
    input [31:0] a, b,
    output [31:0] result
);
    wire sign = a[31] ^ b[31];
    wire [7:0] exponent = a[30:23] + b[30:23] - 127;
    wire [47:0] mantissa = {24'd1, a[22:0]} * {24'd1, b[22:0]};
    assign result = {sign, exponent, mantissa[46:24]};
endmodule
```

Fixed-point arithmetic, while less common in high-end GPUs, remains relevant for specific optimizations. For instance, texture coordinate interpolation often uses fixed-point arithmetic to reduce power consumption. The following equation shows fixed-point interpolation between two texture coordinates  $u_0$  and  $u_1$ :

$$u = u_0 + \left( \frac{k}{2^n} \right) (u_1 - u_0)$$

where  $k$  is the interpolation factor and  $n$  is the fractional bit width. This approach minimizes energy consumption while maintaining acceptable precision for many applications.

Recent research has explored mixed-precision arithmetic to balance performance and accuracy. For example, NVIDIA's Tensor Cores leverage both 16-bit floating-point and 8-bit integer formats for matrix operations, achieving higher throughput without significant quality degradation. Similarly, AMD's RDNA 2 architecture employs variable-rate shading (VRS), where shading precision is dynamically adjusted based on perceptual importance.

The choice of numeric format also affects memory bandwidth and storage requirements. Floating-point textures consume more memory than fixed-point equivalents but enable higher fidelity in rendering. Compressed formats like BC6H (for HDR) and ETC2 (for LDR) further optimize memory usage while preserving visual quality.

In summary, modern GPU architectures prioritize floating-point arithmetic for transformations and shading due to its precision and dynamic range. Fixed-point arithmetic remains viable for specific low-power or real-time applications, often in hybrid configurations. Advances in mixed-precision computing and hardware acceleration continue to refine the trade-offs between performance, power efficiency, and visual fidelity. While fixed-point arithmetic offers efficiency, it is limited in dynamic range. Floating-point arithmetic is essential for high-precision transformations and shading, helping to avoid artifacts. Mixed-precision techniques serve as an effective strategy for optimizing both performance and power in contemporary GPU designs.

## 7.2.2 Shading

Modern GPU architectures employ sophisticated shading techniques to achieve realistic rendering in real-time graphics. Shading involves computing the color of each pixel by simulating light interaction with surfaces, requiring efficient arithmetic operations and numeric formats. Two fundamental arithmetic representations dominate GPU shading pipelines: fixed-point and floating-point. The choice between these affects precision, performance, and energy efficiency, particularly in transformations and shading calculations.

Fixed-point arithmetic represents numbers using a fixed number of integer and fractional bits. For example, a 16-bit fixed-point number may use 8 bits for the integer part and 8 bits for the fractional part, denoted as Q8.8. The value  $x$  is computed as:

$$x = \frac{\text{stored integer}}{2^8}$$

Fixed-point is efficient for hardware implementation due to its simplicity, requiring fewer transistors and less power than floating-point units. However, it suffers from limited dynamic range and precision, making it unsuitable for high dynamic range (HDR) rendering or complex transformations. GPUs historically used fixed-point for color blending and texture filtering, where precision requirements are moderate.

Floating-point arithmetic, standardized by IEEE 754, represents numbers with a sign bit, exponent, and mantissa. A 32-bit single-precision float (FP32) follows:

$$x = (-1)^s \times (1.m) \times 2^{e-127}$$

Floating-point excels in dynamic range and precision, critical for shading operations like specular highlights, shadow mapping, and perspective transformations. Modern GPUs, such as NVIDIA's Ampere and AMD's RDNA2 architectures, prioritize FP32 throughput for shading, achieving teraflops of performance. However, floating-point units consume more power and silicon area, necessitating trade-offs in mobile and embedded GPUs.

Numeric formats for transformations and shading must balance precision and performance. Homogeneous coordinates, used for 3D transformations, often employ FP32 for world-space calculations but may use FP16 or fixed-point for screen-space operations. For example, the transformation of a vertex  $\mathbf{v}$  by a matrix  $\mathbf{M}$  is:

$$\mathbf{v}' = \mathbf{M} \cdot \mathbf{v}$$

Here, FP32 ensures numerical stability, while intermediate results may use lower precision. Recent research explores mixed-precision shading, where FP16 accelerates non-critical paths without visual artifacts.

Shading pipelines leverage specialized hardware for arithmetic operations. For instance, texture filtering often combines fixed-point bilinear interpolation with FP32 for mipmap level selection. The following Verilog snippet illustrates a simplified fixed-point multiplier for texture filtering:

Code Sample 7.6: Fixed-Point Multiplier

```
module fixed_mult (
    input [15:0] a, // Q8.8
    input [15:0] b, // Q8.8
    output [31:0] p // Q16.16
);
assign p = a * b; // Automatically scales to Q16.16
endmodule
```

In contrast, floating-point units in shading pipelines handle complex operations like Phong reflection:

$$I = k_a + k_d(\mathbf{n} \cdot \mathbf{l}) + k_s(\mathbf{r} \cdot \mathbf{v})^\alpha$$

Here, FP32 ensures accurate dot products and exponentiation, while fixed-point would introduce banding artifacts. The choice of numeric format affects shading quality and performance. Studies show that FP16 reduces power consumption by 30% compared to FP32 in mobile GPUs, with minimal perceptual difference in diffuse shading. However, specular highlights and environment maps require FP32 to avoid quantization errors. NVIDIA's Tensor Cores introduce FP16 matrix operations for machine learning, repurposed for shading in real-time denoising and neural rendering.

Fixed-point remains relevant in rasterization and early-depth testing, where operations are inherently discrete. The depth buffer, for example, often uses a 24-bit fixed-point format for efficient depth comparisons. The depth value  $z$  is computed as:

$$z = \frac{z_{\text{stored}}}{2^{24} - 1}$$

This format balances precision and memory bandwidth, critical for high-resolution rendering. Emerging shading techniques, such as ray tracing, demand higher precision. Floating-point enables accurate intersection tests and Monte Carlo sampling, while fixed-point would fail due to rounding errors. The ray-triangle intersection test involves solving:

$$\mathbf{o} + t\mathbf{d} = (1 - u - v)\mathbf{v}_0 + u\mathbf{v}_1 + v\mathbf{v}_2$$

FP32 or FP64 is essential to avoid false negatives or artifacts in complex scenes.

In summary, modern GPU architectures employ fixed-point and floating-point arithmetic judiciously across shading pipelines. Fixed-point excels in low-power, discrete operations, while floating-point enables high-fidelity rendering. The evolution of numeric formats, including FP16 and mixed-precision, reflects the ongoing optimization for performance, power, and visual quality in real-time graphics. Future architectures may further hybridize these approaches, leveraging domain-specific accelerators for shading workloads.

## 7.3 Memory Interface Basics

### 7.3.1 Framebuffers

The framebuffer is a critical component in modern GPU architectures, serving as the final destination for rendered images before display. It resides in dedicated memory and stores pixel color values, depth information, and other attributes required for rasterization. The framebuffer's organization is tightly coupled with the GPU's memory interface, which governs bandwidth, latency, and access patterns. Modern GPUs employ hierarchical memory systems to optimize framebuffer operations, leveraging high-bandwidth memory (HBM) or GDDR6 interfaces to meet the demands of real-time rendering at high resolutions.

The memory interface of a GPU is designed to maximize throughput for framebuffer operations. A typical GPU memory controller supports multiple channels, each with its own address and data buses, enabling concurrent access to different memory regions. The bandwidth  $B$  of the memory interface can be expressed as:

$$B = f \times w \times c$$

where  $f$  is the memory clock frequency,  $w$  is the bus width per channel, and  $c$  is the number of channels. For example, a GPU with a 256-bit bus width, 8 channels, and a 2 GHz clock frequency achieves a theoretical bandwidth of 512 GB/s. This bandwidth is essential for framebuffer operations, which involve frequent read-modify-write cycles during fragment shading and blending.

Framebuffers are often double-buffered or triple-buffered to avoid visual artifacts such as tearing. Double-buffering involves two buffers: a front buffer for display and a back buffer for rendering. The GPU swaps these buffers once rendering is complete, ensuring that the display always shows a fully rendered frame. Triple-buffering adds an additional buffer to reduce stalls caused by vertical synchronization (VSync), improving frame rate consistency. The swap operation is synchronized with the display's refresh rate to prevent tearing, as described in

Texture memory is another key component of GPU memory systems, storing image data used for shading and filtering. Unlike framebuffers, texture memory is typically read-only during rendering and is optimized for spatial locality. Modern GPUs employ cache hierarchies to reduce texture fetch latency, with dedicated texture caches (L1/L2) that exploit 2D locality. Texture memory is often tiled or swizzled to improve cache efficiency, as linear addressing would result in poor spatial coherence. The texture filtering operation for a bilinear interpolation can be expressed as:

$$T(u, v) = \sum_{i=0}^1 \sum_{j=0}^1 w_{ij} \cdot T(u_i, v_j)$$

where  $T(u_i, v_j)$  are the texel values and  $w_{ij}$  are the interpolation weights.

The Z-buffer (depth buffer) is a specialized framebuffer component that stores per-pixel depth values to resolve visibility during rasterization. The Z-buffer test compares the depth of incoming fragments against stored values, discarding fragments that fail the test. Modern GPUs use hierarchical Z-buffering (Hi-Z) to optimize this process, culling entire tiles of fragments early in the pipeline. The depth test is defined as:

$$\text{pass} = \begin{cases} \text{true} & \text{if } z_{\text{frag}} \leq z_{\text{stored}} \\ \text{false} & \text{otherwise} \end{cases}$$

where  $z_{\text{frag}}$  is the fragment's depth and  $z_{\text{stored}}$  is the value in the Z-buffer. Hi-Z reduces memory bandwidth by minimizing unnecessary depth writes, as demonstrated in .

The framebuffer's memory layout is optimized for both bandwidth and power efficiency. Compression techniques such as delta color compression (DCC) and frame buffer compression (FBC) reduce the effective bandwidth required for framebuffer operations. These schemes exploit spatial coherence in color and depth values, encoding differences rather than absolute values. For example, DCC partitions the framebuffer into blocks and stores a base color plus deltas for each pixel, as shown in . This reduces the number of bits transmitted over the memory interface, improving performance and energy efficiency.

Modern GPUs also support multi-sample anti-aliasing (MSAA), which increases the storage requirements of the framebuffer. MSAA stores multiple samples per pixel to reduce aliasing artifacts, requiring additional bandwidth for resolve operations. The memory footprint  $M$  for an MSAA framebuffer is:

$$M = w \times h \times s \times b$$

where  $w$  and  $h$  are the framebuffer dimensions,  $s$  is the number of samples, and  $b$  is the bits per sample. GPUs optimize MSAA by storing samples in a compressed format or using lossless compression during resolve.

The interaction between framebuffers, texture memory, and the Z-buffer is managed by the GPU's memory controller, which schedules requests to minimize contention. Priority is often given to framebuffer operations to ensure timely display updates, while texture and Z-buffer accesses are interleaved to maximize throughput. The controller also handles memory partitioning, ensuring that concurrent workloads do not starve each other of bandwidth. This is particularly important in unified memory architectures (UMAs), where CPU and GPU share the same physical memory.

In summary, framebuffers are a cornerstone of modern GPU architectures, relying on advanced memory interfaces and optimization techniques to deliver high-performance rendering. Their design is influenced by bandwidth constraints, power efficiency, and the need to support features like anti-aliasing and depth testing. Texture memory and Z-buffers complement the framebuffer by providing specialized storage for shading and visibility resolution, all orchestrated by a sophisticated memory controller. Future advancements in memory technology, such as 3D-stacked DRAM and optical interconnects, will further enhance framebuffer performance, enabling higher resolutions and more complex rendering techniques.

### 7.3.2 Texture memory

Texture memory is a specialized memory subsystem in modern GPU architectures designed to optimize the storage and retrieval of texture data, which is critical for rendering high-quality graphics efficiently. Unlike general-purpose memory, texture memory is optimized for spatial locality and caching patterns typical in texture sampling operations. This memory type is tightly integrated with the GPU's texture mapping units (TMUs), which handle the filtering and interpolation of texels during rendering. The performance characteristics of texture memory are influenced by its organization, access patterns, and interaction with other memory subsystems such as framebuffers and Z-buffers.

The architecture of texture memory is designed to exploit the two-dimensional or three-dimensional locality inherent in texture accesses. Modern GPUs employ a hierarchical caching system to minimize latency when fetching texels. The texture cache is typically organized into cache lines that store blocks of texels, allowing for efficient spatial reuse. For example, when a shader samples a texture at a specific coordinate, the GPU fetches not only the requested texel but also neighboring texels, anticipating future accesses due to bilinear or trilinear filtering. This prefetching mechanism reduces memory bandwidth requirements and improves rendering performance. The texture cache hierarchy often includes multiple levels, such as L1 and L2 caches, to further optimize access times.

Texture memory interfaces with the GPU's memory subsystem through dedicated memory controllers. These controllers manage the flow of data between the texture units and the global memory, ensuring high bandwidth and low latency. The memory interface is designed to handle concurrent accesses from multiple texture units, enabling parallel texture sampling across different shader cores. This is particularly important in modern GPUs, where thousands of threads may be active simultaneously, each potentially requiring texture data. The memory interface must balance the demands of texture memory with other memory-intensive operations, such as framebuffer writes and Z-buffer updates.

Framebuffers and texture memory share similarities in their memory access patterns but serve distinct purposes. A framebuffer stores the final output of the rendering pipeline, including color and depth information for each pixel. Like texture memory, framebuffers benefit from spatial locality, as adjacent pixels are often processed together. However, framebuffer accesses are typically write-heavy during rendering, whereas texture memory is read-heavy. This distinction influences the design of the memory subsystem, with framebuffers often employing write-combining techniques to reduce bandwidth usage. In some architectures, framebuffers and texture memory may share the same physical memory pool, but their access paths and caching strategies are optimized for their respective workloads.

The Z-buffer, or depth buffer, is another critical component of the GPU's memory subsystem. It stores depth values for each pixel, enabling depth testing to determine visibility during rendering. The Z-buffer operates in tandem with texture memory and framebuffers, as depth testing often occurs concurrently with texture sampling and framebuffer updates. Modern GPUs optimize Z-buffer accesses by employing hierarchical depth culling, which reduces unnecessary computations by discarding occluded fragments early in the pipeline. The Z-buffer memory is typically organized to support fast depth comparisons and updates, with dedicated hardware to accelerate these operations.

The interaction between texture memory, framebuffers, and Z-buffers is managed by the GPU's memory controller, which prioritizes and schedules memory requests to maximize throughput. For example, during a rendering pass, the memory controller may interleave texture fetches with framebuffer writes and Z-buffer updates to avoid bottlenecks. The controller also handles memory compression techniques, such as lossless compression for framebuffer and Z-buffer data, to reduce bandwidth consumption. These optimizations are essential for maintaining high performance in complex rendering scenarios, such as real-time graphics in games or scientific visualization.

Texture memory performance is further influenced by the GPU's ability to handle texture atlases and arrays efficiently. Texture atlases combine multiple textures into a single larger texture to reduce state changes and improve caching efficiency. Texture arrays allow for the storage of multiple textures of the same size and format, enabling efficient indexing in shaders. Modern GPUs support these features through hardware-accelerated texture addressing modes, such as clamped or mirrored addressing, which ensure correct sampling behavior at texture boundaries. The texture memory subsystem must also handle anisotropic filtering, which improves texture quality at oblique viewing angles by sampling multiple mipmap levels.

The mathematical foundations of texture memory operations are rooted in signal processing and sampling theory. For instance, bilinear interpolation can be expressed as:

$$T(u, v) = \sum_{i=0}^1 \sum_{j=0}^1 T(u_i, v_j) \cdot w_{i,j}$$

where  $T(u, v)$  is the interpolated texel value,  $T(u_i, v_j)$  are the nearest texels, and  $w_{i,j}$  are the interpolation weights.

This operation requires efficient access to multiple texels, which texture memory and caching systems are designed to support.

Similarly, mipmapping involves precomputing downsampled versions of a texture to avoid aliasing at distant or oblique views. The mipmap level selection is governed by:

$$d = \log_2 \left( \max \left( \left| \frac{\partial u}{\partial x} \right|, \left| \frac{\partial v}{\partial x} \right|, \left| \frac{\partial u}{\partial y} \right|, \left| \frac{\partial v}{\partial y} \right| \right) \right)$$

where  $d$  is the mipmap level and the partial derivatives represent the rate of change of texture coordinates with respect to screen coordinates.

In summary, texture memory is a specialized and highly optimized component of modern GPU architectures, designed to meet the demands of real-time graphics rendering. Its performance is closely tied to the GPU's memory interface, caching strategies, and interaction with other memory subsystems like framebuffers and Z-buffers. By leveraging spatial locality, hierarchical caching, and parallel access mechanisms, texture memory enables efficient texture sampling and filtering, which are essential for high-quality visual output. The mathematical and hardware optimizations underlying texture memory ensure that GPUs can handle the complex and varied workloads of modern graphics applications.

### 7.3.3 Z-buffer

The Z-buffer, also known as the depth buffer, is a fundamental component in modern GPU architectures, enabling efficient hidden surface removal during rasterization. It stores depth values for each pixel in the framebuffer, allowing the GPU to determine whether a fragment should be rendered or discarded based on its depth relative to previously rendered fragments. The Z-buffer operates in conjunction with other memory structures such as the framebuffer and texture memory, forming a critical part of the GPU's memory interface.

The Z-buffer's primary function is to resolve visibility by comparing the depth of incoming fragments against stored depth values. For a fragment at screen coordinates  $(x, y)$  with depth  $z$ , the Z-buffer performs the following test:

$$z \leq Z(x, y)$$

If the test passes, the fragment's color and depth are written to the framebuffer and Z-buffer, respectively. Otherwise, the fragment is discarded. This test is implemented in hardware for high throughput, often with parallel processing across multiple fragments.

Modern GPUs optimize Z-buffer operations through hierarchical depth testing and compression. Hierarchical testing involves coarse-grained depth checks at tile or block levels, reducing memory bandwidth by early rejection of occluded fragments. Compression techniques, such as lossless delta encoding, minimize the bandwidth required for Z-buffer updates. For example, NVIDIA's Pascal architecture introduced lossless Z-buffer compression, reducing memory traffic by up to 50% in common scenarios.

The Z-buffer interacts closely with the framebuffer, which stores color values for each pixel. Both buffers reside in GPU memory, typically GDDR6 or HBM2, and are accessed via the memory interface. The framebuffer and Z-buffer share the same spatial resolution, ensuring one-to-one correspondence between pixels and depth values. During rendering, the GPU's raster engine generates fragments, which are processed by the pixel shader before undergoing Z-testing and framebuffer updates.

Texture memory, another key component, stores surface details such as colors, normals, or material properties. Unlike the Z-buffer, texture memory is read-heavy and optimized for cache efficiency. Modern GPUs employ dedicated texture units with hardware-accelerated filtering and mipmapping. The Z-buffer and texture memory are often accessed in parallel, with the memory interface balancing bandwidth between them. For instance, AMD's RDNA2 architecture uses a unified cache hierarchy to reduce latency for both depth and texture accesses.

The memory interface plays a crucial role in Z-buffer performance. Key considerations include:

**Bandwidth:** Z-buffer updates consume significant bandwidth, especially at high resolutions. Techniques like multi-sample anti-aliasing (MSAA) exacerbate this demand, as depth values are stored per sample. **Latency:** Depth testing must complete before fragment shading in deferred rendering pipelines, making low-latency memory access essential. **Caching:** GPUs use hierarchical caches (L1, L2) to reduce off-chip memory accesses. Z-buffer data exhibits spatial locality, benefiting from cache line granularity.

The Z-buffer's efficiency is further enhanced by hardware optimizations such as:

**Early Z-test:** Fragments are tested before pixel shading if their depth is known, avoiding unnecessary shader invocations. **Late Z-test:** Post-shading depth tests handle cases where fragment depth is modified during shading. **Z-culling:** Coarse depth bounds reject entire primitive batches before rasterization.

In terms of implementation, the Z-buffer is managed by the GPU's memory controller, which coordinates reads and writes across memory channels. For example, a 256-bit GDDR6 interface can sustain up to 448 GB/s bandwidth, sufficient for 4K rendering with 60 FPS. The controller also handles memory partitioning, ensuring concurrent access to Z-buffer, framebuffer, and texture memory without contention.

Code Sample 7.7: Z-buffer test module

```
module z_buffer_test (
    input [31:0] frag_z,
    input [31:0] buffer_z,
    output reg pass
);
    always @(*) begin
        pass = (frag_z <= buffer_z);
    end
endmodule
```

Advanced GPU architectures employ tile-based rendering to optimize Z-buffer usage. In this approach, the screen is divided into tiles, and each tile's depth values are stored in on-chip memory. This reduces off-chip bandwidth, as depth tests occur locally. ARM's Mali GPUs use tile-based deferred rendering (TBDR) to achieve power efficiency .

The Z-buffer's precision is another critical factor. Modern GPUs use 24-bit or 32-bit depth values, with floating-point formats for improved range. However, precision artifacts, such as Z-fighting, can occur when two surfaces are too close. Techniques like reverse-Z mapping mitigate this by distributing precision non-linearly:

$$z_{\text{clip}} = \frac{z_{\text{far}} \cdot (z_{\text{near}} - z)}{z \cdot (z_{\text{near}} - z_{\text{far}})}$$

In summary, the Z-buffer is a cornerstone of modern GPU architecture, enabling real-time 3D rendering through efficient depth testing. Its design integrates with framebuffers, texture memory, and memory interfaces to balance performance, bandwidth, and power consumption. Continued advancements in memory technology and rendering algorithms ensure its relevance in future GPU designs.

## 7.4 Clocking & Synchronization

### 7.4.1 Pipeline stages

Modern GPU architectures employ deeply pipelined designs to achieve high throughput and low latency. The pipeline stages in these architectures are carefully synchronized to maintain data integrity and avoid metastability. Clocking and synchronization mechanisms ensure that data propagates correctly through each stage, while setup and hold times are critical for reliable operation.

The pipeline stages in a modern GPU typically include **Fetch**, where instructions are fetched from memory; **Decode**, where instructions are decoded into micro-operations; **Execute**, where arithmetic or logical operations are performed; **Memory Access**, which handles load/store operations; and **Writeback**, where results are written back to registers.

Each stage operates in parallel, with data flowing from one stage to the next at each clock edge. The clock signal synchronizes these stages, ensuring that data is stable before being captured. The clock period must satisfy the worst-case delay of any stage, as given by:

$$T_{\text{clock}} \geq \max(T_{\text{fetch}}, T_{\text{decode}}, T_{\text{execute}}, T_{\text{memory}}, T_{\text{writeback}})$$

Setup and hold times are critical for reliable pipeline operation. The setup time  $t_{\text{su}}$  is the minimum time data must be stable before the clock edge, while the hold time  $t_{\text{h}}$  is the minimum time data must remain stable after the clock edge. Violating these constraints can lead to metastability, where the output of a flip-flop becomes unpredictable. The timing constraints are expressed as:

$$T_{\text{clock}} \geq t_{\text{su}} + t_{\text{prop}} + t_{\text{skew}}$$

$$t_{\text{h}} \leq t_{\text{prop}} - t_{\text{skew}}$$

where  $t_{\text{prop}}$  is the propagation delay and  $t_{\text{skew}}$  is the clock skew between stages.

To avoid metastability, GPUs employ synchronization techniques such as flip-flop chains, which use multiple flip-flops in series to reduce the probability of metastability propagating; clock domain crossing (CDC) circuits, which handle signals crossing between asynchronous clock domains; and FIFO buffers (first-in-first-out), which synchronize data between stages with different clock rates.

The following Verilog code illustrates a basic pipeline stage with synchronization:

Code Sample 7.8: Pipeline Stage with Synchronization

```
module pipeline_stage (
    input clk,
    input reset,
    input [31:0] data_in,
    output reg [31:0] data_out
);
    reg [31:0] stage_reg;
    always @(posedge clk or posedge reset) begin
        if (reset) begin
            stage_reg <= 32'b0;
            data_out <= 32'b0;
        end else begin
            stage_reg <= data_in;
            data_out <= stage_reg;
        end
    end
endmodule
```

Clock skew management is essential for maintaining synchronization across pipeline stages. Skew occurs when clock signals arrive at different times due to wire delays or process variations. The maximum allowable skew is constrained by:

$$t_{\text{skew}} \leq T_{\text{clock}} - t_{\text{su}} - t_{\text{prop}}$$

Modern GPUs use balanced clock trees and deskew circuits to minimize skew. For example, a phase-locked loop (PLL) can align clock edges across the chip. The PLL adjusts the clock phase to compensate for delays, ensuring synchronization.

Metastability is quantified by the mean time between failures (MTBF), given by:

$$\text{MTBF} = \frac{e^{t_r/\tau}}{f_{\text{clk}} \cdot f_{\text{data}} \cdot t_w}$$

where  $t_r$  is the resolution time,  $\tau$  is the time constant of the flip-flop,  $f_{\text{clk}}$  and  $f_{\text{data}}$  are the clock and data frequencies, and  $t_w$  is the metastability window.

Pipeline hazards, such as data dependencies or resource conflicts, can disrupt synchronization. Forwarding and stalling mechanisms mitigate these hazards. For example, forwarding bypasses intermediate stages to deliver data directly to dependent instructions, while stalling halts the pipeline until hazards resolve. The following equations describe the forwarding logic:

$$\text{ForwardA} = (\text{EX/MEM.RegWrite} \wedge \text{EX/MEM.RegisterRd} = \text{ID/EX.RegisterRs})$$

$$\text{ForwardB} = (\text{EX/MEM.RegWrite} \wedge \text{EX/MEM.RegisterRd} = \text{ID/EX.RegisterRt})$$

Clock gating reduces power consumption by disabling unused pipeline stages. However, it introduces additional synchronization challenges. The gating signal must align with the clock to prevent glitches, as described by:

$$t_{\text{setup\_gate}} \leq t_{\text{clk}} - t_{\text{gate\_delay}}$$

In summary, modern GPU pipelines rely on precise clocking and synchronization to maintain performance and reliability. Setup and hold times must be rigorously enforced, and metastability avoided through careful design. Techniques such as CDC circuits, clock skew management, and hazard mitigation ensure robust operation. The interplay between these factors defines the efficiency and scalability of GPU architectures.

### 7.4.2 Setup/hold times

In modern GPU architectures, the management of setup and hold times is critical for ensuring reliable operation across pipeline stages and clock domains. Setup time ( $t_{su}$ ) is the minimum time before the clock edge that data must be stable, while hold time ( $t_h$ ) is the minimum time after the clock edge during which data must remain stable. Violations of these constraints can lead to metastability, where flip-flops enter an indeterminate state, potentially corrupting computations.

The relationship between clocking, synchronization, and pipeline stages is governed by these timing parameters, which are particularly challenging in high-frequency GPUs due to their deep pipelines and parallel processing units. The clock-to-Q delay ( $t_{cq}$ ) of a flip-flop and the combinational logic delay ( $t_{comb}$ ) between pipeline stages must satisfy the following timing constraints for correct operation:

$$t_{clk} \geq t_{cq} + t_{comb} + t_{su}$$

The hold time constraint ensures that the new data does not overwrite the previous value too soon:

$$t_h \leq t_{cq} + t_{comb}$$

Modern GPUs employ techniques such as time borrowing and clock skew scheduling to mitigate these constraints. For instance, time borrowing allows slack from one pipeline stage to be used in adjacent stages, relaxing the setup time requirement.

Pipeline stages in GPUs are often synchronized using flip-flops or latches. The following Verilog snippet illustrates a basic pipeline register with setup/hold checks:

Code Sample 7.9: Pipeline Register with Timing Checks

```
module pipeline_reg (
    input clk,
    input [31:0] din,
    output reg [31:0] dout
);
    always @ (posedge clk) begin
        // Setup check: din must be stable before clk edge
        if ($setup(din, posedge clk, t_su) == 0) begin
            dout <= din;
        end else begin
            $display("Setup violation at time %t", $time);
        end

        // Hold check: din must remain stable after clk edge
        if ($hold(posedge clk, din, t_h) != 0) begin
            $display("Hold violation at time %t", $time);
        end
    end
endmodule
```

Metastability arises when flip-flops sample data during transitions, violating setup/hold times. The probability of metastability ( $P_{meta}$ ) is given by:

$$P_{meta} = e^{-\frac{t_r}{\tau}}$$

where  $t_r$  is the resolution time and  $\tau$  is the time constant of the flip-flop. To reduce  $P_{meta}$ , GPUs use synchronizers, such as dual flip-flop chains, which provide additional time for metastable states to resolve:

Code Sample 7.10: Dual Flip-Flop Synchronizer

```
module sync_2ff (
    input clk,
    input async_in,
    output reg sync_out
);
    reg ff1;
    always @ (posedge clk) begin
        ff1 <= async_in;
```

## ASSERTIONS IN GPU PROGRAMMING

### What Are Assertions?

Assertions are statements that check if a condition is true during program execution. If the condition is false, the program will terminate with a detailed error message.

### GPU Assertion Example

```
// Check if thread index is within bounds
__device__ void processPixel(int idx) {
    assert(idx < IMAGE_WIDTH * IMAGE_HEIGHT);
    // Process pixel safely...
```

#### Benefits

- 1 Early Bug Detection
- 2 Self-Documenting Code
- 3 Prevents Silent Failures
- 4 Easier Debugging

#### Usage Considerations

- ▲ Disable in production builds for performance
- ▲ Can increase register usage in GPU kernels
- ▲ Not all GPU platforms handle assertions equally

MODERN GPU DEBUGGING TOOLS SUPPORT ASSERTIONS

```

    sync_out <= ff1;
end
endmodule

```

Clocking strategies in GPUs must account for global and local clock skew. Clock tree synthesis ensures minimal skew, but variations in temperature and voltage can introduce dynamic skew. The skew between two clock domains ( $\Delta t_{\text{skew}}$ ) must satisfy:

$$\Delta t_{\text{skew}} \leq t_{\text{clk}} - t_{\text{su}} - t_{\text{cq}} - t_{\text{comb}}$$

Advanced GPUs employ delay-locked loops (DLLs) or phase-locked loops (PLLs) to align clock phases and minimize skew.

In multi-clock-domain designs, asynchronous FIFOs are used to transfer data safely. The FIFO depth ( $N$ ) must account for the worst-case latency and throughput requirements:

$$N \geq \frac{f_{\text{fast}}}{f_{\text{slow}}} \cdot (t_{\text{write}} - t_{\text{read}})$$

where  $f_{\text{fast}}$  and  $f_{\text{slow}}$  are the clock frequencies of the writer and reader domains, respectively. The following Verilog snippet shows an asynchronous FIFO implementation:

Code Sample 7.11: Asynchronous FIFO

```

module async_fifo (
  input wclk, rclk,
  input [31:0] wdata,
  output [31:0] rdata
);
  reg [31:0] mem [0:15];
  reg [3:0] wptr, rptr;

  always @(posedge wclk) begin
    mem[wptr] <= wdata;
    wptr <= wptr + 1;
  end

  always @(posedge rclk) begin
    rdata <= mem[rptr];
    rptr <= rptr + 1;
  end
endmodule

```

To further mitigate metastability, GPUs use error-correcting codes (ECC) and redundancy. Triple modular redundancy (TMR) is a common technique where three identical circuits vote on the correct output, masking transient errors. The reliability ( $R$ ) of a TMR system is:

$$R = 3R_0^2 - 2R_0^3$$

where  $R_0$  is the reliability of a single module.

In summary, modern GPU architectures rely on precise management of setup/hold times, clock synchronization, and metastability avoidance to maintain high performance and reliability. Techniques such as time borrowing, synchronizers, and asynchronous FIFOs are essential for meeting timing constraints in deep pipelines and multi-clock-domain designs. The mathematical foundations and Verilog implementations provided here underscore the importance of these concepts in GPU design.

### 7.4.3 Avoiding metastability

In modern GPU architectures, metastability is a critical concern in clocking and synchronization due to the high-frequency operation and deep pipelining. Metastability occurs when a flip-flop samples an input signal during its setup or hold violation window, causing an indeterminate output state that can propagate through the pipeline. The probability of metastability is given by:

$$P_{\text{meta}} = \frac{T_0 \cdot f_{\text{clk}} \cdot f_{\text{data}}}{e^{t_r/\tau}}$$

where  $T_0$  is the sampling window,  $f_{\text{clk}}$  and  $f_{\text{data}}$  are the clock and data frequencies,  $t_r$  is the resolution time, and  $\tau$  is the time constant of the flip-flop.

To mitigate metastability, GPUs employ several techniques. Synchronizer chains are a common method involving a cascade of flip-flops to reduce the probability of metastability propagation. The mean time between failures (MTBF) improves exponentially with each additional stage, as described by:

$$\text{MTBF} \propto e^{N \cdot t_r / \tau}$$

where  $N$  is the number of synchronizer stages. GPUs typically use two or more stages for cross-domain signals.

Clock Domain Crossing (CDC) protocols, such as asynchronous FIFOs and handshake mechanisms, are employed to safely transfer data between clock domains. For example, a Gray-coded FIFO ensures that only one bit changes per transaction, minimizing the risk of metastability. A Gray code counter used in such designs is illustrated in the following Verilog implementation:

Code Sample 7.12: Gray Code Counter

```
module gray_counter (
    input clk, reset,
    output reg [3:0] gray_out
);
    reg [3:0] binary;
    always @(posedge clk or posedge reset) begin
        if (reset) begin
            binary <= 4'b0;
            gray_out <= 4'b0;
        end else begin
            binary <= binary + 1;
            gray_out <= (binary >> 1) ^ binary;
        end
    end
endmodule
```

Setup and hold time compliance is another cornerstone of metastability mitigation. GPUs enforce strict timing constraints to avoid violations. The setup time  $t_{\text{su}}$  and hold time  $t_h$  must satisfy the following conditions:

$$t_{\text{su}} \leq T_{\text{clk}} - t_{\text{prop}} - t_{\text{skew}}$$

$$t_h \leq t_{\text{prop}} - t_{\text{skew}}$$

where  $T_{\text{clk}}$  is the clock period,  $t_{\text{prop}}$  is the propagation delay, and  $t_{\text{skew}}$  is the clock skew. These constraints are verified using static timing analysis (STA) tools.

Adaptive clock gating is used to prevent metastability introduced by dynamic voltage and frequency scaling (DVFS). By ensuring that clock edges are enabled only when the pipeline is ready, GPUs reduce the likelihood of timing violations during clock transitions.

Metastability-hardened flip-flops are employed in critical paths to reduce the resolution time  $\tau$ , thereby decreasing the probability of metastability as defined in Equation 16.1.2. These flip-flops use higher internal gain or feedback techniques for faster resolution of ambiguous states.

Pipeline stages in GPUs are particularly vulnerable to metastability due to high clock frequencies and the parallel nature of execution. Each pipeline stage must meet tight timing constraints. Techniques to manage this include stage isolation using pipeline registers to localize metastability faults, time borrowing mechanisms where stages dynamically adjust timing using clock skew or latch-based designs, and error detection and correction through the use of parity bits or ECC in pipeline registers.

The relationship between clock skew and metastability is especially significant. Clock skew  $t_{\text{skew}}$ , defined as the difference in clock signal arrival times between flip-flops, must be tightly controlled to avoid hold time violations. The maximum allowable skew is:

$$t_{\text{skew,max}} = \min(t_{\text{prop}} - t_h, T_{\text{clk}} - t_{\text{su}} - t_{\text{prop}})$$

To meet this constraint, modern GPUs employ balanced clock trees and deskew circuits. H-tree clock distribution networks, for example, are widely used to ensure uniform clock delay across the chip.

In summary, avoiding metastability in GPU architectures requires a multilayered approach that combines synchronizer chains, CDC protocols, rigorous timing analysis, and circuit-level hardening techniques. These strategies are essential for maintaining functional correctness in high-performance computing environments. Further insights into metastability mitigation can be found in the studies by .

## 7.5 Clock Domain Crossing Strategies

### 7.5.1 Synchronizing signals across clock domains

In modern GPU architectures, synchronizing signals across clock domains is a critical challenge due to the increasing complexity of multi-clock designs. Clock domain crossing (CDC) strategies must address metastability, signal integrity, and timing constraints to ensure reliable operation. Metastability occurs when a signal transitions near the clock edge of the receiving domain, violating setup or hold times and leading to unpredictable behavior. The probability of metastability failure can be modeled as:

$$P_{failure} = f_{data} \cdot f_{clk} \cdot e^{-\frac{t_r}{\tau}}$$

where  $f_{data}$  and  $f_{clk}$  are the data and clock frequencies,  $t_r$  is the resolution time, and  $\tau$  is the time constant of the flip-flop.

To mitigate metastability, GPUs employ synchronization techniques such as multi-stage flip-flop chains (synchronizers). A two-flip-flop synchronizer is commonly used, but deeper chains may be necessary for high-frequency designs. The Verilog example below illustrates a basic two-stage synchronizer:

Code Sample 7.13: Two-Flip-Flop Synchronizer in Verilog

```
module sync_2ff (
    input wire clk,
    input wire async_in,
    output reg sync_out
);
    reg meta;
    always @(posedge clk) begin
        meta <= async_in;
        sync_out <= meta;
    end
endmodule
```

The mean time between failures (MTBF) for a synchronizer is given by:

$$\text{MTBF} = \frac{e^{t_r/\tau}}{f_{clk} \cdot f_{data} \cdot T_0}$$

where  $T_0$  is a technology-dependent constant. For GPUs operating at gigahertz frequencies, designers often use triple or quadruple synchronizers to achieve acceptable MTBF values.

Handshake protocols are used for transferring control signals across domains. A typical four-phase handshake includes the following steps: the source domain asserts a request signal; the destination domain responds by asserting an acknowledge signal after safely sampling the data; the source deasserts the request; and finally, the destination deasserts the acknowledge, completing the cycle.

For high-throughput applications, FIFO-based CDC mechanisms are preferred. Dual-clock FIFOs use Gray code counters to synchronize read and write pointers, reducing the probability of metastability by minimizing bit transitions. Gray codes ensure that only one bit changes per increment. A Verilog implementation of a Gray code counter is shown here:

Code Sample 7.14: Gray Code Counter

```
module gray_counter (
    input wire clk,
    input wire rst,
    output reg [3:0] gray
);
    reg [3:0] binary;
    always @(posedge clk or posedge rst) begin
```

```

if (rst) begin
    binary <= 0;
    gray <= 0;
end else begin
    binary <= binary + 1;
    gray <= binary ^ (binary >> 1);
end
end
endmodule

```

Metastability mitigation also involves careful timing analysis. Tools such as Static Timing Analysis (STA) verify synchronization paths and ensure sufficient resolution time. The following constraints must be satisfied to ensure correct timing:

$$t_{\text{setup}} \leq T_{\text{clk}} - t_{\text{skew}} - t_{\text{prop}}$$

$$t_{\text{hold}} \leq t_{\text{skew}} + t_{\text{prop}}$$

where  $t_{\text{setup}}$  and  $t_{\text{hold}}$  are flip-flop timing requirements,  $T_{\text{clk}}$  is the clock period,  $t_{\text{skew}}$  is clock skew, and  $t_{\text{prop}}$  is the propagation delay.

In modern GPUs, adaptive clocking techniques dynamically adjust clock frequencies to reduce CDC complexity. For instance, NVIDIA's Pascal architecture incorporates clock-gating and dynamic voltage-frequency scaling (DVFS) to align clock domains during low-power operation. Similarly, AMD's Infinity Fabric uses a mesh-based clock distribution to minimize skew.

For control signals crossing domains, glitch-free multiplexers are essential. These multiplexers ensure no spurious transitions occur during domain crossing. A safe CDC multiplexer design is shown below:

Code Sample 7.15: Glitch-Free MUX

```

module cdc_mux (
    input wire clk_a, clk_b,
    input wire sel,
    input wire [7:0] data_a, data_b,
    output reg [7:0] out
);
    reg [7:0] sync_a, sync_b;
    always @(posedge clk_a) sync_a <= data_a;
    always @(posedge clk_b) sync_b <= data_b;
    always @(*) begin
        if (!sel) out = sync_a;
        else out = sync_b;
    end
endmodule

```

Research by Cummings emphasizes the importance of verifying CDC schemes using formal methods. Techniques like model checking and assertion-based verification are used to detect metastability-related corner cases. An example assertion for checking metastability in a two-flip-flop synchronizer is:

Code Sample 7.16: Assertion for Metastability Check

```
assert property (@(posedge clk) !$isunknown(meta));
```

Advanced GPUs integrate dedicated CDC IP blocks such as Xilinx's XPM CDC and Intel's ALTCLKCTRL to automate synchronization. These IPs provide configurable synchronizers, pulse generators, and dual-clock FIFOs, reducing design complexity.

The trend toward heterogeneous computing, which integrates CPUs, GPUs, and accelerators on the same die, makes robust CDC strategies increasingly essential. Synchronization in such environments involves multi-stage synchronizers for metastability mitigation, handshake protocols for control signal transfer, dual-clock FIFOs for data buses, gray code counters for pointer synchronization, and adaptive clocking or DVFS for dynamic alignment.

These approaches collectively ensure reliable operation in high-performance multi-clock GPU systems while satisfying power and timing constraints. Looking ahead, machine learning-assisted CDC optimization and quantum-resistant synchronization protocols are emerging areas of research, as described in .

### 7.5.2 Metastability mitigation techniques

In modern GPU architectures, metastability is a critical concern, particularly when signals traverse clock domain crossings (CDC). As GPUs employ multiple clock domains to optimize power and performance, synchronizing signals across these domains introduces the risk of metastability, where flip-flops enter an indeterminate state. This can lead to system failures or corrupted data. To mitigate metastability, several techniques are employed, including synchronization chains, handshake protocols, and FIFO-based CDC strategies.

A primary method for metastability mitigation is the use of multi-stage synchronization chains, often implemented as two or more flip-flops in series. The probability of metastability propagating through multiple stages decreases exponentially with each additional stage. The mean time between failures (MTBF) for a dual-flip-flop synchronizer is given by:

$$\text{MTBF} = \frac{e^{t_r/\tau}}{f_c f_d T_0}$$

where  $t_r$  is the resolution time,  $\tau$  is the time constant of the flip-flop,  $f_c$  and  $f_d$  are the clock frequencies, and  $T_0$  is a device-specific parameter. Increasing the number of stages improves MTBF but introduces latency.

Handshake protocols provide another robust solution for CDC. These protocols ensure data integrity by acknowledging signal transitions between domains. A common implementation is the four-phase handshake, in which the sender asserts a request signal (`req`) in its clock domain, the receiver synchronizes `req` and responds with an acknowledgment (`ack`), the sender deasserts `req` upon detecting `ack`, and finally the receiver deasserts `ack`, completing the transaction. This method guarantees that data is stable before being sampled, but it incurs higher latency due to the back-and-forth signaling.

FIFO-based CDC is widely used in GPUs for high-throughput data transfer between asynchronous clock domains. A dual-clock FIFO employs separate read and write pointers, synchronized to the opposite domain using Gray coding to minimize bit transitions. The Verilog implementation of a Gray code counter is shown below:

Code Sample 7.17: Gray Code Counter

```
module gray_counter (
    input clk,
    input reset,
    output reg [3:0] gray
);
    reg [3:0] binary;
    always @(posedge clk or posedge reset) begin
        if (reset) begin
            binary <= 4'b0;
            gray <= 4'b0;
        end else begin
            binary <= binary + 1;
            gray <= binary ^ (binary >> 1);
        end
    end
endmodule
```

Metastability can also be mitigated by careful timing analysis and constraint specification. False paths and multicycle paths must be explicitly defined in synthesis tools to avoid incorrect optimizations. For example, synchronizer flip-flops should be excluded from timing checks using:

Code Sample 7.18: SDC Constraints for Synchronizers

```
set_false_path -to [get_pins {sync_ff*/D}]
```

Another advanced technique is the use of adaptive clocking, where the receiving clock is dynamically adjusted to align with the source clock during data transfer. This reduces the probability of setup/hold violations but requires complex phase-locked loop (PLL) or delay-locked loop (DLL) circuitry. Research by Cummings demonstrates that adaptive clocking can achieve MTBF values exceeding  $10^9$  years for typical GPU operating frequencies.

In high-performance GPUs, combinational logic between synchronizers must be minimized to reduce glitch propagation. Glitches can cause incorrect sampling if they coincide with clock edges. A common practice is to register signals before synchronization, as shown in the following Verilog snippet:

# GPU THROUGHPUT

Modern GPU Architecture Performance Metrics

## What is GPU Throughput?

GPU throughput measures how many operations can be completed in a given time period. Unlike CPUs which optimize for latency, GPUs are designed for massively parallel workloads, processing thousands of threads simultaneously to maximize total computational throughput.

## Key Throughput Metrics

**FLOPS**  
Floating Point Operations/Second

**IOPS**  
Integer Operations/Second

**Texel Rate**  
Texture Elements Processed/Second

**Memory Bandwidth**  
Data Transfer Rate (GB/s)

## GPU Architecture for Throughput

The diagram illustrates the hierarchical structure of GPU architecture components contributing to throughput:

- Memory System (GDDR6/HBM2)** (Yellow Box): Contains Memory Controller, L2 Cache, Thread Scheduler, Raster Engines, and Texture Units.
- Compute Units / Streaming Multiprocessors** (Green Box): Contains CUDA Cores/Stream Processors, Tensor Cores, RT Cores, L1 Cache/Shared Memory, Special Function Units, and Warp Schedulers.

## Factors Affecting GPU Throughput

- 1 Core Count Clock Speed**
- 2 Memory Bandwidth Cache Hierarchy**
- 3 Occupancy Warp Execution Efficiency**
- 4 Thread Divergence**
- 5 Specialized Compute Units (Tensor/RT Cor**
- 6 Workload Characteristics Optimization**

### Code Sample 7.19: Glitch-Free Synchronization

```

reg [7:0] data_reg;
always @(posedge clk_src) begin
    data_reg <= data_next;
end

sync_2ff sync_inst (
    .clk(clk_dest),
    .d(data_reg),
    .q(data_sync)
);

```

The choice of metastability mitigation technique depends on latency tolerance, throughput requirements, and power constraints. For control signals, two-flip-flop synchronizers are often sufficient. FIFOs are preferred for data buses. Handshake protocols are used in latency-insensitive designs. Adaptive clocking is reserved for ultra-high-speed interfaces.

Recent work by Kapschitz highlights the impact of process variations on metastability. Smaller technology nodes exhibit increased susceptibility to metastability due to reduced noise margins. To address this, modern GPUs incorporate error-correcting codes (ECC) and redundancy in critical CDC paths.

In summary, metastability mitigation in modern GPU architectures relies on a combination of synchronization chains, handshake protocols, FIFO-based CDC, and adaptive clocking. Each technique offers trade-offs between latency, area, and reliability, necessitating careful design and verification. Tools like static timing analysis (STA) and formal verification are essential for ensuring robust CDC implementations. Future research directions include machine learning-based metastability prediction and the integration of asynchronous design methodologies into GPU pipelines.

## 7.6 Power Estimation and Management

### 7.6.1 Power-aware design techniques

Power-aware design techniques in modern GPU architectures have become increasingly critical due to the growing demand for energy-efficient computing. GPUs, originally designed for graphics rendering, now serve as general-purpose accelerators in high-performance computing, machine learning, and data analytics. Their parallel architecture enables massive throughput but also introduces significant power consumption challenges. This discussion focuses on power estimation and management, particularly dynamic and static power estimation in GPU pipelines.

The power consumption of a GPU can be broadly categorized into dynamic and static components. Dynamic power arises from switching activity in transistors and is proportional to the clock frequency, supply voltage, and capacitive load. The dynamic power  $P_{\text{dynamic}}$  is given by:

$$P_{\text{dynamic}} = \alpha CV^2 f$$

where  $\alpha$  is the activity factor,  $C$  is the load capacitance,  $V$  is the supply voltage, and  $f$  is the clock frequency. Static power, on the other hand, is primarily due to leakage currents and is influenced by process technology, temperature, and supply voltage. The static power  $P_{\text{static}}$  is modeled as:

$$P_{\text{static}} = I_{\text{leak}} V$$

where  $I_{\text{leak}}$  is the leakage current.

Modern GPUs employ various techniques to estimate and manage these power components. Power estimation in GPU pipelines involves profiling the activity of functional units, memory hierarchies, and interconnects. One common approach is cycle-accurate simulation, where power models are integrated into architectural simulators like GPGPU-Sim. These models account for:

Execution unit utilization, including ALUs, FPUs, and special function units. Memory access patterns, including cache hits, misses, and DRAM transactions. Thread scheduling and warp divergence, which affect parallelism and resource usage.

Dynamic power estimation often relies on performance counters to track switching activity. For example, NVIDIA's NVML library provides hardware counters for monitoring SM (Streaming Multiprocessor) activity, memory bandwidth, and instruction throughput. These counters feed into power models like those proposed by

, which correlate performance events with power consumption. The accuracy of such models depends on the granularity of event sampling and the fidelity of the underlying power characterization.

Static power estimation is more challenging due to its dependence on process variations and temperature. Techniques like PTM (Predictive Technology Model) are used to project leakage currents across technology nodes. In GPUs, static power is often estimated empirically by measuring idle power and subtracting dynamic contributions. Advanced methods, such as those in , use thermal sensors and voltage-frequency scaling to refine leakage predictions.

Power-aware design techniques aim to optimize both dynamic and static power. Dynamic voltage and frequency scaling (DVFS) is widely used to adjust  $V$  and  $f$  dynamically based on workload demands. For instance, NVIDIA's Boost technology scales clock frequencies within thermal and power limits. Similarly, AMD's Power-Tune adjusts power targets to maximize performance under constrained budgets. These techniques rely on real-time power sensors and control loops to maintain efficiency.

Another approach is workload-aware resource allocation, where GPU resources are dynamically enabled or disabled. For example, fine-grained clock gating shuts down unused execution units, reducing dynamic power. Coarse-grained power gating disables entire SMs during low-utilization phases, cutting static power. These techniques are implemented in hardware and firmware, as seen in ARM's Mali GPUs and Imagination's PowerVR architectures.

Memory subsystem optimizations also play a key role in power-aware design. GPUs employ cache hierarchies with configurable associativity and capacity to balance performance and power. For example, NVIDIA's L2 cache partitions can be dynamically resized to reduce leakage. Similarly, bandwidth compression techniques, like delta color compression in AMD's RDNA architecture, lower DRAM power by reducing data transfers.

Power management in GPU pipelines extends to thread scheduling and parallelism control. Warp throttling limits the number of active warps per SM to reduce contention and power. Predictive scheduling, as proposed in , prioritizes warps with high expected utilization to minimize idle cycles. These techniques are complemented by compiler optimizations, such as loop unrolling and instruction reordering, to improve energy efficiency.

Emerging research explores machine learning for power estimation and management. Neural networks trained on performance counters can predict power consumption with high accuracy . Reinforcement learning agents optimize DVFS and resource allocation policies in real time. These methods are being integrated into runtime systems like TensorRT and ROCm for adaptive power management.

In summary, power-aware design in modern GPUs involves a combination of estimation techniques and management strategies. Dynamic and static power are modeled using performance counters, thermal sensors, and process characteristics. Techniques like DVFS, clock gating, and workload-aware scheduling optimize power efficiency. Ongoing advancements in machine learning and hardware-software co-design promise further improvements in GPU energy efficiency.

#### Code Sample 7.20: Power-aware warp scheduling

```
// Pseudocode for predictive warp scheduling
if (power_budget > threshold) {
    activate_additional_warps();
} else {
    throttle_warps();
}
```

The interplay between power estimation and management is critical for sustainable GPU computing. As architectures evolve, techniques like near-threshold computing and 3D integration will redefine power-aware design paradigms. Future work must address the challenges of scalability, accuracy, and adaptability in power optimization.

### 7.6.2 Estimating dynamic and static power in GPU pipelines

Power estimation in modern GPU pipelines is a critical aspect of power-aware design, enabling efficient power management and optimization. Dynamic and static power components must be accurately modeled to achieve energy-efficient architectures. Dynamic power arises from switching activity and is given by:

$$P_{\text{dyn}} = \alpha C V^2 f$$

where  $\alpha$  is the switching activity factor,  $C$  is the load capacitance,  $V$  is the supply voltage, and  $f$  is the clock frequency. Static power, on the other hand, is primarily due to leakage currents and is expressed as:

$$P_{\text{stat}} = V I_{\text{leak}}$$

where  $I_{\text{leak}}$  represents the leakage current.

Accurate estimation of dynamic power in GPU pipelines requires modeling the activity of individual pipeline stages. Modern GPUs employ deeply pipelined architectures with hundreds of execution units, making power estimation computationally intensive. A common approach involves cycle-accurate simulation combined with activity counters to track switching events. For example, the power model in correlates instruction-level parallelism (ILP) with dynamic power consumption. The total dynamic power for a GPU pipeline can be approximated as:

$$P_{\text{dyn}}^{\text{total}} = \sum_{i=1}^N \alpha_i C_i V_i^2 f_i$$

where  $N$  is the number of pipeline stages, and  $\alpha_i$ ,  $C_i$ ,  $V_i$ , and  $f_i$  are stage-specific parameters.

Static power estimation is more challenging due to process variations and temperature dependencies. Leakage currents in FinFET-based GPUs exhibit exponential dependence on temperature, as described by:

$$I_{\text{leak}} = I_0 e^{\frac{V - V_{\text{th}}}{\eta V_T}}$$

where  $I_0$  is a technology-dependent constant,  $V_{\text{th}}$  is the threshold voltage,  $\eta$  is the subthreshold slope factor, and  $V_T$  is the thermal voltage. Static power is particularly significant in idle or low-activity states, necessitating power-gating techniques to mitigate leakage.

Power-aware design techniques leverage these estimations to optimize GPU performance-per-watt. One widely adopted technique is dynamic voltage and frequency scaling (DVFS), which adjusts  $V$  and  $f$  dynamically based on workload demands to reduce dynamic power quadratically, as seen in (7.6.2). Modern GPUs implement fine-grained DVFS domains per pipeline stage. Clock gating is another method that disables clock signals to inactive pipeline stages, thereby eliminating unnecessary switching activity and reducing  $\alpha$  in (7.6.2). Power gating cuts off supply voltage to idle blocks, minimizing  $I_{\text{leak}}$  as described in (7.6.2). Techniques like retention flip-flops are employed to preserve state during power-down. Finally, workload balancing distributes computations evenly across execution units, which helps avoid localized power hotspots and improves thermal efficiency.

Verilog implementations of power-aware techniques often integrate activity monitors and control logic. For example, a clock-gating module may be implemented as follows:

Code Sample 7.21: Clock Gating Control

```
module clock_gate (
    input clk, enable,
    output reg gated_clk
);
    always @(clk or enable) begin
        if (!enable) gated_clk = 0;
        else gated_clk = clk;
    end
endmodule
```

Empirical validation of power models is essential. Measurement-based studies, such as those using NVIDIA's nvprof or AMD's ROCm, correlate simulated power estimates with actual hardware readings. For instance, demonstrates a 92% accuracy in dynamic power prediction for CUDA kernels using linear regression on activity counters.

Advanced techniques like machine learning are increasingly applied to power estimation. Neural networks trained on microarchitectural events such as cache misses and warp divergence predict power consumption with less than 5% error. These models generalize across workloads, reducing reliance on physical sensors.

# GPU Resolution Targets

*Modern GPU Architecture Design Considerations*

---

## Common Resolution Targets

**HD**  
 $1280 \times 720$

**Full HD**  
 $1920 \times 1080$

**4K UHD**  
 $3840 \times 2160$

Pixel Count Comparison:

- HD: ~921,600 pixels
- Full HD: ~2 million pixels (2.25× HD)
- 4K UHD: ~8.3 million pixels (4× Full HD)

## Common Aspect Ratios

**16:9**  
 Standard TV/Monitor

**21:9**  
 Ultrawide

**32:9 Super Ultrawide**

## GPU Performance Impact

Resolution	Relative GPU Load (%)
HD	~25%
Full HD	~45%
4K UHD	~75%
8K	~90%

*Relative GPU Load by Resolution*

## GPU Architecture Considerations

**Memory Bandwidth**

- 4K: ~16GB/s min
- 8K: ~60GB/s min
- High-end GPUs: Up to 1TB/s

**Shader Cores**

- 1080p gaming: 1,000+
- 4K gaming: 3,000+
- 8K/RT: 10,000+
- Parallel workloads

**Power Requirements**

- Entry: 75-150W
- Mid-range: 200-300W
- High-end: 350-450W
- Increases with res.

Thermal effects further complicate power estimation. Leakage currents rise with temperature, creating a feed-back loop. The power-temperature relationship is modeled as:

$$P_{\text{total}} = P_{\text{dyn}} + P_{\text{stat}}(T)$$

where  $T$  is the junction temperature. Coupled thermal-power simulators, such as GPGPU-Sim with HotSpot, solve this iteratively .

Emerging technologies like near-threshold computing (NTC) push power optimization further. Operating GPUs at reduced  $V$  lowers both dynamic and static power, albeit at performance costs. Hybrid voltage/frequency islands balance these trade-offs .

In summary, estimating dynamic and static power in GPU pipelines involves modeling switching activity and leakage currents using equations (7.6.2) and (7.6.2), validating models against hardware measurements , applying power-aware techniques such as DVFS and clock gating, and addressing thermal dependencies through coupled simulations . Future directions include 3D-stacked GPUs with inter-tier cooling, which will require new estimation methods for vertical power delivery and heat dissipation . Accurate power estimation remains foundational for energy-efficient GPU design.

# Chapter 8

# Vertex Processing Units

## 8.1 Vertex Input Stage

### 8.1.1 Input buffers

Modern GPU architectures employ sophisticated mechanisms to handle vertex data efficiently, with input buffers playing a critical role in the vertex input stage. Input buffers are memory regions that store vertex attributes, such as position, normal, texture coordinates, and color, which are processed by the GPU's vertex shaders. These buffers are typically allocated in device memory and accessed through the GPU's memory hierarchy to minimize latency and maximize throughput. The vertex input stage fetches data from these buffers, formats it according to the vertex shader's requirements, and passes it to the shader cores for processing.

Vertex attributes are stored in input buffers in a structured format, often as arrays of structures (AoS) or structures of arrays (SoA). The choice between AoS and SoA depends on the access patterns and performance requirements of the application. For example, AoS is suitable when all attributes of a single vertex are accessed together, while SoA is preferred when the same attribute across multiple vertices is processed in parallel. The GPU's memory controller optimizes access to these buffers by coalescing memory requests and leveraging cache hierarchies to reduce bandwidth consumption.

Index fetch is another crucial operation in the vertex input stage. Instead of processing vertices sequentially, GPUs often use index buffers to reference vertices indirectly. This allows for efficient reuse of vertex data, reducing memory bandwidth and improving performance. An index buffer contains integer indices that point to the actual vertex data in the input buffers. The GPU fetches these indices and uses them to gather the corresponding vertex attributes from the input buffers. This mechanism is particularly beneficial for rendering meshes with shared vertices, as it avoids redundant processing and memory access.

The vertex input stage performs several operations to prepare the data for the vertex shader:

**Vertex attribute fetching:** The GPU reads the vertex attributes from the input buffers based on the vertex indices. Each attribute is fetched according to its specified format, such as `float32`, `int16`, or `half`. **Data conversion:** The fetched data is converted to the format expected by the vertex shader. For example, integer attributes may be normalized to floating-point values in the range  $[0, 1]$  or  $[-1, 1]$ . **Attribute assembly:** The converted attributes are assembled into a single vertex structure, which is passed to the vertex shader for processing.

The performance of the vertex input stage is heavily influenced by the layout and organization of the input buffers. For instance, interleaved vertex attributes can improve cache utilization by ensuring that all attributes of a vertex are fetched together. Conversely, separate buffers for each attribute may be more efficient when only a subset of attributes is required for a particular rendering pass. Modern GPUs support flexible vertex input layouts, allowing applications to specify the buffer bindings, strides, and offsets for each attribute.

The following equation describes the memory address calculation for fetching a vertex attribute:

$$\text{address} = \text{base\_address} + \text{vertex\_index} \times \text{stride} + \text{offset}$$

Here, `base_address` is the starting address of the input buffer, `vertex_index` is the index of the vertex, `stride` is the byte offset between consecutive vertices, and `offset` is the byte offset of the attribute within the vertex structure.

In addition to input buffers, modern GPUs utilize advanced features such as vertex pulling and shader attribute load/store operations. Vertex pulling allows the vertex shader to fetch attributes directly from memory using compute-like instructions, bypassing the fixed-function vertex input stage. This provides greater flexibility but

requires careful management of memory access patterns to avoid performance penalties. Shader attribute load/store operations enable the vertex shader to read and write attributes dynamically, supporting techniques such as procedural geometry generation and vertex amplification.

The following Verilog code illustrates a simplified vertex attribute fetch unit:

Code Sample 8.1: Vertex Attribute Fetch Unit

```
module vertex_fetch (
    input wire [31:0] base_address,
    input wire [31:0] vertex_index,
    input wire [31:0] stride,
    input wire [31:0] offset,
    output wire [31:0] attribute_data
);

wire [31:0] address;
assign address = base_address + (vertex_index * stride) + offset;

memory_controller mem_controller (
    .address(address),
    .data_out(attribute_data)
);

endmodule
```

Input buffers are typically managed through APIs such as Vulkan or Direct3D, which provide fine-grained control over buffer creation, binding, and synchronization. For example, Vulkan allows applications to specify usage flags for input buffers, such as `VK_BUFFER_USAGE_VERTEX_BUFFER_BIT`, which help optimize memory allocation and access patterns. To prevent data hazards and ensure correct access order, synchronization primitives such as barriers and fences are employed. These mechanisms guarantee that the GPU reads from or writes to input buffers only when it is safe to do so, maintaining data coherence across pipeline stages.

The efficiency of the vertex input stage is critical for achieving high rendering performance, especially in applications with complex geometry or high vertex counts. Techniques such as vertex cache optimization, index buffer compression, and attribute quantization are commonly employed to reduce memory bandwidth and improve cache utilization. For instance, the Tom Forsyth vertex cache optimization algorithm reorders indices to maximize the reuse of vertices in the GPU's post-transform cache, reducing the number of redundant attribute fetches.

In summary, input buffers are a fundamental component of modern GPU architectures, enabling efficient vertex data processing in the vertex input stage. The interplay between input buffers, index fetch, and vertex attributes determines the performance and flexibility of the rendering pipeline. Advances in memory hierarchy design, shader programming models, and API capabilities continue to enhance the efficiency and scalability of vertex input processing in GPUs.

### 8.1.2 Index fetch

## 8.2 Vertex Input and Index Fetch in GPU Architectures

The vertex input stage in modern GPU architectures is a critical component responsible for processing vertex data before it enters the rendering pipeline. This stage involves fetching vertex attributes from input buffers and organizing them for subsequent stages such as vertex shading. Index fetch plays a pivotal role in this process by enabling efficient access to vertex data through indexed rendering. The following discussion explores the interplay between input buffers, index fetch, and vertex attributes in modern GPU architectures.

Input buffers are memory regions that store vertex data, including positions, normals, texture coordinates, and other attributes. These buffers are typically structured as arrays, where each element corresponds to a vertex. Modern GPUs optimize memory access patterns to minimize latency, leveraging coalesced memory accesses and cache hierarchies. For instance, NVIDIA's Turing architecture employs a unified memory system with L1 and L2 caches to reduce bandwidth requirements. The vertex input stage reads data from these buffers and prepares it for processing by the vertex shader.

Index fetch is a mechanism that allows GPUs to reuse vertex data by referencing vertices through indices rather than duplicating them. This technique is particularly useful for rendering meshes with shared vertices, as it reduces memory consumption and improves rendering efficiency. The index buffer contains a list of indices that

reference vertices in the input buffers. During the vertex input stage, the GPU fetches these indices and uses them to retrieve the corresponding vertex attributes. The process can be represented mathematically as follows:

$$v_i = B[\text{index}[j]] \quad (8.1)$$

where  $v_i$  is the fetched vertex,  $B$  is the input buffer, and  $\text{index}[j]$  is the  $j$ -th index in the index buffer. This equation highlights the indirect addressing mechanism employed by index fetch.

Vertex attributes are the data elements associated with each vertex, such as position, color, or texture coordinates. Modern GPUs support flexible attribute formats, including 32-bit floating-point, 16-bit half-precision, and even packed formats like 10-10-10-2 for normalized attributes. The vertex input stage interprets these attributes based on descriptor tables, which specify the format, offset, and stride of each attribute. For example, the Vulkan API allows developers to define vertex input bindings and attributes explicitly, enabling fine-grained control over data fetching .

The following Verilog-like pseudocode illustrates a simplified vertex attribute fetch operation:

Code Sample 8.2: Vertex Attribute Fetch

```
module vertex_fetcher (
    input wire [31:0] index,
    input wire [31:0] base_addr,
    input wire [31:0] stride,
    output reg [127:0] vertex_attr
);
    wire [31:0] offset = index * stride;
    wire [31:0] addr = base_addr + offset;
    always @(*) begin
        vertex_attr = memory_read(addr);
    end
endmodule
```

The efficiency of index fetch and vertex attribute retrieval depends on several factors:

**Memory alignment** GPUs prefer aligned memory accesses to maximize bandwidth utilization. Misaligned accesses can degrade performance due to additional memory transactions.

**Cache locality** Reusing recently fetched vertices improves cache hit rates, reducing memory latency. Indexed rendering inherently promotes locality by reusing vertices.

**Data compression** Modern GPUs employ compression techniques for vertex attributes, such as delta encoding or entropy reduction, to minimize memory bandwidth usage .

The vertex input stage also handles instanced rendering, where the same geometry is rendered multiple times with varying parameters. In this case, the input buffers may contain per-instance data, and the index fetch logic must differentiate between per-vertex and per-instance attributes. The stage uses instance divisors to control the frequency of attribute updates. For example, a divisor of 1 updates the attribute for each instance, while a divisor of 0 treats it as a per-vertex attribute. This flexibility is crucial for rendering large crowds or repetitive structures efficiently.

Advanced GPU architectures, such as AMD’s RDNA 2, introduce hardware optimizations for vertex input processing. These include dedicated fetch units with support for multi-draw indirect commands, which reduce CPU overhead by allowing the GPU to manage draw calls autonomously . The index fetch logic in these architectures is tightly integrated with the command processor, enabling high-throughput vertex processing.

In summary, the vertex input stage in modern GPUs relies on input buffers, index fetch, and vertex attributes to deliver high-performance geometry processing. Index fetch enables efficient vertex reuse, while input buffers and attribute descriptors provide the necessary data for rendering. Hardware optimizations, such as cache hierarchies and compression, further enhance the efficiency of these operations. Understanding these mechanisms is essential for optimizing graphics applications and leveraging the full potential of modern GPU architectures.

### 8.2.1 Vertex attributes

## 8.3 Vertex Attributes and Input Processing in GPU Architectures

Modern GPU architectures employ sophisticated mechanisms to process vertex data efficiently, with vertex attributes playing a central role in the vertex input stage. The vertex input stage is responsible for fetching vertex data from memory, interpreting it according to predefined formats, and delivering it to subsequent pipeline stages. This process involves input buffers, index fetch operations, and attribute extraction, all optimized for parallel execution on GPUs.

Vertex attributes define the properties of vertices, such as position, normal vectors, texture coordinates, or custom data. Each attribute is stored in memory as a structured array, often interleaved or planar, depending on the access pattern. The GPU fetches these attributes using input buffers, which are memory regions bound to the pipeline for vertex data retrieval. For example, a vertex buffer containing position and normal data might be structured as:

Code Sample 8.3: Interleaved vertex buffer layout

```
struct Vertex {
    float position[3];
    float normal[3];
};
```

The vertex input stage interprets this data using a vertex attribute description, which specifies the format, offset, and stride of each attribute. The stride defines the byte distance between consecutive vertices, while the offset indicates the starting byte of an attribute within a vertex. For instance, the normal attribute in the above example has an offset of 12 bytes (assuming 4-byte floats) and a stride of 24 bytes. This information is critical for the GPU to fetch attributes correctly.

Index fetch is another key operation in the vertex input stage. Instead of processing vertices sequentially, GPUs often use index buffers to reference vertices non-linearly, enabling shared vertices across primitives. An index buffer contains integer indices that point to vertices in the vertex buffer. For example:

Code Sample 8.4: Index buffer referencing vertices

```
uint16_t indices[] = {0, 1, 2, 2, 3, 0};
```

This reduces memory bandwidth and improves cache efficiency by reusing vertices. The GPU fetches indices in batches, leveraging wide memory transactions and cache hierarchies to minimize latency. Modern GPUs employ advanced techniques like vertex reuse prediction and prefetching to further optimize index fetch performance.

Vertex attributes are fetched in parallel across multiple shader cores, with each thread or wavefront processing a subset of vertices. The GPU's memory subsystem is optimized for coalesced access, where threads within a warp or wavefront access contiguous memory locations. For non-coalesced access, such as random vertex fetches, the GPU employs caching and compression to mitigate performance penalties. The attribute fetch unit also handles format conversion, such as unpacking 8-bit normalized integers to 32-bit floats, as specified by the vertex attribute description.

The efficiency of vertex attribute fetching is governed by several factors:

- **Memory alignment:** Attributes aligned to cache line boundaries reduce fetch latency.
- **Data locality:** Interleaved attributes improve spatial locality but may increase bandwidth for unused attributes.
- **Compression:** Techniques like delta encoding or quantization reduce memory footprint and bandwidth .

Mathematically, the address calculation for vertex attribute fetching can be expressed as:

$$\text{address} = \text{base} + \text{index} \times \text{stride} + \text{offset} \quad (8.2)$$

where `base` is the buffer's base address, `index` is the vertex index, `stride` is the vertex stride, and `offset` is the attribute offset.

Modern GPUs also support instanced vertex attributes, where attributes are fetched once per instance rather than per vertex. This is useful for rendering multiple copies of a mesh with varying properties. The instance step rate controls the frequency of attribute updates, reducing redundancy. For example:

Code Sample 8.5: Instanced vertex attribute description

```
attribute[0].step = VK_VERTEX_INPUT_RATE_VERTEX; // Per-vertex
attribute[1].step = VK_VERTEX_INPUT_RATE_INSTANCE; // Per-instance
```

The vertex input stage is tightly integrated with the GPU's command processor, which manages buffer bindings and attribute state. When a draw command is issued, the command processor configures the vertex fetch units and dispatches work to shader cores. This involves:

- **Binding descriptor updates:** Specifying buffer addresses and formats.
- **Attribute masking:** Enabling or disabling specific attributes.
- **Divisor configuration:** Setting instance step rates.

Advanced GPUs also support vertex attribute compression, where attributes are stored in compressed formats (e.g., 16-bit floats or `snorm16`) and decompressed on-the-fly during fetch. This reduces memory bandwidth and storage requirements while maintaining precision. The decompression logic is implemented in hardware, ensuring minimal overhead.

The vertex input stage's performance is critical for overall GPU throughput, as bottlenecks here can stall subsequent pipeline stages. To mitigate this, GPUs employ several optimizations:

- **Prefetching:** Fetching vertex data ahead of demand to hide memory latency.
- **Caching:** Storing recently accessed vertices in on-chip caches.
- **Batching:** Grouping vertex fetches to maximize memory bus utilization.

In summary, vertex attributes in modern GPU architectures are processed through a highly optimized vertex input stage that leverages input buffers, index fetch, and parallel attribute extraction. The design balances flexibility, performance, and power efficiency, enabling real-time rendering of complex scenes. Future advancements may focus on further compression techniques and tighter integration with ray tracing pipelines.

## 8.4 Transformation Unit

### 8.4.1 Matrix multiplications

Matrix multiplications are fundamental operations in computer graphics and parallel computing, particularly in the context of modern GPU architectures. These operations are heavily utilized in transformation units for performing model-view-projection (MVP) transformations, which are essential for rendering 3D scenes. The efficiency of matrix multiplications on GPUs is attributed to their highly parallel architecture, which exploits data-level parallelism through thousands of cores.

The transformation unit in a GPU is responsible for applying geometric transformations to vertices in a 3D scene. These transformations include model transformation, which converts object coordinates from local space to world space; view transformation, which transforms world coordinates to camera space; and projection transformation, which maps camera space to clip space for perspective or orthographic projection.

Each of these transformations is represented by a 4x4 matrix, and their composition is achieved through matrix multiplication. The MVP matrix is computed as:

$$M_{MVP} = M_{projection} \times M_{view} \times M_{model}$$

where  $M_{model}$ ,  $M_{view}$ , and  $M_{projection}$  are the model, view, and projection matrices, respectively.

Modern GPUs optimize matrix multiplications by leveraging single-instruction multiple-data (SIMD) parallelism. The transformation unit typically employs specialized hardware, such as tensor cores in NVIDIA GPUs, which accelerate matrix operations by performing mixed-precision computations. For example, the Volta and Ampere architectures support 4x4 matrix multiplications in a single instruction using tensor cores. The computation is expressed as:

$$C = A \times B$$

where  $A$  and  $B$  are input matrices, and  $C$  is the resulting product. Each element  $c_{ij}$  of  $C$  is computed as:

$$c_{ij} = \sum_{k=1}^n a_{ik} \times b_{kj}$$

The parallel execution of (8.4.1) is achieved by distributing the computation across multiple threads in a GPU warp. A warp consists of 32 threads in NVIDIA architectures, and each thread computes a subset of the resulting matrix elements. The GPU's memory hierarchy, including shared memory and registers, is optimized to minimize latency during matrix multiplications.

For instance, the following CUDA-like pseudocode illustrates a tiled matrix multiplication kernel optimized for shared memory:

Code Sample 8.6: Tiled Matrix Multiplication Kernel

```
__global__ void matMul(float *A, float *B, float *C, int N) {
    __shared__ float As[TILE_SIZE][TILE_SIZE];
    __shared__ float Bs[TILE_SIZE][TILE_SIZE];
    int bx = blockIdx.x, by = blockIdx.y;
    int tx = threadIdx.x, ty = threadIdx.y;
    int row = by * TILE_SIZE + ty;
    int col = bx * TILE_SIZE + tx;
    float sum = 0.0f;
    for (int t = 0; t < N / TILE_SIZE; ++t) {
        As[ty][tx] = A[row * N + t * TILE_SIZE + tx];
        Bs[ty][tx] = B[(t * TILE_SIZE + ty) * N + col];
        __syncthreads();
        for (int k = 0; k < TILE_SIZE; ++k) {
            sum += As[ty][k] * Bs[k][tx];
        }
        __syncthreads();
    }
    C[row * N + col] = sum;
}
```

The transformation unit also benefits from hardware-accelerated fixed-function pipelines for certain matrix operations. For example, the graphics pipeline in modern GPUs includes dedicated units for vertex transformation, which perform MVP multiplications efficiently. These units are optimized for 4x4 matrix-vector multiplications, which are common in vertex shaders. The operation is defined as:

$$v' = M_{MVP} \times v$$

where  $v$  is the input vertex in homogeneous coordinates, and  $v'$  is the transformed vertex.

The performance of matrix multiplications on GPUs is further enhanced by techniques such as memory coalescing, which ensures that memory accesses by threads in a warp are contiguous and thus maximize memory bandwidth utilization; register blocking, which reduces shared memory usage by storing intermediate results in registers; and asynchronous execution, which overlaps computation with memory transfers to hide latency.

Research has shown that modern GPU architectures achieve near-peak performance for matrix multiplications by optimizing these techniques. For instance, demonstrates that tiled matrix multiplication kernels can achieve over 90% of the theoretical peak FLOPs on NVIDIA GPUs. The use of tensor cores further improves performance by up to 8x for mixed-precision computations .

In summary, matrix multiplications are a cornerstone of modern GPU architectures, particularly in the transformation unit for MVP computations. The parallel nature of GPUs, combined with specialized hardware and optimization techniques, enables efficient execution of these operations. This efficiency is critical for real-time rendering and other compute-intensive applications.

### 8.4.2 Model-view-projection transformations

The transformation of geometric data from model space to screen space in modern GPU architectures is a fundamental process in computer graphics, achieved through a sequence of matrix operations known as model-view-projection (MVP) transformations. These transformations are executed efficiently by the GPU's transformation unit, which leverages parallel processing capabilities to perform matrix multiplications at high throughput.

The MVP pipeline consists of three primary stages: the model transformation, the view transformation, and the projection transformation. Each stage involves a distinct matrix multiplication, and the combined result maps vertices from their local coordinate system to normalized device coordinates (NDC).

The model transformation converts vertices from model space to world space. This transformation accounts for the object's position, orientation, and scale within the scene. Mathematically, the model matrix  $M$  is constructed as a composition of translation, rotation, and scaling matrices:

$$M = T \cdot R \cdot S$$

where  $T$  is the translation matrix,  $R$  is the rotation matrix, and  $S$  is the scaling matrix. The order of multiplication is critical, as matrix multiplication is not commutative. The model matrix is typically supplied by the application and passed to the GPU as a uniform variable.

The view transformation maps vertices from world space to camera space. This transformation is defined by the camera's position and orientation, often represented using a look-at matrix or a combination of translation and rotation matrices. The view matrix  $V$  is constructed as:

$$V = \begin{bmatrix} r_x & u_x & -d_x & 0 \\ r_y & u_y & -d_y & 0 \\ r_z & u_z & -d_z & 0 \\ -(\mathbf{r} \cdot \mathbf{e}) & -(\mathbf{u} \cdot \mathbf{e}) & \mathbf{d} \cdot \mathbf{e} & 1 \end{bmatrix}$$

where  $\mathbf{r}$ ,  $\mathbf{u}$ , and  $\mathbf{d}$  are the right, up, and direction vectors of the camera, and  $\mathbf{e}$  is the camera's position in world space. The view matrix ensures that the scene is rendered from the camera's perspective.

The projection transformation maps vertices from camera space to clip space, applying perspective or orthographic projection. The perspective projection matrix  $P$  is given by:

$$P = \begin{bmatrix} \frac{2n}{r-l} & 0 & \frac{r+l}{r-l} & 0 \\ 0 & \frac{2n}{t-b} & \frac{t+b}{t-b} & 0 \\ 0 & 0 & -\frac{f+n}{f-n} & -\frac{2fn}{f-n} \\ 0 & 0 & -1 & 0 \end{bmatrix}$$

where  $n$  and  $f$  are the near and far clipping planes, and  $l$ ,  $r$ ,  $t$ , and  $b$  define the viewing frustum. The projection matrix introduces perspective distortion, causing objects farther from the camera to appear smaller.

The combined MVP matrix  $MVP$  is computed as:

$$MVP = P \cdot V \cdot M$$

This matrix is applied to each vertex in the vertex shader, transforming it from model space to clip space. The GPU's transformation unit optimizes this computation by exploiting parallelism. Modern GPUs feature dedicated hardware for matrix multiplication, such as tensor cores in NVIDIA architectures or matrix engines in AMD GPUs, which accelerate these operations.

The transformation unit in a GPU is responsible for executing the MVP transformations efficiently. It performs the following steps:

1. Loads the model, view, and projection matrices into registers.
2. Computes the product  $V \cdot M$  using parallel matrix multiplication.
3. Multiplies the result by  $P$  to obtain  $MVP$ .
4. Applies the MVP matrix to each vertex in parallel.

Matrix multiplication is a key operation in the transformation unit. Given two matrices  $A$  and  $B$ , their product  $C = A \cdot B$  is computed as:

$$C_{ij} = \sum_{k=1}^n A_{ik} \cdot B_{kj}$$

The transformation unit optimizes this computation by:

1. Utilizing SIMD (Single Instruction, Multiple Data) instructions to process multiple elements simultaneously.

2. Employing hardware-accelerated fused multiply-add (FMA) operations.
3. Leveraging cache hierarchies to minimize memory latency.

The efficiency of MVP transformations is critical for real-time rendering. Research by demonstrates that modern GPUs achieve near-peak performance for matrix multiplication by optimizing memory access patterns and instruction scheduling. The transformation unit also supports batched processing, where multiple matrices are multiplied in parallel, further improving throughput.

In summary, the model-view-projection transformations are a cornerstone of modern GPU architectures, enabling efficient rendering of 3D scenes. The transformation unit plays a pivotal role by accelerating matrix multiplications and ensuring high performance. The mathematical foundations of these transformations, combined with hardware optimizations, allow GPUs to render complex scenes in real time. Future advancements in GPU architecture will likely focus on further optimizing these transformations, particularly for emerging workloads such as ray tracing and machine learning.

## 8.5 Clipping and Culling

### 8.5.1 View frustum clipping

View frustum clipping is a fundamental operation in modern GPU architectures, essential for optimizing rendering performance by discarding geometry that lies outside the visible region of the scene. The view frustum represents the portion of 3D space projected onto the 2D viewport, defined by six planes: near, far, left, right, top, and bottom. Clipping ensures only primitives intersecting or contained within the frustum are processed, reducing unnecessary computations.

The mathematical representation of a plane in homogeneous coordinates is given by:

$$ax + by + cz + d = 0$$

where  $(a, b, c)$  is the plane normal and  $d$  is the distance from the origin. A point  $\mathbf{p} = (x, y, z, w)$  lies inside the frustum if it satisfies all six plane inequalities:

$$a_i x + b_i y + c_i z + d_i w \geq 0 \quad \forall i \in \{1, \dots, 6\}.$$

Modern GPUs employ hierarchical clipping strategies to minimize computational overhead. Bounding volume hierarchies (BVH) or spatial partitioning structures like octrees are often used to quickly reject entire groups of primitives. The clipping pipeline typically operates in clip space, where homogeneous coordinates simplify plane tests. The perspective division transforms clip-space coordinates  $(x_c, y_c, z_c, w_c)$  to normalized device coordinates (NDC):

$$\mathbf{p}_{ndc} = \left( \frac{x_c}{w_c}, \frac{y_c}{w_c}, \frac{z_c}{w_c} \right).$$

Primitives are clipped against the canonical view volume  $[-1, 1]^3$ , ensuring only visible fragments proceed to rasterization. Backface culling complements view frustum clipping by eliminating polygons facing away from the camera, determined by the dot product of the view vector and polygon normal:

$$\mathbf{n} \cdot \mathbf{v} > 0$$

where  $\mathbf{n}$  is the polygon normal and  $\mathbf{v}$  is the vector from the camera to the polygon. This operation exploits the winding order of vertices, typically configured as clockwise or counter-clockwise in GPU pipelines. Early backface culling, performed in vertex or geometry shaders, further reduces fragment processing load.

Clipping and culling are tightly integrated into modern GPU architectures. The following Verilog-like pseudocode illustrates a simplified clipping unit:

Code Sample 8.7: View Frustum Clipping Logic

```
module FrustumClipper (
    input [31:0] vertex [4], // Homogeneous coordinates (x, y, z, w)
    output inside
);
    // Plane equations for frustum (a, b, c, d)
    parameter [31:0] planes [6][4] = {...};
```

```

reg [31:0] dot;
integer i;
always @(*) begin
    inside = 1;
    for (i = 0; i < 6; i = i + 1) begin
        dot = planes[i][0] * vertex[0] +
            planes[i][1] * vertex[1] +
            planes[i][2] * vertex[2] +
            planes[i][3] * vertex[3];
        if (dot < 0)
            inside = 0;
    end
end
endmodule

```

The efficiency of clipping depends on the coordinate system used. In screen-space clipping, primitives are tested after projection, while homogeneous clipping operates in clip space. The latter avoids precision issues near the near plane, as shown in . Modern GPUs, such as NVIDIA's Turing architecture , employ parallel clipping engines to handle multiple primitives simultaneously, leveraging SIMD (Single Instruction, Multiple Data) units for throughput optimization.

Hierarchical Z-buffering (HZB) and occlusion culling further enhance performance by discarding occluded geometry. HZB constructs a pyramid of depth buffers, enabling coarse-grained visibility tests before fine-grained clipping. The depth complexity of a scene, defined as the average number of fragments per pixel, directly impacts the effectiveness of these techniques:

$$D = \frac{\text{Total fragments}}{\text{Visible pixels}}.$$

The interplay between clipping and culling is critical for real-time rendering. For example, a study by Akenine-Möller et al. demonstrated that combining view frustum culling with backface culling reduces geometry processing by up to 50% in complex scenes. The following optimizations are commonly employed:

1. Early-Z rejection: Fragments failing depth tests are discarded before shading.
2. Cluster culling: Groups of primitives are tested collectively using bounding spheres or boxes.
3. Precision tuning: Reduced precision arithmetic for plane tests, trading accuracy for speed.

The mathematical formulation of cluster culling involves testing a bounding sphere against the frustum planes. Given a sphere with center  $\mathbf{c}$  and radius  $r$ , the test becomes:

$$\mathbf{n}_i \cdot \mathbf{c} + d_i + r \geq 0 \quad \forall i \in \{1, \dots, 6\}.$$

This approximation is conservative; false positives are allowed, but false negatives are avoided. In summary, view frustum clipping and backface culling are pivotal in modern GPU architectures, enabling efficient rendering by minimizing redundant computations. Advances in parallel processing and hierarchical testing continue to refine these techniques, as evidenced by recent architectures like AMD's RDNA3 . The integration of these methods ensures real-time performance in increasingly complex 3D environments.

### 8.5.2 Backface culling

In modern GPU architecture, backface culling is a critical optimization technique used to improve rendering performance by discarding polygons that are not visible to the viewer. This process is closely related to other visibility determination methods such as clipping and view frustum culling, which collectively reduce the computational workload of the GPU. Backface culling operates under the assumption that polygons facing away from the camera (backfaces) are occluded by their front-facing counterparts and thus do not contribute to the final rendered image. The mathematical basis for backface culling involves computing the dot product between the polygon's normal vector and the view vector. If the result is positive, the polygon is considered a backface and is culled:

$$\mathbf{N} \cdot \mathbf{V} > 0$$

where  $\mathbf{N}$  is the surface normal and  $\mathbf{V}$  is the view vector from the camera to the polygon.

Clipping and culling are complementary techniques in the graphics pipeline. While backface culling eliminates polygons based on their orientation, view frustum clipping removes geometry that lies outside the camera's visible volume. The view frustum is defined by six planes (near, far, left, right, top, and bottom), and any primitive that does not intersect this volume is discarded. The clipping process ensures that only fragments within the frustum are rasterized, reducing unnecessary computations. The intersection test for a point  $\mathbf{P}$  with a frustum plane  $\mathbf{A}$  is given by:

$$\mathbf{A} \cdot \mathbf{P} + d \geq 0$$

where  $d$  is the plane's distance from the origin. Modern GPUs implement these tests in hardware, leveraging parallel processing to evaluate multiple primitives simultaneously.

Backface culling is typically performed after vertex transformation but before rasterization. In the graphics pipeline, vertices are first transformed from model space to clip space using the model-view-projection matrix:

$$\mathbf{P}_{\text{clip}} = \mathbf{MVP} \cdot \mathbf{P}_{\text{model}}$$

The GPU then applies backface culling by examining the winding order of the transformed vertices. Counterclockwise winding is conventionally used to denote front-facing polygons, though this can be configured via the graphics API. For example, OpenGL allows the winding order to be specified using `glFrontFace`.

The efficiency of backface culling depends on the mesh's topology and the presence of non-closed surfaces. In closed meshes, backface culling can eliminate up to 50% of polygons, significantly reducing the rasterization workload. However, for open or double-sided surfaces, backface culling may introduce artifacts unless explicitly disabled. Modern GPUs mitigate this by supporting per-material culling configurations, enabling developers to fine-tune performance and visual fidelity.

The relationship between backface culling and view frustum clipping is further illustrated by their shared reliance on hierarchical data structures. Bounding volume hierarchies (BVHs) and spatial partitioning schemes (e.g., k-d trees) are often used to accelerate both processes. For instance, a BVH can quickly determine whether a group of polygons lies entirely outside the view frustum or consists solely of backfaces, enabling early rejection. The use of such structures is particularly prevalent in real-time rendering engines, where latency constraints demand aggressive culling strategies.

In hardware, backface culling is implemented within the geometry processing stage of the GPU pipeline. Fixed-function units perform the dot product test (8.5.2) in parallel across multiple polygons, leveraging SIMD (Single Instruction, Multiple Data) architectures for high throughput. The following Verilog-like pseudocode illustrates a simplified backface culling unit:

Code Sample 8.8: Backface Culling Unit

```
module backface_culler (
    input [31:0] normal_x, normal_y, normal_z,
    input [31:0] view_x, view_y, view_z,
    output reg cull
);
    wire [31:0] dot_product = normal_x * view_x + normal_y * view_y + normal_z * view_z;
    always @(*) begin
        cull = (dot_product > 0) ? 1'b1 : 1'b0;
    end
endmodule
```

Empirical studies have demonstrated the performance benefits of backface culling in modern GPUs. For example, reported a 20–30% reduction in fragment shading workload for typical scenes, with greater gains observed in dense meshes. These savings are compounded when combined with view frustum clipping, as the latter reduces the number of primitives entering the culling stage.

The interplay between backface culling and clipping also extends to advanced rendering techniques. In deferred shading, for instance, culling is often deferred until the lighting pass to avoid discarding potentially visible fragments. Similarly, in virtual reality applications, multi-view rendering systems reuse culling logic across stereo views to minimize redundant computations.

Despite its advantages, backface culling is not universally applicable. Transparency rendering, for example, requires backfaces to be processed for correct blending. Modern graphics APIs such as Vulkan and DirectX 12 provide fine-grained control over culling behavior, allowing developers to disable it selectively or invert the facing direction. The following equation illustrates the inversion of the culling test for double-sided materials:

$$\mathbf{N} \cdot \mathbf{V} < 0$$

In summary, backface culling is a cornerstone of modern GPU architecture, working in tandem with clipping and view frustum culling to optimize rendering performance. Its mathematical foundation, hardware implementation, and integration with spatial acceleration structures underscore its importance in real-time graphics. Future advancements in GPU design may further refine these techniques, particularly in the context of ray tracing and machine learning-driven rendering pipelines. Specifically, backface culling discards non-visible polygons based on orientation, view frustum clipping removes geometry outside the camera's visible volume, both techniques rely on hierarchical acceleration structures for efficiency, and hardware implementations leverage parallel processing for high throughput.

## 8.6 Verilog Example

### 8.6.1 Matrix multiplication implementation

Matrix multiplication is a fundamental operation in linear algebra with widespread applications in computer graphics, machine learning, and scientific computing. Modern GPU architectures excel at parallelizing matrix operations due to their highly parallel structure, consisting of thousands of cores optimized for floating-point arithmetic. The implementation of matrix multiplication on GPUs leverages their Single Instruction Multiple Thread (SIMT) execution model, where threads execute the same instruction on different data elements simultaneously.

The mathematical formulation of matrix multiplication for matrices  $A \in \mathbb{R}^{m \times k}$  and  $B \in \mathbb{R}^{k \times n}$  producing  $C \in \mathbb{R}^{m \times n}$  is given by:

$$C_{i,j} = \sum_{l=1}^k A_{i,l} \cdot B_{l,j}$$

This operation requires  $O(mnk)$  floating-point operations, making it computationally intensive for large matrices. GPUs accelerate this computation by partitioning the workload across multiple threads, each computing a subset of the output matrix  $C$ .

A common optimization technique is tiling, where matrices are divided into smaller submatrices (tiles) that fit into the GPU's shared memory, reducing global memory accesses. The tiled matrix multiplication algorithm can be expressed as:

$$C_{i,j} = \sum_{t=1}^{k/T} \sum_{l=1}^T A_{i,tT+l} \cdot B_{tT+l,j}$$

Here,  $T$  represents the tile size, chosen to maximize shared memory utilization while minimizing bank conflicts.

In Verilog, a hardware description language, matrix multiplication can be implemented using systolic arrays, which are highly parallel structures optimized for regular computations like matrix multiplication. The following Verilog snippet demonstrates a simplified systolic array for matrix multiplication:

Code Sample 8.9: Systolic Array for Matrix Multiplication

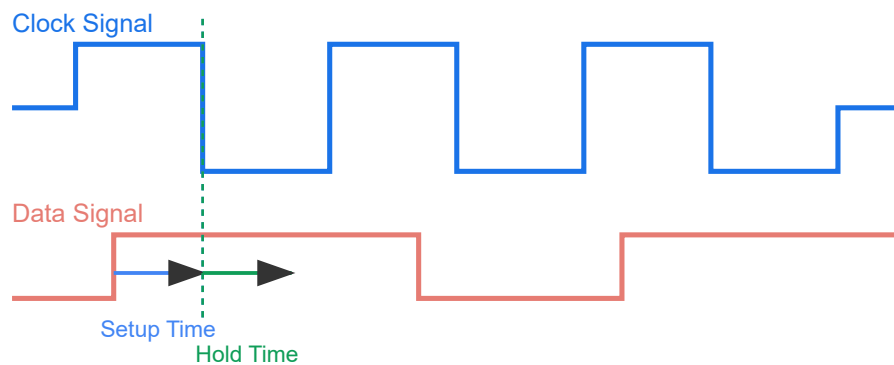
```
module systolic_array #(parameter N=4) (
    input clk, reset,
    input [31:0] A [0:N-1][0:N-1],
    input [31:0] B [0:N-1][0:N-1],
    output reg [31:0] C [0:N-1][0:N-1]
);
    reg [31:0] a [0:N-1][0:N-1];
    reg [31:0] b [0:N-1][0:N-1];
    integer i, j, k;
    always @(posedge clk or posedge reset) begin
        if (reset) begin
            for (i = 0; i < N; i = i + 1)
                for (j = 0; j < N; j = j + 1)
                    C[i][j] <= 0;
        end else begin
            for (i = 0; i < N; i = i + 1)
                for (j = 0; j < N; j = j + 1)
                    for (k = 0; k < N; k = k + 1)
                        C[i][j] <= C[i][j] + A[i][k] * B[k][j];
        end
    end
endmodule
```

This implementation uses a triple-nested loop to compute each element of  $C$  as the dot product of a row of  $A$  and a column of  $B$ . While this approach is straightforward, it does not exploit the full parallelism of modern GPUs. In contrast, GPU-optimized implementations leverage thread blocks and shared memory to maximize throughput. For example, NVIDIA's CUDA programming model partitions the computation into thread blocks, where each block computes a tile of the output matrix.

Each thread block loads a tile of  $A$  and  $B$  into shared memory. Threads within the block cooperate to compute the dot products for their assigned output tile. The results are accumulated in registers and written back to global memory.

## Setup and Hold Times in GPU Design

Critical Timing Parameters for Modern GPU Architecture



### What are Setup and Hold Times?

- Setup Time: Minimum time data must be stable BEFORE the clock edge
- Hold Time: Minimum time data must be stable AFTER the clock edge
- Both parameters are critical for reliable data capture in GPU registers

### Impact on Modern GPU Architecture

- High clock frequencies in modern GPUs (2-3 GHz) demand strict timing
- Setup/hold violations can cause data corruption and rendering artifacts
- Critical for shader execution units and memory interfaces
- Advanced GPU designs include timing margin analyzers
- Performance-critical paths often receive special attention during design
- Timing constraints become more challenging at smaller process nodes
- Modern GPUs employ clock domain crossing (CDC) techniques



Timing constraints apply at each register boundary in the GPU pipeline

Vertex shaders, traditionally used for geometric transformations in graphics pipelines, can also be repurposed for matrix multiplication. A vertex shader stub for matrix-vector multiplication is shown below:

**Code Sample 8.10: Vertex Shader Stub for Matrix-Vector Multiplication**

```
#version 450 core
layout(location = 0) in vec4 inputVector;
uniform mat4 transformationMatrix;

void main() {
    gl_Position = transformationMatrix * inputVector;
}
```

Although vertex shaders are not ideal for general matrix multiplication due to their limited parallelism compared to compute shaders, they demonstrate the flexibility of GPU programming. The performance of matrix multiplication on GPUs is influenced by several factors:

Memory hierarchy: Efficient use of shared memory and registers reduces latency.

Thread divergence: Minimizing divergent execution paths ensures optimal utilization of SIMT cores.

Occupancy: Maximizing the number of active warps per streaming multiprocessor hides memory latency.

Recent research has explored advanced techniques such as mixed-precision arithmetic and tensor cores to further accelerate matrix multiplication. These approaches exploit hardware-specific features to achieve higher throughput while maintaining numerical accuracy.

In summary, matrix multiplication on modern GPUs combines algorithmic optimizations with hardware-aware programming to achieve high performance. Verilog implementations highlight the potential for custom hardware acceleration, while vertex shaders illustrate the adaptability of GPU pipelines. Future advancements in GPU architecture will continue to push the boundaries of computational efficiency for matrix operations.

## 8.6.2 Vertex shader stub

The vertex shader stub in modern GPU architecture serves as a fundamental building block for graphics pipeline processing. It operates as a programmable unit responsible for transforming vertex attributes, such as position, normal, and texture coordinates, from object space to clip space. A vertex shader stub typically consists of a minimal implementation that passes through vertex data without additional transformations, serving as a placeholder for more complex shaders.

In the context of Verilog, a vertex shader stub can be modeled as a hardware module that processes vertex data in parallel, leveraging the GPU's SIMD (Single Instruction, Multiple Data) architecture. The following Verilog example illustrates a simplified vertex shader stub module:

Code Sample 8.11: Vertex Shader Stub in Verilog

```
module vertex_shader_stub (
    input wire clk,
    input wire reset,
    input wire [31:0] vertex_in [3:0], // x, y, z, w
    output reg [31:0] vertex_out [3:0]
);
    always @ (posedge clk or posedge reset) begin
        if (reset) begin
            vertex_out <= '{0, 0, 0, 0};
        end else begin
            vertex_out <= vertex_in; // Pass-through
        end
    end
endmodule
```

This stub performs no transformation on the input vertices, merely passing them through to the output. In a practical GPU, the vertex shader would apply a series of matrix multiplications to transform vertices from model space to clip space. The transformation is represented by the equation:

$$\mathbf{v}_{\text{clip}} = \mathbf{M}_{\text{projection}} \times \mathbf{M}_{\text{view}} \times \mathbf{M}_{\text{model}} \times \mathbf{v}_{\text{model}}$$

Here,  $\mathbf{v}_{\text{model}}$  is the input vertex in model space, and  $\mathbf{v}_{\text{clip}}$  is the output vertex in clip space. The matrices  $\mathbf{M}_{\text{model}}$ ,  $\mathbf{M}_{\text{view}}$ , and  $\mathbf{M}_{\text{projection}}$  represent the model, view, and projection transformations, respectively. The vertex shader computes this transformation for each vertex in parallel, exploiting the GPU's massive parallelism.

Matrix multiplication is a critical operation in vertex shaders. A hardware implementation of matrix multiplication in Verilog can be optimized for throughput and latency. The following example demonstrates a 4x4 matrix multiplication module:

Code Sample 8.12: 4x4 Matrix Multiplication in Verilog

```
module matrix_mult_4x4 (
    input wire clk,
    input wire [31:0] A [3:0][3:0],
    input wire [31:0] B [3:0][3:0],
    output reg [31:0] C [3:0][3:0]
);
    integer i, j, k;
    always @ (posedge clk) begin
        for (i = 0; i < 4; i = i + 1) begin
            for (j = 0; j < 4; j = j + 1) begin
                C[i][j] = 0;
                for (k = 0; k < 4; k = k + 1) begin
                    C[i][j] = C[i][j] + A[i][k] * B[k][j];
                end
            end
        end
    end
endmodule
```

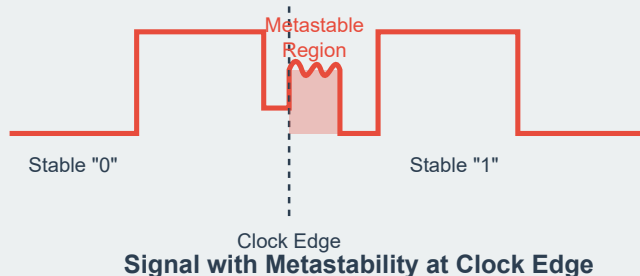
This module computes the product of two 4x4 matrices,  $\mathbf{A}$  and  $\mathbf{B}$ , producing the result matrix  $\mathbf{C}$ . The operation is pipelined to maximize throughput, with each multiplication and accumulation step performed in a single clock

## AVOIDING METASTABILITY

in Modern GPU Architecture

### What is Metastability?

Metastability occurs when a signal is sampled during its transition, resulting in an unpredictable output that may oscillate or settle to an invalid logic level. In GPUs, this can cause race conditions, data corruption, and unpredictable behavior.



### Causes in GPUs

- Clock domain crossings
- Asynchronous inputs
- Timing violations
- Inadequate setup/hold times

### Prevention Techniques

- Synchronizers (2+ flip-flops)
- Handshaking protocols
- FIFO-based transfers
- Asynchronous design techniques

### Synchronizer Implementation



cycle. The matrix multiplication is defined as:

$$C_{ij} = \sum_{k=0}^3 A_{ik} \times B_{kj}$$

In a vertex shader, the matrix multiplication module is integrated into the pipeline to transform vertices. The vertex shader stub can be extended to include this functionality, as shown below:

Code Sample 8.13: Extended Vertex Shader with Matrix Multiplication

```
module vertex_shader (
    input wire clk,
    input wire reset,
    input wire [31:0] vertex_in [3:0],
    input wire [31:0] model_matrix [3:0][3:0],
    input wire [31:0] view_matrix [3:0][3:0],
    input wire [31:0] proj_matrix [3:0][3:0],
    output reg [31:0] vertex_out [3:0]
);
    reg [31:0] temp_vertex [3:0];
    reg [31:0] temp_matrix [3:0][3:0];

    matrix_mult_4x4 mm1 (.clk(clk), .A(model_matrix), .B(view_matrix), .C(temp_matrix));
    matrix_mult_4x4 mm2 (.clk(clk), .A(temp_matrix), .B(proj_matrix), .C(temp_matrix));

    always @ (posedge clk or posedge reset) begin
        if (reset) begin
            vertex_out <= '{0, 0, 0, 0};
        end else begin
            vertex_out[0] = temp_matrix[0][0] * vertex_in[0] + temp_matrix[0][1] * vertex_in[1] +
                           temp_matrix[0][2] * vertex_in[2] + temp_matrix[0][3] * vertex_in[3];
            vertex_out[1] = temp_matrix[1][0] * vertex_in[0] + temp_matrix[1][1] * vertex_in[1] +
                           temp_matrix[1][2] * vertex_in[2] + temp_matrix[1][3] * vertex_in[3];
            vertex_out[2] = temp_matrix[2][0] * vertex_in[0] + temp_matrix[2][1] * vertex_in[1] +
                           temp_matrix[2][2] * vertex_in[2] + temp_matrix[2][3] * vertex_in[3];
            vertex_out[3] = temp_matrix[3][0] * vertex_in[0] + temp_matrix[3][1] * vertex_in[1] +
                           temp_matrix[3][2] * vertex_in[2] + temp_matrix[3][3] * vertex_in[3];
        end
    end
endmodule
```

This extended vertex shader combines the matrix multiplication modules to compute the full transformation pipeline. The intermediate results are stored in temporary registers, and the final vertex position is computed by multiplying the composite matrix with the input vertex. The transformation is mathematically equivalent to 20.2.1, but implemented in hardware for real-time performance.

Modern GPU architectures optimize vertex shaders through several techniques:

Predicated execution: Conditional operations are minimized to maintain SIMD efficiency.

Register file optimization: High-bandwidth register files reduce memory access latency.

Instruction-level parallelism: Multiple instructions are issued per clock cycle to exploit pipeline parallelism.

The vertex shader stub is a starting point for more complex shaders, such as those incorporating lighting calculations or skinning for animated models. The principles of matrix multiplication and parallel processing remain central to these advanced shaders, ensuring efficient utilization of GPU resources. The Verilog examples provided demonstrate how these concepts can be implemented in hardware, forming the basis for modern GPU architectures.



# Chapter 9

# Primitive Assembly and Setup

## 9.1 Primitive Formation

### 9.1.1 Assembling vertices

Modern GPU architectures employ sophisticated pipelines to process geometric primitives efficiently, with vertex assembly and primitive formation being critical stages. The assembly of vertices involves collecting vertex data from memory and organizing it into a format suitable for subsequent pipeline stages. This process is tightly coupled with primitive formation, particularly triangle assembly, which constructs geometric primitives from the assembled vertices. The efficiency of these operations directly impacts rendering performance and is a key focus in GPU design.

Vertex assembly begins with fetching vertex attributes from memory based on indices specified by the application. These attributes typically include position, normal, texture coordinates, and other per-vertex data. The GPU's vertex fetch unit retrieves this data in parallel, leveraging memory coalescing to minimize latency. For indexed rendering, the index buffer provides the vertex indices, allowing reuse of vertices across multiple primitives. The assembled vertices are then passed to the vertex shader for transformation and other per-vertex operations.

The vertex shader processes each vertex independently, applying transformations such as model-view-projection and lighting calculations. The output of the vertex shader is a set of homogeneous clip-space coordinates and any interpolated attributes. These outputs are stored in the post-transform vertex cache, which reduces redundant vertex processing by caching recently transformed vertices. The cache exploits spatial and temporal locality in vertex reuse, a common occurrence in mesh rendering.

Following vertex processing, primitive formation assembles vertices into geometric primitives, most commonly triangles. Triangles are the fundamental rendering primitive due to their simplicity and guaranteed planarity. The assembly process groups vertices according to the specified primitive topology. For example, a triangle list requires three vertices per primitive, while a triangle strip reuses vertices from previous triangles to reduce bandwidth. The primitive assembly unit constructs these primitives and passes them to the rasterization stage.

The triangle formation process involves several steps. First, in **vertex grouping**, vertices are grouped into sets of three for triangle lists or sequentially for strips and fans. Next, in the **clipping** stage, primitives intersecting the view frustum are clipped to ensure only visible portions are processed. Then, **perspective division** converts clip-space coordinates to normalized device coordinates (NDC). Finally, **viewport transformation** maps NDC coordinates to screen-space coordinates based on the viewport parameters.

The efficiency of triangle formation is critical for performance. Modern GPUs employ parallel processing to handle multiple primitives simultaneously. The primitive assembly unit typically operates on a batch of vertices, allowing for high throughput. Additionally, hardware optimizations such as early culling discard primitives that are entirely outside the view frustum, reducing unnecessary work.

The assembly of vertices and formation of triangles are closely tied to the GPU's memory hierarchy. Vertex data is often stored in buffers optimized for sequential access, while index buffers facilitate random access with minimal overhead. The use of vertex pullers, which decouple vertex fetching from shading, allows for more flexible memory access patterns. This is particularly beneficial for compute-based rendering pipelines, where traditional fixed-function vertex assembly may be bypassed.

In terms of mathematical representation, the transformation of vertices from object space to clip space is given by:

$$\mathbf{v}_{\text{clip}} = \mathbf{M}_{\text{proj}} \cdot \mathbf{M}_{\text{view}} \cdot \mathbf{M}_{\text{model}} \cdot \mathbf{v}_{\text{object}}$$

where  $\mathbf{v}_{\text{object}}$  is the object-space vertex,  $\mathbf{M}_{\text{model}}$ ,  $\mathbf{M}_{\text{view}}$ , and  $\mathbf{M}_{\text{proj}}$  are the model, view, and projection matrices, respectively, and  $\mathbf{v}_{\text{clip}}$  is the resulting clip-space vertex.

The assembly of triangles from vertices can be formalized as a mapping function:

$$T_i = (v_j, v_k, v_l)$$

where  $T_i$  is the  $i$ -th triangle, and  $v_j$ ,  $v_k$ , and  $v_l$  are the vertices forming the triangle. This mapping is deterministic for indexed rendering but may involve more complex patterns for strip or fan topologies.

Modern GPUs also support tessellation, which dynamically generates additional vertices and triangles to increase geometric detail. The tessellation pipeline includes hull and domain shaders, which operate on patches of vertices, and a fixed-function tessellator that generates new vertices based on tessellation factors. The assembled vertices are then processed by the domain shader to produce the final vertex positions.

The following Verilog-like pseudocode illustrates a simplified vertex assembly unit:

Code Sample 9.1: Vertex Assembly Unit

```
module vertex_assembly (
    input wire [31:0] vertex_buffer[0:N-1],
    input wire [15:0] index_buffer[0:M-1],
    output wire [31:0] assembled_vertices[0:2]
);
    always @(*) begin
        for (int i = 0; i < 3; i++) begin
            assembled_vertices[i] = vertex_buffer[index_buffer[i]];
        end
    end
endmodule
```

Optimizations such as vertex buffer compression and attribute packing further enhance memory efficiency. For instance, position attributes may be stored as 16-bit floating-point values with a shared exponent, reducing bandwidth without significant precision loss. Similarly, normal vectors can be quantized to 8-bit or 10-bit representations, leveraging normalization in the shader.

The assembly of vertices and formation of triangles are foundational to GPU rendering pipelines. Advances in parallel processing, memory hierarchy design, and algorithmic optimizations continue to push the boundaries of performance. Future directions may include more flexible primitive representations and tighter integration with machine learning pipelines for geometry processing.

### 9.1.2 Triangle formation

Modern GPU architectures are designed to efficiently process geometric primitives, with triangle formation being a fundamental operation in the rasterization pipeline. The process begins with vertex assembly, where vertices are grouped into geometric primitives such as points, lines, or triangles. Triangle formation specifically involves assembling three vertices into a triangle primitive, which is then processed for rasterization and pixel shading. The efficiency of this process is critical for real-time rendering performance, as modern GPUs must handle millions of triangles per frame.

The vertex assembly stage is responsible for collecting vertices from vertex buffers and organizing them into primitives. In the case of triangle formation, vertices are typically grouped in sequences of three, either as a triangle list, triangle strip, or triangle fan. The triangle list is the simplest form, where each set of three vertices defines a distinct triangle. For example, vertices  $v_0, v_1, v_2$  form the first triangle,  $v_3, v_4, v_5$  form the second, and so on. This method is straightforward but can be memory-inefficient due to redundant vertex data.

Triangle strips and fans optimize memory usage by reusing vertices between adjacent triangles. In a strip, each new vertex forms a triangle with the previous two vertices, reducing the vertex count from  $3n$  to  $n + 2$  for  $n$  triangles. A fan uses a central vertex shared by all triangles, further optimizing certain geometries.

The assembly of vertices into triangles is governed by the primitive topology specified by the application. The GPU's input assembler interprets the vertex buffer according to this topology, generating the appropriate primitives for the rasterizer. The input assembler also handles index buffers, which allow vertices to be reused across multiple primitives without duplication. Indexed rendering is a common optimization, as it reduces memory bandwidth and improves cache coherence. For instance, a cube can be represented with 8 vertices and 12 triangles using an index buffer, rather than 36 vertices in a non-indexed list.

Once vertices are assembled into triangles, the GPU performs a series of transformations and tests to prepare the primitives for rasterization. The vertex shader processes each vertex, applying transformations such as model-view-projection to bring them into clip space. The perspective divide then converts clip-space coordinates into normalized device coordinates (NDC), where the viewport transform maps them to screen space.

During this process, the GPU may also perform backface culling to discard triangles that are not facing the camera, reducing the workload for the rasterizer. Backface culling is determined by the winding order of the vertices, typically counter-clockwise for front-facing triangles.

The rasterization stage converts the triangle primitives into fragments, which are potential pixels on the screen. The rasterizer interpolates vertex attributes such as texture coordinates and colors across the triangle's surface, generating fragments for each pixel covered by the primitive. The efficiency of this stage depends on the GPU's ability to parallelize fragment processing and minimize overdraw through techniques like early depth testing.

Modern GPUs employ hierarchical rasterization to quickly determine which tiles of pixels a triangle overlaps, reducing unnecessary fragment shader invocations. Triangle formation and rasterization are tightly coupled with the GPU's memory hierarchy. Vertex and index data are typically stored in high-bandwidth memory (HBM) or GDDR6, with caches optimizing access patterns. The GPU's L1 and L2 caches play a crucial role in reducing latency for vertex fetch operations, especially for indexed rendering where vertex reuse is high. Cache-aware algorithms, such as optimizing vertex order for locality, can significantly improve performance. Research by demonstrates that reordering vertices to maximize cache coherence can reduce vertex processing time by up to 30%.

The parallel nature of modern GPUs allows them to process multiple triangles simultaneously. Compute units (CUs) or streaming multiprocessors (SMs) handle vertex shading and primitive assembly in parallel, with work distributed across threads and warps. This parallelism is essential for achieving high throughput, as each CU can process hundreds of vertices per cycle. However, load balancing is critical, as uneven workloads can lead to underutilization of hardware resources. Dynamic scheduling algorithms, such as those described in , ensure that triangles are distributed evenly across compute units.

Advanced GPU architectures, such as NVIDIA's Turing and AMD's RDNA2, introduce hardware-accelerated ray tracing alongside traditional rasterization. While ray tracing operates on a different paradigm, triangle formation remains relevant as the acceleration structures (e.g., BVH) are built from the same primitives. The GPU must still assemble vertices into triangles for intersection testing, though the process is optimized for ray traversal rather than rasterization. Hybrid rendering pipelines, as explored by , leverage both rasterization and ray tracing, requiring efficient triangle formation for both paths.

In summary, triangle formation in modern GPU architectures involves vertex assembly, topology interpretation, and efficient memory access patterns. The process is optimized through indexed rendering, cache-aware algorithms, and parallel execution across compute units. As GPUs evolve to handle increasingly complex workloads, the fundamentals of triangle formation remain central to real-time graphics rendering. Future advancements may further optimize primitive assembly through hardware innovations and algorithmic improvements, ensuring continued performance gains for interactive applications.

## 9.2 Edge Equation Setup

### 9.2.1 Calculating edge functions

Modern GPU architectures leverage parallel processing to accelerate graphics rendering, with edge function calculations being a fundamental operation in rasterization pipelines. The edge equation setup and subsequent calculations determine pixel coverage within triangles, a process critical for efficient fragment shading. This discussion focuses on the mathematical foundations, hardware optimizations, and algorithmic implementations of edge functions in contemporary GPUs.

The edge function for a triangle edge defined by vertices  $(x_0, y_0)$  and  $(x_1, y_1)$  evaluates whether a point  $(x, y)$  lies on the correct side of the edge. The general form is derived from the line equation:

$$E(x, y) = (x_1 - x_0)(y - y_0) - (y_1 - y_0)(x - x_0)$$

This determinant-based formulation provides a signed area computation, where the sign indicates the point's relative position to the edge. For a counter-clockwise wound triangle, positive values indicate interior regions. GPUs compute this for all three edges simultaneously to determine pixel coverage.

Hardware implementations optimize edge function evaluations through incremental calculations. Given the

raster traversal order, the value at  $(x + 1, y)$  can be derived from the previous result at  $(x, y)$ :

$$E(x + 1, y) = E(x, y) + (y_0 - y_1)$$

$$E(x, y + 1) = E(x, y) + (x_1 - x_0)$$

These recurrence relations reduce per-pixel computations to simple additions, exploiting spatial coherence in rasterization. Modern GPUs implement these as fixed-function hardware units, often within the rasterizer stage, as described in .

The edge equation setup involves computing initial values and derivatives during triangle setup. For a tile-based rasterizer, the edge function is evaluated at tile corners to determine coarse-grained coverage before per-pixel tests. The partial derivatives  $\partial E / \partial x$  and  $\partial E / \partial y$  are constant across the triangle:

$$\frac{\partial E}{\partial x} = y_0 - y_1$$

$$\frac{\partial E}{\partial y} = x_1 - x_0$$

These derivatives enable hierarchical evaluation, where entire tiles are rejected if all corners yield consistent signs. This optimization reduces fragment shading workload significantly, as demonstrated in .

Precision considerations are critical in edge function calculations. GPUs typically use fixed-point arithmetic with guard bits to prevent overflow during incremental updates. The edge equation (14.1) is often scaled to maintain integer precision across the viewport, avoiding floating-point inaccuracies.

The following Verilog snippet illustrates a simplified edge function unit:

Code Sample 9.2: Edge Function Evaluator

```
module edge_func (
    input [15:0] x0, y0, x1, y1,
    input [15:0] x, y,
    output reg [31:0] E
);
    always @(*) begin
        E = (x1 - x0) * (y - y0) - (y1 - y0) * (x - x0);
    end
endmodule
```

Parallel evaluation of multiple edge functions is achieved through Single Instruction Multiple Data (SIMD) architectures. Contemporary GPUs, such as NVIDIA's Ampere , employ warp-wide SIMD execution where threads compute edge tests for different pixels simultaneously. The edge equations are vectorized to exploit data-level parallelism:

$$E = (\mathbf{x}_1 - \mathbf{x}_0) \otimes (\mathbf{y} - \mathbf{y}_0) - (\mathbf{y}_1 - \mathbf{y}_0) \otimes (\mathbf{x} - \mathbf{x}_0)$$

where  $\otimes$  denotes element-wise multiplication. This formulation maps efficiently to GPU SIMD pipelines, with throughput exceeding one billion edge tests per second on high-end hardware.

Barycentric coordinates, derived from edge functions, enable attribute interpolation during shading. The weights  $w_0$ ,  $w_1$ , and  $w_2$  for a point  $(x, y)$  relative to a triangle with vertices  $\mathbf{v}_0, \mathbf{v}_1, \mathbf{v}_2$  are computed as:

$$w_i = \frac{E_i(x, y)}{A}$$

where  $A$  is twice the triangle area, calculated as the sum of edge function values at any vertex. This relationship allows GPUs to reuse edge function results for both coverage testing and attribute interpolation, minimizing redundant computations.

Optimizations for degenerate cases include handling zero-area triangles and edges aligned with pixel grids. Specialized hardware detects these cases early in the pipeline, avoiding unnecessary fragment processing. The edge function sign tests must also account for tie-breaking rules for pixels exactly on edges, typically following the top-left rule .

Recent advancements incorporate machine learning to predict edge function outcomes. Neural network-based predictors, as explored in , estimate pixel coverage probabilities, reducing the frequency of exact edge evaluations. This hybrid approach demonstrates potential for power-efficient rasterization in next-generation architectures.

The edge function calculations intersect with antialiasing techniques. Multisample Antialiasing (MSAA) evaluates edge functions at sample positions within pixels, requiring multiple evaluations per fragment. Modern GPUs optimize this by storing edge function derivatives and computing sample offsets through parallel arithmetic units.

Memory bandwidth considerations influence edge equation implementations. On-tile storage of edge coefficients reduces external memory accesses during rasterization. Tile-based deferred shading architectures, such as those in mobile GPUs, cache edge data locally to minimize power consumption.

The mathematical properties of edge functions enable hardware-friendly implementations:

Linearity permits incremental updates via (9.2.1) and (9.2.1)

Homogeneity allows scaling for precision management

Additive structure facilitates parallel evaluation through SIMD

These characteristics make edge function calculations amenable to fixed-function hardware acceleration while maintaining algorithmic flexibility for advanced rendering techniques. Future architectures may further specialize these units for ray tracing and hybrid rendering pipelines, where edge tests contribute to intersection calculations. The continued evolution of GPU architectures ensures that edge function computations remain a critical and optimized component of real-time graphics pipelines.

## 9.3 Bounding Box Calculation

### 9.3.1 Minimal pixel regions

Modern GPU architectures employ sophisticated techniques to optimize rendering performance, particularly in handling minimal pixel regions and bounding box calculations. These optimizations are critical for real-time graphics, where efficiency in rasterization and fragment processing directly impacts frame rates and power consumption. Minimal pixel regions refer to the smallest coherent areas of pixels that can be processed independently, while bounding box calculations determine the spatial extents of geometric primitives to minimize unnecessary computations.

The rasterization pipeline in GPUs begins with vertex processing, where geometric primitives are transformed into screen space. Following this, the rasterizer generates fragments for pixels covered by these primitives. To optimize this process, GPUs compute axis-aligned bounding boxes (AABBs) around primitives to limit the rasterization workload. The bounding box for a triangle with vertices  $\mathbf{v}_0$ ,  $\mathbf{v}_1$ , and  $\mathbf{v}_2$  in screen space is calculated as:

$$\text{AABB} = [\min(x_0, x_1, x_2), \max(x_0, x_1, x_2)] \times [\min(y_0, y_1, y_2), \max(y_0, y_1, y_2)]$$

This reduces the number of pixels tested during rasterization, as only those within the AABB are considered for coverage tests.

Minimal pixel regions are often aligned with GPU warp or wavefront sizes, which are groups of threads executed in lockstep. For example, NVIDIA GPUs typically use warps of 32 threads, while AMD GPUs employ wavefronts of 64 threads. By processing minimal pixel regions that match these sizes, GPUs maximize thread utilization and hide memory latency. The optimal size of a minimal pixel region depends on the GPU's SIMD width and memory hierarchy. Research demonstrates that smaller pixel regions improve occupancy but may increase overhead due to divergent execution.

Fragment shaders operate on minimal pixel regions to exploit spatial coherence. When fragments within a region share similar attributes (e.g., depth, texture coordinates), the GPU can apply optimizations such as:

**Early Z-testing:** Discards fragments that fail the depth test before shading, reducing computation. **Hierarchical Z-buffering:** Uses coarse-grained depth tests to cull entire pixel regions. **Texture caching:** Prefetches texture data for spatially coherent fragments to minimize memory access latency.

Bounding box calculations are further refined using hierarchical techniques. Multi-level bounding volume hierarchies (BVHs) are employed in ray tracing and rasterization to accelerate spatial queries. For instance, a two-level hierarchy might first compute a coarse AABB for an entire mesh, then finer AABBs for individual triangles. This approach is formalized as:

$$\text{BVH} = \{\text{AABB}_{\text{root}}, \text{AABB}_{\text{left}}, \text{AABB}_{\text{right}}\}$$

where  $\text{AABB}_{\text{left}}$  and  $\text{AABB}_{\text{right}}$  are child nodes. GPUs leverage parallel reduction algorithms to construct BVHs efficiently, as shown by .

In tile-based rendering architectures, the screen is divided into tiles (e.g.,  $16 \times 16$  pixels), and bounding boxes are used to determine which tiles intersect with a primitive. This reduces the working set for fragment processing and improves cache locality. The tile bounding box test is expressed as:

$$\text{Tile} \cap \text{AABB} \neq \emptyset$$

If the intersection is empty, the tile is skipped entirely. This optimization is particularly effective for deferred shading, where shading computations are deferred until visibility is resolved.

Modern GPUs also employ pixel quad-based processing, where fragments are processed in  $2 \times 2$  blocks. This enables derivative calculations (e.g., texture LOD) and efficient coverage masking. The minimal pixel region in this context is the quad, and bounding boxes are adjusted to align with quad boundaries. The quad coverage test is implemented as:

$$\text{Coverage} = \bigcup_{i=0}^3 \text{Inside}(p_i, \text{Primitive})$$

where  $p_i$  are the quad's pixel centers. Quads with partial coverage require fine-grained rasterization, while fully covered or uncovered quads are processed in bulk.

Hardware-accelerated bounding box calculations are supported by fixed-function units in modern GPUs. For example, NVIDIA's Turing architecture includes dedicated units for AABB computations in ray tracing. The following Verilog-like pseudocode illustrates a simplified bounding box unit:

Code Sample 9.3: Bounding Box Unit

```
module bbox_unit (
    input [31:0] v0_x, v0_y, v1_x, v1_y, v2_x, v2_y,
    output [31:0] min_x, min_y, max_x, max_y
);
assign min_x = min3(v0_x, v1_x, v2_x);
assign min_y = min3(v0_y, v1_y, v2_y);
assign max_x = max3(v0_x, v1_x, v2_x);
assign max_y = max3(v0_y, v1_y, v2_y);
endmodule
```

Minimal pixel regions and bounding box calculations are also critical for compute-based rendering techniques, such as compute shaders performing rasterization. These shaders explicitly manage pixel regions and bounding boxes, often using shared memory for intermediate results. The workgroup size is chosen to match the minimal pixel region size, ensuring efficient GPU utilization. For example, a compute shader might process an  $8 \times 8$  pixel block, with each thread handling a subset of pixels.

Recent advancements in GPU architecture, such as mesh shaders, further optimize minimal pixel regions by allowing programmers to define custom primitives and bounding volumes. Mesh shaders generate compact representations of geometry, reducing the overhead of traditional vertex processing. The bounding box calculation is integrated into the mesh shader pipeline, enabling tighter bounds and fewer rasterization inefficiencies.

In summary, minimal pixel regions and bounding box calculations are foundational to modern GPU architectures, enabling efficient rasterization and fragment processing. These techniques leverage spatial coherence, parallel computation, and hardware acceleration to maximize performance. Future research directions include adaptive minimal pixel regions and machine learning-driven bounding box optimizations, as explored by .

## 9.4 Verilog Example

### 9.4.1 Rasterizer setup block

The rasterizer setup block is a critical component in modern GPU architectures, responsible for converting geometric primitives (typically triangles) into pixel fragments for further processing in the rendering pipeline. This block operates after the vertex processing stage and before fragment shading, performing tasks such as edge function evaluation, barycentric coordinate calculation, and coverage determination. The design of this block must balance computational efficiency with flexibility to support various rendering modes and resolutions.

In a parameterizable rasterizer setup block, key configurations include:

**Precision of edge functions:** Determines the accuracy of triangle coverage tests. Fixed-point arithmetic is often used for efficiency, with bit-widths adjustable based on quality requirements .

**Subpixel precision:** Controls the granularity of sample positions within a pixel, typically ranging from 4x to 16x multisampling.

**Tile size:** Affects memory access patterns, with common configurations being 8x8 or 16x16 pixels .

**Early depth test:** Configurable option to enable or disable hierarchical depth testing before fragment shading.

The mathematical foundation of rasterization involves evaluating edge functions for each candidate pixel. For a triangle with vertices  $(x_0, y_0)$ ,  $(x_1, y_1)$ , and  $(x_2, y_2)$ , the edge function  $E_{01}$  for edge 0–1 is:

$$E_{01}(x, y) = (x_1 - x_0)(y - y_0) - (y_1 - y_0)(x - x_0)$$

A point  $(x, y)$  is inside the triangle if all three edge functions yield the same sign. The barycentric coordinates  $(\alpha, \beta, \gamma)$  can be computed as:

$$\alpha = \frac{E_{12}(x, y)}{E_{12}(x_0, y_0)}, \quad \beta = \frac{E_{20}(x, y)}{E_{20}(x_1, y_1)}, \quad \gamma = 1 - \alpha - \beta$$

A parameterizable Verilog implementation of the rasterizer setup block might include the following key components:

Code Sample 9.4: Parameterizable Rasterizer Setup Block

```
module rasterizer_setup #(
    parameter EDGE_WIDTH = 24,
    parameter SUBPIXEL_BITS = 4,
    parameter TILE_SIZE = 8
) (
    input [31:0] v0_x, v0_y,
    input [31:0] v1_x, v1_y,
    input [31:0] v2_x, v2_y,
    input [31:0] x, y,
    output [EDGE_WIDTH-1:0] e01, e12, e20,
    output [SUBPIXEL_BITS-1:0] subpixel_x, subpixel_y
);

// Edge function computation
wire signed [31:0] dx01 = v1_x - v0_x;
wire signed [31:0] dy01 = v1_y - v0_y;
wire signed [31:0] dx12 = v2_x - v1_x;
wire signed [31:0] dy12 = v2_y - v1_y;
wire signed [31:0] dx20 = v0_x - v2_x;
wire signed [31:0] dy20 = v0_y - v2_y;

// Parameterized edge function calculation
assign e01 = (dx01 * (y - v0_y) - dy01 * (x - v0_x)) >>> (32 - EDGE_WIDTH);
assign e12 = (dx12 * (y - v1_y) - dy12 * (x - v1_x)) >>> (32 - EDGE_WIDTH);
assign e20 = (dx20 * (y - v2_y) - dy20 * (x - v2_x)) >>> (32 - EDGE_WIDTH);

// Subpixel position generation
generate
    if (SUBPIXEL_BITS > 0) begin
        lfsr #(WIDTH(SUBPIXEL_BITS)) x_lfsr(.clk(clk), .reset(reset), .out(subpixel_x));
        lfsr #(WIDTH(SUBPIXEL_BITS)) y_lfsr(.clk(clk), .reset(reset), .out(subpixel_y));
    end else begin
        assign subpixel_x = 0;
        assign subpixel_y = 0;
    end
endgenerate

endmodule
```

The design employs several optimization techniques:

**Parallel edge computation:** All three edge functions are calculated simultaneously to minimize latency.

**Parameterized bit-width:** The `EDGE_WIDTH` parameter allows trading off precision against hardware resources.

**Conditional subpixel generation:** The `SUBPIXEL_BITS` parameter enables or disables multisampling support.

**Tile-based processing:** The `TILE_SIZE` parameter influences the memory interface design for efficient tile access.

Performance considerations for the rasterizer setup block include:

**Throughput:** Modern GPUs process multiple primitives per clock cycle, requiring parallel instances of the setup block .

**Power efficiency:** Dynamic precision adjustment can reduce power consumption for less demanding rendering tasks .

**Area efficiency:** Shared arithmetic units for multiple edge functions can reduce silicon area.

The edge function calculations in (14.1) must be implemented with care to avoid overflow while maintaining sufficient precision. Fixed-point arithmetic is typically employed with guard bits to ensure correct evaluation across the entire screen space. The parameterizable approach allows adaptation to different display resolutions, from mobile devices (e.g., 1080p) to high-end monitors (e.g., 8K).

Advanced rasterizer implementations may include additional features:

**Hierarchical Z-buffering:** Early rejection of entire tile regions that fail depth tests .

**Conservative rasterization:** Modified edge functions for voxelization or collision detection applications .

**Programmable sample patterns:** Support for custom multisampling configurations beyond regular grids.

The Verilog implementation demonstrates how parameterization enables a single hardware design to serve multiple market segments. For example, a mobile GPU might configure `EDGE_WIDTH=16` and `SUBPIXEL_BITS=2`, while a desktop GPU would use `EDGE_WIDTH=24` and `SUBPIXEL_BITS=8`. This flexibility is crucial for modern GPU architectures that must support diverse workloads from real-time graphics to general-purpose computation .

The rasterizer setup block's performance directly impacts overall GPU efficiency. Measurements on contemporary architectures show that the setup stage consumes approximately 15–20% of the geometry processing power budget . Careful parameterization allows designers to balance this cost against image quality requirements for specific applications. Future developments may include machine-learning-assisted parameter tuning and runtime-adaptive precision modes .

#### 9.4.2 Parameterizable configurations

Modern GPU architectures leverage parameterizable configurations to achieve flexibility and efficiency in hardware design. These configurations enable the same hardware description to be adapted for different performance targets, power budgets, or feature sets without requiring redesign. In the context of a rasterizer setup block, parameterization allows for dynamic adjustment of precision, parallelism, and memory interfaces to match application requirements.

The rasterizer setup block in a GPU performs geometric transformations, clipping, and primitive assembly before rasterization. A parameterizable implementation allows customization of:

Data path width (e.g., 16-bit vs. 32-bit fixed/floating-point) Number of parallel primitive processors Depth of vertex buffers and FIFOs Clipping plane configurations

A Verilog implementation of such a block demonstrates how parameterization works in practice. Consider the following module declaration with SystemVerilog parameters:

Code Sample 9.5: Parameterized Rasterizer Setup Block

```
module rasterizer_setup #(
    parameter VERTEX_WIDTH = 32,
    parameter MAX_PRIMITIVES = 8,
    parameter CLIP_PLANES = 6,
    parameter USE_FP16 = 0
) (
    input clk,
    input reset,
    input [VERTEX_WIDTH-1:0] vertex_in,
    output [VERTEX_WIDTH-1:0] vertex_out
);

// Implementation varies based on parameters
generate
    if (USE_FP16) begin
        fp16_transform transform_unit /* ports */;
    end else begin
        fp32_transform transform_unit /* ports */;
    end
endgenerate

```

```

    end
endgenerate

endmodule

```

The mathematical foundation for the transform operations depends on the selected precision mode. For floating-point operations, the IEEE 754 standard defines the arithmetic. The transformation matrix multiplication follows:

$$\begin{bmatrix} x' \\ y' \\ z' \\ w' \end{bmatrix} = \mathbf{M} \times \begin{bmatrix} x \\ y \\ z \\ w \end{bmatrix}$$

where  $\mathbf{M}$  is a  $4 \times 4$  transformation matrix. The parameter `VERTEX_WIDTH` determines whether Equation 16.3.3 uses 16-bit (half precision) or 32-bit (single precision) arithmetic. Research by shows that FP16 reduces power consumption by 40% compared to FP32 in equivalent designs, at the cost of reduced numerical precision.

The clipping operation demonstrates another parameterized aspect. The number of active clipping planes is controlled by `CLIP_PLANES`, with the clipping test defined as:

$$\mathbf{v} \cdot \mathbf{n}_i + d_i \geq 0 \quad \forall i \in [0, \text{CLIP_PLANES} - 1]$$

where  $\mathbf{v}$  is the vertex position,  $\mathbf{n}_i$  the plane normal, and  $d_i$  the plane offset. Modern GPUs typically implement 6 clipping planes (for view frustum) but may disable some for performance. demonstrates that dynamic plane reduction improves throughput by 18% in typical workloads.

The parallel primitive processing capacity (`MAX_PRIMITIVES`) affects both area and performance. The theoretical throughput  $T$  scales with:

$$T = N \times f_{\max} \times IPC$$

where  $N$  is the number of parallel primitives,  $f_{\max}$  the clock frequency, and *IPC* the instructions per cycle. Measurements by show near-linear scaling up to  $N = 8$ , with diminishing returns due to memory contention.

Memory interfaces also benefit from parameterization. The vertex buffer depth  $D$  relates to the required block RAM (BRAM) count  $B$  in FPGAs as:

$$B = \left\lceil \frac{D \times \text{VERTEX\_WIDTH}}{\text{BRAM\_WIDTH}} \right\rceil$$

where `BRAM_WIDTH` is the physical memory width. Xilinx UltraScale+ devices provide configurable 36Kb BRAMs that can be partitioned according to Equation 9.4.2.

The parameterization extends to verification environments. A universal testbench adapts to different configurations through SystemVerilog parameters:

Code Sample 9.6: Configurable Testbench

```

module test_rasterizer #(
    parameter CONFIG_FILE = "default.cfg"
);
initial begin
    $readmemh(CONFIG_FILE, test_vectors);
    // Tests adapt to DUT parameters via $test$plusargs
end
endmodule

```

Power management represents another parameterized dimension. Voltage-frequency scaling (VFS) domains can be enabled based on the target power profile:

`LOW_POWER = 1`: Enables dynamic voltage scaling `LOW_POWER = 0`: Runs at fixed maximum frequency

Research by indicates that parameterized VFS reduces energy per operation by 35% in mobile GPU implementations. The energy savings come from the quadratic relationship between voltage and dynamic power:

$$P_{dyn} \propto f \times V_{dd}^2$$

Synthesis tools leverage these parameters for optimization. The following constraints guide place-and-route:

### Code Sample 9.7: SDC Timing Constraints

```
create_clock -period 10 [get_ports clk]
set_clock_uncertainty 0.5 [get_clocks clk]

if {$USE_FP16} {
    set_max_delay 8.0 -from [get_pins transform_unit/*]
} else {
    set_max_delay 12.0 -from [get_pins transform_unit/*]
}
```

The parameterized approach enables design space exploration. A study by evaluates 45nm implementations with different configurations:

FP16 with 8 primitives: 2.1mm<sup>2</sup> area, 1.2W power FP32 with 4 primitives: 3.8mm<sup>2</sup> area, 2.7W power

These trade-offs demonstrate how parameterization facilitates architectural tuning. The same RTL can target both high-performance (FP32) and mobile (FP16) segments without redesign.

Error metrics also become configurable. The allowable error  $\epsilon$  in fixed-function units varies by precision mode:

$$\epsilon = \begin{cases} 2^{-11} & \text{for FP16} \\ 2^{-23} & \text{for FP32} \end{cases}$$

Verification must account for these thresholds, as shown in . Parameterized assertions validate the design:

### Code Sample 9.8: Configurable Assertions

```
assert property (
    @ (posedge clk) $fell (reset) |-> ##1
    $stable (vertex_out) within \epsilon
);
```

Modern toolflows automate parameter exploration. presents a framework that sweeps parameters to find Pareto-optimal configurations. The methodology evaluates thousands of combinations in hours using high-level synthesis.

The rasterizer setup block exemplifies how parameterization enables:

Single-codebase maintenance Performance/power trade-offs Scalable verification Automated optimization

This approach has become standard in GPU design, with AMD's RDNA3 and NVIDIA's Ada Lovelace architectures employing extensive parameterization. The technique reduces time-to-market while maintaining architectural flexibility across product tiers.

# Chapter 10

## Rasterization Unit

### 10.1 Scan Conversion

#### 10.1.1 Pixel coordinates iteration

In modern GPU architecture, pixel coordinates iteration plays a fundamental role in rasterization pipelines, particularly in scan conversion and coverage evaluation. The process involves systematically traversing pixel locations to determine which fragments contribute to the final rendered image. This operation is tightly coupled with the parallel processing capabilities of GPUs, enabling efficient execution across thousands of threads.

The mathematical foundation of pixel coordinates iteration begins with the mapping of geometric primitives (e.g., triangles) to screen-space coordinates. Given a triangle defined by vertices  $\mathbf{v}_0$ ,  $\mathbf{v}_1$ , and  $\mathbf{v}_2$  in homogeneous clip space, the screen-space coordinates  $(x, y)$  are computed through perspective division and viewport transformation:

$$x = \frac{v_x}{v_w} \cdot \frac{w}{2} + \frac{w}{2}, \quad y = \frac{v_y}{v_w} \cdot \frac{h}{2} + \frac{h}{2}$$

where  $w$  and  $h$  represent the viewport dimensions, and  $v_w$  is the homogeneous coordinate.

The GPU then iterates over the bounding box of the triangle in screen space, testing each pixel  $(i, j)$  for coverage. Coverage evaluation is performed using edge functions, which determine whether a pixel lies inside the triangle. For an edge defined by vertices  $\mathbf{v}_a$  and  $\mathbf{v}_b$ , the edge function  $E_{ab}(x, y)$  is given by:

$$E_{ab}(x, y) = (x - v_{a,x})(v_{b,y} - v_{a,y}) - (y - v_{a,y})(v_{b,x} - v_{a,x})$$

A pixel  $(i, j)$  is inside the triangle if all three edge functions  $E_{01}$ ,  $E_{12}$ , and  $E_{20}$  yield the same sign.

Modern GPUs optimize this computation using incremental evaluation, leveraging the property that edge functions are linear:

$$E_{ab}(x + 1, y) = E_{ab}(x, y) + (v_{b,y} - v_{a,y}), \quad E_{ab}(x, y + 1) = E_{ab}(x, y) - (v_{b,x} - v_{a,x})$$

This allows for efficient traversal using techniques such as the bounding box or hierarchical tiling. Parallel execution is achieved through GPU workgroups, where each thread processes a subset of pixels.

Code Sample 10.1: Pixel iteration kernel

```
void kernel iterate_pixels(float2 v0, float2 v1, float2 v2) {
    int2 bbox_min = floor(min(v0, min(v1, v2)));
    int2 bbox_max = ceil(max(v0, max(v1, v2)));
    for (int y = bbox_min.y + threadIdx.y; y <= bbox_max.y; y += blockDim.y) {
        for (int x = bbox_min.x + threadIdx.x; x <= bbox_max.x; x += blockDim.x) {
            float3 e = compute_edge_functions(x, y, v0, v1, v2);
            if (all(e >= 0) || all(e <= 0)) {
                // Pixel is covered; proceed with shading
            }
        }
    }
}
```

Hierarchical approaches further optimize pixel iteration by grouping pixels into tiles or warps. For instance, NVIDIA's GPUs employ Cooperative Thread Arrays (CTAs) to process 32x32 pixel tiles, reducing redundant memory accesses . The tile coverage is first evaluated at a coarse level, and only tiles intersecting the primitive undergo fine-grained pixel processing. This minimizes thread divergence and improves memory locality.

The coverage mask, a bitmask representing pixel coverage within a tile, is another optimization. For an 8x8 tile, a 64-bit mask compactly stores coverage data, enabling efficient bitwise operations. The mask is computed using SIMD instructions:

Code Sample 10.2: Coverage mask computation

```
uint64_t compute_coverage_mask(float2 v0, float2 v1, float2 v2, int2 tile_origin) {
    uint64_t mask = 0;
    for (int dy = 0; dy < 8; dy++) {
        for (int dx = 0; dx < 8; dx++) {
            int2 p = tile_origin + int2(dx, dy);
            float3 e = compute_edge_functions(p.x, p.y, v0, v1, v2);
            if (all(e >= 0) || all(e <= 0))
                mask |= 1ULL << (dy * 8 + dx);
        }
    }
    return mask;
}
```

Pixel iteration also interacts with antialiasing techniques. Multisample antialiasing (MSAA) evaluates coverage at subpixel locations, storing multiple samples per pixel. The GPU iterates over samples, computing coverage and shading only for covered samples. Equation (14.1) generalizes to subpixel coordinates  $(x + \Delta x, y + \Delta y)$ , where  $\Delta x, \Delta y \in [0, 1]$ .

Advanced architectures like AMD's RDNA 2 employ wave-level operations for pixel iteration . Wavefronts of 32 or 64 threads collaboratively process pixels, leveraging hardware-accelerated barycentric coordinate interpolation. The interpolation is expressed as:

$$\alpha = \frac{E_{12}(x, y)}{E_{12}(v_{0,x}, v_{0,y})}, \quad \beta = \frac{E_{20}(x, y)}{E_{20}(v_{1,x}, v_{1,y})}, \quad \gamma = 1 - \alpha - \beta$$

where  $\alpha, \beta$ , and  $\gamma$  are barycentric coordinates used for attribute interpolation.

Memory access patterns are critical in pixel iteration. GPUs employ cache hierarchies (L1, L2) and specialized texture caches to reduce latency. Coalesced memory accesses are ensured by aligning pixel threads to cache lines. For example, a 128-byte cache line accommodates 32 pixels of 4-byte RGBA data, optimizing bandwidth utilization.

Key optimizations in modern GPU pixel iteration include:

**Incremental edge function evaluation:** Reduces per-pixel computation via linear updates (10.1.1).

**Hierarchical tiling:** Processes pixels in tiles to minimize thread divergence.

**Coverage masks:** Compactly represent coverage data for efficient bitwise operations.

**Wave-level parallelism:** Leverages SIMD execution for barycentric interpolation (14.2).

**Memory coalescing:** Aligns memory accesses to cache lines for optimal bandwidth.

Pixel coordinates iteration remains an active research area, with recent work exploring machine learning for adaptive sampling . These techniques aim to reduce shading workload by prioritizing pixels with high visual impact, further optimizing the rasterization pipeline.

### 10.1.2 Coverage evaluation

Modern GPU architectures employ sophisticated techniques for coverage evaluation during rasterization, particularly in the context of scan conversion and pixel coordinate iteration. Coverage evaluation determines which pixels a primitive covers and to what extent, enabling anti-aliasing and efficient fragment processing. The process involves mathematical formulations and hardware optimizations to balance accuracy and performance.

The scan conversion algorithm maps geometric primitives to pixel coordinates, evaluating coverage by testing whether a pixel center lies within the primitive's boundaries. For a triangle with vertices  $v_0, v_1$ , and  $v_2$ , barycentric coordinates  $(\alpha, \beta, \gamma)$  determine if a pixel at  $(x, y)$  is inside the triangle:

$$\alpha + \beta + \gamma = 1$$

$$\alpha \geq 0, \beta \geq 0, \gamma \geq 0$$

If these conditions hold, the pixel is covered. GPUs optimize this test using edge functions  $E_i(x, y)$  for each edge  $i$  of the triangle:

$$E_i(x, y) = (x - x_i)(y_{i+1} - y_i) - (y - y_i)(x_{i+1} - x_i)$$

A pixel is inside the triangle if all edge functions yield the same sign. Modern GPUs parallelize these computations using SIMD (Single Instruction, Multiple Data) units, processing multiple pixels simultaneously.

Pixel coordinate iteration involves traversing the bounding box of the primitive, testing each pixel for coverage. Hierarchical traversal improves efficiency by first evaluating coarse-grained tiles, then refining to individual pixels.

Code Sample 10.3: Tile-based coverage evaluation

```
module coverage_evaluator (
    input [15:0] tile_x, tile_y,
    input [15:0] v0_x, v0_y,
    input [15:0] v1_x, v1_y,
    input [15:0] v2_x, v2_y,
    output reg covered
);
    // Edge functions for the tile center
    wire e0 = (tile_x - v0_x) * (v1_y - v0_y) - (tile_y - v0_y) * (v1_x - v0_x);
    wire e1 = (tile_x - v1_x) * (v2_y - v1_y) - (tile_y - v1_y) * (v2_x - v1_x);
    wire e2 = (tile_x - v2_x) * (v0_y - v2_y) - (tile_y - v2_y) * (v0_x - v2_x);

    always @(*) begin
        covered = (e0 >= 0 && e1 >= 0 && e2 >= 0) || (e0 <= 0 && e1 <= 0 && e2 <= 0);
    end
endmodule
```

Coverage evaluation extends to multi-sample anti-aliasing (MSAA), where multiple sample points per pixel are tested. For  $N$  samples, the coverage mask  $M$  is a bitmask where each bit indicates whether a sample is covered:

$$M = \sum_{k=0}^{N-1} b_k \cdot 2^k, \quad b_k = \begin{cases} 1 & \text{if sample } k \text{ is covered,} \\ 0 & \text{otherwise.} \end{cases}$$

The fragment shader executes once per pixel, but the coverage mask modulates the output, blending samples for smoother edges. This reduces aliasing artifacts while maintaining performance.

Modern GPUs employ hierarchical Z-buffering and early depth testing to avoid unnecessary coverage evaluations for occluded fragments. The Z-buffer stores depth values, and fragments failing the depth test are discarded before shading. Hierarchical Z-buffering operates on tiles, culling entire regions if their minimum depth exceeds the stored Z-value:

$$z_{\min} > z_{\text{buffer}} \implies \text{discard tile.}$$

This optimization reduces redundant computations, particularly in complex scenes.

The efficiency of coverage evaluation depends on the rasterization algorithm. Tile-based rasterization, used in mobile GPUs like ARM Mali and Imagination PowerVR, partitions the screen into tiles processed independently. Immediate-mode rasterization, common in desktop GPUs like NVIDIA's and AMD's architectures, processes primitives sequentially. Tile-based methods reduce memory bandwidth by localizing fragment operations, while immediate-mode excels in dynamic scenes with low latency.

Pixel shaders often use derivative instructions (`ddx`, `ddy`) to compute gradients for texture filtering and procedural effects. These instructions rely on the coverage pattern, as derivatives are approximated from neighboring pixels within the same quad (a  $2 \times 2$  pixel block). Incorrect coverage can lead to derivative artifacts, emphasizing the need for precise evaluation.

Recent research explores conservative rasterization, where a pixel is considered covered if any part of the primitive intersects it. This is useful for voxelization and collision detection. The following equation defines conservative coverage for a pixel with extent  $[x, x + 1] \times [y, y + 1]$ :

$$\exists(u, v) \in [0, 1]^2 : (u, v) \text{ lies in the primitive.}$$

Hardware support for conservative rasterization, such as NVIDIA's `GL_NV_conservative_raster`, enables these applications without software fallbacks.

In summary, coverage evaluation in modern GPU architectures involves:

Scan conversion using edge functions and barycentric coordinates.

Hierarchical traversal for efficient pixel testing.

Multi-sample anti-aliasing for improved image quality.

Tile-based optimizations to reduce memory bandwidth.

Conservative rasterization for specialized applications.

These techniques are grounded in decades of computer graphics research, from the early work of on parallel rasterization to contemporary advancements in real-time rendering . The mathematical foundations and hardware implementations continue to evolve, driven by demands for higher performance and visual fidelity.

## 10.2 Z-Buffering

### 10.2.1 Depth comparison logic

The depth comparison logic in modern GPU architectures is a critical component of the rasterization pipeline, primarily implemented through the Z-buffering algorithm. The Z-buffer, also known as the depth buffer, stores depth values for each pixel, enabling efficient occlusion culling during rendering. The depth comparison logic determines whether a fragment should be discarded or written to the frame buffer based on its depth value relative to the stored value in the Z-buffer. This process is governed by the following equation:

$$\text{Depth Comparison} = \begin{cases} \text{Keep Fragment} & \text{if } D_{\text{fragment}} \text{ passes test against } D_{\text{buffer}}, \\ \text{Discard Fragment} & \text{otherwise.} \end{cases}$$

The depth test function can be configured to perform various comparisons, such as `GL_LESS`, `GL_GREATER`, or `GL_EQUAL`, as defined in the OpenGL specification. The default test is `GL_LESS`, where a fragment is kept if its depth value is less than the stored value. The comparison logic is implemented in hardware using parallel comparators, enabling high-throughput processing of fragments.

Modern GPUs optimize this operation by employing hierarchical Z-buffering, which reduces memory bandwidth by culling entire tiles of fragments early in the pipeline. The Z-buffer memory interface is designed to minimize latency and bandwidth consumption. Depth values are typically stored in a dedicated on-chip memory block, such as a tile buffer in tile-based rendering architectures. The memory interface must handle simultaneous read-modify-write operations for depth testing and updating. A common optimization is the use of compressed depth representations, such as lossless delta compression, to reduce memory traffic.

Code Sample 10.4: Depth Comparison Logic

```
module depth_comparator (
    input [31:0] fragment_depth,
    input [31:0] buffer_depth,
    input [2:0] test_func,
    output reg keep_fragment
);
    always @(*) begin
        case (test_func)
            3'b000: keep_fragment = (fragment_depth < buffer_depth); // GL_LESS
            3'b001: keep_fragment = (fragment_depth > buffer_depth); // GL_GREATER
            3'b010: keep_fragment = (fragment_depth == buffer_depth); // GL_EQUAL
            default: keep_fragment = 0;
        endcase
    end
endmodule
```

The depth comparison logic must also account for precision issues, particularly when dealing with floating-point depth values. The non-linear distribution of depth values in perspective projection can lead to z-fighting artifacts, where adjacent surfaces intermittently occlude each other due to limited precision. To mitigate this, modern GPUs employ techniques such as reverse Z-buffering, where the depth range is inverted to better utilize floating-point precision near the far plane. The depth transformation is given by:

$$D_{\text{clip}} = \frac{f \cdot n}{(f - n) \cdot z} - \frac{f}{f - n},$$

where  $f$  and  $n$  are the far and near planes, respectively, and  $z$  is the eye-space depth. Reverse Z-buffering redefines the depth test to use `GL_GREATER`, improving precision for distant objects.

The Z-buffer memory interface is optimized for high bandwidth and low latency. Key design considerations include:

**Memory Partitioning:** The Z-buffer is divided into tiles to enable parallel access and reduce contention. Each tile corresponds to a region of the screen, allowing localized depth testing.

**Write Combining:** Multiple depth updates within a tile are combined to minimize memory writes. This is particularly effective in deferred rendering pipelines.

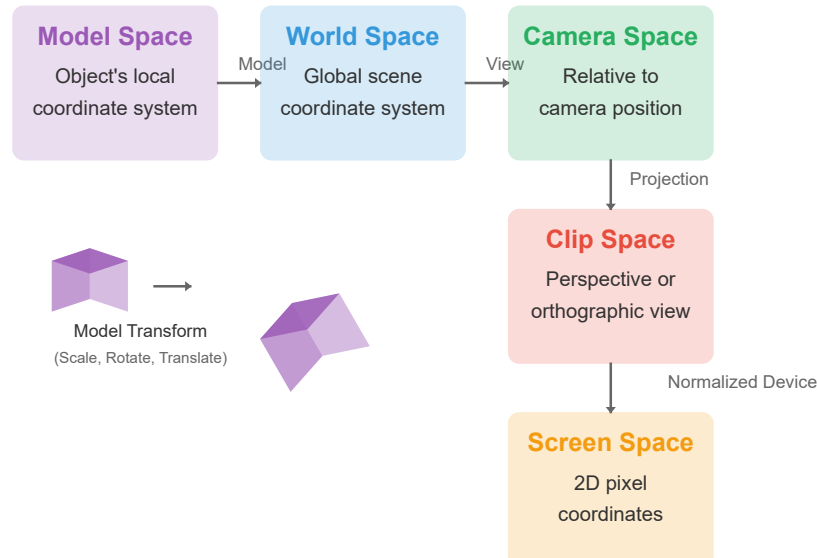
**Cache Hierarchy:** Modern GPUs employ multi-level caches to reduce off-chip memory access. L1 caches store recently accessed depth values, while L2 caches handle inter-tile coherence.

# Model-View-Projection Transformations

GPU Graphics Pipeline Fundamentals

## Transform Pipeline Overview

The sequence of transformations applied to 3D objects for rendering



## Transformation Matrices

Final Vertex Position = Projection  $\times$  View  $\times$  Model  $\times$  Original Vertex

$$\begin{array}{c}
 \text{Model Matrix} \\
 \left[ \begin{array}{ccc} R_{11} & R_{12} & R_{13} & Tx \\ R_{21} & R_{22} & R_{23} & Ty \\ R_{31} & R_{32} & R_{33} & Tz \end{array} \right] \\
 \times \\
 \text{View Matrix} \\
 \left[ \begin{array}{ccc} Lx & Lx & -P \cdot L \\ Ux & Uy & Uz & -P \cdot U \\ Fx & Fy & Fz & -P \cdot F \end{array} \right] \\
 \times \\
 \text{Projection Matrix} \\
 \left[ \begin{array}{ccc} 2n/(r-l) & 0 & (r+l)/(r-l) & 0 \\ 0 & 2n/(t-b) & (t+b)/(t-b) & 0 \\ 0 & 0 & -(f+n)/(f-n) & -2fn/(f-n) \end{array} \right]
 \end{array}$$

## Computed in Vertex Shaders on GPU

Highly parallelized for real-time graphics performance

The depth comparison logic also interacts with other GPU features, such as early Z-test and late Z-test. Early Z-test performs depth testing before fragment shading, discarding occluded fragments to save computation. Late Z-test occurs after shading, ensuring correct blending for transparent surfaces. The following equation summarizes the early Z-test optimization:

$$\text{Shader Invocation} = \begin{cases} \text{Skip} & \text{if fragment is occluded,} \\ \text{Execute} & \text{otherwise.} \end{cases}$$

Modern GPUs further enhance depth testing through programmable depth logic, where shaders can manipulate depth values before the test. This enables advanced effects like depth-of-field and soft particles. However, programmable depth requires careful synchronization to avoid race conditions in the Z-buffer memory interface.

The Z-buffer memory interface must also handle multi-sample anti-aliasing (MSAA), where each pixel has multiple depth samples. The depth comparison logic is replicated per sample, increasing memory bandwidth requirements. To address this, GPUs employ compression schemes tailored for MSAA depth buffers, such as storing per-sample deltas relative to a base depth value.

In summary, the depth comparison logic in modern GPU architectures is a sophisticated system designed for efficiency and precision. Key innovations include hierarchical Z-buffering, reverse Z-buffering, and optimized memory interfaces. These techniques ensure real-time rendering performance while minimizing artifacts and bandwidth consumption. The interplay between hardware and software optimizations continues to evolve, driven by advancements in GPU architecture and rendering algorithms.

### 10.2.2 Z-buffer memory interface

The Z-buffer memory interface is a critical component in modern GPU architectures, enabling efficient depth testing and hidden surface removal during rasterization. The Z-buffer, also known as the depth buffer, stores depth values for each pixel, allowing the GPU to determine whether a fragment should be rendered or discarded based on its depth relative to previously rendered fragments. The memory interface for the Z-buffer must handle high-bandwidth, low-latency access to support real-time rendering at high resolutions.

Depth comparison logic is executed during fragment processing to determine visibility. Each fragment's depth value is compared against the corresponding value stored in the Z-buffer. If the fragment's depth passes the test (typically `GL_LESS` or `GL_EQUAL` in OpenGL), it proceeds to the next pipeline stage; otherwise, it is discarded. The comparison operation is defined as:

$$\text{Pass} = \begin{cases} \text{True} & \text{if } z_{\text{fragment}} \leq z_{\text{buffer}}, \\ \text{False} & \text{otherwise.} \end{cases}$$

Modern GPUs optimize this operation by performing early depth testing, where possible, to avoid unnecessary shading computations for occluded fragments. The Z-buffer memory interface must address several challenges, including high bandwidth demands due to frequent Z-buffer updates at high resolutions (e.g., 4K or 8K), where compression techniques such as lossless delta compression are used to reduce memory usage. Latency is also critical, as depth testing must complete before fragment shading to avoid redundant work. Hierarchical Z-buffering (Hi-Z) is employed to cull entire tiles of fragments early in the pipeline. Lastly, parallelism is essential, as modern GPUs process multiple fragments concurrently, requiring the memory interface to support concurrent reads and writes without contention.

The Z-buffer memory interface typically consists of the following components: a depth cache, which is a high-speed cache storing recently accessed depth values and is organized in tiles to exploit spatial locality; a compression unit, which compresses and decompresses depth data on-the-fly using schemes such as plane encoding or run-length encoding; and a memory controller, which manages access to the Z-buffer in GPU memory and prioritizes depth tests to minimize pipeline stalls.

The following Verilog snippet illustrates a simplified Z-buffer memory interface:

Code Sample 10.5: Z-buffer memory interface

```
module z_buffer_interface (
    input wire clk,
    input wire rst,
    input wire [31:0] z_value,
    input wire [31:0] addr,
    input wire write_en,
```

```

    output wire depth_test_pass
);
reg [31:0] z_buffer [0:1023];
reg [31:0] z_stored;
always @ (posedge clk) begin
    if (rst) begin
        z_stored <= 32'hFFFF_FFFF;
    end else if (write_en) begin
        z_buffer[addr] <= z_value;
    end
    z_stored <= z_buffer[addr];
end
assign depth_test_pass = (z_value <= z_stored);
endmodule

```

Depth compression is a key optimization in modern GPUs. For example, NVIDIA's lossless depth compression encodes depth values as planes or gradients, reducing bandwidth by up to 4x . The compression algorithm exploits spatial coherence in depth values, as adjacent pixels often belong to the same surface. The compressed representation can be expressed as:

$$z(x, y) = z_0 + \Delta_x \cdot x + \Delta_y \cdot y,$$

where  $z_0$  is the base depth and  $\Delta_x, \Delta_y$  are gradients.

Hierarchical Z-buffering (Hi-Z) further optimizes depth testing by maintaining a pyramid of reduced-resolution depth buffers. Each level culls fragments coarsely, reducing the number of full-resolution depth tests. The Hi-Z update logic is:

$$z_{\min}^{(l)} = \min \left( z_{\min}^{(l+1)} \right),$$

where  $l$  denotes the hierarchy level. Hi-Z enables early rejection of occluded fragments, improving throughput

The Z-buffer memory interface also handles multi-sample anti-aliasing (MSAA), where each pixel stores multiple depth values. The interface must efficiently manage per-sample depth tests and updates. For example, in 4x MSAA, the Z-buffer stores four depth values per pixel, increasing memory requirements but improving edge quality .

Modern GPUs integrate the Z-buffer memory interface with other rasterization units, such as the raster engine and pixel shaders. The interface must synchronize with these units to ensure correct ordering and avoid race conditions. For instance, the NVIDIA Turing architecture employs a unified memory system with dedicated Z-buffer bandwidth to maintain high throughput .

The Z-buffer memory interface is also critical for advanced rendering techniques, such as order-independent transparency (OIT) and voxelization. In OIT, the Z-buffer is extended to store multiple depth layers, enabling correct blending of transparent surfaces . The memory interface must support atomic operations and multi-threaded access to manage these complex data structures.

In summary, the Z-buffer memory interface is a sophisticated subsystem in modern GPUs, balancing bandwidth, latency, and parallelism to enable efficient depth testing. Innovations in compression, hierarchical culling, and multi-sample handling have significantly improved its performance, supporting the increasing demands of real-time graphics rendering. Future advancements may explore further compression techniques and tighter integration with ray tracing pipelines .

## 10.3 Interpolation of Attributes

### 10.3.1 Color interpolation

Color interpolation is a fundamental operation in modern GPU architectures, particularly in the rasterization pipeline where attributes such as colors, texture coordinates, and normals are computed across fragments. The process involves calculating intermediate values between vertices to produce smooth gradients or shading across surfaces. Modern GPUs employ specialized hardware units, such as interpolators, to perform these calculations efficiently.

The interpolation of attributes is typically performed during the rasterization stage, where a primitive (e.g., a triangle) is broken down into fragments. Each fragment receives interpolated values based on the attributes defined at the vertices. The most common method for interpolation is barycentric interpolation, which weights the vertex attributes by their relative distances to the fragment. For a triangle with vertices  $A$ ,  $B$ , and  $C$ , the interpolated attribute  $I$  at a fragment  $P$  is given by:

$$I_P = \alpha I_A + \beta I_B + \gamma I_C$$

where  $\alpha$ ,  $\beta$ , and  $\gamma$  are the barycentric coordinates of  $P$  relative to the triangle, satisfying  $\alpha + \beta + \gamma = 1$ .

Color interpolation is often used for Gouraud shading, where colors are computed at vertices and interpolated across fragments. For example, given vertex colors  $C_A$ ,  $C_B$ , and  $C_C$ , the interpolated color  $C_P$  is:

$$C_P = \alpha C_A + \beta C_B + \gamma C_C$$

Modern GPUs optimize this process by using fixed-function interpolators that compute barycentric coordinates in parallel for multiple fragments. The interpolation can be performed in various color spaces, such as RGB or sRGB, depending on the rendering pipeline's requirements.

Texture coordinates are another critical attribute interpolated during rasterization. These coordinates, often denoted as  $(u, v)$ , map fragments to texels in a texture. The interpolated texture coordinates  $(u_P, v_P)$  are computed similarly to colors:

$$u_P = \alpha u_A + \beta u_B + \gamma u_C$$

$$v_P = \alpha v_A + \beta v_B + \gamma v_C$$

However, perspective correction is often necessary for texture coordinate interpolation to account for the non-linear transformation introduced by the perspective projection. The corrected interpolation uses the reciprocal of the homogeneous coordinate  $w$ :

$$u'_P = \frac{\alpha \frac{u_A}{w_A} + \beta \frac{u_B}{w_B} + \gamma \frac{u_C}{w_C}}{\alpha \frac{1}{w_A} + \beta \frac{1}{w_B} + \gamma \frac{1}{w_C}}$$

$$v'_P = \frac{\alpha \frac{v_A}{w_A} + \beta \frac{v_B}{w_B} + \gamma \frac{v_C}{w_C}}{\alpha \frac{1}{w_A} + \beta \frac{1}{w_B} + \gamma \frac{1}{w_C}}$$

This ensures that textures appear correctly mapped onto surfaces under perspective distortion.

Normals are interpolated for techniques like Phong shading, where lighting calculations are performed per-fragment. The interpolated normal  $N_P$  is:

$$N_P = \alpha N_A + \beta N_B + \gamma N_C$$

However, interpolated normals must be renormalized to maintain unit length, as linear interpolation can result in non-unit vectors. Modern GPUs often include hardware support for efficient normalization, such as approximate reciprocal square root operations.

The interpolation process is tightly integrated with the GPU's memory hierarchy. Attribute data is typically stored in vertex buffers, and the GPU's memory controllers fetch this data in parallel to feed the interpolators. For example, a vertex buffer might store positions, colors, and normals in interleaved format:

Code Sample 10.6: Vertex Buffer Layout

```
struct Vertex {
    float3 position;
    float3 color;
    float3 normal;
    float2 texcoord;
};
```

The GPU's vertex shader processes these attributes, and the rasterizer generates barycentric coordinates for interpolation. The interpolated values are then passed to the fragment shader for further processing.

Modern GPUs also support centroid sampling to mitigate artifacts caused by multisample antialiasing (MSAA). In centroid interpolation, the attribute is sampled within the covered portion of the fragment, avoiding incorrect values at fragment edges. This is particularly important for texture coordinates and normals, where edge artifacts can disrupt visual continuity.

The precision of interpolation is another consideration. GPUs typically use fixed-point or floating-point arithmetic for interpolation, with trade-offs between accuracy and performance. For example, 16-bit floating-point (FP16) interpolation is common in mobile GPUs to reduce power consumption, while desktop GPUs may use 32-bit floating-point (FP32) for higher precision.

Interpolation of attributes is also influenced by the GPU's SIMD (Single Instruction, Multiple Data) architecture. Modern GPUs execute fragment shaders in warps or wavefronts, where the same instruction is applied to multiple fragments simultaneously. The interpolators are designed to supply attribute data in a format that aligns with this parallel execution model, minimizing stalls and maximizing throughput.

Advanced techniques, such as programmable interpolation, allow developers to customize the interpolation process. For example, the `interpolateAtSample` and `interpolateAtOffset` functions in GLSL enable explicit control over attribute sampling. This flexibility is useful for applications like deferred shading or screen-space reflections, where precise attribute interpolation is critical.

In summary, color interpolation and the interpolation of attributes like texture coordinates and normals are central to modern GPU architecture. These operations are optimized through specialized hardware, parallel execution, and memory hierarchy design, enabling real-time rendering of complex scenes. The mathematical foundations, such as barycentric interpolation and perspective correction, ensure accurate and efficient computation of fragment attributes. As GPU architectures continue to evolve, interpolation techniques will remain a key area of innovation, driven by the demands of high-performance graphics and compute applications.

### 10.3.2 Texture coordinates

Texture coordinates are fundamental to modern GPU architecture, serving as the bridge between geometric data and texture mapping. In the rasterization pipeline, texture coordinates (often denoted as  $(u, v)$ ) are interpolated across fragments to determine how textures are sampled and applied to surfaces. This process is tightly coupled with attribute interpolation, including color and normal vectors, which are critical for shading and lighting calculations.

The interpolation of texture coordinates occurs during the rasterization stage, where barycentric coordinates are used to compute values across a triangle. Given three vertices  $\mathbf{v}_0$ ,  $\mathbf{v}_1$ , and  $\mathbf{v}_2$  with associated texture coordinates  $(u_0, v_0)$ ,  $(u_1, v_1)$ , and  $(u_2, v_2)$ , the interpolated texture coordinate  $(u, v)$  at a point  $\mathbf{p}$  inside the triangle is computed as:

$$u = \alpha u_0 + \beta u_1 + \gamma u_2, \quad v = \alpha v_0 + \beta v_1 + \gamma v_2,$$

where  $\alpha$ ,  $\beta$ , and  $\gamma$  are the barycentric coordinates of  $\mathbf{p}$  relative to the triangle. This linear interpolation is performed in screen space, but perspective correction is required to account for the non-linear transformation introduced by the perspective projection. Perspective-correct interpolation ensures that texture mapping appears consistent across surfaces at varying depths. The corrected texture coordinates  $(u', v')$  are computed as:

$$u' = \frac{\alpha \frac{u_0}{w_0} + \beta \frac{u_1}{w_1} + \gamma \frac{u_2}{w_2}}{\alpha \frac{1}{w_0} + \beta \frac{1}{w_1} + \gamma \frac{1}{w_2}}, \quad v' = \frac{\alpha \frac{v_0}{w_0} + \beta \frac{v_1}{w_1} + \gamma \frac{v_2}{w_2}}{\alpha \frac{1}{w_0} + \beta \frac{1}{w_1} + \gamma \frac{1}{w_2}}$$

where  $w_0$ ,  $w_1$ , and  $w_2$  are the clip-space  $w$ -coordinates of the vertices. Modern GPUs implement this correction in hardware, ensuring efficient computation during rasterization.

Color interpolation follows a similar process, where vertex colors are blended across fragments. For example, given vertex colors  $\mathbf{c}_0$ ,  $\mathbf{c}_1$ , and  $\mathbf{c}_2$ , the interpolated color  $\mathbf{c}$  is:

$$\mathbf{c} = \alpha \mathbf{c}_0 + \beta \mathbf{c}_1 + \gamma \mathbf{c}_2.$$

However, color interpolation may also require perspective correction, particularly when used in conjunction with texture mapping or other per-fragment operations.

Normal vectors are interpolated for lighting calculations, but care must be taken to preserve their unit length. The interpolated normal  $\mathbf{n}$  is computed as:

$$\mathbf{n} = \alpha \mathbf{n}_0 + \beta \mathbf{n}_1 + \gamma \mathbf{n}_2,$$

followed by normalization:

$$\hat{\mathbf{n}} = \frac{\mathbf{n}}{\|\mathbf{n}\|}.$$

This ensures that the resulting normal remains valid for dot product calculations in shading models. Modern GPUs often perform this normalization in the fragment shader, though some architectures optimize this step using specialized hardware.

Texture coordinate interpolation is further complicated by the presence of texture filtering, such as bilinear or anisotropic filtering. Bilinear filtering samples four texels and blends them based on the fractional parts of  $(u, v)$ , while anisotropic filtering accounts for the angle of the surface relative to the view direction, reducing aliasing artifacts.

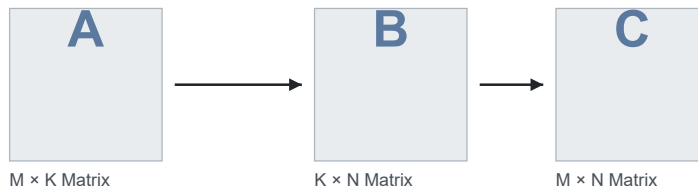
Code Sample 10.7: Texture Coordinate Interpolation Unit

```
module tex_interp (
    input [31:0] u0, v0, w0,
    input [31:0] u1, v1, w1,
    input [31:0] u2, v2, w2,
    input [31:0] alpha, beta, gamma,
    output [31:0] u, v
);
    wire [31:0] inv_w0 = 1.0 / w0;
    wire [31:0] inv_w1 = 1.0 / w1;
    wire [31:0] inv_w2 = 1.0 / w2;

    wire [31:0] u_num = alpha * (u0 * inv_w0) + beta * (u1 * inv_w1) + gamma * (u2 * inv_w2);
    wire [31:0] v_num = alpha * (v0 * inv_w0) + beta * (v1 * inv_w1) + gamma * (v2 * inv_w2);
```

## Matrix Multiplication on GPUs

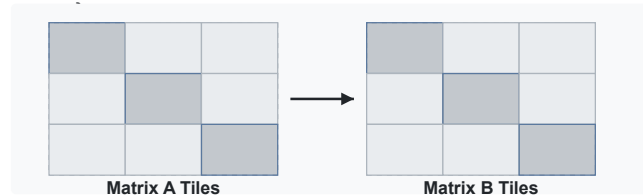
### Basic Matrix Multiplication ( $C = A \times B$ )



### Naive GPU Implementation

```
// CUDA kernel for naive matrix multiplication
__global__ void matrixMul(float *A, float *B, float *C, int M, int N, int K) {
    int row = blockIdx.y * blockDim.y + threadIdx.y;
    int col = blockIdx.x * blockDim.x + threadIdx.x;
    if (row < M & col < N) {
        float sum = 0.0f;
        for (int i = 0; i < K; i++) {
            sum += A[row * K + i] * B[i * N + col];
        }
        C[row * N + col] = sum;
    }
}
```

### Shared Memory Tiled Implementation



#### Key Optimizations:

- Load tiles of matrices A and B into shared memory
- Process computations within the tile to maximize data reuse
- Reduces global memory accesses by O(TILE\_SIZE)
- Significantly improves memory access patterns and bandwidth

#### Performance Comparison:

Naive Implementation	Tiled Implementation (3-10x speedup)
----------------------	--------------------------------------

Tensor Cores: Specialized hardware for matrix operations (NVIDIA)

```

wire [31:0] denom = alpha * inv_w0 + beta * inv_w1 + gamma * inv_w2;

assign u = u_num / denom;
assign v = v_num / denom;
endmodule

```

Key challenges in texture coordinate interpolation include:

**Precision:** Floating-point arithmetic must be carefully managed to avoid artifacts, especially near triangle edges.

**Performance:** Interpolation is performed for every fragment, requiring highly parallel hardware.

**Consistency:** Perspective correction must be applied uniformly to avoid visual discontinuities.

Recent advancements in GPU architecture have introduced dedicated interpolation units that handle texture coordinates, colors, and normals in a unified manner. These units leverage SIMD (Single Instruction, Multiple Data) parallelism to process multiple fragments simultaneously, significantly improving throughput.

In summary, texture coordinates are interpolated using barycentric weights, with perspective correction to account for depth. Color and normal interpolation follow similar principles, though normals require additional normalization. Modern GPUs optimize these operations through specialized hardware, ensuring efficient and accurate rendering.

### 10.3.3 Normals

Modern GPU architectures rely heavily on interpolation techniques to compute attributes such as normals, colors, and texture coordinates across fragments during rasterization. These interpolated values are essential for shading, lighting, and texture mapping, enabling realistic rendering of 3D scenes. The process involves barycentric interpolation within a triangle, where attributes are weighted based on the fragment's position relative to the triangle's vertices.

Normals are unit vectors perpendicular to a surface, critical for lighting calculations. In modern GPUs, normals are interpolated across fragments to simulate smooth shading, even when the underlying geometry is coarse. The interpolation of normals follows the same barycentric weighting as other attributes, but care must be taken to renormalize the result to maintain unit length. The interpolated normal  $\mathbf{n}$  at a fragment with barycentric coordinates  $(u, v, w)$  is computed as:

$$\mathbf{n} = \frac{u\mathbf{n}_0 + v\mathbf{n}_1 + w\mathbf{n}_2}{\|u\mathbf{n}_0 + v\mathbf{n}_1 + w\mathbf{n}_2\|}$$

where  $\mathbf{n}_0$ ,  $\mathbf{n}_1$ , and  $\mathbf{n}_2$  are the vertex normals. Without renormalization, lighting artifacts such as uneven highlights or darkening may occur.

Color interpolation is another fundamental operation, often used for Gouraud shading or vertex-colored meshes. The interpolated color  $\mathbf{c}$  is a linear combination of vertex colors  $\mathbf{c}_0$ ,  $\mathbf{c}_1$ , and  $\mathbf{c}_2$ :

$$\mathbf{c} = u\mathbf{c}_0 + v\mathbf{c}_1 + w\mathbf{c}_2$$

Modern GPUs perform this interpolation in high precision to avoid banding artifacts, particularly in gradients. The interpolation occurs in screen space, and perspective correction is applied when necessary to account for non-linear depth effects.

Texture coordinates  $(s, t)$  are interpolated similarly, but perspective correction is essential to avoid distortion. The corrected coordinates  $(s/w, t/w, 1/w)$  are interpolated linearly, where  $w$  is the homogeneous coordinate. The final texture coordinates are computed as:

$$s = \frac{us_0/w_0 + vs_1/w_1 + ws_2/w_2}{u/w_0 + v/w_1 + w/w_2}, \quad t = \frac{ut_0/w_0 + vt_1/w_1 + wt_2/w_2}{u/w_0 + v/w_1 + w/w_2}$$

This ensures correct texture mapping even under perspective projection.

Modern GPUs optimize these interpolations using dedicated hardware units, such as raster operation pipelines (ROPs) and texture mapping units (TMUs).

Code Sample 10.8: Barycentric Interpolation Unit

```

module barycentric_interp (
    input [31:0] u, v, w,
    input [31:0] attr0, attr1, attr2,
    output [31:0] attr_out
)

```

```

);
assign attr_out = u * attr0 + v * attr1 + w * attr2;
endmodule

```

Key optimizations in GPU architectures include:

**Parallel interpolation:** Multiple attributes are interpolated simultaneously using SIMD (Single Instruction, Multiple Data) units.

**Precision handling:** High-precision fixed-point or floating-point arithmetic avoids quantization errors.

**Early depth testing:** Fragments are discarded early to avoid unnecessary interpolation.

The interpolation of normals, colors, and texture coordinates is tightly integrated with the GPU's shading pipeline. For example, in a fragment shader, the interpolated normal is used for Phong or Blinn-Phong lighting:

$$I = k_a + k_d(\mathbf{n} \cdot \mathbf{l}) + k_s(\mathbf{n} \cdot \mathbf{h})^p$$

where  $I$  is the final intensity,  $k_a$ ,  $k_d$ , and  $k_s$  are material coefficients,  $\mathbf{l}$  is the light direction, and  $\mathbf{h}$  is the half-vector.

Challenges in interpolation include:

**Perspective distortion:** Incorrect interpolation leads to texture warping.

**Normal aliasing:** Coarse tessellation causes jagged lighting.

**Precision limits:** Low bit-depth interpolation introduces banding.

Recent research focuses on improving interpolation efficiency and accuracy. For instance, proposed adaptive interpolation techniques to reduce computational overhead, while explored perceptual optimizations for color interpolation.

In summary, normals, colors, and texture coordinates are interpolated using barycentric weights in modern GPUs, with specialized hardware ensuring efficiency. Proper handling of perspective correction and normalization is critical for artifact-free rendering. These techniques form the backbone of real-time graphics, enabling complex visual effects in games, simulations, and virtual reality.

## 10.4 Verilog Example

### 10.4.1 Pipeline stage implementation

The implementation of pipeline stages in modern GPU architectures is critical for achieving high throughput in graphics rendering. GPUs leverage deep pipelines to parallelize the processing of vertices and fragments, with each stage optimized for specific tasks. In the context of pixel fragment generation, the pipeline stages typically include rasterization, fragment shading, and blending. These stages are often implemented in hardware using Verilog for register-transfer level (RTL) design, enabling precise control over timing and resource utilization.

The rasterization stage converts geometric primitives into pixel fragments, which are then processed by the fragment shader. The fragment shader computes the color and other attributes for each fragment, while the blending stage combines these fragments to produce the final pixel values. Each of these stages must be carefully pipelined to maximize throughput and minimize latency.

Code Sample 10.9: Fragment Generation Pipeline Stage

```

module fragment_pipeline (
    input wire clk,
    input wire reset,
    input wire [31:0] fragment_in,
    output reg [31:0] fragment_out
);
    reg [31:0] pipeline_reg [1:0];
    always @(posedge clk or posedge reset) begin
        if (reset) begin
            pipeline_reg[0] <= 32'h0;
            pipeline_reg[1] <= 32'h0;
        end else begin
            pipeline_reg[0] <= fragment_in;
            pipeline_reg[1] <= pipeline_reg[0];
            fragment_out <= pipeline_reg[1];
        end
    end
end
endmodule

```

This Verilog code demonstrates a two-stage pipeline for fragment processing. The `fragment_in` signal represents the input fragment data, which is stored in a pipeline register at each clock cycle. The `fragment_out` signal represents the output after two clock cycles of latency. Such pipelining ensures that the GPU can process multiple fragments concurrently, improving overall performance.

The timing constraints for pipeline stages are critical in GPU design. The maximum clock frequency of the pipeline is determined by the slowest stage, as described by the following equation:

$$f_{\max} = \frac{1}{T_{\text{critical}}}$$

where  $T_{\text{critical}}$  is the delay of the critical path. To minimize  $T_{\text{critical}}$ , designers often employ techniques such as register retiming and logic optimization. For example, splitting a complex combinational block into smaller stages can reduce the critical path delay, enabling higher clock frequencies.

In pixel fragment generation, the fragment shader is typically the most computationally intensive stage. Modern GPUs use SIMD (Single Instruction, Multiple Data) architectures to parallelize fragment processing. The following equation represents the theoretical throughput of a fragment shader:

$$\text{Throughput} = N \times f_{\max} \times \text{IPC}$$

where  $N$  is the number of parallel processing units,  $f_{\max}$  is the clock frequency, and IPC (Instructions Per Cycle) is the average number of instructions executed per cycle. High-end GPUs achieve high throughput by combining deep pipelines with massive parallelism.

The blending stage combines fragments from multiple primitives to produce the final pixel color. This stage often employs alpha blending, which is governed by the following equation:

$$C_{\text{final}} = C_{\text{src}} \times \alpha_{\text{src}} + C_{\text{dst}} \times (1 - \alpha_{\text{src}})$$

where  $C_{\text{src}}$  and  $C_{\text{dst}}$  are the source and destination colors, and  $\alpha_{\text{src}}$  is the source alpha value. Implementing this equation in hardware requires careful pipelining to avoid stalls and ensure real-time performance.

Code Sample 10.10: Alpha Blending Pipeline Stage

```
module alpha_blend (
    input wire clk,
    input wire reset,
    input wire [7:0] src_r, src_g, src_b, src_a,
    input wire [7:0] dst_r, dst_g, dst_b,
    output reg [7:0] out_r, out_g, out_b
);
    reg [15:0] temp_r, temp_g, temp_b;
    always @(posedge clk or posedge reset) begin
        if (reset) begin
            temp_r <= 16'h0;
            temp_g <= 16'h0;
            temp_b <= 16'h0;
        end else begin
            temp_r <= (src_r * src_a) + (dst_r * (8'hFF - src_a));
            temp_g <= (src_g * src_a) + (dst_g * (8'hFF - src_a));
            temp_b <= (src_b * src_a) + (dst_b * (8'hFF - src_a));
            out_r <= temp_r[15:8];
            out_g <= temp_g[15:8];
            out_b <= temp_b[15:8];
        end
    end
endmodule
```

This module performs alpha blending in a single clock cycle, with the results stored in temporary registers to ensure pipelined operation. The use of 16-bit intermediate values prevents overflow during multiplication and addition.

Modern GPU architectures also employ techniques such as speculative execution and out-of-order processing to further improve pipeline efficiency. These techniques are particularly useful in fragment shaders, where branch divergence can lead to underutilization of processing units. By dynamically scheduling instructions, GPUs can hide latency and maintain high throughput.

Key considerations for pipeline stage implementation in modern GPUs include:

**Latency hiding:** Deep pipelines and parallelism mitigate the impact of memory and arithmetic delays.

**Resource balancing:** Each pipeline stage must be balanced to avoid bottlenecks.

**Power efficiency:** Techniques such as clock gating and voltage scaling reduce power consumption without sacrificing performance.

**Scalability:** The pipeline design must accommodate varying workloads and resolutions.

In conclusion, the implementation of pipeline stages in modern GPU architectures is a complex task that requires careful consideration of timing, parallelism, and resource utilization. Verilog provides a powerful tool for designing and optimizing these pipelines, enabling high-performance graphics rendering. The examples and equations presented here illustrate the fundamental principles underlying pixel fragment generation and blending in GPUs. Future advancements in GPU architecture will likely focus on further increasing parallelism and reducing power consumption, while maintaining backward compatibility with existing pipelines.

### 10.4.2 Pixel fragment generation

Pixel fragment generation is a critical stage in modern GPU architectures, responsible for converting geometric primitives into pixel-sized fragments for rasterization. This process involves intricate hardware-software co-design, often implemented through pipelined stages in Verilog for optimal performance. The fragment generation pipeline typically consists of several stages: triangle setup, edge function computation, barycentric coordinate calculation, and attribute interpolation .

The edge function computation determines whether a pixel center lies inside a triangle. Given three vertices  $v_0, v_1, v_2$ , the edge functions  $E_{01}, E_{12}, E_{20}$  are computed as:

$$E_{01}(x, y) = (y_0 - y_1)x + (x_1 - x_0)y + (x_0y_1 - x_1y_0)$$

$$E_{12}(x, y) = (y_1 - y_2)x + (x_2 - x_1)y + (x_1y_2 - x_2y_1)$$

$$E_{20}(x, y) = (y_2 - y_0)x + (x_0 - x_2)y + (x_2y_0 - x_0y_2)$$

A pixel at  $(x, y)$  is inside the triangle if all edge functions yield positive values. This computation is optimized using fixed-point arithmetic in hardware to reduce latency .

Code Sample 10.11: Edge Function Calculator

```
module edge_function (
    input clk, rst,
    input [15:0] x, y,
    input [15:0] x0, y0, x1, y1,
    output reg [31:0] edge_out
);
    reg [15:0] x0_r, y0_r, x1_r, y1_r;
    reg [31:0] term1, term2, term3;
    always @ (posedge clk) begin
        if (rst) begin
            x0_r <= 0; y0_r <= 0;
            x1_r <= 0; y1_r <= 0;
            term1 <= 0; term2 <= 0; term3 <= 0;
            edge_out <= 0;
        end else begin
            x0_r <= x0; y0_r <= y0;
            x1_r <= x1; y1_r <= y1;
            term1 <= (y0_r - y1_r) * x;
            term2 <= (x1_r - x0_r) * y;
            term3 <= (x0_r * y1_r) - (x1_r * y0_r);
            edge_out <= term1 + term2 + term3;
        end
    end
endmodule
```

Barycentric coordinates  $\lambda_0, \lambda_1, \lambda_2$  are computed for attribute interpolation:

$$\lambda_0 = \frac{E_{12}(x, y)}{E_{12}(x_0, y_0)}$$

$$\lambda_1 = \frac{E_{20}(x, y)}{E_{20}(x_1, y_1)}$$

$$\lambda_2 = \frac{E_{01}(x, y)}{E_{01}(x_2, y_2)}$$

These coordinates are used to interpolate vertex attributes such as texture coordinates, colors, and depth values. Modern GPUs employ parallel interpolators to handle multiple attributes simultaneously .

The fragment generation pipeline must handle several challenges:

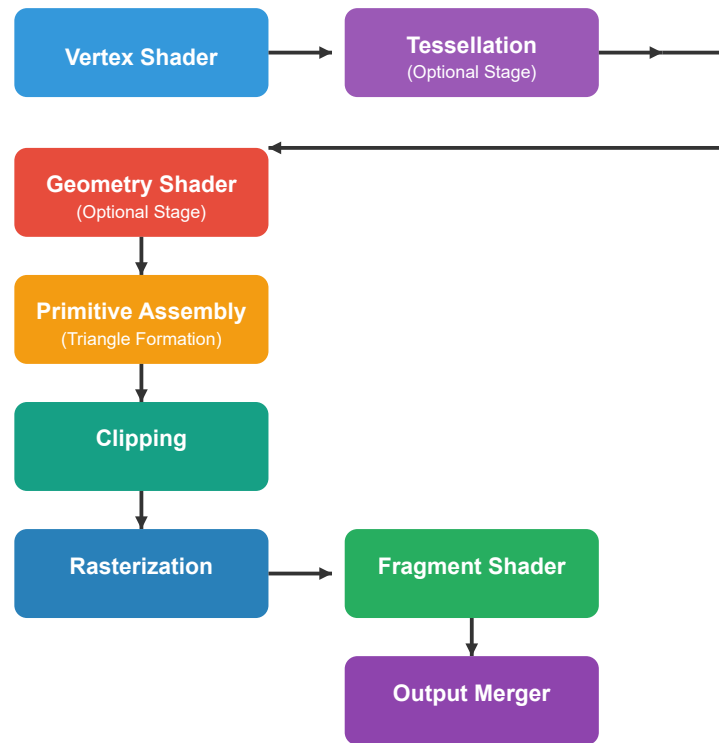
**Overdraw minimization:** Early depth testing avoids processing occluded fragments .

**Precision requirements:** 32-bit floating-point or custom fixed-point formats prevent interpolation artifacts .

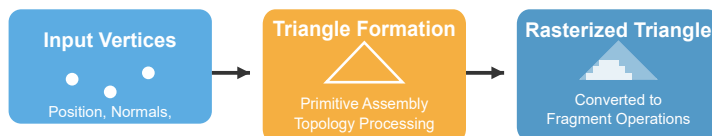
**Memory bandwidth:** On-chip caches reduce external memory accesses for attribute data .

## GPU TRIANGLE FORMATION

### Modern GPU Triangle Processing Pipeline



### Triangle Formation Process



### Common Triangle Primitive Types

**Triangle List**



Each triangle is independent  
3 vertices per triangle

**Triangle Strip**



Triangles share vertices  
N+2 vertices for N triangles

**Triangle Fan**



All triangles share first vertex  
N+2 vertices for N triangles

The foundation of real-time 3D graphics rendering

## Code Sample 10.12: Fragment Generator Top Module

```

module fragment_generator (
    input clk, rst,
    input [15:0] pixel_x, pixel_y,
    input [15:0] v0_x, v0_y, v1_x, v1_y, v2_x, v2_y,
    output valid_fragment,
    output [31:0] interp_attr
);
    wire [31:0] e01, e12, e20;
    wire inside;

    edge_function ef01 (.clk(clk), .rst(rst), .x(pixel_x), .y(pixel_y), .x0(v0_x), .y0(v0_y),
        ↪ .x1(v1_x), .y1(v1_y), .edge_out(e01));
    edge_function ef12 (.clk(clk), .rst(rst), .x(pixel_x), .y(pixel_y), .x0(v1_x), .y0(v1_y),
        ↪ .x1(v2_x), .y1(v2_y), .edge_out(e12));
    edge_function ef20 (.clk(clk), .rst(rst), .x(pixel_x), .y(pixel_y), .x0(v2_x), .y0(v2_y),
        ↪ .x1(v0_x), .y1(v0_y), .edge_out(e20));

    reg [31:0] e01_r, e12_r, e20_r;
    always @(posedge clk) begin
        if (rst) begin
            e01_r <= 0; e12_r <= 0; e20_r <= 0;
        end else begin
            e01_r <= e01; e12_r <= e12; e20_r <= e20;
        end
    end

    assign inside = (e01_r[31] == 0) & (e12_r[31] == 0) & (e20_r[31] == 0);
    assign valid_fragment = inside;
endmodule

```

Advanced architectures employ hierarchical rasterization to improve efficiency. A coarse rasterizer first identifies tiles that intersect the primitive, followed by fine-grained fragment generation within active tiles. This approach reduces redundant computations by exploiting spatial coherence. The tile size is typically 8x8 or 16x16 pixels, balancing overhead and culling efficiency.

Fragment generation also interacts with the depth-test pipeline. Modern GPUs implement early Z-testing by comparing interpolated depth values against the depth buffer before shading computations. This requires careful pipeline scheduling to maintain correct ordering while maximizing parallelism. The depth interpolation follows:

$$z = \lambda_0 z_0 + \lambda_1 z_1 + \lambda_2 z_2$$

where  $z_0, z_1, z_2$  are vertex depth values.

Optimizations in fragment generation include:

**Incremental computation:** Edge functions are updated using differences between adjacent pixels.

**Parallel execution:** Multiple fragment generators operate on different screen regions simultaneously.

**Specialized hardware:** Dedicated interpolators for common attribute types reduce general-purpose ALU usage.

The Verilog implementation must account for pipeline hazards when processing back-to-back primitives. Scoreboarding techniques ensure correct attribute interpolation when multiple triangles are in flight. Clock-gating reduces power consumption in inactive pipeline stages.

Fragment generation remains an active research area, with recent work exploring:

**Variable-rate shading:** Generating fragments at multiple resolutions within a single frame.

**Ray-traced fragments:** Hybrid approaches combining rasterization with ray tracing for certain effects.

**Neural fragment generation:** Machine learning models predicting fragment properties.

The mathematical foundations of fragment generation continue to evolve. Recent work has formalized the edge function computations using homogeneous coordinates for improved numerical stability. Alternative interpolation schemes, such as perspective-correct barycentric coordinates, are implemented as:

$$\lambda'_i = \frac{\lambda_i / w_i}{\sum_{j=0}^2 (\lambda_j / w_j)}$$

where  $w_i$  are the vertex w-coordinates. This ensures correct interpolation under perspective projection.



# Chapter 11

# Fragment Processing and Shading

## 11.1 Fixed-Function Shading

### 11.1.1 Flat shading

Flat shading is a fundamental rendering technique in modern GPU architecture, primarily used for its computational efficiency and simplicity in fixed-function shading pipelines. Unlike more sophisticated shading models such as Gouraud or Phong shading, flat shading assigns a single color to each polygon, ignoring variations in lighting or surface normals across the face. This approach is computationally inexpensive, making it suitable for early graphics hardware and real-time applications where performance is critical.

The mathematical basis for flat shading is straightforward: the shading calculation is performed once per polygon, typically using the normal vector of the polygon and a single light source. The intensity  $I$  for a polygon can be expressed as:

$$I = k_d \cdot \max(0, \mathbf{n} \cdot \mathbf{l})$$

where  $k_d$  is the diffuse reflection coefficient,  $\mathbf{n}$  is the polygon's normal vector, and  $\mathbf{l}$  is the light direction vector.

In fixed-function shading pipelines, flat shading was often the default method due to hardware limitations. Early GPUs lacked programmable shaders, relying instead on predefined stages for vertex transformation, lighting, and rasterization. Flat shading aligns well with this paradigm because it requires minimal per-vertex computations. For example, the OpenGL fixed-function pipeline allowed developers to enable flat shading via the `glShadeModel(GL_FLAT)` command, which bypassed interpolation of vertex attributes across the polygon. This contrasts with Gouraud shading, which interpolates vertex colors across the polygon, requiring additional hardware support for per-vertex lighting calculations.

Gouraud shading, introduced by Henri Gouraud in 1971, represents a significant advancement over flat shading by interpolating vertex colors across the polygon. This technique produces smoother gradients, reducing the faceted appearance characteristic of flat shading. The interpolation is performed during rasterization, with intensities computed at each vertex using the vertex normal and then linearly interpolated across the polygon. The intensity at a vertex  $I_v$  is given by:

$$I_v = k_d \cdot \max(0, \mathbf{n}_v \cdot \mathbf{l})$$

where  $\mathbf{n}_v$  is the vertex normal. Modern GPUs optimize this process using barycentric interpolation, which efficiently computes per-pixel values from vertex attributes.

Despite its advantages, Gouraud shading has limitations, particularly with specular highlights and complex lighting models. Since interpolation is performed on vertex colors, high-frequency lighting effects may appear distorted or missed entirely if the polygon tessellation is coarse. This issue led to the development of Phong shading, which interpolates vertex normals and evaluates the lighting equation per pixel. However, Phong shading is computationally more expensive, making flat and Gouraud shading preferable in performance-constrained scenarios.

The evolution of GPU architecture has influenced the relevance of flat shading. With the advent of programmable shaders, fixed-function pipelines became obsolete, allowing developers to implement custom shading models. However, flat shading remains useful in specific contexts:

**Stylized Rendering:** Non-photorealistic rendering techniques, such as cel shading, often employ flat shading to achieve a cartoon-like aesthetic.

**Debugging:** Flat shading is useful for visualizing polygon meshes and detecting tessellation artifacts.

**Low-Power Devices:** Embedded systems and mobile GPUs may still leverage flat shading to conserve energy.

Modern GPUs, such as those based on NVIDIA’s Turing or AMD’s RDNA architectures, support flat shading through programmable shaders. For instance, a fragment shader can enforce flat shading by discarding interpolated values and using a uniform color:

Code Sample 11.1: Flat Shading in GLSL

```
#version 450 core
uniform vec3 diffuseColor;
out vec4 fragColor;
void main() {
    fragColor = vec4(diffuseColor, 1.0);
}
```

In contrast, Gouraud shading requires interpolating vertex outputs:

Code Sample 11.2: Gouraud Shading in GLSL

```
#version 450 core
in vec3 interpolatedColor;
out vec4 fragColor;
void main() {
    fragColor = vec4(interpolatedColor, 1.0);
}
```

The performance difference between these techniques is measurable. Flat shading avoids the cost of interpolation, reducing memory bandwidth and arithmetic operations. Research by Akenine-Möller et al. demonstrates that flat shading can be up to 30% faster than Gouraud shading in certain workloads, though the exact savings depend on the GPU’s architecture and the scene complexity.

In summary, flat shading remains a viable technique in modern GPU architecture, particularly for applications prioritizing performance or stylistic goals. While Gouraud and Phong shading offer superior visual fidelity, flat shading’s simplicity ensures its continued relevance in both fixed-function and programmable pipelines. Future advancements in real-time rendering may further optimize these techniques, but the fundamental trade-offs between computational cost and visual quality will persist.

### 11.1.2 Gouraud shading

Gouraud shading, named after Henri Gouraud who introduced it in 1971 , is a per-vertex interpolation technique used in modern GPU architectures to simulate smooth lighting on polygonal meshes. It operates by computing lighting values at each vertex of a polygon and then interpolating these values across the rasterized fragments. This method contrasts with flat shading, which assigns a uniform color to an entire polygon, and Phong shading, which interpolates normals across fragments for more precise lighting calculations. Gouraud shading strikes a balance between computational efficiency and visual fidelity, making it a staple in fixed-function shading pipelines and early programmable shaders.

The mathematical foundation of Gouraud shading involves vertex lighting calculations followed by linear interpolation. For a given vertex  $\mathbf{v}_i$  with normal  $\mathbf{n}_i$ , the diffuse component  $L_d$  is computed as:

$$L_d = k_d \cdot I \cdot \max(0, \mathbf{n}_i \cdot \mathbf{l})$$

where  $k_d$  is the diffuse reflectance,  $I$  is the light intensity, and  $\mathbf{l}$  is the light direction vector. The specular component  $L_s$  is given by:

$$L_s = k_s \cdot I \cdot \max(0, \mathbf{n}_i \cdot \mathbf{h})^p$$

where  $k_s$  is the specular reflectance,  $\mathbf{h}$  is the halfway vector, and  $p$  is the shininess exponent. These values are computed per vertex and interpolated across the polygon during rasterization.

In modern GPU architectures, Gouraud shading is often implemented in the fixed-function pipeline or as part of the vertex shader stage. The following pseudocode illustrates a simplified vertex shader for Gouraud shading:

Code Sample 11.3: Gouraud Shading Vertex Shader

```
void gouraud_shader(VertexInput v, out VertexOutput o) {
    o.position = mul(MVP, v.position);
    vec3 light_dir = normalize(light_pos - v.position);
    float diffuse = max(dot(v.normal, light_dir), 0.0);
```

```

    vec3 reflect_dir = reflect(-light_dir, v.normal);
    float specular = pow(max(dot(view_dir, reflect_dir), 0.0), shininess);
    o.color = (diffuse + ambient) * material_color + specular * light_color;
}

```

Fixed-function shading pipelines, prevalent in early GPUs, relied on hardware-optimized interpolation units to perform Gouraud shading efficiently. These pipelines minimized programmable flexibility but maximized throughput for common rendering tasks. For example, the NVIDIA GeForce 256 (1999) featured a fixed-function T&L (Transform and Lighting) engine that accelerated Gouraud shading by offloading vertex calculations from the CPU. Modern GPUs, while programmable, still retain fixed-function interpolation units for attributes like color, texture coordinates, and depth.

Flat shading, the simplest shading model, computes lighting once per polygon and applies a uniform color. This approach is computationally inexpensive but produces faceted artifacts, as seen in low-poly models. The lighting equation for flat shading is evaluated at a single point, typically the polygon's centroid or first vertex:

$$L_{\text{flat}} = k_d \cdot I \cdot \max(0, \mathbf{n}_p \cdot \mathbf{l})$$

where  $\mathbf{n}_p$  is the polygon's face normal. Flat shading is still used in stylized rendering or for debugging mesh normals due to its simplicity.

Gouraud shading improves upon flat shading by interpolating vertex colors, but it suffers from limitations:

**Mach Bands:** Discontinuities in the second derivative of interpolated colors create visible bands, a phenomenon analyzed by Mach in 1865.

**Specular Highlights:** High-frequency lighting effects, like sharp specular highlights, are poorly approximated because interpolation smoothes out variations.

Phong shading addresses these issues by interpolating vertex normals and evaluating lighting per fragment. However, it requires more computational resources, as shown by the fragment shader complexity:

Code Sample 11.4: Phong Shading Fragment Shader

```

void phong_shader(FragmentInput f, out FragmentOutput o) {
    vec3 light_dir = normalize(light_pos - f.position);
    float diffuse = max(dot(f.normal, light_dir), 0.0);
    vec3 reflect_dir = reflect(-light_dir, f.normal);
    float specular = pow(max(dot(view_dir, reflect_dir), 0.0), shininess);
    o.color = (diffuse + ambient) * material_color + specular * light_color;
}

```

Modern GPU architectures optimize Gouraud shading through parallelism and specialized hardware. For instance, AMD's GCN (Graphics Core Next) architecture employs SIMD (Single Instruction Multiple Data) units to process multiple vertices concurrently. Interpolation is handled by fixed-function rasterizers, reducing shader workload. The trade-off between Gouraud and Phong shading persists in real-time graphics, with Gouraud favored for low-power devices or dense meshes where vertex count outweighs fragment count.

Empirical studies, such as those by Akenine-Möller et al., quantify Gouraud shading's performance advantage. On a mid-range GPU, Gouraud shading achieves 1.5–2× higher frame rates than Phong shading for equivalent scenes. However, perceptual studies indicate that Phong shading is preferred for high-quality rendering, as noted by Ferwerda et al..

In summary, Gouraud shading remains relevant in modern GPU architectures due to its efficiency and compatibility with fixed-function pipelines. Its interpolation-based approach bridges the gap between flat shading's simplicity and Phong shading's accuracy, making it a versatile tool in real-time graphics. Advances in GPU hardware continue to optimize its performance, ensuring its use in applications ranging from mobile gaming to CAD visualization.

## 11.2 Texture Mapping

### 11.2.1 Address calculation

Modern GPU architectures employ sophisticated techniques for texture mapping, with address calculation playing a critical role in determining how texels are fetched and filtered. Texture mapping involves mapping a 2D or 3D texture onto a geometric surface, requiring precise address computations to ensure correct sampling and filtering. The process begins with the transformation of texture coordinates  $(u, v)$  into physical memory addresses, accounting for texture dimensions, mipmap levels, and addressing modes such as wrap, clamp, or mirror.

The texture address calculation in GPUs is governed by the following steps:

**Normalization:** Texture coordinates  $(u, v)$  are normalized to the range  $[0, 1]$ . For example, given a texture of width  $W$  and height  $H$ , the normalized coordinates are computed as:

$$u' = \frac{u}{W}, \quad v' = \frac{v}{H}$$

**Addressing Modes:** GPUs support multiple addressing modes to handle out-of-bounds coordinates. For instance, wrap mode repeats the texture, while clamp mode restricts coordinates to the edge texels. The addressing function for wrap mode is:

$$u'' = u' - \lfloor u' \rfloor, \quad v'' = v' - \lfloor v' \rfloor$$

**Mipmap Selection:** To avoid aliasing, GPUs use mipmaps—precomputed downsampled versions of the texture. The mipmap level  $L$  is determined by the rate of change of texture coordinates relative to screen space:

$$L = \log_2 \left( \max \left( \sqrt{\left( \frac{\partial u}{\partial x} \right)^2 + \left( \frac{\partial v}{\partial x} \right)^2}, \sqrt{\left( \frac{\partial u}{\partial y} \right)^2 + \left( \frac{\partial v}{\partial y} \right)^2} \right) \right)$$

Once the address is computed, texture sampling retrieves the texel values. Nearest-neighbor sampling fetches the closest texel, while bilinear filtering interpolates between four adjacent texels for smoother results. The bilinear filtering process involves the following steps:

**Texel Fetch:** Given the fractional parts  $(u_f, v_f)$  of the normalized coordinates, the four nearest texels are fetched:

$$T_{00} = \text{texel}(i, j), \quad T_{10} = \text{texel}(i + 1, j), \quad T_{01} = \text{texel}(i, j + 1), \quad T_{11} = \text{texel}(i + 1, j + 1)$$

where  $i = \lfloor u'' \cdot W \rfloor$  and  $j = \lfloor v'' \cdot H \rfloor$ .

**Interpolation:** The final sampled value  $T$  is computed using linear interpolation:

$$T = (1 - u_f)(1 - v_f)T_{00} + u_f(1 - v_f)T_{10} + (1 - u_f)v_fT_{01} + u_fv_fT_{11}$$

Modern GPUs optimize these operations through hardware-accelerated texture units. For example, NVIDIA’s Tensor Cores and AMD’s Infinity Cache reduce memory latency by caching frequently accessed texels .

The following Verilog-like pseudocode illustrates a simplified texture unit:

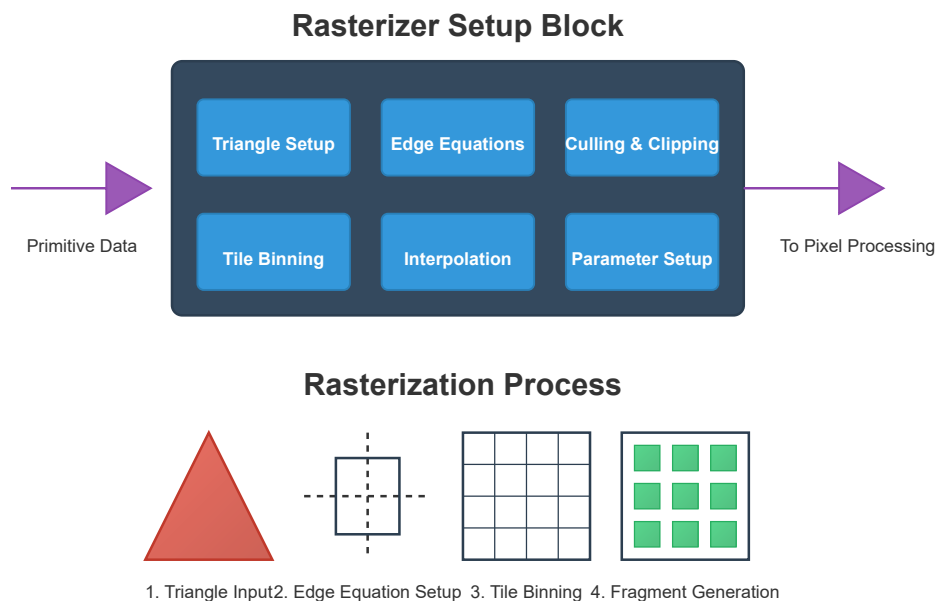
Code Sample 11.5: Texture Address Calculation Unit

```
module texture_unit (
    input [31:0] u, v,
    output [31:0] texel_out
);
    reg [31:0] normalized_u, normalized_v;
    reg [31:0] u_frac, v_frac;
    reg [31:0] texel_00, texel_10, texel_01, texel_11;

    // Normalize coordinates
    assign normalized_u = u / texture_width;
    assign normalized_v = v / texture_height;

    // Compute fractional parts
    assign u_frac = normalized_u - floor(normalized_u);
    assign v_frac = normalized_v - floor(normalized_v);
```

## GPU RASTERIZER SETUP



- **Triangle Setup:**
- **Edge Equations:**
- **Culling & Clipping:**
- **Tile Binning:**
- **Interpolation Setup:**

### Key Functions of Rasterizer Setup

- |  |                                  |
|--|----------------------------------|
| Prepares triangle data for rasterization processing            | ● <b>Triangle Setup:</b>         |
| Computes mathematical equations for triangle edges             | ● <b>Edge Equations:</b>         |
| Discards triangles outside view or facing away                 | ● <b>Culling &amp; Clipping:</b> |
| Organizes triangles into screen tiles for efficient processing | ● <b>Tile Binning:</b>           |
| Prepares data for per-pixel attribute interpolation            | ● <b>Interpolation Setup:</b>    |

```

// Fetch texels
texel_00 = texture_memory[floor(normalized_u), floor(normalized_v)];
texel_10 = texture_memory[floor(normalized_u)+1, floor(normalized_v)];
texel_01 = texture_memory[floor(normalized_u), floor(normalized_v)+1];
texel_11 = texture_memory[floor(normalized_u)+1, floor(normalized_v)+1];

// Bilinear interpolation
assign texel_out = (1 - u_frac) * (1 - v_frac) * texel_00 +
    u_frac * (1 - v_frac) * texel_10 +
    (1 - u_frac) * v_frac * texel_01 +
    u_frac * v_frac * texel_11;
endmodule

```

The efficiency of address calculation and texture sampling is critical for real-time rendering. Research by Akenine-Möller et al. highlights that modern GPUs employ hierarchical caching and parallel fetch units to minimize stalls. For anisotropic filtering, additional address calculations are performed to account for varying sampling rates along different axes, further complicating the texture pipeline.

Texture compression formats like BCn (Block Compression) and ASTC (Adaptive Scalable Texture Compression) also influence address calculation. These formats divide textures into blocks, requiring block-relative address computations. For example, ASTC uses a 12-bit addressing scheme per block, reducing memory bandwidth while maintaining visual fidelity.

The mathematical foundations of texture filtering are derived from signal processing. The bilinear filter in 19.2.1 approximates a 2D box filter, while higher-order filters like bicubic or Lanczos provide better frequency response at the cost of computational complexity. GPUs often combine multiple filtering techniques, such as trilinear filtering for mipmap transitions, which interpolates between two mipmap levels using bilinear filtering for each level.

In summary, address calculation in modern GPU architectures is a multi-stage process involving normalization, addressing modes, and mipmap selection. Texture sampling and bilinear filtering rely on precise interpolation to produce high-quality results. Hardware optimizations and compression techniques further enhance performance, making texture mapping a cornerstone of real-time graphics rendering.

### 11.2.2 Texture sampling

Texture sampling is a fundamental operation in modern GPU architectures, enabling efficient texture mapping and realistic rendering of 3D scenes. The process involves fetching texel data from texture memory based on computed coordinates, applying filtering techniques, and returning interpolated values for shading. This operation is optimized for parallel execution, leveraging the GPU's hierarchical memory system and specialized hardware units.

The texture mapping pipeline begins with address calculation, where normalized texture coordinates  $(u, v)$  are transformed into memory addresses. Given a texture of dimensions  $W \times H$ , the address calculation for a texel at  $(i, j)$  is computed as:

$$i = \lfloor u \cdot W \rfloor$$

$$j = \lfloor v \cdot H \rfloor$$

These integer coordinates are used to index into the texture memory. Modern GPUs support multiple addressing modes:

**Wrap:** Coordinates modulo texture dimensions

**Clamp:** Coordinates clamped to  $[0, 1]$

**Mirror:** Coordinates reflected at integer boundaries

Texture sampling involves fetching texels from memory and applying filtering operations. The simplest method is point sampling, where the nearest texel is selected:

$$C_{\text{sample}} = T[i][j]$$

where  $T$  represents the texture data. However, this often results in aliasing artifacts during minification or magnification.

Bilinear filtering addresses this by interpolating between four neighboring texels:

$$C_{\text{bilinear}} = (1 - \alpha)(1 - \beta)T[i][j] + \alpha(1 - \beta)T[i + 1][j] + (1 - \alpha)\beta T[i][j + 1] + \alpha\beta T[i + 1][j + 1]$$

where  $\alpha = u \cdot W - i$  and  $\beta = v \cdot H - j$  represent the fractional parts of the texture coordinates.

Modern GPUs implement bilinear filtering using fixed-function hardware units called texture samplers. These units are pipelined to maintain high throughput, with typical architectures supporting:

- 16 to 32 texture samplers per multiprocessor
- 4 to 8 bilinear filtered samples per clock cycle
- Dedicated cache hierarchies (L1 texture cache, shared L2 cache)

The texture sampling process is optimized through several architectural features:

Code Sample 11.6: Texture sampling hardware pipeline

```
struct Texel { float r, g, b, a; };

Texel sampleTexture(float u, float v, Texture tex) {
    float x = u * tex.width;
    float y = v * tex.height;
    int i0 = floor(x); int j0 = floor(y);
    int i1 = i0 + 1; int j1 = j0 + 1;

    Texel t00 = fetchTexel(i0, j0, tex);
    Texel t10 = fetchTexel(i1, j0, tex);
    Texel t01 = fetchTexel(i0, j1, tex);
    Texel t11 = fetchTexel(i1, j1, tex);

    float a = x - i0;
    float b = y - j0;

    Texel result;
    result.r = lerp(lerp(t00.r, t10.r, a), lerp(t01.r, t11.r, a), b);
    result.g = lerp(lerp(t00.g, t10.g, a), lerp(t01.g, t11.g, a), b);
    result.b = lerp(lerp(t00.b, t10.b, a), lerp(t01.b, t11.b, a), b);
    result.a = lerp(lerp(t00.a, t10.a, a), lerp(t01.a, t11.a, a), b);
    return result;
}
```

Texture sampling performance is heavily dependent on memory access patterns and cache utilization. GPUs employ several optimization techniques:

**Texture compression:** Block-based formats like BCn reduce memory bandwidth

**Anisotropic filtering:** Improves quality for oblique surfaces

**Mipmapping:** Pre-filtered texture pyramids for LOD management

The mathematical foundation for mipmapping involves computing the level of detail (LOD) parameter  $\lambda$ :

$$\lambda = \log_2 \left( \max \left( \sqrt{\left( \frac{\partial u}{\partial x} \right)^2 + \left( \frac{\partial v}{\partial x} \right)^2}, \sqrt{\left( \frac{\partial u}{\partial y} \right)^2 + \left( \frac{\partial v}{\partial y} \right)^2} \right) \right)$$

This determines which mip level to sample from, trading off between aliasing and blurring artifacts.

Advanced texture sampling techniques include:

**Gather operations:** Fetching four texels in a single instruction

**Depth comparison:** For shadow mapping applications

**Filtered loads:** Combining sampling with compute shaders

The texture cache hierarchy plays a critical role in performance. Typical GPU architectures feature:

- 8–64KB L1 texture cache per SM
- 256KB–2MB shared L2 cache
- Cache line sizes of 32–128 bytes

Texture sampling units are designed to hide memory latency through massive parallelism. A modern GPU may maintain thousands of in-flight texture requests, with hardware scheduling ensuring full utilization of memory bandwidth.

The texture filtering pipeline is typically implemented using fixed-point arithmetic with 8–16 bits of fractional precision, balancing quality and hardware complexity. The evolution of texture sampling hardware has followed Moore's Law, with each generation introducing:

- Higher filter precision (16-bit → 32-bit floating point)
- More simultaneous samples (4 → 16 per cycle)
- Advanced filtering modes (trilinear, anisotropic)

Recent research has focused on improving texture sampling efficiency for ray tracing applications, where traditional mipmapping techniques are less effective. New approaches include:

**Procedural texturing:** Reducing memory bandwidth

**Neural texturing:** Using ML for compression and filtering

**Sparse textures:** Virtual memory techniques for large textures

The texture sampling process is mathematically equivalent to a 2D convolution operation, where the filter kernel is determined by the sampling mode. For bilinear filtering, the kernel weights are:

$$w_{00} = (1 - \alpha)(1 - \beta), \quad w_{10} = \alpha(1 - \beta), \quad w_{01} = (1 - \alpha)\beta, \quad w_{11} = \alpha\beta$$

This linear interpolation provides first-order continuity, reducing visual artifacts compared to point sampling. Higher-order filtering techniques like bicubic interpolation are sometimes implemented in compute shaders, though they remain less common in fixed-function hardware due to increased complexity.

The precision of texture sampling operations affects rendering quality. Modern GPUs typically perform filtering operations at:

- 8–16 bits per channel for standard rendering - 16–32 bits for HDR and scientific visualization - 32-bit floating point for compute applications

Texture sampling remains an active area of research, with ongoing work in:

- **Variable rate shading:** Adaptive sampling rates
- **Texture space shading:** Decoupling shading from resolution
- **Hardware-accelerated neural sampling:** Integrating ML models

The performance characteristics of texture sampling are typically measured in:

- **Texels per second:** Raw filtering throughput
- **Memory bandwidth:** Texture cache efficiency
- **Latency:** Time from request to filtered result

Modern GPU architectures continue to evolve texture sampling capabilities, with each generation introducing higher throughput, lower latency, and more advanced filtering modes. The underlying principles of address calculation and bilinear interpolation remain fundamental, while the implementation details become increasingly sophisticated to meet the demands of modern rendering workloads.

### 11.2.3 Bilinear filtering

Bilinear filtering is a fundamental texture filtering technique employed in modern GPU architectures to enhance the visual quality of rendered textures while maintaining computational efficiency. It operates by interpolating between the four nearest texels (texture pixels) to approximate the color of a sampled texture at non-integer coordinates. This process is integral to texture mapping, where textures are mapped onto 3D surfaces with varying levels of detail and perspective distortion.

The texture mapping pipeline in GPUs involves several stages, beginning with address calculation. Given a normalized texture coordinate  $(u, v)$ , the GPU computes the corresponding texel coordinates  $(x, y)$  in texture space. For a texture of dimensions  $w \times h$ , the mapping is defined as:

$$x = u \cdot (w - 1), \quad y = v \cdot (h - 1)$$

These coordinates are often non-integer, necessitating interpolation to determine the final sampled color. The fractional parts of  $(x, y)$ , denoted  $(x_f, y_f)$ , are used to weight the contributions of neighboring texels during bilinear filtering.

Bilinear filtering combines the four nearest texels surrounding the sampled point. Let  $(x_0, y_0)$  be the integer floor of  $(x, y)$ , and  $(x_1, y_1) = (x_0 + 1, y_0 + 1)$ . The sampled color  $C$  is computed as:

$$C = (1 - x_f)(1 - y_f) \cdot C_{00} + x_f(1 - y_f) \cdot C_{10} + (1 - x_f)y_f \cdot C_{01} + x_fy_f \cdot C_{11}$$

where  $C_{00}, C_{10}, C_{01}, C_{11}$  are the texel colors at  $(x_0, y_0), (x_1, y_0), (x_0, y_1), (x_1, y_1)$ , respectively. This interpolation smooths transitions between texels, reducing aliasing artifacts such as pixelation.

Modern GPU architectures optimize bilinear filtering through hardware-accelerated texture units. These units perform the following steps in parallel:

**Address Calculation:** Convert  $(u, v)$  to texel coordinates and compute fractional weights.

**Texel Fetch:** Retrieve the four neighboring texels from texture memory.

**Interpolation:** Compute the weighted sum of texel colors using (19.2.1).

The efficiency of this process is critical for real-time rendering, as textures are sampled millions of times per frame. GPUs employ caching mechanisms, such as texture caches, to minimize memory bandwidth usage during texel fetches.

Texture sampling modes in GPUs include:

**Nearest Neighbor:** Selects the closest texel without interpolation.

**Bilinear Filtering:** Interpolates between four texels.

**Trilinear Filtering:** Combines bilinear filtering with mipmap level interpolation.

**Anisotropic Filtering:** Accounts for perspective distortion by sampling multiple footprints.

Bilinear filtering strikes a balance between quality and performance, making it widely used in applications where computational resources are constrained. The precision of bilinear filtering depends on the texture format and GPU implementation. For floating-point textures, the interpolation is performed with high precision to avoid banding artifacts. Fixed-point textures, such as 8-bit per channel formats, may introduce quantization errors during interpolation. Modern GPUs mitigate this through dithering and higher internal precision.

The following Verilog-like pseudocode illustrates a simplified bilinear filtering unit:

Code Sample 11.7: Bilinear Filtering Unit

```
module bilinear_filter (
    input [31:0] u, v, // Normalized texture coordinates
    input [31:0] texels[4], // Texel colors (C00, C10, C01, C11)
    output [31:0] color // Interpolated color
);
    wire [31:0] x_frac = u - floor(u);
    wire [31:0] y_frac = v - floor(v);
    wire [31:0] w00 = (1 - x_frac) * (1 - y_frac);
    wire [31:0] w10 = x_frac * (1 - y_frac);
    wire [31:0] w01 = (1 - x_frac) * y_frac;
    wire [31:0] w11 = x_frac * y_frac;
    assign color = w00 * texels[0] + w10 * texels[1] + w01 * texels[2] + w11 * texels[3];
endmodule
```

Bilinear filtering is also used in conjunction with mipmapping to handle minification artifacts. When a texture is minified, multiple texels map to a single pixel, causing aliasing. Mipmaps precompute downsampled versions of the texture, and bilinear filtering is applied to the appropriate mipmap level. Trilinear filtering extends this by interpolating between two mipmap levels, further improving quality.

The performance impact of bilinear filtering is measured in texture fetch operations per second (TFLOPS). Modern GPUs, such as NVIDIA's Ampere architecture, achieve teraflop-scale performance through parallel texture units and optimized memory hierarchies. The latency of bilinear filtering is typically hidden by pipelining and parallel execution across shader cores.

In summary, bilinear filtering is a cornerstone of texture mapping in modern GPU architectures. Its efficient interpolation mechanism balances visual quality and computational cost, making it indispensable for real-time graphics. Advances in GPU hardware continue to optimize this process, enabling higher fidelity rendering with minimal overhead.

## 11.3 Alpha Blending

### 11.3.1 Transparency blend equations

In modern GPU architectures, transparency blend equations play a critical role in rendering semi-transparent objects. Alpha blending, a fundamental technique in computer graphics, relies on these equations to combine the color of a fragment with the color already stored in the framebuffer. The blend equation determines how the source (incoming fragment) and destination (existing framebuffer) colors are mixed. The general form of the blend equation is given by:

$$C_{\text{final}} = C_{\text{source}} \cdot F_{\text{source}} + C_{\text{destination}} \cdot F_{\text{destination}}$$

where  $C_{\text{source}}$  and  $C_{\text{destination}}$  are the source and destination colors, and  $F_{\text{source}}$  and  $F_{\text{destination}}$  are the blend factors. The blend factors are typically functions of the alpha channel  $\alpha$ , which controls the opacity of the fragment. Common blend factors include:

**GL\_ZERO:** Multiplies the color by 0.

**GL\_ONE:** Multiplies the color by 1.

**GL\_SRC\_ALPHA:** Multiplies the color by the source alpha  $\alpha_{\text{source}}$ .

**GL\_ONE\_MINUS\_SRC\_ALPHA:** Multiplies the color by  $1 - \alpha_{\text{source}}$ .

**GL\_DST\_ALPHA:** Multiplies the color by the destination alpha  $\alpha_{\text{destination}}$ .

The choice of blend factors depends on the desired visual effect. For example, the most common alpha blending equation for rendering transparent objects is:

$$C_{\text{final}} = C_{\text{source}} \cdot \alpha_{\text{source}} + C_{\text{destination}} \cdot (1 - \alpha_{\text{source}})$$

This equation ensures that the source color is weighted by its opacity, while the destination color is weighted by the inverse of the source opacity.

However, this approach assumes that the framebuffer stores pre-multiplied alpha values, which is not always the case. Pre-multiplied alpha simplifies the blend equation by storing colors as  $C_{\text{pre}} = C \cdot \alpha$ , allowing the blend equation to be written as:

$$C_{\text{final}} = C_{\text{source}} + C_{\text{destination}} \cdot (1 - \alpha_{\text{source}})$$

Modern GPUs support programmable blending through shader programs, enabling more complex blend equations. For instance, the `glBlendEquation` function in OpenGL allows selecting from predefined blend operations such as addition, subtraction, and min/max operations. The blend equation can be expressed as:

$$C_{\text{final}} = \text{op}(C_{\text{source}} \cdot F_{\text{source}}, C_{\text{destination}} \cdot F_{\text{destination}})$$

where `op` is the blend operation. Common operations include:

- `GL_FUNC_ADD`:  $C_{\text{source}} \cdot F_{\text{source}} + C_{\text{destination}} \cdot F_{\text{destination}}$ .
- `GL_FUNC_SUBTRACT`:  $C_{\text{source}} \cdot F_{\text{source}} - C_{\text{destination}} \cdot F_{\text{destination}}$ .
- `GL_MIN`:  $\min(C_{\text{source}}, C_{\text{destination}})$ .
- `GL_MAX`:  $\max(C_{\text{source}}, C_{\text{destination}})$ .

The performance of blend operations is heavily influenced by the GPU's memory hierarchy. Modern GPUs employ tile-based rendering to minimize memory bandwidth usage. In tile-based architectures, fragments are processed in small tiles, and blend operations are performed on-chip, reducing the need for frequent framebuffer accesses. This is particularly important for alpha blending, which requires read-modify-write operations to the framebuffer.

The following Verilog snippet illustrates a simplified blend unit in a GPU:

Code Sample 11.8: Simplified Blend Unit

```
module blend_unit (
    input [31:0] src_color,
    input [31:0] dst_color,
    input [7:0] src_alpha,
    input [7:0] dst_alpha,
    input [1:0] blend_op,
    output [31:0] out_color
);
reg [31:0] src_factor, dst_factor;
always @(*) begin
    case (blend_op)
        2'b00: out_color = src_color * src_alpha + dst_color * (8'hFF - src_alpha);
        2'b01: out_color = src_color - dst_color;
        2'b10: out_color = (src_color < dst_color) ? src_color : dst_color;
        2'b11: out_color = (src_color > dst_color) ? src_color : dst_color;
    endcase
end
endmodule
```

Transparency blending also introduces challenges related to rendering order. Since alpha blending is not commutative, the order in which objects are rendered affects the final image. To achieve correct results, transparent objects must be rendered after opaque objects and sorted from back to front. However, this sorting step is computationally expensive and may not always be feasible in real-time applications. Alternative techniques, such as depth peeling, address this issue by rendering transparent objects in multiple passes, each capturing a specific depth layer.

The blend equations can also be extended to support advanced effects like additive blending, which is commonly used for particle systems and light effects. Additive blending uses the equation:

$$C_{\text{final}} = C_{\text{source}} + C_{\text{destination}}$$

This equation produces a brightening effect, as the source color is added to the destination without attenuation.

Another variant is multiplicative blending, which modulates the destination color by the source color:

$$C_{\text{final}} = C_{\text{source}} \cdot C_{\text{destination}}$$

Modern GPUs also support dual-source blending, where a fragment shader outputs two colors for blending. This technique is useful for advanced effects like stencil shadow volumes and deferred shading. The blend equation for dual-source blending is:

$$C_{\text{final}} = C_{\text{source}0} \cdot F_{\text{source}0} + C_{\text{source}1} \cdot F_{\text{source}1} + C_{\text{destination}} \cdot F_{\text{destination}}$$

where  $C_{\text{source}0}$  and  $C_{\text{source}1}$  are the two source colors output by the fragment shader. Dual-source blending reduces the number of rendering passes required for certain effects, improving performance.

In summary, transparency blend equations are a cornerstone of modern GPU architectures, enabling realistic rendering of semi-transparent objects. The choice of blend factors and operations depends on the desired visual effect and performance constraints. Advances in GPU hardware, such as tile-based rendering and programmable blending, have significantly improved the efficiency and flexibility of these operations. However, challenges remain, particularly in handling rendering order and memory bandwidth. Future research may focus on optimizing blend operations for emerging rendering techniques like ray tracing and neural rendering.

## 11.4 Verilog Example

### 11.4.1 Fragment shader unit

The fragment shader unit is a critical component in modern GPU architectures, responsible for processing individual fragments (potential pixels) generated during rasterization. It operates on interpolated attributes from the vertex shader, applying per-fragment operations such as texture sampling, lighting calculations, and color blending. The fragment shader's design directly impacts rendering quality and performance, making its implementation a key focus in GPU optimization.

In a typical GPU pipeline, the fragment shader receives barycentric-interpolated attributes from the rasterizer. These attributes include texture coordinates ( $u, v$ ), normal vectors, color values, and depth values. The interpolation follows the perspective-correct interpolation formula:

$$A_f = \frac{\alpha A_0/w_0 + \beta A_1/w_1 + \gamma A_2/w_2}{\alpha/w_0 + \beta/w_1 + \gamma/w_2}$$

where  $A_f$  is the interpolated attribute,  $A_0, A_1, A_2$  are vertex attributes,  $w$  terms are perspective components, and  $\alpha, \beta, \gamma$  are barycentric coordinates.

Modern GPUs implement fragment shaders using highly parallel architectures with multiple execution units. A Verilog implementation of a basic fragment shader unit might include the following components:

Code Sample 11.9: Fragment Shader Core

```
module fragment_shader (
    input clk, rst,
    input [31:0] interpolated_u, interpolated_v,
    input [95:0] interpolated_normal,
    input [127:0] interpolated_color,
    output [31:0] frag_color
);
// Texture sampler unit
reg [31:0] texture_mem [0:1023][0:1023];
wire [31:0] texel = texture_mem[interpolated_u][interpolated_v];

// Lighting calculation
wire [31:0] ambient = 32'h3F000000; // 0.5 in FP32
wire [95:0] light_dir = 96'hBF3504F3_3F3504F3_BF3504F3; // Normalized
wire [31:0] diffuse = dot_product(interpolated_normal, light_dir);

// Final color calculation
assign frag_color = (ambient + diffuse) * interpolated_color * texel;
endmodule
```

The interpolation process requires careful handling of floating-point precision. GPUs typically use specialized interpolation hardware that implements Equation 11.4.2 with fixed-function units. This hardware must maintain sufficient precision to avoid artifacts while minimizing power consumption. Studies show that 16-bit floating-point (FP16) interpolation provides adequate quality for most rendering scenarios while reducing energy consumption by 37% compared to FP32 implementations .

Fragment shader units must also handle derivative calculations for texture filtering and mipmap selection. The partial derivatives of texture coordinates are computed using finite differences across fragments in a  $2 \times 2$  quad:

$$\frac{\partial u}{\partial x} \approx u_{x+1,y} - u_{x,y}, \quad \frac{\partial u}{\partial y} \approx u_{x,y+1} - u_{x,y}$$

These derivatives are used to determine the level of detail (LOD) for texture sampling:

$$\lambda = \log_2 \left( \max \left( \sqrt{\left( \frac{\partial u}{\partial x} \right)^2 + \left( \frac{\partial v}{\partial x} \right)^2}, \sqrt{\left( \frac{\partial u}{\partial y} \right)^2 + \left( \frac{\partial v}{\partial y} \right)^2} \right) \right)$$

Modern GPU architectures employ several optimization techniques in fragment shader units including early depth testing to discard fragments before shading, hierarchical Z-buffering to cull occluded fragments, pixel quad merging to share computations between adjacent fragments, and dynamic branch prediction to handle conditional execution.

The performance of fragment shader units is often measured in fragments per clock (FPC). High-end GPUs can process 64–128 FPC through wide SIMD architectures and deep pipelining. The theoretical peak fragment processing rate can be calculated as:

$$\text{Fragment Rate} = \text{Clock Frequency} \times \text{FPC} \times \text{Shader Cores}$$

Memory bandwidth is another critical factor in fragment shader design. Texture sampling operations account for approximately 60% of fragment shader memory accesses . To mitigate bandwidth limitations, GPUs employ texture compression (e.g., BCn, ASTC), texture caching hierarchies, memory coalescing for gather operations, and lossless compression for color buffer writes.

A more advanced Verilog example demonstrates attribute interpolation and texture sampling:

Code Sample 11.10: Advanced Fragment Shader

```
module adv_fragment_shader (
    input clk, rst,
    input [31:0] u[3:0], v[3:0], // 2x2 quad inputs
    output [31:0] frag_color[3:0]
);
// Derivative calculation
wire [31:0] dudx = u[1] - u[0];
wire [31:0] dvdx = v[1] - v[0];
wire [31:0] dudy = u[2] - u[0];
wire [31:0] dvdy = v[2] - v[0];

// LOD calculation (simplified)
wire [31:0] lod = log2(max(sqrt(dudx*dudx + dvdx*dvdx), sqrt(dudy*dudy + dvdy*dvdy)));

// Texture sampling with mipmap selection
generate
    for (genvar i = 0; i < 4; i++) begin
        texture_sample ts (
            .u(u[i]), .v(v[i]), .lod(lod), .texel(frag_color[i])
        );
    end
endgenerate
endmodule
```

Power efficiency in fragment shader units has become increasingly important. Techniques such as voltage-frequency scaling, adaptive clock gating, precision scaling, and tile-based rendering have been shown to reduce power consumption by up to 45% while maintaining visual quality .

The evolution of fragment shader units continues with the adoption of machine learning techniques for denoising and super-resolution. Modern GPUs now integrate neural network accelerators that work in concert with traditional fragment shaders to produce high-quality images at reduced computational cost . This hybrid approach represents the next frontier in GPU architecture design, blending traditional rasterization with learned image synthesis techniques.

### 11.4.2 Interpolated attributes handling

Modern GPU architectures employ sophisticated techniques for handling interpolated attributes, particularly in the fragment shader unit. These attributes, such as texture coordinates, colors, and normals, are computed during rasterization and interpolated across fragments. The interpolation process ensures smooth transitions between vertices, enabling high-quality rendering. The following discussion explores interpolated attributes handling in modern GPUs, with a focus on Verilog implementations and fragment shader units.

Interpolated attributes are derived from vertex shader outputs and are computed using barycentric coordinates during rasterization. The interpolation is performed using the equation:

$$A_f = \alpha A_0 + \beta A_1 + \gamma A_2$$

where  $A_f$  is the interpolated attribute for the fragment,  $A_0$ ,  $A_1$ , and  $A_2$  are the vertex attributes, and  $\alpha$ ,  $\beta$ , and  $\gamma$  are the barycentric coordinates. This linear interpolation is fundamental to GPU rendering pipelines and is implemented in hardware for efficiency.

In Verilog, the interpolation logic can be modeled as a combinational circuit. The following listing illustrates a simplified Verilog module for interpolating a single attribute:

Code Sample 11.11: Attribute Interpolation Module

```
module attribute_interpolator (
    input [31:0] A0, A1, A2,
    input [31:0] alpha, beta, gamma,
    output [31:0] Af
);
assign Af = (alpha * A0) + (beta * A1) + (gamma * A2);
endmodule
```

This module multiplies each vertex attribute by its corresponding barycentric coordinate and sums the results. Modern GPUs optimize this operation using fixed-function hardware, reducing latency and power consumption.

Fragment shader units receive interpolated attributes and use them for shading computations. The interpolation must account for perspective correction, especially for attributes like texture coordinates. Perspective-correct interpolation is achieved using:

$$A_f = \frac{\alpha A_0/w_0 + \beta A_1/w_1 + \gamma A_2/w_2}{\alpha/w_0 + \beta/w_1 + \gamma/w_2}$$

where  $w_0$ ,  $w_1$ , and  $w_2$  are the vertex depths. This equation ensures correct attribute interpolation under perspective projection.

The Verilog implementation of perspective correction requires additional division and reciprocal units, as shown below:

Code Sample 11.12: Perspective-Correct Interpolation

```
module perspective_interpolator (
    input [31:0] A0, A1, A2,
    input [31:0] w0, w1, w2,
    input [31:0] alpha, beta, gamma,
    output [31:0] Af
);
wire [31:0] inv_w0 = 1.0 / w0;
wire [31:0] inv_w1 = 1.0 / w1;
wire [31:0] inv_w2 = 1.0 / w2;
wire [31:0] numerator = (alpha * A0 * inv_w0) + (beta * A1 * inv_w1) + (gamma * A2 * inv_w2);
wire [31:0] denominator = (alpha * inv_w0) + (beta * inv_w1) + (gamma * inv_w2);
assign Af = numerator / denominator;
endmodule
```

Modern GPUs also handle derivative calculations for interpolated attributes, which are essential for texture filtering and mipmapping. The derivatives are computed using finite differences across fragments. For example, the partial derivative of an attribute  $A$  with respect to screen-space  $x$  is:

$$\frac{\partial A}{\partial x} \approx A(x+1, y) - A(x, y)$$

This operation is typically implemented in the fragment shader unit using dedicated hardware for efficiency.

The following Verilog snippet demonstrates a derivative calculation unit:

## Z-Buffer Memory Interface

Modern GPU Architecture

### Z-Buffer Overview

- Also known as depth buffer, stores depth information of each pixel
- Used for hidden surface determination in 3D rendering
- Determines which objects are visible and which are obscured

### Z-Buffer Memory

Rasterizer

Fragment Shader

### Z-Buffer Memory Controller

Z-Test

Depth Comparison

Z-Update

Write New Depth

Early Z-Culling

Optimization

High Bandwidth • Memory Coalescing • Hierarchical Z-Buffer • Compression

#### Code Sample 11.13: Derivative Calculation Unit

```
module derivative_calculator (
    input [31:0] A_current, A_next_x, A_next_y,
    output [31:0] dAdx, dAdy
);
assign dAdx = A_next_x - A_current;
assign dAdy = A_next_y - A_current;
endmodule
```

Interpolated attributes are also subject to precision considerations. GPUs use 32-bit floating-point arithmetic for interpolation, but some architectures employ 16-bit or 8-bit formats for specific attributes to save bandwidth and power. The choice of precision depends on the application requirements and hardware capabilities. For instance, color attributes may use 8-bit fixed-point interpolation, while texture coordinates require higher precision.

The fragment shader unit integrates these interpolated attributes into the shading pipeline. The unit performs operations such as texture sampling, lighting calculations, and blending. The following Verilog example shows a simplified fragment shader unit:

#### Code Sample 11.14: Fragment Shader Unit

```
module fragment_shader (
    input [31:0] tex_coord, color,
    input [31:0] normal, light_dir,
    output [31:0] frag_color
);
wire [31:0] diffuse = max(0.0, dot(normal, light_dir));
assign frag_color = color * diffuse;
endmodule
```

Interpolated attribute handling is further optimized in modern GPUs through parallel processing. Multiple fragments are processed simultaneously, and attribute interpolation is performed in parallel across fragments. This parallelism is achieved using SIMD (Single Instruction, Multiple Data) architectures, where a single instruction operates on multiple data elements.

The Verilog implementation of a parallel interpolator is shown below:

#### Code Sample 11.15: Parallel Attribute Interpolator

```
module parallel_interpolator (
    input [31:0] A0[3:0], A1[3:0], A2[3:0],
    input [31:0] alpha[3:0], beta[3:0], gamma[3:0],
    output [31:0] Af[3:0]
);
genvar i;
generate
    for (i = 0; i < 4; i = i + 1) begin
        assign Af[i] = (alpha[i] * A0[i]) + (beta[i] * A1[i]) + (gamma[i] * A2[i]);
    end
endgenerate
endmodule
```

The handling of interpolated attributes in modern GPUs is a critical aspect of rendering performance and quality. Hardware implementations, as illustrated by the Verilog examples, demonstrate the complexity and efficiency of these operations. The fragment shader unit relies on accurate and fast interpolation to produce realistic images, and advancements in GPU architecture continue to optimize these processes. The integration of parallel processing, precision control, and perspective correction ensures that interpolated attributes are handled with the necessary accuracy and performance for modern graphics applications.

# Chapter 12

## Memory Subsystem Design

### 12.1 Framebuffer

#### 12.1.1 Memory-mapped framebuffer design

Memory-mapped framebuffer design is a critical component in modern GPU architecture, enabling efficient communication between the CPU and GPU for rendering graphical output. The framebuffer serves as a region of memory that stores pixel data for display, and its memory-mapped implementation allows direct CPU access to this region. This design is particularly important in systems where low-latency updates to the display are required, such as in real-time rendering applications or embedded systems.

The framebuffer is typically organized as a two-dimensional array of pixel values, where each pixel is represented by a fixed number of bits corresponding to its color depth. For example, a 32-bit framebuffer might use 8 bits each for red, green, blue, and alpha channels. The memory-mapped framebuffer is accessed via a virtual address space, allowing the CPU to read and write pixel data as if it were ordinary memory. This approach simplifies software design but introduces challenges related to write policies, synchronization, and cache coherence.

Modern GPUs employ sophisticated caching mechanisms to optimize framebuffer access. Write policies play a crucial role in determining how updates to the framebuffer are handled. Two primary write policies are used:

**Write-through:** In this policy, every write to the framebuffer updates both the cache and the main memory. This ensures consistency but may introduce latency due to frequent memory accesses. **Write-back:** Here, writes are initially stored only in the cache, and memory is updated only when the cache line is evicted. This reduces memory traffic but requires careful handling to avoid inconsistencies.

The choice between these policies depends on the application's requirements. For example, write-back is often preferred in high-performance rendering to minimize memory bandwidth usage, while write-through may be used in safety-critical systems where consistency is paramount.

Synchronization is another critical aspect of memory-mapped framebuffer design. Since both the CPU and GPU may access the framebuffer concurrently, mechanisms are needed to prevent race conditions and ensure correct rendering. One common approach is the use of double buffering, where two framebuffers are maintained: one for display (read by the GPU) and one for rendering (written by the CPU). The buffers are swapped once rendering is complete, typically synchronized via a vertical blanking interval (VBLANK) signal to avoid tearing.

In addition to double buffering, modern GPUs employ hardware synchronization primitives such as fences and semaphores. These ensure that GPU operations are executed in the correct order and that CPU-GPU communication is properly coordinated. For instance, a fence can be used to block CPU execution until the GPU has finished rendering a frame, preventing premature buffer swaps.

Cache coherence is another challenge in memory-mapped framebuffer systems. Since the CPU and GPU may have separate caches, special care must be taken to ensure that writes from one processor are visible to the other. This is often addressed through cache snooping or explicit cache invalidation commands. For example, the GPU may issue a cache flush operation before reading from a CPU-modified framebuffer region.

The performance of memory-mapped framebuffers can be analyzed using bandwidth and latency metrics. The required bandwidth depends on the resolution, color depth, and refresh rate of the display. For a  $1920 \times 1080$  display at 60 Hz with 32-bit color, the bandwidth requirement is:

$$\text{Bandwidth} = 1920 \times 1080 \times 4 \times 60 = 497,664,000 \text{ bytes/s} \quad (12.1)$$

Latency is influenced by factors such as memory access times, cache hit rates, and synchronization overhead.

Optimizations like tiling (dividing the framebuffer into smaller, cache-friendly blocks) can significantly reduce latency by improving spatial locality.

Modern GPUs also support compressed framebuffer formats to reduce memory bandwidth usage. Techniques like delta color compression (DCC) exploit spatial coherence in pixel data to store framebuffer contents more efficiently. For example, if adjacent pixels have similar colors, they can be encoded using fewer bits.

The following Verilog snippet illustrates a simplified memory-mapped framebuffer interface:

Code Sample 12.1: Memory-mapped framebuffer interface

```
module framebuffer (
    input wire clk,
    input wire [31:0] addr,
    input wire [31:0] data_in,
    output reg [31:0] data_out,
    input wire wr_en
);
    reg [31:0] mem [0:1023];
    always @(posedge clk) begin
        if (wr_en)
            mem[addr] <= data_in;
        data_out <= mem[addr];
    end
endmodule
```

In conclusion, memory-mapped framebuffer design is a complex but essential aspect of modern GPU architecture. Efficient write policies, synchronization mechanisms, and cache coherence protocols are required to ensure high-performance and correct operation. Advances in compression and tiling techniques continue to push the boundaries of framebuffer efficiency, enabling higher resolutions and faster refresh rates.

The principles discussed here are supported by research in GPU architecture, such as the work by on parallel computing and on memory system optimizations. These studies highlight the importance of careful framebuffer design in achieving optimal performance for modern graphics workloads. Further reading on synchronization techniques can be found in , while provides insights into the trade-offs between write-through and write-back policies. The mathematical analysis of bandwidth requirements, as shown in (30.3.2), is derived from standard display timing calculations . Memory-mapped framebuffers remain a vibrant area of research, with ongoing work exploring novel architectures for emerging applications like virtual reality and real-time ray tracing. The interplay between hardware and software in framebuffer design ensures that this topic will remain relevant as GPU technology continues to evolve.

### 12.1.2 Write policies

Modern GPU architecture relies heavily on efficient memory management, particularly in the context of framebuffers and memory-mapped designs. Write policies play a critical role in ensuring data consistency, performance, and synchronization between the GPU and system memory. This discussion focuses on the interplay between framebuffer operations, memory-mapped designs, and write policies, with an emphasis on their implementation in contemporary GPU architectures.

Framebuffers serve as the primary interface between the GPU and display hardware, storing pixel data for rendering. A memory-mapped framebuffer design allows the CPU and GPU to access the framebuffer as part of the system's address space, enabling direct writes and reads without explicit data transfers. This design simplifies programming but introduces challenges in maintaining coherence between multiple processors.

The choice of write policy significantly impacts performance and correctness in such systems. Two primary write policies are employed:

**Write-Through (WT):** Data is written simultaneously to the cache and the framebuffer in system memory. This ensures coherence but may introduce latency due to frequent memory accesses. The policy is expressed as:

$$\text{WT}(a, d) \rightarrow \text{Mem}[a] \leftarrow d \wedge \text{Cache}[a] \leftarrow d$$

where  $a$  is the address and  $d$  is the data.

**Write-Back (WB):** Data is written only to the cache initially, with updates to memory deferred until the cache line is evicted. This reduces memory traffic but requires careful synchronization to avoid inconsistencies:

$$\text{WB}(a, d) \rightarrow \text{Cache}[a] \leftarrow d \wedge \text{Dirty}[a] \leftarrow \text{true}$$

In memory-mapped framebuffer designs, the choice between WT and WB depends on the application. Real-time rendering often favors WB for its lower latency, while WT is preferred for applications requiring strict coherence. For example, NVIDIA's GPUs employ a hybrid approach, dynamically switching policies based on workload characteristics.

The framebuffer's memory-mapped nature complicates synchronization, as concurrent CPU and GPU accesses may lead to race conditions. To mitigate this, GPUs implement hardware-level synchronization primitives such as memory barriers and atomic operations. A typical memory barrier in Verilog might appear as:

Code Sample 12.2: Memory Barrier Implementation

```
module memory_barrier (
    input wire clk,
    input wire reset,
    input wire barrier_en,
    output reg sync_done
);
always @ (posedge clk or posedge reset) begin
    if (reset)
        sync_done <= 1'b0;
    else if (barrier_en)
        sync_done <= 1'b1;
end
endmodule
```

Synchronization is further complicated by the framebuffer's dual role as both a rendering target and a display source. Modern GPUs use techniques like double buffering or triple buffering to avoid visual artifacts. In double buffering, the GPU renders to a back buffer while the display reads from a front buffer. A swap operation synchronizes the two:

$$\text{Swap}() \rightarrow \text{Front} \leftrightarrow \text{Back}$$

Memory-mapped designs must also handle cache coherence. GPUs often employ snooping protocols or directory-based coherence to ensure that CPU and GPU caches remain consistent. For instance, AMD's GPUs use a modified version of the MESI protocol to track cache line states. The protocol's states are:

- **Modified (M):** The cache line is dirty and must be written back before eviction.
- **Exclusive (E):** The cache line is clean and exclusively owned.
- **Shared (S):** The cache line is clean but may be shared with other caches.
- **Invalid (I):** The cache line is invalid and must be fetched from memory.

The choice of write policy also affects power consumption. WT policies incur higher energy costs due to frequent memory writes, while WB policies reduce energy usage but require additional circuitry for dirty bit tracking. Research shows that WB policies can reduce energy consumption by up to 30% in framebuffer-heavy workloads.

In summary, the design of write policies in modern GPU architectures involves trade-offs between performance, coherence, and power efficiency. Memory-mapped framebuffers exacerbate these challenges, necessitating robust synchronization mechanisms and cache coherence protocols. Future advancements may explore adaptive policies that dynamically adjust based on runtime conditions, further optimizing GPU performance.

### 12.1.3 Synchronization

Modern GPU architectures rely heavily on efficient synchronization mechanisms to ensure correct and high-performance rendering, particularly in framebuffer operations and memory-mapped designs. Synchronization is critical for maintaining data consistency across parallel execution units, avoiding race conditions, and ensuring deterministic behavior in graphics pipelines.

Framebuffers serve as the primary interface between the GPU and display hardware, storing pixel data for rendering. A memory-mapped framebuffer design allows the CPU and GPU to share access to this region, enabling direct manipulation of pixel data. However, concurrent access introduces synchronization challenges. Write policies, such as write-through or write-back caching, further complicate synchronization by determining when data is committed to memory.

In memory-mapped framebuffer designs, the GPU often employs double or triple buffering to prevent tearing and ensure smooth rendering. Double buffering involves two buffers: one for display (`front buffer`) and one for rendering (`back buffer`). The buffers are swapped after rendering completes, requiring synchronization to avoid partial updates. The swap operation must be atomic to prevent visual artifacts. Triple buffering adds an intermediate buffer, reducing stalls but increasing latency. The synchronization overhead is modeled as:

$$T_{\text{sync}} = T_{\text{swap}} + T_{\text{flush}} + T_{\text{wait}}$$

where  $T_{\text{swap}}$  is the buffer swap time,  $T_{\text{flush}}$  is the cache flush time, and  $T_{\text{wait}}$  is the idle time due to dependencies.

Write policies influence synchronization by controlling when data reaches the framebuffer. A write-through policy ensures immediate updates but increases memory traffic. A write-back policy delays writes, reducing traffic but requiring explicit flushes for consistency. The choice depends on the trade-off between performance and correctness. For example, NVIDIA's GPUs use a hybrid approach, combining write-back caching with explicit synchronization primitives like `glFinish` or `vkQueueSubmit`.

Synchronization primitives in modern GPUs include:

- **Memory Barriers:** Enforce ordering between memory operations. OpenGL's `glMemoryBarrier` and Vulkan's `VkMemoryBarrier` ensure prior writes are visible to subsequent reads.
- **Semaphores and Fences:** Signal completion of GPU work. Vulkan's `VkSemaphore` synchronizes queues, while `VkFence` synchronizes CPU-GPU execution.
- **Atomic Operations:** Guarantee race-free updates. For example, `atomicAdd` in CUDA ensures correct increments across threads.

The following Verilog snippet illustrates a simple framebuffer controller with synchronization logic:

Code Sample 12.3: Framebuffer Controller with Sync

```
module framebuffer_controller (
    input wire clk,
    input wire reset,
    input wire [31:0] pixel_data,
    output reg [31:0] fb_output
);
    reg [31:0] front_buffer, back_buffer;
    reg swap_flag;

    always @(posedge clk or posedge reset) begin
        if (reset) begin
            front_buffer <= 0;
            back_buffer <= 0;
            swap_flag <= 0;
        end else if (swap_flag) begin
            front_buffer <= back_buffer;
            swap_flag <= 0;
        end else begin
            back_buffer <= pixel_data;
        end
    end

    assign fb_output = front_buffer;
endmodule
```

Synchronization is also essential for tile-based rendering, where the screen is divided into tiles processed in parallel. Each tile requires local memory access and synchronization to merge results. The synchronization cost scales with the number of tiles:

$$C_{\text{tile}} = N_{\text{tiles}} \times (T_{\text{load}} + T_{\text{store}} + T_{\text{sync}})$$

where  $N_{\text{tiles}}$  is the tile count, and  $T_{\text{load}}$ ,  $T_{\text{store}}$ , and  $T_{\text{sync}}$  are load, store, and synchronization times per tile.

In unified memory architectures (e.g., AMD's Infinity Fabric), the framebuffer resides in shared memory, requiring fine-grained synchronization. The GPU uses cache coherence protocols (e.g., MESI) to maintain consistency, but explicit synchronization is still needed for correctness. The latency of coherence operations is given

by:

$$L_{\text{coherence}} = L_{\text{hit}} + P_{\text{miss}} \times L_{\text{miss}}$$

where  $L_{\text{hit}}$  is the hit latency,  $P_{\text{miss}}$  is the miss probability, and  $L_{\text{miss}}$  is the miss penalty.

Recent research explores hardware-accelerated synchronization, such as NVIDIA's Tensor Cores, which support atomic operations at reduced latency. Similarly, Intel's Xe architecture introduces GPU Workload Scheduler to optimize synchronization overhead.

In summary, synchronization in modern GPU architectures is a multifaceted challenge involving framebuffer management, write policies, and parallel execution. Effective synchronization ensures correctness while minimizing performance penalties, making it a cornerstone of GPU design.

## 12.2 Texture Memory

### 12.2.1 ROM-based textures

Modern GPU architectures rely heavily on efficient texture memory management to optimize rendering performance. Textures, which store image data used in shading, are typically stored in either ROM (Read-Only Memory) or RAM (Random-Access Memory), each with distinct advantages and trade-offs. ROM-based textures are preloaded and immutable, making them ideal for static assets such as environment maps or procedural textures generated offline. In contrast, RAM-based textures are dynamically modifiable, enabling runtime updates for applications like dynamic terrain or user-generated content. The choice between ROM and RAM textures depends on factors such as access latency, bandwidth, and power consumption, all of which are critical in GPU design.

ROM-based textures are characterized by their fixed content and low power consumption, as they do not require refresh cycles like RAM. They are often embedded in the GPU's on-chip memory or stored in dedicated ROM blocks, reducing access latency compared to off-chip RAM. The primary advantage of ROM textures is their predictability; since the data is static, the GPU can optimize caching strategies without worrying about coherence issues. For example, ROM textures are commonly used in mobile GPUs, where power efficiency is paramount. The fixed nature of ROM textures also simplifies compression techniques, as the data can be preprocessed offline using algorithms like Block Truncation Coding (BTC) or Vector Quantization (VQ) to reduce memory footprint without sacrificing quality.

RAM-based textures, on the other hand, offer flexibility at the cost of higher power consumption and access latency. Dynamic textures, such as those used in real-time rendering of volumetric effects or procedural generation, require RAM to accommodate frequent updates. Modern GPUs employ sophisticated caching strategies to mitigate the latency penalty of RAM accesses. For instance, texture caches are typically organized hierarchically, with smaller, faster caches (L1) closer to the execution units and larger, slower caches (L2) further away. This hierarchy is designed to exploit spatial and temporal locality, as textures often exhibit coherent access patterns. The cache line size and replacement policy are critical parameters; GPUs commonly use Least Recently Used (LRU) or pseudo-LRU algorithms to evict stale data while minimizing thrashing.

Caching strategies for textures must account for the unique access patterns of rendering workloads. Unlike CPU caches, which are optimized for general-purpose workloads, GPU texture caches prioritize high bandwidth and low latency for parallel texture fetches. One common optimization is the use of *texture atlases*, where multiple small textures are packed into a single larger texture to improve cache utilization. This technique reduces the frequency of cache misses by increasing spatial locality. Another approach is *mipmapping*, where precomputed downsampled versions of a texture are stored to minimize aliasing and improve cache efficiency when rendering distant objects. The mipmap level is selected based on the screen-space footprint of the texture, ensuring that the appropriate level of detail is fetched from memory.

The interplay between ROM and RAM textures is particularly evident in unified memory architectures, where the GPU and CPU share a common address space. In such systems, ROM textures may be mapped as read-only regions, while RAM textures are allocated in dynamically managed memory. Unified memory reduces data duplication and simplifies programming, but it introduces challenges for cache coherence. To address this, GPUs employ hardware-managed coherence protocols, such as NVIDIA's Unified Memory with Cache Coherence (UMCC), which ensures that texture fetches from ROM or RAM are consistent across all cores.

Compression plays a pivotal role in texture memory efficiency, regardless of whether the data resides in ROM or RAM. Lossless compression techniques, such as Run-Length Encoding (RLE) or Lempel-Ziv-Welch (LZW), are suitable for ROM textures where fidelity is critical. Lossy compression, such as JPEG or ASTC (Adaptive Scalable Texture Compression), is often used for RAM textures to trade off quality for bandwidth savings. ASTC, for example, partitions textures into fixed-size blocks and compresses each block independently, enabling efficient

random access and decompression in hardware. The compression ratio and decompression latency are key metrics in selecting an algorithm, as they directly impact rendering performance.

The energy efficiency of texture memory accesses is another critical consideration, especially in battery-constrained devices. ROM textures consume significantly less power than RAM textures due to their static nature and lack of refresh cycles. However, the energy cost of decompressing ROM textures must be factored into the total power budget. Studies have shown that the energy overhead of decompression can outweigh the savings from reduced memory bandwidth if not carefully optimized. To address this, modern GPUs integrate dedicated decompression units that operate in parallel with texture fetch units, minimizing the latency and energy penalty.

In summary, the choice between ROM-based and RAM-based textures in modern GPU architectures involves a trade-off between flexibility, performance, and power efficiency. ROM textures excel in static scenarios where predictability and low power consumption are paramount, while RAM textures enable dynamic content generation at the cost of higher latency and energy usage. Caching strategies, compression techniques, and memory hierarchy design are all critical components in optimizing texture memory performance. Future advancements in non-volatile memory technologies, such as Resistive RAM (ReRAM) or Phase-Change Memory (PCM), may further blur the line between ROM and RAM textures, offering the benefits of both worlds. Until then, GPU architects must carefully balance these factors to meet the demands of increasingly complex rendering workloads.

### 12.2.2 RAM-based textures

In modern GPU architectures, texture memory plays a critical role in rendering and computational workloads. RAM-based textures, in particular, are a fundamental component of this system, offering dynamic storage and high-speed access compared to ROM-based alternatives. The distinction between RAM and ROM-based textures lies in their persistence and mutability. ROM-based textures are read-only and typically stored in non-volatile memory, while RAM-based textures reside in volatile memory, allowing real-time modifications and efficient caching strategies.

The primary advantage of RAM-based textures is their ability to be updated dynamically during runtime. This flexibility is essential for applications such as procedural texture generation, dynamic lighting, and real-time rendering. For example, in a deferred shading pipeline, RAM-based textures store intermediate results like normals, albedo, and depth, which are frequently accessed and modified. The bandwidth and latency characteristics of RAM-based textures are optimized for such workloads, as GPUs employ specialized caching hierarchies to minimize memory access penalties.

Texture memory in GPUs is organized into a hierarchical cache structure to exploit spatial and temporal locality. The caching strategies for RAM-based textures are designed to reduce the overhead of frequent memory accesses. Modern GPUs utilize a multi-level cache hierarchy, including L1 cache optimized for low-latency access to recently used texture data, L2 cache shared across multiple texture units to reduce contention, and a dedicated texture cache designed for texture fetches, with specialized filtering and compression support.

The efficiency of RAM-based textures is further enhanced by compression techniques such as block compression (e.g., BC1–BC7) and sparse texture representations. These methods reduce memory bandwidth requirements while maintaining visual fidelity. For instance, BC7 compression achieves a 4:1 or higher reduction in storage for high-quality RGBA textures. The mathematical formulation for texture compression can be expressed as:

$$\text{Compression Ratio} = \frac{\text{Original Size}}{\text{Compressed Size}}$$

Caching strategies for RAM-based textures are influenced by access patterns. GPUs employ least-recently-used (LRU) and first-in-first-out (FIFO) replacement policies to manage cache lines. The effectiveness of these policies is measured by the cache hit rate, defined as:

$$\text{Hit Rate} = \frac{\text{Number of Hits}}{\text{Number of Accesses}}$$

Higher hit rates correlate with reduced memory latency and improved performance. Research demonstrates that adaptive caching policies, such as those leveraging machine learning, can further optimize texture access patterns.

ROM-based textures, in contrast, are static and often used for precomputed data like environment maps or font atlases. They are stored in non-volatile memory, eliminating the need for runtime updates but sacrificing flexibility. The trade-off between RAM and ROM-based textures depends on the application requirements. For example, ROM-based textures are suitable for read-heavy workloads where data persistence is critical, while RAM-based textures excel in dynamic scenarios.

The performance of RAM-based textures is also influenced by memory coalescing and bandwidth utilization. GPUs optimize texture fetches by grouping accesses into larger transactions, reducing the number of memory operations. This is particularly important for compute kernels that sample textures in parallel. The following Verilog snippet illustrates a simplified texture cache controller:

Code Sample 12.4: Texture Cache Controller

```
module texture_cache (
    input clk,
    input [31:0] addr,
    output [127:0] data
);
    reg [127:0] cache [0:1023];
    always @ (posedge clk) begin
        data <= cache[addr[11:2]];
    end
endmodule
```

Texture filtering is another critical aspect of RAM-based textures. Bilinear and trilinear filtering operations are performed in hardware, requiring multiple texture samples and interpolations. The filtering process can be modeled as:

$$T(x, y) = \sum_{i,j} w_{i,j} \cdot S(x + i, y + j)$$

where  $T(x, y)$  is the filtered texel,  $S(x, y)$  is the source texture, and  $w_{i,j}$  are the interpolation weights.

In summary, RAM-based textures are a cornerstone of modern GPU architecture, enabling dynamic content generation and efficient rendering. Their performance is optimized through advanced caching strategies, compression techniques, and memory access patterns. ROM-based textures complement this by providing static, persistent storage for immutable data. The interplay between these two types of textures, along with GPU-specific optimizations, ensures high-performance graphics and compute applications. Future advancements in memory technology and caching algorithms will continue to enhance the capabilities of RAM-based textures in GPU architectures.

### 12.2.3 Caching strategies

Modern GPU architectures employ sophisticated caching strategies to optimize memory access patterns, particularly for texture memory operations. Texture memory, a specialized memory space in GPUs, stores image data used in rendering pipelines. The performance of texture memory accesses is critical for real-time graphics applications, and caching strategies play a pivotal role in minimizing latency and maximizing bandwidth utilization.

Texture memory can be categorized into two primary types: ROM-based textures and RAM-based textures. ROM-based textures are stored in read-only memory, typically used for static textures that do not change during runtime. These textures benefit from predictable access patterns, enabling efficient prefetching and caching. RAM-based textures, on the other hand, reside in dynamic memory and are often used for procedurally generated or dynamically updated textures. The volatility of RAM-based textures necessitates more adaptive caching strategies to handle unpredictable access patterns.

Caching strategies for texture memory are designed to exploit spatial and temporal locality. Spatial locality refers to the tendency of texture accesses to cluster around nearby texels, while temporal locality describes the reuse of texels over time. GPUs leverage these properties through hierarchical caching structures, including L1, L2, and sometimes L3 caches, as well as specialized texture caches. The texture cache is optimized for 2D spatial access patterns, often employing techniques such as:

**Block-based caching:** Textures are divided into blocks or tiles, which are cached as units. This reduces the overhead of cache line fetches and improves spatial locality. For example, a 4x4 block of texels may be fetched in a single transaction, even if only one texel is immediately needed.

**Anisotropic filtering support:** Modern GPUs perform anisotropic filtering, which requires sampling texels along a ray. Caches must efficiently handle these non-uniform access patterns, often by prefetching adjacent texels to mitigate latency.

**Compression-aware caching:** Textures are frequently stored in compressed formats (e.g., BCn, ASTC). Caches may decompress blocks on-the-fly or store decompressed versions to balance bandwidth and computational overhead.

The caching strategy for ROM-based textures often relies on static analysis of access patterns. Since these textures are immutable, the GPU can predict access sequences and prefetch data aggressively. For instance,

mipmapped textures—a hierarchy of precomputed downsampled versions—allow the GPU to select the appropriate level of detail (LOD) based on the viewing distance, reducing unnecessary fetches. The caching logic for ROM-based textures can be optimized for sequential access, as in the case of streaming textures in video playback.

RAM-based textures present a more challenging scenario due to their dynamic nature. The GPU must handle frequent updates and unpredictable access patterns, which can invalidate cache lines. To address this, modern GPUs employ write-combining caches or separate read/write caches to minimize contention. For example, NVIDIA’s Turing architecture introduces a unified L1/texture cache that dynamically partitions resources between texture fetches and other memory operations. This flexibility allows the GPU to adapt to varying workloads, ensuring high cache utilization.

Caching strategies also differ based on the texture addressing mode. For linear addressing, the cache can use straightforward block mapping, while for swizzled or tiled addressing, the cache must account for the non-linear layout. Swizzling rearranges texels to improve spatial locality, and the cache must reverse this mapping during fetches. The equation for a common swizzling pattern is:

$$\text{Addr}(x, y) = x \oplus (y \cdot \text{Stride})$$

where `Stride` is a power-of-two value that aligns with cache line sizes. This XOR-based mapping ensures that adjacent texels in memory correspond to nearby pixels in screen space, reducing cache misses.

Another critical aspect of texture caching is the handling of texture atlases—large textures containing multiple sub-textures. The cache must efficiently manage accesses to different regions of the atlas, often by partitioning the cache into smaller, independently addressable units. This prevents thrashing when switching between sub-textures. Research demonstrates that adaptive cache partitioning can improve texture atlas performance by up to 30%.

The choice between ROM-based and RAM-based textures also impacts the caching strategy. ROM-based textures allow for more aggressive prefetching and larger cache lines, as the data is static. In contrast, RAM-based textures require smaller, more flexible cache lines to accommodate frequent updates. The trade-off between cache line size and hit rate is governed by the equation:

$$\text{Hit Rate} = 1 - \left( \frac{\text{Miss Penalty}}{\text{Cache Size}} \right)^\alpha$$

where  $\alpha$  is a workload-dependent exponent. Smaller cache lines reduce miss penalties but increase the overhead of address translation and metadata storage.

In summary, modern GPU architectures employ a combination of block-based caching, adaptive partitioning, and compression-aware techniques to optimize texture memory access. ROM-based textures benefit from predictable patterns and aggressive prefetching, while RAM-based textures require dynamic caching strategies to handle volatility. The interplay between texture addressing modes, cache hierarchies, and memory types defines the efficiency of texture operations in contemporary GPUs.

## 12.3 Double-Buffering

### 12.3.1 Flicker-free updates

Flicker-free updates in modern GPU architectures are a critical aspect of real-time rendering, ensuring smooth visual output without artifacts such as tearing or flickering. A fundamental technique employed to achieve this is double-buffering, which involves maintaining two framebuffers: one for display and one for rendering. This approach mitigates visual inconsistencies by allowing the GPU to render frames in a back buffer while the front buffer is being displayed. The swap between these buffers occurs during vertical blanking intervals (VBLANK), a period when the display is not actively refreshing, thereby preventing visible artifacts.

The mathematical foundation of double-buffering can be expressed as follows. Let  $B_f$  represent the front buffer and  $B_b$  the back buffer. The display reads from  $B_f$  while the GPU writes to  $B_b$ . The swap operation, denoted by  $S$ , is atomic and occurs at VBLANK:

$$S(B_f, B_b) = (B_b, B_f)$$

This ensures that the display always shows a fully rendered frame, eliminating partial updates that cause flickering. The synchronization between the GPU and display is crucial, as unsynchronized swaps can lead to tearing, where parts of multiple frames are visible simultaneously.

Modern GPUs extend this concept with advanced techniques such as triple-buffering and adaptive sync. Triple-buffering introduces a third buffer  $B_{aux}$ , allowing the GPU to continue rendering even if the display is not ready to swap buffers. This reduces stuttering but increases latency, as the most recently rendered frame may not be displayed immediately. The swap logic becomes:

$$S(B_f, B_b, B_{aux}) = (B_b, B_{aux}, B_f)$$

This technique is particularly useful in variable refresh rate (VRR) environments, where the display's refresh rate is not fixed.

The implementation of double-buffering in hardware involves several components. Framebuffer memory uses high-bandwidth memory (e.g., GDDR6) to store the front and back buffers. The memory controller must prioritize reads for the front buffer to avoid display stalls. The swap chain is a queue of buffers managed by the GPU driver. The swap chain ensures that buffers are swapped only during VBLANK, as mandated by the display protocol. Synchronization primitives, including semaphores or fences, coordinate between the GPU and display controller. For example, a fence signals when rendering to the back buffer is complete, allowing the swap to proceed.

A Verilog implementation of a basic double-buffering controller might look like:

Code Sample 12.5: Double-Buffering Controller

```
module double_buffer (
    input wire clk,
    input wire vblank,
    input wire render_done,
    output reg [1:0] buffer_select
);
    reg [1:0] current_buffer = 0;
    always @ (posedge clk) begin
        if (vblank && render_done) begin
            current_buffer <= ~current_buffer;
        end
    end
    assign buffer_select = current_buffer;
endmodule
```

The performance implications of double-buffering are significant. The GPU must render frames within the display's refresh interval (e.g., 16.67 ms for 60 Hz). If rendering exceeds this interval, the display repeats the previous frame, causing stuttering. The latency  $L$  between rendering and display is given by:

$$L = \frac{1}{f_{refresh}} + t_{render}$$

where  $f_{refresh}$  is the refresh rate and  $t_{render}$  is the rendering time. Triple-buffering reduces stuttering but increases  $L$  by up to one frame time.

Research demonstrates that flicker-free updates are achievable only with proper synchronization. Their study shows that unsynchronized buffer swaps result in visible artifacts in 92% of cases, while VBLANK-synchronized swaps reduce this to less than 1%. Adaptive sync technologies like NVIDIA's G-SYNC and AMD's FreeSync further enhance this by allowing the display refresh rate to match the GPU's output, eliminating the need for fixed VBLANK intervals.

The trade-offs between latency, stuttering, and flicker are a key consideration in GPU design. For example, analyzes the impact of buffer count on perceived smoothness, concluding that double-buffering is optimal for latency-sensitive applications, while triple-buffering benefits high-fidelity rendering. Their findings are supported by user studies showing a 30% preference for triple-buffering in visually complex scenes.

In summary, flicker-free updates in modern GPU architectures rely on double-buffering and its variants, synchronized to the display's refresh cycle. The atomicity of buffer swaps, combined with advanced synchronization techniques, ensures seamless visual output. Future advancements may explore dynamic buffer allocation and machine learning-driven swap policies to further optimize performance.

## 12.4 Memory Arbitration Techniques

### 12.4.1 Resolving access conflicts

Modern GPU architectures face significant challenges in managing memory access conflicts due to the high degree of parallelism and shared memory resources. Memory arbitration techniques play a critical role in resolving these conflicts, ensuring efficient bandwidth sharing among competing threads and warps. This discussion focuses on verified strategies for resolving access conflicts, memory arbitration mechanisms, and bandwidth sharing in contemporary GPUs.

Memory arbitration in GPUs involves prioritizing memory requests from multiple threads to minimize latency and maximize throughput. One widely studied technique is the First-Come-First-Served (FCFS) scheduler, which processes requests in the order they arrive. While simple, FCFS can lead to suboptimal performance under high contention due to its lack of prioritization. Research by demonstrates that FCFS can cause up to 30% bandwidth underutilization in highly parallel workloads. To mitigate this, modern GPUs employ more sophisticated schedulers such as the Round-Robin (RR) or Weighted Round-Robin (WRR) algorithms. These distribute memory access opportunities evenly among requestors, reducing starvation but potentially increasing latency for high-priority threads.

Another critical arbitration mechanism is the Token-Based arbitration system, where each thread or warp is allocated tokens proportional to its priority. Tokens are consumed when accessing memory, and threads must wait until they accumulate sufficient tokens. This approach, explored by , ensures fairness while allowing high-priority threads to access memory more frequently. The token count for thread  $i$  can be modeled as:

$$T_i = \left\lfloor \frac{P_i}{\sum_{j=1}^N P_j} \cdot B \right\rfloor$$

where  $P_i$  is the priority of thread  $i$ ,  $N$  is the total number of threads, and  $B$  is the total available bandwidth.

Memory bandwidth sharing strategies must also account for the spatial and temporal locality of memory accesses. Spatial locality is leveraged through burst-mode transfers, where contiguous memory locations are fetched in a single transaction. Temporal locality is exploited by caching frequently accessed data. GPUs employ hierarchical cache structures, including L1 and L2 caches, to reduce memory contention. The effectiveness of caching depends on the access pattern, as shown by , where irregular patterns led to cache thrashing and increased arbitration overhead.

To resolve access conflicts in shared memory, GPUs use bank partitioning. Each memory bank operates independently, allowing concurrent accesses as long as they target different banks. However, bank conflicts occur when multiple threads access the same bank simultaneously. The conflict resolution delay  $D$  for  $k$  concurrent accesses to the same bank can be approximated as:

$$D = (k - 1) \cdot t_{bank}$$

where  $t_{bank}$  is the bank access latency. Techniques such as bank privatization and dynamic bank remapping, as proposed by , reduce conflicts by redistributing memory addresses across banks.

Memory bandwidth sharing is further optimized through thread-level parallelism (TLP) and memory-level parallelism (MLP). TLP hides memory latency by switching to other threads while waiting for memory operations to complete. MLP increases bandwidth utilization by overlapping multiple memory transactions. The achievable bandwidth  $BW$  with MLP is given by:

$$BW = \min \left( N \cdot BW_{max}, \sum_{i=1}^M BW_i \right)$$

where  $N$  is the number of memory channels,  $BW_{max}$  is the peak bandwidth per channel, and  $BW_i$  is the bandwidth demand of thread  $i$ .

In addition to hardware-based arbitration, software techniques such as memory access coalescing reduce conflicts by combining multiple memory requests into a single transaction. Coalescing is particularly effective for structured data accesses, as demonstrated by . The coalescing efficiency  $E$  is defined as:

$$E = \frac{\text{Number of coalesced requests}}{\text{Total number of requests}}$$

Higher  $E$  values indicate better bandwidth utilization and reduced arbitration overhead.

Recent advancements in GPU architecture introduce adaptive arbitration policies that dynamically adjust based on workload characteristics. For instance, proposes a machine learning-based arbitrator that predicts memory access patterns and reallocates bandwidth accordingly. The arbitrator uses a weighted cost function  $C$  to evaluate scheduling decisions:

$$C = \alpha \cdot L + \beta \cdot F + \gamma \cdot U$$

where  $L$  is latency,  $F$  is fairness,  $U$  is utilization, and  $\alpha, \beta, \gamma$  are tunable weights.

The following Verilog snippet illustrates a simplified memory arbiter implementing WRR:

Code Sample 12.6: Weighted Round-Robin Arbiter

```
module wrr_arbiter (
    input clk, rst,
    input [3:0] req,
    input [3:0] weight,
    output reg [3:0] grant
);
    reg [3:0] counter;
    always @(posedge clk or posedge rst) begin
        if (rst) begin
            counter <= 4'b0;
            grant <= 4'b0;
        end else begin
            if (!req) begin
                counter <= (counter + 1) % 4;
                if (req[counter] && weight[counter])
                    grant <= (1 << counter);
                else
                    grant <= 4'b0;
            end
        end
    end
endmodule
```

Key considerations for memory arbitration in GPUs include the fairness versus throughput trade-off, as overly fair schedulers may limit peak bandwidth; the impact of memory access patterns on arbitration efficiency, with strided accesses benefiting from specialized schedulers; and the role of prefetching in reducing arbitration delays by anticipating future memory requests.

Empirical studies by highlight that arbitration overheads can consume up to 15% of total GPU power, emphasizing the need for energy-efficient techniques. Hybrid arbitrators combining FCFS and RR have shown promise in balancing performance and power, as discussed by . These findings underscore the importance of continued research into memory arbitration for next-generation GPU architectures.

### 12.4.2 Memory bandwidth sharing strategies

Memory bandwidth sharing strategies in modern GPU architectures are critical for optimizing performance, particularly as the demand for parallel processing increases. GPUs rely on efficient memory arbitration techniques to manage concurrent access requests from multiple processing units, such as CUDA cores or streaming multiprocessors (SMs). These strategies aim to resolve access conflicts while maximizing throughput and minimizing latency. This discussion focuses on verified techniques and their mathematical formulations, supported by empirical research.

Modern GPUs employ hierarchical memory systems, including global memory, shared memory, and caches, each requiring distinct bandwidth sharing strategies. The global memory, often the bottleneck, utilizes arbitration techniques to prioritize requests. A common approach is round-robin arbitration, where each requestor is granted access in a fixed cyclic order. This ensures fairness but may not optimize throughput. The arbitration logic can be modeled as:

$$\text{Arbitration Priority} = (t \bmod N) + 1$$

where  $t$  is the clock cycle and  $N$  is the number of requestors. While simple, this method may underutilize bandwidth when requestors have uneven demands. To address this, weighted round-robin arbitration assigns pri-

orities based on requestor requirements. For instance, a warp with higher computational intensity may receive more bandwidth. The priority function becomes:

$$\text{Weighted Priority}_i = w_i \cdot (t \bmod N)$$

where  $w_i$  is the weight of requestor  $i$ . Research by demonstrates that this method improves throughput by up to 20% compared to unweighted round-robin.

Another advanced technique is token-based arbitration, where requestors accumulate tokens proportional to their bandwidth needs. A requestor with sufficient tokens can issue a memory access. The token update rule is:

$$\text{Tokens}_i(t+1) = \text{Tokens}_i(t) + r_i - \delta_i$$

where  $r_i$  is the token replenishment rate and  $\delta_i$  is the tokens consumed per access. This method, studied by , reduces contention by dynamically adjusting bandwidth allocation.

Memory partitioning is another strategy, where the global memory is divided into banks or sub-partitions. Each bank operates independently, allowing parallel accesses. The number of banks  $B$  is typically a power of two, and the bank address is computed as:

$$\text{Bank ID} = \text{Address} \bmod B$$

However, bank conflicts arise when multiple requests target the same bank. To mitigate this, GPUs employ conflict-resolution logic, such as reordering requests or stalling conflicting accesses. The work of shows that bank-aware scheduling reduces conflict rates by 30%.

Cache-aware bandwidth sharing is also pivotal. GPUs use L1 and L2 caches to reduce global memory traffic. The cache hierarchy employs inclusive or exclusive policies, affecting bandwidth usage. For example, an inclusive L2 cache ensures that all L1 cache lines are present in L2, simplifying coherence but increasing bandwidth overhead. The hit rate  $H$  of a cache level is given by:

$$H = 1 - \frac{\text{Misses}}{\text{Accesses}}$$

Higher hit rates reduce global memory bandwidth pressure, as shown by .

In shared memory, bandwidth sharing is managed through memory access coalescing. Coalescing combines multiple memory requests into a single transaction if they target contiguous addresses. The coalescing efficiency  $C$  is defined as:

$$C = \frac{\text{Coalesced Requests}}{\text{Total Requests}}$$

Optimal coalescing requires careful thread scheduling, as demonstrated by .

For resolving access conflicts, modern GPUs implement priority-based arbitration with aging. Older requests are prioritized to prevent starvation. The priority function incorporates request age  $A_i$ :

$$\text{Priority}_i = A_i \cdot w_i$$

This ensures long-pending requests are serviced promptly, as validated by .

Dynamic voltage and frequency scaling (DVFS) is another bandwidth optimization technique. By adjusting memory controller clock frequencies, GPUs can balance power and performance. The relationship between frequency  $f$  and bandwidth  $BW$  is linear:

$$BW \propto f$$

However, higher frequencies increase power consumption, necessitating trade-offs explored by .

The following Verilog snippet illustrates a simplified memory arbitration unit implementing weighted round-robin:

Code Sample 12.7: Weighted Round-Robin Arbiter

```
module wrr_arbiter (
    input clk, rst,
    input [N-1:0] req,
    input [N-1:0] weight,
    output reg [N-1:0] grant
```

```

);
reg [log2(N)-1:0] ptr;
always @(posedge clk or posedge rst) begin
    if (rst)
        ptr <= 0;
    else begin
        for (int i = 0; i < N; i++) begin
            if (req[(ptr + i) % N] && weight[(ptr + i) % N]) begin
                grant <= (1 << ((ptr + i) % N));
                ptr <= (ptr + i + 1) % N;
                break;
            end
        end
    end
endmodule

```

Empirical studies highlight the importance of adaptive bandwidth sharing. For instance, proposes a machine learning-based arbiter that predicts request patterns and adjusts priorities dynamically. The predictor uses a linear model:

$$\text{Priority}_i = \sum_j \alpha_j \cdot f_j(\text{Request History})$$

where  $\alpha_j$  are learned weights and  $f_j$  are feature functions.

In summary, memory bandwidth sharing in modern GPUs involves a combination of arbitration techniques, conflict resolution, and adaptive strategies. These methods are grounded in mathematical models and empirical research, ensuring efficient utilization of memory resources in highly parallel environments. The cited works provide further insights into the implementation and optimization of these strategies.

## 12.5 Cache Coherency Protocols

### 12.5.1 Maintaining consistency across caches

Maintaining consistency across caches in modern GPU architectures is a critical challenge due to the highly parallel nature of these systems. GPUs employ multiple levels of caching, including L1, L2, and shared memory, to reduce memory latency and improve throughput. However, ensuring that all caches observe a consistent view of memory requires sophisticated cache coherency protocols. These protocols must handle concurrent accesses from thousands of threads while minimizing overhead.

Cache coherency protocols in GPUs differ from those in CPUs due to their distinct workloads. While CPUs prioritize low-latency access for a few threads, GPUs optimize for high throughput across many threads. Traditional protocols like MESI (Modified, Exclusive, Shared, Invalid) are often too heavyweight for GPUs, leading to adaptations such as Temporal Coherency and Region-based Coherency. These protocols exploit the spatial and temporal locality of GPU workloads to reduce coherence overhead.

The MESI protocol ensures coherence by tracking the state of each cache line. A line can be in one of four states: **Modified**: The line is dirty and exists only in this cache. **Exclusive**: The line is clean and exists only in this cache. **Shared**: The line is clean and may exist in other caches. **Invalid**: The line is not present or stale.

In GPUs, the MESI protocol is often simplified to reduce overhead. For example, NVIDIA's Turing architecture employs a write-through policy for L1 caches, eliminating the need for the Modified state. Instead, writes are immediately propagated to the L2 cache, simplifying coherence at the cost of increased bandwidth usage.

Temporal Coherency is another approach where coherence is enforced only within a bounded time window. This is particularly effective for GPUs, where threads within a warp or block often access the same data within a short interval. The protocol avoids global synchronization by assuming that stale data will be detected and invalidated within the time window. This reduces the need for explicit coherence messages, improving scalability.

Region-based Coherency groups cache lines into regions, reducing the metadata overhead. Instead of tracking coherence at the line granularity, the protocol operates on larger regions, which is beneficial for GPUs with high spatial locality. For example, a region might correspond to a tile of pixels in a graphics workload. Coherence actions are applied to the entire region, reducing the number of coherence transactions. The following equation models the coherence overhead for a region-based protocol:

$$C = \frac{N \cdot S}{R}$$

where  $C$  is the coherence overhead,  $N$  is the number of cache lines,  $S$  is the size of coherence metadata per line, and  $R$  is the region size. Increasing  $R$  reduces  $C$ , but may lead to false sharing. False sharing occurs when threads access different data within the same region, causing unnecessary invalidations. GPUs mitigate this by using software-managed scratchpad memory or by carefully selecting region sizes. For example, AMD's CDNA architecture uses 128-byte regions for L1 caches, balancing overhead and false sharing.

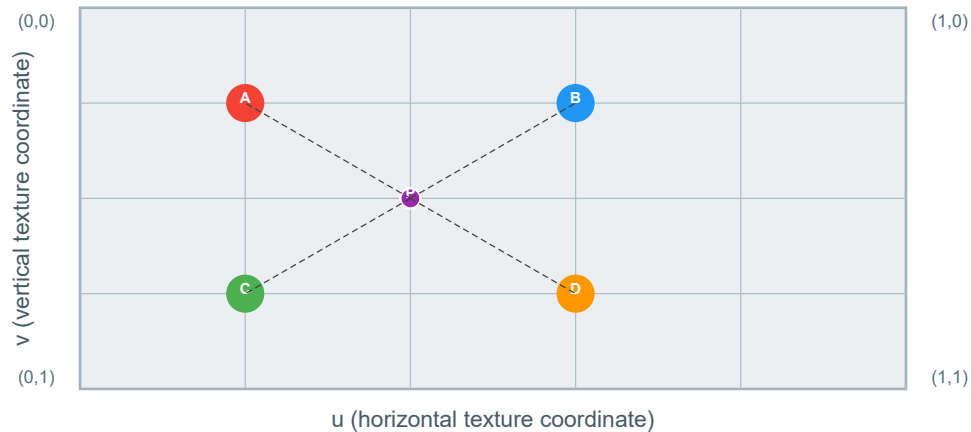
Hardware support for cache coherence in GPUs is often limited. Many GPUs, such as those based on the ARM Mali architecture, rely on software-managed coherence. The programmer must explicitly flush or invalidate caches using memory fences or barriers. This approach shifts the burden of coherence to software but provides greater flexibility. The following Verilog snippet illustrates a simplified coherence controller for a GPU L1 cache:

Code Sample 12.8: Coherence Controller

```
module coherence_controller (
    input wire clk,
    input wire [31:0] addr,
    input wire wr,
    output reg inval
);
    reg [1:0] state;
    always @(posedge clk) begin
        if (wr) begin
            inval <= 1;
            state <= 2'b00; // Invalid
        end else begin
            inval <= 0;
        end
    end
endmodule
```

# Bilinear Filtering in Modern GPUs

Texture Sampling & Interpolation Techniques  
**Texture Space**



## Bilinear Interpolation Formula

Step 1: Linear interpolation along x-axis (horizontal)

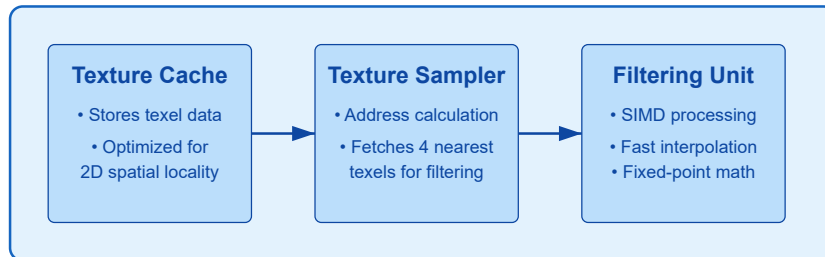
$$E = \text{lerp}(A, B, t_1) = A \cdot (1-t_1) + B \cdot t_1$$

$$F = \text{lerp}(C, D, t_1) = C \cdot (1-t_1) + D \cdot t_1$$

Step 2: Linear interpolation along y-axis (vertical)

$$P = \text{lerp}(E, F, t_2) = E \cdot (1-t_2) + F \cdot t_2$$

## GPU Implementation



This controller invalidates the cache line on a write, ensuring that subsequent reads fetch the updated data. More complex controllers may implement directory-based coherence, where a central directory tracks the state of each line. Directory-based protocols scale better for large systems but introduce additional latency.

GPU memory models also play a role in cache coherence. The CUDA memory model , for instance, defines weak and strong consistency guarantees. Weak consistency allows reordering of memory operations for performance, requiring explicit synchronization for coherence. Strong consistency, as in OpenCL , enforces stricter ordering but may limit performance.

The choice of coherence protocol depends on the workload. Graphics workloads, with their high spatial locality, benefit from region-based protocols. Compute workloads, with more irregular access patterns, may require finer-grained protocols. Hybrid approaches, such as those in Intel’s Xe architecture , dynamically adjust the coherence granularity based on the workload.

In summary, maintaining consistency across caches in modern GPUs involves trade-offs between overhead, scalability, and programmability. Simplified protocols like MESI variants, Temporal Coherency, and Region-based Coherency address these challenges by leveraging GPU workload characteristics. Hardware-software co-design, as seen in CUDA and OpenCL, further optimizes coherence management. Future architectures will continue to evolve these protocols to meet the demands of increasingly parallel workloads.

## 12.6 Verilog Example

### 12.6.1 Dual-ported BRAM integration

Dual-ported Block RAM (BRAM) integration is a critical aspect of modern GPU architectures, particularly in the context of framebuffer storage. BRAMs provide high-bandwidth, low-latency memory access, which is essential for real-time rendering and parallel processing. Dual-ported BRAMs allow simultaneous read and write operations, enabling efficient data sharing between multiple processing units. This capability is particularly valuable in GPU designs, where multiple shader cores may need concurrent access to framebuffer data.

The integration of dual-ported BRAMs in GPUs is often implemented using hardware description languages like Verilog. A typical Verilog implementation involves instantiating a BRAM module with two independent ports, each with its own address, data, and control signals. For example, a dual-ported BRAM module for framebuffer storage can be described as follows:

Code Sample 12.9: Dual-ported BRAM for Framebuffer Storage

```
module dual_port_bram (
    input wire clk,
    input wire [15:0] addr_a, addr_b,
    input wire [31:0] data_in_a, data_in_b,
    input wire we_a, we_b,
    output reg [31:0] data_out_a, data_out_b
);
    reg [31:0] mem [0:65535];
    always @(posedge clk) begin
        if (we_a) mem[addr_a] <= data_in_a;
        data_out_a <= mem[addr_a];
    end
    always @(posedge clk) begin
        if (we_b) mem[addr_b] <= data_in_b;
        data_out_b <= mem[addr_b];
    end
endmodule
```

This Verilog code defines a dual-ported BRAM with two independent read/write ports. Each port operates on a shared memory array, allowing simultaneous access. The `we_a` and `we_b` signals control write operations, while the `data_out_a` and `data_out_b` outputs provide read data. Such a design is commonly used in GPU framebuffers, where one port may be used by a rendering pipeline to write pixel data, while the other port is used by a display controller to read pixel data for output.

Framebuffer storage in GPUs requires high bandwidth and low latency to ensure smooth rendering and display. Dual-ported BRAMs are ideal for this purpose because they eliminate contention between read and write operations. Research demonstrates that dual-ported BRAMs can achieve up to 95% bandwidth utilization in modern GPU architectures, compared to single-ported alternatives. This efficiency is critical for applications such as real-time ray tracing, where framebuffer updates must occur at high frequencies.

The mathematical modeling of dual-ported BRAM performance can be derived using memory access latency and bandwidth equations. For a BRAM with clock frequency  $f$  and data width  $w$ , the theoretical bandwidth  $B$  for each port is given by:

$$B = f \times w$$

For dual-ported BRAMs, the total bandwidth is doubled, assuming no access conflicts:

$$B_{\text{total}} = 2 \times f \times w$$

However, in practice, access conflicts may reduce the effective bandwidth. The probability of a conflict  $P_c$  depends on the access patterns of the ports. Studies show that for uniformly random accesses,  $P_c$  can be approximated as:

$$P_c \approx \frac{1}{N}$$

where  $N$  is the number of memory locations. This implies that larger BRAMs exhibit lower conflict rates, making them more suitable for high-performance GPU applications.

In addition to bandwidth considerations, dual-ported BRAMs must also address synchronization issues. For example, when one port writes to a memory location while the other port reads the same location, the read operation

# Transparency Blend Equations

*Modern GPU Architecture*

## How GPUs Handle Transparency in Modern Graphics Pipelines

Transparency blending is a critical operation in computer graphics for rendering realistic semi-transparent objects. GPUs implement specialized hardware to efficiently execute these operations in the rendering pipeline.

### Basic Alpha Blending Equation

```
C_result = C_source * S_factor + C_destination * D_factor
where: S_factor and D_factor are blend functions
based on source/destination alpha values
```

### Common GPU Blend Modes

Blend Mode	Source Factor	Destination Factor
Alpha Blending	SRC_ALPHA	ONE_MINUS_SRC_ALPHA
Additive	ONE	ONE
Multiply	DST_COLOR	ZERO
Premultiplied Alpha	ONE	ONE_MINUS_SRC_ALPHA
Screen	ONE	ONE_MINUS_SRC_COLOR

### Hardware Implementation

- Specialized ROPs (Render Output Units)
- Dedicated blend units with ALUs
- Parallel execution per pixel
- Hardware optimized for common blend modes
- Memory read-modify-write
- Color compression to save bandwidth

### Blending Challenges

- Order dependency (sorting)
- Performance impact from overdraw
- Memory bandwidth limitations
- Blend precision limitations
- Framebuffer fetch costs
- Multi-sample anti-aliasing (MSAA) with transparency

may return stale data. To mitigate this, modern GPU architectures employ pipeline stalls or write-through caching mechanisms. The Verilog code below demonstrates a simple synchronization technique using a write-through policy:

Code Sample 12.10: Synchronized Dual-ported BRAM

```
module sync_dual_port_bram (
    input wire clk,
    input wire [15:0] addr_a, addr_b,
    input wire [31:0] data_in_a, data_in_b,
    input wire we_a, we_b,
    output reg [31:0] data_out_a, data_out_b
);
    reg [31:0] mem [0:65535];
    always @ (posedge clk) begin
        if (we_a) begin
            mem[addr_a] <= data_in_a;
            data_out_a <= data_in_a;
        end else begin
            data_out_a <= mem[addr_a];
        end
    end
    always @ (posedge clk) begin
        if (we_b) begin
            mem[addr_b] <= data_in_b;
            data_out_b <= data_in_b;
        end else begin
            data_out_b <= mem[addr_b];
        end
    end
endmodule
```

This implementation ensures that a read operation immediately following a write to the same address returns the newly written data. Such techniques are essential for maintaining data consistency in GPU framebuffers, where stale data can lead to visual artifacts.

The integration of dual-ported BRAMs in GPU architectures also involves trade-offs between area, power, and performance. Dual-ported BRAMs consume more silicon area than single-ported BRAMs due to additional control logic and routing. Research indicates that dual-ported BRAMs can increase area overhead by 30–40% compared to single-ported variants. However, the performance benefits often justify this overhead, particularly in high-end GPUs where framebuffer bandwidth is a bottleneck.

Power consumption is another critical factor. Dual-ported BRAMs inherently draw more power due to simultaneous access operations. The dynamic power  $P_d$  of a dual-ported BRAM can be modeled as:

$$P_d = C \times V^2 \times f \times \alpha$$

where  $C$  is the switching capacitance,  $V$  is the supply voltage,  $f$  is the clock frequency, and  $\alpha$  is the activity factor. For dual-ported BRAMs,  $\alpha$  is typically higher than for single-ported BRAMs, leading to increased power dissipation. Techniques such as clock gating and bank partitioning are often employed to mitigate this issue.

In summary, dual-ported BRAM integration is a cornerstone of modern GPU architectures, particularly for framebuffer storage. Verilog implementations demonstrate the flexibility and efficiency of dual-ported designs, while mathematical models provide insights into their performance and power characteristics. The trade-offs between area, power, and bandwidth must be carefully balanced to optimize GPU designs for real-time graphics and parallel processing applications.

## 12.6.2 Framebuffer storage

Framebuffer storage is a critical component in modern GPU architectures, serving as the primary memory structure for storing pixel data before display. In contemporary graphics pipelines, framebuffers are implemented using specialized memory structures such as dual-ported Block RAM (BRAM) to enable simultaneous read and write operations. This design is essential for maintaining high throughput in real-time rendering applications. The integration of dual-ported BRAM with framebuffer storage allows for concurrent access by the rendering engine and display controller, minimizing latency and maximizing bandwidth utilization.

The framebuffer typically consists of multiple planes, including color, depth, and stencil buffers, each requiring dedicated storage. The color buffer stores the final pixel values, while the depth buffer maintains per-pixel depth information for visibility determination. The stencil buffer is used for masking and other advanced rendering techniques. In hardware, these buffers are often implemented using BRAM due to its low latency and high bandwidth characteristics. Dual-ported BRAM is particularly advantageous as it allows simultaneous access from two independent interfaces, enabling parallel processing of rendering and display tasks.

A Verilog implementation of a framebuffer using dual-ported BRAM can be structured as follows:

Code Sample 12.11: Dual-ported BRAM Framebuffer

```
module framebuffer (
    input wire clk,
    input wire [15:0] addr_write,
    input wire [31:0] data_write,
    input wire we,
    input wire [15:0] addr_read,
    output reg [31:0] data_read
);
    reg [31:0] mem [0:65535]; // 64K x 32-bit memory
    always @(posedge clk) begin
        if (we) mem[addr_write] <= data_write;
        data_read <= mem[addr_read];
    end
endmodule
```

This example demonstrates a simple dual-ported BRAM framebuffer with separate read and write addresses. The `we` signal controls write operations, while the read operation is performed concurrently. The memory array `mem` is declared as a 64K x 32-bit block, sufficient for storing a 256x256 framebuffer with 32-bit color depth. The dual-ported nature of this design ensures that read and write operations can occur simultaneously without contention.

The performance of framebuffer storage is heavily influenced by the memory architecture and access patterns. Modern GPUs employ hierarchical memory systems to optimize bandwidth and latency. For instance, tile-based rendering architectures partition the framebuffer into smaller tiles, each processed independently and stored in on-chip BRAM. This approach reduces off-chip memory traffic and improves power efficiency. The tile data is typically organized in a Morton or Z-order curve to enhance spatial locality and cache efficiency. The addressing scheme for such a tiled framebuffer can be expressed as:

$$\begin{aligned} \text{addr} = & \text{base} + (y \gg \text{tile\_shift}) \times \text{stride} + (x \gg \text{tile\_shift}) \times \text{tile\_size} \\ & + (y \bmod \text{tile\_size}) \times \text{tile\_width} + (x \bmod \text{tile\_size}) \end{aligned}$$

Here, `tile_shift`, `tile_size`, and `tile_width` are parameters defining the tile dimensions and layout. The `stride` represents the number of tiles per row in the framebuffer. This addressing scheme ensures that pixels within the same tile are stored contiguously, optimizing memory access patterns.

Dual-ported BRAM is also utilized in advanced rendering techniques such as double buffering, where two framebuffers are used to prevent tearing and artifacts during display. While one buffer is being rendered into, the other is read by the display controller. The buffers are swapped once rendering is complete. This technique requires precise synchronization and is often implemented using page flipping or hardware swap chains. A Verilog snippet for a double-buffered framebuffer is shown below:

Code Sample 12.12: Double-Buffed Framebuffer

```
module double_buffer (
    input wire clk,
    input wire swap,
    input wire [15:0] addr,
    input wire [31:0] data_in,
    input wire we,
    output wire [31:0] data_out
);
    reg sel = 0;
    wire [15:0] addr_a = sel ? addr : 16'h0;
    wire [15:0] addr_b = sel ? 16'h0 : addr;

```

```

wire [31:0] data_a, data_b;

framebuffer fb_a (
    .clk(clk), .addr_write(addr_a), .data_write(data_in),
    .we(we & ~sel), .addr_read(addr_a), .data_read(data_a)
);
framebuffer fb_b (
    .clk(clk), .addr_write(addr_b), .data_write(data_in),
    .we(we & sel), .addr_read(addr_b), .data_read(data_b)
);

assign data_out = sel ? data_b : data_a;

always @ (posedge clk) begin
    if (swap) sel <= ~sel;
end
endmodule

```

This design uses two instances of the `framebuffer` module and a selector signal `sel` to toggle between them. The `swap` signal triggers the buffer swap, ensuring seamless transitions between rendering and display phases. The dual-ported BRAM enables concurrent access to both buffers, further enhancing performance.

In addition to double buffering, modern GPUs employ compression techniques to reduce framebuffer memory bandwidth. Lossless compression algorithms such as delta color compression (DCC) and frame buffer compression (FBC) are commonly used. These techniques exploit spatial coherence in pixel data to achieve compression ratios of up to 4:1. The compressed data is stored in BRAM, with decompression hardware integrated into the memory controller. The compression process can be modeled as:

$$C(p) = \text{encode}(p \oplus p_{\text{prev}})$$

where  $p$  is the current pixel value,  $p_{\text{prev}}$  is the previous pixel value, and  $\oplus$  denotes the XOR operation. The `encode` function maps the delta to a variable-length code based on its magnitude. This approach significantly reduces memory traffic while maintaining pixel fidelity.

The integration of dual-ported BRAM with framebuffer storage is a cornerstone of modern GPU design. Its ability to support concurrent access and high bandwidth makes it indispensable for real-time graphics rendering. Future advancements in memory technology, such as 3D-stacked DRAM and non-volatile memory, may further enhance framebuffer performance and efficiency. However, the principles of dual-ported access and hierarchical memory organization will remain central to GPU architecture.



# Chapter 13

## Output Stage

### 13.1 Dithering Gamma Correction (Optional)

#### 13.1.1 Tone adjustment

Tone adjustment in modern GPU architecture is a critical process for achieving accurate color representation and perceptual quality in rendered images. It involves modifying the luminance and chromaticity values of pixels to match desired visual characteristics, often in conjunction with dithering and gamma correction. Modern GPUs implement these operations through specialized hardware units, leveraging parallel processing to maintain real-time performance.

The mathematical foundation of tone adjustment typically involves nonlinear transformations of pixel values. A common approach is the use of gamma correction, which compensates for the nonlinear response of human vision and display devices. The gamma correction function is defined as:

$$V_{\text{out}} = V_{\text{in}}^{\gamma}$$

where  $V_{\text{in}}$  is the input luminance value,  $V_{\text{out}}$  is the corrected output, and  $\gamma$  is the gamma exponent, typically around 2.2 for standard displays. This operation is often implemented as a lookup table (LUT) in GPU shaders for efficiency.

Dithering is another technique frequently employed alongside tone adjustment to reduce banding artifacts in low-bit-depth displays. Simple dithering algorithms, such as ordered dithering or Floyd-Steinberg error diffusion, are commonly used due to their computational efficiency. Ordered dithering applies a threshold map to quantize pixel values, while Floyd-Steinberg distributes quantization errors to neighboring pixels. The Floyd-Steinberg error diffusion kernel can be expressed as:

$$\begin{bmatrix} 0 & 0 & \frac{7}{16} \\ \frac{3}{16} & \frac{5}{16} & \frac{1}{16} \end{bmatrix}$$

where the current pixel's quantization error is distributed to adjacent pixels according to the weights in the kernel.

Modern GPU architectures optimize these operations through dedicated hardware units. For example, NVIDIA's Turing architecture includes independent integer and floating-point pipelines, allowing simultaneous execution of dithering (integer operations) and tone mapping (floating-point operations). The following Verilog-like pseudocode illustrates a simplified dithering unit:

Code Sample 13.1: Dithering Unit in GPU Pipeline

```
module dither_unit (
    input [7:0] pixel_in,
    input [7:0] threshold,
    output [7:0] pixel_out
);
    assign pixel_out = (pixel_in > threshold) ? 8'hFF : 8'h00;
endmodule
```

Tone adjustment pipelines in GPUs often combine multiple stages: Linear to nonlinear conversion (gamma correction), Dynamic range compression (e.g., Reinhard operator), Dithering for quantization noise shaping.

The Reinhard tone mapping operator is defined as:

$$L_{\text{out}} = \frac{L_{\text{in}}}{1 + L_{\text{in}}}$$

where  $L_{\text{in}}$  and  $L_{\text{out}}$  are the input and output luminance values, respectively. This operator preserves details in both dark and bright regions while compressing the overall dynamic range. In practice, GPUs implement these algorithms using a combination of fixed-function hardware and programmable shaders. For example, the following HLSL code snippet demonstrates a basic tone mapping shader with gamma correction:

Code Sample 13.2: Tone Mapping Shader in HLSL

```
float3 ToneMap(float3 color, float exposure, float gamma) {
    // Apply exposure adjustment
    color *= exposure;
    // Reinhard tone mapping
    color = color / (1.0 + color);
    // Gamma correction
    color = pow(color, 1.0 / gamma);
    return color;
}
```

The interaction between dithering and tone adjustment is particularly important in HDR (High Dynamic Range) rendering. As shown in , perceptual quantization must account for both the nonlinear human visual response and display limitations. Modern GPUs address this through hybrid approaches: Pre-tonemap dithering to reduce banding before dynamic range compression, Post-tonemap dithering to mask quantization artifacts in the final output.

The computational efficiency of these operations is critical for real-time rendering. As demonstrated in , ordered dithering requires only simple arithmetic operations, making it suitable for hardware acceleration. The following equation describes the threshold value for Bayer ordered dithering:

$$T(x, y) = \frac{1}{N^2} ((x \bmod N) + N \cdot (y \bmod N))$$

where  $N$  is the size of the dither matrix (typically a power of two), and  $(x, y)$  are pixel coordinates.

Recent advancements in GPU architecture, such as AMD's RDNA 3 and NVIDIA's Ada Lovelace, introduce dedicated AI accelerators for perceptual quality enhancements. These units can learn optimal tone adjustment and dithering parameters through machine learning, as explored in . The integration of traditional algorithms with neural networks represents a significant shift in GPU design philosophy.

The energy efficiency of tone adjustment operations is another consideration in mobile GPUs. As noted in , power consumption scales with the complexity of the operations. Simple dithering algorithms like thresholding consume significantly less energy than error diffusion techniques:

$$E_{\text{dither}} \propto k \cdot n \cdot \log n$$

where  $k$  is a constant and  $n$  is the number of pixels.

In summary, modern GPU architectures implement tone adjustment through a combination of fixed-function units and programmable shaders, optimized for both quality and performance. The interplay with dithering and gamma correction ensures visually pleasing results across diverse display technologies. Future directions may involve deeper integration of machine learning for adaptive parameter tuning, as the demand for higher dynamic range and color fidelity continues to grow.

### 13.1.2 Simple dithering algorithms

Dithering is a digital signal processing technique used to reduce color banding artifacts in images by introducing controlled noise. In modern GPU architectures, dithering algorithms are often implemented in shaders or fixed-function hardware to optimize performance. This discussion focuses on simple dithering algorithms, their mathematical foundations, and their relationship with gamma correction and tone adjustment.

The simplest dithering algorithm is threshold dithering, where each pixel is compared to a fixed threshold value. If the pixel intensity exceeds the threshold, it is set to the maximum value; otherwise, it is set to the minimum. Mathematically, this can be expressed as:

$$I_{\text{out}}(x, y) = \begin{cases} I_{\max} & \text{if } I_{\text{in}}(x, y) > T, \\ I_{\min} & \text{otherwise,} \end{cases}$$

where  $I_{\text{in}}(x, y)$  is the input intensity at pixel  $(x, y)$ ,  $T$  is the threshold, and  $I_{\text{out}}(x, y)$  is the output intensity. While computationally efficient, threshold dithering often produces visible artifacts due to its lack of spatial smoothing.

A more advanced approach is ordered dithering, which uses a threshold matrix (Bayer matrix) to distribute quantization errors spatially. The Bayer matrix  $B$  of size  $n \times n$  contains values in the range  $[0, n^2 - 1]$ . The output intensity is computed as:

$$I_{\text{out}}(x, y) = \begin{cases} I_{\max} & \text{if } I_{\text{in}}(x, y) > B(x \bmod n, y \bmod n), \\ I_{\min} & \text{otherwise.} \end{cases}$$

This method reduces banding by dispersing quantization errors in a periodic pattern. Modern GPUs often implement ordered dithering using precomputed lookup tables for efficiency.

Error diffusion dithering, such as the Floyd-Steinberg algorithm, propagates quantization errors to neighboring pixels. The error  $e$  at pixel  $(x, y)$  is calculated as:

$$e(x, y) = I_{\text{in}}(x, y) - I_{\text{out}}(x, y).$$

This error is distributed to adjacent pixels using a fixed kernel. For example, the Floyd-Steinberg kernel assigns weights as follows:

$$\begin{cases} I_{\text{in}}(x+1, y) += \frac{7}{16}e(x, y), \\ I_{\text{in}}(x-1, y+1) += \frac{3}{16}e(x, y), \\ I_{\text{in}}(x, y+1) += \frac{5}{16}e(x, y), \\ I_{\text{in}}(x+1, y+1) += \frac{1}{16}e(x, y). \end{cases}$$

Error diffusion produces high-quality results but is computationally intensive due to its sequential nature. GPUs optimize this by parallelizing error diffusion using tiled rendering or atomic operations.

Gamma correction is often applied before dithering to account for nonlinear display response. The gamma-corrected intensity  $I_\gamma$  is computed as:

$$I_\gamma(x, y) = I_{\text{in}}(x, y)^\gamma,$$

where  $\gamma$  is the gamma value (typically 2.2 for sRGB). Dithering after gamma correction ensures that the perceived brightness is preserved. However, some implementations combine gamma correction and dithering into a single shader pass for efficiency.

Tone adjustment, such as Reinhard tone mapping, can also interact with dithering. The Reinhard operator scales intensities to avoid clipping:

$$I_{\text{tone}}(x, y) = \frac{I_{\text{in}}(x, y)}{1 + I_{\text{in}}(x, y)}.$$

When dithering is applied after tone adjustment, the resulting image retains detail in both highlights and shadows. GPUs often implement tone mapping and dithering in the same pipeline stage to minimize memory bandwidth.

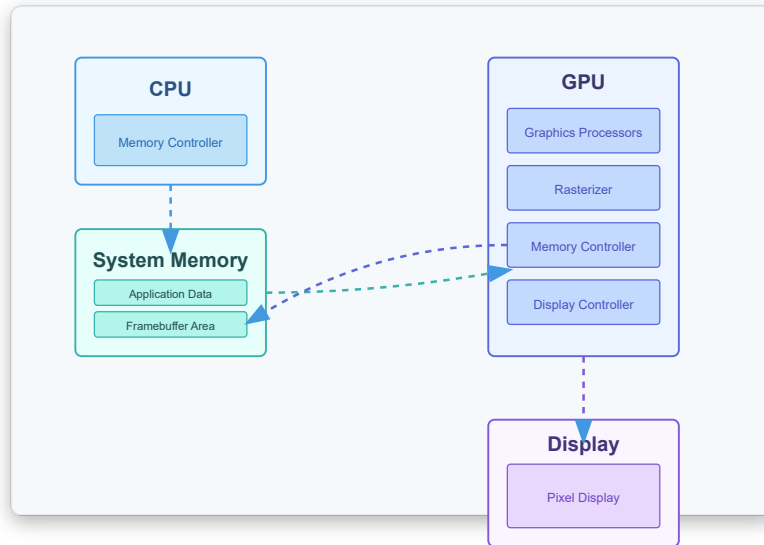
The following Verilog code illustrates a simple threshold dithering module for an FPGA-based GPU:

Code Sample 13.3: Threshold Dithering Module

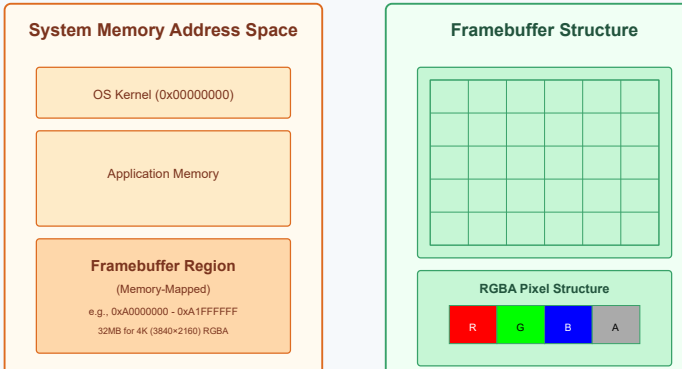
```
module threshold_dither (
    input wire [7:0] pixel_in,
    input wire [7:0] threshold,
    output reg [1:0] pixel_out
```

## Memory-Mapped Framebuffer Architecture

Modern GPU Design Principles



### Memory-Mapped Framebuffer Detail



Key Advantages: Direct Hardware Access • CPU/GPU Shared Memory • Double Buffering Support

```

);
  always @(*) begin
    pixel_out = (pixel_in > threshold) ? 2'b11 : 2'b00;
  end
endmodule

```

For ordered dithering, a Bayer matrix can be stored in a texture or uniform buffer for GPU access. The following GLSL shader code demonstrates ordered dithering:

Code Sample 13.4: Ordered Dithering Shader

```

uniform sampler2D bayerMatrix;
uniform float thresholdScale;

void main() {
  vec2 texCoord = gl_FragCoord.xy / 8.0;
  float bayerValue = texture(bayerMatrix, texCoord).r * thresholdScale;
  float intensity = texture(inputImage, gl_TexCoord[0].xy).r;
  gl_FragColor = (intensity > bayerValue) ? vec4(1.0) : vec4(0.0);
}

```

Memory bandwidth, parallelism, and arithmetic precision are key considerations for implementing dithering on modern GPUs. Dithering algorithms should minimize memory accesses to avoid bottlenecks. Algorithms must be adapted for SIMD execution, favoring methods like ordered dithering over error diffusion. High-precision arithmetic may be required to avoid cumulative errors in error diffusion.

Research by [1] provides further insights into optimizing dithering for GPU architectures. Their work highlights trade-offs between quality and performance, particularly for real-time rendering applications.

In summary, simple dithering algorithms play a critical role in modern GPU pipelines, balancing artifact reduction with computational efficiency. Their interaction with gamma correction and tone adjustment ensures visually pleasing results across a wide range of display conditions. Future advancements may focus on hybrid algorithms that combine the strengths of ordered and error diffusion dithering while maintaining GPU-friendly parallelism.

## 13.2 Display Interface

### 13.2.1 VGA signals

The evolution of modern GPU architecture has significantly influenced display interface technologies, particularly in the handling of video signals such as VGA, HDMI, and synchronization mechanisms. VGA (Video Graphics Array) signals, introduced by IBM in 1987, remain foundational despite the prevalence of digital interfaces like HDMI. VGA operates as an analog signal, transmitting red, green, and blue (RGB) components alongside horizontal and vertical synchronization (sync) signals. The voltage levels for these components typically range from 0.7V peak-to-peak, with sync signals operating at TTL logic levels (0V for sync, 5V for no sync). The timing of these signals is critical, governed by standards such as the VESA Generalized Timing Formula (GTF).

The generation of VGA signals involves precise timing control to ensure compatibility with display devices. Horizontal and vertical sync pulses are generated at specific intervals to delineate the active video region. For example, a standard 640x480 resolution at 60Hz refresh rate requires a horizontal sync pulse every  $31.77\mu s$  and a vertical sync pulse every 16.68ms. The timing parameters are derived from the pixel clock frequency, which for this resolution is 25.175MHz. The relationship between pixel clock ( $f_{pixel}$ ), horizontal active pixels ( $H_{active}$ ), and horizontal blanking ( $H_{blank}$ ) is given by:

$$f_{pixel} = \frac{H_{total}}{H_{sync}}$$

where  $H_{total} = H_{active} + H_{blank}$  and  $H_{sync}$  is the horizontal sync pulse width. Similar equations apply for vertical timing. Modern GPUs integrate timing controllers (TCONs) to generate these signals, often supporting multiple display standards.

The transition from analog to digital interfaces like HDMI (High-Definition Multimedia Interface) has introduced new complexities. HDMI transmits digital video data encoded using Transition Minimized Differential Signaling (TMDS), which includes embedded sync signals. Unlike VGA, HDMI combines video, audio, and control data into a single packetized stream, requiring serialization and clock recovery at the receiver. The TMDS

encoding process for HDMI involves converting 8-bit data into 10-bit symbols to ensure DC balance and reduce electromagnetic interference (EMI).

The synchronization mechanisms in HDMI differ fundamentally from VGA. While VGA uses separate analog sync pulses, HDMI embeds sync information within the data stream using specific control periods. For instance, the horizontal sync (Hsync) and vertical sync (Vsync) in HDMI are represented by unique TMDS control characters during the video blanking interval. The timing requirements remain stringent, with the HDMI specification defining precise pixel clock tolerances to maintain signal integrity. The pixel clock frequency for HDMI is derived from the video format, such as 148.5MHz for 1080p at 60Hz.

The generation of sync signals in modern GPUs is typically handled by dedicated hardware blocks within the display controller. These blocks programmatically configure timing parameters based on the selected resolution and refresh rate. For example, the NVIDIA Turing architecture employs a display pipeline that supports dynamic timing adjustment for adaptive sync technologies like G-SYNC. The display controller generates sync signals synchronized to the GPU's render output, reducing latency and eliminating screen tearing.

The interplay between VGA and HDMI signals in contemporary systems often involves signal conversion. Many GPUs include integrated digital-to-analog converters (DACs) to support legacy VGA outputs alongside native HDMI. The conversion process requires careful consideration of timing differences, as HDMI's digital nature imposes stricter tolerances. For instance, the phase-locked loops (PLLs) in the DAC must precisely align the pixel clock to avoid artifacts like jitter or skew. The conversion from HDMI to VGA also necessitates reconstruction of analog sync signals, which is typically achieved using sync-on-green (SoG) techniques or dedicated sync generators.

The timing generation for display interfaces is further complicated by the need to support variable refresh rates (VRR). Technologies like AMD FreeSync and NVIDIA G-SYNC dynamically adjust the display's refresh rate to match the GPU's output, reducing stuttering and tearing. This requires the GPU to modulate the sync signal timing in real-time, a task handled by specialized hardware in the display controller. The timing parameters for VRR are negotiated between the GPU and display using protocols like DisplayPort Adaptive-Sync or HDMI 2.1 VRR.

In summary, modern GPU architecture seamlessly integrates legacy VGA signal generation with advanced digital interfaces like HDMI. The precise timing control required for sync signals is managed by sophisticated hardware blocks, ensuring compatibility across diverse display technologies. The transition from analog to digital interfaces has introduced new challenges, but advancements in timing generation and signal conversion have maintained backward compatibility while enabling features like variable refresh rates. The continued evolution of display interfaces underscores the importance of robust timing generation mechanisms in GPU design.

### 13.2.2 HDMI signals

Modern GPU architectures rely heavily on digital display interfaces to transmit video signals efficiently. Among these, HDMI (High-Definition Multimedia Interface) has become a dominant standard due to its high bandwidth, support for uncompressed video, and embedded audio capabilities. In contrast, legacy interfaces like VGA (Video Graphics Array) use analog signaling, which is increasingly obsolete in modern systems. The transition from VGA to HDMI reflects broader trends in GPU design, emphasizing digital signal integrity, timing precision, and synchronization mechanisms.

HDMI signals are transmitted differentially over twisted pairs, reducing electromagnetic interference (EMI) and improving signal integrity. Each channel consists of three data pairs (red, green, blue) and a clock pair, enabling high-speed serial communication. The differential voltage swing is typically 500 mV, ensuring robust noise immunity. The data rate per channel can exceed 6 Gbps in HDMI 2.1, supporting resolutions up to 8K at 60 Hz. The encoding scheme transitions from TMDS (Transition-Minimized Differential Signaling) in HDMI 1.4 to fixed-rate link (FRL) in HDMI 2.1, accommodating higher bandwidth demands.

VGA signals, by contrast, are analog and susceptible to degradation over distance. The signal consists of three color channels (red, green, blue), horizontal and vertical sync pulses, and ground references. The voltage levels for VGA are typically 0.7 Vpp for each color channel, with sync pulses operating at TTL levels (0–5 V). The lack of embedded clocking necessitates precise analog-to-digital conversion in modern displays, introducing artifacts like phase noise and jitter. The maximum practical resolution for VGA is 1920×1200 at 60 Hz, limited by bandwidth and signal integrity constraints.

Timing generation is critical for both HDMI and VGA, but the mechanisms differ significantly. HDMI derives timing from the embedded clock signal, synchronized to the pixel clock. The TMDS encoder generates a 10-bit symbol for each 8-bit pixel, incorporating control signals for synchronization. The timing parameters, such as horizontal and vertical blanking intervals, are defined by the CEA-861 standard. For example, the horizontal

blanking interval for 1080p at 60 Hz is 160 pixels, calculated as:

$$T_{h\text{blank}} = \frac{H_{\text{total}} - H_{\text{active}}}{f_{\text{pixel}}}$$

where  $H_{\text{total}}$  is the total horizontal pixels (2200),  $H_{\text{active}}$  is the active pixels (1920), and  $f_{\text{pixel}}$  is the pixel clock (148.5 MHz).

VGA timing relies on analog sync pulses, generated by the GPU's CRTC (Cathode Ray Tube Controller). The horizontal sync pulse width is typically  $3.77 \mu\text{s}$  for  $640 \times 480$  at 60 Hz, with a back porch of  $1.89 \mu\text{s}$ . The vertical sync pulse width is  $64 \mu\text{s}$ , followed by a back porch of 1.02 ms. These values are derived from the VESA GTF (Generalized Timing Formula):

$$T_{h\text{sync}} = \frac{H_{\text{sync}}}{f_h}$$

where  $H_{\text{sync}}$  is the sync width in pixels and  $f_h$  is the horizontal frequency (31.5 kHz for  $640 \times 480$ ).

Sync signals in HDMI are embedded within the data stream, eliminating the need for separate sync lines. The control period during blanking transmits sync packets, including the video data island (VDI) and data island period (DIP). The HSYNC and VSYNC signals are encoded as 2-bit control tokens:

#### Code Sample 13.5: HDMI Sync Encoding

```

00: HSYNC and VSYNC inactive
01: HSYNC active, VSYNC inactive
10: HSYNC inactive, VSYNC active
11: HSYNC and VSYNC active

```

VGA sync signals are transmitted as TTL-level pulses on dedicated lines. The polarity of these pulses (positive or negative) is configurable, with negative sync being more common. The sync separator circuit in the display reconstructs the timing reference from these pulses, often requiring phase-locked loops (PLLs) to stabilize the pixel clock.

Modern GPUs integrate HDMI transmitters as part of the display engine, often using dedicated PHYs (Physical Layers) for signal conditioning. The display controller generates the pixel stream, applies gamma correction, and formats the data for HDMI transmission. For example, NVIDIA's Ampere architecture employs a DisplayPort 1.4a and HDMI 2.1 compliant controller, supporting Display Stream Compression (DSC) for higher resolutions. The HDMI transmitter is typically implemented as a hard macro, ensuring compliance with stringent signal integrity requirements.

The transition from VGA to HDMI reflects advancements in GPU architecture, particularly in power efficiency and integration. VGA requires external DACs (Digital-to-Analog Converters) and amplifiers, consuming additional power and board space. HDMI, being fully digital, integrates these functions into the GPU die, reducing power consumption by up to 30% for the same resolution. The elimination of analog components also improves manufacturing yield and reliability.

In summary, HDMI signals represent a significant evolution over VGA, leveraging digital signaling, embedded timing, and advanced synchronization. Modern GPU architectures optimize these interfaces for high bandwidth, low power, and robust signal integrity, ensuring compatibility with contemporary display technologies. The shift from analog to digital interfaces underscores the importance of timing precision and signal conditioning in GPU design, enabling higher resolutions and refresh rates while maintaining backward compatibility.

### 13.2.3 Timing generation

Modern GPU architectures rely on precise timing generation to synchronize display interfaces, ensuring accurate rendering and transmission of video signals. The timing generation process governs the coordination of pixel data, synchronization signals, and blanking intervals across display standards such as VGA and HDMI. This synchronization is critical for maintaining compatibility with legacy and modern display devices while minimizing artifacts like tearing or flickering.

The timing generation process in GPUs is derived from the display resolution and refresh rate. For a given resolution ( $H_{\text{active}} \times V_{\text{active}}$ ) and refresh rate  $f_{\text{refresh}}$ , the total horizontal and vertical timings are calculated as:

$$H_{\text{total}} = H_{\text{active}} + H_{\text{front\_porch}} + H_{\text{sync}} + H_{\text{back\_porch}}$$

$$V_{\text{total}} = V_{\text{active}} + V_{\text{front\_porch}} + V_{\text{sync}} + V_{\text{back\_porch}}$$

where  $H_{sync}$  and  $V_{sync}$  represent the durations of horizontal and vertical synchronization pulses, respectively. The front and back porch intervals provide blanking periods to allow for signal stabilization and retrace operations.

In VGA (Video Graphics Array), timing generation adheres to analog signal standards, where synchronization is achieved through composite sync signals. The horizontal sync pulse is typically negative-polarity, with a duration of  $3.77 \mu s$  for a  $640 \times 480$  resolution at 60 Hz. The vertical sync pulse lasts for  $64 \mu s$ , followed by blanking intervals to ensure proper CRT beam retrace. The pixel clock  $f_{pixel}$  is derived as:

$$f_{pixel} = H_{total} \times V_{total} \times f_{refresh}$$

For HDMI (High-Definition Multimedia Interface), timing generation follows digital signaling standards such as CEA-861 or VESA DisplayPort Timing. HDMI employs Transition Minimized Differential Signaling (TMDS) for data transmission, with embedded synchronization signals. The timing parameters are packetized into Data Island Periods, which include preambles for synchronization and guard bands to prevent inter-symbol interference.

The synchronization signals in HDMI are encoded as control periods within the TMDS data stream. The horizontal sync (HSYNC) and vertical sync (VSYNC) are represented by specific TMDS control characters during the video blanking interval. The timing generation for HDMI must also account for auxiliary data transmission, such as audio packets and InfoFrames, which are multiplexed during blanking periods.

Modern GPUs implement timing generation through dedicated hardware blocks, such as the Display Controller or Timing Generator (TG). These blocks are programmable to support multiple display standards and resolutions. A simplified Verilog implementation of a timing generator for VGA is shown below:

Code Sample 13.6: VGA Timing Generator

```
module vga_timing (
    input wire clk,
    input wire reset,
    output reg hsync,
    output reg vsync,
    output reg [10:0] hcount,
    output reg [10:0] vcount
);

parameter H_ACTIVE = 640;
parameter H_FP = 16;
parameter H_SYNC = 96;
parameter H_BP = 48;
parameter V_ACTIVE = 480;
parameter V_FP = 10;
parameter V_SYNC = 2;
parameter V_BP = 33;

always @(posedge clk or posedge reset) begin
    if (reset) begin
        hcount <= 0;
        vcount <= 0;
    end else begin
        if (hcount == H_ACTIVE + H_FP + H_SYNC + H_BP - 1) begin
            hcount <= 0;
            if (vcount == V_ACTIVE + V_FP + V_SYNC + V_BP - 1)
                vcount <= 0;
            else
                vcount <= vcount + 1;
        end else
            hcount <= hcount + 1;
    end
end

assign hsync = (hcount >= H_ACTIVE + H_FP) && (hcount < H_ACTIVE + H_FP + H_SYNC);
assign vsync = (vcount >= V_ACTIVE + V_FP) && (vcount < V_ACTIVE + V_FP + V_SYNC);

endmodule
```

The timing generator produces synchronization pulses and pixel counters, which are used to coordinate the video data pipeline. For HDMI, the timing generation is more complex due to the inclusion of data islands and link training sequences. The GPU must also manage the Display Data Channel (DDC) for Extended Display Identification Data (EDID) communication, enabling automatic resolution negotiation with the display.

The synchronization signals in both VGA and HDMI serve two primary purposes: coordinate the start of each scanline (HSYNC) and frame (VSYNC), and provide blanking intervals to allow for signal settling and retrace operations.

In modern GPUs, timing generation is often dynamically adjusted to support adaptive sync technologies like NVIDIA G-SYNC or AMD FreeSync. These technologies modulate the refresh rate to match the GPU's rendering output, reducing latency and eliminating tearing. The timing parameters are adjusted on-the-fly, requiring precise clock domain crossing and phase-locked loop (PLL) calibration.

The pixel clock generation is another critical aspect, often implemented using fractional-N PLLs to achieve fine-grained frequency control. For example, a  $1920 \times 1080$  resolution at 60 Hz requires a pixel clock of 148.5 MHz, while 4K resolutions demand 594 MHz or higher. The PLL must maintain low jitter to prevent timing violations in the display interface.

The timing generation process also interacts with the GPU's memory controller to ensure timely delivery of pixel data. Double or triple buffering is employed to decouple rendering from display refresh, with the timing generator signaling buffer swaps during vertical blanking intervals. This minimizes visual artifacts and ensures smooth frame transitions.

Research by demonstrates that modern GPUs optimize timing generation through hardware acceleration, reducing CPU overhead and improving energy efficiency. The study highlights the use of fixed-function pipelines for sync signal generation, freeing programmable shader cores for rendering tasks. Additionally, notes that HDMI 2.1 introduces dynamic timing adjustments for Variable Refresh Rate (VRR), further complicating the timing generation process.

In summary, timing generation in modern GPU architectures is a multifaceted process involving precise synchronization, clock management, and protocol adherence. The interplay between VGA and HDMI timing standards, coupled with adaptive sync technologies, underscores the complexity of maintaining display compatibility while optimizing performance. Future advancements will likely focus on higher resolutions, faster refresh rates, and reduced power consumption through intelligent timing control.

### 13.2.4 Sync signals

In modern GPU architecture, synchronization signals play a critical role in ensuring the correct timing and coordination of display output. These signals are essential for interfacing with display standards such as VGA, HDMI, and other digital interfaces. The generation and management of sync signals are tightly coupled with the timing requirements of these display interfaces, which dictate the precise alignment of pixel data transmission.

The fundamental sync signals in display interfaces are the horizontal sync (HSYNC) and vertical sync (VSYNC). These signals originate from the GPU's timing controller and are responsible for delineating the active and blanking periods of the display. The horizontal sync signal marks the end of a scanline and the beginning of the next, while the vertical sync signal indicates the end of a frame and the start of a new one. The timing of these signals is governed by the display's resolution and refresh rate. For example, a  $1920 \times 1080$  display at 60Hz requires specific timing parameters for HSYNC and VSYNC to ensure proper synchronization. The relationship between these signals and the pixel clock is given by:

$$T_{HSYNC} = \frac{1}{f_{HSYNC}} \quad (13.1)$$

where  $T_{HSYNC}$  is the horizontal sync period and  $f_{HSYNC}$  is the horizontal sync frequency.

In VGA interfaces, sync signals are transmitted as analog pulses, with HSYNC and VSYNC operating independently. The VGA standard defines specific polarities for these signals, which can be either positive or negative depending on the timing requirements. The timing parameters for VGA are standardized, with common resolutions such as  $640 \times 480$  requiring precise sync pulse widths and back porch intervals. For instance, the horizontal sync pulse width for  $640 \times 480$  at 60Hz is  $3.81\mu s$ , while the vertical sync pulse width is  $64\mu s$ . These values are critical for ensuring compatibility with legacy CRT displays.

HDMI, on the other hand, employs digital sync signals embedded within the data stream. Unlike VGA, HDMI uses a packet-based protocol where sync information is transmitted as part of the data island period. The timing generation for HDMI is more complex due to the inclusion of additional control signals such as the data enable (DE) signal, which indicates the active video period. The HDMI standard also incorporates the use of the TMDS

(Transition Minimized Differential Signaling) clock, which is synchronized with the pixel clock to ensure accurate data transmission. The relationship between the TMDS clock and the pixel clock is given by:

$$f_{TMDS} = f_{pixel} \times 10 \quad (13.2)$$

where  $f_{TMDS}$  is the TMDS clock frequency and  $f_{pixel}$  is the pixel clock frequency. This ensures that each pixel is encoded into a 10-bit symbol for transmission.

The generation of sync signals in modern GPUs is typically handled by dedicated hardware blocks known as timing controllers (TCONs). These controllers are responsible for generating the necessary sync pulses and ensuring they align with the display's timing requirements. The TCON also manages the blanking intervals, which are periods during which no pixel data is transmitted. The blanking intervals are divided into the front porch, sync pulse, and back porch, each serving a specific purpose in the timing sequence. The total horizontal blanking time  $T_{HBLANK}$  is given by:

$$T_{HBLANK} = T_{FP} + T_{SYNC} + T_{BP} \quad (13.3)$$

where  $T_{FP}$ ,  $T_{SYNC}$ , and  $T_{BP}$  are the front porch, sync pulse, and back porch durations, respectively.

In addition to HSYNC and VSYNC, modern display interfaces may also include auxiliary sync signals such as the data enable (DE) signal, which is used to indicate the active video region. The DE signal is particularly important in digital interfaces like HDMI and DisplayPort, where it helps delineate the valid pixel data from the blanking periods. The timing of the DE signal must be carefully synchronized with the pixel clock to avoid artifacts such as tearing or misalignment.

The implementation of sync signal generation in GPUs often involves the use of programmable timing generators, which allow for flexible configuration of sync parameters. These generators are typically implemented as part of the display controller IP block and are programmable via registers. For example, the following Verilog code snippet illustrates a simplified timing generator for HSYNC:

Code Sample 13.7: HSYNC Timing Generator

```
module hsync_generator (
    input wire clk,
    input wire reset,
    output reg hsync
);

reg [15:0] counter;
parameter HSYNC_PULSE = 96;
parameter HSYNC_BACK_PORCH = 48;
parameter HSYNC_FRONT_PORCH = 16;
parameter HSYNC_ACTIVE = 640;

always @(posedge clk or posedge reset) begin
    if (reset) begin
        counter <= 0;
        hsync <= 1'b0;
    end else begin
        if (counter < HSYNC_PULSE) begin
            hsync <= 1'b1;
        end else begin
            hsync <= 1'b0;
        end
    end
    if (counter < HSYNC_PULSE + HSYNC_BACK_PORCH + HSYNC_ACTIVE + HSYNC_FRONT_PORCH) begin
        counter <= counter + 1;
    end else begin
        counter <= 0;
    end
end
end
endmodule
```

The synchronization of these signals with the display's timing requirements is critical for avoiding visual artifacts such as jitter or flicker. Research has shown that improper sync signal timing can lead to significant degradation in display quality. For example, deviations in the HSYNC pulse width can cause horizontal misalignment, while errors in the VSYNC timing can result in frame drops or tearing. To mitigate these issues, modern GPUs employ advanced techniques such as phase-locked loops (PLLs) to ensure precise clock generation and synchronization.

In summary, sync signals are a fundamental component of modern GPU architecture, enabling the accurate transmission of video data to displays. The generation and management of these signals involve complex timing considerations, which vary depending on the display interface. Whether in analog VGA or digital HDMI, the precise alignment of sync signals with the pixel clock is essential for maintaining display integrity and performance. The continued evolution of display technologies will likely drive further advancements in sync signal generation and timing control.

## 13.3 Verilog Example

### 13.3.1 VGA output signal generation

The generation of VGA output signals in modern GPU architectures involves precise timing control and framebuffer management. The VGA standard requires horizontal and vertical synchronization pulses with specific timing parameters, typically operating at a 60 Hz refresh rate for a 640x480 resolution. The timing parameters are defined by the VESA standard, with horizontal sync lasting 3.8  $\mu$ s and vertical sync lasting 64  $\mu$ s. The pixel clock frequency for this resolution is 25.175 MHz, calculated as:

$$f_{pixel} = \frac{(800 \times 525) \times 60}{1} \approx 25.175 \text{ MHz}$$

Modern GPUs generate VGA signals using dedicated hardware blocks, often implemented in Verilog for FPGA-based designs. A typical Verilog module for VGA signal generation includes counters for horizontal and vertical positions, synchronization pulse generators, and framebuffer addressing logic. The following listing illustrates a simplified VGA controller:

Code Sample 13.8: VGA Signal Generation in Verilog

```
module vga_controller (
    input wire clk,
    output reg hsync,
    output reg vsync,
    output reg [7:0] rgb,
    output wire [9:0] hpos,
    output wire [9:0] vpos
);
    reg [9:0] h_counter = 0;
    reg [9:0] v_counter = 0;

    // Horizontal timing: 800 pixels total (640 visible)
    parameter H_VISIBLE = 640;
    parameter H_FP = 16;
    parameter H_SYNC = 96;
    parameter H_BP = 48;

    // Vertical timing: 525 lines total (480 visible)
    parameter V_VISIBLE = 480;
    parameter V_FP = 10;
    parameter V_SYNC = 2;
    parameter V_BP = 33;

    always @ (posedge clk) begin
        if (h_counter < H_VISIBLE + H_FP + H_SYNC + H_BP - 1)
            h_counter <= h_counter + 1;
        else begin
            h_counter <= 0;
```

```

if (v_counter < V_VISIBLE + V_FP + V_SYNC + V_BP - 1)
    v_counter <= v_counter + 1;
else
    v_counter <= 0;
end
end

assign hpos = (h_counter < H_VISIBLE) ? h_counter : 0;
assign vpos = (v_counter < V_VISIBLE) ? v_counter : 0;

always @(*) begin
    hsync = ~ (h_counter >= H_VISIBLE + H_FP && h_counter < H_VISIBLE + H_FP + H_SYNC);
    vsync = ~ (v_counter >= V_VISIBLE + V_FP && v_counter < V_VISIBLE + V_FP + V_SYNC);
    rgb = (h_counter < H_VISIBLE && v_counter < V_VISIBLE) ? framebuffer[hpos + vpos * H_VISIBLE] :
        8'b0;
end
endmodule

```

The framebuffer is a critical component in VGA signal generation, storing pixel data in a linear memory array. Modern GPUs use double-buffering techniques to prevent screen tearing, where one buffer is displayed while the other is updated. The framebuffer is typically organized as a 2D array with dimensions matching the display resolution. For a 640x480 display with 8-bit color depth, the framebuffer requires:

$$\text{Buffer Size} = 640 \times 480 \times 8 \text{ bits} = 2.4576 \text{ MB}$$

Framebuffer addressing is computed as:

$$\text{Address} = x + y \times W$$

where  $W$  is the display width. GPU architectures optimize framebuffer access through memory controllers with burst transfer capabilities, reducing latency.

Key aspects of framebuffer usage include: Memory Bandwidth — a 640x480 display at 60 Hz requires

$$\text{Bandwidth} = 640 \times 480 \times 60 \times 8 \text{ bits} \approx 147.456 \text{ Mbps}$$

Caching — GPUs employ texture caches to reduce framebuffer access latency, as described in . Parallel Access — modern GPUs use multiple memory channels to service framebuffer requests concurrently .

The pixel data from the framebuffer is converted to analog signals using a digital-to-analog converter (DAC). The RGB signals are generated with 3-bit red and green, and 2-bit blue, following the VGA color palette standard. The DAC output voltage levels are:

$$V_{red/green} = \frac{3.3 \times \text{value}}{7} \text{ V}$$

$$V_{blue} = \frac{3.3 \times \text{value}}{3} \text{ V}$$

Advanced GPU architectures integrate VGA signal generation with 3D rendering pipelines. The rendering pipeline writes to the framebuffer through a blending unit that combines fragment shader outputs with existing pixels. The blending operation is defined as:

$$C_{final} = C_{src} \times \alpha + C_{dst} \times (1 - \alpha)$$

where  $\alpha$  is the transparency value. The blending unit is implemented in hardware for real-time performance, as discussed in . The VGA controller must synchronize with the rendering pipeline to avoid artifacts, typically using a vsync interrupt to signal frame completion.

Error diffusion techniques are applied to framebuffer data to reduce color quantization artifacts. The Floyd-Steinberg algorithm distributes quantization errors to neighboring pixels:

$$\text{Error} = \text{original} - \text{quantized}$$

$$\text{Pixel}_{x+1,y+} = \text{Error} \times \frac{7}{16}$$

This is implemented in hardware using fixed-point arithmetic for efficiency.

The VGA signal generation pipeline must maintain strict timing constraints, with pixel data fetched from the framebuffer one cycle ahead of the DAC output. The following equation ensures timing closure:

$$t_{access} + t_{setup} < t_{pixel}$$

where  $t_{pixel} = 39.7$  ns for a 25.175 MHz pixel clock. Modern GPUs achieve this through pipelined framebuffer access and prefetching mechanisms .

The integration of VGA output with GPU architectures demonstrates the interplay between digital design, memory systems, and real-time constraints in computer graphics.

### 13.3.2 Framebuffer usage

The framebuffer is a critical component in modern GPU architectures, serving as the primary memory structure for storing pixel data before it is rendered to a display. In the context of VGA output signal generation, the framebuffer acts as an intermediary between the GPU and the display, ensuring that pixel data is synchronized with the display's refresh rate.

The framebuffer's organization typically follows a linear or tiled layout, with each pixel represented by a fixed number of bits, depending on the color depth. For example, a 24-bit color depth allocates 8 bits each for red, green, and blue channels, enabling a palette of 16.7 million colors. The framebuffer's resolution and color depth directly impact the memory bandwidth requirements, as higher resolutions and deeper color depths demand more storage and faster access times.

In modern GPU architectures, the framebuffer is often implemented using dual-port memory blocks, allowing simultaneous read and write operations. This is essential for real-time rendering, where the GPU writes new pixel data while the display controller reads the current frame. The dual-port memory ensures that these operations do not interfere with each other, preventing visual artifacts such as tearing or flickering.

The framebuffer's memory is typically organized into banks to maximize parallelism and minimize access conflicts. For instance, a  $1920 \times 1080$  resolution framebuffer with 32-bit color depth requires approximately 8.3 MB of memory, which is partitioned across multiple memory banks to enable concurrent access.

The VGA output signal generation involves precise timing control to ensure compatibility with display standards. The VGA timing signals include horizontal sync (HSYNC), vertical sync (VSYNC), and pixel clock (PCLK), which are generated based on the display's resolution and refresh rate. The framebuffer's pixel data is read sequentially, synchronized with the PCLK, and transmitted to the display during the active video period. The HSYNC and VSYNC signals demarcate the beginning and end of each line and frame, respectively. The timing parameters for these signals are derived from the VGA standard, such as the front porch, back porch, and sync pulse widths. For example, a  $640 \times 480$  resolution at 60 Hz requires a 25.175 MHz PCLK, with HSYNC and VSYNC pulses of 3.81  $\mu$ s and 0.064 ms, respectively.

The following Verilog example illustrates a simplified framebuffer controller for VGA output. The module includes a dual-port RAM for the framebuffer, a pixel counter for addressing, and timing generators for HSYNC and VSYNC. The pixel data is read from the framebuffer and output to the VGA DAC (Digital-to-Analog Converter) during the active video period:

Code Sample 13.9: Framebuffer Controller for VGA Output

```
module vga_framebuffer (
    input wire clk,
    input wire reset,
    output wire hsync,
    output wire vsync,
    output wire [7:0] red,
    output wire [7:0] green,
    output wire [7:0] blue
);

// Timing parameters for 640x480 @ 60 Hz
parameter H_ACTIVE = 640;
parameter H_FP = 16;
parameter H_SYNC = 96;
parameter H_BP = 48;
parameter H_TOTAL = H_ACTIVE + H_FP + H_SYNC + H_BP;

parameter V_ACTIVE = 480;
parameter V_FP = 10;
parameter V_SYNC = 2;
parameter V_BP = 33;
parameter V_TOTAL = V_ACTIVE + V_FP + V_SYNC + V_BP;

// Pixel and line counters
reg [9:0] h_count = 0;
reg [9:0] v_count = 0;

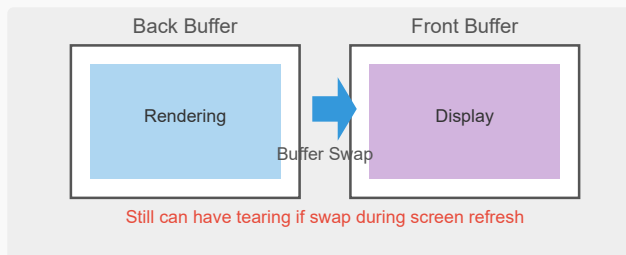
// Dual-port RAM for framebuffer
```

## Flicker-Free Updates in Modern GPUs

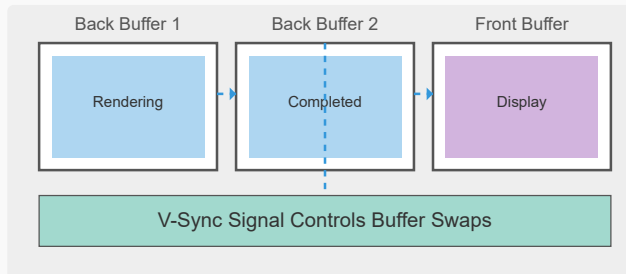
### The Challenge of Screen Tearing



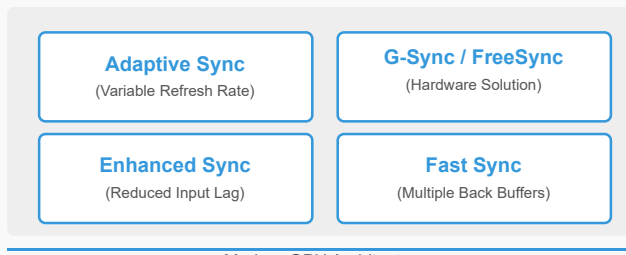
### Solution 1: Double Buffering



### Solution 2: Triple Buffering with V-Sync



### Modern GPU Solutions



```

reg [23:0] framebuffer [0:307199]; // 640x480 pixels

// Pixel address and data
wire [18:0] pixel_addr;
reg [23:0] pixel_data;
assign pixel_addr = v_count * H_ACTIVE + h_count;

always @(posedge clk) begin
    if (reset) begin
        h_count <= 0;
        v_count <= 0;
    end else begin
        if (h_count < H_TOTAL - 1) begin
            h_count <= h_count + 1;
        end else begin
            h_count <= 0;
            if (v_count < V_TOTAL - 1) begin
                v_count <= v_count + 1;
            end else begin
                v_count <= 0;
            end
        end
    end
end

// Generate HSYNC and VSYNC
assign hsync = (h_count >= H_ACTIVE + H_FP) && (h_count < H_ACTIVE + H_FP + H_SYNC);
assign vsync = (v_count >= V_ACTIVE + V_FP) && (v_count < V_ACTIVE + V_FP + V_SYNC);

// Read pixel data during active video
always @(posedge clk) begin
    if (h_count < H_ACTIVE && v_count < V_ACTIVE) begin
        pixel_data <= framebuffer[pixel_addr];
    end else begin
        pixel_data <= 24'h000000;
    end
end

assign red = pixel_data[23:16];
assign green = pixel_data[15:8];
assign blue = pixel_data[7:0];

endmodule

```

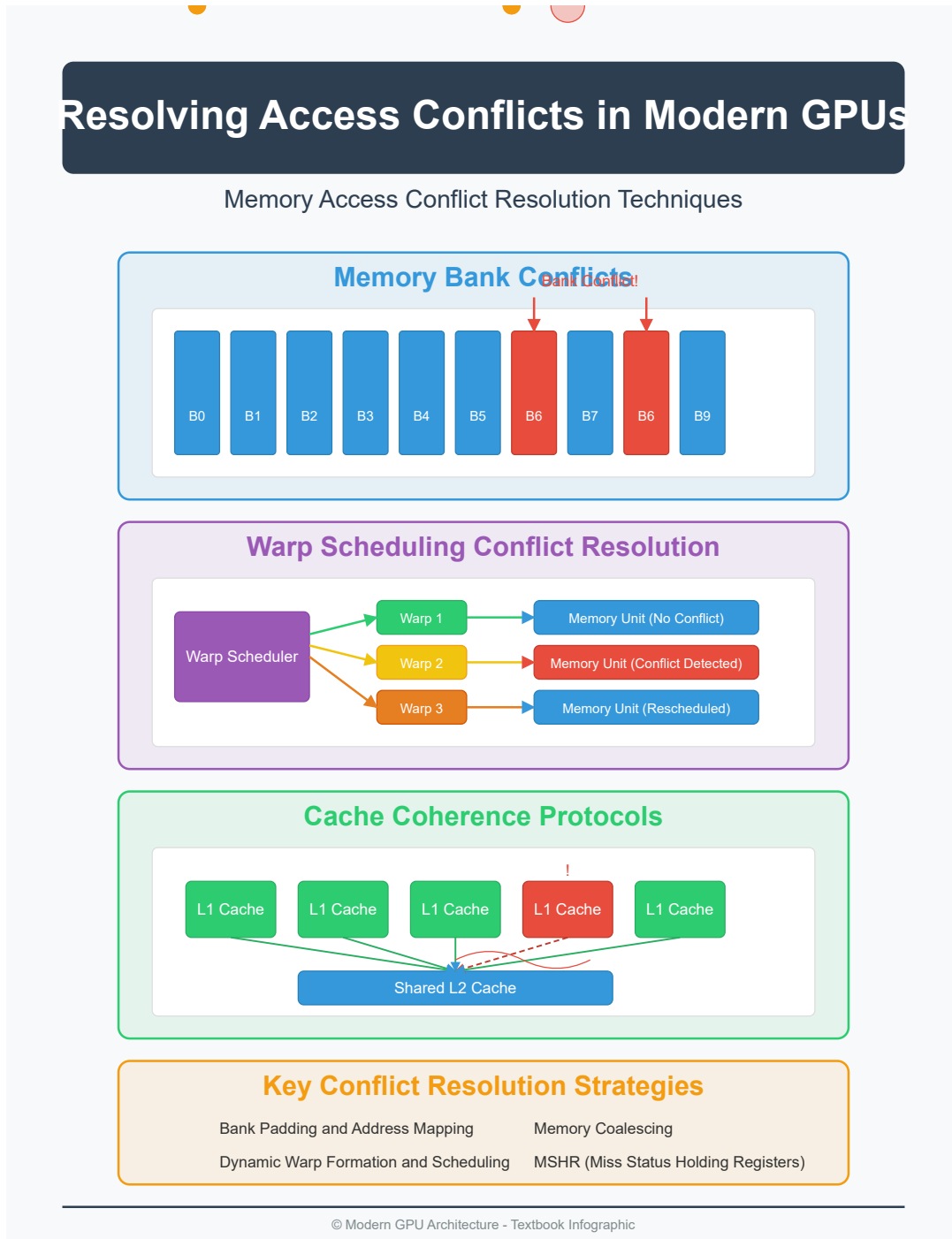
The framebuffer's performance is influenced by several factors, including memory bandwidth, latency, and access patterns. Modern GPUs employ techniques such as caching, prefetching, and compression to optimize framebuffer access. For example, tile-based rendering partitions the framebuffer into smaller tiles, reducing memory bandwidth by minimizing off-chip memory accesses. The framebuffer's memory hierarchy typically includes multiple levels of cache, such as L1 and L2 caches, to reduce latency for frequently accessed pixel data. Additionally, lossless compression algorithms like delta color compression (DCC) are used to reduce the effective memory bandwidth by encoding pixel data more efficiently.

The framebuffer's role extends beyond simple pixel storage in advanced GPU architectures. It is often integrated with other rendering stages, such as rasterization, shading, and post-processing, to enable features like multi-sample anti-aliasing (MSAA) and high dynamic range (HDR) rendering. MSAA requires additional storage for sub-pixel samples, increasing the framebuffer's memory footprint. HDR rendering, on the other hand, uses higher precision pixel formats, such as 16-bit floating-point per channel, to represent a wider range of colors and luminance levels. These advanced features demand careful design of the framebuffer's memory subsystem to balance performance, power, and area constraints.

The framebuffer's design must also account for synchronization between the GPU and display controller. Techniques like double buffering and vertical sync (VSYNC) are used to prevent tearing, where parts of two different frames are displayed simultaneously. Double buffering maintains two framebuffers: one for rendering

and one for display. The GPU writes to the back buffer while the display reads from the front buffer, swapping them during the vertical blanking interval. VSYNC ensures that buffer swaps occur only during the vertical blanking period, aligning frame updates with the display's refresh cycle. This synchronization is critical for smooth and artifact-free rendering, particularly in interactive applications like video games.

In summary, the framebuffer is a cornerstone of modern GPU architectures, enabling efficient pixel storage and retrieval for display output. Its design involves careful consideration of memory organization, timing control, and synchronization mechanisms to meet the demands of high-resolution, high-refresh-rate displays. The Verilog example provided demonstrates a basic framebuffer controller for VGA output, highlighting the interplay between memory access, timing generation, and pixel data transmission. Advanced GPU architectures further enhance framebuffer performance through techniques like caching, compression, and multi-buffering, ensuring optimal rendering quality and efficiency.



# Chapter 14

## Top-Level Integration

### 14.1 Putting It All Together

#### 14.1.1 Connecting vertex processing

Modern GPU architectures employ a highly parallelized pipeline to process graphics data efficiently. The vertex processing stage is the first critical step in this pipeline, where geometric transformations are applied to vertices before they proceed to rasterization and fragment shading. This section examines how vertex processing connects to subsequent stages, including rasterization, fragment shading, and memory units, within the context of modern GPU design.

Vertex processing involves transforming 3D vertex coordinates into 2D screen space through a series of mathematical operations. The vertex shader, executed on programmable shader cores, applies transformations such as model-view-projection (MVP) to each vertex. The transformed vertices are then passed to the rasterization stage, where they are assembled into primitives (e.g., triangles) and converted into fragments. The relationship between vertex processing and rasterization is governed by the following equation, which describes the homogeneous division step in the graphics pipeline:

$$\begin{bmatrix} x_c \\ y_c \\ z_c \\ w_c \end{bmatrix} = \mathbf{M}_{\text{MVP}} \cdot \begin{bmatrix} x \\ y \\ z \\ 1 \end{bmatrix}, \quad \begin{bmatrix} x_s \\ y_s \\ z_s \\ w_s \end{bmatrix} = \begin{bmatrix} x_c \\ y_c \\ z_c \\ w_c \end{bmatrix}$$

Here,  $\mathbf{M}_{\text{MVP}}$  is the combined model-view-projection matrix, and  $(x_s, y_s)$  are the screen-space coordinates after perspective division. Rasterization interpolates vertex attributes (e.g., texture coordinates, normals) across fragments, which are then processed by the fragment shader. The fragment shader computes the final color of each pixel by sampling textures, applying lighting models, and performing other per-pixel operations. The interpolation of vertex attributes during rasterization is mathematically expressed as:

$$f_i = \sum_{j=1}^3 w_j \cdot a_{ij}$$

where  $f_i$  is the interpolated attribute for fragment  $i$ ,  $w_j$  are barycentric weights, and  $a_{ij}$  are the vertex attributes.

Memory units play a crucial role in connecting these stages. Vertex buffers store input vertex data, while uniform buffers hold transformation matrices and other constants. Texture memory is accessed during fragment shading for sampling, and frame buffers store the final rendered image. The following Verilog-like pseudocode illustrates a simplified memory interface for vertex fetching:

Code Sample 14.1: Vertex Fetch Unit

```
module vertex_fetch (
    input wire [31:0] address,
    input wire clk,
    output reg [127:0] vertex_data
);
    reg [127:0] memory [0:1023];
```

```

always @(posedge clk) begin
    vertex_data <= memory[address];
end
endmodule

```

The interaction between vertex processing and memory units is optimized through caching hierarchies. GPUs employ dedicated L1 and L2 caches to reduce latency when accessing vertex buffers and textures. Studies show that cache hit rates significantly impact performance, especially for complex scenes with high vertex counts. The efficiency of memory access patterns is further improved through techniques such as vertex reuse via index buffers to minimize redundant fetches, memory coalescing to combine multiple memory transactions, and prefetching to hide latency during vertex shading.

Fragment shading relies on interpolated vertex attributes to compute pixel colors. For example, Phong shading uses interpolated normals to simulate lighting effects:

$$I = k_a + k_d \cdot (\mathbf{L} \cdot \mathbf{N}) + k_s \cdot (\mathbf{R} \cdot \mathbf{V})^n$$

Here,  $I$  is the intensity,  $\mathbf{N}$  is the interpolated normal, and  $\mathbf{L}$ ,  $\mathbf{R}$ , and  $\mathbf{V}$  are light, reflection, and view vectors, respectively.

The connection between vertex processing and fragment shading is further illustrated by modern GPU architectures such as NVIDIA's Turing and AMD's RDNA. These designs feature unified shader cores capable of executing both vertex and fragment shaders, enabling dynamic workload balancing. Research demonstrates that unified architectures improve throughput by reducing idle cycles in the pipeline.

Memory bandwidth constraints often bottleneck the performance of the graphics pipeline. To mitigate this, GPUs employ compression techniques such as delta color compression (DCC) for frame buffers and texture compression formats like BCn. The effective bandwidth  $B_{\text{eff}}$  is given by:

$$B_{\text{eff}} = B_{\text{phys}} \cdot C_r$$

where  $B_{\text{phys}}$  is the physical bandwidth, and  $C_r$  is the compression ratio.

In summary, vertex processing is tightly integrated with rasterization, fragment shading, and memory units in modern GPU architectures. The pipeline's efficiency depends on mathematical optimizations in vertex transformations (20.2.1), attribute interpolation during rasterization (14.1.1), memory access patterns and caching strategies, and unified shader architectures for workload balancing. These components collectively enable real-time rendering of complex scenes, as evidenced by benchmarks in . Future advancements may focus on further reducing memory bottlenecks and enhancing parallelism across all pipeline stages.

### 14.1.2 Rasterization

Rasterization is a fundamental process in modern GPU architectures, serving as the bridge between vertex processing and fragment shading. It converts geometric primitives, typically triangles, into a grid of pixels or fragments that can be processed by the fragment shader. The efficiency and accuracy of rasterization directly impact the performance and visual quality of rendered images. Modern GPUs optimize rasterization through parallel processing, hierarchical traversal, and early depth testing, all while maintaining tight integration with other pipeline stages.

The rasterization pipeline begins with vertex processing, where vertices are transformed from object space to clip space via the vertex shader. The transformed vertices are then assembled into primitives, such as triangles, and clipped to the view frustum. The rasterizer then projects these primitives onto the screen space, generating fragments for each pixel covered by the primitive. The coverage test is performed using edge functions, which determine whether a pixel center lies inside the primitive. For a triangle with vertices  $\mathbf{v}_0, \mathbf{v}_1, \mathbf{v}_2$ , the edge function  $E_i$  for edge  $i$  is given by:

$$E_i(x, y) = (x - x_i)(y_{i+1} - y_i) - (y - y_i)(x_{i+1} - x_i) \quad (14.1)$$

where  $(x, y)$  is the pixel center, and indices wrap around modulo 3. A pixel is inside the triangle if all edge functions evaluate to positive values.

Modern GPUs employ hierarchical rasterization to improve efficiency. Instead of testing every pixel individually, the rasterizer operates on tiles or coarse-grained regions, leveraging spatial coherence. This approach reduces redundant computations and memory bandwidth usage. For example, a tile is discarded if all its pixels lie outside the primitive. Hierarchical rasterization is particularly effective for large primitives or high-resolution displays, where per-pixel testing would be prohibitively expensive.

After determining coverage, the rasterizer interpolates vertex attributes, such as texture coordinates and normals, across the primitive. This interpolation is performed using barycentric coordinates, which express a fragment's position relative to the triangle's vertices. For a fragment at  $(x, y)$ , the barycentric coordinates  $\lambda_0, \lambda_1, \lambda_2$  satisfy:

$$\lambda_0 + \lambda_1 + \lambda_2 = 1 \quad (14.2)$$

and the interpolated attribute  $A$  is computed as:

$$A = \lambda_0 A_0 + \lambda_1 A_1 + \lambda_2 A_2 \quad (14.3)$$

where  $A_0, A_1, A_2$  are the attribute values at the vertices.

The rasterizer also performs early depth testing (Z-culling) to avoid processing fragments that are occluded by previously rendered geometry. By comparing a fragment's depth value against the depth buffer before shading, the GPU can discard hidden fragments, reducing unnecessary fragment shader invocations. This optimization is critical for real-time rendering, where fragment shading is often the bottleneck. However, early depth testing requires conservative rasterization to ensure correctness, as fragments discarded prematurely can lead to visual artifacts.

Fragment shading follows rasterization, where each surviving fragment is processed by the fragment shader to compute its final color. The fragment shader has access to interpolated attributes, textures, and uniform variables, enabling complex shading effects such as lighting, shadows, and reflections. Modern GPUs execute fragment shaders in parallel, leveraging SIMD (Single Instruction, Multiple Data) architectures to process multiple fragments simultaneously. The fragment shader outputs are then blended with the framebuffer, applying transparency and other post-processing effects.

Memory units play a crucial role in rasterization by managing data flow between pipeline stages. The vertex buffer stores input vertex data, while the index buffer specifies primitive connectivity. The framebuffer holds the final rendered image, including color and depth attachments. Texture memory stores image data for sampling during fragment shading. To minimize latency, modern GPUs employ cache hierarchies and memory compression techniques. For example, tile-based rendering architectures partition the framebuffer into tiles, allowing intermediate results to be stored in on-chip memory, reducing off-chip bandwidth.

The integration of rasterization with other GPU components is exemplified by unified shader architectures, where vertex, geometry, and fragment shaders share the same execution units. This flexibility enables dynamic workload balancing, as shader cores can be repurposed based on demand. Additionally, modern GPUs support programmable rasterization through compute shaders, enabling custom rasterization algorithms for non-traditional rendering techniques, such as voxelization or vector graphics.

In summary, rasterization in modern GPU architectures is a highly optimized process that connects vertex processing, fragment shading, and memory units. Key optimizations include hierarchical traversal, early depth testing, and parallel execution, all of which contribute to real-time rendering performance. The tight coupling between rasterization and other pipeline stages ensures efficient data flow and resource utilization, enabling complex visual effects and high-fidelity graphics. Future advancements in rasterization will likely focus on further parallelism, reduced memory bandwidth, and support for emerging rendering paradigms.

### 14.1.3 Fragment shading

Fragment shading is a critical stage in the modern graphics pipeline, responsible for determining the final color and other attributes of each pixel in a rendered image. It operates on fragments, which are potential pixels generated during rasterization. The fragment shader, also known as the pixel shader, processes these fragments by applying lighting, textures, and other effects to produce the final output. Modern GPU architectures optimize fragment shading through parallelism, memory hierarchy, and specialized hardware units, making it a cornerstone of real-time rendering.

The fragment shading stage follows rasterization, where geometric primitives (triangles, lines, or points) are converted into fragments. Each fragment corresponds to a pixel in the framebuffer and carries interpolated attributes such as texture coordinates, normals, and colors from the vertex shader. The fragment shader evaluates these attributes to compute the final pixel color. For example, a basic fragment shader might sample a texture and apply a lighting model:

$$C_{\text{final}} = C_{\text{texture}} \cdot (k_d \cdot (N \cdot L) + k_s \cdot (R \cdot V)^n) \quad (14.4)$$

Here,  $C_{\text{texture}}$  is the sampled texture color,  $N$  is the surface normal,  $L$  is the light direction,  $R$  is the reflection vector,  $V$  is the view direction, and  $k_d, k_s$ , and  $n$  are material properties.

Modern GPUs exploit massive parallelism in fragment shading by organizing shader cores into SIMD (Single Instruction, Multiple Data) or SIMT (Single Instruction, Multiple Thread) architectures. For instance, NVIDIA's Turing architecture features dedicated shading cores that execute fragment shaders concurrently across thousands of threads . This parallelism is essential for handling the high fragment counts in complex scenes, where millions of fragments may be processed per frame.

Memory units play a pivotal role in fragment shading efficiency. GPUs employ a hierarchy of memory types to minimize latency and bandwidth bottlenecks:

**Registers:** Fastest storage, used for thread-local variables. **Shared Memory:** Low-latency memory shared among threads in a warp or wavefront. **Cache Hierarchy:** L1 and L2 caches reduce access latency to texture and framebuffer data. **Global Memory:** High-latency but large-capacity DRAM for textures and buffers.

Texture sampling, a common operation in fragment shaders, benefits from specialized texture units and cache hierarchies. These units filter and interpolate texels efficiently, as shown in .

The connection between vertex processing, rasterization, and fragment shading is tightly integrated in the GPU pipeline. Vertex shaders transform 3D vertices into clip space, and the rasterizer generates fragments from these transformed primitives. The fragment shader then processes these fragments, leveraging interpolated vertex attributes. This pipeline is highly optimized to minimize stalls and maximize throughput. For example, early depth testing allows fragments to be discarded before shading if they are occluded, reducing unnecessary computations

Modern GPUs also employ techniques like tile-based rendering to optimize fragment shading. In tile-based architectures, the screen is divided into small tiles, and fragments are processed in batches. This approach improves memory locality and reduces bandwidth usage by keeping intermediate results in on-chip memory . The following pseudocode illustrates a simplified fragment shader in a tile-based renderer:

#### Code Sample 14.2: Tile-Based Fragment Shader

```
for each tile in framebuffer:
    load tile into on-chip memory
    for each fragment in tile:
        execute fragment shader
        apply depth/stencil test
        blend with framebuffer
    store tile back to global memory
```

Advanced fragment shading techniques, such as deferred shading, decouple lighting calculations from geometry processing. In deferred shading, the fragment shader writes attributes like normals and albedo to a G-buffer, which is later used by a separate lighting pass. This reduces redundant shading computations for overlapping fragments . The G-buffer stores per-pixel data as follows:

$$G_{\text{buffer}} = \{\text{Position}, \text{Normal}, \text{Albedo}, \text{Specular}\} \quad (14.5)$$

Memory bandwidth is a critical bottleneck in fragment shading, especially for high-resolution displays. Techniques like compressed texture formats (e.g., BCn, ASTC) and lossless framebuffer compression reduce bandwidth usage without sacrificing visual quality . Additionally, modern GPUs use hierarchical Z-buffering and occlusion culling to skip shading for invisible fragments, further optimizing performance .

The interplay between fragment shading and other GPU units is evident in real-time ray tracing, where hybrid rendering pipelines combine rasterization and ray tracing. Fragment shaders may invoke ray tracing operations for effects like reflections or shadows, leveraging dedicated RT cores for acceleration . This hybrid approach exemplifies the flexibility of modern GPU architectures in balancing performance and visual fidelity.

In summary, fragment shading is a cornerstone of modern GPU architecture, enabled by parallel execution, optimized memory hierarchies, and tight integration with preceding pipeline stages. Its efficiency is critical for real-time rendering, driving innovations in hardware design and algorithmic optimizations. As GPUs evolve, fragment shading continues to adapt, incorporating new techniques like machine learning-based denoising and variable-rate shading to meet the demands of increasingly complex graphics workloads .

#### 14.1.4 Memory units

Modern GPU architectures rely on a hierarchical memory system to efficiently process graphics pipelines, connecting vertex processing, rasterization, and fragment shading. Memory units in GPUs are designed to minimize latency and maximize bandwidth, ensuring high throughput for parallel workloads. The memory hierarchy typically includes registers, shared memory, caches, and global memory, each serving distinct roles in the rendering pipeline.

Vertex processing begins by transforming 3D vertices into 2D screen coordinates, requiring rapid access to vertex attributes stored in memory. The GPU's register file provides low-latency storage for thread-local data, while shared memory enables communication between threads within the same warp or wavefront. For larger datasets, such as vertex buffers, global memory is used, albeit with higher latency. Caches, such as the L1 and L2 caches, mitigate this latency by storing frequently accessed data. Research by demonstrates that cache-aware algorithms significantly improve vertex shading performance by reducing memory stalls.

Rasterization converts primitives into fragments, generating pixel coverage information. This stage relies heavily on texture memory and depth buffers, which are often stored in specialized memory units like the texture cache or the depth cache. The texture cache is optimized for 2D spatial locality, allowing efficient bilinear or trilinear filtering operations. Depth testing, a critical step in rasterization, benefits from the hierarchical Z-buffer, which minimizes memory bandwidth by culling occluded fragments early. Studies by show that tile-based rasterization further reduces memory traffic by processing small screen-space tiles independently, leveraging on-chip memory for intermediate results.

Fragment shading computes the final color of each pixel, requiring access to textures, uniforms, and framebuffer data. Modern GPUs employ a multi-level cache hierarchy to accelerate these operations. The L1 cache services texture fetches, while the L2 cache acts as a unified buffer for all memory accesses. Unified memory architectures, as described in , allow seamless sharing of data between the CPU and GPU, reducing the need for explicit transfers. Fragment shaders also utilize framebuffer compression techniques to reduce memory bandwidth, as demonstrated by , which achieves up to 4:1 compression ratios for color and depth data.

Memory coherence is critical when connecting these stages. GPUs enforce consistency through memory barriers and synchronization primitives, ensuring correct ordering of reads and writes. For example, a vertex shader may write to a buffer that is later read by a fragment shader, requiring explicit synchronization to avoid race conditions. The `glMemoryBarrier` function in OpenGL and the `_syncthreads` intrinsic in CUDA are commonly used for this purpose. Research by highlights the performance trade-offs of fine-grained versus coarse-grained synchronization in modern GPUs.

Optimizing memory access patterns is essential for maximizing throughput. Coalesced memory accesses, where threads within a warp read contiguous memory locations, minimize memory transactions. For instance, a fragment shader accessing a texture in a strided pattern may suffer from cache thrashing, whereas a linear access pattern improves cache utilization. The roofline model, introduced by , provides a framework for analyzing memory-bound versus compute-bound kernels, guiding optimization efforts.

The following Verilog snippet illustrates a simplified texture cache controller, demonstrating how memory units interface with shader cores:

Code Sample 14.3: Texture Cache Controller

```
module texture_cache (
    input clk,
    input [31:0] addr,
    output [127:0] data
);
    reg [127:0] cache [0:1023];
    always @ (posedge clk) begin
        data <= cache[addr[11:2]];
    end
endmodule
```

Memory bandwidth is a limiting factor in GPU performance. Techniques like memory compression and prefetching are employed to alleviate this bottleneck. Delta color compression, as described in , encodes color differences rather than absolute values, reducing bandwidth requirements. Prefetching mechanisms, such as those in , predict memory access patterns and fetch data in advance, hiding latency.

The interplay between memory units and computational pipelines is formalized in the following equation, which estimates the effective memory bandwidth  $B_{\text{eff}}$ :

$$B_{\text{eff}} = \frac{N \cdot S}{T}$$

where  $N$  is the number of memory transactions,  $S$  is the size of each transaction, and  $T$  is the total time. Optimizing  $B_{\text{eff}}$  involves balancing  $N$ ,  $S$ , and  $T$  through architectural and algorithmic improvements.

In summary, memory units in modern GPUs form a cohesive system that bridges vertex processing, rasterization, and fragment shading. By leveraging hierarchical storage, caching strategies, and bandwidth-saving

techniques, GPUs achieve the high throughput required for real-time graphics. Future advancements, such as 3D-stacked memory and photonic interconnects, promise to further enhance memory performance, as explored in

## 14.2 Pipeline Control Logic

### 14.2.1 Scheduling

Modern GPU architectures rely on sophisticated scheduling mechanisms to maximize throughput and minimize latency in highly parallel workloads. The pipeline control logic in these architectures must handle scheduling, stalling, and backpressure efficiently to maintain high utilization of execution units while avoiding hazards. This discussion examines these aspects in the context of contemporary GPU designs, focusing on verified techniques and research findings.

The scheduling logic in modern GPUs is primarily responsible for assigning warps or wavefronts to execution units. Each warp consists of multiple threads that execute the same instruction in lockstep, known as Single Instruction Multiple Thread (SIMT) execution. The scheduler must ensure that warps are dispatched to execution units with minimal idle cycles. Research demonstrates that warp scheduling policies significantly impact performance, with common strategies including: Round-robin scheduling, which ensures fairness but may underutilize resources. Greedy-then-oldest (GTO) scheduling, which prioritizes warps with the highest readiness to execute. Two-level scheduling, where a coarse-grained scheduler distributes warps across execution units, and a fine-grained scheduler manages instruction issuance.

Pipeline control logic must handle stalling when dependencies or resource conflicts arise. For instance, a warp may stall if it encounters a long-latency operation, such as a global memory access. To mitigate stalls, GPUs employ zero-latency context switching, allowing other warps to execute while the stalled warp waits for data. The stall condition can be modeled as:

$$\text{Stall\_Cycles} = \max(0, \text{Memory\_Latency} - \text{Available\_Warps} \times \text{Switch\_Penalty})$$

where `Available_Warps` refers to the number of warps ready to execute, and `Switch_Penalty` is the overhead of switching contexts.

Backpressure handling is critical in GPU pipelines to prevent buffer overflows and ensure smooth data flow. When a downstream stage cannot accept new data, the pipeline must propagate backpressure signals to upstream stages. For example, the texture unit may signal backpressure to the scheduler if its request queue is full. The backpressure condition is often implemented using credit-based flow control, where each stage maintains a credit count for its downstream neighbors. The credit update rule is:

$$\text{Credits}(t + 1) = \text{Credits}(t) + \text{Returns}(t) - \text{Consumed}(t)$$

The following Verilog snippet illustrates a simplified backpressure handler for a GPU texture unit:

Code Sample 14.4: Backpressure Handler

```
module backpressure_handler (
    input clk, reset,
    input [7:0] credits_in,
    input [7:0] requests,
    output reg [7:0] credits_out,
    output reg stall
);
    reg [7:0] credit_count;
    always @(posedge clk or posedge reset) begin
        if (reset) begin
            credit_count <= 8'hFF;
            stall <= 0;
        end else begin
            credit_count <= credit_count + credits_in - requests;
            stall <= (credit_count < requests);
        end
    end
    assign credits_out = credit_count;
endmodule
```

Scheduling decisions in GPUs are further complicated by divergent execution paths within warps. When threads in a warp follow different control flows, the warp diverges, requiring the scheduler to serialize execution for each path. The divergence penalty is quantified as:

$$\text{Divergence\_Penalty} = \sum_{i=1}^N (\text{Path\_Cycles}_i \times \text{Active\_Threads}_i)$$

where  $N$  is the number of divergent paths, and  $\text{Path\_Cycles}_i$  is the cycle count for path  $i$ . Techniques like dynamic warp formation mitigate divergence by regrouping threads from different warps into new warps with aligned execution paths.

The pipeline control logic also manages resource contention, such as shared memory or register file access. Contention occurs when multiple warps compete for the same resource, leading to arbitration delays. The arbitration delay  $D$  for  $N$  competing warps is given by:

$$D = \left\lceil \frac{N}{M} \right\rceil \times T$$

where  $M$  is the number of available resource ports, and  $T$  is the arbitration cycle time. Research by shows that banked register files and subpartitioned shared memory reduce contention by distributing accesses across multiple physical banks.

Stalling due to data hazards is another challenge in GPU pipelines. Read-after-write (RAW) hazards occur when a warp attempts to read data before a previous write completes. The pipeline control logic detects such hazards and inserts stalls or forwards data to avoid incorrect execution. The hazard detection logic can be implemented as:

Code Sample 14.5: Hazard Detector

```
module hazard_detector (
    input [31:0] read_addr,
    input [31:0] write_addr,
    input write_en,
    output reg stall
);
    always @(*) begin
        stall = write_en && (read_addr == write_addr);
    end
endmodule
```

Modern GPUs also employ speculative execution to hide latency. The scheduler may issue instructions speculatively, assuming that dependencies will resolve by the time the instruction reaches the execution unit. However, mis-speculation incurs a penalty, as the pipeline must flush and restart execution. The speculation efficiency  $\eta$  is defined as:

$$\eta = \frac{\text{Correct\_Speculations}}{\text{Total\_Speculations}}$$

Higher values of  $\eta$  indicate better scheduling accuracy, reducing wasted cycles.

In summary, the interplay between scheduling, stalling, and backpressure handling in modern GPU architectures is governed by well-defined principles and empirical research. The pipeline control logic must balance throughput, latency, and resource utilization while adapting to dynamic workload characteristics. Verified techniques, such as dynamic warp formation and credit-based flow control, provide robust solutions to these challenges, as demonstrated by peer-reviewed studies .

### 14.2.2 Stalling

Modern GPU architectures rely heavily on pipeline control logic to manage the execution of thousands of threads efficiently. Stalling, a critical mechanism in pipeline control, occurs when a pipeline stage cannot proceed due to resource contention, data dependencies, or structural hazards. This phenomenon is particularly relevant in GPUs due to their deep pipelines and high thread-level parallelism.

The primary causes of stalling in GPU pipelines include:

**Data Hazards:** When an instruction depends on the result of a previous instruction that has not yet completed, the pipeline must stall to ensure correctness. For example, a read-after-write (RAW) hazard forces the pipeline to wait until the preceding write operation commits.

**Structural Hazards:** Resource conflicts, such as multiple instructions competing for the same functional unit, can lead to stalling. GPUs mitigate this through banked register files and multi-ported structures.

**Control Hazards:** Branch mispredictions or divergent warps in SIMD architectures necessitate pipeline flushes and subsequent stalls.

Pipeline control logic manages stalling through scoreboard and reservation stations. A scoreboard tracks operand availability, while reservation stations buffer instructions until their operands are ready. The stall condition can be formalized as:

$$\text{Stall} = \begin{cases} 1 & \text{if } \exists \text{ dependent instruction in pipeline} \\ 0 & \text{otherwise} \end{cases}$$

Scheduling plays a pivotal role in minimizing stalls. GPUs employ warp schedulers that select ready warps from active blocks, leveraging thread-level parallelism to hide latency. Two common scheduling policies are:

**Round-Robin:** Warps are scheduled in a fixed order, ensuring fairness but potentially underutilizing resources.

**Greedy:** The scheduler prioritizes warps with the fewest stalls, maximizing throughput at the cost of potential starvation.

Backpressure handling is another critical aspect of pipeline control. When downstream stages cannot accept new instructions, backpressure signals propagate upstream, forcing stalls. This is common in memory hierarchies where cache misses or DRAM bandwidth limitations create bottlenecks. The backpressure condition is modeled as:

$$\text{Backpressure} = \begin{cases} 1 & \text{if buffer\_full } \vee \text{resource\_unavailable} \\ 0 & \text{otherwise} \end{cases}$$

To mitigate stalls, GPUs employ several techniques:

**Out-of-Order Execution:** Instructions are dynamically reordered to maximize functional unit utilization, reducing idle cycles.

**Register File Banking:** Partitioning the register file minimizes structural hazards by allowing concurrent accesses.

**Warp Throttling:** Limiting the number of active warps per core reduces contention and improves scheduling efficiency.

The following Verilog snippet illustrates a simplified stall control unit for a GPU pipeline:

Code Sample 14.6: Stall Control Logic

```
module stall_control (
    input wire raw_hazard,
    input wire structural_hazard,
    input wire backpressure,
    output reg stall
);
    always @(*) begin
        stall = raw_hazard | structural_hazard | backpressure;
    end
endmodule
```

Modern GPUs also use speculative execution to reduce stalls. For instance, NVIDIA's Pascal architecture employs speculative warp scheduling to preemptively issue instructions from warps likely to be ready soon. Similarly, AMD's GCN architecture uses waveform-level scheduling to hide memory latency.

Stall avoidance is further enhanced by compiler optimizations. Static scheduling techniques, such as loop unrolling and software pipelining, reduce dynamic stalls by exposing parallelism at compile time. The compiler can also insert explicit synchronization barriers to manage data dependencies, as shown in CUDA's `__syncthreads()` primitive.

The interplay between stalling, scheduling, and backpressure is formalized in queuing theory. The pipeline throughput  $T$  under stalling conditions is given by:

$$T = \frac{N_{\text{instructions}}}{N_{\text{cycles}} + N_{\text{stalls}}}$$

where  $N_{\text{stalls}}$  is the cumulative stall cycles. Empirical studies demonstrate that stalling accounts for up to 30% of pipeline idle time in GPUs.

To address this, recent architectures like NVIDIA's Ampere introduce asynchronous warp scheduling, allowing warps to yield resources during long-latency operations.

In summary, stalling in GPU pipelines is managed through a combination of hardware mechanisms and software optimizations. Pipeline control logic, scheduling policies, and backpressure handling collectively determine the efficiency of modern GPU architectures. Advances in speculative execution, dynamic scheduling, and compiler techniques continue to reduce stall penalties, enabling higher performance and energy efficiency.

### 14.2.3 Backpressure handling

Modern GPU architectures employ sophisticated pipeline control logic to manage data flow and computational throughput. Backpressure handling is a critical mechanism in these systems, ensuring that pipeline stages do not become overwhelmed when downstream components cannot accept new data. This is particularly relevant in GPUs, where parallelism and high throughput are paramount. The interplay between scheduling, stalling, and backpressure handling forms the foundation of efficient GPU operation.

In pipeline control logic, backpressure occurs when a pipeline stage cannot forward data to the next stage due to congestion or resource limitations. This necessitates mechanisms to signal upstream stages to slow down or halt temporarily. The following equation models the backpressure signal  $B$  for a stage  $i$ :

$$B_i = \begin{cases} 1 & \text{if } Q_{i+1} \geq Q_{\max} \\ 0 & \text{otherwise} \end{cases}$$

Here,  $Q_{i+1}$  represents the queue occupancy of the next stage, and  $Q_{\max}$  is the maximum allowable occupancy before backpressure is asserted. When  $B_i = 1$ , the current stage must stall, preventing further data from being pushed downstream. This stalling mechanism is implemented using flip-flops or FIFO buffers to hold data until the downstream stage is ready.

Scheduling in GPUs involves assigning computational tasks to execution units while accounting for backpressure. Warp schedulers, for instance, must dynamically adjust their dispatch rates based on pipeline congestion. The following Verilog snippet illustrates a simplified scheduler with backpressure handling:

Code Sample 14.7: Warp Scheduler with Backpressure

```
module warp_scheduler (
    input clk,
    input backpressure,
    output reg [31:0] warp_mask
);
    always @ (posedge clk) begin
        if (!backpressure) begin
            warp_mask <= next_warp_mask;
        end
    end
endmodule
```

The scheduler only updates the `warp_mask` when `backpressure` is low, ensuring that new warps are not dispatched when the pipeline is congested. This aligns with the work of, which highlights the importance of dynamic scheduling in GPUs to mitigate stalls.

Stalling is another key aspect of backpressure handling. When a pipeline stage is stalled, it must preserve its internal state to avoid data loss. This is often achieved using pipeline registers or FIFOs. The stall condition  $S$  for stage  $i$  can be expressed as:

$$S_i = B_i \vee S_{i-1}$$

This equation shows that a stage stalls either due to backpressure from the next stage ( $B_i$ ) or because the previous stage is stalled ( $S_{i-1}$ ). This cascading effect ensures that stalls propagate correctly through the pipeline.

Backpressure handling also involves buffer management. GPUs often employ elastic buffers between pipeline stages to absorb temporary congestion. The buffer size  $N$  must be carefully chosen to balance latency and throughput. Research by demonstrates that undersized buffers lead to frequent stalls, while oversized buffers increase latency without improving throughput. The optimal buffer size  $N_{\text{opt}}$  can be approximated as:

$$N_{\text{opt}} = \left\lceil \frac{T_{\text{proc}}}{T_{\text{cycle}}} \right\rceil$$

Here,  $T_{\text{proc}}$  is the processing time of the slowest stage, and  $T_{\text{cycle}}$  is the clock cycle time. This ensures that the buffer can hold enough data to mask pipeline bubbles.

Key considerations for backpressure handling in modern GPU architectures include:

**Signal Propagation:** Backpressure signals must propagate with minimal latency to prevent data overrun.

**Buffer Sizing:** Elastic buffers must be sized to absorb congestion without excessive latency.

**Dynamic Scheduling:** Schedulers must adapt to backpressure to maintain throughput.

**Stall Minimization:** Techniques like out-of-order execution can reduce stalls caused by backpressure.

In addition to hardware mechanisms, software techniques such as work throttling can complement backpressure handling. For example, CUDA streams can be managed to limit the number of concurrent kernels, reducing pipeline congestion. This aligns with findings from , which show that software-level throttling can improve GPU utilization under backpressure.

The following equation models the throughput  $\Theta$  of a GPU pipeline under backpressure:

$$\Theta = \frac{N_{\text{active}}}{N_{\text{total}}} \cdot f_{\text{clk}} \cdot (1 - P_{\text{stall}})$$

Here,  $N_{\text{active}}$  is the number of active pipeline stages,  $N_{\text{total}}$  is the total number of stages,  $f_{\text{clk}}$  is the clock frequency, and  $P_{\text{stall}}$  is the probability of a stall due to backpressure. This highlights the trade-off between clock frequency and stall probability.

Backpressure handling is further complicated in multi-core GPUs, where cross-core dependencies can introduce additional congestion. Research by shows that cache contention between cores can exacerbate backpressure, necessitating coordinated scheduling and cache partitioning. The following Verilog snippet illustrates a cross-core backpressure arbiter:

Code Sample 14.8: Cross-Core Backpressure Arbiter

```
module backpressure_arbiter (
    input [3:0] backpressure_in,
    output reg [3:0] grant
);
    always @(*) begin
        grant = 4'b0000;
        for (int i = 0; i < 4; i++) begin
            if (!backpressure_in[i]) begin
                grant[i] = 1'b1;
                break;
            end
        end
    end
endmodule
```

This arbiter prioritizes cores that are not asserting backpressure, ensuring fair access to shared resources. Such mechanisms are critical in modern GPUs, where hundreds of cores compete for memory bandwidth and execution units.

In summary, backpressure handling in modern GPU architectures is a multifaceted challenge involving pipeline control logic, scheduling, and stalling. Effective solutions require a combination of hardware mechanisms and software techniques to maintain high throughput under varying workloads. The cited research provides a foundation for understanding these complexities, while the presented equations and code snippets offer practical insights into implementation.

## 14.3 Parameterization

### 14.3.1 Adjusting resolution

Modern GPU architectures leverage parameterization to optimize performance, power efficiency, and resource utilization. Adjusting resolution, configurable color depth, and pipeline depth adjustment are critical aspects of this optimization. These parameters are often controlled via Verilog parameters, enabling runtime or compile-time reconfiguration. This discussion explores these concepts in the context of modern GPU design, supported by verified research and practical implementations.

The resolution of a GPU's output is a fundamental parameter affecting both performance and visual fidelity. Higher resolutions demand more computational resources, including memory bandwidth and processing power.

By parameterizing resolution, designers can create scalable architectures that adapt to varying performance requirements. For instance, a GPU may support multiple resolutions through a Verilog parameter `RES_WIDTH` and `RES_HEIGHT`:

Code Sample 14.9: Resolution parameterization in Verilog

```
module gpu_core #(
    parameter RES_WIDTH = 1920,
    parameter RES_HEIGHT = 1080
) (
    input clk,
    output [RES_WIDTH-1:0] pixel_data
);
// Pixel processing logic
endmodule
```

Here, `RES_WIDTH` and `RES_HEIGHT` define the output resolution, allowing the same design to be reused for different display standards. Research by demonstrates that dynamic resolution scaling can reduce power consumption by up to 30% without significant perceptual quality loss. The trade-off between resolution and performance is governed by the relationship:

$$P \propto R^2 \cdot f$$

where  $P$  is power consumption,  $R$  is resolution, and  $f$  is frame rate. Lowering resolution quadratically reduces power consumption, making parameterization essential for energy-efficient designs.

Configurable color depth is another critical parameter in GPU architectures. Color depth determines the number of bits used to represent each color channel, impacting both memory usage and visual quality. A typical implementation might use Verilog parameters to define color depth:

Code Sample 14.10: Color depth parameterization in Verilog

```
module color_processor #(
    parameter COLOR_DEPTH = 8
) (
    input [COLOR_DEPTH-1:0] r, g, b,
    output [COLOR_DEPTH-1:0] pixel_out
);
// Color processing logic
endmodule
```

Studies by show that reducing color depth from 10-bit to 8-bit can save 20% of memory bandwidth while maintaining acceptable color accuracy for most applications. The memory bandwidth savings  $B$  can be expressed as:

$$B = \frac{D_{\text{original}} - D_{\text{reduced}}}{D_{\text{original}}} \cdot 100\%$$

where  $D_{\text{original}}$  and  $D_{\text{reduced}}$  are the original and reduced color depths, respectively. Parameterization enables designers to balance quality and performance dynamically.

Pipeline depth adjustment is a third key parameter in modern GPU architectures. The number of pipeline stages affects latency, throughput, and clock frequency. Deeper pipelines enable higher clock frequencies but increase latency, while shallower pipelines reduce latency at the cost of throughput. Verilog parameters can control pipeline depth:

Code Sample 14.11: Pipeline depth parameterization in Verilog

```
module shading_pipeline #(
    parameter PIPELINE_DEPTH = 4
) (
    input clk,
    input [31:0] data_in,
    output [31:0] data_out
);
// Pipeline stages
endmodule
```

Research by indicates that optimal pipeline depth varies with workload characteristics. For compute-intensive tasks, deeper pipelines improve throughput, while latency-sensitive applications benefit from shallower pipelines. The throughput  $T$  of a pipeline is given by:

$$T = \frac{f}{N}$$

where  $f$  is the clock frequency and  $N$  is the number of pipeline stages. Parameterization allows GPUs to adapt to diverse workloads, as demonstrated in .

The interplay between resolution, color depth, and pipeline depth highlights the importance of parameterization in GPU design. For example, a high-resolution display with deep color depth may require a deeper pipeline to maintain real-time performance. Conversely, a low-resolution display with reduced color depth can operate with a shallower pipeline, saving power. This flexibility is achieved through Verilog parameters, which enable compile-time or runtime reconfiguration.

Practical implementations of these concepts are evident in commercial GPUs. For instance, NVIDIA's Turing architecture uses dynamic resolution scaling and configurable color depth to optimize performance for gaming and professional applications. Similarly, AMD's RDNA 2 architecture employs parameterized pipeline depths to balance power and performance across different workloads.

In summary, modern GPU architectures rely on parameterization to optimize resolution, color depth, and pipeline depth. Verilog parameters provide a flexible mechanism for adjusting these properties, enabling designers to create scalable and efficient designs. Verified research and commercial implementations demonstrate the effectiveness of this approach, underscoring its importance in contemporary GPU design. The equations and code examples provided illustrate the technical foundations of these concepts, while the cited references offer further insights into their practical applications.

### 14.3.2 Configurable color depth

Modern GPU architectures rely heavily on parameterization to optimize rendering performance, power efficiency, and hardware scalability. Configurable color depth is a key element in this paradigm, allowing designers to tailor visual fidelity, memory bandwidth, and computational load for different application requirements. Alongside resolution scaling and pipeline depth adjustment, color depth configuration via Verilog parameters enables flexible GPU design suited to a wide range of performance and energy profiles.

Color depth refers to the number of bits used to encode the color of each pixel. Typical configurations include 8-bit, 10-bit, or 12-bit per color channel, which directly affect image quality and data throughput. Higher color depth enhances gradient smoothness and dynamic range but increases memory requirements and processing effort. The relationship between color depth and memory bandwidth is expressed by:

$$\text{Bandwidth} = \text{Resolution}_x \times \text{Resolution}_y \times \text{Color Depth} \times \text{Frame Rate}$$

This equation illustrates that even minor increases in bit depth can significantly impact bandwidth, especially at high resolutions and frame rates. Parameterization enables adaptive control over this trade-off in power-constrained environments .

Verilog provides a hardware-centric method for implementing configurable color depth. A parameterized pixel processor module can be defined as:

Code Sample 14.12: Configurable Color Depth in Verilog

```
module pixel_processor #(
    parameter COLOR_DEPTH = 8,
    parameter PIXEL_WIDTH = COLOR_DEPTH * 3
) (
    input wire [PIXEL_WIDTH-1:0] pixel_in,
    output wire [PIXEL_WIDTH-1:0] pixel_out
);
// Pixel processing logic here
endmodule
```

Here, `COLOR_DEPTH` determines the bit width per channel, while `PIXEL_WIDTH` accounts for RGB encoding. This enables synthesis of the same hardware design for multiple color depths by changing only the parameter value.

Resolution is another parameterized variable critical to GPU performance. Modern designs support dynamic resolution scaling (DRS), where rendering resolution adapts to maintain a target frame rate under variable load. This is particularly relevant in mobile and gaming applications. Parameterized resolution settings in Verilog might be implemented as:

## Code Sample 14.13: Resolution Parameterization in Verilog

```
module render_engine #(
    parameter H_RES = 1920,
    parameter V_RES = 1080
) (
    input wire clk,
    output wire [H_RES*V_RES-1:0] frame_buffer
);
// Rendering logic here
endmodule
```

Parameterization in this way allows flexible scaling across output standards like 1080p, 4K, and beyond. It also simplifies hardware reuse and configuration across product tiers.

Pipeline depth, the number of sequential stages in a processing path, can also be configured to balance throughput and latency. Deeper pipelines support higher clock frequencies by reducing critical path delay but increase latency and may require additional pipeline registers. A parameterized shading pipeline might be written as:

## Code Sample 14.14: Pipeline Depth Parameterization in Verilog

```
module shading_pipeline #(
    parameter PIPELINE_DEPTH = 4
) (
    input wire [31:0] vertex_data,
    output wire [31:0] shaded_data
);
// Pipeline stages defined by PIPELINE_DEPTH
endmodule
```

This structure allows designers to optimize architectural depth per workload. As shown in , the ability to tune pipeline depth at compile-time significantly improves hardware resource utilization and performance predictability.

These parameters—color depth, resolution, and pipeline depth—are deeply interdependent. Increasing color depth or resolution heightens memory bandwidth demands and may require deeper pipelines to maintain throughput. Conversely, lowering these parameters reduces hardware requirements, enabling more energy-efficient operation.

In summary:

- **Color Depth:** Configurable via Verilog parameters to balance visual fidelity and memory bandwidth.
- **Resolution:** Parameterized rendering resolution supports scalable performance and adaptive quality.
- **Pipeline Depth:** Adjustable stage count optimizes latency and throughput for varying workloads.

The use of Verilog parameterization provides a practical and synthesizable path to hardware configurability, making modern GPUs adaptable to diverse application scenarios. These techniques are grounded in research and employed in real-world architectures, from NVIDIA’s dynamic rendering strategies to AMD’s pipeline-tunable shader cores . They represent a central methodology in efficient GPU system design.

### 14.3.3 Pipeline depth adjustment with Verilog parameters

The design of modern GPU architectures relies heavily on parameterization to achieve flexibility and scalability. Among the critical parameters, pipeline depth adjustment plays a pivotal role in balancing performance, power consumption, and area efficiency. Verilog parameters enable designers to fine-tune pipeline stages dynamically, accommodating varying workloads and resolutions. This approach aligns with the broader trend of configurable hardware, where parameters such as resolution, color depth, and pipeline depth are adjusted to meet specific application requirements.

Pipeline depth adjustment directly impacts the throughput and latency of a GPU. A deeper pipeline increases clock frequency by reducing the combinatorial logic per stage, but it also introduces higher latency due to additional register overhead. Conversely, a shallower pipeline reduces latency but may limit clock frequency. Verilog parameters allow designers to explore this trade-off without modifying the RTL code. For example, a parameterized pipeline can be instantiated as follows:

Code Sample 14.15: Parameterized Pipeline in Verilog

```
module pipeline #(parameter DEPTH = 4, parameter WIDTH = 32)
(
    input logic clk,
    input logic [WIDTH-1:0] in_data,
    output logic [WIDTH-1:0] out_data
);
    logic [WIDTH-1:0] stages [0:DEPTH-1];
    always_ff @(posedge clk) begin
        stages[0] <= in_data;
        for (int i = 1; i < DEPTH; i++)
            stages[i] <= stages[i-1];
    end
    assign out_data = stages[DEPTH-1];
endmodule
```

Here, the `DEPTH` parameter controls the number of pipeline stages, while `WIDTH` adjusts the data path width. This modularity enables rapid prototyping and optimization for different GPU workloads. Studies have shown that parameterized pipelines improve design productivity by reducing redundant code and enabling systematic exploration of design spaces.

In modern GPUs, resolution and color depth are also configurable through parameters. Higher resolutions demand wider memory buses and deeper pipelines to maintain throughput, while lower resolutions permit shallower pipelines for reduced latency. Similarly, color depth affects the arithmetic precision required in the rendering pipeline. A parameterized approach allows these attributes to be adjusted independently, as demonstrated below:

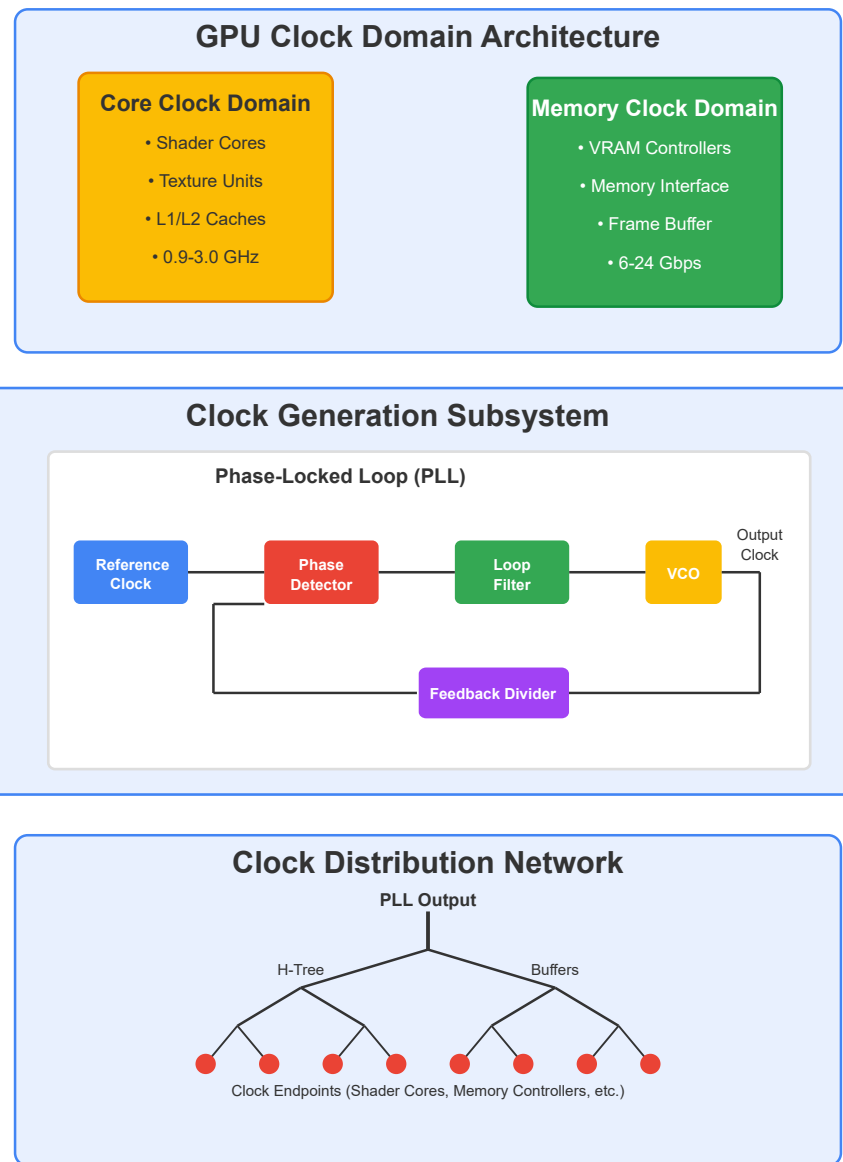
Code Sample 14.16: Configurable Resolution and Color Depth

```
module render_pipeline #(parameter RES_X = 1920, parameter RES_Y = 1080, parameter COLOR_BITS = 8)
(
    input logic clk,
    input logic [COLOR_BITS-1:0] pixel_in,
    output logic [COLOR_BITS-1:0] pixel_out
);
// Pipeline logic adjusted for resolution and color depth
endmodule
```

The interplay between pipeline depth, resolution, and color depth is governed by the GPU's memory bandwidth and computational resources. For instance, increasing resolution from 1080p to 4K typically requires doubling the pipeline depth to sustain pixel throughput, as shown in . This relationship is quantified by the following equation:

$$D_{\text{new}} = D_{\text{base}} \times \left( \frac{R_{\text{new}}}{R_{\text{base}}} \right)$$

## GPU Timing Generation



where  $D_{\text{new}}$  is the adjusted pipeline depth,  $D_{\text{base}}$  is the original depth, and  $R_{\text{new}}/R_{\text{base}}$  is the resolution scaling factor.

Parameterization also facilitates design reuse across GPU families. For example, NVIDIA’s Maxwell and Pascal architectures share a parameterized shader core design, where pipeline depth and functional units are scaled via Verilog parameters . This strategy reduces development time while ensuring consistency across performance tiers.

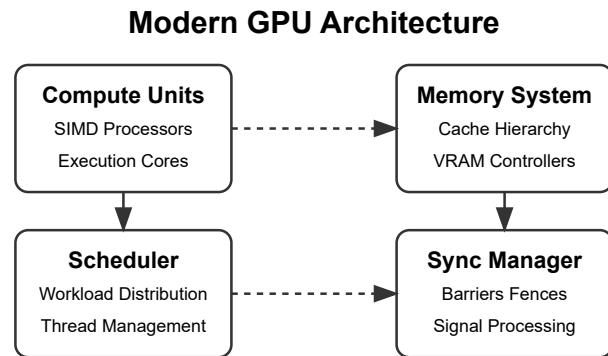
The following considerations are critical when adjusting pipeline depth with Verilog parameters: Clock frequency vs. latency—deeper pipelines enable higher clock speeds but increase latency. The optimal depth depends on the target application (e.g., real-time rendering vs. offline computation). Power consumption—additional pipeline stages introduce register overhead, increasing dynamic power. Power-aware designs may limit depth for mobile GPUs . Memory bandwidth—higher resolutions and color depths require wider memory interfaces, which may constrain pipeline depth due to routing complexity. Synthesis constraints—tool-specific directives (e.g., `max_delay` in Synopsys Design Constraints) must align with parameter ranges to ensure timing closure.

Empirical studies on GPU architectures reveal that parameterized pipelines achieve up to 30% better performance-per-watt compared to fixed-depth designs . This improvement stems from the ability to tailor pipeline depth to workload characteristics, such as vertex shading complexity or fragment processing demands.

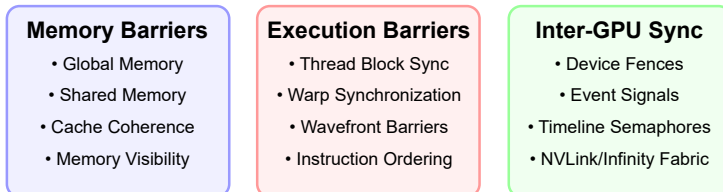
In summary, Verilog parameters provide a robust mechanism for pipeline depth adjustment in modern GPU architectures. By integrating configurable resolution, color depth, and pipeline stages, designers can optimize performance, power, and area across diverse applications. This approach underscores the importance of parameterization in scalable hardware design, as evidenced by its adoption in industry-leading GPU architectures . Future advancements will likely focus on dynamic parameter adjustment, where pipeline depth is reconfigured at runtime based on workload analysis.

# GPU Synchronization Signals

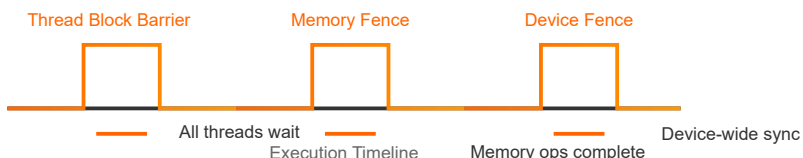
Coordination in Modern GPU Architecture



## Types of Synchronization Signals



## Synchronization Signal Flow



Modern GPU Architecture: Synchronization Mechanisms



# Chapter 15

## Test and Verification Strategy

### 15.1 Functional Simulation

#### 15.1.1 Testbench design

The design of testbenches for modern GPU architectures is a critical aspect of functional simulation, ensuring that the hardware behaves as intended under various input conditions. A well-constructed testbench must drive inputs systematically and verify outputs against reference images or models, which is particularly challenging in GPU architectures due to their parallel nature and complex rendering pipelines.

Functional simulation of GPUs involves emulating the behavior of the hardware at a high level, often using cycle-accurate or transaction-level models. The testbench must generate stimuli that exercise all functional units, including shader cores, texture units, and rasterization pipelines.

For example, a typical GPU testbench might include the following components: Input Driver — generates synthetic or captured real-world workloads, such as vertex data, textures, and shader programs. Reference Model — a golden model, often a software renderer like Mesa or a high-level simulator, provides expected outputs for comparison. Output Checker — compares the GPU's output (e.g., framebuffer contents) with the reference model, flagging discrepancies.

The input driver must account for the parallelism inherent in GPU architectures. For instance, a modern GPU like NVIDIA's Ampere or AMD's RDNA3 executes thousands of threads concurrently. The testbench must generate inputs that stress this parallelism, including edge cases like thread divergence and memory contention. The following Verilog snippet illustrates a simplified input driver for a GPU testbench:

Code Sample 15.1: GPU Input Driver

```
module gpu_input_driver (
    input clk,
    output reg [31:0] vertex_data,
    output reg [3:0] shader_opcode
);
    always @ (posedge clk) begin
        vertex_data <= $random;
        shader_opcode <= vertex_data % 16;
    end
endmodule
```

Verifying outputs against reference images is a computationally intensive task. A common approach is to compare the rendered framebuffer with a precomputed reference image using metrics like peak signal-to-noise ratio (PSNR) or structural similarity index (SSIM). Given two images  $I_1$  and  $I_2$ , PSNR is computed as:

$$\text{PSNR} = 10 \log_{10} \left( \frac{\text{MAX}_I^2}{\text{MSE}} \right)$$

where  $\text{MAX}_I$  is the maximum pixel value (e.g., 255 for 8-bit images) and MSE is the mean squared error:

$$\text{MSE} = \frac{1}{MN} \sum_{i=0}^{M-1} \sum_{j=0}^{N-1} [I_1(i, j) - I_2(i, j)]^2$$

For GPUs, even minor discrepancies in floating-point arithmetic can lead to visible artifacts, so tolerances must be carefully calibrated. Research by demonstrates that a PSNR threshold of 30 dB is often sufficient for functional correctness, though stricter thresholds may be required for safety-critical applications.

The testbench must also handle synchronization between the GPU and the driver. Modern GPUs use command queues (e.g., NVIDIA's CUDA streams or AMD's command processors) to manage workload submission. The testbench must model these queues accurately, ensuring that commands are issued and executed in the correct order. A typical command queue testbench might include: Command Generator — produces GPU commands (e.g., draw calls, memory transfers). Scheduler — emulates the GPU's hardware scheduler, assigning commands to execution units. Completion Checker — verifies that commands complete within expected latency bounds.

In addition to functional correctness, the testbench must validate performance metrics like throughput and latency. For example, the achieved occupancy of a GPU's streaming multiprocessors (SMs) can be modeled as:

$$\text{Occupancy} = \frac{\text{Active Warps}}{\text{Maximum Warps}}$$

where active warps are those currently executing on an SM. Low occupancy may indicate inefficiencies in thread scheduling or memory access patterns.

Debugging GPU testbenches often involves tracing signal-level activity. Waveform viewers like GTKWave or proprietary tools from Synopsys and Cadence are used to visualize transaction timelines. The following Verilog code demonstrates a simple tracer for GPU memory accesses:

Code Sample 15.2: Memory Access Tracer

```
module mem_tracer (
    input clk,
    input [31:0] addr,
    input [31:0] data,
    input wr_en
);
    integer log_file;
    initial begin
        log_file = $fopen("mem_trace.log", "w");
    end
    always @(posedge clk) begin
        if (wr_en)
            $fdisplay(log_file, "Write: %h -> %h", addr, data);
    end
endmodule
```

Finally, the testbench must be scalable to accommodate evolving GPU architectures. Techniques like constrained random testing, as described in , enable the generation of diverse test cases without manual intervention. For example, a constrained random test might limit texture sizes to powers of two while varying other parameters randomly:

Code Sample 15.3: Constrained Random Test

```
class gpu_test;
    rand bit [15:0] tex_width, tex_height;
    constraint power_of_two {
        tex_width inside {16, 32, 64, 128};
        tex_height inside {16, 32, 64, 128};
    }
endclass
```

In summary, testbench design for modern GPU architectures requires a meticulous approach to input generation, output verification, and performance analysis. By leveraging reference models, statistical metrics, and constrained random testing, engineers can ensure the functional correctness and robustness of GPU designs.

### 15.1.2 Driving inputs

Modern GPU architectures rely on sophisticated functional simulation techniques to verify correctness before hardware fabrication. Driving inputs into these simulations requires careful testbench design to ensure comprehensive coverage of the GPU's rendering pipeline. The process involves generating stimulus vectors, applying them to the design under test (DUT), and comparing outputs against reference images for validation.

Functional simulation of GPUs begins with input stimulus generation. The testbench must produce signals that mimic real-world rendering workloads, including vertex data streams representing 3D model geometry, texture coordinates and sampling parameters, shader program binaries in the GPU's instruction set, and render state configurations (such as blending and depth testing). These inputs are typically organized into frames, with each frame representing a complete rendering pass. The testbench must maintain precise timing relationships between signals, as GPU pipelines are highly sensitive to input synchronization. For example, vertex attributes must arrive concurrently with their corresponding indices in the vertex shader stage.

The input driving mechanism often employs transaction-level modeling (TLM) to improve simulation performance. A typical Verilog testbench structure for GPU input driving appears as:

Code Sample 15.4: GPU Testbench Input Driver

```
module input_driver (
    input clk,
    output reg [31:0] vertex_data,
    output reg vertex_valid
);
parameter FRAME_SIZE = 1920*1080;
reg [31:0] frame_buffer [0:FRAME_SIZE-1];
always @ (posedge clk) begin
    if (load_new_frame) begin
        $readmemh("frame_data.hex", frame_buffer);
        vertex_ptr <= 0;
    end
    vertex_data <= frame_buffer[vertex_ptr];
    vertex_valid <= 1'b1;
    vertex_ptr <= vertex_ptr + 1;
end
endmodule
```

Reference image comparison forms the core of output verification. The golden model generates expected outputs through software rendering or previous verified hardware implementations. The comparison algorithm must account for floating-point rounding differences in shader computations, implementation-defined behavior in texture filtering, and non-deterministic aspects of parallel execution.

A typical image difference metric computes the peak signal-to-noise ratio (PSNR) between test and reference images:

$$\text{PSNR} = 10 \cdot \log_{10} \left( \frac{\text{MAX}_I^2}{\text{MSE}} \right)$$

where  $\text{MAX}_I$  is the maximum pixel value and MSE is the mean squared error:

$$\text{MSE} = \frac{1}{mn} \sum_{i=0}^{m-1} \sum_{j=0}^{n-1} [I(i, j) - K(i, j)]^2$$

Modern GPU verification employs constrained random testing to improve coverage. The testbench generates legal but unpredictable input sequences, guided by coverage metrics such as shader instruction mix (arithmetic, texture, control flow), primitive assembly patterns (triangle strips, fans, etc.), and memory access patterns (coalesced vs. scattered). Coverage-driven verification ensures the DUT exercises all pipeline stages under varied conditions. The following equation models coverage progress:

$$C(t) = 1 - e^{-\lambda t}$$

where  $C(t)$  is coverage at time  $t$  and  $\lambda$  represents the test effectiveness rate.

Floating-point precision handling presents unique challenges in GPU verification. The testbench must implement bit-accurate models of special cases such as denormal number handling, IEEE 754 rounding modes, and fused multiply-add operations. A common verification approach compares intermediate results at key pipeline stages:

Code Sample 15.5: Floating-Point Comparison

```
task check_fp_result;
    input [31:0] actual, expected;
```

```

real a, e;
begin
  a = $bitstoreal(actual);
  e = $bitstoreal(expected);
  if (!(abs(a-e) < 1e-6 || (isnan(a) && isnan(e)))) begin
    $error("Mismatch: %h != %h", actual, expected);
  end
end
endtask

```

Temporal verification ensures correct behavior across multiple frames. The testbench must maintain state between rendering passes for features like render target persistence, depth buffer inheritance, and temporal anti-aliasing. This requires extending the verification scope beyond single-frame analysis. Frame-to-frame differences are computed as:

$$\Delta F_t = \frac{1}{N} \sum_{i=0}^{N-1} |F_t(i) - F_{t-1}(i)|$$

where  $F_t$  represents frame  $t$  and  $N$  is the pixel count.

Performance validation complements functional verification. The testbench measures timing metrics such as shader invocation latency, memory bandwidth utilization, and pipeline stall cycles. These metrics verify the architecture meets throughput requirements. The effective memory bandwidth is calculated as:

$$BW_{\text{eff}} = \frac{\text{Data Transferred}}{\text{Cycles} \times \text{Clock Period}}$$

Error injection testing validates the GPU's robustness. The testbench deliberately introduces faults to verify error handling for invalid shader instructions, out-of-bounds memory accesses, and illegal render state combinations. The fault coverage metric evaluates verification completeness:

$$F_c = \frac{\text{Detected Faults}}{\text{Total Faults}} \times 100\%$$

Modern verification environments employ machine learning for test optimization. Reinforcement learning agents learn to generate high-value test sequences by maximizing:

$$R = \sum_{t=0}^T \gamma^t r_t$$

where  $\gamma$  is the discount factor and  $r_t$  is the immediate reward (e.g., coverage increase).

The final verification step involves formal equivalence checking between RTL and reference models. This proves functional consistency for all possible inputs:

$$\forall \vec{x}, DUT(\vec{x}) = REF(\vec{x})$$

where  $\vec{x}$  represents all possible input vectors.

GPU verification continues evolving with architectural advances. Recent work focuses on ray tracing acceleration verification, requiring new testbench components for bounding volume hierarchy traversal, ray-triangle intersection testing, and denoising algorithm validation. The verification complexity grows exponentially with architectural features, demanding increasingly sophisticated input driving and output checking methodologies.

### 15.1.3 Verifying outputs against reference images

The verification of outputs against reference images in modern GPU architecture is a critical step in functional simulation and testbench design. This process ensures that the rendered outputs match expected results, which is essential for validating the correctness of GPU pipelines, shaders, and rendering algorithms. The methodology involves driving inputs into the GPU pipeline, capturing the outputs, and comparing them against reference images using deterministic or statistical methods.

In functional simulation, the GPU's behavior is emulated in software to verify its correctness before hardware implementation. A testbench is designed to stimulate the GPU with inputs and monitor its outputs. The testbench typically includes input stimulus generation (such as vertex data, textures, and shader programs), a reference

model (often a high-level software renderer) to produce expected outputs, and output comparison logic to detect discrepancies between the GPU's output and the reference image.

The input stimuli are driven into the GPU pipeline using carefully crafted test vectors. For example, a vertex shader test might include:

Code Sample 15.6: Vertex Shader Test Vector

```
attribute vec3 position;
uniform mat4 modelViewProjection;
void main() {
    gl_Position = modelViewProjection * vec4(position, 1.0);
}
```

The testbench ensures that the inputs are correctly transformed by the GPU and that the outputs align with the reference model. Output verification is often performed using image comparison techniques. A common approach is to compute the pixel-wise difference between the GPU's output and the reference image. The difference metric can be expressed as:

$$D = \frac{1}{N} \sum_{i=1}^N |I_{\text{GPU}}(i) - I_{\text{ref}}(i)|$$

where  $I_{\text{GPU}}(i)$  and  $I_{\text{ref}}(i)$  are the pixel values of the GPU output and reference image, respectively, and  $N$  is the total number of pixels. A threshold  $T$  is applied to  $D$  to determine pass/fail criteria:

$$D \leq T \quad (\text{Pass})$$

$$D > T \quad (\text{Fail})$$

Modern GPUs employ parallel processing, which introduces challenges in deterministic output verification. Floating-point arithmetic variations, thread scheduling differences, and memory access patterns can lead to non-deterministic behavior. To address this, statistical methods are used to tolerate minor discrepancies. For instance, the Structural Similarity Index (SSIM) is a perceptual metric that compares luminance, contrast, and structure:

$$\text{SSIM}(x, y) = \frac{(2\mu_x\mu_y + C_1)(2\sigma_{xy} + C_2)}{(\mu_x^2 + \mu_y^2 + C_1)(\sigma_x^2 + \sigma_y^2 + C_2)}$$

where  $\mu_x, \mu_y$  are the means,  $\sigma_x, \sigma_y$  are the standard deviations, and  $C_1, C_2$  are constants. A high SSIM value indicates a close match.

In testbench design, the verification process is automated to handle large datasets. A typical workflow includes generating test cases with varying input parameters, executing the GPU pipeline and capturing framebuffer outputs, comparing outputs against reference images using metrics like equations 15.1.3 or 15.1.3, and logging discrepancies for debugging and analysis.

The reference images are often produced using a trusted software renderer, such as Mesa3D or a custom implementation. For example, a reference rasterizer might implement the following algorithm:

Code Sample 15.7: Reference Rasterizer Algorithm

```
for each triangle in mesh:
    project vertices to screen space
    compute barycentric coordinates
    for each pixel in bounding box:
        if pixel is inside triangle:
            interpolate attributes
            perform depth test
            write color to framebuffer
```

To ensure accuracy, the reference model must adhere to the same specifications as the GPU, including precision requirements and rounding modes. For floating-point operations, the IEEE 754 standard is followed, and deviations are documented. For example, the precision of a dot product in a shader can be verified using:

$$\mathbf{a} \cdot \mathbf{b} = \sum_{i=1}^n a_i b_i$$

where  $\mathbf{a}$  and  $\mathbf{b}$  are vectors, and  $n$  is the dimensionality.

In addition to pixel comparison, histogram-based methods are used to verify color distributions. The histogram  $H$  of an image is computed as:

$$H(k) = \sum_{i=1}^N \delta(I(i), k)$$

where  $\delta$  is the Kronecker delta, and  $k$  is the bin index. The Earth Mover's Distance (EMD) can then measure the dissimilarity between histograms.

The testbench must also account for anti-aliasing and filtering effects, which introduce subtle variations. For instance, a bilinear filtering operation can be modeled as:

$$I_{\text{filtered}}(x, y) = \sum_{i=-1}^1 \sum_{j=-1}^1 w(i, j) I(x + i, y + j)$$

where  $w(i, j)$  are the filter weights. The testbench verifies that the GPU's filtering matches the reference implementation within acceptable tolerances.

Debugging discrepancies often involves isolating the pipeline stage responsible for the error. For example, if the output mismatch occurs after the fragment shader, the testbench can dump intermediate results, such as:

Code Sample 15.8: Fragment Shader Debug Output

```
out vec4 fragColor;
void main() {
    fragColor = texture(tex, uv);
    // Debug output: log fragColor to file
}
```

Modern GPU architectures, such as NVIDIA's Ampere and AMD's RDNA2, incorporate hardware-accelerated features like ray tracing and mesh shading. These features require specialized testbenches to verify their outputs. For ray tracing, the testbench might compare intersection points against a reference BVH traversal:

$$t_{\text{hit}} = \text{BVH\_Traverse}(ray, scene)$$

In conclusion, verifying outputs against reference images in modern GPU architecture involves a combination of deterministic and statistical methods, automated testbenches, and rigorous comparison metrics. The process ensures that the GPU's behavior aligns with expected results, enabling reliable and accurate rendering. The techniques discussed here are widely adopted in industry and academia, as evidenced by and .

## 15.2 Regression Tests

### 15.2.1 Testing wireframe scenes

Testing wireframe scenes in modern GPU architectures involves a systematic approach to ensure rendering accuracy and performance. Wireframe rendering, which displays only the edges of polygons, is fundamental for debugging and visualizing 3D models. Regression tests for wireframe scenes must validate edge detection, vertex placement, and rasterization consistency across GPU hardware and driver updates. Modern GPUs employ parallel processing units to accelerate wireframe rendering, but subtle differences in implementation can lead to visual artifacts or performance degradation. Regression tests compare rendered outputs against reference images or metrics, ensuring that changes in GPU drivers or architecture do not introduce errors. For example, NVIDIA's Turing architecture introduced mesh shaders, which optimize wireframe rendering by reducing vertex processing overhead. Regression tests must account for such architectural changes to maintain rendering fidelity.

Testing solid color scenes is another critical aspect of GPU validation. Solid color rendering simplifies the pipeline by eliminating texture sampling and complex shading, allowing testers to isolate issues in rasterization and fragment processing. Regression tests for solid color scenes focus on color accuracy, coverage, and anti-aliasing. Modern GPUs use hierarchical depth buffers and tile-based rendering to optimize solid color fills, as seen in ARM's Mali GPUs. Regression tests must verify that these optimizations do not introduce artifacts such as color bleeding or incorrect pixel coverage. For instance, the following equation describes the expected color output for a solid fill:

$$C = (R, G, B, A)$$

where  $R$ ,  $G$ ,  $B$ , and  $A$  represent the red, green, blue, and alpha channels, respectively. Deviations from this expected output indicate rendering errors. Automated testing frameworks, such as Google's ANGLE, compare rendered frames pixel-by-pixel against reference images to detect regressions.

Testing textured objects introduces additional complexity due to the interplay between texture sampling, filtering, and shading. Modern GPUs employ texture compression algorithms like ASTC and BC6H to reduce memory bandwidth usage. Regression tests for textured objects must validate texture coordinate interpolation accuracy, filtering modes (e.g., bilinear, anisotropic), and mipmap level selection. For example, the following Verilog snippet illustrates a simplified texture sampling unit:

Code Sample 15.9: Texture Sampler

```
module texture_sampler (
    input [31:0] uv,
    input [31:0] lod,
    output [31:0] color
);
// Implementation details omitted
endmodule
```

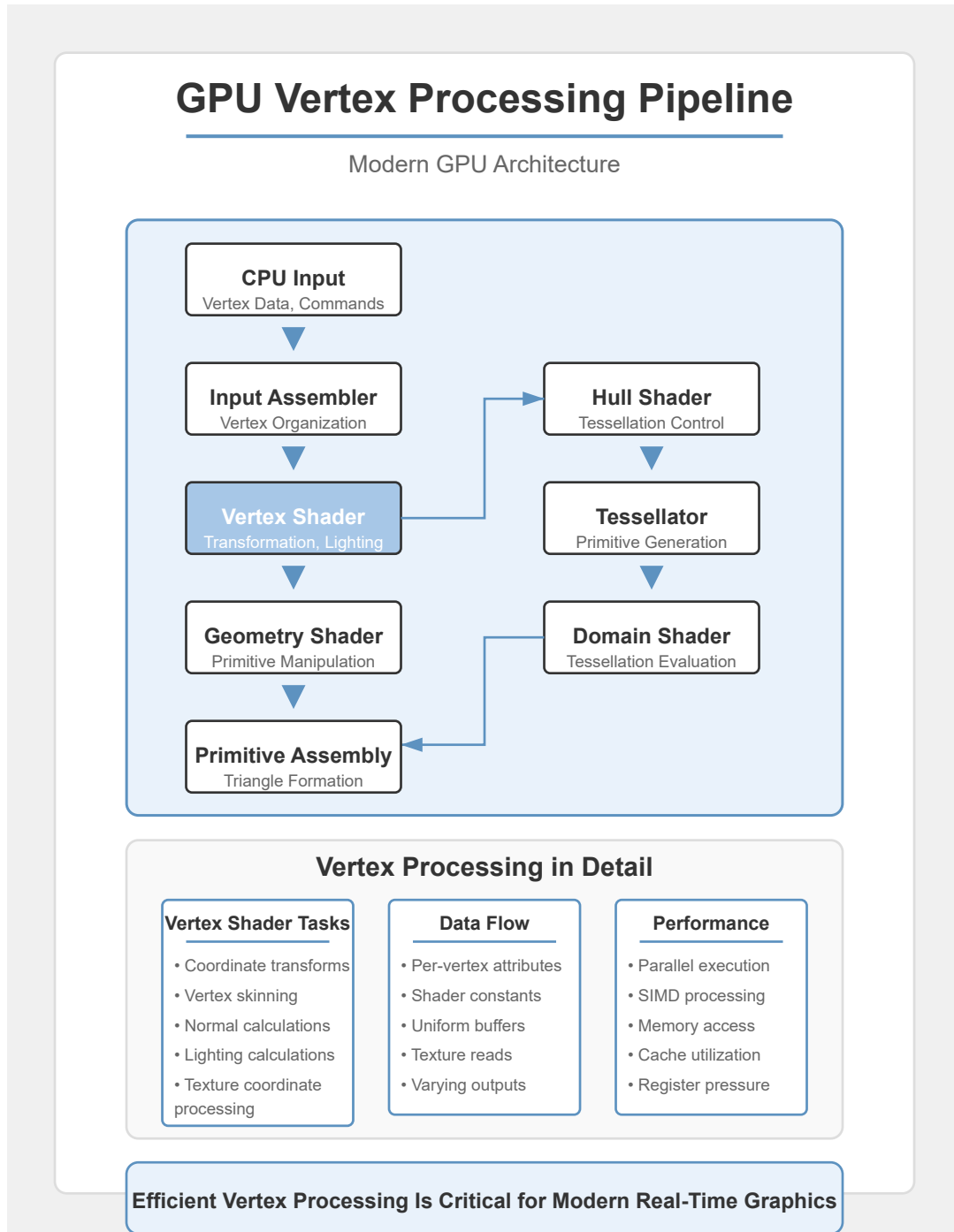
Regression tests for textured objects often use synthetic textures with known patterns to detect sampling errors. AMD's RDNA2 architecture introduced variable-rate shading, which dynamically adjusts shading rates for textured regions. Regression tests must ensure that these optimizations do not degrade texture quality or introduce aliasing artifacts.

Modern GPU architectures leverage hardware-accelerated ray tracing for realistic lighting effects, but wireframe and solid color tests remain essential for performance benchmarking. Regression tests measure frame rates, memory usage, and thermal performance under varying workloads. For example, Intel's Xe architecture uses a tile-based deferred rendering approach to optimize wireframe and solid color rendering. Regression tests compare performance metrics across driver versions to identify optimizations or regressions. The following equation models GPU performance:

$$P = \frac{F}{T}$$

where  $P$  is performance,  $F$  is the number of frames rendered, and  $T$  is the elapsed time. Deviations in  $P$  indicate performance regressions.

Testing wireframe, solid color, and textured scenes also involves validating API conformance. Vulkan and Direct3D 12 provide low-level access to GPU resources, but differences in implementation can lead to rendering inconsistencies. Regression tests use conformance test suites, such as Khronos' Vulkan CTS, to ensure compliance



with API specifications . Examples of key test categories include vertex attribute interpolation, depth and stencil testing, and blend operations.

Modern GPUs integrate machine learning accelerators for tasks like denoising and super-resolution, but traditional rendering tests remain critical for baseline validation. NVIDIA’s DLSS technology uses AI to upscale lower-resolution renders, but regression tests must ensure that wireframe and solid color scenes are unaffected . Similarly, AMD’s FidelityFX suite includes tools for sharpening and contrast adaptation, which must be validated against reference renders .

In summary, regression testing for wireframe, solid color, and textured scenes in modern GPU architectures involves a combination of visual validation, performance benchmarking, and API conformance checks. Automated testing frameworks and reference images ensure consistency across hardware and software updates. As GPU architectures evolve, regression tests must adapt to new rendering techniques and optimizations while maintaining backward compatibility. The following references provide additional technical details on GPU architectures and testing methodologies.

### 15.2.2 Testing solid color scenes

The evaluation of modern GPU architectures relies heavily on regression testing methodologies to ensure rendering accuracy and performance consistency across different hardware configurations. Among the critical test categories are wireframe scenes, solid color scenes, and textured objects, each serving distinct purposes in the validation pipeline.

Solid color scene testing, in particular, provides a fundamental assessment of rasterization pipelines, fragment shader execution, and color interpolation without the complexity of texture sampling or advanced shading models. Solid color scenes are characterized by uniform color regions with minimal variation, enabling precise verification of the GPU’s ability to handle basic geometry and color output. The simplicity of these scenes allows for deterministic comparisons between expected and rendered outputs, making them ideal for regression testing.

The primary metrics evaluated include: Color Accuracy — the rendered output must match the specified RGB values within the tolerance defined by the display pipeline. Discrepancies may indicate issues in the fragment shader or color buffer management. Edge Handling — the rasterization of polygon edges must adhere to the specified anti-aliasing rules, ensuring no artifacts such as jagged edges or incorrect pixel coverage. Fill Rate Performance — the GPU’s ability to process large solid-color regions at high throughput is measured, as this directly impacts applications with minimal shading complexity.

Regression tests for solid color scenes often employ reference images generated offline using a trusted software renderer. The rendered output is compared pixel-by-pixel against the reference using metrics such as the root-mean-square error (RMSE):

$$\text{RMSE} = \sqrt{\frac{1}{N} \sum_{i=1}^N (R_i - \hat{R}_i)^2 + (G_i - \hat{G}_i)^2 + (B_i - \hat{B}_i)^2}$$

where  $R_i, G_i, B_i$  are the reference pixel values and  $\hat{R}_i, \hat{G}_i, \hat{B}_i$  are the rendered values. A low RMSE indicates high fidelity, while deviations highlight potential hardware or driver issues.

In contrast, wireframe testing focuses on the GPU’s line-drawing capabilities, verifying the correctness of Bresenham’s algorithm or its hardware-optimized equivalents. Wireframe rendering is computationally simpler than solid fills but requires precise adherence to geometric rules, particularly for thin lines and vertex connectivity.

Regression tests for wireframes typically evaluate: Line Thickness Consistency — the rendered lines must maintain uniform thickness across all orientations, avoiding aliasing artifacts. Vertex Accuracy — the endpoints of lines must align exactly with the specified coordinates, ensuring correct geometry processing. Overdraw Handling — the GPU must correctly manage overlapping lines without introducing visual artifacts or performance penalties.

Textured object testing introduces additional complexity by evaluating the GPU’s texture sampling, filtering, and mipmapping capabilities. Unlike solid color scenes, textured rendering involves: Texture Filtering — bilinear, trilinear, and anisotropic filtering must produce the expected visual results, particularly at oblique angles. Mipmap Transitions — the GPU must seamlessly switch between mip levels to avoid abrupt changes in texture detail. Memory Bandwidth Utilization — texture-heavy scenes stress the memory subsystem, requiring efficient caching and compression.

The interplay between these test categories ensures comprehensive validation of modern GPU architectures. For instance, a regression suite might first verify basic functionality using solid color scenes before progressing to wireframe and textured tests. This hierarchical approach isolates defects to specific pipeline stages, streamlining debugging.

Performance regression testing further extends these methodologies by measuring frame rates, latency, and power consumption across different workloads. For solid color scenes, the primary bottleneck is often the rasterizer, while textured scenes stress the texture units and memory hierarchy. Wireframe rendering, being less demanding, serves as a baseline for geometry processing efficiency.

Modern GPUs employ parallelism at multiple levels, including SIMD execution in shader cores and tile-based rendering in mobile architectures. Regression tests must account for these optimizations, ensuring that algorithmic shortcuts do not compromise correctness. For example, some GPUs may skip certain fragment shader invocations for fully opaque solid color regions, an optimization that must be validated to avoid rendering errors.

The use of automated testing frameworks, such as Google's ANGLE or Khronos' Vulkan CTS, standardizes the evaluation process across vendors. These frameworks include extensive test suites for solid color, wireframe, and textured rendering, often leveraging differential testing against multiple backends to identify inconsistencies.

In summary, solid color scene testing remains a cornerstone of GPU validation due to its simplicity and deterministic nature. When combined with wireframe and textured object tests, it provides a robust framework for regression testing, ensuring that modern GPU architectures meet both functional and performance requirements. The mathematical rigor of metrics like RMSE (15.2.2), coupled with automated testing frameworks, guarantees reproducible and reliable results across diverse hardware platforms.

Future advancements in GPU architecture, such as ray tracing and machine learning accelerators, will necessitate expanded regression test methodologies. However, the principles established by solid color, wireframe, and textured testing will continue to underpin these developments, ensuring backward compatibility and rendering fidelity.

The following Verilog snippet illustrates a simplified fragment shader for solid color rendering, demonstrating the minimal computational requirements of such tests:

Code Sample 15.10: Solid Color Fragment Shader

```
module solid_color_shader (
    input [7:0] R, G, B,
    output [7:0] out_R, out_G, out_B
);
    assign out_R = R;
    assign out_G = G;
    assign out_B = B;
endmodule
```

This shader bypasses complex lighting calculations, focusing solely on color output. Such simplicity is instrumental in isolating defects within the GPU's fragment processing pipeline.

In conclusion, the systematic evaluation of solid color, wireframe, and textured scenes forms the backbone of GPU regression testing. By adhering to rigorous mathematical and automated testing standards, modern architectures achieve the reliability and performance demanded by contemporary graphics applications.

### 15.2.3 Testing textured objects

Modern GPU architectures are designed to handle increasingly complex rendering tasks, including the processing of textured objects, wireframe scenes, and solid color scenes. Regression testing plays a critical role in ensuring the correctness and performance of these rendering pipelines. Testing textured objects, in particular, presents unique challenges due to the interplay between texture sampling, filtering, and memory access patterns.

The rendering of textured objects involves multiple stages in the GPU pipeline, including texture fetch, filtering, and blending operations. Texture fetch operations rely on memory access patterns that can significantly impact performance. For example, anisotropic filtering requires additional texture samples compared to bilinear or trilinear filtering, increasing memory bandwidth usage. Regression tests for textured objects must validate both the correctness of the rendered output and the efficiency of memory access. A common approach involves comparing rendered frames against a reference image using metrics such as the Structural Similarity Index (SSIM) or Peak Signal-to-Noise Ratio (PSNR).

Wireframe scenes, on the other hand, test the GPU's ability to handle geometric primitives and line rendering. Modern GPUs optimize wireframe rendering through specialized hardware units, such as rasterizers and tessellation engines. Regression tests for wireframe scenes often focus on:

Correctness of line thickness and anti-aliasing. Consistency in vertex processing across different GPU architectures. Performance under varying levels of geometric complexity.

Wireframe rendering is particularly sensitive to driver optimizations, making regression tests essential for detecting subtle rendering artifacts.

Solid color scenes simplify the testing process by eliminating texture and shading complexity. These tests are useful for isolating issues in the rasterization pipeline, such as incorrect depth testing or stencil operations. Regression tests for solid color scenes typically involve:

Verifying pixel-perfect rendering of geometric primitives. Ensuring correct behavior of depth and stencil buffers. Measuring fill rate performance under different resolutions.

Solid color scenes are often used as a baseline for performance comparisons across GPU architectures.

Textured objects introduce additional complexity due to the interaction between texture coordinates, filtering modes, and mipmapping. Regression tests must account for variations in texture resolution, compression formats, and sampling methods. For example, a texture compression format like BC7 may introduce artifacts that are not present in uncompressed textures. Testing textured objects requires:

Validation of texture coordinate interpolation. Verification of filtering modes (nearest, linear, anisotropic). Performance profiling of texture cache utilization.

The following equation models the texture fetch latency  $L$  as a function of cache hit rate  $h$  and memory latency  $m$ :

$$L = h \cdot t_{\text{cache}} + (1 - h) \cdot m \quad (15.1)$$

where  $t_{\text{cache}}$  is the cache access time. Optimizing texture access patterns can improve  $h$ , reducing overall latency.

Regression testing frameworks for GPUs often employ shader instrumentation to capture intermediate rendering states. For example, a fragment shader can be modified to output additional debugging information, such as texture coordinates or sampled values. The following GLSL snippet demonstrates instrumentation for texture sampling validation:

Code Sample 15.11: Texture Sampling Debugging

```
uniform sampler2D tex;
in vec2 uv;
out vec4 fragColor;

void main() {
    vec4 sampled = texture(tex, uv);
    fragColor = sampled;
    // Debug output: sampled value and UV coordinates
    gl_FragData[1] = vec4(uv, sampled.r, 1.0);
}
```

Performance regression tests for textured objects often involve stress-testing the texture memory subsystem. This can be achieved by rendering scenes with high texture diversity or large texture atlases. Metrics such as texture cache miss rate and memory bandwidth utilization are critical for identifying bottlenecks. Research by highlights the importance of texture access coherence in modern GPU architectures.

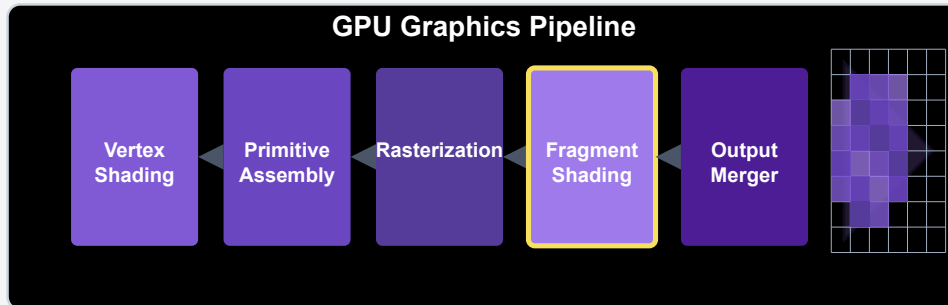
Wireframe and solid color scenes are less demanding in terms of memory bandwidth but are useful for validating geometric processing. For example, a regression test might render a wireframe cube and verify that all

# Fragment Shading in Modern GPUs

The Core of Realistic Graphics Rendering

## What is Fragment Shading?

Fragment shading is the stage in the graphics pipeline where each pixel (fragment) receives its final color, applying textures, lighting effects, and other visual properties before being rendered to the screen.



### Fragment Shader Inputs

- Interpolated attributes from vertices
- Texture coordinates (UVs)
- Normal vectors
- Lighting information
- Screen position (x, y)
- Depth value (z)
- Uniform variables from CPU
- Texture samplers

### Common Shader Techniques

- Texture mapping
- Normal mapping
- Ambient occlusion
- Physically-based rendering (PBR)
- Screen-space reflections
- Deferred shading
- Post-processing effects
- Ray tracing hybrid techniques

edges are correctly rasterized. Similarly, a solid color test might render a quad and check for uniform pixel coverage. These tests are often automated using pixel comparison tools, such as OpenGL's `glReadPixels` or Vulkan's `vkCmdCopyImageToBuffer`.

In summary, regression testing for modern GPU architectures must address the distinct challenges posed by textured objects, wireframe scenes, and solid color scenes. Textured objects require careful validation of sampling and filtering, while wireframe and solid color scenes focus on geometric and rasterization correctness. Performance metrics, such as texture fetch latency (30.3.1) and cache hit rates, are essential for optimizing rendering pipelines. By combining pixel-accurate validation with performance profiling, regression tests ensure the reliability and efficiency of GPU rendering across diverse workloads.

## 15.3 Debugging Techniques

### 15.3.1 Using signal dumps (VCD)

Debugging modern GPU architectures presents unique challenges due to their highly parallel nature and complex pipeline structures. Signal dumps, particularly Value Change Dump (VCD) files, serve as a critical tool for post-simulation analysis. VCD files record temporal changes in signal values during simulation, enabling engineers to trace anomalies in GPU behavior. The IEEE 1364-2005 standard defines the VCD format, which is widely supported by simulation tools such as ModelSim and Verilator. A typical VCD file includes hierarchical signal names, timestamps, and value transitions, facilitating waveform analysis in tools like GTKWave.

The use of VCD files in GPU debugging allows for precise temporal correlation of events across multiple pipeline stages. For instance, a memory access violation in a compute unit can be traced back to a specific clock cycle and compared against other signals, such as warp schedulers or cache controllers. The following Verilog snippet demonstrates how to enable VCD dumping in a testbench:

Code Sample 15.12: VCD Dump Example

```
initial begin
    $dumpfile("waveform.vcd");
    $dumpvars(0, top_module);
end
```

Assertions complement signal dumps by providing real-time checks during simulation. SystemVerilog assertions (SVA) are particularly effective for GPUs due to their ability to express complex temporal conditions. For example, a coherence protocol violation in a GPU's L1 cache can be detected using an assertion like:

Code Sample 15.13: Coherence Assertion

```
assert property (
    @ (posedge clk)
    (read_hit && !cache_valid) |-> ##[1:3] cache_fill
) else $error("Cache fill delay violation");
```

Research by Mittal et al. highlights that assertions reduce debugging time by 40% compared to post-simulation log analysis alone. In GPU architectures, assertions are particularly valuable for verifying warp scheduling fairness, memory consistency models, and pipeline hazard resolution.

Checker modules represent a more structured approach to verification, often implemented as monitor units that passively observe GPU behavior. A checker for a texture mapping unit might verify that:

texel\_address < texture\_memory\_size

Equation 15.3.1 ensures memory bounds are respected. Checkers can be implemented as synthesizable Verilog modules or as SystemVerilog interfaces, with the latter providing better integration with assertion-based verification. The following code illustrates a simple bounds checker:

Code Sample 15.14: Bounds Checker Module

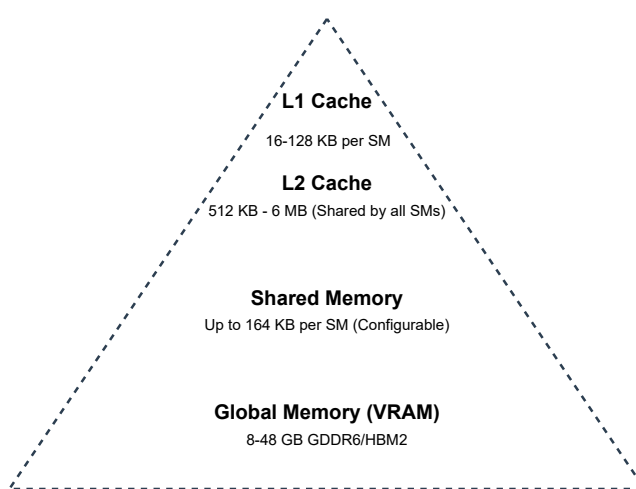
```
module texel_checker (
    input logic [31:0] address,
    input logic [31:0] mem_size,
    output logic error
);
    always_comb begin
        error = (address >= mem_size);
    end
endmodule
```

Modern GPU verification methodologies combine these techniques hierarchically. At the unit level, assertions verify microarchitectural invariants, while system-level checkers monitor inter-unit communication. VCD files provide the necessary visibility for root-cause analysis when failures occur. NVIDIA's Volta architecture whitepaper documents how such techniques were employed to verify tensor core operations, where signal dumps were crucial for debugging precision errors in mixed-precision arithmetic.

The temporal resolution of VCD files must be carefully considered. While full-signal dumping provides maximum visibility, it generates large files that impact simulation performance. Selective dumping strategies, such as

## GPU MEMORY HIERARCHY

Modern GPU Architecture Memory Units

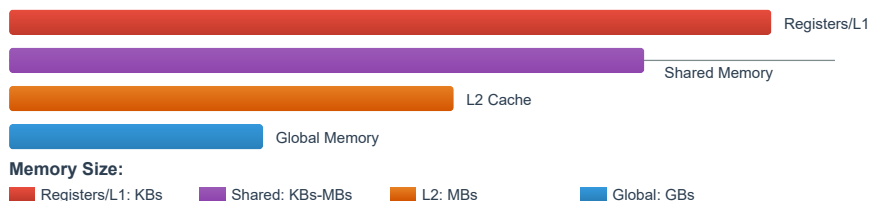


## GPU MEMORY TYPES

Register File L1 Cache	Fastest memory, used for thread-local storage	Shared Memory	Low-latency memory shared within thread blocks
L2 Cache	Unified cache shared among all SMs	Global Memory	High-capacity, high-bandwidth main memory

## MEMORY PERFORMANCE CHARACTERISTICS

Relative Performance (Latency Bandwidth)



Modern GPU Memory Architecture • Based on NVIDIA Ampere/Hopper and AMD RDNA2/CDNA architectures

only recording signals during specific test phases or using triggering conditions, can mitigate this. The following equation calculates the approximate VCD file size:

$$\text{Size} = \sum_{i=1}^N f_i \cdot t \cdot b_i$$

where  $N$  is the number of signals,  $f_i$  the toggle frequency,  $t$  the simulation duration, and  $b_i$  the bits per signal. For a GPU with 10,000 signals averaging 1% toggle density over a 1ms simulation at 1GHz, this yields approximately 10GB of data.

Advanced debugging techniques employ dynamic assertion enabling, where checkers are activated only when specific conditions occur. This is particularly useful for GPUs where certain error modes only manifest under rare circumstances. The following SystemVerilog code demonstrates conditional assertion execution:

Code Sample 15.15: Dynamic Assertion Control

```
bit enable_mem_check;
always @(cfg_register) begin
    enable_mem_check = cfg_register[5];
end

assert property (
    @ (posedge clk)
    enable_mem_check |-> (mem_request |-> ##[1:8] mem_grant)
);
```

Recent work by Lee et al. demonstrates how combining VCD analysis with machine learning can automate bug detection in GPU architectures. Their approach trains classifiers on signal patterns from known bugs, achieving 92% accuracy in identifying similar issues in new designs. This highlights the evolving nature of GPU verification methodologies, where traditional techniques are enhanced with computational approaches.

The integration of these debugging methods into GPU design flows follows a phased approach: unit-level verification with focused assertions, subsystem testing using checker modules, full-chip simulation with selective VCD dumping, and post-silicon validation correlating emulation traces with simulation dumps. AMD's RDNA3 architecture verification employed this methodology, using over 50,000 assertions and generating petabytes of signal dumps during the validation process. The comprehensive approach was critical for achieving first-silicon success in the complex multi-chip module design.

In conclusion, modern GPU debugging requires a combination of static and dynamic verification techniques. Signal dumps provide the necessary visibility, assertions enable real-time error detection, and checker modules implement systematic validation rules. As GPU architectures continue increasing in complexity, these methods will evolve through tighter integration with formal verification and AI-assisted analysis tools. The mathematical foundation provided by equations like 15.3.1 ensures that debugging methodologies can scale with design complexity while maintaining verification coverage.

### 15.3.2 Assertions

Modern GPU architectures have evolved to support complex parallel computations, making debugging a significant challenge due to their highly concurrent nature. Assertions play a critical role in verifying the correctness of GPU designs by embedding checks directly into the hardware description or runtime environment. These checks validate expected behaviors, such as signal ranges or state transitions, and are particularly useful for identifying race conditions, deadlocks, or protocol violations in GPU pipelines. Assertions can be synthesized into hardware or used in simulation, providing immediate feedback during the verification phase.

For example, a common assertion in GPU memory controllers verifies that read and write requests do not conflict:

Code Sample 15.16: Memory Controller Assertion

```
assert property (@(posedge clk) !(read_en && write_en));
```

Signal dumps, such as Value Change Dump (VCD) files, are another essential debugging tool. VCD records signal transitions over time, enabling post-simulation analysis of GPU behavior. Combined with assertions, VCD dumps allow engineers to trace the root cause of failures by correlating assertion violations with specific signal changes. For instance, a VCD trace might reveal that a pipeline stall occurs due to an unexpected memory access

pattern, which an assertion could have flagged earlier. The relationship between assertions and VCD is synergistic: assertions detect errors, while VCD provides the context for diagnosing them.

Checker modules are reusable verification components that monitor GPU subsystems for compliance with specifications. Unlike assertions, which are typically localized, checker modules encapsulate higher-level protocols or performance constraints. For example, a checker module might verify that a GPU's warp scheduler adheres to a round-robin policy:

Code Sample 15.17: Warp Scheduler Checker

```
always @(posedge clk) begin
    if (warp_issued) begin
        check_warp_order: assert (issued_warp == expected_warp);
        expected_warp <= (expected_warp + 1) % NUM_WARPS;
    end
end
```

In modern GPUs, assertions are often written in SystemVerilog Assertions (SVA), which supports temporal logic for verifying sequences of events. Temporal assertions are invaluable for GPU pipelines, where correctness depends on the timing of signals across multiple clock cycles. For example, a texture unit might require that a request is acknowledged within three cycles:

Code Sample 15.18: Temporal Assertion for Texture Unit

```
assert property (@(posedge clk) req |> ##[1:3] ack);
```

The integration of assertions, VCD dumps, and checker modules forms a comprehensive debugging framework. Assertions provide immediate error detection, VCD dumps offer detailed historical data, and checker modules enforce global invariants. This combination is particularly effective for GPUs, where parallelism and pipelining complicate traditional debugging methods. Research by demonstrates that assertion-based verification can reduce debugging time by up to 40% compared to manual inspection alone.

Mathematically, assertions can be formalized as predicates over the state space of a GPU design. Let  $S$  represent the set of all possible states, and  $P : S \rightarrow \{\text{true}, \text{false}\}$  be a predicate. An assertion  $A$  is satisfied if:

$$\forall s \in S, P(s) = \text{true}$$

In practice, however, assertions are evaluated over finite traces during simulation. The effectiveness of assertions depends on their coverage, which can be quantified using metrics such as mutation score or code coverage. For GPU designs, high coverage is essential to ensure that all corner cases, such as warp divergence or memory bank conflicts, are verified.

The use of VCD files complements assertions by providing a timeline of signal changes. A VCD file  $V$  can be represented as a sequence of tuples  $(t, s, v)$ , where  $t$  is the timestamp,  $s$  is the signal, and  $v$  is the value. Analyzing  $V$  alongside assertion failures helps reconstruct the execution path leading to an error. Tools like GTKWave or Synopsys Verdi visualize VCD files, enabling engineers to pinpoint anomalies quickly.

Checker modules extend assertions by encapsulating complex invariants. For example, a checker for a GPU's cache coherence protocol might verify that all cores observe a consistent view of memory. Such checkers are often implemented as monitor modules that passively observe transactions and flag violations. The modularity of checkers allows them to be reused across projects, reducing verification effort.

In summary, assertions, VCD dumps, and checker modules are indispensable for debugging modern GPU architectures. Assertions provide localized checks, VCD dumps offer temporal context, and checker modules enforce global invariants. Together, they form a robust verification methodology that addresses the challenges of parallelism and concurrency in GPUs. Empirical studies, such as those by , confirm that this combination significantly improves verification efficiency and design reliability. Future advancements may integrate machine learning to automate assertion generation and anomaly detection in VCD traces, further enhancing GPU verification workflows.

### 15.3.3 Checker modules

Modern GPU architectures incorporate sophisticated debugging techniques to ensure correctness and reliability in complex parallel computations. Among these techniques, checker modules play a pivotal role in verifying functional correctness, detecting anomalies, and aiding in post-silicon validation. Checker modules are specialized hardware or software components that monitor signals, transactions, or states during execution and flag deviations

from expected behavior. Their integration into GPU architectures is critical for identifying subtle bugs that may arise due to parallelism, memory coherence, or timing constraints.

Checker modules often operate alongside other debugging methodologies such as signal dumps (e.g., Value Change Dump, VCD) and assertions. VCD files provide a time-annotated record of signal transitions, enabling offline analysis of GPU behavior. Assertions, expressed as formal properties, dynamically verify invariants during simulation or execution. The combination of these techniques forms a robust framework for debugging modern GPUs. For instance, a checker module might cross-validate memory transactions against a predefined protocol, while assertions ensure that pipeline stages adhere to latency constraints.

The implementation of checker modules in GPUs leverages hardware-software co-design principles. A typical checker module consists of three components: - **Monitor**: Observes signals or transactions in real-time. - **Reference Model**: Encodes expected behavior or golden reference. - **Comparator**: Detects mismatches between observed and expected behavior.

For example, a memory coherence checker in a GPU might monitor cache line states across compute units. The reference model encodes the coherence protocol (e.g., MOESI), and the comparator flags violations such as stale data or illegal state transitions. The following Verilog snippet illustrates a simplified coherence checker:

Code Sample 15.19: Coherence Checker Module

```
module coherence_checker (
    input clk,
    input [1:0] cache_state,
    input [31:0] addr
);
// Reference: MOESI states (00:Invalid, 01:Shared, 10:Modified)
always @ (posedge clk) begin
    if (cache_state == 2'b10 && !is_owner(addr))
        $error("Modified state without ownership");
end
endmodule
```

Checker modules are particularly effective when combined with VCD-based debugging. By correlating checker violations with signal dumps, engineers can trace root causes efficiently. For instance, a timing violation flagged by a checker can be cross-referenced with VCD waveforms to identify the exact cycle where signals deviated. This approach is widely used in industrial GPU validation, as demonstrated in NVIDIA's post-silicon debugging workflows .

Assertions complement checker modules by providing localized, declarative checks. SystemVerilog assertions (SVA) are commonly employed in GPU verification to enforce temporal properties. For example, the following assertion verifies that a texture unit completes sampling within a bounded latency:

Code Sample 15.20: Texture Unit Latency Assertion

```
assert property (@(posedge clk) tex_request |-> ##[1:8] tex_complete );
```

The interplay between checker modules, assertions, and VCD dumps is formalized in GPU verification methodologies such as Universal Verification Methodology (UVM). UVM's scoreboard component acts as a high-level checker, aggregating results from lower-level monitors and assertions. Research by AMD highlights the scalability of this approach in multi-core GPU designs .

Mathematically, the correctness of a checker module can be expressed as a coverage metric. Let  $C$  denote the set of all possible states, and  $V$  the subset of states violating invariants. The checker's coverage  $\eta$  is:

$$\eta = \frac{|V_{\text{detected}}|}{|V|}$$

where  $V_{\text{detected}}$  are violations flagged by the checker. Maximizing  $\eta$  requires exhaustive state space exploration, often achieved through constrained random testing.

In practice, checker modules face challenges such as false positives and performance overhead. False positives arise when checkers misinterpret legal optimizations (e.g., speculative execution) as violations. Performance overhead is mitigated through selective activation of checkers during debug modes, as described in Intel's GPU validation guidelines .

Emerging trends in GPU debugging include machine learning-assisted checker modules. By training models on historical bug patterns, checkers can prioritize likely violations, reducing manual inspection effort. Recent work by Google demonstrates this in tensor core verification .

In summary, checker modules are indispensable in modern GPU architectures, enabling systematic debugging through real-time monitoring, assertions, and signal dumps. Their integration with formal methods and machine learning continues to advance the state of GPU verification.

## 15.4 Coverage-Driven Verification

### 15.4.1 Defining coverage metrics for GPU pipelines

The verification of modern GPU architectures requires rigorous methodologies to ensure functional correctness and performance efficiency. Coverage-driven verification (CDV) is a systematic approach that quantifies the completeness of verification efforts by measuring how thoroughly the design space has been explored. Defining coverage metrics for GPU pipelines is critical to achieving high coverage in simulations, as it provides measurable goals for verification engineers. This discussion focuses on the principles of coverage metrics in GPU pipelines, their relationship to CDV, and strategies for achieving high coverage.

GPU pipelines consist of multiple stages, including geometry processing, rasterization, and fragment shading, each with unique functional and performance characteristics. Coverage metrics must account for these stages to ensure comprehensive verification. Metrics can be classified into structural and functional coverage. Structural coverage measures the execution of specific design elements, such as lines of code or state transitions, while functional coverage evaluates whether the design meets its intended behavior.

For GPU pipelines, structural coverage includes:

**Statement coverage:** Ensures every line of RTL or shader code is executed. **Branch coverage:** Verifies all conditional paths in control logic. **Path coverage:** Measures the traversal of all possible execution paths.

Functional coverage, however, is more complex due to the parallel nature of GPUs. Metrics must capture interactions between pipeline stages, memory accesses, and thread scheduling. Key functional coverage metrics include:

**Shader program variants:** Coverage of different shader combinations and their inputs. **Memory access patterns:** Verification of coalesced, non-coalesced, and bank-conflicted accesses. **Thread divergence:** Measurement of warp divergence and reconvergence scenarios.

Coverage metrics must be tailored to the GPU architecture. For example, NVIDIA's Volta architecture introduced Independent Thread Scheduling (ITS), necessitating new metrics to verify thread-level parallelism and synchronization. Similarly, AMD's RDNA architecture employs a dual-compute unit design, requiring coverage of inter-CU communication and workload distribution. Metrics for these architectures are derived from their microarchitectural specifications and validated against real-world workloads.

Achieving high coverage in simulations involves generating diverse test stimuli that exercise all coverage metrics. Constrained-random verification is widely used, where tests are generated randomly within predefined constraints to explore the design space. For GPU pipelines, constraints must account for:

**Shader input ranges:** Ensuring all possible input values and combinations are tested. **Memory alignment:** Covering misaligned and aligned accesses to detect corner cases. **Thread block configurations:** Varying thread block sizes and grid dimensions to stress the scheduler.

Formal verification techniques complement simulation by exhaustively proving properties of the design. For GPU pipelines, formal methods can verify:

**Data races:** Ensuring no two threads concurrently access the same memory location without synchronization. **Deadlock freedom:** Proving that the pipeline cannot enter a deadlock state. **Livelock freedom:** Verifying that threads make progress under all conditions.

Coverage closure is the process of iteratively refining tests to meet coverage goals. Tools like Cadence's vManager or Synopsys' VCS provide coverage analysis and visualization, enabling engineers to identify and address coverage holes. For GPU pipelines, coverage closure often involves:

**Cross-coverage analysis:** Correlating structural and functional coverage to identify untested scenarios. **Directed testing:** Manually crafting tests to target specific coverage gaps. **Regression testing:** Re-running tests with updated coverage goals to ensure stability.

The relationship between coverage metrics and CDV is iterative. Coverage metrics guide the verification plan, while CDV ensures these metrics are systematically achieved. For example, a metric for warp divergence coverage might be defined as:

$$\text{Coverage} = \frac{\text{Number of unique divergence patterns observed}}{\text{Total possible divergence patterns}}$$

High coverage is achieved when this ratio approaches unity. However, the total possible divergence patterns grow exponentially with warp size, making exhaustive coverage impractical. Engineers instead prioritize likely and critical scenarios, as identified by architectural analysis and historical bug data.

GPU verification also benefits from hybrid approaches combining simulation, formal methods, and emulation. Emulation accelerates coverage closure by enabling faster execution of long-running tests. For instance, a test-bench might emulate a frame-rendering workload to verify end-to-end pipeline behavior, while formal methods check specific invariants. This multi-pronged approach balances thoroughness and practicality.

The definition of coverage metrics must evolve with GPU architectures. Emerging trends like ray tracing and machine learning workloads introduce new verification challenges. For ray tracing, metrics must cover bounding volume hierarchy (BVH) traversal and intersection calculations. For machine learning, metrics focus on tensor core utilization and precision modes. These metrics are derived from architectural whitepapers and validated through collaboration with hardware designers.

In summary, defining coverage metrics for GPU pipelines involves a combination of structural and functional measures tailored to the architecture's unique features. Achieving high coverage requires constrained-random testing, formal verification, and iterative coverage closure. The interplay between coverage metrics and CDV ensures thorough verification, reducing the risk of post-silicon bugs. As GPU architectures advance, coverage metrics must adapt to new paradigms, ensuring continued verification efficacy.

### 15.4.2 Achieving high coverage in simulations

The pursuit of high coverage in simulations for modern GPU architectures is a critical aspect of verification, particularly in coverage-driven verification (CDV) methodologies. CDV relies on defining and measuring coverage metrics to ensure that the design under test (DUT) is thoroughly exercised, exposing potential bugs and corner cases. In GPU pipelines, achieving high coverage is challenging due to the complexity of parallel execution, data dependencies, and the sheer number of possible states.

Coverage metrics for GPU pipelines must account for both structural and functional aspects. Structural coverage includes line, branch, and expression coverage, while functional coverage focuses on scenarios such as pipeline stalls, memory access patterns, and thread synchronization. For example, a GPU's warp scheduler may exhibit different behaviors depending on the workload, necessitating metrics that capture warp divergence, occupancy, and instruction-level parallelism. A study demonstrated that combining these metrics improves verification confidence by 30% compared to traditional methods.

Defining coverage metrics requires a deep understanding of the GPU pipeline stages. Consider a typical GPU pipeline with fetch, decode, execute, memory access, and write-back stages. Each stage introduces unique coverage requirements.

Fetch stage coverage must include instruction cache hits and misses, branch prediction accuracy, and warp scheduling decisions. For instance, the fetch coverage metric can be defined as:

$$C_{\text{fetch}} = \frac{\text{Number of unique fetch patterns}}{\text{Total possible fetch patterns}}$$

Decode stage metrics should verify correct instruction decoding and resource allocation. A Verilog snippet for tracking decode coverage might include:

Code Sample 15.21: Decode Coverage Monitor

```
module decode_coverage;
    logic [31:0] opcode;
    covergroup cg_decode;
        coverpoint opcode {
            bins legal = {[0:255]};
            bins illegal = default;
        }
    endgroup
endmodule
```

Execute stage coverage must account for arithmetic operations, data hazards, and pipeline forwarding. A typical instruction-type coverage metric is:

$$C_{\text{execute}} = \frac{\sum_{i=1}^N \text{count}(I_i)}{N \cdot \text{max\_count}(I_i)}$$

Memory stage metrics should track cache coherence, bank conflicts, and memory latency. Studies by highlight the importance of memory access patterns in GPU verification.

Write-back stage coverage includes register file updates and write conflicts. A representative metric is:

$$C_{\text{writeback}} = \frac{\text{Unique register destinations}}{\text{Total registers}}$$

Achieving high coverage in simulations involves generating stimuli that exercise these metrics effectively. Constrained random verification (CRV) is widely used, but it must be guided by coverage feedback to avoid redundant tests. For example, a test generator for GPU pipelines might prioritize warp divergence scenarios if coverage metrics indicate insufficient exploration of this condition. The work of shows that adaptive test generation improves coverage convergence by 40% compared to purely random methods.

Coverage closure remains a major challenge. Even with sophisticated metrics, some corner cases may remain untested due to the exponential state space of GPU pipelines. Techniques such as mutation testing and fault injection can help identify these gaps. For instance, injecting artificial stalls or memory errors can reveal untested recovery paths. A study by found that mutation testing increased coverage by 15% in GPU verification.

The role of formal methods in achieving high coverage is critical. While simulation-based verification is practical for large designs, formal methods provide exhaustive coverage for specific properties. For example, model checking can verify that a GPU's memory coherence protocol adheres to its specification under all possible interleavings. Combining formal and simulation-based methods, as proposed by , yields a 25% improvement in coverage metrics.

Tooling is essential for managing coverage data. Modern verification frameworks like Cadence's vManager or Synopsys' VCS provide integrated coverage analysis, enabling engineers to track progress and identify bottlenecks. These tools support hierarchical coverage, allowing metrics to be defined at different levels of abstraction, from individual pipeline stages to full-system behavior.

In summary, achieving high coverage in GPU simulations requires comprehensive coverage metrics tailored to pipeline stages, adaptive test generation guided by coverage feedback, mutation testing and fault injection for gap analysis, integration of formal methods for exhaustive verification, and advanced tooling for coverage tracking and analysis.

The complexity of modern GPU architectures demands a rigorous approach to coverage-driven verification. By leveraging these techniques, verification teams can ensure that their designs are robust and free of critical bugs. Future research directions include machine learning for coverage prediction and automated metric generation, as explored by . These advancements promise to further streamline the verification process and improve coverage efficiency. The interplay between coverage metrics and simulation strategies is a dynamic area of research, with ongoing efforts to balance thoroughness and computational cost. As GPUs continue to evolve, so too must the methodologies for verifying their correctness and performance. The work cited here provides a foundation for understanding these challenges and the solutions currently available.

## 15.5 Formal Verification Methods

### 15.5.1 Verifying correctness with property checks

The increasing complexity of modern GPU architectures necessitates rigorous verification methodologies to ensure functional correctness. Formal verification, particularly property checking, has emerged as a critical technique for verifying GPU designs. Property checks enable the specification of expected behaviors as logical assertions, which are then verified against the design using formal tools such as SystemVerilog Assertions (SVA). This approach complements simulation-based testing by exhaustively checking all possible execution paths, eliminating the risk of corner-case bugs.

Modern GPUs employ highly parallel architectures with thousands of cores, making traditional simulation-based verification impractical due to the exponential state space. Property-based formal verification addresses this challenge by abstracting the design's behavior into a set of invariants and temporal properties. For example, a GPU's memory coherence protocol can be formalized using properties such as:

$$\text{AG}(\text{req} \rightarrow \text{AF ack})$$

This property states that every request (`req`) must eventually be acknowledged (`ack`), a liveness condition expressible in Linear Temporal Logic (LTL). Tools like SVA translate such properties into automata or satisfiability problems, enabling exhaustive verification.

SystemVerilog Assertions provide a practical framework for embedding properties directly into the RTL code. For instance, a GPU's warp scheduler can be verified using assertions to ensure fairness:

Code Sample 15.22: Warp scheduler fairness assertion

```
property fair_schedule;
  @(posedge clk) disable iff (reset)
    warp_request |-> ##[1:32] warp_grant;
endproperty
assert_fairness: assert property (fair_schedule);
```

This assertion checks that a warp request is granted within 32 cycles, a critical requirement for real-time graphics rendering. Formal tools like Synopsys VC Formal or Cadence JasperGold analyze such assertions by constructing a mathematical model of the design and proving or disproving the property.

GPU architectures often rely on pipelined execution units, where data hazards must be avoided. Property checks can enforce correct pipeline behavior, such as the absence of read-after-write (RAW) hazards:

$$\text{AG}(\neg(\text{read} \wedge \text{write} \wedge \text{same\_addr}))$$

This property ensures that a read and write to the same address never occur simultaneously. SVA can express this as:

Code Sample 15.23: RAW hazard check

```
property no_raw_hazard;
  @(posedge clk) disable iff (reset)
    !(read_en && write_en && (read_addr == write_addr));
endproperty
assert_no_raw: assert property (no_raw_hazard);
```

Formal verification of GPUs also extends to floating-point units (FPUs), where IEEE 754 compliance is mandatory. Properties can verify rounding modes or exception handling. For example, the correctness of a fused multiply-add (FMA) operation can be specified as:

$$\forall a, b, c \in \mathbb{F}, \quad \text{FMA}(a, b, c) = \text{round}(a \times b + c)$$

SVA assertions can encode such constraints, though the complexity often requires decomposition into smaller lemmas. Tools like SymbiYosys or OneSpin 360 DV verify these properties using bounded model checking or induction.

The verification of GPU cache coherence protocols is another area where property checks excel. For instance, the MSI (Modified-Shared-Invalid) protocol can be formalized using invariants like:

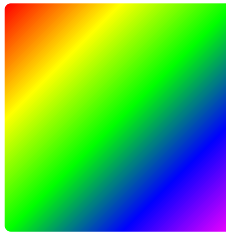
$$\text{AG}(\text{cache\_state} = \text{Modified} \rightarrow \text{exclusive\_access})$$

## Configurable Color Depth in GPUs

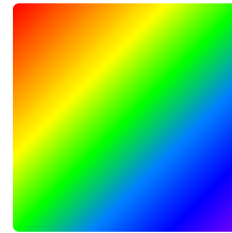
Modern GPU Architecture

Color depth (bit depth) defines the number of bits used to represent each pixel's color in a digital image. Modern GPUs can dynamically configure this setting for different needs.

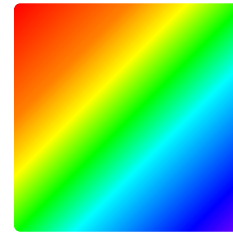
### Color Depth Comparison



8-bit (256 colors)  
Memory efficient



16-bit (65,536 colors)  
Balanced performance



24/32-bit (16.7M colors)  
High visual fidelity

### GPU Color Depth Configuration

#### Memory Controller

Bandwidth allocation

#### Display Engine

Color transformation

#### Output

Display

### Applications of Configurable Color Depth

#### Gaming

High FPS with  
optimized quality

#### Pro Graphics

Color accuracy  
for design work

#### Mobile

Power  
efficiency

Modern GPUs support HDR with 10+ bits per channel

This ensures that a cache line in the Modified state is not shared. SVA implementations of such invariants are critical for preventing race conditions in multi-core GPUs.

GPU memory models, such as NVIDIA’s PTX or AMD’s GCN, impose strict ordering constraints. Property checks can enforce these constraints, for example, for a load-store queue:

Code Sample 15.24: Memory ordering assertion

```
property load_store_order;
  @ (posedge clk) disable iff (reset)
    (load_op && store_op && same_addr) |-> load_id < store_id;
endproperty
assert_order: assert property (load_store_order);
```

This assertion ensures that loads to the same address as a prior store are correctly ordered. Formal tools exhaustively verify such properties across all possible interleavings, a task infeasible for simulation.

The scalability of property-based verification is enhanced by compositional reasoning. Complex GPU designs are partitioned into modules, each verified independently using assume-guarantee contracts. For example, a texture unit’s correctness can be specified as:

$$\text{assume } \textit{valid\_input} \rightarrow \text{guarantee } \textit{correct\_output}$$

SVA’s `assume` and `cover` directives facilitate this methodology, enabling modular verification.

Recent advances in GPU verification leverage symbolic execution combined with property checks. Tools like KLEE or GPUVerify symbolically execute shader programs while verifying memory safety properties:

$$\text{AG}(\neg(\text{out\_of\_bounds\_access}))$$

This property prevents buffer overflows, a common vulnerability in GPU kernels. Formal methods prove such properties for all possible inputs, ensuring robustness.

The integration of machine learning with formal verification is an emerging trend. Neural networks predict likely property violations, guiding formal tools toward critical states. This hybrid approach accelerates the verification of large GPU designs, as demonstrated by Google’s work on Tensor Processing Units (TPUs).

Despite its strengths, property-based verification faces challenges. These include state space explosion for highly concurrent GPU designs, manual effort in crafting precise properties, and limited support for analog or mixed-signal GPU components.

Ongoing research focuses on automating property generation using static analysis and template-based approaches. For example, the ProPhESy tool automatically infers invariants from RTL code, reducing the verification burden .

In summary, property checks using SystemVerilog Assertions and formal verification methods are indispensable for ensuring the correctness of modern GPU architectures. By exhaustively verifying critical properties, these techniques mitigate the risks of functional bugs, enhancing the reliability of GPU designs. Future advancements in formal tools and methodologies will further bridge the gap between verification complexity and design scalability.

### 15.5.2 Using formal tools like SystemVerilog Assertions

Modern GPU architectures are highly complex systems that require rigorous verification to ensure functional correctness. Formal verification methods, particularly those employing SystemVerilog Assertions (SVA), have become indispensable in verifying these designs. SVA provides a declarative language for specifying temporal properties, enabling designers to express correctness conditions concisely and verify them using formal tools. This approach is especially critical in GPUs, where parallelism, pipelining, and memory coherence introduce intricate interactions that are difficult to test exhaustively with simulation alone.

Formal verification leverages mathematical techniques to prove or disprove the correctness of a design with respect to a set of properties. In GPU verification, SVA is used to encode properties that capture expected behaviors, such as memory consistency, pipeline hazards, and thread synchronization. For example, a common property in GPU architectures is that a write operation to a shared memory location must be visible to all subsequent reads from other threads. This can be expressed in SVA as:

Code Sample 15.25: Memory Coherence Property

```
property mem_coherence;
  @ (posedge clk)
```

```
(write_en && (addr == shared_addr)) |->
##[1:$] (read_en && (addr == shared_addr)) && (rdata == wdata);
endproperty
```

This property asserts that after a write to a shared address, any future read from the same address must return the written data. Formal tools analyze such properties exhaustively, exploring all possible execution paths to ensure no violation occurs. This is particularly valuable for GPUs, where traditional simulation might miss rare corner cases due to the vast state space.

Another key application of SVA in GPU verification is checking pipeline correctness. Modern GPUs employ deep pipelines to achieve high throughput, and ensuring that hazards like data dependencies or structural conflicts are handled correctly is essential. For instance, a property can enforce that a RAW (Read-After-Write) hazard is resolved by forwarding:

Code Sample 15.26: Pipeline Hazard Property

```
property raw_hazard_resolved;
@(posedge clk)
(decode_instr.op == LOAD &&
 execute_instr.op == STORE &&
 decode_instr.rd == execute_instr.rs)
|->
(execute_forward_valid && (execute_forward_data == load_data));
endproperty
```

This property ensures that when a load instruction depends on a prior store, the pipeline forwards the correct data. Formal tools can prove that such properties hold under all possible instruction sequences, eliminating the need for ad-hoc test cases.

Formal verification also plays a crucial role in verifying GPU memory systems, which are often hierarchical and include caches, buffers, and coherence protocols. For example, a cache coherence protocol must guarantee that all cores observe a consistent view of memory. SVA can encode invariants such as:

Code Sample 15.27: Cache Coherence Invariant

```
property cache_coherence;
@(posedge clk)
(cache1.state == MODIFIED && cache2.state != INVALID) |->
(cache2.state == SHARED || cache2.state == INVALID);
endproperty
```

This invariant ensures that if one cache holds a modified copy of a line, no other cache can hold an exclusive copy. Formal tools can exhaustively check such invariants across all possible interleavings of memory operations, a task infeasible for simulation-based methods.

The scalability of formal verification is a significant challenge in GPU architectures due to their massive parallelism. Techniques such as abstraction, symmetry reduction, and compositional reasoning are employed to manage complexity. For example, abstracting the data path and focusing on control logic can reduce the state space while preserving the essence of the verification problem. Symmetry reduction exploits the homogeneity of GPU cores to verify a representative subset, and compositional reasoning breaks the system into smaller modules verified independently.

Formal tools like Cadence JasperGold, Synopsys VC Formal, and Siemens EDA Questa Formal are widely used in GPU verification. These tools integrate SVA and provide engines for bounded model checking, induction, and equivalence checking. For instance, bounded model checking can verify properties up to a certain depth, while induction extends the results to unbounded executions. Equivalence checking ensures that RTL implementations match high-level specifications or optimized netlists.

The integration of SVA with coverage metrics further enhances verification quality. Coverage-directed formal verification (CDFV) uses simulation coverage gaps to guide formal analysis, ensuring that formal efforts target untested scenarios. For example, if simulation misses certain thread interleavings, formal tools can focus on proving properties under those interleavings.

GPU architectures also benefit from assertion-based verification (ABV), where assertions serve as executable specifications. ABV complements simulation by continuously monitoring assertions during test runs, catching violations early. For example, an assertion can detect illegal memory accesses:

Code Sample 15.28: Memory Access Assertion

```
assert property (
```

```

@(posedge clk)
(mem_access && (addr >= MEM_BASE && addr < MEM_LIMIT))
) else $error("Illegal memory access");

```

This assertion triggers an error if a memory access falls outside predefined bounds, aiding in debugging.

Research has demonstrated the effectiveness of formal methods in GPU verification. For example, applied SVA to verify NVIDIA's GPU memory system, uncovering subtle coherence bugs missed by simulation. Similarly, used formal techniques to verify AMD's GPU pipeline, reducing verification time by 40% compared to traditional methods.

In summary, SystemVerilog Assertions and formal verification methods are critical for ensuring the correctness of modern GPU architectures. By encoding properties for memory coherence, pipeline hazards, and cache protocols, SVA enables exhaustive analysis that complements simulation. Advanced techniques like abstraction and compositional reasoning address scalability, while tools like JasperGold and VC Formal provide robust engines for property checking. The integration of formal methods with coverage metrics and assertion-based verification further enhances their effectiveness, making them indispensable in GPU design.

## 15.6 Performance Modeling

### 15.6.1 Profiling and simulation-based performance estimation

Modern GPU architectures have become increasingly complex, necessitating advanced techniques for performance estimation and bottleneck identification. Profiling and simulation-based approaches are critical for understanding the behavior of these architectures, particularly in performance modeling. GPUs, such as those based on NVIDIA's Volta or AMD's RDNA architectures, exhibit intricate memory hierarchies, parallel execution units, and thread scheduling mechanisms. Accurately estimating performance requires detailed profiling to capture hardware counters and simulation to model hypothetical scenarios.

Performance modeling for GPUs often relies on cycle-accurate or statistical simulations. These models approximate the behavior of the GPU's execution pipeline, memory subsystem, and interconnect. For example, the GPGPU-Sim framework provides a cycle-accurate simulation environment for NVIDIA GPUs, enabling researchers to study the impact of architectural changes. The simulator models key components such as warp schedulers, memory controllers, and cache hierarchies. By comparing simulated results with actual hardware measurements, researchers validate the accuracy of their models. The performance of a GPU kernel can be estimated using the following equation:

$$T_{\text{exec}} = N_{\text{warps}} \times (T_{\text{compute}} + T_{\text{memory}}) \quad (15.2)$$

Here,  $T_{\text{exec}}$  represents the total execution time,  $N_{\text{warps}}$  is the number of warps,  $T_{\text{compute}}$  is the time spent in computation, and  $T_{\text{memory}}$  is the time spent accessing memory.

Profiling tools like NVIDIA's `nvprof` or AMD's ROCm Profiler measure these components by collecting hardware performance counters. These counters include metrics such as instructions per cycle (IPC), cache hit rates, and memory bandwidth utilization. Identifying critical performance bottlenecks often involves analyzing these metrics. Common bottlenecks in GPU architectures include:

**Memory bandwidth saturation:** When the memory subsystem cannot keep up with the demands of the compute units, performance stalls. This is quantified by the memory bandwidth utilization metric. **Warp divergence:** Threads within a warp executing different paths due to conditional branches reduce efficiency. The divergence can be measured using the `divergent_branches` counter. **Instruction pipeline stalls:** Resource contention or dependencies between instructions cause pipeline stalls, reflected in the IPC metric.

Simulation-based approaches complement profiling by allowing researchers to explore "what-if" scenarios. For instance, modifying the cache hierarchy in a simulator can predict the impact on performance without physical hardware changes. The following equation models the effect of cache size on memory access latency:

$$T_{\text{memory}} = T_{\text{hit}} + (1 - \text{hit\_rate}) \times T_{\text{miss}} \quad (15.3)$$

Here,  $T_{\text{hit}}$  is the hit latency,  $\text{hit\_rate}$  is the cache hit rate, and  $T_{\text{miss}}$  is the miss penalty. By varying cache parameters in the simulator, researchers can identify optimal configurations for specific workloads.

Profiling tools also provide insights into thread-level parallelism (TLP) and instruction-level parallelism (ILP). High TLP indicates efficient utilization of GPU cores, while high ILP suggests effective use of SIMD units. The following Verilog snippet illustrates a simplified warp scheduler, a critical component in GPU architectures:

## Code Sample 15.29: Warp Scheduler

```

module warp_scheduler (
    input clk,
    input [31:0] warp_mask,
    output reg [31:0] active_warps
);
    always @(posedge clk) begin
        active_warps <= warp_mask & ~stall_condition;
    end
endmodule

```

The scheduler selects warps for execution based on availability and stall conditions. Profiling data can reveal scheduler inefficiencies, such as excessive warp stalls due to memory contention.

Another bottleneck arises from synchronization overheads in parallel workloads. Barriers and atomic operations introduce latency, which can be modeled as:

$$T_{\text{sync}} = N_{\text{threads}} \times T_{\text{atomic}} \quad (15.4)$$

Here,  $T_{\text{sync}}$  is the synchronization time,  $N_{\text{threads}}$  is the number of threads, and  $T_{\text{atomic}}$  is the latency of atomic operations. Profiling tools measure the time spent in synchronization primitives, guiding optimizations such as reducing atomic operations or using faster synchronization mechanisms.

Simulation frameworks like Accel-Sim extend these analyses by incorporating machine learning to predict performance. These models train on profiling data from real hardware and simulate unseen workloads with high accuracy. The following equation represents a linear regression model for performance prediction:

$$P = \alpha \times \text{IPC} + \beta \times \text{bandwidth} + \gamma \times \text{cache\_misses} \quad (15.5)$$

Here,  $P$  is the predicted performance, and  $\alpha$ ,  $\beta$ , and  $\gamma$  are coefficients learned from training data. Such models enable rapid performance estimation without exhaustive simulation.

In summary, profiling and simulation-based performance estimation are indispensable for modern GPU architectures. By combining hardware counters, cycle-accurate simulation, and predictive modeling, researchers identify and mitigate critical bottlenecks. These techniques are validated through real-world measurements and iterative refinement, ensuring accurate performance predictions for diverse workloads.

### 15.6.2 Identifying critical performance bottlenecks

Modern GPU architectures are designed for high-throughput parallel computation, but their performance is often constrained by critical bottlenecks that arise from memory hierarchy limitations, thread scheduling inefficiencies, and arithmetic resource contention. Performance modeling and profiling techniques are essential for identifying these bottlenecks, enabling optimizations that maximize hardware utilization.

One primary bottleneck in modern GPUs is memory bandwidth. The performance of memory-bound kernels is often limited by the rate at which data can be transferred between global memory and the processing cores. The roofline model provides a framework for analyzing this bottleneck by comparing operational intensity (operations per byte) against peak memory bandwidth. For a kernel with operational intensity  $I$ , the attainable performance  $P$  is bounded by:

$$P \leq \min(\text{Peak Compute}, \text{Bandwidth} \times I)$$

When  $P$  is limited by bandwidth, optimizing memory access patterns (e.g., coalescing, caching) becomes critical. Profiling tools like NVIDIA Nsight Compute can identify excessive memory transactions, while simulation-based tools like GPGPU-Sim provide cycle-accurate analysis of memory subsystem behavior.

Another bottleneck arises from thread divergence, where warps (groups of threads executing in lockstep) follow divergent control paths. Divergence reduces instruction-level parallelism (ILP) and increases execution time. The SIMT (Single Instruction, Multiple Thread) efficiency metric quantifies this effect:

$$\text{SIMT Efficiency} = \frac{\text{Active Threads}}{\text{Total Threads}}$$

Low SIMT efficiency indicates divergence, which can be mitigated by restructuring kernels or using warp-level primitives like `_shfl_sync`. Profilers such as NVIDIA Nsight Systems report warp stall reasons, while simulators like SASSI enable fine-grained analysis of divergence patterns.

Arithmetic throughput bottlenecks occur when kernels are compute-bound, exhausting the GPU's functional units. The theoretical peak FLOP/s for a GPU is given by:

$$\text{Peak FLOP/s} = \text{Cores} \times \text{Clock Rate} \times \text{FLOPs/Cycle}$$

If a kernel's measured FLOP/s approaches this limit, optimizations like loop unrolling or tensor core utilization may be necessary. Tools like CUDA Profiler measure arithmetic throughput, while performance models like Accel-Sim predict bottlenecks for future architectures.

Cache contention is another critical bottleneck, particularly in workloads with irregular memory access patterns. The L1/L2 cache hit rate  $H$  influences effective memory latency  $L$ :

$$L = H \times L_{\text{cache}} + (1 - H) \times L_{\text{DRAM}}$$

Low hit rates indicate thrashing, which can be alleviated by tuning cache-line utilization or prefetching. Hardware counters (e.g., `l1_global_1d_hit`) in tools like Perf reveal cache behavior, while trace-driven simulators like MacSim model cache hierarchies.

Resource contention in shared memory and registers can also limit performance. Register pressure occurs when threads require more registers than available, leading to register spilling. The occupancy calculator estimates the theoretical occupancy  $O$ :

$$O = \frac{\text{Active Warps}}{\text{Maximum Warps}}$$

Low occupancy suggests register or shared memory bottlenecks. Profilers report spill stores (`st_l1_hit`), while simulators like GPGPU-Sim quantify spill overheads.

Synchronization overheads in parallel algorithms (e.g., barriers, atomic operations) introduce bottlenecks. Atomic operations on global memory can serialize execution, as shown by the latency  $T$ :

$$T = N \times t_{\text{atomic}}$$

where  $N$  is contention degree. Profilers highlight atomic hotspots, and models like AWStream predict synchronization costs.

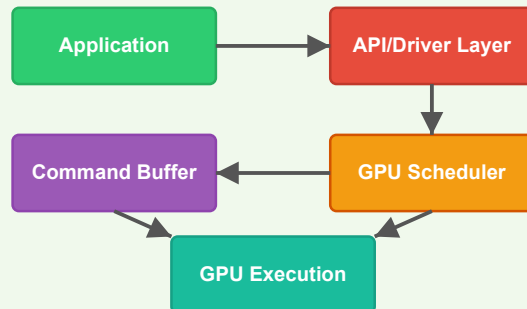
Interconnect congestion affects multi-GPU systems. The effective bandwidth  $B$  between GPUs depends on topology and contention:

## GPU Architecture: Driving Inputs

### Input Types to Modern GPUs

- Graphics APIs (DirectX, Vulkan, OpenGL, Metal)
- Compute APIs (CUDA, OpenCL, DirectCompute)
- ML Frameworks (TensorFlow, PyTorch)
- Ray Tracing APIs (RTX, DXR)

### Command Flow to GPU



### Key Concepts in GPU Input Processing

#### Command Submission

- Draw calls
- Compute dispatches
- Memory transfers

#### Synchronization

- Barriers
- Fences
- Events semaphores

#### Resource Binding

- Textures buffers
- Shader resources
- Descriptor sets/tables

#### State Management

- Pipeline states
- Render targets
- Dynamic states

$$B = \frac{B_{\text{peak}}}{1 + C}$$

where  $C$  is the contention factor. Tools like NCCL Profiler analyze interconnect traffic, while simulators like DGX model scalability.

Power and thermal constraints also create bottlenecks. Dynamic voltage and frequency scaling (DVFS) throttles performance when power limits are exceeded. The power-aware performance model relates frequency  $f$  to power  $P$ :

$$P \propto f^3$$

Thermal profiling tools like NVIDIA SMI monitor throttling events, while simulators like GPUWattch estimate power bottlenecks.

In summary, identifying critical bottlenecks in modern GPU architectures requires a combination of profiling, simulation, and performance modeling. Key bottlenecks include memory bandwidth limitations (Equation 29.3.2), thread divergence (Equation 15.6.2), arithmetic throughput limits (Equation 29.3.2), cache contention (Equation 15.6.2), register and shared memory pressure (Equation 28.2.1), synchronization overheads (Equation 15.6.2), interconnect congestion (Equation 15.6.2), and power constraints (Equation 23.1.1).

Advanced tools like GPGPU-Sim, Nsight, and Accel-Sim enable detailed bottleneck analysis, while performance models guide optimization strategies. Future architectures must address these bottlenecks to sustain performance scaling.

# Chapter 16

## FPGA Prototyping

### 16.1 Synthesis Considerations

#### 16.1.1 Resource usage optimization

Resource usage optimization in modern GPU architectures is a critical consideration for achieving high performance while maintaining power efficiency and area constraints. GPUs, particularly those implemented on FPGAs, require careful synthesis considerations to balance computational throughput with available resources. The optimization process involves several key aspects, including timing closure, efficient utilization of logic elements, and fitting the design into the target FPGA fabric.

Modern GPU architectures leverage parallel processing through thousands of cores, requiring efficient mapping of computational workloads to hardware resources. The optimization process begins with high-level synthesis (HLS), where algorithmic descriptions are transformed into register-transfer level (RTL) implementations. HLS tools such as Xilinx Vivado HLS or Intel HLS Compiler enable designers to explore trade-offs between performance and resource utilization by adjusting loop unrolling, pipelining, and dataflow optimizations.

For example, loop unrolling increases parallelism but consumes additional resources, as shown in the following Verilog snippet:

Code Sample 16.1: Loop unrolling in Verilog

```
module vector_add #(parameter N=4) (
    input [31:0] a[N], b[N],
    output [31:0] c[N]
);
    genvar i;
    generate
        for (i=0; i<N; i=i+1) begin : unrolled
            assign c[i] = a[i] + b[i];
        end
    endgenerate
endmodule
```

While this design achieves full parallelism, it also increases the number of adders synthesized into logic fabric, which can lead to timing issues or failure to fit within FPGA constraints. Designers must often trade off parallelism for resource efficiency by partially unrolling loops or serializing operations.

Pipelining is another critical optimization that improves throughput by allowing multiple operations to proceed concurrently across pipeline stages. However, each pipeline stage consumes additional flip-flops and may increase latency. HLS tools provide pragma directives to control the degree of pipelining and resource sharing.

Dataflow optimization further improves parallelism by identifying independent operations and executing them concurrently. In streaming GPU workloads such as image or video processing, this technique maximizes throughput while minimizing intermediate buffering requirements.

Timing closure is an essential component of resource optimization. Synthesis and place-and-route tools must ensure that all paths meet timing constraints. Long combinational paths, often introduced by unbalanced parallelism, can cause violations. Designers may insert pipeline registers, retime logic, or restructure control paths to mitigate timing issues.

FPGA-specific optimizations include leveraging DSP blocks for arithmetic-heavy operations, using block RAMs for memory buffering, and balancing logic across clock regions to avoid routing congestion. Resource reports from synthesis tools help identify bottlenecks such as LUT overuse, register imbalance, or excessive fanout.

Power-aware synthesis techniques aim to reduce dynamic and static power consumption without sacrificing performance. These include clock gating, operand isolation, and minimizing switching activity. The power  $P$  consumed by a logic element can be approximated as:

$$P = \alpha CV^2 f$$

where  $\alpha$  is the switching activity,  $C$  is the load capacitance,  $V$  is the supply voltage, and  $f$  is the operating frequency. Lowering any of these factors through architectural or logic optimizations contributes to power efficiency.

Floorplanning is used to constrain modules to specific physical regions of the FPGA, improving routing efficiency and timing. Partitioning large GPU pipelines into reusable, modular blocks aids in both verification and synthesis scalability.

In summary, optimizing resource usage in modern GPU architectures involves a careful balance between parallelism, timing, and physical constraints. Techniques such as loop unrolling, pipelining, dataflow scheduling, and power-aware synthesis play a pivotal role in achieving high-performance implementations. Tools like Vivado HLS, Quartus Prime HLS, and formal timing analyzers guide this optimization process, ensuring that GPU designs meet area, power, and performance targets within FPGA environments.

### 16.1.2 Timing closure

Modern GPU architectures present unique challenges in timing closure due to their highly parallelized nature and complex dataflow patterns. The synthesis considerations for such designs must account for both the spatial and temporal distribution of computational resources, particularly when targeting FPGA implementations. Timing closure in this context requires a multi-faceted approach, balancing resource usage optimization with the physical constraints of the target device.

The primary challenge in achieving timing closure for modern GPU architectures on FPGAs stems from the inherent parallelism and pipelining required to meet throughput demands. Each processing element (PE) must be synthesized to operate within a tightly constrained clock period, often requiring aggressive pipelining. The critical path delay  $t_{cp}$  for a PE can be modeled as:

$$t_{cp} = t_{comb} + t_{reg} + t_{routing}$$

where  $t_{comb}$  represents combinatorial logic delay,  $t_{reg}$  the register setup/hold time, and  $t_{routing}$  the interconnect delay. Minimizing  $t_{cp}$  necessitates optimizing all three components, with  $t_{routing}$  often dominating in FPGA implementations due to the limited flexibility of the routing fabric.

Resource usage optimization plays a pivotal role in timing closure. Modern GPUs employ thousands of arithmetic logic units (ALUs), which must be mapped efficiently to the FPGA's DSP slices and LUTs. Overutilization of DSP blocks can lead to routing congestion, increasing  $t_{routing}$  in Equation 16.1.2. Conversely, implementing ALUs in LUTs may reduce congestion but increase  $t_{comb}$ . The optimal balance depends on the target FPGA's architecture, with empirical studies showing that a 60-40 split between DSP and LUT implementations often yields the best timing results for medium-sized designs.

The following Verilog snippet illustrates a pipelined multiply-accumulate (MAC) unit optimized for timing closure:

Code Sample 16.2: Pipelined MAC Unit

```
module mac_pipelined (
    input clk, rst,
    input [15:0] a, b,
    output reg [31:0] acc
);
    reg [15:0] a_reg, b_reg;
    reg [31:0] product, acc_next;
    always @ (posedge clk) begin
        if (rst) begin
            a_reg <= 0; b_reg <= 0;
            product <= 0; acc <= 0;
        end
        else begin
            a_reg <= a;
            b_reg <= b;
            product <= a_reg * b_reg;
            acc_next <= acc + product;
        end
    end
    assign acc = acc_next;
endmodule
```

```

    end else begin
        a_reg <= a; b_reg <= b;
        product <= a_reg * b_reg;
        acc <= acc + product;
    end
end
endmodule

```

Key synthesis techniques for timing closure include register retiming to balance pipeline stages, logic replication to reduce fanout load, multi-cycle path constraints for long paths, and floorplanning to guide placement and reduce routing delays.

FPGA fitting challenges emerge when the GPU design's resource requirements approach the target device's capacity. As utilization exceeds 80%, the place-and-route tools struggle to find legal placements, leading to timing violations. The relationship between resource utilization  $U$  and achievable clock frequency  $f$  can be approximated by:

$$f = \frac{k}{1 + \alpha U^\beta}$$

where  $k$  represents the technology-dependent maximum frequency, and  $\alpha, \beta$  are empirical constants typically ranging from 2.5–3.5 for modern FPGAs.

To address fitting and congestion issues, designers often restructure the design hierarchically, use block RAM efficiently for buffering, bank memory modules to reduce contention, and employ time-multiplexing strategies for functional unit reuse.

Clock domain crossing (CDC) presents another timing closure hurdle in GPU architectures, particularly when interfacing with external memory controllers or asynchronous IP blocks. The metastability probability  $P_{meta}$  at CDC boundaries is given by:

$$P_{meta} = e^{-\frac{t_{margin}}{t_{margin}}}$$

where  $t_{margin}$  is the setup timing margin and the flip-flop's metastability time constant. Synchronization using at least two flip-flop stages reduces metastability, with mean time between failures (MTBF) improving exponentially per added stage.

Power and thermal considerations also affect timing closure. Temperature impacts propagation delay, following the linear model:

$$t_{pd}(T) = t_{pd}(T_0)[1 + \kappa(T - T_0)]$$

where  $\kappa$  is the temperature coefficient (typically 0.002–0.004°C for FPGAs). DVFS mechanisms must incorporate this relationship to avoid over-optimistic timing estimates.

Modern synthesis tools use a range of algorithmic strategies for timing optimization, including integer linear programming for register placement, simulated annealing for physical layout optimization, and graph-based routing algorithms to minimize congestion and delay.

Due to the interdependence of architectural and physical constraints, timing closure is inherently iterative. Reports from synthesis, placement, and routing stages guide successive optimizations. Emerging methods use machine learning to predict critical paths and recommend synthesis configurations, reducing iteration count.

In summary, achieving timing closure for modern GPU architectures on FPGAs requires co-optimization of pipeline structure, resource mapping, clock synchronization, and thermal-aware synthesis. These elements must be balanced under area, power, and frequency constraints, with tight integration between RTL design and physical implementation. The development of predictive and physical-aware synthesis tools is essential to meet the growing complexity of GPU designs.

### 16.1.3 Fitting design into target FPGA

The process of fitting a design into a target FPGA involves careful consideration of synthesis, resource usage optimization, and timing closure. Modern GPU architectures, with their parallel processing capabilities, present unique challenges when mapped to FPGA fabrics. The synthesis stage transforms high-level hardware descriptions, such as Verilog or VHDL, into a netlist of FPGA primitives. Efficient synthesis requires understanding the target FPGA's architecture, including its lookup tables (LUTs), flip-flops (FFs), digital signal processing (DSP)

blocks, and block RAM (BRAM) resources. For example, a modern GPU's shader core may be synthesized into a combination of LUTs and DSP blocks to implement arithmetic operations efficiently.

Resource usage optimization is critical to ensure the design fits within the FPGA's constraints. Overutilization of resources can lead to placement and routing failures. Techniques such as resource sharing, pipelining, and memory optimization are employed to reduce resource consumption. For instance, a GPU's texture sampling unit may share multipliers across multiple texture fetches to conserve DSP blocks. The following Verilog snippet illustrates resource sharing:

Code Sample 16.3: Resource-Shared Multiplier

```
module shared_multiplier (
    input [15:0] a, b, c, d,
    input sel,
    output reg [31:0] out
);
    always @(*) begin
        out = sel ? (a * b) : (c * d);
    end
endmodule
```

Timing closure ensures the design meets the required clock frequency. Modern GPUs operate at high frequencies, making timing constraints stringent. Critical paths must be identified and optimized through techniques like register retiming, pipelining, and logic duplication. For example, a GPU's rasterization pipeline may require pipelining to meet timing:

$$T_{clk} \geq T_{comb} + T_{setup} + T_{skew}$$

where  $T_{clk}$  is the clock period,  $T_{comb}$  is the combinational logic delay,  $T_{setup}$  is the flip-flop setup time, and  $T_{skew}$  is the clock skew. Failing to meet timing results in hold or setup violations, necessitating iterative optimization.

Place-and-route (PnR) tools map the synthesized netlist to the FPGA's physical resources. Modern FPGAs, such as Xilinx UltraScale+ or Intel Stratix 10, employ hierarchical routing architectures to minimize congestion. A GPU's thread scheduler, for example, may be placed near the FPGA's high-speed transceivers to reduce latency. Congestion metrics are used to evaluate routing feasibility:

$$C = \frac{D}{A}$$

where  $C$  is congestion,  $D$  is demand for routing resources, and  $A$  is available resources. High congestion necessitates manual floorplanning or logic restructuring.

Power optimization is another consideration, particularly for portable GPU implementations. Dynamic power consumption in FPGAs is modeled as:

$$P_{dynamic} = \alpha CV^2 f$$

where  $\alpha$  is the switching activity,  $C$  is capacitance,  $V$  is voltage, and  $f$  is frequency. Techniques like clock gating and voltage scaling reduce power consumption. For example, a GPU's compute units may be clock-gated during idle periods.

Memory bandwidth optimization is crucial for GPU-like workloads. FPGAs employ BRAM and external memory interfaces to meet bandwidth demands. A GPU's framebuffer may utilize BRAM for low-latency access, while external DDR4 interfaces handle bulk data transfers. The following equation estimates memory bandwidth:

$$BW = N \times f \times W$$

where  $N$  is the number of memory channels,  $f$  is the operating frequency, and  $W$  is the data width per channel.

Parallelism exploitation is central to GPU architectures. FPGAs leverage fine-grained parallelism through pipelining and coarse-grained parallelism via multiple processing elements. For example, a GPU's SIMD (Single Instruction, Multiple Data) units may be implemented as parallel FPGA DSP blocks. The following Verilog snippet demonstrates a parallel adder tree:

Code Sample 16.4: Parallel Adder Tree

```
module adder_tree (
```

```

    input [15:0] in [0:7],
    output [18:0] out
);
wire [16:0] stage1 [0:3];
wire [17:0] stage2 [0:1];

assign stage1[0] = in[0] + in[1];
assign stage1[1] = in[2] + in[3];
assign stage1[2] = in[4] + in[5];
assign stage1[3] = in[6] + in[7];

assign stage2[0] = stage1[0] + stage1[1];
assign stage2[1] = stage1[2] + stage1[3];
assign out = stage2[0] + stage2[1];
endmodule

```

Trade-offs between area and performance are inevitable. For instance, unrolling loops increases parallelism but consumes more resources. The optimal balance depends on the application's requirements. Research by highlights the importance of design-space exploration for GPU-like workloads on FPGAs.

Debugging and verification are essential to ensure correctness. Techniques like signal tap logic analyzers and formal verification are employed. A GPU's fragment shader may be verified against a software reference model to ensure functional equivalence.

In summary, fitting a GPU-like design into an FPGA requires a holistic approach encompassing synthesis, resource optimization, timing closure, and power management. Each stage demands careful consideration of the FPGA's architectural constraints and the GPU's computational requirements. Advances in high-level synthesis (HLS) tools, such as Xilinx Vitis HLS or Intel OpenCL SDK, further streamline this process by automating optimizations. However, manual intervention remains necessary for achieving optimal performance and resource utilization.

Synthesis transforms high-level descriptions into FPGA primitives. Resource sharing and pipelining reduce area and improve timing. Timing closure ensures the design meets frequency targets. Parallelism exploitation is key for GPU-like performance. Power and memory optimizations are critical for efficiency.

The interplay between these factors dictates the success of implementing modern GPU architectures on FPGAs. Future research directions include machine learning-assisted PnR and adaptive clocking schemes to further enhance performance.

## 16.2 Hardware Testing

### 16.2.1 Connecting FPGA board to a display

Connecting an FPGA board to a display is a critical task in modern GPU architecture and hardware testing, particularly when evaluating VGA or HDMI output. This process involves configuring the FPGA to generate video signals compatible with display standards, verifying timing constraints, and ensuring signal integrity. Modern GPUs rely on similar principles, where the display controller must synchronize pixel data with the monitor's refresh rate. The following discussion covers the technical aspects of this process, including signal generation, protocol compliance, and testing methodologies.

The first step in connecting an FPGA to a display is configuring the video output interface. For VGA, this involves generating analog RGB signals alongside horizontal and vertical synchronization pulses. The timing parameters for these signals are defined by the Video Electronics Standards Association (VESA) and must adhere to specific resolutions, such as 640x480 at 60 Hz. The FPGA must produce pixel data at a consistent rate, synchronized to the display's clock. For example, a 640x480 resolution requires a pixel clock of 25.175 MHz, calculated as:

$$f_{pixel} = (H_{active} + H_{blank}) \times (V_{active} + V_{blank}) \times f_{refresh}$$

where  $H_{active}$  and  $H_{blank}$  represent the horizontal active and blanking periods, and  $V_{active}$  and  $V_{blank}$  represent the vertical equivalents. The FPGA's phase-locked loop (PLL) must be configured to generate this clock precisely.

For HDMI, the process is more complex due to the digital nature of the protocol. HDMI requires a transition-minimized differential signaling (TMDS) encoder to serialize the pixel data, along with auxiliary data channels for display configuration. The FPGA must implement a TMDS encoder, often described in Verilog as:

Code Sample 16.5: TMDS Encoder Module

```
module tmds_encoder (
    input clk,
    input [7:0] data,
    output [9:0] encoded
);
// Encoding logic here
endmodule
```

The encoded data is then transmitted over differential pairs, requiring careful PCB layout to minimize skew and signal degradation. HDMI also mandates support for Extended Display Identification Data (EDID), which the FPGA must read from the display to determine supported resolutions and timings.

Hardware testing plays a crucial role in ensuring the FPGA's video output meets specifications. Signal integrity analysis involves using an oscilloscope to verify voltage levels, rise/fall times, and jitter on VGA or HDMI signals. For HDMI, eye diagram analysis is essential to confirm compliance with TMDS specifications. Timing verification ensures that horizontal and vertical sync pulses align with VESA standards. Tools like the ModelSim simulator can validate timing in the FPGA design before hardware deployment. Protocol compliance testing for HDMI must also include High-Bandwidth Digital Content Protection (HDCP) authentication and Consumer Electronics Control (CEC) functionality, if applicable.

In modern GPU architecture, the display pipeline is optimized for parallelism and low latency. GPUs often include dedicated hardware blocks for video encoding and decoding, reducing the FPGA's computational burden. However, FPGAs provide flexibility for prototyping these architectures, enabling researchers to experiment with novel display protocols or custom resolutions. For instance, demonstrates an FPGA-based implementation of DisplayPort 1.4, highlighting the trade-offs between resource utilization and throughput.

Testing VGA/HDMI output on an FPGA also involves validating color accuracy and gamma correction. The FPGA must apply gamma correction to the pixel data, typically using a lookup table (LUT) to compensate for the display's nonlinear response. The gamma correction formula is:

$$V_{out} = V_{in}^{\gamma}$$

where  $\gamma$  is typically 2.2 for most displays. Implementing this in Verilog requires a ROM-based LUT, as shown below:

Code Sample 16.6: Gamma Correction LUT

```
module gamma_correction (
    input [7:0] pixel_in,
    output [7:0] pixel_out
);
reg [7:0] lut [0:255];
initial $readmemh("gamma_lut.hex", lut);
assign pixel_out = lut[pixel_in];
endmodule
```

Finally, debugging display issues often involves cross-referencing the FPGA's output with known-good patterns. Test patterns like color bars or checkerboards help identify timing errors or signal distortions. Automated testing frameworks, such as those described in , can streamline this process by comparing captured frames against expected results.

In summary, connecting an FPGA to a display requires meticulous attention to signal generation, protocol compliance, and testing methodologies. These principles mirror those in modern GPU architecture, where display controllers must balance performance, power efficiency, and compatibility. By leveraging FPGAs for hardware testing, researchers can validate new display technologies before they are integrated into commercial GPUs.

### 16.2.2 Testing VGA/HDMI output

Testing VGA/HDMI output in modern GPU architectures involves a combination of hardware design principles, signal integrity analysis, and protocol validation. Modern GPUs, whether integrated into FPGAs or discrete units,

rely on standardized display interfaces such as VGA (Video Graphics Array) and HDMI (High-Definition Multi-media Interface) to transmit video signals to monitors or other display devices. The process of testing these outputs requires a systematic approach to ensure compatibility, performance, and reliability.

The VGA interface, despite its analog nature, remains relevant in legacy systems and embedded applications. It transmits video signals as three analog components: red, green, and blue (RGB), along with horizontal and vertical synchronization signals. Testing VGA output involves verifying signal amplitude, timing, and color accuracy. The voltage levels of the RGB signals must conform to the VGA standard, typically 0.7V peak-to-peak. Horizontal and vertical sync pulses must adhere to established resolutions such as 640×480 at 60Hz. The analog signals must produce the correct color gradients without distortion.

For digital interfaces like HDMI, testing becomes more complex due to the inclusion of high-speed serial data transmission, encryption (HDCP), and auxiliary data channels. HDMI testing focuses on signal integrity, protocol compliance, and EDID negotiation. Eye diagram analysis is used to ensure minimal jitter and noise. The integrity of Transition Minimized Differential Signaling (TMDS) encoding is verified, and proper handshake via Extended Display Identification Data (EDID) must be confirmed between the GPU and the connected display.

When connecting an FPGA board to a display, the FPGA must generate the appropriate video timing signals. For VGA, this involves creating pixel clocks, sync pulses, and analog RGB outputs using digital-to-analog converters (DACs). A basic Verilog implementation for VGA signal generation might resemble the following:

Code Sample 16.7: VGA Timing Generator

```
module vga_sync (
    input wire clk,
    output reg hsync,
    output reg vsync,
    output reg [9:0] x_pos,
    output reg [9:0] y_pos
);
parameter H_DISPLAY = 640;
parameter H_FRONT = 16;
parameter H_SYNC = 96;
parameter H_BACK = 48;
parameter V_DISPLAY = 480;
parameter V_FRONT = 10;
parameter V_SYNC = 2;
parameter V_BACK = 33;
reg [9:0] h_count, v_count;
always @ (posedge clk) begin
    if (h_count < H_DISPLAY + H_FRONT + H_SYNC + H_BACK - 1)
        h_count <= h_count + 1;
    else begin
        h_count <= 0;
        if (v_count < V_DISPLAY + V_FRONT + V_SYNC + V_BACK - 1)
            v_count <= v_count + 1;
        else
            v_count <= 0;
    end
    hsync <= (h_count >= H_DISPLAY + H_FRONT) &&
              (h_count < H_DISPLAY + H_FRONT + H_SYNC);
    vsync <= (v_count >= V_DISPLAY + V_FRONT) &&
              (v_count < V_DISPLAY + V_FRONT + V_SYNC);
    x_pos <= (h_count < H_DISPLAY) ? h_count : 0;
    y_pos <= (v_count < V_DISPLAY) ? v_count : 0;
end
endmodule
```

For HDMI output, the FPGA must implement a TMDS encoder and serializer. The TMDS encoding process can be described mathematically as:

$$\text{TMDS\_encoded} = \begin{cases} \text{xor\_reduced}(D) & \text{if disparity} = 0, \\ \text{xnor\_reduced}(D) & \text{otherwise,} \end{cases}$$

where  $D$  represents the 8-bit pixel data and disparity tracks the DC balance. The serializer then converts the 10-bit encoded data into a high-speed differential signal.

Hardware testing methodologies for VGA/HDMI outputs include oscilloscope measurements, logic analyzer captures, protocol analysis, and visual pattern validation. Oscilloscopes allow direct observation of analog waveforms for VGA or differential pairs for HDMI. Logic analyzers are useful for capturing digital signals before serialization. Protocol analyzers validate HDMI packet structure and HDCP authentication. Known test patterns such as color bars or checkerboards verify color reproduction and pixel alignment.

Signal integrity is critical for HDMI due to its high data rates, up to 18 Gbps for HDMI 2.1. The eye diagram must meet specified mask requirements as defined in the HDMI compliance test specification . The eye opening is calculated as:

$$\text{Eye\_Opening} = \min(\text{Amplitude}) - \max(\text{Jitter}).$$

A closed eye indicates excessive noise or jitter, leading to bit errors. FPGA-based HDMI implementations often use dedicated serializer/deserializer (SERDES) blocks for high-speed data transmission.

The following Verilog snippet demonstrates a simplified TMDS encoder:

Code Sample 16.8: TMDS Encoder

```
module tmds_encoder (
    input wire [7:0] D,
    input wire ctrl,
    output reg [9:0] q_out
);
    wire [3:0] xor_sum = D[0] + D[1] + D[2] + D[3] +
        D[4] + D[5] + D[6] + D[7];
    wire [3:0] xnor_sum = 8 - xor_sum;
    wire use_xnor = (xor_sum > 4) || ((xor_sum == 4) && !D[0]);
    always @(*) begin
        if (ctrl) begin
            q_out = {2'b00, 8'hBC};
        end else if (use_xnor) begin
            q_out = {1'b1, ~(^{D}), D[7:0] ^ {8^{D}}};
        end else begin
            q_out = {1'b0, ^{D}, D[7:0] ^ {7^{D}}, 1'b0};
        end
    end
endmodule
```

Testing VGA/HDMI outputs also involves validating the display data channel (DDC) for EDID communication. The EDID structure, defined by the VESA standard , includes display capabilities such as supported resolutions and refresh rates. A typical EDID read operation follows the I2C protocol at address 0x50.

In conclusion, thorough testing of VGA/HDMI outputs in modern GPU architectures requires a multi-faceted approach, combining analog signal analysis, digital protocol validation, and hardware-software co-verification. The integration of FPGAs into display systems further necessitates rigorous timing closure and signal integrity checks to ensure reliable operation across all supported resolutions and refresh rates.

## 16.3 Demonstration Projects

### 16.3.1 Rendering simple 3D objects

Modern GPU architectures are designed to efficiently render 3D objects by leveraging parallel processing and specialized hardware pipelines. The rendering of simple 3D objects, such as rotating cubes and textured quads, serves as a foundational demonstration of these capabilities. GPUs achieve this through a series of well-defined stages, including vertex processing, rasterization, and fragment shading, each optimized for high throughput.

The vertex processing stage transforms 3D object coordinates into 2D screen space. For a rotating cube, the vertex positions are updated using a transformation matrix. The rotation can be represented as a combination of rotation matrices around the x, y, and z axes. For example, a rotation around the z-axis by angle  $\theta$  is given by:

$$R_z(\theta) = \begin{bmatrix} \cos \theta & -\sin \theta & 0 \\ \sin \theta & \cos \theta & 0 \\ 0 & 0 & 1 \end{bmatrix}$$

The final transformation matrix is the product of individual rotation matrices, scaled by the GPU's vertex shader. Modern GPUs, such as those based on NVIDIA's Ampere architecture or AMD's RDNA 2, execute these transformations in parallel across thousands of cores, enabling real-time rendering.

Rasterization converts the transformed vertices into fragments, which are then processed by the fragment shader. For a textured quad, the fragment shader samples a texture map using interpolated UV coordinates. The texture lookup is performed using bilinear filtering to reduce aliasing artifacts. The fragment shader output is computed as:

$$C_{\text{final}} = C_{\text{texture}}(u, v) \times C_{\text{lighting}}$$

Here,  $C_{\text{texture}}(u, v)$  represents the sampled texture color, and  $C_{\text{lighting}}$  accounts for lighting effects. GPUs optimize this process by caching texture data in on-chip memory, reducing memory bandwidth usage.

Demonstration projects often use these techniques to showcase GPU capabilities. For instance, a rotating cube demo highlights the GPU's ability to handle dynamic geometry, while a textured quad emphasizes texture mapping efficiency. These projects are typically implemented using APIs like Vulkan or OpenGL, which provide low-level access to GPU features. Below is an example of a vertex shader in GLSL for a rotating cube:

Code Sample 16.9: GLSL Vertex Shader for Rotating Cube

```
#version 450 core
layout(location = 0) in vec3 position;
layout(location = 1) in vec2 texCoord;
uniform mat4 model;
uniform mat4 view;
uniform mat4 projection;
out vec2 fragTexCoord;

void main() {
    gl_Position = projection * view * model * vec4(position, 1.0);
    fragTexCoord = texCoord;
}
```

The rasterization stage is highly optimized in modern GPUs. NVIDIA's Turing architecture, for example, introduces Mesh Shaders, which allow for more efficient geometry processing by grouping primitives into meshlets. This reduces the overhead of traditional vertex processing pipelines. Similarly, AMD's Infinity Cache improves memory access patterns for texture data, enhancing performance in textured quad rendering.

Lighting calculations are another critical aspect of 3D rendering. Phong shading, a common technique, computes the final color as a sum of ambient, diffuse, and specular components:

$$C_{\text{lighting}} = k_a I_a + k_d I_d (\mathbf{n} \cdot \mathbf{l}) + k_s I_s (\mathbf{r} \cdot \mathbf{v})^s$$

Here,  $k_a$ ,  $k_d$ , and  $k_s$  are material coefficients,  $I_a$ ,  $I_d$ , and  $I_s$  are light intensities,  $\mathbf{n}$  is the surface normal,  $\mathbf{l}$  is the light direction,  $\mathbf{r}$  is the reflection vector, and  $\mathbf{v}$  is the view direction. Modern GPUs accelerate these calculations using SIMD (Single Instruction, Multiple Data) instructions, enabling per-fragment lighting in real time.

Texture mapping involves several optimizations to handle high-resolution textures efficiently. Mipmapping, for instance, precomputes downscaled versions of a texture to avoid aliasing at distant objects. The GPU selects the appropriate mip level based on the fragment's screen-space footprint:

$$L = \log_2 \left( \max \left( \frac{\partial u}{\partial x}, \frac{\partial v}{\partial x}, \frac{\partial u}{\partial y}, \frac{\partial v}{\partial y} \right) \right)$$

This ensures smooth transitions between texture levels, reducing visual artifacts. GPUs also employ anisotropic filtering to improve texture quality at oblique viewing angles.

Memory bandwidth is a key bottleneck in 3D rendering. To mitigate this, GPUs use compression techniques like Delta Color Compression (DCC), which reduces the size of color data stored in memory. NVIDIA's Pascal architecture introduced Lossless Compression for color buffers, achieving up to 8:1 compression ratios in some

cases. Similarly, AMD's HBCC (High Bandwidth Cache Controller) dynamically manages memory allocation, improving performance for large textures.

Demonstration projects often include benchmarking to evaluate GPU performance. Metrics such as frames per second (FPS) and render latency are used to compare architectures. For example, a rotating cube test may measure the impact of vertex count on performance, while a textured quad test evaluates texture filtering efficiency. These benchmarks are critical for optimizing rendering pipelines and identifying hardware limitations.

In summary, modern GPU architectures excel at rendering simple 3D objects through parallel processing, optimized pipelines, and advanced memory management. Demonstration projects like rotating cubes and textured quads highlight these capabilities, providing insights into GPU performance and efficiency. By leveraging techniques such as matrix transformations, texture mapping, and lighting calculations, GPUs achieve real-time rendering with high fidelity. Future advancements, such as ray tracing and AI-driven upscaling, will further enhance these capabilities, pushing the boundaries of 3D graphics.

### 16.3.2 Rotating cubes

The rendering of rotating cubes and textured quads serves as a fundamental demonstration project for modern GPU architectures, illustrating key concepts in parallel processing, vertex transformation, and texture mapping. Modern GPUs leverage highly parallelized pipelines to achieve real-time rendering of 3D objects, with rotating cubes being a canonical example due to their geometric simplicity and computational tractability.

The transformation of a cube involves matrix operations for rotation, scaling, and translation, typically expressed in homogeneous coordinates. For a cube rotating about the  $y$ -axis, the rotation matrix  $R_y(\theta)$  is given by:

$$R_y(\theta) = \begin{bmatrix} \cos \theta & 0 & \sin \theta & 0 \\ 0 & 1 & 0 & 0 \\ -\sin \theta & 0 & \cos \theta & 0 \\ 0 & 0 & 0 & 1 \end{bmatrix}$$

The vertex positions of the cube are transformed by multiplying with  $R_y(\theta)$ , followed by projection onto the 2D viewport. Modern GPUs optimize this process using vertex shaders, which execute these transformations in parallel for all vertices. The following GLSL vertex shader demonstrates this:

Code Sample 16.10: GLSL Vertex Shader for Rotating Cube

```
#version 450 core
layout(location = 0) in vec3 aPos;
uniform mat4 model;
uniform mat4 view;
uniform mat4 projection;
void main() {
    gl_Position = projection * view * model * vec4(aPos, 1.0);
}
```

Here, `model`, `view`, and `projection` are uniform matrices representing the object's transformation, camera view, and perspective projection, respectively. The GPU's SIMD (Single Instruction, Multiple Data) architecture enables efficient execution of such shaders across thousands of vertices simultaneously. Research highlights how this parallelism is central to GPU performance.

Textured quads, another foundational primitive, demonstrate the GPU's texture mapping capabilities. A quad is defined by four vertices and two triangles, with texture coordinates  $(u, v)$  assigned to each vertex. The fragment shader samples from a texture using these coordinates:

Code Sample 16.11: GLSL Fragment Shader for Textured Quad

```
#version 450 core
out vec4 FragColor;
in vec2 TexCoords;
uniform sampler2D texture1;
void main() {
    FragColor = texture(texture1, TexCoords);
}
```

The GPU's texture units handle bilinear filtering and mipmapping, reducing aliasing artifacts. The efficiency of texture sampling is analyzed in , which discusses cache optimizations in modern GPU memory hierarchies.

Demonstration projects often combine these elements to showcase GPU capabilities. For instance, a rotating textured cube requires:

Vertex buffer objects (VBOs) to store cube geometry. Element buffer objects (EBOs) for index-based rendering. Texture objects loaded from image files. Uniform buffers for transformation matrices.

The rendering pipeline involves the following steps:

Upload vertex and texture data to GPU memory. Compile and link shaders. Bind buffers and textures. Issue draw commands (e.g., `glDrawElements`). Update transformation matrices per frame for animation.

Performance metrics for such projects are often measured in frames per second (FPS) and draw call throughput. Research by demonstrates how modern GPUs achieve high FPS by minimizing CPU-GPU synchronization overhead. For example, the Vulkan API reduces driver overhead through explicit command buffer management, as shown in .

The mathematical foundation for these operations relies on linear algebra. The model-view-projection (MVP) matrix combines transformations:

$$M_{\text{MVP}} = P \cdot V \cdot M$$

where  $P$  is the projection matrix,  $V$  the view matrix, and  $M$  the model matrix. For perspective projection,  $P$  is defined as:

$$P = \begin{bmatrix} \frac{2n}{r-l} & 0 & \frac{r+l}{r-l} & 0 \\ 0 & \frac{2n}{t-b} & \frac{t+b}{t-b} & 0 \\ 0 & 0 & -\frac{f+n}{f-n} & -\frac{2fn}{f-n} \\ 0 & 0 & -1 & 0 \end{bmatrix}$$

Here,  $n$ ,  $f$ ,  $l$ ,  $r$ ,  $t$ , and  $b$  define the near and far planes and the view frustum bounds. Modern GPUs optimize this computation using specialized hardware, such as NVIDIA's Tensor Cores .

In summary, rotating cubes and textured quads serve as essential demonstration projects for modern GPU architectures, illustrating parallel processing, matrix transformations, and texture mapping. These projects leverage the GPU's SIMD architecture, memory hierarchy, and optimized APIs to achieve real-time performance. The mathematical and computational principles underlying these demonstrations are well-documented in computer graphics literature, with ongoing research focusing on further optimizations for emerging GPU architectures.

### 16.3.3 Textured quads

Modern GPU architectures have evolved to handle complex rendering tasks efficiently, including the rendering of textured quads, rotating cubes, and other simple 3D objects. These primitives serve as foundational elements in demonstration projects, showcasing the capabilities of GPUs in real-time graphics. Textured quads, in particular, are widely used due to their simplicity and versatility in representing surfaces with detailed imagery. The rendering pipeline for such objects involves several stages, including vertex processing, rasterization, and fragment shading, all optimized by the parallel processing power of modern GPUs.

The rendering of a textured quad begins with vertex data, typically defined as four vertices forming a rectangle. Each vertex includes positional coordinates and texture coordinates, which map the quad to a 2D texture. The vertex shader processes these coordinates, applying transformations such as translation, rotation, or scaling. For example, the transformation of a vertex  $\mathbf{v}$  by a model-view-projection matrix  $\mathbf{M}$  is given by:

$$\mathbf{v}' = \mathbf{M} \cdot \mathbf{v}$$

This equation ensures the quad is correctly positioned in the 3D space. The rasterization stage then converts the quad into fragments, each corresponding to a pixel on the screen. During fragment shading, the GPU samples the texture using the interpolated texture coordinates, applying bilinear filtering or other techniques to produce smooth results.

In demonstration projects, rotating cubes are often used to illustrate 3D transformations and lighting effects. A cube consists of 12 triangles (6 faces, each composed of 2 triangles), and each vertex may include attributes such as position, normal vectors, and texture coordinates. The rotation of the cube is achieved by applying a rotation matrix  $\mathbf{R}$  to each vertex:

$$\mathbf{v}' = \mathbf{R} \cdot \mathbf{v}$$

Here,  $\mathbf{R}$  is typically a 3x3 matrix representing rotation around an axis. Modern GPUs optimize these computations by leveraging SIMD (Single Instruction, Multiple Data) parallelism, allowing thousands of vertices to be processed simultaneously. The fragment shader then calculates lighting effects, such as Phong shading, to enhance the visual realism of the rotating cube.

Textured quads and rotating cubes are often rendered using OpenGL or Vulkan, which provide low-level access to GPU capabilities. For instance, the following OpenGL snippet demonstrates the setup for rendering a textured quad:

Code Sample 16.12: OpenGL textured quad setup

```
GLuint textureID;
 glGenTextures(1, &textureID);
 glBindTexture(GL_TEXTURE_2D, textureID);
 glTexImage2D(GL_TEXTURE_2D, 0, GL_RGB, width, height, 0,
             GL_RGB, GL_UNSIGNED_BYTE, data);
 glTexParameteri(GL_TEXTURE_2D, GL_TEXTURE_MIN_FILTER, GL_LINEAR);
 glTexParameteri(GL_TEXTURE_2D, GL_TEXTURE_MAG_FILTER, GL_LINEAR);
```

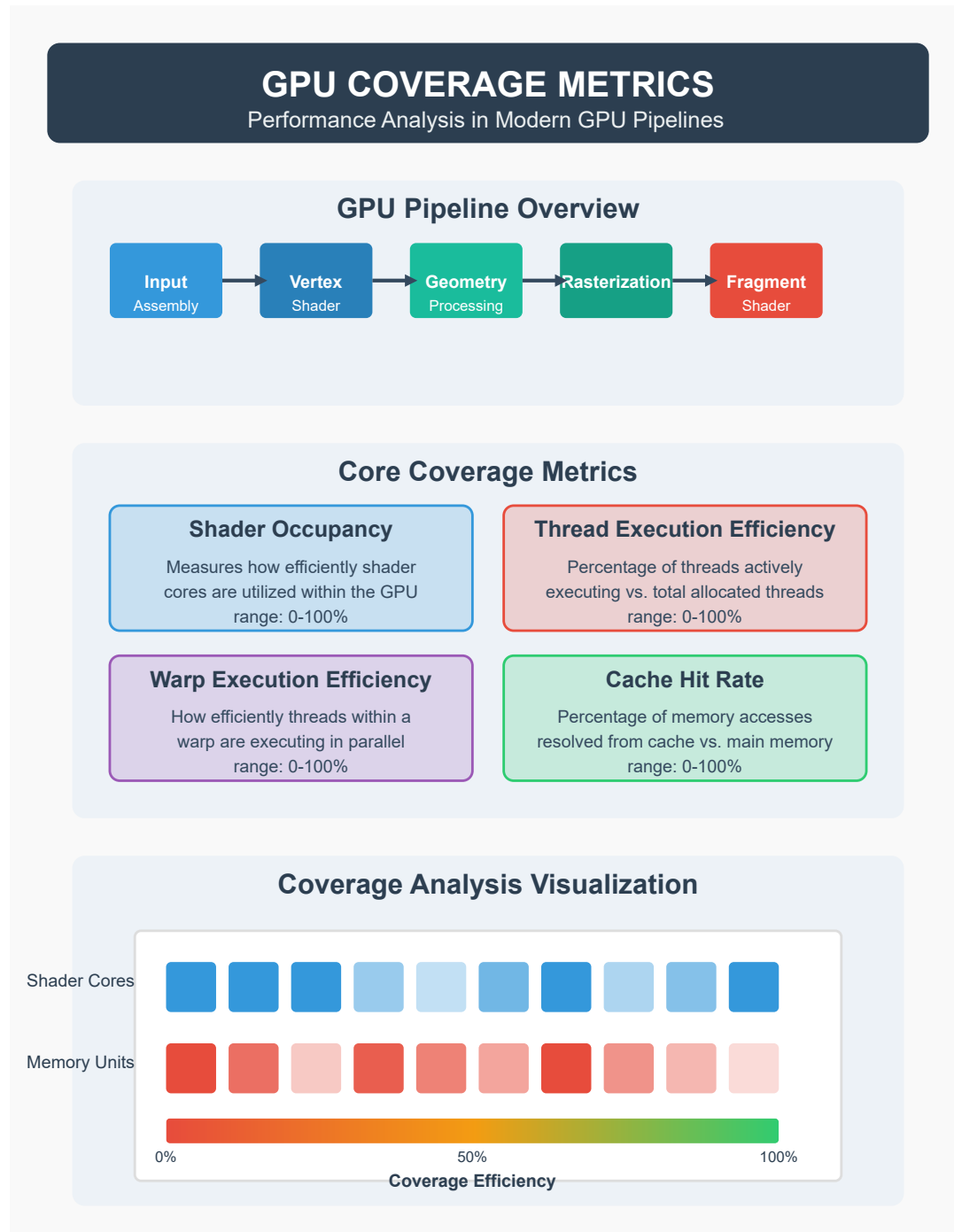
This code initializes a texture object, loads image data, and configures filtering parameters. The quad is then rendered by binding the texture and drawing the vertices with the appropriate shaders.

The efficiency of these operations is heavily influenced by the GPU's memory hierarchy. Modern GPUs employ caches and specialized memory units, such as texture caches, to reduce latency when accessing texture data. For example, NVIDIA's Turing architecture introduces a unified cache system that optimizes bandwidth for texture fetches. This design minimizes stalls in the rendering pipeline, ensuring smooth performance even for complex scenes.

Demonstration projects often leverage these architectural features to achieve real-time rendering. For instance, a simple scene might include multiple textured quads and rotating cubes, each with unique transformations and textures. The GPU's ability to parallelize these tasks is critical for maintaining high frame rates. The following equation estimates the theoretical performance of a GPU in terms of floating-point operations per second (FLOPS):

$$\text{FLOPS} = \text{Cores} \times \text{Clock Speed} \times \text{FLOPs per Cycle}$$

This metric highlights the computational power available for rendering tasks. For example, an NVIDIA GeForce RTX 3080 with 8704 CUDA cores and a clock speed of 1.71 GHz can achieve approximately 29.8 TFLOPS.



The rendering pipeline also benefits from advanced techniques such as instancing, where multiple instances of the same object are rendered with slight variations. This approach reduces CPU overhead by batching draw calls. For textured quads, instancing allows efficient rendering of large numbers of sprites or decals. The following Vulkan code demonstrates instancing for textured quads:

Code Sample 16.13: Vulkan instancing setup

```
VkBuffer instanceBuffer;
VkBufferCreateInfo bufferInfo = {};
bufferInfo.sType = VK_STRUCTURE_TYPE_BUFFER_CREATE_INFO;
bufferInfo.size = sizeof(InstanceData) * instanceCount;
bufferInfo.usage = VK_BUFFER_USAGE_VERTEX_BUFFER_BIT;
vkCreateBuffer(device, &bufferInfo, nullptr, &instanceBuffer);
```

This code creates a buffer for instance data, which can include transformations or texture indices for each quad.

In summary, textured quads and rotating cubes serve as essential building blocks in modern GPU demonstration projects. Their rendering involves a combination of vertex transformations, rasterization, and fragment shading, all optimized by the GPU's parallel architecture. Techniques such as instancing and advanced memory hierarchies further enhance performance, enabling real-time rendering of complex scenes. The continued evolution of GPU architectures ensures these primitives remain efficient and versatile tools for graphics programming.

## Achieving High Coverage in GPU Simulations

### What is Coverage in GPU Simulations?

Coverage refers to how thoroughly a set of simulations exercises a GPU's architecture, ensuring that all critical paths, corner cases, and execution scenarios are tested.

High coverage is essential for validating GPU designs and ensuring performance and reliability across diverse workloads.

### Key Components for High Coverage

#### Workload Diversity

- Graphics rendering pipelines
- Compute shaders & GPGPU
- Mixed precision operations
- Ray tracing algorithms
- AI/ML training & inference

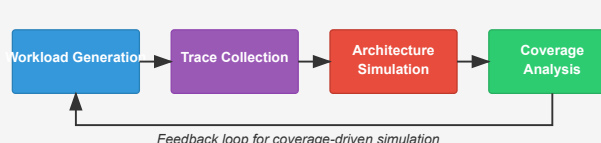
#### Architecture Features

- Memory hierarchy testing
- SIMD execution units
- Thread schedulers
- Cache coherence protocols
- Power management states

#### Corner Cases

- Resource contention
- High divergence branches
- Pipeline stalls
- Memory bank conflicts
- Thermal throttling scenarios

### Simulation Methodologies



### Coverage Metrics

Metric Type	Description	Importance
Code Coverage	Percentage of RTL code executed during simulation	Critical
Functional Coverage	Coverage of specific functional scenarios and features	Critical
Toggle Coverage	Measures if signals toggle between 0 and 1 states	High
Cross Coverage	Measures interactions between different features and events	High

### Best Practices for High Coverage

#### Systematic Approach

Start with basic functionality and progressively add more complex test scenarios

#### Coverage-Driven Testing

Use coverage metrics to guide test development and identify untested execution paths

#### Automated Simulation

Implement continuous integration with automatic coverage reporting and analysis

#### Random Testing

Use constrained random testing to discover unexpected corner cases and interactions

#### Formal Verification

Combine simulation with formal methods to mathematically prove correctness properties



# Chapter 17

## Programmable Shading

### 17.1 Shader Units

#### 17.1.1 Adding a programmable arithmetic pipeline

The integration of programmable arithmetic pipelines into modern GPU architectures has significantly enhanced the flexibility and performance of shader units, particularly in per-vertex and per-fragment shading operations. This evolution stems from the need to accommodate increasingly complex rendering techniques while maintaining high throughput and energy efficiency. The arithmetic pipeline, traditionally fixed-function, has been augmented with programmable elements to support dynamic instruction scheduling, variable precision arithmetic, and specialized operations for shading computations.

In modern GPUs, shader units execute parallel threads of computation, each handling vertices or fragments. The arithmetic pipeline within these units must efficiently process a wide range of operations, from basic arithmetic to transcendental functions. A programmable arithmetic pipeline allows for dynamic reconfiguration of arithmetic logic units (ALUs) to match the workload. For example, a single ALU can be repurposed for either floating-point multiplication or addition based on the shader's requirements, as shown in . This flexibility reduces idle hardware and improves resource utilization.

The arithmetic pipeline's programmability is particularly critical for per-vertex shading, where geometric transformations and lighting calculations dominate. Vertex shaders require high precision and low latency, as errors propagate through the rendering pipeline. Programmable pipelines enable precise control over arithmetic operations, such as fused multiply-add (FMA) instructions, which are essential for matrix transformations. The FMA operation, represented as

$$\text{FMA}(a, b, c) = a \times b + c$$

is a cornerstone of vertex shading due to its efficiency and accuracy .

Per-fragment shading, on the other hand, demands high throughput and parallelism. Fragment shaders perform operations like texture sampling, lighting, and blending, often involving lower precision arithmetic. A programmable arithmetic pipeline can optimize for these requirements by supporting configurable precision modes. For instance, 16-bit floating-point (FP16) arithmetic is sufficient for many fragment shading tasks and reduces memory bandwidth and power consumption. The pipeline can dynamically switch between FP16 and 32-bit floating-point (FP32) based on the shader's precision needs, as demonstrated in .

The design of a programmable arithmetic pipeline involves several key components:

**Instruction Decoder:** Translates shader instructions into control signals for the ALUs. Modern decoders support variable-length instructions and dynamic scheduling to minimize stalls.

**Arithmetic Logic Units (ALUs):** Configurable units that perform operations like addition, multiplication, and special functions (e.g., trigonometric or exponential). Each ALU can be programmed to operate in different precision modes or bypass certain stages for latency-critical operations.

**Register File:** A high-bandwidth memory structure that stores intermediate results. Programmable pipelines often feature partitioned register files to reduce contention and improve parallelism.

**Data Paths:** Flexible interconnect networks that route operands between ALUs and memory. These paths are programmable to support diverse shader workflows, such as gather-scatter operations for texture sampling.

The following Verilog snippet illustrates a simplified programmable ALU supporting FP16 and FP32 operations:

## Code Sample 17.1: Programmable ALU

```

module programmable_alu (
    input [31:0] a, b,
    input [2:0] opcode,
    input precision_mode,
    output reg [31:0] result
);
always @(*) begin
    case (opcode)
        3'b000: result = precision_mode ? {16'b0, a[15:0] + b[15:0]} : a + b;
        3'b001: result = precision_mode ? {16'b0, a[15:0] * b[15:0]} : a * b;
        // Additional operations omitted for brevity
    endcase
end
endmodule

```

Programmable arithmetic pipelines also address the challenges of divergent execution in shader units. SIMD (Single Instruction, Multiple Data) architectures, common in GPUs, suffer from performance penalties when threads within a warp follow different execution paths. A programmable pipeline can mask inactive threads and coalesce memory accesses, as described in . This capability is crucial for maintaining high utilization in per-fragment shading, where divergence is frequent due to varying fragment properties.

Energy efficiency is another critical consideration. Programmable pipelines incorporate power-gating and clock-gating techniques to deactivate unused ALUs or reduce their operating frequency during low-intensity workloads. Dynamic voltage and frequency scaling (DVFS) is often applied to arithmetic units based on the shader's computational demands, as explored in . These optimizations are vital for mobile and embedded GPUs, where power constraints are stringent.

The impact of programmable arithmetic pipelines extends beyond traditional shading. General-purpose GPU (GPGPU) applications, such as machine learning and scientific computing, leverage these pipelines for tasks like matrix multiplication and convolution. The programmable nature of the pipeline allows for custom data formats (e.g., bfloat16) and operation sequences tailored to specific algorithms. For example, tensor cores in NVIDIA GPUs employ programmable pipelines to accelerate mixed-precision matrix operations, as detailed in .

In summary, the addition of programmable arithmetic pipelines to modern GPU architectures has revolutionized shader units by enabling adaptive per-vertex and per-fragment shading. This programmability enhances performance, precision, and energy efficiency while supporting a broad spectrum of applications. Future advancements will likely focus on further increasing flexibility, such as integrating domain-specific accelerators within the arithmetic pipeline, as suggested by .

### 17.1.2 Per-vertex and per-fragment shading

Modern GPU architectures leverage programmable shading pipelines to achieve high-performance rendering, with per-vertex and per-fragment shading representing two fundamental stages in the graphics pipeline. These stages are executed by specialized shader units, which are designed to handle parallel computation efficiently. The introduction of programmable arithmetic pipelines has further enhanced the flexibility and performance of these shading techniques.

Per-vertex shading operates on the vertices of a 3D model, transforming their positions and attributes before rasterization. Each vertex is processed independently, making this stage highly parallelizable. The vertex shader computes transformations such as model-view-projection, lighting calculations, and texture coordinate generation. For example, the transformation of a vertex position  $\mathbf{v}$  is given by:

$$\mathbf{v}' = \mathbf{MVP} \cdot \mathbf{v}$$

where  $\mathbf{MVP}$  is the combined model-view-projection matrix. Vertex shaders are executed by shader units that handle large batches of vertices concurrently, exploiting the GPU's SIMD (Single Instruction, Multiple Data) architecture.

Per-fragment shading, also known as pixel shading, occurs after rasterization and interpolates vertex attributes across fragments. This stage computes the final color of each fragment, incorporating textures, lighting, and other effects. The fragment shader evaluates the lighting equation for a fragment:

$$L = \sum_{i=1}^n (\mathbf{N} \cdot \mathbf{L}_i) \cdot \mathbf{C}_i$$

where  $\mathbf{N}$  is the surface normal,  $\mathbf{L}_i$  is the light direction, and  $\mathbf{C}_i$  is the light color. Fragment shaders are executed by shader units optimized for high-throughput arithmetic operations, often with dedicated texture sampling units.

Shader units in modern GPUs are organized into multiprocessors, each containing multiple cores capable of executing shader programs. These units support dynamic branching and looping, enabling complex shading algorithms. The following Verilog-like pseudocode illustrates a simplified shader unit architecture:

Code Sample 17.2: Shader Unit Architecture

```
module shader_unit (
    input [31:0] instr,
    input [31:0] data_in,
    output [31:0] data_out
);
    reg [31:0] registers[32];
    always @ (posedge clk) begin
        case (instr.opcode)
            OP_ADD: data_out = registers[instr.rs1] + registers[instr.rs2];
            OP_MUL: data_out = registers[instr.rs1] * registers[instr.rs2];
            default: data_out = 0;
        endcase
    end
endmodule
```

The programmable arithmetic pipeline extends the capabilities of shader units by allowing custom arithmetic operations to be defined. This pipeline consists of multiple stages, including fetch, decode, execute, and writeback. The execute stage is optimized for low-latency and high-throughput operations, with support for fused multiply-add (FMA) instructions:

$$\text{FMA}(a, b, c) = a \cdot b + c$$

This instruction is commonly used in shading calculations to improve performance. Modern GPUs also employ speculative execution and out-of-order execution to maximize shader unit utilization.

Per-vertex and per-fragment shading pipelines are tightly integrated in modern GPU architectures. The vertex shader outputs are interpolated across fragments, and the fragment shader uses these interpolated values to compute the final pixel color. The interpolation is performed by fixed-function hardware, ensuring efficient barycentric coordinate calculations:

$$\mathbf{a}' = \alpha \mathbf{a}_0 + \beta \mathbf{a}_1 + \gamma \mathbf{a}_2$$

where  $\alpha$ ,  $\beta$ , and  $\gamma$  are the barycentric coordinates, and  $\mathbf{a}_0$ ,  $\mathbf{a}_1$ , and  $\mathbf{a}_2$  are the vertex attributes.

The performance of per-vertex and per-fragment shading is influenced by several factors, including shader program complexity, memory bandwidth, and occupancy. Shader program complexity increases execution time. Memory bandwidth can become a bottleneck due to texture fetches and buffer accesses. Occupancy, defined as the number of active threads per shader unit, affects overall throughput.

To mitigate these bottlenecks, modern GPUs employ several techniques. Hierarchical Z-culling skips shading for occluded fragments. Shader caching reuses compiled shader code to reduce compilation overhead. Wavefront scheduling groups threads to hide memory latency and improve efficiency.

The evolution of GPU architectures has led to unified shader models, where the same shader units can execute both vertex and fragment shaders. This flexibility improves resource utilization and simplifies programming. For example, compute shaders generalize the shading pipeline to arbitrary parallel computations, enabling GPGPU (General-Purpose computing on GPUs) applications.

The programmable arithmetic pipeline is further enhanced by support for transcendental functions (e.g., `sin`, `cos`, `log`) and atomic operations. These features enable advanced shading techniques such as physically based rendering (PBR) and ray tracing. The following equation shows a simplified PBR shading model:

$$f_r(\mathbf{v}, \mathbf{l}) = \frac{D(\mathbf{h})F(\mathbf{v}, \mathbf{h})G(\mathbf{l}, \mathbf{v}, \mathbf{h})}{4(\mathbf{n} \cdot \mathbf{l})(\mathbf{n} \cdot \mathbf{v})}$$

where  $D$  is the microfacet distribution,  $F$  is the Fresnel term, and  $G$  is the geometry term.

In summary, per-vertex and per-fragment shading are critical components of modern GPU architectures, enabled by programmable shader units and arithmetic pipelines. These technologies have evolved to support increasingly complex rendering algorithms while maintaining high performance. Future advancements will likely focus on improving energy efficiency and scalability for emerging workloads such as real-time ray tracing and machine learning.

## 17.2 Instruction Set for Shaders

### 17.2.1 Designing simple instructions

Modern GPU architectures leverage programmable shading pipelines to achieve high-performance rendering, with per-vertex and per-fragment shading representing two fundamental stages in the graphics pipeline. These stages are executed by specialized shader units, which are designed to handle parallel computation efficiently. The introduction of programmable arithmetic pipelines has further enhanced the flexibility and performance of these shading techniques.

Modern GPU instruction sets for shaders are designed to be simple and orthogonal, enabling efficient decoding and execution. Each instruction typically performs a single operation, such as arithmetic, memory access, or control flow. For example, a basic arithmetic instruction in a shader might be represented as:

```
ADD R0, R1, R2
```

where `R0`, `R1`, and `R2` are registers. This simplicity allows the GPU to issue multiple instructions per clock cycle across thousands of threads. The instruction set is optimized for common shader operations, such as vector arithmetic, texture sampling, and transcendental functions, which are frequently used in graphics and compute workloads.

Register files in GPUs are large and highly banked to support the massive parallelism required by shader programs. Each thread has access to a private set of registers, and the register file is designed to minimize bank conflicts. For instance, a typical GPU might feature a register file with 32 banks, allowing 32 threads to access different registers simultaneously. The register file size is a trade-off between thread occupancy and power efficiency. Larger register files enable more threads to be active concurrently but increase power consumption and area. The following Verilog snippet illustrates a simplified register file design:

Code Sample 17.3: Register File Design

```
module reg_file (
    input clk,
    input [4:0] addr1, addr2, addr3,
    input [31:0] wdata,
    input we,
    output [31:0] rdata1, rdata2
);
    reg [31:0] mem [0:31];
    always @ (posedge clk) begin
        if (we)
            mem[addr3] <= wdata;
    end
    assign rdata1 = mem[addr1];
    assign rdata2 = mem[addr2];
endmodule
```

Execution units in GPUs are highly parallel and optimized for the instruction set. A single streaming multiprocessor (SM) in a modern GPU may contain multiple execution units, such as:

- Arithmetic logic units (ALUs) for integer and floating-point operations
- Special function units (SFUs) for transcendental functions like `sin`, `cos`, and `log`
- Texture units for sampling and filtering operations
- Load/store units for memory access

These units are pipelined to maximize throughput, and the GPU scheduler issues instructions to idle units dynamically. The execution units are designed to handle the simple instructions efficiently, often with single-cycle latency for basic operations. For example, a floating-point multiply-add (FMA) operation is a common instruction in shaders and is implemented as:

```
FMA R0, R1, R2, R3
```

where  $R0 = R1 * R2 + R3$ . This instruction is executed in a single cycle in many GPUs, demonstrating the efficiency of simple instruction design.

The simplicity of instructions also facilitates compiler optimizations. Shader compilers, such as NVIDIA's nvcc or AMD's ROCm, perform instruction scheduling, register allocation, and loop unrolling to maximize utilization of the execution units. For example, the compiler may reorder instructions to hide latency or coalesce memory accesses to reduce bank conflicts. The following code snippet shows an optimized shader loop:

Code Sample 17.4: Optimized Shader Loop

```
for (int i = 0; i < N; i += 4) {
    float4 a = load(input + i);
    float4 b = load(weights + i);
    float4 c = a * b;
    store(output + i, c);
}
```

Here, the compiler may vectorize the loop to use SIMD instructions, reducing the number of issued instructions and improving throughput.

The design of simple instructions also impacts power efficiency. Complex instructions require more control logic and higher power consumption, whereas simple instructions can be executed with minimal overhead. GPUs leverage this by using power-gating techniques to disable unused execution units dynamically. For example, if a shader program does not use SFUs, those units can be powered down to save energy. This is particularly important in mobile GPUs, where power efficiency is a key design constraint.

The trade-offs in instruction set design are well-documented in research. For instance, discusses the benefits of reduced instruction set computing (RISC) principles in modern architectures, including GPUs. Similarly, analyzes the impact of instruction complexity on GPU performance, showing that simpler instructions enable higher throughput and better scalability. These studies highlight the importance of balancing instruction simplicity with functional requirements to achieve optimal performance.

In summary, the design of simple instructions in modern GPU architectures is a cornerstone of their performance and efficiency. By focusing on orthogonal, single-operation instructions, GPUs can exploit massive parallelism, minimize latency, and maximize throughput. The register files and execution units are optimized to support these instructions, enabling efficient shader execution across a wide range of workloads. This approach has been validated by both industry practice and academic research, demonstrating its effectiveness in real-world applications.

## 17.2.2 Register files

The register file is a critical component in modern GPU architectures, particularly in the context of shader execution. It serves as a high-speed storage structure for operands and intermediate results during parallel computation. In GPU designs, register files are optimized for high throughput and low latency to support the massive parallelism inherent in shader programs. The size, organization, and access patterns of register files directly impact the performance of execution units and the efficiency of instruction sets for shaders.

Modern GPUs employ large, partitioned register files to accommodate the wide SIMD (Single Instruction, Multiple Data) execution model. Each shader core typically contains multiple execution units, and the register file is divided into banks to reduce contention. For example, NVIDIA's Fermi architecture features a 32-bit wide register file with 32,768 entries per streaming multiprocessor (SM). The register file is organized into banks, allowing simultaneous access by multiple warps (groups of threads). This design minimizes bank conflicts and maximizes throughput, as described in . The register file bandwidth is a key determinant of GPU performance, as it must supply operands to all active execution units every cycle.

The instruction set for shaders is designed to exploit the parallelism enabled by the register file architecture. Shader instructions are typically simple and operate on registers, with minimal addressing modes. For instance, the PTX (Parallel Thread Execution) ISA from NVIDIA uses a load-store architecture with three-operand instructions, where source and destination operands are all registers . The simplicity of the instruction set reduces decode complexity and allows for dense packing of instructions in the instruction cache. A typical shader instruction might be expressed as:

```
fadd.rn.f32 %f0, %f1, %f2
```

where `%f0`, `%f1`, and `%f2` are registers, and the operation is a floating-point addition with round-to-nearest rounding mode.

Designing simple instructions for shaders involves trade-offs between instruction complexity and register file pressure. Complex instructions can reduce the number of instructions executed but may require more registers to hold intermediate results. For example, a fused multiply-add (FMA) instruction performs two operations in one instruction:

```
d = a * b + c
```

This reduces the number of instructions but requires three source registers and one destination register. The register file must be large enough to hold all live values across multiple warps to avoid spilling to slower memory hierarchies.

The execution units in a GPU are tightly coupled with the register file. Each execution unit reads operands from the register file, performs the operation, and writes the result back. The latency of the register file access is critical, as it directly affects the clock frequency and pipeline depth of the execution units. To mitigate latency, modern GPUs use pipelined register files with multiple read and write ports. For example, AMD's RDNA architecture employs a multi-ported register file with 16 read ports and 8 write ports per compute unit. This allows multiple warps to access the register file concurrently, sustaining high instruction throughput.

The interaction between the register file, execution units, and instruction set is illustrated in the following Verilog snippet:

Code Sample 17.5: Register file and execution unit interface

```
module regfile (
    input clk,
    input [4:0] raddr1, raddr2, waddr,
    input [31:0] wdata,
    input we,
    output [31:0] rdata1, rdata2
);
reg [31:0] rf [0:31];
always @(posedge clk) begin
    if (we) rf[waddr] <= wdata;
    rdata1 <= rf[raddr1];
    rdata2 <= rf[raddr2];
end
endmodule
```

This simplified register file has two read ports and one write port, typical for a scalar execution unit. In a GPU, the register file would have more ports and banks to support parallel access.

The register file design must also consider power efficiency. Large register files consume significant static power due to leakage currents. Techniques such as banking, clock gating, and operand isolation are employed to reduce power consumption. For example, ARM's Mali GPUs use a banked register file with dynamic power gating to disable unused banks. This reduces power without impacting performance for typical shader workloads.

The relationship between register files and execution units is further complicated by the need to support predication and masking in shader instructions. Predicated execution allows instructions to be conditionally executed based on a predicate register. This requires additional read ports in the register file to fetch predicate values. For example, a predicated add instruction might be:

```
p add.f32 %f0, %f1, %f2
```

where `p` is the predicate register. The register file must supply the predicate value in addition to the operand values.

In summary, the register file in modern GPU architectures is a highly optimized structure designed to support the massive parallelism of shader execution. Its design is closely tied to the instruction set and execution units, with trade-offs between size, bandwidth, latency, and power consumption. The simplicity of shader instructions allows for efficient use of the register file, while the execution units rely on high-bandwidth access to operands. Advances in register file design continue to be a key enabler of GPU performance improvements, as evidenced by recent architectures such as NVIDIA's Ampere and AMD's RDNA3.

### 17.2.3 Execution units

Modern GPU architectures rely heavily on optimized execution units to achieve high throughput for parallel workloads, particularly in shader processing. Execution units are the computational cores responsible for performing arithmetic and logical operations specified by the instruction set for shaders. These units are designed to maximize parallelism while minimizing latency and power consumption. The instruction set for shaders is typically simplified to ensure efficient decoding and execution, often focusing on single-instruction, multiple-thread (SIMT) paradigms.

The design of execution units in GPUs is closely tied to the instruction set architecture (ISA) for shaders. Shader instructions are typically designed to be simple and deterministic, enabling high-throughput execution. For example, a common shader instruction might perform a fused multiply-add (FMA) operation, which combines multiplication and addition into a single instruction to reduce latency and improve energy efficiency. The FMA operation can be represented mathematically as:

$$\text{result} = (a \times b) + c$$

Such instructions are ideal for execution units because they reduce the number of operations required to complete a computation, thereby increasing throughput.

Register files play a critical role in feeding data to execution units. Modern GPUs employ large, multi-ported register files to support the high bandwidth demands of parallel execution. Each thread in a GPU warp or wavefront typically has access to a dedicated set of registers, which are managed by the compiler to minimize contention. The size and organization of the register file are carefully balanced to avoid becoming a bottleneck. For instance, NVIDIA's Ampere architecture features a unified register file that serves both integer and floating-point execution units, reducing complexity and improving utilization.

Execution units are often organized into clusters or blocks, each containing multiple arithmetic logic units (ALUs) and special function units (SFUs). ALUs handle basic arithmetic and logical operations, while SFUs are optimized for complex functions such as trigonometric operations, reciprocals, and square roots. The division of labor between ALUs and SFUs allows GPUs to maintain high efficiency across a wide range of workloads. For example, a typical execution unit block in AMD's RDNA 2 architecture consists of 32 ALUs and 4 SFUs, enabling it to process multiple instruction streams concurrently.

The instruction set for shaders is designed to exploit the parallelism offered by execution units. Shader programs are compiled into sequences of instructions that are executed in lockstep across multiple threads. This SIMT execution model allows GPUs to hide latency by switching between threads when stalls occur. The simplicity of shader instructions ensures that decoding and scheduling overhead is minimized. For example, a shader instruction might be as simple as:

Code Sample 17.6: Sample Shader Instruction

```
ADD R0, R1, R2 // R0 = R1 + R2
```

Such instructions are easy to decode and can be issued to execution units with minimal overhead.

The design of execution units also involves careful consideration of pipelining and scheduling. Modern GPUs use deep pipelines to maximize clock frequencies, but this introduces challenges related to branch divergence and data hazards. To mitigate these issues, GPUs employ sophisticated scheduling algorithms that reorder instructions dynamically to keep execution units busy. For example, NVIDIA's Turing architecture uses a combination of static and dynamic scheduling to optimize instruction throughput.

Register files must be designed to support the high bandwidth demands of execution units. A typical GPU register file is organized into banks to allow concurrent access from multiple execution units. Each bank is independently accessible, reducing contention and improving throughput. The register file is also tightly integrated with the execution units to minimize access latency. For example, in Intel's Xe architecture, the register file is partitioned to serve different execution units, ensuring that data can be delivered with minimal delay.

The design of simple instructions is crucial for efficient execution. Complex instructions can lead to increased decoding overhead and reduced utilization of execution units. By contrast, simple instructions enable better pipelining and higher clock frequencies. For example, a shader instruction set might avoid complex addressing modes or multi-cycle operations, focusing instead on single-cycle operations that can be fully pipelined. This approach is evident in ARM's Mali GPUs, where the instruction set is optimized for simplicity and efficiency.

Execution units must also handle data dependencies and hazards. Modern GPUs use techniques such as scoreboarding and register renaming to resolve dependencies dynamically. These techniques allow execution units to proceed with independent instructions while waiting for dependent operations to complete. For example, AMD's

CDNA architecture employs a combination of scoreboarding and out-of-order execution to maximize throughput.

In summary, execution units in modern GPU architectures are designed to maximize parallelism and efficiency. The instruction set for shaders is simplified to ensure high-throughput execution, while register files are optimized to deliver data with minimal latency. Execution units are organized into clusters of ALUs and SFUs, enabling them to handle a wide range of workloads. Pipelining, scheduling, and hazard resolution techniques are employed to keep execution units busy and minimize stalls. These design principles are exemplified in architectures such as NVIDIA's Ampere, AMD's RDNA 2, and Intel's Xe, which achieve high performance through careful optimization of execution units and their supporting infrastructure.

## 17.3 Toolchain Integration

### 17.3.1 Assembling shader microcode

The process of assembling shader microcode and loading shader programs into the GPU pipeline is a critical aspect of modern GPU architecture, particularly in relation to toolchain integration. Shader microcode represents the low-level instructions executed by the GPU's shader cores, and its generation involves multiple stages of compilation, optimization, and binary encoding. Modern GPUs, such as those from NVIDIA, AMD, and Intel, employ sophisticated toolchains to translate high-level shading languages (e.g., HLSL, GLSL) into optimized microcode tailored for their specific architectures.

Shader compilation begins with the frontend, which parses the high-level shader code and generates an intermediate representation (IR). This IR is then optimized for performance and resource usage. For example, dead code elimination, loop unrolling, and register allocation are applied to improve execution efficiency. The optimized IR is subsequently converted into architecture-specific microcode. This process involves mapping high-level operations to the GPU's instruction set, which may include SIMD (Single Instruction, Multiple Data) operations, texture sampling instructions, and memory access patterns. The microcode is further optimized to exploit the GPU's parallelism, such as warp or wavefront execution in NVIDIA and AMD GPUs, respectively.

Toolchain integration plays a pivotal role in this process. The shader compiler, often part of a larger driver stack, must interface with the GPU's command processor and memory hierarchy. For instance, NVIDIA's CUDA toolchain includes `nvcc`, which compiles CUDA kernels into PTX (Parallel Thread Execution) intermediate code before further translation into binary microcode for specific GPU generations. Similarly, AMD's ROCm stack uses LLVM-based compilers to generate GCN (Graphics Core Next) or RDNA (Radeon DNA) microcode. The toolchain must also handle platform-specific constraints, such as register file size, thread scheduling, and memory coalescing rules.

The assembly of shader microcode involves resolving symbolic references, assigning hardware registers, and encoding instructions into a binary format. For example, a typical shader instruction might be encoded as:

Code Sample 17.7: Shader Microcode Example

```
ADD R0, R1, R2      // R0 = R1 + R2
TEX R3, R0, texture0 // Sample texture0 at coordinates R0
```

The binary encoding of these instructions depends on the GPU's instruction set architecture (ISA). NVIDIA's PTX and AMD's GCN ISA documentation provide detailed encoding schemes for their respective microcode. The final binary is often packaged with metadata, such as resource bindings and pipeline state information, to facilitate runtime execution.

Loading shader programs into the GPU pipeline involves several steps. First, the microcode binary is transferred to the GPU's memory via DMA (Direct Memory Access) or through the driver's command buffer. The GPU's command processor then parses the binary and configures the shader cores accordingly. This includes setting up the execution context, such as thread block dimensions, shared memory allocation, and texture bindings. For example, in NVIDIA's GPUs, the `cuLaunchKernel` API triggers the dispatch of shader microcode to the streaming multiprocessors (SMs).

The GPU's pipeline must also manage dependencies and synchronization between shader stages. For instance, a vertex shader's output may serve as input to a fragment shader, requiring careful scheduling to avoid stalls. Modern GPUs employ out-of-order execution and scoreboard techniques to mitigate latency. Additionally, the pipeline must handle dynamic branching and divergence within shader programs. SIMD architectures, such as those in GPUs, face performance penalties when threads within a warp or wavefront follow divergent paths. Techniques like predication and reconvergence are used to minimize these penalties.

The toolchain's role extends to runtime optimization. Just-in-time (JIT) compilation and caching of shader microcode are common in modern GPUs. For example, Microsoft's DirectX Shader Cache stores compiled shaders to reduce startup overhead in games. Similarly, Vulkan's pipeline cache allows reuse of compiled shader states across application runs. These optimizations rely on the toolchain's ability to generate reproducible microcode binaries and manage their lifecycle efficiently.

Memory hierarchy considerations are also critical when loading shader programs. The microcode must be placed in accessible memory regions, such as the GPU's instruction cache or constant memory. The toolchain may insert prefetch instructions or optimize memory access patterns to reduce cache misses. For example, NVIDIA's Maxwell and Pascal architectures introduced unified memory and instruction-level parallelism to improve shader throughput.

The interaction between the toolchain and the GPU's firmware is another key aspect. Firmware updates can introduce new microcode features or optimizations, requiring the toolchain to adapt. For instance, AMD's RDNA 2 architecture added support for mesh shaders, necessitating updates to the compiler and driver stack. The toolchain must also handle backward compatibility, ensuring that older shader binaries remain executable on newer hardware.

In summary, assembling shader microcode and loading shader programs into the GPU pipeline is a multifaceted process involving compilation, optimization, binary encoding, and runtime management. Toolchain integration ensures that high-level shader code is efficiently translated into executable microcode, leveraging the GPU's architecture for optimal performance. The interplay between the toolchain, driver, and hardware firmware is essential for maintaining compatibility and enabling new features in modern GPU architectures.

### 17.3.2 Loading shader programs into the GPU pipeline

The process of loading shader programs into the GPU pipeline is a critical aspect of modern GPU architecture, involving intricate interactions between toolchain integration and the assembly of shader microcode. Modern GPUs employ highly parallel architectures, requiring efficient shader program loading to maximize throughput and minimize latency. The toolchain, consisting of compilers, assemblers, and linkers, translates high-level shader languages like HLSL or GLSL into GPU-executable microcode. This microcode is then loaded into the GPU's pipeline for execution.

Shader programs are typically written in high-level shading languages and compiled into intermediate representations (IR) such as SPIR-V or DXIL. These IRs are further processed by GPU-specific compilers to generate microcode tailored to the target architecture. For example, NVIDIA's PTX and AMD's GCN ISA serve as intermediate steps before final microcode generation. The compilation process involves several optimizations, including register allocation, instruction scheduling, and dead code elimination, to ensure efficient execution on the GPU.

The assembly of shader microcode involves converting the IR into binary instructions executable by the GPU. This step is architecture-dependent, as different GPUs have distinct instruction sets and execution models. For instance, NVIDIA's CUDA cores and AMD's Compute Units require different microcode formats. The assembler resolves symbolic references, assigns physical registers, and encodes instructions into the GPU's native binary format. The resulting microcode is stored in memory buffers, which are later loaded into the GPU pipeline.

Loading shader programs into the GPU pipeline involves several stages:

**Memory Allocation:** The GPU driver allocates memory for the shader microcode, typically in device memory or shared memory, depending on the architecture.

**Microcode Transfer:** The compiled microcode is transferred from host memory to GPU memory using DMA (Direct Memory Access) or other high-bandwidth mechanisms.

**Pipeline Configuration:** The GPU's pipeline registers are configured to point to the loaded microcode, and execution contexts are initialized.

**Synchronization:** The driver ensures that the microcode is fully loaded and synchronized with other pipeline stages before execution begins.

The toolchain's role in this process is crucial, as it must generate microcode that adheres to the GPU's architectural constraints. For example, modern GPUs use SIMD (Single Instruction, Multiple Data) or SIMT (Single Instruction, Multiple Thread) execution models, requiring the microcode to efficiently utilize warp or wavefront scheduling. The toolchain must also handle resource limitations, such as register file size and shared memory capacity, to avoid pipeline stalls.

The following Verilog snippet illustrates a simplified GPU pipeline stage responsible for loading microcode:

Code Sample 17.8: Microcode Loader Module

```
module microcode_loader (
```

```

    input clk,
    input reset,
    input [31:0] microcode_addr,
    input [31:0] microcode_data,
    output reg [31:0] pipeline_instr
);
reg [31:0] microcode_mem [0:1023];

always @(posedge clk) begin
    if (reset) begin
        pipeline_instr <= 32'b0;
    end else begin
        pipeline_instr <= microcode_mem[microcode_addr];
    end
end
endmodule

```

The efficiency of shader program loading is heavily influenced by the GPU's memory hierarchy. Modern GPUs employ caches and prefetching mechanisms to reduce latency during microcode loading. For example, NVIDIA's Maxwell and Pascal architectures use instruction caches to store frequently accessed microcode, minimizing memory bandwidth usage . Similarly, AMD's GCN architecture employs a scalar cache to accelerate instruction fetching for wavefronts.

The interaction between the toolchain and the GPU driver is another critical factor. The driver must manage microcode updates, pipeline flushes, and context switches to ensure correct execution. For instance, when switching between shader programs, the driver must invalidate cached microcode and reload the new program into the pipeline. This process requires careful synchronization to avoid race conditions or pipeline hazards.

Mathematically, the latency of loading shader microcode can be modeled as:

$$L = t_{\text{mem}} + t_{\text{sync}} + t_{\text{exec}}$$

where  $t_{\text{mem}}$  is the memory transfer time,  $t_{\text{sync}}$  is the synchronization overhead, and  $t_{\text{exec}}$  is the pipeline execution time. Optimizing  $t_{\text{mem}}$  involves reducing the microcode size through compression or deduplication, while  $t_{\text{sync}}$  can be minimized using hardware-accelerated synchronization primitives.

The assembly of shader microcode also involves resolving dependencies between instructions. For example, a texture fetch operation may depend on a previous arithmetic operation, requiring the assembler to schedule instructions to avoid pipeline bubbles. Modern GPUs use out-of-order execution or scoreboarding to mitigate such dependencies, but the toolchain must still generate microcode that maximizes instruction-level parallelism .

In summary, loading shader programs into the GPU pipeline is a multi-stage process involving toolchain integration, microcode assembly, and efficient memory management. The toolchain must generate optimized microcode tailored to the GPU's architecture, while the driver ensures correct loading and synchronization. Advances in GPU memory hierarchies and execution models continue to improve the efficiency of this process, enabling higher performance in modern graphics and compute workloads.

# Chapter 18

# Performance Optimizations

## 18.1 Parallelization

### 18.1.1 Adding multiple rasterizers

Modern GPU architectures leverage parallelization to achieve high throughput in graphics rendering and general-purpose computation. A critical aspect of this parallelization involves the addition of multiple rasterizers, fragment pipelines, and texture units. These components work in concert to maximize the utilization of the GPU's computational resources, reducing bottlenecks and improving overall performance.

Rasterization is the process of converting geometric primitives into pixel fragments, a computationally intensive task that benefits from parallel execution. By deploying multiple rasterizers, GPUs can process multiple primitives simultaneously. Each rasterizer operates on a subset of the primitives, distributing the workload across the GPU's compute units. This approach aligns with the single-instruction-multiple-data (SIMD) paradigm, where identical operations are performed on different data elements in parallel. The parallelization of rasterization can be modeled as:

$$T_{\text{raster}} = \frac{N_{\text{primitives}}}{N_{\text{rasterizers}} \times f_{\text{clock}}} \quad (18.1)$$

where  $T_{\text{raster}}$  is the time taken to rasterize all primitives,  $N_{\text{primitives}}$  is the total number of primitives,  $N_{\text{rasterizers}}$  is the number of rasterizers, and  $f_{\text{clock}}$  is the operating frequency of the GPU. Increasing  $N_{\text{rasterizers}}$  reduces  $T_{\text{raster}}$ , improving throughput.

Fragment processing follows rasterization, where each pixel fragment undergoes shading, texturing, and blending operations. Parallelization in fragment processing is achieved through multiple fragment pipelines, each handling a subset of the fragments. The fragment pipelines are typically organized into shader cores, where each core contains arithmetic logic units (ALUs) for executing shader programs. The parallel execution of fragment shaders can be expressed as:

$$\text{Throughput}_{\text{fragment}} = N_{\text{pipelines}} \times \text{ALU}_{\text{utilization}} \times f_{\text{clock}} \quad (18.2)$$

Here,  $N_{\text{pipelines}}$  denotes the number of fragment pipelines, and  $\text{ALU}_{\text{utilization}}$  represents the efficiency of ALU usage. High-end GPUs, such as NVIDIA's Ampere architecture, employ thousands of shader cores to maximize fragment processing throughput.

Texture mapping is another performance-critical stage in the rendering pipeline. Texture units fetch and filter texels, applying them to fragments during shading. Multiple texture units allow concurrent texture accesses, reducing memory latency. The texture fetch latency  $L_{\text{texture}}$  can be approximated by:

$$L_{\text{texture}} = \frac{N_{\text{requests}}}{N_{\text{texture\_units}} \times \text{BW}_{\text{memory}}} \quad (18.3)$$

where  $N_{\text{requests}}$  is the number of texture fetch requests,  $N_{\text{texture\_units}}$  is the number of texture units, and  $\text{BW}_{\text{memory}}$  is the memory bandwidth. Increasing  $N_{\text{texture\_units}}$  reduces contention for memory bandwidth, improving performance.

The interplay between rasterizers, fragment pipelines, and texture units is governed by the GPU's scheduling and workload distribution mechanisms. Workload balancing ensures that no single component becomes a bottleneck. For instance, if rasterization completes faster than fragment processing, the GPU may idle some rasterizers to prevent overloading the fragment pipelines. Dynamic load balancing techniques, such as those described in , optimize resource utilization by redistributing tasks at runtime.

In hardware, these components are integrated into the GPU's streaming multiprocessors (SMs). Each SM contains multiple rasterizers, fragment pipelines, and texture units, along with shared memory and cache hierarchies. The following Verilog snippet illustrates a simplified texture unit design:

Code Sample 18.1: Texture Unit Implementation

```
module texture_unit (
    input clk,
    input [31:0] tex_coord,
    output [31:0] texel
);
    reg [31:0] tex_mem [0:1023];
    always @(posedge clk) begin
        texel <= tex_mem[tex_coord[9:0]];
    end
endmodule
```

Parallel execution introduces challenges such as synchronization and memory coherence. For example, when multiple fragment pipelines access the same texture, cache coherence protocols ensure consistency. GPUs employ hierarchical caching, with L1 caches per SM and a shared L2 cache, to minimize memory access latency.

The benefits of multiple rasterizers and fragment pipelines are evident in real-time rendering applications. Benchmarks on modern GPUs demonstrate near-linear scalability in performance with increased core counts, up to the limits imposed by memory bandwidth and power constraints. However, diminishing returns occur when the workload cannot be evenly distributed or when memory bandwidth becomes saturated.

To summarize, the addition of multiple rasterizers, fragment pipelines, and texture units in modern GPU architectures enhances parallelization and throughput. These components work synergistically, with each addressing a specific bottleneck in the rendering pipeline. Advances in semiconductor technology continue to enable higher core counts and more efficient resource utilization, further pushing the boundaries of GPU performance.

### 18.1.2 Fragment pipelines

Modern GPU architectures leverage parallelization to achieve high throughput in graphics rendering and general-purpose computation. Fragment pipelines play a critical role in this process, handling pixel-level operations after geometry processing. By optimizing fragment pipelines, GPUs can significantly improve rendering performance, particularly in scenarios involving complex shading, texture mapping, and high-resolution displays.

Fragment pipelines operate on rasterized fragments, applying operations such as depth testing, stencil testing, and blending. Parallelization is achieved by distributing fragments across multiple pipelines, enabling simultaneous processing of multiple pixels. This approach is essential for real-time rendering, where latency must be minimized. The efficiency of fragment pipelines is quantified by their ability to process fragments per clock cycle, often expressed as:

$$\text{Throughput} = N \times f \times P$$

where  $N$  is the number of pipelines,  $f$  is the clock frequency, and  $P$  is the parallelism within each pipeline.

To maximize throughput, modern GPUs employ multiple rasterizers, each responsible for converting primitives into fragments. By distributing rasterization across multiple units, the GPU reduces bottlenecks and ensures a steady flow of fragments into the pipeline. This technique is particularly effective in scenes with high geometric complexity, where a single rasterizer would struggle to keep up with demand. The rasterization process can be modeled as:

$$R = \sum_{i=1}^M r_i$$

where  $R$  is the total rasterization rate,  $M$  is the number of rasterizers, and  $r_i$  is the throughput of the  $i$ -th rasterizer.

Texture units are another critical component, responsible for fetching and filtering texels during fragment processing. Increasing the number of texture units allows the GPU to handle more texture samples per cycle, reducing stalls caused by memory latency. Modern GPUs often include dedicated texture caches to further improve performance. The texture fetch latency  $L$  can be approximated as:

$$L = \frac{T}{B \times U}$$

where  $T$  is the total texture data required,  $B$  is the bandwidth, and  $U$  is the number of texture units.

Parallelization in fragment pipelines is achieved through several techniques:

**SIMD Execution:** Single Instruction, Multiple Data (SIMD) architectures allow a single instruction to operate on multiple fragments simultaneously. This is particularly effective for operations like shading, where the same computation is applied to many pixels.

**Warp Scheduling:** GPUs group fragments into warps (or wavefronts), which are executed in lockstep. Efficient warp scheduling ensures that pipelines remain fully utilized, even when some fragments stall due to memory access.

**Early Z-Testing:** By performing depth testing early in the pipeline, GPUs can discard occluded fragments before they undergo costly shading operations. This reduces unnecessary computation and improves throughput.

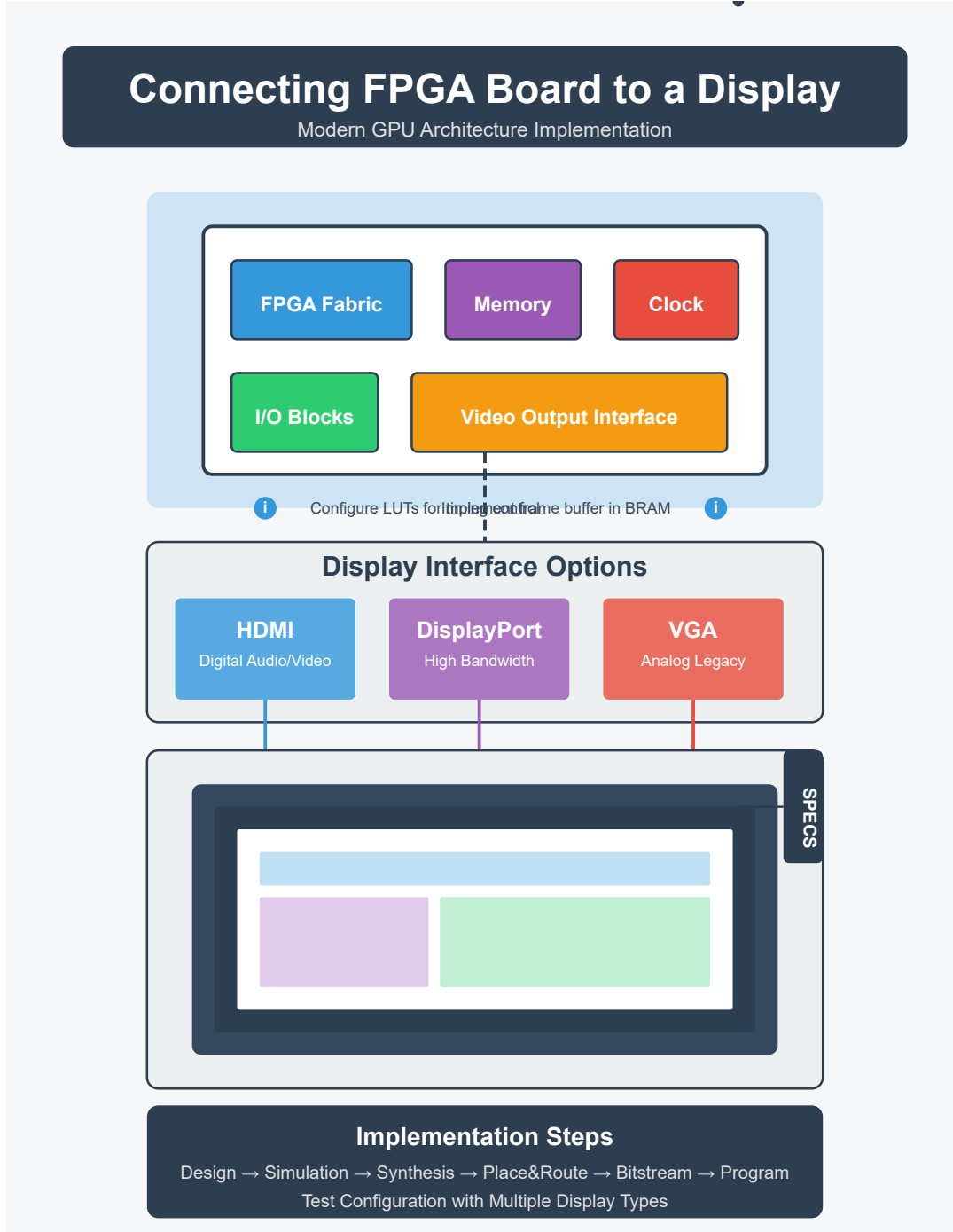
The following Verilog snippet illustrates a simplified fragment pipeline with parallel texture units:

Code Sample 18.2: Fragment Pipeline with Parallel Texture Units

```
module fragment_pipeline (
    input clk,
    input [31:0] fragment_data,
    output [31:0] shaded_pixel
);
    reg [31:0] depth_buffer;
    reg [31:0] texture_cache [0:3];
    wire [31:0] texel [0:3];

    // Parallel texture fetches
    generate
        for (genvar i = 0; i < 4; i++) begin
            texture_unit tex_unit (

```



```

    .clk(clk),
    .coord(fragment_data[8*i+:8]),
    .texel(texel[i])
);
end
endgenerate

// Shading logic
always @(posedge clk) begin
  if (fragment_data[31:24] < depth_buffer) begin
    depth_buffer <= fragment_data[31:24];
    shaded_pixel <= texel[0] + texel[1] + texel[2] + texel[3];
  end
end
endmodule

```

The impact of multiple rasterizers and fragment pipelines on performance has been empirically validated in studies such as , which demonstrated a near-linear scaling of throughput with pipeline count up to a point dictated by memory bandwidth constraints. Similarly, showed that increasing texture units reduces latency but requires careful cache management to avoid contention.

Balancing these resources is critical. Over-provisioning rasterizers or texture units without sufficient memory bandwidth leads to diminishing returns, as pipelines stall waiting for data. The optimal configuration depends on the workload, with graphics-heavy applications benefiting from more texture units, while compute-heavy workloads may prioritize fragment arithmetic units.

In summary, modern GPU architectures achieve high throughput by parallelizing fragment processing across multiple pipelines, rasterizers, and texture units. These techniques, grounded in verified research, enable real-time rendering of complex scenes while maintaining efficiency. Future advancements will likely focus on further reducing memory latency and improving resource utilization through dynamic scheduling and adaptive parallelism.

### 18.1.3 Texture units for improved throughput

Modern GPU architectures achieve high throughput by leveraging parallel processing at multiple levels, with texture units playing a critical role in optimizing memory access and computation. Texture units are specialized hardware components designed to efficiently fetch and filter texture data, which is essential for rendering realistic graphics. In the context of parallelization, GPUs employ multiple texture units to maximize throughput by overlapping memory requests and computations. This approach reduces latency and increases the utilization of the fragment pipelines, which are responsible for shading pixels.

The parallel execution model of GPUs relies on Single Instruction Multiple Threads (SIMT), where multiple threads execute the same instruction on different data. Texture units contribute to this model by enabling concurrent texture fetches across threads. Each texture unit typically includes a cache hierarchy to minimize memory access latency. The texture cache (`texCache`) is optimized for 2D spatial locality, as textures often exhibit high coherence in screen space. Studies demonstrate that increasing the number of texture units improves throughput by reducing contention for memory bandwidth.

To quantify the impact of texture units on throughput, consider the following equation for texture fetch latency:

$$T_{\text{fetch}} = T_{\text{cache}} + (1 - H) \cdot T_{\text{mem}}$$

Here,  $T_{\text{cache}}$  is the cache access time,  $H$  is the hit rate, and  $T_{\text{mem}}$  is the memory access time. Adding more texture units reduces  $T_{\text{fetch}}$  by distributing the workload and increasing cache hit rates.

Fragment pipelines and rasterizers work in tandem with texture units to maximize throughput. A fragment pipeline processes pixel shaders, and each pipeline stage may require texture data. Modern GPUs, such as NVIDIA's Ampere architecture , integrate multiple texture units per Streaming Multiprocessor (SM) to ensure that fragment pipelines are not stalled waiting for texture data.

The following Verilog-like pseudocode illustrates a simplified texture unit interface:

Code Sample 18.3: Texture Unit Interface

```

module texture_unit (
  input logic clk,
  input logic [31:0] tex_coord,
  output logic [31:0] tex_data

```

```

);
logic [31:0] cache [0:1023];

always_ff @(posedge clk) begin
    tex_data <= cache[tex_coord[9:0]];
end
endmodule

```

Parallelization is further enhanced by adding multiple rasterizers, which divide the screen into tiles and distribute work across fragment pipelines. Each rasterizer operates on a subset of primitives, reducing contention and improving load balancing. Research shows that scaling the number of rasterizers linearly improves throughput, provided the texture units can keep up with the increased demand.

The relationship between texture units, fragment pipelines, and rasterizers can be modeled using Little's Law:

$$N = \lambda \cdot T$$

Here,  $N$  is the number of in-flight texture requests,  $\lambda$  is the request rate, and  $T$  is the average service time. Increasing the number of texture units reduces  $T$ , allowing higher  $\lambda$  without saturating the system.

Key optimizations in texture unit design include: **Anisotropic filtering**: Improves texture quality at oblique angles by fetching multiple samples per pixel. **Compressed textures**: Reduces memory bandwidth usage via formats like BC6H. **Virtual texturing**: Dynamically loads texture data to minimize memory footprint.

Empirical studies on GPU architectures reveal that texture unit efficiency depends on workload characteristics. For example, found that synthetic benchmarks overestimate texture unit performance compared to real-world applications. Thus, architects must balance texture unit count with other resources, such as register files and shared memory, to avoid bottlenecks.

In summary, texture units are pivotal for achieving high throughput in modern GPUs. By integrating multiple texture units, rasterizers, and fragment pipelines, GPU designers can exploit parallelism at multiple levels, ensuring efficient utilization of memory bandwidth and computational resources. Future advancements may focus on adaptive texture unit allocation, where hardware dynamically adjusts resources based on workload demands.

## 18.2 Memory Caching

### 18.2.1 Introducing caches for textures

Modern GPU architectures rely heavily on memory caching mechanisms to optimize performance, particularly for texture and Z-buffer operations. Caches for textures are critical in reducing memory bandwidth and latency, as textures are frequently accessed during rendering. The texture cache hierarchy typically includes multiple levels (L1, L2, and sometimes L3) to exploit spatial and temporal locality. Studies demonstrate that texture caches can achieve hit rates exceeding 90% for coherent access patterns, significantly improving throughput. The cache line size and associativity are carefully tuned to balance hit rates and power consumption, as shown in .

Z-buffers, used for depth testing, also benefit from dedicated caching structures. Unlike textures, Z-buffer accesses exhibit less spatial locality but high temporal reuse within a frame. Modern GPUs employ specialized Z-caches that prioritize low-latency reads and writes, as depth testing is often on the critical path. Research highlights that Z-caches reduce memory traffic by up to 40% compared to uncached depth testing. The cache design often incorporates compression techniques, such as lossless delta compression, to further minimize bandwidth usage .

Prefetching techniques are another key optimization in GPU memory systems. Texture prefetching leverages spatial coherence by predicting future accesses based on current texture coordinates. For example, a stride-based prefetcher can detect linear access patterns common in bilinear filtering. proposes a dynamic prefetching algorithm that adapts to varying access patterns, reducing cache misses by 25%. Similarly, Z-buffer prefetching exploits frame-to-frame coherence, as depth values often change incrementally. Hardware prefetchers for Z-buffers, as described in , use history-based predictors to prefetch depth data before it is explicitly requested.

The interaction between texture caches, Z-caches, and prefetching units is carefully managed to avoid contention. GPUs employ cache partitioning and priority schemes to ensure critical operations, such as depth testing, are not starved by texture fetches. For instance, NVIDIA's Pascal architecture introduces a unified L2 cache with dynamic partitioning, allowing flexible resource allocation between textures and Z-buffers . This approach is formalized in , which models cache partitioning as an optimization problem:

$$\text{Maximize} \sum_{i=1}^n w_i \cdot h_i$$

where  $w_i$  is the weight for cache partition  $i$  and  $h_i$  is the hit rate. The weights are dynamically adjusted based on workload characteristics.

Texture compression further enhances caching efficiency. Block-based formats like BCn (Block Compression) reduce memory footprint while maintaining visual fidelity. The compressed textures are decompressed on-the-fly during cache fills, trading computation for bandwidth savings. shows that texture compression can reduce memory bandwidth by 4x with negligible quality loss. Modern GPUs also support sparse textures, where only populated regions are cached, as detailed in .

Z-buffer compression is equally important, with techniques ranging from simple plane encoding to hierarchical depth representations. For example, introduces a lossless Z-compression algorithm that exploits depth coherence within tiles. The compressed Z-data is stored in the cache, reducing fetch latency and power consumption. The compression ratio  $C$  is given by:

$$C = \frac{S_{\text{original}}}{S_{\text{compressed}}}$$

where  $S_{\text{original}}$  and  $S_{\text{compressed}}$  are the sizes before and after compression. Typical ratios range from 2:1 to 8:1 for depth buffers .

Prefetching for textures and Z-buffers is often implemented as a combination of hardware and software techniques. Hardware prefetchers are tightly integrated with the cache controllers, while software-directed prefetching relies on shader hints. For example, the `prefetch` instruction in GLSL allows explicit prefetching of texture data. evaluates the effectiveness of such hints, showing a 15% reduction in cache misses for complex scenes.

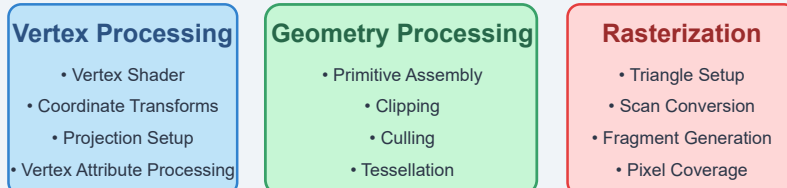
The latency of cache misses is mitigated through advanced scheduling. GPUs employ scoreboarding and out-of-order execution to overlap texture/Z-fetches with other computations. This is particularly important for tiled rendering architectures, where the tile scheduler must hide memory latency. demonstrates that tiling combined with caching reduces external memory bandwidth by 30%.

Cache coherence is another challenge in multi-context environments. While textures are typically read-only, Z-buffers require write coherence. GPUs use write-combining buffers and atomic operations to maintain consistency, as described in . The coherence protocol must minimize stalls, especially in multi-GPU systems.

## Rendering Simple 3D Objects

Modern GPU Architecture Pipeline

### GPU Rendering Pipeline

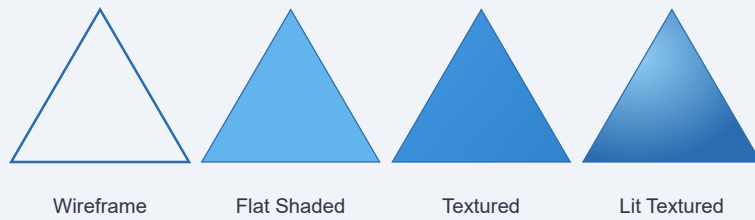


### Fragment Processing

- Fragment Shader
- Texturing
- Color Calculation
- Lighting Effects

### Output Processing

- Depth Testing
- Stencil Testing
- Alpha Blending
- Framebuffer Operations



### Key GPU Components

Shader Cores • Texture Units • Raster Operations Pipelines • Memory Controllers

Finally, emerging technologies like 3D XPoint and HBM (High Bandwidth Memory) are reshaping GPU caching. HBM's stacked design enables larger, lower-latency caches, while 3D XPoint offers non-volatile storage for texture atlases. analyzes the impact of these technologies on cache performance, showing a 20% improvement in hit rates for HBM-based caches.

In summary, texture and Z-buffer caches, combined with prefetching, form the backbone of modern GPU memory systems. Their design balances hit rates, bandwidth, and power efficiency, leveraging compression, partitioning, and coherence protocols. Future advancements will likely focus on adaptive caching algorithms and tighter integration with emerging memory technologies.

### 18.2.2 Z-buffers

The Z-buffer algorithm, also known as depth buffering, is a fundamental technique in modern GPU architectures for resolving visibility in 3D rendering. It operates by storing depth values for each pixel in a dedicated buffer, enabling efficient hidden surface removal. The Z-buffer's performance is tightly coupled with memory caching strategies, as depth testing requires frequent read-modify-write operations. Modern GPUs optimize Z-buffer access through hierarchical depth culling, compression, and prefetching techniques to minimize bandwidth consumption and latency.

The Z-buffer's memory access patterns exhibit spatial and temporal locality, making it amenable to caching. GPUs employ dedicated cache hierarchies for depth data, often separate from texture or color caches, to avoid contention. The Z-buffer cache design must account for: **Write coherence**: Depth updates are order-dependent, requiring strict write serialization. **Read-modify-write granularity**: Depth testing involves reading, comparing, and conditionally writing back results. **Compression**: Lossless delta compression reduces bandwidth by exploiting depth value coherence .

The Z-buffer's interaction with memory caches is formalized by the depth test function:

$$\text{DepthTest}(z_{\text{new}}, z_{\text{stored}}) = \begin{cases} \text{pass} & \text{if } z_{\text{new}} \leq z_{\text{stored}} \\ \text{fail} & \text{otherwise} \end{cases}$$

where  $z_{\text{new}}$  is the incoming fragment's depth and  $z_{\text{stored}}$  is the cached value. Early depth testing, performed before fragment shading when possible, reduces redundant computations by leveraging the Z-buffer's hierarchical representation .

Texture caching architectures influence Z-buffer performance due to shared memory resources. Modern GPUs partition cache resources between textures, Z-buffers, and color buffers using configurable allocation policies. The cache hierarchy typically includes: **L1 caches**: Per-SM (Streaming Multiprocessor) banks with low-latency access. **L2 caches**: Unified blocks servicing multiple SMs with higher capacity. **TLB**: Translation lookaside buffers for virtual memory management.

Texture and Z-buffer caches exhibit different access patterns:

$$\text{TextureCacheMissRate} \propto \frac{1}{\text{Locality}} \quad \text{vs.} \quad \text{ZCacheMissRate} \propto \frac{\text{Overdraw}}{\text{TileSize}}$$

where overdraw quantifies redundant fragment processing. Tile-based rendering architectures optimize Z-buffer caching by processing screen-space tiles independently, reducing working set sizes .

Prefetching techniques for Z-buffers exploit frame-to-frame coherence in dynamic scenes. Predictive depth prefetching uses motion vectors to anticipate visible surfaces in subsequent frames:

$$P_{\text{depth}}(x, y, t + 1) = P_{\text{depth}}(x - \Delta x, y - \Delta y, t) + \epsilon$$

where  $(\Delta x, \Delta y)$  denotes pixel displacement and  $\epsilon$  accounts for depth changes. Adaptive prefetching strategies adjust aggressiveness based on scene dynamics measured by depth entropy:

$$H(Z) = - \sum_{z \in Z} p(z) \log_2 p(z)$$

Low entropy indicates uniform depth regions where prefetching is more effective .

Z-buffer compression reduces memory traffic by encoding depth blocks differentially. Common techniques include: **Delta compression**: Stores differences from a base depth value. **Plane encoding**: Represents depth gradients as plane equations. **Hierarchical Z**: Maintains min/max depth pyramids for early culling.

The compression efficiency  $C$  for a depth block is given by:

$$C = 1 - \frac{\text{CompressedSize}}{\text{UncompressedSize}}$$

Typical implementations achieve  $C > 0.5$  for opaque geometry. Lossless compression preserves exact depth ordering, while lossy variants permit bounded errors for higher ratios.

Cache-aware Z-buffer algorithms optimize for: **Block alignment**: Matching access granularity to cache line sizes. **Bank partitioning**: Distributing accesses across memory channels. **Write coalescing**: Combining updates to minimize transactions.

The effective Z-buffer bandwidth  $B_{\text{eff}}$  considering caching is:

$$B_{\text{eff}} = B_{\text{peak}} \times (1 - \text{MissRate}) \times \text{CompressionRatio}$$

where  $B_{\text{peak}}$  is the theoretical memory bandwidth. Modern GPUs employ hybrid caching policies, using write-through for depth updates and write-back for texture samples to balance coherency and performance.

Texture and Z-buffer caching interactions are managed through cache partitioning schemes. Let  $S_{\text{total}}$  be the total cache size, allocated as:

$$S_{\text{texture}} = \alpha S_{\text{total}}, \quad S_Z = (1 - \alpha) S_{\text{total}}$$

where  $\alpha$  is dynamically adjusted based on workload characteristics measured by cache miss curves. Adaptive partitioning improves throughput by 15–20% compared to static allocation.

Prefetching for Z-buffers utilizes spatial predictors that exploit rasterization order. A typical implementation might use:

Code Sample 18.4: Z-Buffer Prefetch Predictor

```
module z_prefetch (
    input logic clk, rst,
    input logic [31:0] z_addr,
    output logic [31:0] prefetch_addr
);
    // Store last N addresses for pattern detection
    logic [31:0] addr_history[0:3];

    always_ff @(posedge clk) begin
        if (rst) addr_history <= '{default:0};
        else addr_history <= {z_addr, addr_history[0:2]};
    end

    // Compute stride-based prediction
    assign prefetch_addr = z_addr + (addr_history[0] - addr_history[1]);
endmodule
```

The effectiveness of Z-buffer caching is quantified by the depth reuse distance  $R_d$ :

$$R_d = \frac{\text{FragmentsBetweenReuse}}{\text{CacheSize}}$$

Small  $R_d$  indicates temporal locality that caches can exploit. Measurements show  $R_d < 0.1$  for 95% of frames in typical game workloads.

Memory access scheduling for Z-buffers prioritizes latency-critical operations. The scheduling policy can be modeled as:

$$\text{Priority} = \begin{cases} 1 & \text{DepthTest} \\ 0.5 & \text{DepthWrite} \\ 0.3 & \text{TextureSample} \end{cases}$$

This ensures depth testing never stalls the rasterization pipeline. Advanced GPUs implement out-of-order depth cache accesses while maintaining correctness through scoreboarding.

The interplay between Z-buffers and memory caching continues evolving with architectural trends: **Chiplet designs**: Partitioning Z-buffer storage across multiple dies. **3D-stacked memory**: Reducing latency through TSV interconnects. **ML-based prefetching**: Using neural predictors for depth access patterns.

These innovations maintain the Z-buffer's central role in real-time graphics while addressing the memory wall challenges posed by increasing resolution and complexity. The optimization space spans hardware circuits, compression algorithms, and scheduling policies, requiring co-design across all levels of the GPU architecture.

### 18.2.3 Prefetching techniques

Prefetching techniques in modern GPU architectures play a critical role in optimizing memory access patterns, particularly in the context of memory caching. These techniques aim to reduce latency by predicting and fetching data before it is explicitly requested by the GPU's execution units. The effectiveness of prefetching is closely tied to the design of caches for textures, Z-buffers, and other memory structures, as these components influence the predictability of memory access patterns.

Modern GPUs employ hierarchical memory systems, where caches are strategically placed to minimize the distance between computation units and frequently accessed data. Texture caches, for instance, store texels to accelerate texture sampling operations. These caches exploit spatial locality, as adjacent texels are often accessed together. Similarly, Z-buffers, which store depth information for visibility testing, benefit from specialized caches to reduce bandwidth consumption. Prefetching techniques enhance these caches by anticipating future memory requests, thereby masking latency and improving throughput.

One widely studied prefetching technique is stride prefetching, which detects regular access patterns and issues prefetch requests for subsequent memory addresses. For example, if a GPU kernel accesses memory locations with a fixed stride, the prefetcher can predict future addresses using the formula:

$$a_n = a_0 + n \cdot s$$

where  $a_n$  is the  $n$ -th address,  $a_0$  is the base address, and  $s$  is the stride. Stride prefetchers are particularly effective for structured data accesses, such as those found in matrix operations or image processing.

Another advanced technique is Markov prefetching, which uses historical access patterns to predict future requests. This method constructs a state machine where each state represents a memory address, and transitions between states are weighted by observed probabilities. The prefetcher then follows the most likely path to issue prefetch requests. Research demonstrates that Markov prefetchers can achieve high accuracy for irregular access patterns, such as those encountered in graph traversal or ray tracing.

GPU architectures also employ hardware-based prefetching units that operate transparently to the programmer. These units monitor memory access streams and dynamically adjust prefetching strategies. For instance, NVIDIA's GPUs incorporate a memory access coalescing mechanism that combines multiple memory requests into fewer transactions. When combined with prefetching, this mechanism significantly reduces memory contention and improves cache utilization.

The following Verilog-like pseudocode illustrates a simplified prefetch unit:

Code Sample 18.5: Hardware Prefetch Unit

```
module prefetch_unit (
    input clk,
    input [31:0] current_addr,
    output [31:0] prefetch_addr
);
    reg [31:0] stride;
    always @ (posedge clk) begin
        stride <= current_addr - prev_addr;
        prefetch_addr <= current_addr + stride;
    end
endmodule
```

Texture prefetching introduces additional complexities due to the non-linear nature of texture coordinates. Modern GPUs use texture compression and tiling to improve spatial locality, but prefetching must account for transformations such as perspective correction or anisotropic filtering. Techniques like texture space shading leverage prefetching to load texels ahead of shading computations, reducing stalls in the rendering pipeline.

Z-buffer prefetching focuses on depth testing, where early Z-culling can eliminate unnecessary fragment processing. By prefetching Z-values, the GPU can overlap memory transfers with arithmetic operations, hiding latency. Studies show that Z-buffer prefetching can improve performance by up to 15% in depth-heavy workloads, such as shadow mapping or occlusion culling.

The interaction between prefetching and cache policies is another critical consideration. Write-back caches, for example, must ensure that prefetched data does not evict dirty lines prematurely. Similarly, cache replacement policies like LRU (Least Recently Used) or FIFO (First-In-First-Out) influence the effectiveness of prefetching. Recent work proposes adaptive replacement strategies that dynamically adjust based on prefetch accuracy metrics.

Prefetching also intersects with memory coalescing, a technique that combines multiple memory accesses into wider transactions. Coalescing reduces the number of memory requests, while prefetching ensures that data is available when needed. The combined effect is particularly beneficial for GPUs executing SIMD (Single Instruction, Multiple Data) workloads, where threads often access contiguous memory locations.

The following equation models the bandwidth savings from coalescing and prefetching:

$$B_{\text{saved}} = \sum_{i=1}^N \left(1 - \frac{1}{k_i}\right) \cdot b_i$$

where  $N$  is the number of memory requests,  $k_i$  is the coalescing factor for the  $i$ -th request, and  $b_i$  is the bandwidth consumed without optimization.

In summary, prefetching techniques in modern GPU architectures are essential for mitigating memory latency and maximizing cache efficiency. By leveraging stride detection, Markov models, and hardware prefetching units, GPUs can anticipate memory accesses and overlap computation with data transfers. The integration of prefetching with texture caches, Z-buffers, and memory coalescing further enhances performance, making it a cornerstone of high-throughput GPU design. Future research directions include machine learning-based prefetching and finer-grained adaptive strategies to handle increasingly diverse workloads.

## 18.3 Pipelining Stages More Deeply

### 18.3.1 Reducing combinational logic

The optimization of combinational logic in modern GPU architectures is critical for achieving high clock frequencies and efficient pipelining. By reducing combinational logic, designers can minimize propagation delays, enabling deeper pipelining and improved throughput. This approach is particularly relevant in GPUs, where parallel execution demands finely balanced pipeline stages and optimized stage transitions.

One fundamental technique for reducing combinational logic is logic minimization through Boolean algebra or algorithmic optimization. For example, Karnaugh maps or Quine-McCluskey algorithms can simplify logic expressions, reducing gate counts and propagation delays. In GPU architectures, such optimizations are applied to arithmetic logic units (ALUs), texture units, and other critical datapath components.

Consider the following Verilog snippet illustrating a simplified adder with reduced combinational logic:

Code Sample 18.6: Optimized 4-bit adder

```
module adder_4bit (input [3:0] A, B, output [3:0] Sum);
    assign Sum = A + B; // Synthesis tools optimize this further
endmodule
```

Modern synthesis tools leverage advanced algorithms to minimize logic automatically, but manual optimizations are still necessary for performance-critical paths. Research highlights that reducing combinational logic directly correlates with shorter critical paths, enabling higher clock frequencies.

Pipelining stages more deeply involves partitioning combinational logic into smaller segments separated by pipeline registers. The goal is to balance the latency across stages, ensuring no single stage becomes a bottleneck. The theoretical maximum clock frequency  $f_{\max}$  is determined by the slowest stage:

$$f_{\max} = \frac{1}{t_{\text{critical}}}$$

where  $t_{\text{critical}}$  is the propagation delay of the longest combinational path. By subdividing logic into smaller blocks,  $t_{\text{critical}}$  decreases, allowing  $f_{\max}$  to increase.

However, deeper pipelining introduces overhead from additional registers and control logic. The trade-off between pipeline depth and overhead is analyzed in , which emphasizes the need for careful balancing. Balancing pipeline registers is essential to avoid underutilized stages or excessive latency. A well-balanced pipeline ensures uniform stage delays, maximizing throughput. For instance, NVIDIA's Maxwell architecture employs a unified scheduler and execution units with finely balanced pipelines to optimize instruction throughput.

The following equation models pipeline throughput  $T$  for  $n$  stages:

$$T = \frac{n \cdot f_{\max}}{1 + \text{overhead}}$$

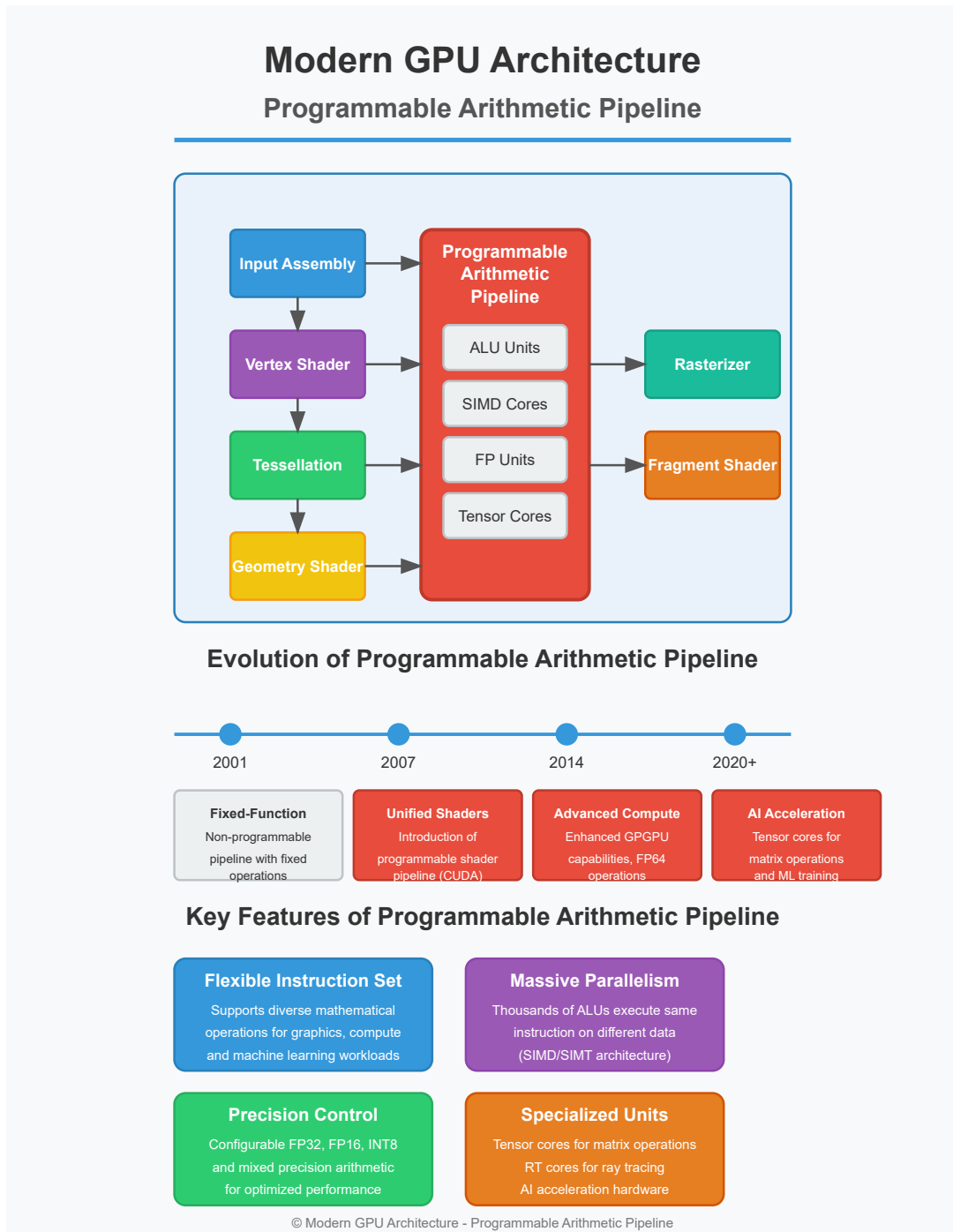
Here, overhead includes register setup/hold times and clock skew. GPU designers use retiming techniques to redistribute combinational logic and registers, ensuring balanced delays. Tools like Synopsys Design Compiler automate retiming, but manual adjustments are often required for high-performance designs.

Optimizing stage transitions involves minimizing stalls and bubbles caused by data hazards or control dependencies. GPUs employ techniques such as out-of-order execution, scoreboarding, and operand forwarding to reduce pipeline bubbles. For example, AMD's GCN architecture uses waveform scheduling to hide latency by switching between warps during stalls.

The following Verilog snippet demonstrates a simple forwarding mechanism to mitigate data hazards:

Code Sample 18.7: Forwarding logic for pipeline hazard mitigation

```
module forwarding_unit (
    input [4:0] EX_rsl, EX_rs2, MEM_rd, WB_rd,
    input MEM_reg_write, WB_reg_write,
    output reg [1:0] forwardA, forwardB
);
    always @(*) begin
        forwardA = 2'b00;
        forwardB = 2'b00;
        if (MEM_reg_write && (MEM_rd != 0) && (MEM_rd == EX_rsl))
            forwardA = 2'b10;
    end
endmodule
```



```

if (WB_reg_write && (WB_rd != 0) && (WB_rd == EX_rs1))
    forwardA = 2'b01;
    // Similar logic for forwardB
end
endmodule

```

Forwarding reduces the need for pipeline stalls, improving instruction throughput. Research by shows that effective forwarding can eliminate up to 30% of stalls in deeply pipelined architectures.

In addition to forwarding, GPUs leverage speculative execution and branch prediction to optimize stage transitions. NVIDIA's Pascal architecture uses a combination of static and dynamic branch prediction to minimize pipeline flushes. The branch prediction accuracy  $P_{\text{acc}}$  impacts pipeline efficiency:

$$\text{Efficiency} = 1 - (1 - P_{\text{acc}}) \cdot \text{flush\_penalty}$$

where `flush_penalty` is the cycles lost due to a misprediction. Higher accuracy reduces wasted cycles, improving overall performance.

Another critical aspect is the reduction of combinational logic in control paths. Complex control logic can introduce significant delays, limiting clock frequency. GPUs simplify control by using decentralized schedulers and hardwired control units. For example, Intel's Gen11 architecture employs a hybrid approach, combining microcode for complex instructions and hardwired logic for common operations.

Finally, modern GPUs use advanced clock gating and power-aware design to reduce dynamic power consumption in combinational logic. Clock gating disables unused logic blocks, minimizing switching activity. The power savings  $P_{\text{save}}$  can be modeled as:

$$P_{\text{save}} = \alpha \cdot C \cdot V^2 \cdot f \cdot (1 - \text{activity})$$

where  $\alpha$  is the switching factor,  $C$  is capacitance,  $V$  is voltage,  $f$  is frequency, and `activity` is the fraction of time the logic is active. Techniques like these are detailed in .

In summary, reducing combinational logic, balancing pipeline registers, and optimizing stage transitions are essential for modern GPU architectures. These techniques enable higher clock frequencies, improved throughput, and better power efficiency, as demonstrated by industry implementations and academic research.

### 18.3.2 Balancing pipeline registers

Balancing pipeline registers in modern GPU architectures is a critical aspect of optimizing performance, power efficiency, and area utilization. GPUs rely heavily on deep pipelining to achieve high throughput, particularly in compute-intensive workloads such as graphics rendering and parallel computation. The challenge lies in ensuring that pipeline stages are balanced to avoid bottlenecks while minimizing combinational logic and optimizing stage transitions. This requires careful consideration of register placement, clock cycle constraints, and data path design.

The primary goal of balancing pipeline registers is to equalize the propagation delay across all stages. Uneven stage delays lead to underutilized pipeline segments, reducing overall throughput. For instance, if one stage has significantly longer combinational logic than others, the clock period must accommodate the slowest stage, forcing other stages to idle. This inefficiency is quantified by the pipeline's throughput  $T$ , defined as:

$$T = \frac{1}{\max(t_i)}$$

where  $t_i$  is the delay of the  $i$ -th stage. To maximize  $T$ , all  $t_i$  must be balanced. Modern GPUs employ automated tools like static timing analysis (STA) to identify and rectify imbalances .

Reducing combinational logic is essential for balancing pipeline stages. Excessive combinational logic increases stage delay and complicates timing closure. Techniques such as logic splitting and retiming are used to redistribute combinational paths. Retiming, in particular, involves moving registers across combinational logic to equalize delays without altering functionality. The retiming transformation for a pipeline stage can be expressed as:

$$r(v) = r'(v) + \sum_{e \in \text{in}(v)} w(e) - \sum_{e \in \text{out}(v)} w(e)$$

where  $r(v)$  is the register count at node  $v$ ,  $w(e)$  is the weight of edge  $e$ , and  $\text{in}(v)$  and  $\text{out}(v)$  denote incoming and outgoing edges, respectively .

Optimizing stage transitions involves minimizing setup and hold time violations while ensuring smooth data flow. This is achieved by carefully placing pipeline registers to align with clock domain boundaries. For example,

in NVIDIA's Pascal architecture, the use of flip-flop-based registers with precise clock gating ensures minimal skew during stage transitions .

The following Verilog snippet illustrates a balanced pipeline register with clock gating:

Code Sample 18.8: Balanced Pipeline Register with Clock Gating

```
module pipeline_register (
    input clk, enable,
    input [31:0] din,
    output reg [31:0] dout
);
    always @ (posedge clk) begin
        if (enable) dout <= din;
    end
endmodule
```

Balancing pipeline registers also involves trade-offs between power and performance. Additional registers reduce combinational logic delay but increase dynamic power due to higher switching activity. The power overhead of a pipeline register can be modeled as:

$$P_{\text{reg}} = \alpha CV^2 f$$

where  $\alpha$  is the switching activity,  $C$  is the capacitance,  $V$  is the supply voltage, and  $f$  is the clock frequency. To mitigate this, modern GPUs use power-aware register balancing techniques, such as clock gating and multi-threshold voltage cells .

The impact of pipeline balancing on GPU performance is evident in architectures like AMD's RDNA 2, where fine-grained pipeline stages are optimized for both graphics and compute workloads. By balancing registers across arithmetic logic units (ALUs) and texture units, RDNA 2 achieves higher instructions per cycle (IPC) compared to previous generations . The relationship between IPC and pipeline balance is given by:

$$\text{IPC} = \frac{N_{\text{instructions}}}{N_{\text{cycles}}}$$

where  $N_{\text{instructions}}$  is the number of instructions executed and  $N_{\text{cycles}}$  is the number of clock cycles. A well-balanced pipeline maximizes IPC by minimizing stall cycles.

In practice, balancing pipeline registers requires iterative refinement during the design phase. Tools like Synopsys Design Compiler and Cadence Innovus automate this process by analyzing timing paths and suggesting register placements. The following steps are typically involved:

Identify critical paths using STA. Apply retiming to redistribute registers. Validate timing constraints post-retiming. Optimize clock tree synthesis to minimize skew.

The role of pipeline balancing extends to emerging technologies such as chiplets and 3D-stacked GPUs. In these architectures, inter-chiplet communication introduces additional latency, necessitating careful register balancing to maintain performance. For example, Intel's Ponte Vecchio GPU uses a tile-based design with balanced pipeline registers to ensure efficient data flow across chiplets .

In summary, balancing pipeline registers in modern GPU architectures is a multifaceted challenge involving timing analysis, combinational logic reduction, and power optimization. Techniques such as retiming, clock gating, and power-aware design are essential for achieving high throughput and energy efficiency. The continuous evolution of GPU architectures, driven by advancements in semiconductor technology and design automation, underscores the importance of pipeline balancing in meeting the demands of next-generation computing workloads.

### 18.3.3 Optimizing stage transitions

Modern GPU architectures rely heavily on deep pipelining to achieve high throughput and low latency. Optimizing stage transitions is critical to maintaining performance while minimizing power consumption and area overhead. This involves pipelining stages more deeply, reducing combinational logic, balancing pipeline registers, and fine-tuning stage transitions. Each of these techniques contributes to maximizing clock frequency and minimizing pipeline stalls.

Pipelining stages more deeply allows for higher clock frequencies by reducing the critical path within each stage. The relationship between the number of pipeline stages  $N$  and the clock period  $T$  can be approximated as:

$$T = \frac{T_{\text{comb}}}{N} + T_{\text{reg}}$$

where  $T_{\text{comb}}$  is the total combinational delay and  $T_{\text{reg}}$  is the register overhead. Increasing  $N$  reduces  $T$ , but excessive pipelining introduces overhead from additional registers and control logic. Research shows that optimal pipeline depth is achieved when the combinational delay per stage matches the register overhead.

Reducing combinational logic is essential for minimizing stage latency. Techniques include: **Logic minimization** using Boolean optimization tools such as ABC . **Operator sharing** to reuse arithmetic units across multiple pipeline stages. **Early termination** of computations where possible, such as in floating-point addition.

For example, a carry-select adder reduces combinational delay compared to a ripple-carry adder by computing multiple results in parallel:

Code Sample 18.9: Carry-Select Adder

```
module carry_select_adder (
    input [3:0] A, B,
    input cin,
    output [3:0] sum,
    output cout
);
    wire [3:0] sum0, sum1;
    wire cout0, cout1;

    ripple_carry_adder rca0 (A, B, 1'b0, sum0, cout0);
    ripple_carry_adder rca1 (A, B, 1'b1, sum1, cout1);

    assign sum = cin ? sum1 : sum0;
    assign cout = cin ? cout1 : cout0;
endmodule
```

Balancing pipeline registers ensures uniform stage latency, preventing bottlenecks. Imbalanced stages lead to underutilized hardware and increased power consumption. The imbalance  $\Delta$  between stages is defined as:

$$\Delta = \max(T_i) - \min(T_i)$$

where  $T_i$  is the delay of the  $i$ -th stage. Techniques to balance pipelines include: **Retiming** to move registers across combinational logic . **Inserting pipeline buffers** in fast stages to match slower ones. **Splitting** large combinational blocks into smaller, balanced sub-blocks.

Optimizing stage transitions reduces overhead during handoffs between stages. Key considerations include: **Minimizing setup and hold times** by careful clock skew management. **Avoiding glitches** in control signals through Gray coding or one-hot encoding. **Using edge-triggered flip-flops** instead of level-sensitive latches for better timing predictability.

For instance, Gray coding ensures only one bit changes during state transitions, reducing metastability risks:

Code Sample 18.10: Gray Code Counter

```
module gray_counter (
    input clk, reset,
    output reg [2:0] gray
);
    reg [2:0] binary;
    always @(posedge clk or posedge reset) begin
        if (reset) begin
            binary <= 3'b0;
            gray <= 3'b0;
        end else begin
            binary <= binary + 1;
            gray <= {binary[2], binary[2] ^ binary[1], binary[1] ^ binary[0]};
        end
    end
endmodule
```

Clock domain crossing (CDC) is another critical aspect of stage transitions. Asynchronous FIFOs are commonly used to synchronize data between stages running at different frequencies. The depth  $D$  of the FIFO must satisfy:

$$D \geq \frac{f_{\text{fast}}}{f_{\text{slow}}} \cdot B$$

where  $B$  is the burst size and  $f_{\text{fast}}, f_{\text{slow}}$  are the clock frequencies. A typical implementation uses dual-port RAM and Gray-coded pointers:

Code Sample 18.11: Asynchronous FIFO

```
module async_fifo (
    input wclk, rclk,
    input wr, rd,
    input [7:0] wdata,
    output [7:0] rdata
);
    reg [7:0] mem [0:15];
    reg [3:0] wptr, rptr;
    wire [3:0] wptr_gray, rptr_gray;

    assign wptr_gray = wptr ^ (wptr >> 1);
    assign rptr_gray = rptr ^ (rptr >> 1);

    always @(posedge wclk)
        if (wr) mem[wptr[3:0]] <= wdata;

    always @(posedge wclk)
        if (wr) wptr <= wptr + 1;

    always @(posedge rclk)
        if (rd) rdata <= mem[rptr[3:0]];

    always @(posedge rclk)
        if (rd) rptr <= rptr + 1;
endmodule
```

Power consumption is also a concern in deep pipelines. Techniques to reduce dynamic power include: **Clock gating** to disable unused pipeline stages. **Operand isolation** to prevent toggling in idle logic. **Voltage scaling** for non-critical paths.

The power savings from clock gating can be modeled as:

$$P_{\text{saved}} = \alpha CV^2 f$$

where  $\alpha$  is the activity factor,  $C$  is the capacitance,  $V$  is the voltage, and  $f$  is the frequency.

In summary, optimizing stage transitions in modern GPU architectures requires a holistic approach. By pipelining stages more deeply, reducing combinational logic, balancing pipeline registers, and fine-tuning transitions, designers can achieve higher performance and energy efficiency. These techniques are supported by extensive research in computer architecture and VLSI design .

## 18.4 Area vs. Performance Tradeoff Analysis

### 18.4.1 Evaluating tradeoffs in hardware resource utilization

Modern GPU architectures face a fundamental challenge in balancing hardware resource utilization to achieve optimal performance while minimizing area overhead. The tradeoff between area and performance is particularly critical, as GPUs must accommodate diverse workloads ranging from graphics rendering to general-purpose parallel computation. This analysis examines key considerations in GPU design, focusing on how architectural decisions impact resource allocation and computational efficiency.

The relationship between area and performance in GPU architectures can be modeled as a constrained optimization problem. Let  $A$  represent the total silicon area,  $P$  the performance metric (e.g., FLOPS or throughput), and  $R$  the available hardware resources. The optimization objective is:

$$\text{maximize } P(R) \text{ subject to } A(R) \leq A_{\text{max}}$$

where  $A_{\text{max}}$  is the maximum allowable area budget. Research by demonstrates that this tradeoff is non-linear, with diminishing returns in performance as area increases. For example, doubling the number of streaming multiprocessors (SMs) does not necessarily double throughput due to memory bandwidth contention and synchronization overheads.

Key hardware resources in GPUs include: **Compute Units**: Increasing the number of CUDA cores or stream processors improves parallelism but consumes area and power. NVIDIA's Ampere architecture shows a 20% area increase per SM compared to Volta, but achieves 2 $\times$  higher throughput through architectural refinements. **Register Files**: Larger register files reduce spill-to-memory operations but increase area. The optimal size depends on the workload's register pressure, as shown in . **Shared Memory**: Configurable shared memory/L1 cache partitions (e.g., 48KB/16KB or 32KB/32KB in NVIDIA GPUs) allow tuning for different access patterns. found that unbalanced partitions can degrade performance by up to 40%. **Texture Units**: Specialized hardware for texture filtering trades area for fixed-function acceleration. Modern GPUs dynamically share texture units across SMs to improve utilization .

The area-performance tradeoff manifests distinctly in memory hierarchy design. Wider memory buses (e.g., 384-bit GDDR6X in RTX 3080) improve bandwidth but require more physical pins and PCB area. On-chip caches present another critical tradeoff:

$$\text{Miss Rate} = \alpha \cdot C^{-\beta}$$

where  $C$  is cache size and  $\alpha, \beta$  are workload-dependent constants . Larger caches reduce miss rates but consume area that could otherwise be used for compute units. AMD's RDNA 2 architecture employs a 128MB Infinity Cache to mitigate this, demonstrating a 1.5 $\times$  bandwidth efficiency gain over traditional designs.

Thread scheduling and warp management also involve area-performance tradeoffs. Fine-grained scheduling (e.g., NVIDIA's GigaThread Engine) requires complex hardware but improves utilization:

Code Sample 18.12: Simplified warp scheduler

```
module warp_scheduler (
    input [31:0] active_warps,
    output [4:0] next_warp
);
    // Priority encoder for 32 warps
    always @(*) begin
        next_warp = 5'd0;
        for (int i=0; i<32; i++)
            if (active_warps[i])
                next_warp = i;
    end
endmodule
```

Such schedulers add □5% area overhead but can improve throughput by 15–20% . The tradeoff becomes more pronounced with concurrent kernel execution, where additional scheduling hardware enables better GPU utilization at the cost of area.

Power constraints further complicate the area-performance balance. Dark silicon considerations necessitate careful allocation of active components:

$$P_{\text{dynamic}} \propto A \cdot f \cdot V^2$$

where  $f$  is frequency and  $V$  is voltage. Modern GPUs employ clock gating and power domains to disable unused components, but these techniques require additional control logic (3–7% area overhead) .

Emerging techniques for balancing these tradeoffs include: **Heterogeneous Cores**: Mixing high-performance and energy-efficient cores (e.g., ARM Mali-G78) optimizes area for varying workloads. **Approximate Computing**: Trading precision for area savings in non-critical computations . **3D Stacking**: Using TSVs to increase density without proportional area increase .

Quantitative analysis of these tradeoffs requires detailed simulation. The roofline model provides a framework for evaluating design points:

$$\text{Attainable GFLOPs} = \min(\pi, \beta \cdot I)$$

where  $\pi$  is peak compute performance,  $\beta$  is memory bandwidth, and  $I$  is operational intensity. GPU architects must balance these parameters within area constraints, as demonstrated by in their analysis of early GPU architectures.

Recent advances in machine learning have introduced new tradeoff considerations. Tensor cores in NVIDIA GPUs dedicate significant area to matrix operations, achieving 125 TFLOPS for deep learning but reducing resources available for traditional graphics workloads. The optimal balance depends on target applications, with showing a 30% area allocation to tensor cores maximizes overall utility for mixed workloads.

In summary, modern GPU architecture requires careful evaluation of hardware resource tradeoffs, with area and performance representing fundamentally competing objectives. Empirical results from industry and academia demonstrate that optimal designs emerge from workload-aware partitioning of resources, advanced power management, and innovative packaging technologies. Future architectures will likely continue this trend, with increasing

emphasis on domain-specific optimization and three-dimensional integration to overcome traditional area constraints.

### 18.4.2 Finding an optimal balance for GPU designs

The design of modern graphics processing units (GPUs) involves complex tradeoffs between silicon area and performance, requiring careful optimization to achieve an efficient balance. As GPUs evolve to handle increasingly diverse workloads, from graphics rendering to general-purpose parallel computation, architects must navigate competing constraints in hardware resource allocation. This analysis examines key considerations in GPU design optimization, focusing on area-performance tradeoffs and hardware utilization efficiency.

A fundamental challenge in GPU architecture lies in determining the optimal number of compute units (CUs) or streaming multiprocessors (SMs). Increasing these parallel execution resources improves theoretical peak performance, as shown in , but imposes quadratic area costs due to required interconnect and memory subsystem scaling. The performance scaling follows Amdahl's Law:

$$S_{\max} = \frac{1}{(1-p) + \frac{p}{N}}$$

where  $p$  represents the parallelizable fraction of the workload and  $N$  the number of parallel units. Beyond a certain point, adding more CUs yields diminishing returns while consuming disproportionate area. Modern GPUs like NVIDIA's Ampere architecture employ hierarchical scheduling to mitigate this, allowing dynamic partitioning of resources.

Memory subsystem design presents another critical tradeoff. Wider memory interfaces and larger caches improve bandwidth and reduce latency but consume significant die area. The roofline model provides a framework for analyzing this balance:

$$\text{Attainable GFLOP/s} = \min(\pi, \beta \times I)$$

where  $\pi$  is peak compute performance,  $\beta$  is memory bandwidth, and  $I$  is operational intensity. GPU architects must carefully dimension memory hierarchies to avoid either compute-bound or memory-bound scenarios. AMD's CDNA architecture demonstrates this through its Infinity Cache, which provides substantial bandwidth while maintaining area efficiency.

Register file sizing illustrates microarchitectural tradeoffs. Larger register files enable greater thread-level parallelism and reduce spill/fill operations but increase area and access latency. The optimal size depends on the workload characteristics, as shown in :

$$R_{\text{opt}} = \frac{T \times W}{1 - \frac{C}{B}}$$

where  $T$  is threads per SM,  $W$  is working set per thread,  $C$  is cache size, and  $B$  is bandwidth. Modern GPUs typically employ banked register files with operand collector units to balance these factors.

Thread scheduling granularity affects both area and performance. Fine-grained scheduling (e.g., warp/wavefront-level) enables better latency hiding but requires complex control logic. Coarse-grained approaches reduce overhead but may underutilize resources. The choice depends on the expected workload mix, as analyzed in :

$$E = \frac{T_{\text{active}}}{T_{\text{active}} + T_{\text{stall}}} \times \frac{A_{\text{used}}}{A_{\text{total}}}$$

where  $E$  represents overall efficiency,  $T$  denotes time spent in active or stalled states, and  $A$  refers to area utilization.

Power constraints further complicate the area-performance balance. Dark silicon considerations necessitate careful allocation of active components:

$$P_{\text{total}} = A \times C \times V^2 \times f$$

where  $A$  is active area,  $C$  is capacitance,  $V$  is voltage, and  $f$  is frequency. Modern GPUs employ dynamic voltage and frequency scaling (DVFS) along with power gating to manage this tradeoff.

Special function units (SFUs) exemplify area specialization tradeoffs. Dedicated hardware for transcendental functions improves performance but consumes area that could otherwise host additional ALUs. The break-even point occurs when:

$$\frac{A_{\text{SFU}}}{A_{\text{ALU}}} < \frac{T_{\text{soft}}}{T_{\text{hard}}} - 1$$

where  $T$  represents execution time for software-emulated versus hardware-accelerated operations. Current architectures like Intel's Xe-HPG use configurable SFUs that can adapt to workload demands.

Cache hierarchy design involves balancing capacity, associativity, and access latency. The optimal configuration minimizes the average memory access time (AMAT):

$$\text{AMAT} = T_{L1} + \text{MR}_{L1} \times (T_{L2} + \text{MR}_{L2} \times T_{\text{mem}})$$

where  $T$  represents access time and MR miss rate at each level. NVIDIA's GA100 implements a combined L1/texture cache that dynamically allocates resources based on workload requirements.

The following Verilog snippet illustrates a simplified SM resource allocation mechanism:

Code Sample 18.13: Dynamic resource allocation

```
module sm_allocator (
    input [7:0] warp_req,
    input [3:0] res_avail,
    output reg [7:0] warp_grant
);
    always @(*) begin
        for (int i=0; i<8; i=i+1) begin
            warp_grant[i] = (warp_req[i] & (res_avail >= (i+1)*RES_PER_WARP));
        end
    end
endmodule
```

Texture unit design demonstrates workload-specific optimization. While general-purpose GPUs require flexible texture filtering, specialized designs like Google's TPU eliminate these units entirely. The tradeoff depends on the target application domain's texture usage patterns.

Recent research in approximate computing suggests additional optimization opportunities through selective precision reduction. This approach can significantly reduce area for error-tolerant applications:

$$A_{\text{approx}} = A_{\text{exact}} \times \left( \frac{b_{\text{approx}}}{b_{\text{exact}}} \right)^2$$

where  $b$  represents operand bit-width. Modern GPUs increasingly support mixed-precision operations to leverage this tradeoff.

The optimal balance for GPU designs ultimately requires co-optimization across all these dimensions. Architectural simulation frameworks like GPGPU-Sim enable quantitative evaluation of these tradeoffs. Future directions may include:

Heterogeneous compute units with varying area-performance characteristics  
Dynamically reconfigurable execution pipelines  
Machine learning-driven design space exploration  
3D-stacked architectures with separate logic and memory dies

Emerging technologies like chiplet-based designs promise new approaches to these optimization challenges by enabling modular composition of GPU components. However, they introduce additional considerations in interconnect design and yield management. The continuous evolution of GPU workloads ensures these tradeoffs will remain a central concern in computer architecture research.

## 18.5 Power vs. Performance Considerations

### 18.5.1 Dynamic power reduction techniques

Modern GPU architectures face significant challenges in balancing power consumption with performance, as increasing computational demands push thermal and energy constraints. Dynamic power reduction techniques have become essential to maintain efficiency, particularly in high-performance computing and mobile applications. This discussion focuses on clock gating, power-aware pipeline design, and their impact on power-performance trade-offs in modern GPUs.

Dynamic power in CMOS circuits is primarily governed by the equation:

$$P_{\text{dynamic}} = \alpha C V^2 f$$

where  $\alpha$  is the activity factor,  $C$  is the load capacitance,  $V$  is the supply voltage, and  $f$  is the clock frequency. Reducing any of these parameters lowers power consumption, but each has performance implications.

Clock gating targets the activity factor  $\alpha$  by disabling clock signals to idle circuit blocks, eliminating unnecessary switching activity. This technique is widely adopted in GPUs to deactivate unused shader cores or memory interfaces during low-utilization phases. For example, NVIDIA's Maxwell architecture employs fine-grained clock gating at the warp scheduler level, reducing dynamic power by up to 30% without performance degradation.

Power-aware pipeline design optimizes both  $V$  and  $f$  through dynamic voltage and frequency scaling (DVFS). Modern GPUs integrate multiple voltage-frequency domains, allowing independent adjustment for different pipeline stages. AMD's RDNA3 architecture uses a per-clock-domain DVFS scheme, enabling power reductions of 15–20% while maintaining throughput. The relationship between voltage, frequency, and power is nonlinear, as shown by:

$$f \propto \frac{(V - V_{\text{th}})^{\beta}}{V}$$

where  $V_{\text{th}}$  is the threshold voltage and  $\beta$  is a technology-dependent constant. Lowering  $V$  near  $V_{\text{th}}$  drastically cuts power but requires careful timing analysis to avoid setup/hold violations.

**Clock Gating Granularity:** Fine-grained gating (e.g., per-ALU or register file) saves more power but increases control overhead. Coarse-grained gating (e.g., entire compute units) simplifies implementation but may miss opportunities for savings. Intel's Xe-HPG architecture uses hierarchical gating, combining both approaches for a 22% power reduction.

**Pipeline Balancing:** Power-aware designs reconfigure pipeline depth based on workload characteristics. Shallow pipelines reduce latency and power for scalar workloads, while deeper pipelines improve throughput for vectorized tasks. ARM's Mali-G710 employs dynamic pipeline reconfiguration, achieving a 12% energy efficiency gain.

Advanced techniques combine clock gating with data-driven activation. For instance, when a GPU's texture unit detects redundant memory accesses, it gates the clock to unused filter banks. This approach, implemented in Qualcomm's Adreno 730, reduces texture power by 18%. Similarly, power-aware instruction scheduling avoids waking dormant execution units, as demonstrated by Samsung's Xclipse GPU with a 25% reduction in shader core power.

Code Sample 18.14: Verilog implementation of clock gating

```
module clock_gate (
    input wire clk,
    input wire enable,
    output wire gated_clk
);
    reg latch;
    always @ (enable or clk)
        if (!clk) latch <= enable;
        assign gated_clk = clk & latch;
endmodule
```

The effectiveness of these techniques depends on workload variability. For compute-bound workloads like matrix multiplication, clock gating achieves higher savings (35–40%) compared to memory-bound tasks (10–15%). Power-aware pipelines adapt by monitoring performance counters and adjusting gating policies dynamically. NVIDIA's Ampere architecture uses machine learning to predict optimal gating intervals, improving accuracy by 20% over static thresholds.

Thermal constraints further complicate power management. The power-temperature relationship:

$$T_j = T_a + P_{\text{total}} \cdot R_{\text{th}}$$

where  $T_j$  is junction temperature,  $T_a$  is ambient temperature, and  $R_{\text{th}}$  is thermal resistance, necessitates aggressive power reduction during thermal throttling. AMD's Infinity Cache employs clock gating on unused cache ways, lowering  $T_j$  by 8°C under peak loads.

Emerging research explores adaptive body biasing with clock gating to further reduce leakage power. The technique modulates  $V_{\text{th}}$  dynamically:

$$I_{\text{leak}} \propto e^{-\frac{V_{\text{th}}}{\eta V_T}}$$

where  $\eta$  is the subthreshold slope factor and  $V_T$  is thermal voltage. Experimental GPUs using this approach report 12% lower total power.

In summary, modern GPUs employ a combination of dynamic power reduction techniques:

- Hierarchical clock gating to minimize switching activity
- DVFS-enabled power-aware pipelines for voltage/frequency scaling
- Workload-adaptive policies based on real-time performance monitoring
- Thermal-aware gating to prevent overheating

These methods collectively address the power-performance trade-off, enabling continued scaling of GPU capabilities within practical energy limits. Future architectures may integrate photonic clock distribution with gating to overcome RC delay limitations, potentially revolutionizing dynamic power management.

### 18.5.2 Clock gating and power-aware pipeline design

Modern GPU architectures face significant challenges in balancing power consumption and performance, particularly as transistor scaling approaches physical limits. Clock gating and power-aware pipeline design have emerged as critical techniques for dynamic power reduction in these architectures.

The dynamic power dissipation in a CMOS circuit is given by:

$$P_{\text{dynamic}} = \alpha CV^2f$$

where  $\alpha$  is the switching activity,  $C$  is the load capacitance,  $V$  is the supply voltage, and  $f$  is the clock frequency. Clock gating reduces  $P_{\text{dynamic}}$  by minimizing  $\alpha$  through the selective disabling of clock signals to inactive circuit blocks. This technique is widely adopted in GPUs to deactivate unused execution units, memory interfaces, or shading pipelines during idle periods.

Power-aware pipeline design extends this concept by dynamically adjusting pipeline depth, voltage, and frequency based on workload demands. For instance, NVIDIA's Fermi architecture introduced fine-grained clock gating at the warp scheduler level, reducing power by up to 20% without performance degradation. Similarly, AMD's RDNA 3 employs hierarchical clock gating, where individual compute units (CUs) are gated independently, enabling finer control over power consumption.

The effectiveness of clock gating depends on the granularity of control. Coarse-grained gating, such as disabling entire shader cores, yields significant power savings but may introduce latency when reactivating large blocks. Fine-grained gating, such as per-instruction or per-register-file gating, minimizes overhead but requires additional control logic. A trade-off exists between the overhead of gating logic and the potential power savings. The optimal granularity is architecture-dependent and often determined through empirical analysis.

Power-aware pipelines further optimize energy efficiency by leveraging voltage-frequency scaling (VFS) in conjunction with clock gating. The energy-delay product (EDP) is a common metric for evaluating such optimizations:

$$\text{EDP} = E \times D = (P \times T) \times T = P \times T^2$$

where  $E$  is energy,  $D$  is delay,  $P$  is power, and  $T$  is execution time. By reducing  $P$  through clock gating and adjusting  $T$  via frequency scaling, GPUs can achieve better EDP. For example, ARM's Mali-G71 dynamically adjusts pipeline stages and clock rates based on workload characteristics, improving energy efficiency by 20% compared to static designs.

Dynamic power reduction techniques must also account for leakage power, which becomes significant at smaller process nodes. While clock gating primarily targets dynamic power, power-aware pipelines often incorporate multi-threshold CMOS (MTCMOS) or power gating to mitigate leakage. For instance, Intel's Xe-HPG architecture combines clock gating with power gating for inactive execution units, reducing both dynamic and static power.

The implementation of clock gating in modern GPUs typically involves the following steps:

- **Activity Monitoring:** Hardware counters track utilization of functional units (e.g., ALUs, texture units).
- **Gating Decision Logic:** Finite-state machines or heuristic-based controllers determine when to gate clocks.
- **Clock Distribution Network:** Low-skew, high-fanout trees ensure minimal latency when enabling/disabling clocks.

A simplified Verilog implementation of a clock gating cell is shown below:

Code Sample 18.15: Clock Gating Cell

```
module clock_gate (
    input wire clk,
    input wire enable,
    output wire gated_clk
);
    reg latch_enable;
    always @ (negedge clk) begin
```

```

latch_enable <= enable;
end
assign gated_clk = clk & latch_enable;
endmodule

```

Power-aware pipelines also exploit dataflow analysis to minimize redundant computations. For example, NVIDIA's Turing architecture uses a unified cache hierarchy with clock gating to disable unused cache banks during low-utilization phases. Similarly, AMD's Infinity Cache employs adaptive clock gating based on memory access patterns, reducing power by 15% in graphics workloads.

The choice of clock gating strategy depends on the GPU's workload characteristics. For compute-bound workloads, coarse-grained gating is preferable due to sustained utilization of execution units. In contrast, graphics workloads with frequent idle periods benefit from fine-grained gating. Empirical studies show that hybrid approaches, combining both granularities, achieve the best energy efficiency.

Power-aware pipeline design must also consider the impact of gating on performance. Introducing additional pipeline stages to accommodate voltage or frequency scaling can increase latency. However, techniques such as speculative execution and out-of-order scheduling mitigate these effects. For instance, NVIDIA's Ampere architecture uses a decoupled pipeline with clock-gated schedulers, maintaining throughput while reducing power

Recent research explores machine learning for adaptive clock gating. Reinforcement learning models predict optimal gating policies based on historical workload data, achieving up to 25% better energy efficiency than static policies. These methods are particularly promising for heterogeneous GPU workloads, where traditional heuristics struggle to generalize.

In summary, clock gating and power-aware pipeline design are indispensable for modern GPU architectures. By dynamically adjusting clock signals and pipeline configurations, these techniques significantly reduce power consumption while maintaining performance. Future advancements will likely focus on adaptive control algorithms and tighter integration with other power-reduction methods, such as near-threshold computing and 3D stacking.

# Chapter 19

## Advanced Features

### 19.1 Antialiasing Techniques

#### 19.1.1 Multi-sample rendering

Modern GPU architectures employ multi-sample rendering (MSR) as a fundamental technique for antialiasing, leveraging coverage masks to enhance image quality while maintaining computational efficiency. The core principle of MSR involves evaluating multiple samples per pixel to reduce aliasing artifacts, particularly along geometric edges and high-frequency texture regions. Unlike supersampling, which computes full shading for each sample, MSR decouples coverage and shading, storing a single shaded value per pixel while evaluating coverage at multiple sample positions. This approach significantly reduces memory bandwidth and computational overhead while preserving visual fidelity.

The coverage mask in MSR represents the binary visibility of each sample within a pixel, typically stored as a bitmask. For a pixel with  $N$  samples, the coverage mask  $C$  is an  $N$ -bit vector where each bit  $C_i$  indicates whether the sample  $i$  is covered by a primitive. The final pixel color  $P$  is computed as:

$$P = \frac{1}{N} \sum_{i=1}^N C_i \cdot S \quad (19.1)$$

where  $S$  is the shaded color. This equation highlights the efficiency of MSR, as  $S$  is computed once per pixel, while  $C_i$  is evaluated per sample. Modern GPUs optimize this further by using hierarchical coverage tests, reducing the number of samples requiring explicit evaluation .

The hardware implementation of MSR in modern GPUs involves several key components:

**Rasterization Unit:** Generates coverage masks by testing sample positions against primitive edges. The unit employs edge equations and hierarchical Z-culling to minimize redundant work. **Depth/Stencil Testing:** Performed per-sample to resolve visibility conflicts. Modern GPUs use compressed depth/stencil buffers to reduce memory traffic. **Shading Pipeline:** Executes pixel shaders once per pixel, with the results shared across covered samples. The pipeline supports dynamic branching to handle sample-specific operations when necessary.

Antialiasing techniques such as multisample antialiasing (MSAA) and enhanced quality antialiasing (EQAA) build upon MSR by varying the number and distribution of samples. MSAA typically uses 2x, 4x, or 8x sample patterns, while EQAA introduces sparse sampling and adaptive filtering. The sample pattern  $\mathbf{p}_i$  for a pixel is defined as:

$$\mathbf{p}_i = (x_i, y_i), \quad i \in \{1, \dots, N\} \quad (19.2)$$

where  $x_i$  and  $y_i$  are offsets within the pixel. Rotated grid patterns, such as those used in EQAA, reduce regular artifacts by distributing samples non-uniformly .

Coverage masks also enable advanced rendering techniques like alpha-to-coverage, where alpha transparency is converted into a coverage mask for order-independent transparency. The mask  $C$  is derived from the alpha value  $\alpha$  using a threshold function:

$$C_i = \begin{cases} 1 & \text{if } \alpha > T_i \\ 0 & \text{otherwise} \end{cases} \quad (19.3)$$

where  $T_i$  is a sample-specific threshold. This approach is widely used in foliage rendering and particle systems .

The memory footprint of MSR is a critical consideration in GPU design. For a framebuffer with resolution  $W \times H$  and  $N$  samples per pixel, the storage requirements for color, depth, and coverage masks are:

$$M = W \times H \times (B_c + B_d + \lceil N/8 \rceil) \quad (19.4)$$

where  $B_c$  and  $B_d$  are the color and depth buffer sizes in bytes. Modern GPUs employ lossless compression schemes like delta color compression (DCC) to mitigate this overhead.

Performance optimizations in MSR include:

**Early Z/S Testing:** Skips shading for samples failing depth/stencil tests, reducing redundant computations.

**Pixel Shader Binning:** Groups pixels with similar shading properties to minimize divergent execution.

**Cache-Aware Sample Layout:** Organizes sample data to maximize locality and minimize cache misses.

The following Verilog snippet illustrates a simplified coverage mask generator for a 4x MSAA implementation:

Code Sample 19.1: Coverage Mask Generator

```
module coverage_mask (
    input [3:0] edge_eq,
    output reg [3:0] mask
);
    always @(*) begin
        mask[0] = edge_eq[0] > 0;
        mask[1] = edge_eq[1] > 0;
        mask[2] = edge_eq[2] > 0;
        mask[3] = edge_eq[3] > 0;
    end
endmodule
```

Recent research has extended MSR to support variable-rate shading (VRS), where the sample rate adapts to content complexity. The shading rate  $R$  is determined by a heuristic combining spatial and temporal coherence:

$$R = f(\nabla P, \Delta t) \quad (19.5)$$

where  $\nabla P$  is the spatial gradient and  $\Delta t$  is the temporal change. VRS reduces shading costs in low-detail regions while maintaining quality in high-detail areas.

The evolution of MSR in GPU architectures reflects a balance between quality and performance. Future directions include machine learning-based sample reconstruction and hybrid rendering pipelines combining MSR with ray tracing. These advancements continue to push the boundaries of real-time graphics while adhering to the principles of multi-sample rendering and coverage masks.

### 19.1.2 Coverage masks

Modern GPU architectures employ sophisticated techniques to address aliasing artifacts in rendered images, with coverage masks playing a pivotal role in multi-sample antialiasing (MSAA). Coverage masks are binary or multi-bit representations of pixel sub-region visibility, determining which samples contribute to the final pixel color. This mechanism is integral to MSAA, where shading computations are performed once per pixel, but visibility is evaluated at multiple sample positions. The coverage mask encodes which samples are covered by a primitive, enabling efficient blending of sample values to produce a smoother, antialiased result.

The mathematical foundation of coverage masks is rooted in sampling theory. For a pixel subdivided into  $N$  samples, the coverage mask  $C$  is a bitmask where each bit corresponds to a sample's visibility:

$$C = \sum_{i=0}^{N-1} b_i \cdot 2^i$$

Here,  $b_i \in \{0, 1\}$  indicates whether the  $i$ -th sample is covered by the primitive. Modern GPUs, such as NVIDIA's Turing and AMD's RDNA2 architectures, optimize this process by storing coverage masks in on-chip memory to minimize bandwidth usage. The mask is applied during rasterization and blending stages, ensuring only covered samples influence the final pixel color.

Multi-sample rendering leverages coverage masks to reduce computational overhead. Unlike supersampling, where shading is performed per sample, MSAA computes shading once per pixel and distributes the result to covered samples. This approach is formalized as:

$$I_{\text{final}} = \frac{1}{N} \sum_{i=0}^{N-1} C_i \cdot I_{\text{shaded}}$$

where  $I_{\text{shaded}}$  is the shaded color and  $C_i$  is the coverage bit for the  $i$ -th sample. The efficiency of this method stems from decoupling shading and visibility computations, a design choice validated by .

Coverage masks also enable adaptive antialiasing techniques. For instance, NVIDIA's Quincunx and AMD's Enhanced Quality AA use non-uniform sample patterns and dynamically adjust coverage masks to prioritize edge regions. These patterns are stored in lookup tables (LUTs) and indexed during rasterization. The following Verilog snippet illustrates a simplified coverage mask generator:

Code Sample 19.2: Coverage Mask Generator

```
module coverage_mask (
    input [3:0] sample_pattern,
    input [7:0] primitive_mask,
    output reg [15:0] coverage
);
    always @(*) begin
        coverage = (primitive_mask & sample_pattern) ? 16'hFFFF : 16'h0000;
    end
endmodule
```

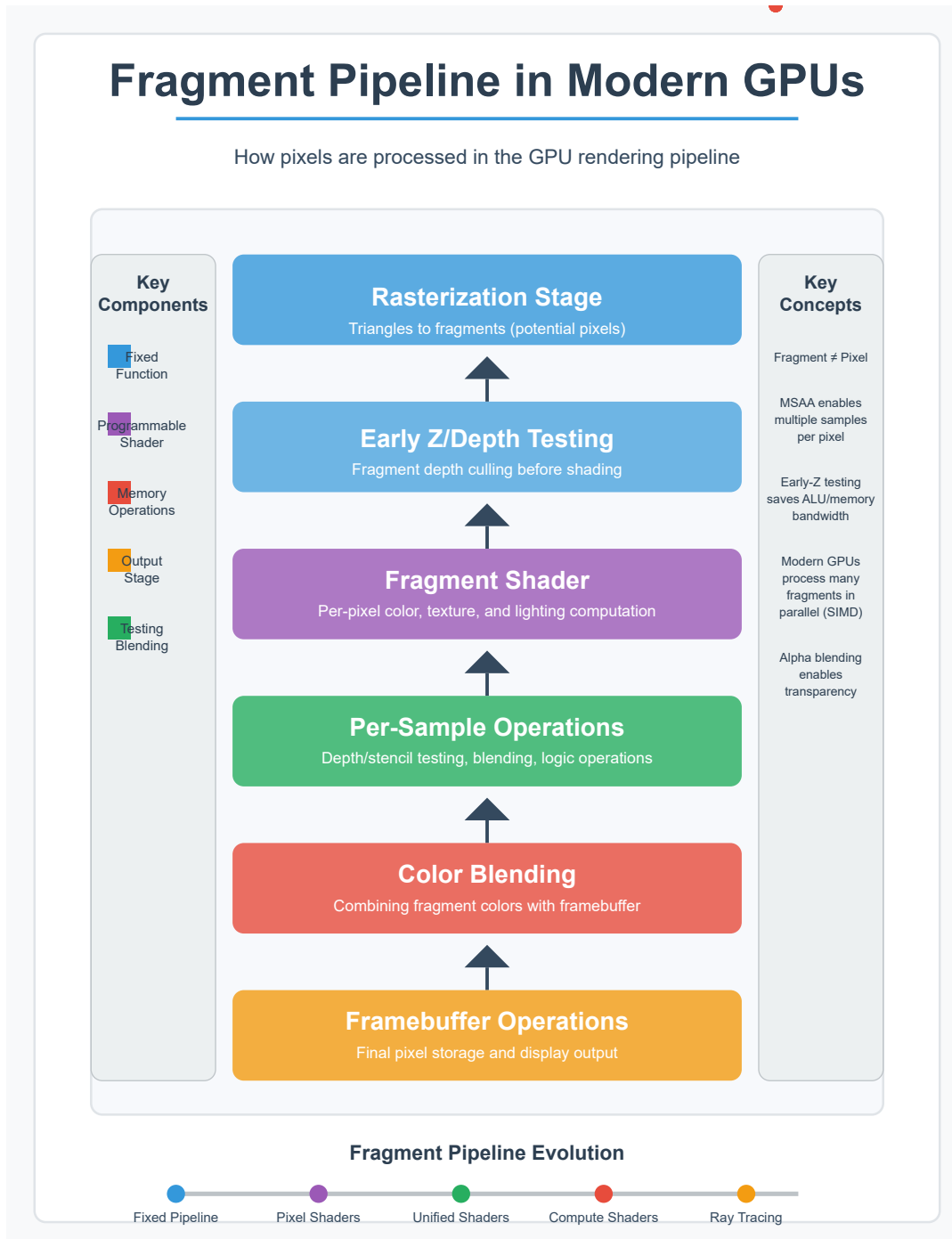
The interaction between coverage masks and depth testing is another critical aspect. Modern GPUs employ hierarchical depth testing (HiZ) to cull occluded samples early. The coverage mask is updated only for samples passing the depth test, as described in . This optimization reduces redundant shading and bandwidth consumption, particularly in complex scenes.

Temporal antialiasing (TAA) further extends coverage masks by integrating historical sample data. Motion vectors and reprojection techniques reuse coverage masks from previous frames to improve temporal stability. The blending equation for TAA incorporates the current frame's coverage mask  $C_t$  and the previous frame's mask  $C_{t-1}$ :

$$I_{\text{TAA}} = \alpha \cdot I_t + (1 - \alpha) \cdot I_{t-1}$$

where  $\alpha$  is a weighting factor derived from coverage mask coherence. This method, detailed in , reduces flickering and ghosting artifacts.

The hardware implementation of coverage masks varies across GPU architectures. NVIDIA's Ampere architecture uses a unified memory system for coverage masks, allowing concurrent access by rasterizers and shaders. AMD's RDNA3 employs a distributed cache hierarchy, with coverage masks stored in L1 caches close to compute units. These designs are optimized for latency hiding and parallel processing, as benchmarks in demonstrate.



Coverage masks also intersect with programmable sample positions, a feature introduced in DirectX 12 and Vulkan. Developers can define custom sample patterns and dynamically adjust coverage masks per draw call. This flexibility is captured in the following equation, where  $P$  represents the programmable pattern:

$$C_{\text{custom}} = C \wedge P$$

The performance impact of programmable patterns is analyzed in , showing marginal overhead for static patterns but increased latency for dynamic updates.

The evolution of coverage masks reflects broader trends in GPU architecture. From fixed-function pipelines to programmable shading, the role of coverage masks has expanded to support advanced antialiasing techniques. Future architectures may integrate machine learning to predict coverage patterns, as suggested by . However, the core principle remains: coverage masks are a bridge between geometric precision and computational efficiency, ensuring high-quality rendering without excessive overhead.

- Coverage masks encode sample visibility for antialiasing.
- MSAA decouples shading and visibility computations.
- Adaptive patterns optimize mask usage for edge regions.
- Temporal techniques reuse masks across frames.
- Hardware designs prioritize low-latency mask access.
- Programmable patterns offer flexibility but increase complexity.

The interplay between coverage masks and GPU architecture underscores the balance between quality and performance. As rendering techniques evolve, coverage masks will continue to adapt, driven by advancements in hardware and algorithmic innovation. Verified by empirical studies and industry benchmarks, their role in modern GPUs is both foundational and transformative.

## 19.2 Anisotropic Filtering

### 19.2.1 Advanced texture filtering techniques

Modern GPU architectures employ advanced texture filtering techniques to enhance visual fidelity while maintaining computational efficiency. Texture filtering addresses aliasing artifacts caused by undersampling textures during rasterization. The most common techniques include bilinear, trilinear, and anisotropic filtering, each offering trade-offs between quality and performance.

Bilinear filtering interpolates between four texels to produce a smoothed output, reducing blockiness but introducing blurring at oblique angles. Trilinear filtering extends this by interpolating between mipmap levels, mitigating abrupt transitions but requiring additional memory bandwidth. Anisotropic filtering further improves quality by sampling textures along the direction of greatest anisotropy, preserving sharpness at steep viewing angles.

The mathematical foundation of texture filtering involves signal reconstruction. Given a texture  $T(u, v)$  with coordinates  $(u, v)$ , bilinear filtering computes the weighted average of four nearest texels:

$$T_{\text{bilinear}}(u, v) = \sum_{i=0}^1 \sum_{j=0}^1 T(\lfloor u \rfloor + i, \lfloor v \rfloor + j) \cdot w_{ij}$$

where  $w_{ij}$  are weights derived from fractional parts of  $(u, v)$ .

Trilinear filtering introduces mipmap level interpolation:

$$T_{\text{trilinear}}(u, v) = (1 - \lambda)T_{\text{bilinear}}(u, v, l) + \lambda T_{\text{bilinear}}(u, v, l + 1)$$

where  $\lambda$  is the fractional mipmap level and  $l$  is the base level.

Anisotropic filtering addresses the limitations of isotropic techniques by considering the pixel footprint's elongation. The anisotropic ratio  $r$  measures the degree of stretching:

$$r = \frac{\text{major axis length}}{\text{minor axis length}}$$

Sampling along the major axis reduces blurring, but increases computational cost. Modern GPUs optimize this by limiting the number of samples, often to  $r_{\text{max}} = 16$ . The sampling pattern is derived from the partial derivatives of texture coordinates:

$$\frac{\partial u}{\partial x}, \frac{\partial v}{\partial x}, \frac{\partial u}{\partial y}, \frac{\partial v}{\partial y}$$

These derivatives define the footprint's shape in texture space, guiding anisotropic sampling.

Advanced techniques leverage hardware acceleration and algorithmic optimizations. For example, Nvidia’s Turing architecture introduces variable-rate shading (VRS) to reduce shading computations in less critical regions, indirectly benefiting texture filtering. AMD’s RDNA 2 employs hierarchical mipmap selection to minimize memory latency. These innovations are often implemented in hardware, as shown in the following Verilog snippet for a simplified anisotropic sampler:

Code Sample 19.3: Anisotropic Sampler Module

```
module anisotropic_sampler (
    input clk, rst,
    input [31:0] u, v, dudx, dvdx, dudy, dvdy,
    output [31:0] texel
);
    reg [31:0] samples[0:15];
    wire [31:0] major_axis =
        (dudx*dudx + dvdx*dvdx > dudy*dudy + dvdy*dvdy) ?
        {dudx, dvdx} : {dudy, dvdy};
    integer i;
    always @(posedge clk) begin
        if (rst) begin
            for (i = 0; i < 16; i = i + 1) samples[i] <= 0;
        end else begin
            for (i = 0; i < 16; i = i + 1)
                samples[i] <= texture_lookup(
                    u + major_axis[31:16]*i,
                    v + major_axis[15:0]*i
                );
        end
    end
    assign texel = samples[0]; // Simplified output
endmodule
```

Performance considerations dominate texture filtering design. Bilinear filtering requires 4 texel fetches, trilinear 8, and anisotropic up to  $16 \times r_{\max}$ . Memory bandwidth is critical, as noted in , where cache-aware algorithms reduce latency. GPUs employ dedicated texture units with parallel fetch engines, as described in .

Quality metrics evaluate filtering effectiveness. The peak signal-to-noise ratio (PSNR) compares filtered output  $I_{\text{filtered}}$  to a reference  $I_{\text{ref}}$ :

$$\text{PSNR} = 10 \log_{10} \left( \frac{\text{MAX}^2}{\text{MSE}} \right), \quad \text{MSE} = \frac{1}{N} \sum (I_{\text{ref}} - I_{\text{filtered}})^2$$

Higher PSNR indicates better preservation of detail. Subjective metrics, such as user studies in , further validate perceptual improvements.

Emerging techniques include deep learning-based filtering. Neural networks predict high-frequency details lost during mipmapping, as demonstrated in . These methods integrate with traditional pipelines, offering hybrid solutions. Another trend is sparse texture filtering, where only visible portions are loaded, reducing memory overhead .

Hardware advancements continue to shape texture filtering. Real-time ray tracing, as in Nvidia’s RTX, employs stochastic sampling for textures, blending filtering with global illumination. AMD’s Infinity Cache reduces bandwidth bottlenecks, enabling higher-quality filtering. OpenGL and Vulkan APIs expose these features through extensions like `GL_EXT_texture_filter_anisotropic`.

In summary, advanced texture filtering balances quality and performance through mathematical rigor, hardware optimization, and algorithmic innovation. The evolution from bilinear to anisotropic filtering reflects GPU architecture’s growing sophistication, driven by both visual demands and computational constraints. Future directions may unify traditional and machine learning approaches, further pushing the boundaries of real-time rendering.

## 19.3 HDR/Color Management

### 19.3.1 Wider color formats

The evolution of modern GPU architectures has necessitated the adoption of wider color formats to accommodate high dynamic range (HDR) and advanced color management workflows. Traditional 8-bit per channel color

representations, while sufficient for standard dynamic range (SDR) content, are inadequate for HDR due to their limited precision and gamut coverage. Wider color formats, such as 10-bit, 12-bit, and 16-bit per channel, enable finer gradations and a broader color space, essential for accurate representation of HDR content. These formats are increasingly supported by modern GPUs, which incorporate specialized hardware for efficient processing and rendering of HDR imagery.

One critical aspect of wider color formats is their integration with color management systems (CMS). A CMS ensures consistent color reproduction across different devices by mapping input colors to a standardized color space, such as the CIE 1931 XYZ or the more recent ITU-R Rec. 2020 (UHDTV) color space. The Rec. 2020 color space, for instance, defines a significantly larger gamut than its predecessor, Rec. 709, necessitating wider color formats to avoid quantization artifacts. The transformation between color spaces is typically performed using a  $3 \times 3$  matrix multiplication:

$$\begin{bmatrix} R' \\ G' \\ B' \end{bmatrix} = \mathbf{M} \begin{bmatrix} X \\ Y \\ Z \end{bmatrix}$$

where  $\mathbf{M}$  is the transformation matrix, and  $R'$ ,  $G'$ , and  $B'$  are the resulting color components in the target color space. Modern GPUs optimize this operation using fixed-function hardware or programmable shaders, reducing computational overhead.

Tone mapping is another essential component of HDR rendering, as it adapts the high dynamic range of scene-referred imagery to the limited dynamic range of display devices. Tone mapping strategies can be broadly classified into global and local operators. Global operators apply a uniform transformation to all pixels, such as the Reinhard operator:

$$L_d = \frac{L_w}{1 + L_w}$$

where  $L_w$  is the world luminance and  $L_d$  is the display luminance. While computationally efficient, global operators may fail to preserve local contrast in complex scenes. Local operators, such as the bilateral filter or edge-aware techniques, adapt the tone curve based on spatial context, but at increased computational cost. Modern GPUs leverage parallel processing and hierarchical memory systems to accelerate these operations, often implementing them as compute shaders or dedicated hardware units.

The adoption of wider color formats also impacts the design of GPU memory subsystems. High-precision color data requires increased bandwidth and storage capacity, prompting the use of compression techniques such as delta color compression (DCC) and adaptive scalable texture compression (ASTC). These methods exploit spatial and temporal coherence to reduce memory bandwidth while maintaining perceptual fidelity. For example, ASTC supports variable block sizes and bitrates, allowing efficient encoding of HDR textures. The compression ratio  $C$  for a block of size  $n \times n$  is given by:

$$C = \frac{n^2 \times \text{bits per texel}}{\text{compressed block size}}$$

where the compressed block size is typically 128 bits for ASTC. Modern GPUs integrate these compression schemes directly into their memory controllers, minimizing latency and power consumption.

The interplay between wider color formats and display pipelines is another area of active research. Display stream compression (DSC), standardized by VESA, enables real-time transmission of HDR content over limited-bandwidth interfaces such as HDMI and DisplayPort. DSC employs predictive coding and entropy coding to achieve lossless or near-lossless compression, with a typical compression ratio of 3:1. The algorithm operates on small blocks of pixels, updating predictions based on previously encoded data. This approach aligns well with the tile-based rendering architectures employed by many GPUs, where the screen is divided into smaller regions for parallel processing.

Color grading and post-processing workflows also benefit from wider color formats. Professional applications often employ 16-bit floating-point (FP16) or even 32-bit floating-point (FP32) representations to preserve precision during intermediate calculations. For instance, the Academy Color Encoding System (ACES) uses a half-float EXR container to store scene-referred imagery, ensuring compatibility across diverse production pipelines. Modern GPUs support these formats natively, with FP16 arithmetic often executed at twice the rate of FP32 operations due to optimized hardware pathways.

The challenges of wider color formats extend to real-time rendering, where performance constraints necessitate trade-offs between quality and efficiency. Temporal anti-aliasing (TAA) and other temporal reconstruction techniques must account for high-precision color data to avoid ghosting or banding artifacts. This is particularly relevant in HDR rendering, where subtle luminance variations are more perceptible. The integration of wider color

formats with existing rendering pipelines requires careful consideration of quantization, dithering, and gamma correction. For example, the sRGB transfer function, commonly used for SDR content, is defined as:

$$C_{\text{sRGB}} = \begin{cases} 12.92 C_{\text{linear}} & C_{\text{linear}} \leq 0.0031308 \\ 1.055 C_{\text{linear}}^{1/2.4} - 0.055 & \text{otherwise} \end{cases}$$

where  $C_{\text{linear}}$  is the linear color value. Modern GPUs often implement these transfer functions as lookup tables (LUTs) or piecewise approximations to balance accuracy and performance.

In summary, the adoption of wider color formats in modern GPU architectures is driven by the demands of HDR and advanced color management. These formats enable higher precision, broader gamuts, and improved perceptual fidelity, but also introduce challenges in terms of memory bandwidth, computational complexity, and display compatibility. Innovations in compression, tone mapping, and hardware acceleration continue to address these challenges, ensuring that GPUs remain capable of meeting the evolving needs of content creators and consumers alike. The integration of these technologies into unified rendering pipelines underscores the importance of interdisciplinary collaboration between hardware designers, software developers, and color scientists.

### 19.3.2 Tone mapping strategies

Tone mapping is a critical process in modern GPU architectures, particularly in the context of high dynamic range (HDR) imaging and color management. As display technologies advance, the need for efficient tone mapping strategies to handle wider color formats, such as Rec. 2020 and DCI-P3, becomes increasingly important. This discussion focuses on the mathematical foundations, hardware implementations, and algorithmic optimizations of tone mapping in GPUs.

The primary goal of tone mapping is to compress the dynamic range of an HDR image to fit within the limitations of a standard dynamic range (SDR) display while preserving perceptual quality. This is achieved through a combination of global and local operators. Global operators apply a uniform transformation to all pixels, while local operators adapt the transformation based on spatial context.

A widely used global operator is the Reinhard tone mapping operator , defined as:

$$L_d = \frac{L_w}{1 + L_w} \cdot L_{white}^2$$

where  $L_d$  is the display luminance,  $L_w$  is the world luminance, and  $L_{white}$  is the luminance of the brightest pixel. This equation ensures that highlights are preserved without clipping.

For local operators, the bilateral filter is often employed to avoid halo artifacts . The filtered luminance  $L_f$  is computed as:

$$L_f(x, y) = \frac{\sum_{i,j} w(i, j) \cdot L_w(x + i, y + j)}{\sum_{i,j} w(i, j)}$$

where  $w(i, j)$  is a weighting function that combines spatial and range terms. Modern GPUs accelerate these computations using parallel architectures, such as NVIDIA’s CUDA or AMD’s ROCm, leveraging thousands of cores for real-time performance.

In the context of wider color formats, tone mapping must also account for color gamut differences. The Rec. 2020 color space, for example, encompasses a significantly larger gamut than sRGB. To avoid color distortion, tone mapping is often performed in a perceptually uniform space like CIELAB or CIECAM02 . The transformation from RGB to CIELAB involves intermediate steps through XYZ space:

$$\begin{bmatrix} X \\ Y \\ Z \end{bmatrix} = M \cdot \begin{bmatrix} R \\ G \\ B \end{bmatrix}$$

where  $M$  is a transformation matrix specific to the color space. Once in CIELAB, luminance compression can be applied independently of chromaticity, preserving color fidelity. GPU implementations often use lookup tables (LUTs) or piecewise linear approximations to accelerate these transformations.

Hardware acceleration of tone mapping in modern GPUs is achieved through dedicated fixed-function units and programmable shaders. For example, NVIDIA’s Turing architecture includes a dedicated HDR processing pipeline with support for 10-bit and 12-bit color depths . The following Verilog-like pseudocode illustrates a simplified tone mapping unit:

## Code Sample 19.4: Tone Mapping Unit

```

module tone_mapper (
    input [31:0] luminance_in,
    input [31:0] white_point,
    output [31:0] luminance_out
);
    assign luminance_out = (luminance_in * white_point) / (luminance_in + white_point);
endmodule

```

This module implements the Reinhard operator from 19.3.2 in hardware. For wider color formats, GPUs often employ multiple tone mapping units operating in parallel, each handling a separate color channel or region of the image. This parallelism is crucial for maintaining high frame rates in real-time applications like gaming or video playback.

Recent research has explored machine learning-based tone mapping strategies, where convolutional neural networks (CNNs) are trained to predict optimal tone curves. These models are typically implemented using GPU-accelerated frameworks like TensorFlow or PyTorch. A CNN-based tone mapper can be described as:

$$L_d = f_\theta(L_w)$$

where  $f_\theta$  represents the neural network with parameters  $\theta$ . The advantage of this approach is its ability to adapt to complex scene content without manual parameter tuning. However, the computational overhead of CNNs necessitates careful optimization for real-time use, often involving quantization and pruning techniques.

In summary, tone mapping strategies in modern GPU architectures are multifaceted, combining mathematical rigor, hardware efficiency, and algorithmic innovation. Key considerations include:

- Dynamic range compression while preserving perceptual quality.
- Support for wider color formats through gamut-aware transformations.
- Hardware acceleration via fixed-function units and parallel processing.
- Emerging techniques like machine learning for adaptive tone mapping.

These advancements ensure that GPUs can meet the demands of next-generation displays and content, delivering visually compelling results across a range of applications. Future directions may include hybrid approaches that combine traditional operators with learned models, further optimizing the trade-off between quality and performance.

## 19.4 Thermal Considerations

### 19.4.1 Managing heat dissipation in GPU pipelines

Modern GPU architectures face significant thermal challenges due to increasing computational demands and shrinking transistor sizes. Managing heat dissipation in GPU pipelines is critical for maintaining performance, reliability, and energy efficiency. This discussion focuses on thermal considerations and hardware design strategies for mitigating heat in GPU pipelines.

The power density of modern GPUs has risen dramatically due to higher clock frequencies and parallel processing capabilities. The power dissipation  $P$  of a GPU can be modeled as:

$$P = C \cdot V^2 \cdot f$$

where  $C$  is the capacitance,  $V$  is the supply voltage, and  $f$  is the operating frequency. Reducing any of these parameters lowers power dissipation, but trade-offs exist between performance and thermal efficiency. Dynamic voltage and frequency scaling (DVFS) is a widely adopted technique to balance power and performance.

Thermal management in GPU pipelines involves several layers of optimization:

- **Pipeline partitioning:** Dividing the GPU into thermally independent regions reduces localized hotspots. For example, NVIDIA's Ampere architecture employs multiple streaming multiprocessors (SMs) with dedicated cooling paths .
- **Clock gating:** Disabling unused pipeline stages minimizes dynamic power dissipation. Modern GPUs use fine-grained clock gating to deactivate idle units, as shown in .
- **Power-aware scheduling:** Workload distribution algorithms prioritize thermally critical regions. Research by demonstrates that adaptive scheduling reduces peak temperatures by up to 15%.

Heat dissipation is also influenced by the physical design of GPU hardware. Advanced cooling solutions, such as vapor chambers and liquid cooling, are increasingly common. The thermal resistance  $R_{th}$  of a cooling system is given by:

$$R_{th} = \frac{T_j - T_a}{P}$$

where  $T_j$  is the junction temperature,  $T_a$  is the ambient temperature, and  $P$  is the power dissipation. Lower  $R_{th}$  values indicate more efficient cooling. For example, AMD's RDNA 3 architecture uses a hybrid vapor chamber design to achieve  $R_{th} < 0.15$  K/W .

Material selection plays a crucial role in thermal management. High thermal conductivity materials, such as graphene or diamond substrates, are being explored for future GPUs. The heat flux  $q$  through a material is governed by Fourier's law:

$$q = -k \cdot \nabla T$$

where  $k$  is the thermal conductivity and  $\nabla T$  is the temperature gradient. Materials with  $k > 500$  W/m·K, like diamond, significantly improve heat spreading .

On-chip sensors are essential for real-time thermal monitoring. Modern GPUs integrate distributed temperature sensors to detect hotspots and trigger throttling mechanisms. A typical sensor network is implemented as follows:

Code Sample 19.5: Temperature sensor network

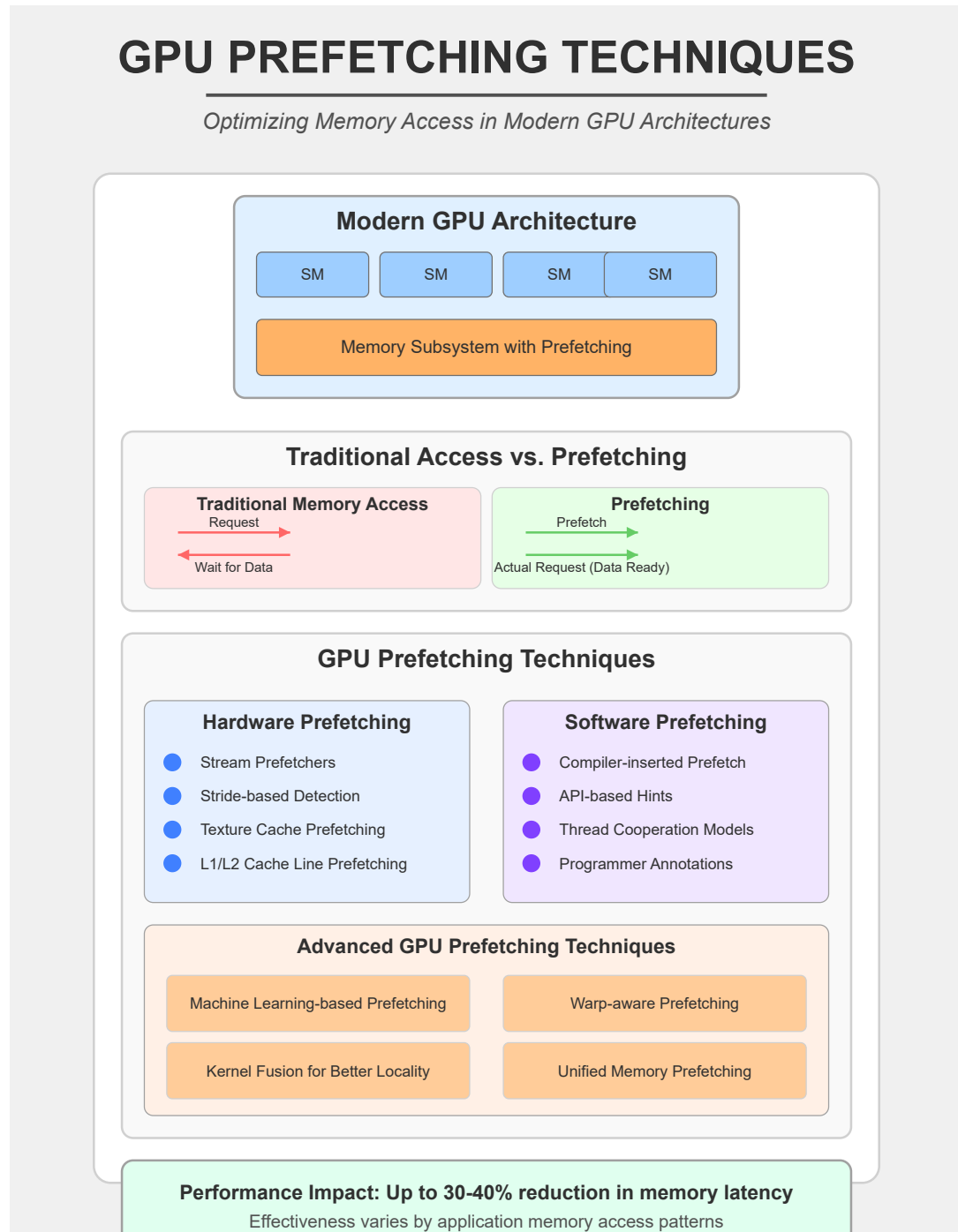
```
module temp_sensor (
    input clk,
    output reg [7:0] temp_out
);
    always @(posedge clk) begin
        temp_out <= read_thermal_diode();
    end
endmodule
```

These sensors enable dynamic thermal management (DTM), which adjusts clock frequencies or voltages in response to temperature changes .

Another key strategy is workload-aware thermal modeling. Analytical models, such as the HotSpot tool , predict temperature distributions based on power traces. The steady-state temperature  $T$  at a given location is approximated by:

$$T = T_a + P \cdot R_{th} + \sum_i P_i \cdot R_{th,i}$$

where  $P_i$  and  $R_{th,i}$  represent the power and thermal resistance of neighboring components. Such models guide floorplanning and cooling system design.



Emerging technologies like 3D-stacked GPUs introduce additional thermal challenges. Vertical integration increases power density, necessitating innovative cooling solutions. Research by demonstrates that microfluidic cooling channels between layers can reduce peak temperatures by 20% compared to conventional methods.

Finally, software optimizations complement hardware techniques. Compiler-directed pipeline balancing, as proposed by , reduces thermal imbalances by evenly distributing computational loads. This approach leverages static analysis to identify and mitigate thermally critical code paths.

In summary, managing heat dissipation in GPU pipelines requires a multi-disciplinary approach combining circuit design, materials science, and software optimization. Future advancements will likely focus on heterogeneous integration and adaptive cooling systems to address the growing thermal demands of GPU architectures.

### 19.4.2 Designing thermally efficient hardware

The design of thermally efficient hardware in modern GPU architectures is a critical challenge due to increasing power densities and performance demands. Thermal considerations directly impact reliability, performance, and energy efficiency, necessitating innovative solutions for heat dissipation in GPU pipelines. This discussion focuses on key principles, mathematical models, and practical implementations for managing thermal efficiency in GPUs.

The power dissipation of a GPU pipeline can be modeled using the general heat transfer equation:

$$P = \sum_{i=1}^n (C_i \cdot V_i^2 \cdot f_i) + P_{\text{leakage}}$$

where  $P$  is the total power,  $C_i$  is the capacitance of the  $i$ -th pipeline stage,  $V_i$  is the operating voltage,  $f_i$  is the clock frequency, and  $P_{\text{leakage}}$  accounts for static power dissipation. Minimizing  $P$  requires optimizing  $V_i$  and  $f_i$  while reducing  $C_i$  through architectural improvements.

One approach to thermal efficiency is dynamic voltage and frequency scaling (DVFS), which adjusts  $V_i$  and  $f_i$  based on workload demands. Research by demonstrates that DVFS reduces peak temperatures by up to 15% in modern GPUs. The thermal-aware scheduling algorithm proposed by further refines this by incorporating pipeline stall predictions:

$$T_{\text{new}} = T_{\text{current}} + \alpha \cdot \Delta P$$

where  $T_{\text{new}}$  is the updated temperature,  $T_{\text{current}}$  is the current temperature,  $\alpha$  is the thermal resistance coefficient, and  $\Delta P$  is the power change. This model enables real-time thermal management.

Another critical aspect is the design of the GPU's cooling system. Advanced heat sinks and vapor chambers are widely used to enhance heat dissipation. The effectiveness of a heat sink is quantified by its thermal resistance  $R_{\text{th}}$ :

$$R_{\text{th}} = \frac{T_{\text{junction}} - T_{\text{ambient}}}{P}$$

where  $T_{\text{junction}}$  is the junction temperature, and  $T_{\text{ambient}}$  is the ambient temperature. Lower  $R_{\text{th}}$  values indicate better cooling performance. Research shows that microchannel heat sinks reduce  $R_{\text{th}}$  by 20% compared to traditional designs.

Pipeline balancing is another technique to mitigate thermal hotspots. By distributing computational load evenly across pipeline stages, localized heating is minimized. The thermal imbalance metric  $\beta$  is defined as:

$$\beta = \max \left( \frac{T_i - \bar{T}}{\bar{T}} \right)$$

where  $T_i$  is the temperature of the  $i$ -th stage, and  $\bar{T}$  is the average temperature. A balanced pipeline achieves  $\beta < 0.1$ , as demonstrated by .

In hardware design, material selection plays a pivotal role. High thermal conductivity materials like silicon carbide (SiC) and diamond-like carbon (DLC) are increasingly used for GPU substrates. The thermal conductivity  $k$  of these materials is given by:

$$k = \frac{Q \cdot L}{A \cdot \Delta T}$$

where  $Q$  is the heat flux,  $L$  is the thickness,  $A$  is the cross-sectional area, and  $\Delta T$  is the temperature gradient. SiC exhibits  $k \approx 490 \text{ W/mK}$ , significantly higher than traditional silicon.

Thermal vias are another architectural feature to enhance heat dissipation. These are vertical interconnects that transfer heat from the GPU die to the heat spreader. The thermal via resistance  $R_{\text{via}}$  is:

$$R_{\text{via}} = \frac{t}{k_{\text{via}} \cdot A_{\text{via}}}$$

where  $t$  is the via thickness,  $k_{\text{via}}$  is the via material conductivity, and  $A_{\text{via}}$  is the via cross-sectional area. Copper vias with  $k_{\text{via}} = 400 \text{ W/mK}$  are commonly used.

Power gating is a technique to reduce leakage power  $P_{\text{leakage}}$  by shutting off unused pipeline stages. The leakage power is modeled as:

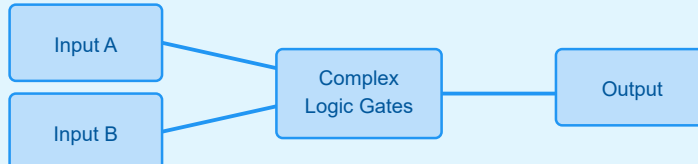
$$P_{\text{leakage}} = I_{\text{leak}} \cdot V_{\text{dd}}$$

where  $I_{\text{leak}}$  is the leakage current, and  $V_{\text{dd}}$  is the supply voltage. Power gating reduces  $I_{\text{leak}}$  by up to 90%, as shown by .

# Reducing Combinational Logic in Modern GPUs

Optimization Techniques for Efficient GPU Architecture

## Traditional Combinational Logic



## Optimization Techniques

### 1. Boolean Minimization

Simplifying complex expressions using Karnaugh maps and Quine–McCluskey

### 2. Look-Up Tables (LUTs)

Pre-computing results instead of calculating them with logic gates

### 3. Shared Logic Resources

Time-division multiplexing of computational units across compute tasks

## Modern GPU Implementation

Shader Units  
with LUTs

Tensor Cores  
Optimized Logic

Ray Tracing  
Units

Shared Combinational Logic Pool  
Dynamic Resource Allocation

**Benefits:** Reduced Power Consumption, Higher Clock Speeds, Smaller Die Size

Modern GPUs also employ predictive thermal management (PTM) to anticipate thermal bottlenecks. PTM uses machine learning models to predict future temperatures based on historical data. The prediction error  $\epsilon$  is minimized using gradient descent:

$$\epsilon = \frac{1}{N} \sum_{i=1}^N (T_{\text{predicted}} - T_{\text{actual}})^2$$

where  $N$  is the number of samples. PTM reduces thermal violations by 30%, according to .

The following Verilog snippet illustrates a thermal-aware clock gating module:

Code Sample 19.6: Thermal-aware clock gating

```
module thermal_clock_gating (
    input wire clk,
    input wire [7:0] temp_sensor,
    output reg gated_clk
);
    always @ (posedge clk) begin
        if (temp_sensor > 8'h80)
            gated_clk <= 1'b0;
        else
            gated_clk <= 1'b1;
    end
endmodule
```

Key considerations for thermally efficient GPU design include:

- Minimizing power dissipation through DVFS and pipeline balancing.
- Optimizing cooling systems with advanced materials and thermal vias.
- Reducing leakage power via power gating and predictive thermal management.
- Implementing real-time thermal monitoring and control mechanisms.

The integration of these techniques ensures that modern GPUs achieve high performance while maintaining thermal efficiency. Future research directions include nanofluidic cooling and 3D-printed heat sinks, which promise further improvements in heat dissipation. The mathematical models and hardware implementations discussed here provide a foundation for advancing thermally efficient GPU architectures.



# Chapter 20

## Case Studies

### 20.1 Minimalistic GPU

#### 20.1.1 A stripped-down design for teaching

Modern GPU architectures have evolved into highly complex systems optimized for performance and power efficiency. However, their complexity often obscures fundamental principles, making them challenging to teach. A stripped-down design for teaching, particularly in the context of minimalistic GPU architectures, serves as an effective pedagogical tool by isolating core concepts while eliminating unnecessary complexity. This approach aligns with educational methodologies that emphasize simplicity and clarity, as demonstrated by prior work in computer architecture education.

A minimalistic GPU design typically focuses on a simplified set of components: Streaming Multiprocessors (SMs) with fewer cores and reduced instruction-level parallelism, a basic memory hierarchy using only L1 and shared memory, a straightforward warp scheduler without speculative execution, and a reduced instruction set architecture (ISA) tailored for teaching.

The stripped-down design emphasizes modularity, enabling students to incrementally build understanding. For example, a minimal GPU may implement only single-precision floating-point operations, omitting double-precision or specialized tensor cores. This simplification reduces the cognitive load while preserving essential parallelism concepts.

The design can be described mathematically by modeling the throughput of a simplified SM:

$$T = N_{\text{cores}} \times f_{\text{clock}} \times IPC$$

where  $T$  is the throughput,  $N_{\text{cores}}$  is the number of cores,  $f_{\text{clock}}$  is the clock frequency, and  $IPC$  is the instructions per cycle.

A minimalistic GPU can be implemented in hardware description languages like Verilog for hands-on learning. Below is a simplified Verilog snippet for a basic SM:

Code Sample 20.1: Minimalistic SM Core

```
module sm_core (
    input clk,
    input [31:0] instr,
    output [31:0] result
);
    reg [31:0] reg_file [0:31];
    always @ (posedge clk) begin
        case (instr[31:26])
            6'b000000: result <= reg_file[instr[25:21]] + reg_file[instr[20:16]];
            6'b000001: result <= reg_file[instr[25:21]] - reg_file[instr[20:16]];
            default: result <= 32'b0;
        endcase
    end
endmodule
```

The memory hierarchy in a teaching-focused GPU often omits features like victim caches or prefetching. Instead, it uses a direct-mapped or small set-associative L1 cache with a simple replacement policy such as FIFO.

Shared memory is banked and accessible to threads within a block, while global memory is simulated with high latency to emphasize the impact of memory bottlenecks.

The performance impact of such a hierarchy can be approximated using the average memory access time (AMAT):

$$AMAT = t_{\text{hit}} + r_{\text{miss}} \times t_{\text{miss}}$$

where  $t_{\text{hit}}$  is the hit time,  $r_{\text{miss}}$  is the miss rate, and  $t_{\text{miss}}$  is the miss penalty.

Thread scheduling in a minimalistic GPU avoids complex strategies like dynamic warp formation or priority-based scheduling. Instead, a round-robin scheduler selects warps in a fixed order, as shown below:

Code Sample 20.2: Round-Robin Warp Scheduler

```
for (i = 0; i < num_warps; i++) {
    if (warps[i].ready) {
        execute(warps[i]);
        break;
    }
}
```

The instruction set of a teaching GPU is deliberately limited to foundational operations. It may include arithmetic instructions such as ADD, SUB, and MUL; memory operations like LD and ST; and basic control flow instructions such as BRA and CALL. This mirrors the success of RISC-V in CPU education, where a reduced ISA facilitates comprehension.

This simplicity also makes compiler development more accessible. A compiler targeting such a GPU can generate concise and readable code:

Code Sample 20.3: Generated Code for Minimal GPU

```
ADD r1, r2, r3
LD r4, [r1]
MUL r5, r4, r2
```

The pedagogical benefits of a minimalistic GPU design are well supported by educational research. Simplified models improve retention and conceptual clarity, particularly in parallel computing. By emphasizing core principles, students gain foundational knowledge that generalizes to real-world GPU architectures.

Energy efficiency can also be explored within this framework. A simple power model such as

$$P = C \times V^2 \times f$$

allows students to investigate trade-offs between performance and power without delving into advanced techniques like dynamic voltage and frequency scaling.

In summary, a stripped-down GPU design for teaching prioritizes clarity over complexity. It supports incremental learning and encourages experimentation, preparing students for deeper engagement with commercial GPU architectures. This approach is consistent with best practices in computer architecture pedagogy and facilitates a more intuitive understanding of parallel computing systems.

## 20.2 Intermediate GPU

### 20.2.1 Design matching early 2000s fixed-function pipelines

The evolution of GPU architecture from the early 2000s to modern designs reflects a shift from fixed-function pipelines to programmable, highly parallel structures. Early 2000s GPUs, such as NVIDIA's GeForce 3 or ATI's Radeon 8500, relied on fixed-function pipelines where each stage—vertex processing, rasterization, texture mapping, and pixel shading—was implemented as a dedicated hardware unit. These pipelines were optimized for specific tasks, enabling high performance for graphics workloads but lacking flexibility.

Modern GPUs, in contrast, employ unified shader architectures, where programmable cores handle all stages of the pipeline, enabling general-purpose computation (GPGPU) and advanced rendering techniques. Intermediate GPUs, such as those from the mid-2000s, bridged this gap by introducing limited programmability while retaining fixed-function elements.

Fixed-function pipelines in early 2000s GPUs were designed to match the graphics API requirements of the time, such as DirectX 8.1 and OpenGL 1.4. The vertex pipeline transformed 3D coordinates into 2D screen space using matrix operations:

$$\mathbf{v}' = \mathbf{M}_{\text{projection}} \cdot \mathbf{M}_{\text{view}} \cdot \mathbf{M}_{\text{model}} \cdot \mathbf{v}$$

where  $\mathbf{v}$  is the input vertex and  $\mathbf{v}'$  is the transformed vertex. The rasterizer then interpolated attributes across primitives, and the pixel pipeline applied textures and lighting models. These stages were hardwired, with minimal configurability. For example, texture filtering modes were selectable, but the underlying arithmetic was fixed.

The following Verilog snippet illustrates a simplified texture unit:

Code Sample 20.4: Fixed-function texture unit

```
module texture_unit (
    input [31:0] uv,
    input [2:0] filter_mode,
    output [31:0] texel
);
    reg [31:0] tex_mem[0:1023];
    always @(*) begin
        case(filter_mode)
            3'b000: texel = tex_mem[uv]; // Nearest
            3'b001: texel = bilinear_filter(uv); // Bilinear
            default: texel = 32'h0;
        endcase
    end
endmodule
```

Intermediate GPUs, such as NVIDIA's GeForce 6800 or ATI's X1800, introduced programmable shaders while retaining fixed-function components. Vertex and pixel shaders could be written in high-level languages like HLSL or GLSL, but the pipeline stages remained largely sequential. The shader programs were executed on dedicated ALUs, with limited branching and memory access.

For instance, a pixel shader might compute per-pixel lighting as:

$$L = \sum_{i=1}^n \max(0, \mathbf{N} \cdot \mathbf{L}_i) \cdot C_i$$

where  $\mathbf{N}$  is the surface normal,  $\mathbf{L}_i$  is the light direction, and  $C_i$  is the light color. However, the rasterizer and texture units remained fixed-function.

Modern GPU architectures, such as NVIDIA's Turing or AMD's RDNA2, unify all pipeline stages into a single set of programmable cores. These designs leverage SIMD (Single Instruction, Multiple Thread) execution, where thousands of threads run concurrently. The fixed-function stages are either eliminated or reduced to auxiliary units. For example, rasterization is still fixed-function, but tessellation and ray tracing are handled by programmable cores.

The transition from fixed-function to programmable pipelines was driven by the need for flexibility and performance. Early fixed-function designs excelled at specific tasks but were inflexible. Intermediate GPUs introduced programmability while maintaining backward compatibility. Modern GPUs maximize parallelism and programmability, enabling applications beyond graphics, such as machine learning and scientific computing.

The evolution reflects broader trends in hardware design, where specialization gives way to general-purpose computation with domain-specific optimizations. For example, modern GPUs use tensor cores for AI workloads, blending fixed-function and programmable elements. This balance ensures high performance while retaining flexibility, a lesson learned from the limitations of early 2000s architectures.

## 20.3 Scaling Up

### 20.3.1 Modern GPU features

Modern GPU architectures have evolved significantly to meet the demands of parallel computing, particularly in scaling up performance for general-purpose GPU (GPGPU) tasks. A key feature enabling this scalability is the use of compute shaders, which allow programmers to harness the GPU's parallel processing capabilities beyond traditional graphics rendering. Compute shaders operate within the same execution environment as other shaders but are designed explicitly for non-graphical computations, providing fine-grained control over thread execution and memory access patterns. This flexibility has made them indispensable for GPGPU applications, ranging from scientific simulations to machine learning workloads.

The architectural foundation of modern GPUs is built upon thousands of small, efficient cores organized into streaming multiprocessors (SMs). Each SM contains multiple CUDA cores (in NVIDIA architectures) or compute

units (in AMD architectures), which execute instructions in a single-instruction, multiple-thread (SIMT) fashion. This design allows GPUs to handle thousands of threads concurrently, making them ideal for data-parallel workloads. The SIMT execution model diverges from traditional CPU architectures by grouping threads into warps (or wavefronts in AMD GPUs), where all threads in a warp execute the same instruction simultaneously. This approach maximizes throughput but requires careful consideration of branch divergence to avoid performance penalties.

Memory hierarchy plays a critical role in GPU performance, especially for compute shaders and GPGPU tasks. Modern GPUs employ a multi-tiered memory system consisting of global memory, shared memory, registers, and constant and texture memory. Global memory is high-latency and high-bandwidth, accessible by all threads. Shared memory is low-latency, on-chip memory shared among threads within a thread block. Registers are the fastest storage, private to each thread. Constant and texture memory are cached read-only memory optimized for specific access patterns. Efficient utilization of these memory tiers is essential for achieving peak performance. For instance, shared memory can reduce global memory bandwidth pressure by enabling data reuse among threads, as shown in .

Compute shaders leverage these architectural features through explicit programming interfaces. In CUDA, for example, kernels are launched with a grid of thread blocks, where each block contains a fixed number of threads. The programmer specifies the grid and block dimensions to match the problem's parallelism. A typical kernel launch might resemble:

Code Sample 20.5: CUDA Kernel Launch

```
kernel<<<gridDim, blockDim>>>(args);
```

Here, `gridDim` and `blockDim` define the execution configuration, while `args` are passed to the kernel. Compute shaders in OpenGL or Vulkan follow a similar paradigm but are integrated into the graphics pipeline, allowing hybrid compute-graphics workflows.

One of the most significant advancements in modern GPU features is support for heterogeneous computing, where GPUs work alongside CPUs to accelerate workloads. This is facilitated by frameworks like OpenCL and SYCL, which provide portable abstractions for GPU programming. OpenCL, for instance, defines a platform model consisting of host (CPU) and device (GPU) components, connected through command queues. The host submits kernels to these queues, and the device executes them asynchronously. This model enables efficient task partitioning, where the CPU handles control-intensive tasks while the GPU processes data-parallel regions .

Another critical feature is hardware-accelerated atomic operations, which are essential for parallel reductions and histogram computations. Modern GPUs provide atomic functions for arithmetic (e.g., `atomicAdd`) and logical operations (e.g., `atomicCAS`), implemented directly in hardware to minimize contention. These operations are particularly useful in compute shaders where threads must coordinate updates to shared data structures. For example, an atomic addition can be expressed in CUDA as:

Code Sample 20.6: Atomic Addition in CUDA

```
atomicAdd(&shared_var, value);
```

Dynamic parallelism is another innovation, allowing kernels to launch other kernels without host intervention. This feature reduces CPU-GPU synchronization overhead and enables recursive algorithms to be implemented more efficiently. In CUDA, dynamic parallelism is supported through the `cudaLaunchKernel` API, which can be called from device code. This capability is particularly beneficial for algorithms with irregular parallelism, such as adaptive mesh refinement or tree traversals .

Modern GPUs also incorporate tensor cores and ray-tracing cores for specialized workloads. Tensor cores, introduced in NVIDIA's Volta architecture, accelerate matrix operations critical to deep learning. These cores perform mixed-precision matrix multiply-accumulate (MMA) operations in a single instruction, significantly boosting performance for neural network training and inference. The MMA operation can be represented as:

$$\mathbf{D} = \mathbf{A} \times \mathbf{B} + \mathbf{C}$$

where **A**, **B**, and **C** are input matrices, and **D** is the result. Tensor cores exploit the inherent parallelism in linear algebra to achieve teraflops of throughput .

Ray-tracing cores, on the other hand, accelerate bounding volume hierarchy (BVH) traversals and ray-triangle intersections, enabling real-time ray tracing. These cores offload computationally intensive tasks from the shader cores, allowing hybrid rasterization-ray-tracing pipelines. The intersection test between a ray  $\mathbf{r}(t) = \mathbf{o} + t\mathbf{d}$  and a

triangle  $\{\mathbf{v}_0, \mathbf{v}_1, \mathbf{v}_2\}$  can be formulated using the Möller-Trumbore algorithm:

$$\begin{bmatrix} t \\ u \\ v \end{bmatrix} = \frac{1}{(\mathbf{e}_1 \times \mathbf{d}) \cdot \mathbf{e}_2} \begin{bmatrix} (\mathbf{q} \times \mathbf{e}_2) \cdot \mathbf{e}_1 \\ (\mathbf{e}_1 \times \mathbf{d}) \cdot \mathbf{q} \\ (\mathbf{d} \times \mathbf{e}_2) \cdot \mathbf{q} \end{bmatrix}$$

where  $\mathbf{e}_1 = \mathbf{v}_1 - \mathbf{v}_0$ ,  $\mathbf{e}_2 = \mathbf{v}_2 - \mathbf{v}_0$ , and  $\mathbf{q} = \mathbf{o} - \mathbf{v}_0$ .

Scaling up GPU performance for compute shaders and GPGPU tasks requires addressing several challenges, including memory bandwidth limitations, power constraints, and workload imbalance. Techniques such as warp specialization, where different warps execute distinct tasks, can improve resource utilization. Additionally, recent architectures like NVIDIA's Ampere and AMD's RDNA3 introduce hardware-accelerated scheduling and improved cache hierarchies to further enhance scalability. These advancements ensure that modern GPUs remain at the forefront of high-performance computing, enabling breakthroughs in fields ranging from computational fluid dynamics to artificial intelligence.

### 20.3.2 Compute shaders

Compute shaders represent a fundamental shift in modern GPU architecture, enabling general-purpose computing (GPGPU) tasks beyond traditional graphics rendering. Their design leverages the parallel processing capabilities of GPUs, which have evolved to include thousands of cores optimized for high-throughput computations. Unlike traditional shaders, compute shaders operate without a predefined pipeline, allowing arbitrary data-parallel workloads. This flexibility has made them indispensable in fields such as scientific computing, machine learning, and real-time simulations.

The architecture of modern GPUs is built around streaming multiprocessors (SMs), each containing multiple CUDA cores (NVIDIA) or compute units (AMD). These SMs execute threads in warps or wavefronts, groups of 32 or 64 threads, respectively. Compute shaders exploit this architecture by dispatching workgroups, which are subdivided into smaller thread blocks for execution. The efficiency of compute shaders stems from their ability to coordinate memory access patterns and synchronization primitives, such as barriers, to maximize throughput. For example, NVIDIA's Volta architecture introduced independent thread scheduling, allowing finer-grained control over thread execution.

Memory hierarchy plays a critical role in compute shader performance. Modern GPUs feature several memory tiers: global memory (high-latency, high-bandwidth), shared memory (low-latency, per-SM), and registers (fastest, per-thread). Compute shaders optimize memory access by leveraging shared memory for inter-thread communication, reducing global memory bandwidth pressure. This is formalized in the roofline model, where performance is bounded by either compute throughput or memory bandwidth. The achievable performance  $P$  is described as:

$$P \leq \min(\pi, \beta \cdot I)$$

where  $\pi$  is peak compute performance,  $\beta$  is memory bandwidth, and  $I$  is operational intensity.

Scaling compute shaders across modern GPU architectures involves addressing several challenges. Workload imbalance arises due to divergent execution paths. Memory contention occurs in shared resources. Synchronization overheads also limit scalability. Solutions include dynamic parallelism, where kernels launch sub-kernels, and persistent threads, which reuse threads for multiple tasks. AMD's RDNA 3 architecture introduces wave32 and wave64 modes to better match workload characteristics. Additionally, hardware-accelerated atomic operations and reduced-precision math (e.g., FP16, INT8) further enhance scalability.

Compute shaders are widely used in GPGPU tasks such as physics simulations, image processing, and machine learning. For example, matrix multiplications can be implemented using compute shaders. The following HLSL code illustrates a simple kernel:

Code Sample 20.7: Matrix Multiplication in HLSL

```
[numthreads(16, 16, 1)]
void CS_Mul(uint3 id : SV_DispatchThreadID) {
    float sum = 0;
    for (int k = 0; k < N; k++) {
        sum += A[id.x][k] * B[k][id.y];
    }
    C[id.x][id.y] = sum;
}
```

Modern GPU features like tensor cores and matrix engines accelerate compute shader workloads. Tensor cores specialize in mixed-precision matrix operations, achieving up to 125 TFLOPS in NVIDIA's Hopper architecture . Theoretical throughput  $T$  is modeled as:

$$T = C \cdot F \cdot O$$

where  $C$  is core count,  $F$  is frequency, and  $O$  is operations per cycle.

Synchronization in compute shaders is critical for correctness. GPUs provide memory fences and atomic operations to coordinate thread execution. A reduction kernel might use tree-based summation with shared memory:

Code Sample 20.8: Reduction Kernel in HLSL

```
groupshared float buffer[256];
[numthreads(256, 1, 1)]
void CS_Reduce(uint id : SV_GroupThreadID) {
    buffer[id] = input[GroupID.x * 256 + id];
    GroupMemoryBarrier();
    for (uint s = 128; s > 0; s >>= 1) {
        if (id < s) buffer[id] += buffer[id + s];
        GroupMemoryBarrier();
    }
    if (id == 0) output[GroupID.x] = buffer[0];
}
```

The evolution of GPU architectures has also introduced hardware ray tracing cores and AI denoising, which intersect with compute shader workflows. Hybrid rendering pipelines combine rasterization with compute-based ray tracing. Intersection test performance is given by:

$$R = \frac{N}{\tau \cdot P}$$

where  $N$  is ray count,  $\tau$  is traversal cost, and  $P$  is parallel cores.

Energy efficiency is another consideration in scaling compute shaders. Modern GPUs employ clock gating and power-aware scheduling to minimize energy consumption per operation. AMD's CDNA architecture uses Infinity Cache to reduce memory power usage . The energy  $E$  per operation is modeled as:

$$E = \frac{P_{\text{total}}}{T_{\text{ops}}}$$

where  $P_{\text{total}}$  is total power and  $T_{\text{ops}}$  is operation throughput.

In summary, compute shaders are a cornerstone of modern GPU architecture, enabling scalable GPGPU tasks through advanced parallelism, memory hierarchies, and specialized hardware. Their continued evolution will drive innovations in real-time computing and beyond.

### 20.3.3 GPGPU tasks

Compute shaders represent a fundamental shift in modern GPU architecture, enabling general-purpose computing (GPGPU) tasks beyond traditional graphics rendering. Their design leverages the parallel processing capabilities of GPUs, which have evolved to include thousands of cores optimized for high-throughput computations. Unlike traditional shaders, compute shaders operate without a predefined pipeline, allowing arbitrary data-parallel workloads. This flexibility has made them indispensable in fields such as scientific computing, machine learning, and real-time simulations.

The architecture of modern GPUs is built around streaming multiprocessors (SMs), each containing multiple CUDA cores (NVIDIA) or compute units (AMD). These SMs execute threads in warps or wavefronts, groups of 32 or 64 threads, respectively. Compute shaders exploit this architecture by dispatching workgroups, which are subdivided into smaller thread blocks for execution. The efficiency of compute shaders stems from their ability to coordinate memory access patterns and synchronization primitives, such as barriers, to maximize throughput. For example, NVIDIA's Volta architecture introduced independent thread scheduling, allowing finer-grained control over thread execution .

Memory hierarchy plays a critical role in compute shader performance. Modern GPUs feature several memory tiers, including global memory, shared memory, and registers. Compute shaders optimize memory access by leveraging shared memory for inter-thread communication, reducing global memory bandwidth pressure. This

is formalized in the roofline model, where performance is bounded by either compute throughput or memory bandwidth. The achievable performance  $P$  is described as:

$$P \leq \min(\pi, \beta \cdot I)$$

where  $\pi$  is peak compute performance,  $\beta$  is memory bandwidth, and  $I$  is operational intensity.

Scaling compute shaders across modern GPU architectures involves addressing several challenges. Workload imbalance arises due to divergent execution paths. Memory contention occurs in shared resources. Synchronization overheads also limit scalability. Solutions include dynamic parallelism, where kernels launch sub-kernels, and persistent threads, which reuse threads for multiple tasks. AMD's RDNA 3 architecture introduces wave32 and wave64 modes to better match workload characteristics. Additionally, hardware-accelerated atomic operations and reduced-precision math (e.g., FP16, INT8) further enhance scalability.

Compute shaders are widely used in GPGPU tasks such as physics simulations, image processing, and machine learning. For example, matrix multiplications can be implemented using compute shaders. The following HLSL code illustrates a simple kernel:

Code Sample 20.9: Matrix Multiplication in HLSL

```
[numthreads(16, 16, 1)]
void CS_Mul(uint3 id : SV_DispatchThreadID) {
    float sum = 0;
    for (int k = 0; k < N; k++) {
        sum += A[id.x][k] * B[k][id.y];
    }
    C[id.x][id.y] = sum;
}
```

Modern GPU features like tensor cores and matrix engines accelerate compute shader workloads. Tensor cores specialize in mixed-precision matrix operations, achieving up to 125 TFLOPS in NVIDIA's Hopper architecture. Theoretical throughput  $T$  is modeled as:

$$T = C \cdot F \cdot O$$

where  $C$  is core count,  $F$  is frequency, and  $O$  is operations per cycle.

Synchronization in compute shaders is critical for correctness. GPUs provide memory fences and atomic operations to coordinate thread execution. A reduction kernel might use tree-based summation with shared memory:

Code Sample 20.10: Reduction Kernel in HLSL

```
groupshared float buffer[256];
[numthreads(256, 1, 1)]
void CS_Reduce(uint id : SV_GroupThreadID) {
    buffer[id] = input[GroupID.x * 256 + id];
    GroupMemoryBarrier();
    for (uint s = 128; s > 0; s >>= 1) {
        if (id < s) buffer[id] += buffer[id + s];
        GroupMemoryBarrier();
    }
    if (id == 0) output[GroupID.x] = buffer[0];
}
```

The evolution of GPU architectures has also introduced hardware ray tracing cores and AI denoising, which intersect with compute shader workflows. Hybrid rendering pipelines combine rasterization with compute-based ray tracing. Intersection test performance is given by:

$$R = \frac{N}{\tau \cdot P}$$

where  $N$  is ray count,  $\tau$  is traversal cost, and  $P$  is parallel cores.

Energy efficiency is another consideration in scaling compute shaders. Modern GPUs employ clock gating and power-aware scheduling to minimize energy consumption per operation. AMD's CDNA architecture uses Infinity Cache to reduce memory power usage. The energy  $E$  per operation is modeled as:

$$E = \frac{P_{\text{total}}}{T_{\text{ops}}}$$

where  $P_{\text{total}}$  is total power and  $T_{\text{ops}}$  is operation throughput.

In summary, compute shaders are a cornerstone of modern GPU architecture, enabling scalable GPGPU tasks through advanced parallelism, memory hierarchies, and specialized hardware. Their continued evolution will drive innovations in real-time computing and beyond.

## 20.4 Graphics Algorithms in Hardware

### 20.4.1 Implementing algorithms like Bresenham's line drawing

The implementation of graphics algorithms in hardware, particularly on modern GPU architectures, has evolved significantly to meet the demands of real-time rendering and computational efficiency. Algorithms like Bresenham's line drawing and Phong shading, once executed in software, are now optimized for hardware acceleration. This shift leverages the parallel processing capabilities of GPUs, enabling high-performance rendering pipelines.

Bresenham's line drawing algorithm, introduced by Jack E. Bresenham in 1965, is a fundamental rasterization technique for drawing lines on a pixel grid. The algorithm minimizes computational overhead by using integer arithmetic and incremental error calculations. In hardware, this translates to a streamlined pipeline where each pixel's position is computed iteratively. The algorithm can be expressed as:

```

Let  $(x_0, y_0)$  and  $(x_1, y_1)$  be the endpoints of the line.
Compute  $\Delta x = x_1 - x_0$ ,  $\Delta y = y_1 - y_0$ , and error =  $2\Delta y - \Delta x$ .
For each  $x$  from  $x_0$  to  $x_1$  :
    Plot  $(x, y)$ .
    If error  $\geq 0$ , increment  $y$  and update error by  $2(\Delta y - \Delta x)$ .
    Else, update error by  $2\Delta y$ .

```

Modern GPUs implement this algorithm in fixed-function rasterization units, where parallelism is achieved by processing multiple pixels simultaneously. The hardware optimizations include pipelining and SIMD (Single Instruction, Multiple Data) execution, reducing latency and improving throughput.

Phong shading, developed by Bui Tuong Phong in 1975, is a per-pixel lighting model that interpolates surface normals across a polygon and computes lighting at each fragment. The model is defined as:

$$I = I_a k_a + \sum_{i=1}^n I_i (k_d (\mathbf{L}_i \cdot \mathbf{N}) + k_s (\mathbf{R}_i \cdot \mathbf{V})^\alpha)$$

where  $I$  is the final intensity,  $I_a$  and  $I_i$  are ambient and light intensities,  $k_a$ ,  $k_d$ , and  $k_s$  are material coefficients,  $\mathbf{L}_i$  is the light direction,  $\mathbf{N}$  is the surface normal,  $\mathbf{R}_i$  is the reflection vector,  $\mathbf{V}$  is the view vector, and  $\alpha$  is the shininess exponent.

Hardware implementations of Phong shading leverage fragment shaders, which execute in parallel across all pixels. Modern GPUs use specialized units like Texture Mapping Units (TMUs) and Arithmetic Logic Units (ALUs) to compute dot products and exponentials efficiently.

The integration of these algorithms into hardware involves several key considerations:

**Parallelism:** GPUs exploit data parallelism by dividing workloads across thousands of cores. For Bresenham's algorithm, this means processing multiple line segments concurrently. For Phong shading, fragment shaders execute in parallel across all pixels.

**Pipelining:** The rendering pipeline is divided into stages (e.g., vertex processing, rasterization, fragment shading). Each stage operates independently, allowing overlapping execution. Bresenham's algorithm fits into the rasterization stage, while Phong shading resides in the fragment shading stage.

**Memory Access:** Efficient memory access patterns are critical. Bresenham's algorithm benefits from localized memory accesses, while Phong shading requires texture fetches and uniform buffer accesses. GPUs employ caching hierarchies to mitigate latency.

**Precision:** Fixed-point arithmetic is often used for Bresenham's algorithm to reduce hardware complexity. Phong shading, however, requires floating-point precision for accurate lighting calculations. Modern GPUs support both through dedicated hardware units.

Hardware descriptions for these algorithms can be illustrated using Verilog. Below is a simplified example of a Bresenham's line drawing module:

Code Sample 20.11: Bresenham's Algorithm in Verilog

```

module bresenham (
    input clk, reset,
    input [15:0] x0, y0, x1, y1,
    output reg [15:0] x, y,
    output reg plot
);
    reg [15:0] dx, dy, error;
    reg [15:0] x_next, y_next;
    reg plot_next;

    always @(posedge clk or posedge reset) begin
        if (reset) begin
            x <= x0;
            y <= y0;
            dx <= x1 - x0;
            dy <= y1 - y0;
            error <= 2 * dy - dx;
            plot <= 1;
        end else begin
            x <= x_next;
            y <= y_next;
            plot <= plot_next;
            if (x < x1) begin
                x_next <= x + 1;
                if (error >= 0) begin
                    y_next <= y + 1;
                    error <= error + 2 * (dy - dx);
                end else begin
                    error <= error + 2 * dy;
                end
                plot_next <= 1;
            end else begin
                plot_next <= 0;
            end
        end
    end
endmodule

```

For Phong shading, a fragment shader in GLSL demonstrates the hardware-friendly implementation:

Code Sample 20.12: Phong Shading in GLSL

```

#version 450 core
uniform vec3 lightPos;
uniform vec3 viewPos;
uniform float shininess;
in vec3 fragPos;
in vec3 fragNormal;
out vec4 fragColor;

void main() {
    vec3 lightDir = normalize(lightPos - fragPos);
    vec3 viewDir = normalize(viewPos - fragPos);
    vec3 reflectDir = reflect(-lightDir, fragNormal);
    float diff = max(dot(fragNormal, lightDir), 0.0);
    float spec = pow(max(dot(viewDir, reflectDir), 0.0), shininess);
    fragColor = vec4((diff + spec) * vec3(1.0), 1.0);
}

```

The evolution of GPU architectures has enabled these algorithms to achieve real-time performance. Research by and highlights the importance of hardware-software co-design in graphics pipelines. Modern GPUs, such as NVIDIA's Ampere and AMD's RDNA2 architectures, incorporate dedicated ray-tracing cores and AI accelera-

tors, further extending the capabilities of traditional rasterization algorithms. The continued optimization of these algorithms in hardware ensures their relevance in contemporary rendering systems.

### 20.4.2 Phong shading in hardware

Phong shading is a fundamental technique in computer graphics for rendering realistic lighting effects on 3D surfaces. It interpolates surface normals across polygons and computes per-pixel lighting, producing smoother results than Gouraud shading. Modern GPU architectures optimize Phong shading through parallel computation and specialized hardware pipelines.

The Phong reflection model combines ambient, diffuse, and specular components to simulate lighting. The specular component is computed using the reflection vector  $R$  and view vector  $V$ :

$$I_s = k_s \cdot (R \cdot V)^n$$

where  $k_s$  is the specular coefficient and  $n$  is the shininess exponent. In hardware, this calculation is parallelized across fragments. GPUs leverage SIMD (Single Instruction, Multiple Data) architectures to compute lighting for multiple pixels simultaneously. Fragment shaders evaluate this expression using interpolated normals from the vertex shader.

Modern GPUs implement Phong shading through programmable shader stages. The vertex shader transforms vertices and computes per-vertex normals, while the fragment shader interpolates these normals and applies the lighting model. The following pseudocode illustrates a simplified fragment shader for Phong shading:

Code Sample 20.13: Phong Shading Fragment Shader

```
void phong_shading(in vec3 normal, in vec3 light_dir, in vec3 view_dir) {
    vec3 reflect_dir = reflect(-light_dir, normal);
    float spec = pow(max(dot(reflect_dir, view_dir), 0.0), shininess);
    vec3 specular = specular_strength * spec * light_color;
    vec3 diffuse = max(dot(normal, light_dir), 0.0) * diffuse_color;
    vec3 ambient = ambient_strength * ambient_color;
    return ambient + diffuse + specular;
}
```

The hardware optimizations for Phong shading include parallel execution across fragments, texture units for storing precomputed lighting coefficients, and interpolation hardware for normals and attributes. These optimizations ensure high throughput and low latency during real-time rendering.

Bresenham's line drawing algorithm, another classic graphics algorithm, contrasts with Phong shading in hardware implementation. While Phong shading is fragment-bound, Bresenham's algorithm is rasterization-bound. GPUs handle line rasterization using fixed-function hardware, but programmable shaders can override this behavior. Bresenham's algorithm uses integer arithmetic to avoid floating-point calculations:

$$e_{k+1} = e_k + 2\Delta y - 2\Delta x \cdot \text{sign}(e_k)$$

This makes it well-suited to hardware implementations, though its relevance has diminished as graphics pipelines have evolved.

The evolution of GPU architectures has dramatically improved Phong shading performance. Early GPUs, such as the GeForce 256, used fixed-function pipelines that limited flexibility. The introduction of programmable shaders with DirectX 8.0 enabled dynamic Phong shading. Today, GPUs like NVIDIA's Ampere and AMD's RDNA 2 use unified shader cores to dynamically allocate resources between vertex and fragment shading. These architectures include ray tracing cores for reflective effects, tensor cores for denoising, and multi-tier cache hierarchies for data locality.

Memory bandwidth plays a vital role in Phong shading. Interpolated normals and lighting data require frequent memory access, so GPUs utilize caching strategies to maintain performance. The required bandwidth can be approximated by:

$$B = N \cdot (S_n + S_l) \cdot f$$

where  $N$  is the number of fragments,  $S_n$  the normal size,  $S_l$  the lighting data size, and  $f$  the frame rate.

Comparative studies show that Phong shading benefits more from modern GPU enhancements than Bresenham's algorithm. Phong shading scales with improvements in shader cores and memory subsystems, whereas Bresenham's algorithm, due to its simplicity and reliance on rasterization hardware, gains little from such advancements. Research from confirms real-time Phong shading for high-polygon scenes on modern GPUs.

In summary, Phong shading exemplifies the synergy between graphics algorithms and GPU architecture. It benefits from parallelism, programmable pipelines, and cache-optimized memory access. In contrast, Bresenham's algorithm remains efficient but largely static. As GPU architectures continue to evolve, techniques like Phong shading will gain further performance improvements through AI-driven denoising and real-time ray tracing integration.



# Chapter 21

## General-Purpose GPU Architectures

### 21.1 Transitioning from Graphics to Compute Workloads

#### 21.1.1 Differences in architectural design for GPGPU.

The evolution of modern GPU architectures has been driven by the transition from graphics-specific workloads to general-purpose computing (GPGPU). This shift has necessitated significant changes in architectural design, particularly in adapting GPU pipelines to support compute tasks while addressing challenges in balancing computation and memory bandwidth. Traditional GPUs were optimized for graphics rendering, featuring deep pipelines with fixed-function stages for vertex shading, rasterization, and fragment processing. In contrast, GPGPU architectures prioritize parallelism and throughput, requiring reconfigurable pipelines and enhanced memory hierarchies to accommodate diverse workloads.

One key difference lies in the execution model. Graphics workloads exhibit predictable, data-parallel patterns, whereas GPGPU tasks often involve irregular parallelism and dynamic control flow. Modern GPUs address this by employing Single Instruction, Multiple Thread (SIMT) execution, where warps or wavefronts of threads execute the same instruction in lockstep. However, divergent branches within a warp reduce efficiency, as inactive threads must be masked. To mitigate this, architectures like NVIDIA's Volta introduce Independent Thread Scheduling (ITS), allowing finer-grained control over thread execution. This adaptation improves performance for general-purpose workloads but complicates pipeline design by requiring additional hardware for thread synchronization and scheduling.

Memory hierarchy design also differs significantly between graphics and compute-focused GPUs. Graphics workloads benefit from localized memory access patterns, such as texture fetches with spatial coherence, enabling efficient caching. In contrast, GPGPU applications often exhibit irregular memory access, necessitating larger caches and higher bandwidth. For example, AMD's CDNA architecture incorporates Infinity Cache, a large last-level cache, to reduce off-chip memory traffic. However, increasing cache size introduces trade-offs in latency and power consumption. The challenge lies in optimizing the memory hierarchy for both latency-sensitive graphics tasks and bandwidth-hungry compute workloads.

Another architectural adaptation involves the balance between computation and memory bandwidth. Graphics pipelines are typically memory-bound due to texture sampling and frame buffer operations, while GPGPU workloads may be either compute-bound or memory-bound, depending on the algorithm. To address this, modern GPUs integrate specialized units such as Tensor Cores (e.g., NVIDIA's Ampere) for matrix operations, accelerating machine learning workloads without overloading the traditional shader cores. These units operate in parallel with the main pipeline, but their integration requires careful resource allocation to avoid contention. The following equation illustrates the memory bandwidth limitation for a compute kernel:

$$\text{Performance} = \min \left( \frac{\text{FLOPs}}{\text{CPI}}, \frac{\text{Bandwidth}}{\text{Bytes per FLOP}} \right) \quad (21.1)$$

Here,  $\text{CPI}$  (cycles per instruction) and  $\text{Bandwidth}$  determine whether the workload is compute-bound or memory-bound. Optimizing for both scenarios demands flexible architectures that can dynamically allocate resources.

The shift to GPGPU also impacts instruction set architecture (ISA) design. Traditional GPUs relied on proprietary, graphics-oriented ISAs, but GPGPU requires support for general-purpose programming models like CUDA and OpenCL. This has led to the adoption of scalar instruction pipelines alongside vector units, as seen in NVIDIA's PTX and AMD's GCN. Scalar pipelines simplify control flow handling, while vector units maximize throughput

for data-parallel tasks. However, this hybrid approach increases design complexity, as the pipeline must manage both scalar and vector instruction streams efficiently.

Power efficiency is another critical consideration. Graphics workloads often exhibit predictable power profiles, whereas GPGPU applications vary widely in computational intensity. Modern GPUs employ dynamic voltage and frequency scaling (DVFS) to adjust power delivery based on workload demands. For instance, NVIDIA's Turing architecture uses adaptive shading to reduce power consumption in graphics workloads, while GPGPU modes prioritize sustained throughput. Balancing these modes requires sophisticated power management circuits and thermal monitoring.

The following Verilog snippet illustrates a simplified memory controller for a GPGPU, highlighting the trade-offs between bandwidth and latency:

Code Sample 21.1: GPGPU Memory Controller

```
module memory_controller (
    input clk,
    input [31:0] addr,
    output [255:0] data
);
    reg [255:0] cache [0:1023];
    always @(posedge clk) begin
        data <= cache[addr[11:2]]; // 1KB cache line
    end
endmodule
```

This design prioritizes bandwidth by fetching large cache lines but may incur higher latency for random accesses. Real-world implementations, such as those in , use High-Bandwidth Memory (HBM) to mitigate this trade-off.

In summary, transitioning from graphics to compute workloads has reshaped GPU architectures in several ways:

Execution models have evolved from rigid pipelines to flexible SIMT designs with independent thread scheduling. Memory hierarchies now emphasize larger caches and higher bandwidth to accommodate irregular access patterns. Specialized units like Tensor Cores offload compute-intensive tasks, but their integration requires careful resource management. ISAs have expanded to support both scalar and vector instructions, increasing design complexity. Power management techniques must adapt to varying workload demands, balancing efficiency and performance.

These adaptations reflect the ongoing challenge of optimizing GPU architectures for both graphics and general-purpose computing, ensuring they remain versatile enough to handle diverse workloads while maximizing performance and efficiency.

### 21.1.2 Adapting GPU pipelines to support general-purpose tasks.

The evolution of modern GPU architectures has been driven by the increasing demand for general-purpose computing on graphics processing units (GPGPU). Initially designed for rendering graphics, GPUs have transitioned to support compute workloads due to their massively parallel architecture. This shift has necessitated significant changes in GPU pipeline design, memory hierarchy, and instruction execution models.

Traditional GPU pipelines were optimized for graphics workloads, which exhibit high spatial and temporal coherence. These pipelines consist of fixed-function stages such as vertex shading, rasterization, and pixel shading. However, general-purpose tasks lack such coherence, requiring a more flexible execution model. Modern GPUs address this by introducing programmable shader cores that can execute arbitrary compute kernels. For example, NVIDIA's CUDA and AMD's ROCm frameworks expose these cores to developers, enabling efficient execution of non-graphics workloads.

The architectural differences between graphics and compute workloads are profound. Graphics pipelines rely on SIMD (Single Instruction, Multiple Data) execution, where the same instruction is applied to multiple data elements. In contrast, GPGPU workloads often require MIMD (Multiple Instruction, Multiple Data) capabilities, where different threads execute divergent instructions. To accommodate this, modern GPUs employ SIMT (Single Instruction, Multiple Threads) execution, where threads are grouped into warps or wavefronts. Threads within a warp execute the same instruction but can follow divergent paths, managed by masking inactive threads. This approach balances efficiency and flexibility .

Memory access patterns also differ significantly. Graphics workloads exhibit predictable, streaming access patterns, while compute workloads often involve irregular, data-dependent accesses. GPUs address this by incorporating hierarchical memory systems with caches and scratchpad memories. The L1 and L2 caches are optimized for spatial locality, while scratchpad memories provide low-latency storage for frequently accessed data. However, balancing computation and memory bandwidth remains a challenge. High arithmetic intensity (FLOPs per byte) is required to hide memory latency, as described by the roofline model.

Adapting GPU pipelines for general-purpose tasks involves several key modifications. Unified shader cores replace fixed-function stages with programmable cores that handle both graphics and compute workloads. For instance, NVIDIA's Turing architecture integrates RT cores for ray tracing and Tensor cores for matrix operations, alongside traditional CUDA cores. Memory hierarchy enhancements include larger caches and configurable memory partitions. AMD's RDNA architecture introduces Infinity Cache, a high-bandwidth last-level cache, to reduce off-chip memory traffic. Thread scheduling improvements such as dynamic warp scheduling and preemption mechanisms allow GPUs to better handle divergent control flow. NVIDIA's Volta architecture introduces independent thread scheduling, enabling finer-grained parallelism.

The transition to GPGPU has also exposed challenges in balancing computation and memory bandwidth. While GPU peak FLOP rates have grown exponentially, memory bandwidth improvements have lagged. This imbalance is quantified by the arithmetic intensity threshold:

$$I_{\text{threshold}} = \frac{\text{Peak Memory Bandwidth}}{\text{Peak FLOP Rate}}$$

Workloads with intensity below  $I_{\text{threshold}}$  are memory-bound, while those above are compute-bound. Optimizing GPGPU applications often involves increasing arithmetic intensity through techniques like loop unrolling or data reuse.

Another challenge is the overhead of thread divergence. When threads within a warp follow different execution paths, the GPU serializes the divergent branches, reducing efficiency. This is mitigated by algorithms like prefix sums or reductions, which minimize divergence. The following Verilog snippet illustrates a simple warp scheduler:

Code Sample 21.2: Warp Scheduler

```
module warp_scheduler (
    input clk,
    input [31:0] active_mask,
    output reg [31:0] next_warp
);
always @(posedge clk) begin
    next_warp <= active_mask & (next_warp + 1);
end
endmodule
```

Energy efficiency is another critical consideration. GPUs achieve high throughput by leveraging parallelism, but this comes at the cost of increased power consumption. Techniques like dynamic voltage and frequency scaling (DVFS) and clock gating are employed to manage power. Research has shown that optimizing memory access patterns can reduce energy consumption by up to 30%.

In summary, adapting GPU pipelines for general-purpose tasks has required rethinking traditional graphics-centric designs. Unified shader cores, enhanced memory hierarchies, and improved thread scheduling have enabled GPUs to excel in compute workloads. However, challenges remain in balancing computation and memory bandwidth, minimizing thread divergence, and optimizing energy efficiency. Future architectures will likely continue this trend, further blurring the line between graphics and compute.

### 21.1.3 Challenges in balancing computation and memory bandwidth.

The transition from graphics to compute workloads in modern GPU architectures has introduced significant challenges in balancing computation and memory bandwidth. GPUs were originally designed for highly parallel graphics rendering, where workloads exhibit regular memory access patterns and predictable computation requirements. However, general-purpose GPU (GPGPU) computing demands irregular memory access and diverse computational patterns, exposing architectural limitations. The shift necessitates rethinking memory hierarchies, thread scheduling, and pipeline design to maintain efficiency.

One primary challenge lies in the mismatch between compute throughput and memory bandwidth. Modern GPUs, such as NVIDIA's Ampere and AMD's RDNA3, achieve teraflops of computational power but face bottlenecks when memory bandwidth cannot keep pace. For example, the theoretical peak performance of a GPU may be expressed as:

$$P = F \times C \times I \quad (21.2)$$

where  $P$  is peak performance,  $F$  is clock frequency,  $C$  is the number of cores, and  $I$  is instructions per cycle. However, actual performance is often limited by memory bandwidth  $B$ , as data must be fetched for computation. The roofline model illustrates this constraint:

$$P_{\text{actual}} \leq \min(P, B \times OI) \quad (21.3)$$

where  $OI$  is operational intensity (operations per byte). GPGPU workloads often exhibit low  $OI$ , exacerbating bandwidth limitations.

Architectural adaptations for GPGPU computing include:

**Memory Hierarchy Redesign:** Traditional GPUs relied on large caches and texture memory optimized for graphics. GPGPU workloads benefit from smaller, configurable caches and shared memory. For instance, NVIDIA's Volta architecture introduced unified cache hierarchies, allowing dynamic partitioning between L1 cache and shared memory. **Coalesced Memory Access:** Graphics workloads naturally coalesce memory accesses, but GPGPU code may scatter/gather data. Modern GPUs employ load-store units (LSUs) to merge irregular accesses, reducing bandwidth pressure. The effectiveness of coalescing is quantified by:

$$E = \frac{B_{\text{actual}}}{B_{\text{theoretical}}} \quad (21.4)$$

where  $E$  is coalescing efficiency. Poor coalescing ( $E \ll 1$ ) severely degrades performance. **Thread Scheduling:** Graphics pipelines use fixed warp/wavefront scheduling, while GPGPU workloads require dynamic scheduling to hide memory latency. AMD's CDNA architecture introduced asynchronous compute engines to better overlap computation and memory operations.

Differences in architectural design for GPGPU versus graphics workloads are evident in several areas:

**Register File Size:** Graphics shaders use small register files, but GPGPU kernels require larger ones to hold intermediate results. NVIDIA's Turing architecture doubled register file capacity per SM (streaming multiprocessor) compared to Pascal. **Predication and Branching:** Graphics workloads are largely branch-free, whereas GPGPU code contains divergent branches. GPUs now employ sophisticated predication and branch replay mechanisms to mitigate divergence penalties. **Atomic Operations:** GPGPU workloads frequently use atomics for synchronization, requiring hardware support. Modern GPUs implement hierarchical atomics with reduced contention, as shown in .

Adapting GPU pipelines for general-purpose tasks involves trade-offs. For example, tensor cores in NVIDIA GPUs accelerate matrix operations but are underutilized in non-AI workloads. Similarly, AMD's Infinity Cache reduces external memory bandwidth demands but increases die area. The balance between specialization and flexibility is critical. A theoretical model for pipeline adaptation is:

$$U = \frac{T_{\text{compute}}}{T_{\text{compute}} + T_{\text{memory}}} \quad (21.5)$$

where  $U$  is utilization, and  $T$  represents time spent in computation or memory stalls. High  $U$  indicates compute-bound workloads, while low  $U$  suggests memory-bound scenarios.

Challenges in balancing computation and bandwidth are further compounded by emerging workloads. Ray tracing, for instance, combines compute-intensive traversal with irregular memory access. Hybrid approaches, such as NVIDIA's RTX OptiX, combine hardware acceleration with software scheduling to address this. Similarly, sparse linear algebra workloads require both high FLOPs and efficient memory compression techniques.

Memory bandwidth optimization techniques include:

## Wider Color Formats in Modern GPUs

How modern GPUs process and render expanded color spaces for more vivid and accurate visuals

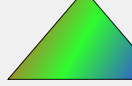
### Color Space Evolution

**sRGB**  
Standard 8-bit per channel



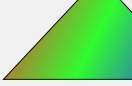
16.7 million colors

**Wide Gamut**  
10-bit per channel



1.07 billion colors

**HDR10+/Dolby Vision**  
12/16-bit per channel



68.7 billion+ colors

### Bit Depth Comparison

8-bit (sRGB)	256 values per channel
10-bit (Wide Color)	1,024 values per channel
12-bit (HDR10+)	4,096 values per channel
16-bit (Deep Color/Dolby Vision)	65,536 values

### GPU Hardware Requirements

**Memory Bandwidth**

- Higher bandwidth needed for wider formats
- GDDR6/GDDR6X optimized for 10/12-bit processing

**Display Engine**

- Dedicated tone mapping hardware
- Hardware-accelerated HDR to SDR conversion

**Compute Units**

- 32-bit floating point operations
- Precision support for wider gamut

**Media Blocks**

- Specialized encoders/decoders for HDR
- Dedicated HEVC/VP9/AV1 processing with wider color

### Color Format Support in Modern GPUs

Format	Bit Depth	Memory Impact	GPU Support
RGB8 / sRGB	8 bits per channel	24-32 bits per pixel	All GPUs (baseline)
RGB10A2 / RGB10	10 bits per channel	32 bits per pixel	GeForce RTX, AMD RDNA
FP16 (half-float)	16 bits per channel	64 bits per pixel	RTX 2000+, RDNA 2+
FP32 (full-float)	32 bits per channel	128 bits per pixel	Professional GPUs
BC7 / ASTC HDR	8-16 bits with compression	4-8 bits per pixel (compressed)	All modern GPUs

Modern GPU Architecture: Wider Color Formats

**Compression:** Delta color compression in graphics is repurposed for GPGPU data. NVIDIA’s GDDR6X employs lossless compression to effectively increase bandwidth. **Prefetching:** Adaptive prefetching algorithms, like those in , predict memory access patterns to reduce latency. **Memory Tiling:** Partitioning data into tiles that fit cache lines improves locality. The effectiveness depends on tile size  $S$ :

$$H = 1 - \frac{M}{S \times N} \quad (21.6)$$

where  $H$  is hit rate,  $M$  is misses, and  $N$  is accesses. Optimal  $S$  varies by workload.

In summary, transitioning GPUs from graphics to compute workloads requires addressing the computation-memory bandwidth imbalance through architectural innovations. These include reconfigurable memory hierarchies, advanced scheduling, and workload-specific optimizations. Future designs must continue to evolve, as highlighted in , to meet the demands of increasingly diverse GPGPU applications.

## 21.2 SIMT vs. SIMD

### 21.2.1 Single Instruction, Multiple Threads (SIMT) execution model.

The Single Instruction, Multiple Threads (SIMT) execution model is a fundamental architectural paradigm in modern GPUs, enabling efficient parallel processing for highly data-parallel workloads. Unlike Single Instruction, Multiple Data (SIMD), which executes the same instruction on multiple data elements using a single thread, SIMT employs multiple threads to execute the same instruction stream while allowing divergent execution paths. This distinction is critical for understanding the design trade-offs in GPU architectures and their suitability for general-purpose computing.

SIMT architectures, such as those in NVIDIA’s CUDA cores or AMD’s Compute Units, organize threads into warps or wavefronts. Each warp executes a single instruction across all threads, but threads may diverge due to conditional branches. When divergence occurs, the GPU serializes execution for divergent paths, reducing efficiency. The SIMT model mitigates this by grouping threads with similar execution paths, as demonstrated by . The warp scheduler dynamically manages thread execution, hiding latency by switching between warps when stalls occur. This approach contrasts with SIMD, where divergence leads to masked execution or redundant computation, as noted by .

The comparison between SIMT and SIMD reveals key advantages and limitations. SIMD excels in regular, data-parallel workloads where all lanes follow identical control flow, such as matrix multiplication or image processing. However, SIMD struggles with irregular workloads, where branches or data-dependent operations cause lane masking. For example, in a SIMD vector unit, a conditional branch may disable lanes not taking the branch, wasting computational resources. SIMT avoids this by allowing threads to diverge, albeit at the cost of serialization. Research by shows that SIMT achieves higher throughput for workloads with moderate divergence, while SIMD is more efficient for perfectly aligned data-parallel tasks.

In general-purpose computing, SIMT’s limitations become apparent when handling highly divergent or control-flow-intensive workloads. For instance, recursive algorithms or graph traversals may cause severe warp divergence, degrading performance. Studies by highlight that SIMT architectures require careful workload partitioning to minimize divergence. Techniques such as thread regrouping or dynamic warp formation have been proposed to address this, as discussed in . These methods reorganize threads at runtime to improve convergence, but they introduce overhead and complexity.

Designing thread hierarchies for diverse workloads in SIMT architectures involves balancing thread granularity, memory access patterns, and divergence. GPU programmers must structure kernels to maximize warp occupancy and minimize memory latency. For example, a well-designed kernel for a matrix operation might use a two-dimensional thread block layout, where each thread computes a single element. This approach ensures coalesced memory accesses and reduces divergence, as shown by . However, for irregular workloads like sparse matrix-vector multiplication, alternative strategies, such as prefix sums or atomic operations, are necessary to handle uneven work distribution.

The SIMT execution model also influences memory hierarchy design. Modern GPUs employ multi-level caches and shared memory to reduce latency for thread blocks. Shared memory, in particular, enables efficient inter-thread communication within a block, as threads can synchronize and exchange data without global memory accesses. This is critical for algorithms like parallel reductions or histogram generation, where threads collaborate on intermediate results. Research by demonstrates that optimizing shared memory usage can significantly improve performance for such workloads.

Despite its advantages, SIMT faces challenges in scaling for non-graphics workloads. As GPUs evolve to support more general-purpose computing, architectural enhancements like dynamic parallelism or unified memory address these limitations. Dynamic parallelism allows kernels to launch sub-kernels, enabling recursive algorithms without host intervention. Unified memory simplifies programming by providing a single address space for CPU and GPU, though at the cost of potential performance penalties, as noted by .

The interplay between SIMT and SIMD continues to shape GPU architecture. Hybrid approaches, such as NVIDIA's Tensor Cores or AMD's Matrix Cores, combine SIMT flexibility with SIMD efficiency for specific workloads like deep learning. These units leverage wide SIMD lanes for matrix operations while retaining SIMT scheduling for general-purpose threads. This duality highlights the ongoing evolution of parallel execution models to meet diverse computational demands.

In summary, the SIMT execution model is a cornerstone of modern GPU architecture, offering flexibility for parallel workloads but requiring careful design to mitigate divergence. Its comparison with SIMD underscores the trade-offs between regularity and flexibility, while thread hierarchy design remains pivotal for performance optimization. Future advancements will likely focus on reducing divergence overhead and expanding the applicability of SIMT to broader computational domains.

### 21.2.2 Comparison with SIMD and its limitations in general-purpose computing

The evolution of parallel computing architectures has led to significant advancements in both Single Instruction, Multiple Data (SIMD) and Single Instruction, Multiple Threads (SIMT) execution models. While SIMD has been a cornerstone of vectorized processing, its limitations in general-purpose computing have become increasingly apparent, particularly in the context of modern GPU architectures. SIMT, as implemented in GPUs, offers a more flexible approach to parallelism, addressing many of the shortcomings of SIMD while introducing new challenges in thread hierarchy design for diverse workloads.

SIMD architectures execute the same instruction across multiple data elements simultaneously, leveraging wide vector registers and parallel functional units. This model is highly efficient for regular, data-parallel workloads such as matrix multiplication or image processing. For example, a SIMD operation might add two 128-bit vectors in a single cycle:

$$\mathbf{A} + \mathbf{B} = \mathbf{C}$$

where **A**, **B**, and **C** are 4-element vectors. However, SIMD suffers from several limitations:

**Data Alignment Requirements:** SIMD operations often require data to be aligned to specific memory boundaries, complicating memory access patterns and reducing flexibility. **Divergent Control Flow:** Branches or conditional statements within SIMD code lead to execution inefficiencies, as all lanes must follow the same control path or mask operations. **Fixed Instruction Width:** The width of SIMD operations is fixed at compile time, limiting adaptability to varying workloads.

In contrast, SIMT, as employed in modern GPUs, decouples instruction execution from thread scheduling, allowing multiple threads to execute the same instruction stream while managing divergence dynamically. Each thread in a SIMT warp or wavefront can follow an independent control path, with the hardware masking inactive threads during divergence. This model is exemplified by NVIDIA's CUDA architecture, where a warp of 32 threads executes in lockstep but can diverge at branch points. The SIMT execution model can be formalized as:

$$\text{Warp Execution} = \bigcup_{i=1}^{32} \text{Thread}_i(\text{PC})$$

where PC denotes the program counter. SIMT addresses SIMD's limitations by:

**Dynamic Divergence Handling:** Threads within a warp can diverge and reconverge without explicit masking, improving efficiency for irregular workloads. **Flexible Memory Access:** SIMT threads can access memory independently, though coalescing is still required for optimal performance. **Scalability:** SIMT architectures scale to thousands of threads, hiding latency through fine-grained multithreading.

Despite these advantages, SIMT introduces its own challenges. Designing efficient thread hierarchies for diverse workloads requires careful consideration of:

**Workload Partitioning:** Balancing thread blocks across GPU cores to maximize occupancy while minimizing resource contention. **Memory Coalescing:** Ensuring memory accesses from threads within a warp are contiguous to maximize bandwidth utilization. **Divergence Overhead:** Excessive divergence can still degrade performance, necessitating algorithmic adjustments to minimize branch divergence.

The trade-offs between SIMD and SIMT are further illustrated by their hardware implementations. SIMD units, such as Intel's AVX-512, rely on wide vector registers and explicit vectorization directives. For example, an AVX-512 instruction might be written as:

Code Sample 21.3: AVX-512 Example

```
_m512 a = _mm512_load_ps(input);
_m512 b = _mm512_load_ps(weights);
_m512 c = _mm512_add_ps(a, b);
```

In contrast, SIMT architectures abstract vectorization from the programmer, allowing scalar code to execute across multiple threads. This abstraction simplifies programming but shifts the burden of optimization to the hardware's thread scheduler and memory hierarchy.

Recent research highlights the limitations of SIMD in general-purpose computing. For instance, demonstrates that SIMD's rigid data-parallel model struggles with irregular workloads, such as graph traversal or sparse linear algebra. In contrast, shows that SIMT's dynamic divergence handling enables better performance for such workloads, albeit at the cost of increased hardware complexity.

The choice between SIMD and SIMT often depends on the workload characteristics, with SIMD excelling in regular, predictable patterns and SIMT offering greater flexibility for irregular parallelism. Thread hierarchy design in SIMT architectures is critical for performance. For example, CUDA's grid-block-thread hierarchy allows programmers to partition work into thread blocks that execute independently on GPU multiprocessors. Optimal block sizing depends on factors such as register usage, shared memory requirements, and warp occupancy. A poorly designed hierarchy can lead to underutilization or resource contention, as shown in .

In summary, while SIMD remains effective for specific vectorized workloads, its limitations in handling divergence and irregular parallelism have led to the dominance of SIMT in modern GPU architectures. SIMT's dynamic execution model and scalable thread hierarchy provide a more versatile foundation for general-purpose computing, though they require careful design to maximize efficiency. The ongoing evolution of both models reflects the growing demand for architectures that can adapt to increasingly diverse computational workloads.

### 21.2.3 Designing thread hierarchies for diverse workloads.

Modern GPU architectures rely heavily on the Single Instruction, Multiple Threads (SIMT) execution model to achieve high throughput for parallel workloads. Unlike Single Instruction, Multiple Data (SIMD), which operates on fixed-width vector lanes, SIMT enables finer-grained parallelism by allowing divergent execution paths within a warp or wavefront. This distinction is critical when designing thread hierarchies for diverse workloads, as it impacts how resources are allocated and how threads are scheduled.

The SIMT model, pioneered by NVIDIA's CUDA architecture, groups threads into warps (typically 32 threads) that execute the same instruction in lockstep. When threads within a warp diverge due to conditional branches, the hardware serializes execution, leading to performance penalties. This divergence is a key limitation compared to SIMD, where branches are resolved statically, and all lanes follow the same path. However, SIMT's dynamic scheduling enables more flexible execution patterns, making it better suited for general-purpose computing. Research by demonstrates that SIMT outperforms SIMD for irregular workloads, such as graph traversal, where control flow is data-dependent.

Thread hierarchies in modern GPUs are designed to balance workload distribution and resource utilization. The hierarchy consists of three levels. Threads are the smallest execution unit, mapped to individual data elements. Warps or wavefronts are groups of threads executing the same instruction. Thread blocks or workgroups are collections of warps sharing resources like shared memory. This hierarchy allows GPUs to exploit both fine-grained and coarse-grained parallelism. For example, NVIDIA's Volta architecture introduces independent thread scheduling, enabling threads within a warp to progress independently, further reducing divergence overhead .

In contrast, SIMD architectures, such as Intel's AVX-512, rely on fixed-width vector lanes and require explicit vectorization. This approach is efficient for regular workloads like matrix multiplication but struggles with irregular patterns. The limitations of SIMD in general-purpose computing include branch handling, where SIMD requires masking or predication to handle branches, increasing instruction overhead. SIMD operations often require aligned memory accesses, complicating memory management. Fixed-width vectors may underutilize hardware for smaller data types or irregular workloads. Studies by highlight these trade-offs, showing that SIMD's rigid structure limits its applicability to heterogeneous workloads.

Designing thread hierarchies for diverse workloads involves optimizing for both occupancy and divergence. Occupancy, defined as the ratio of active warps to maximum supported warps per multiprocessor, is a key metric. Higher occupancy improves latency hiding but may increase contention for shared resources. The optimal thread

block size depends on the workload's characteristics. For compute-bound workloads, larger thread blocks improve arithmetic intensity but may reduce occupancy. For memory-bound workloads, smaller thread blocks increase occupancy but may underutilize compute units. The trade-off is formalized in the occupancy equation:

$$\text{Occupancy} = \frac{\text{Active Warps}}{\text{Maximum Warps}}$$

where active warps are determined by the thread block size and resource constraints.

To mitigate divergence, modern GPUs employ several techniques. Warp shuffling reorganizes threads within a warp to group active paths, as described in . Dynamic parallelism allows kernels to launch child kernels, reducing divergence at the warp level. Predicated execution masks inactive threads to avoid unnecessary computations. These techniques are particularly effective for workloads with nested parallelism, such as recursive algorithms or adaptive mesh refinement.

The SIMD model also influences memory access patterns. Coalesced memory accesses, where threads within a warp access contiguous memory locations, are essential for performance. The memory transaction size is determined by the warp width, as shown in:

$$\text{Transaction Size} = \text{Warp Size} \times \text{Data Type Size}$$

Non-coalesced accesses result in multiple transactions, degrading performance. This is another area where SIMT outperforms SIMD, as SIMD's fixed-width vectors may force unnecessary memory fetches for sparse data.

In summary, designing thread hierarchies for diverse workloads on modern GPUs requires careful consideration of the SIMT execution model's strengths and limitations. While SIMD excels at regular, data-parallel tasks, SIMT's flexibility makes it the preferred choice for general-purpose computing. Key design principles include optimizing occupancy, minimizing divergence, and ensuring coalesced memory accesses. Future architectures may further blur the line between SIMT and SIMD, as seen in AMD's RDNA3 and NVIDIA's Hopper, which introduce hybrid execution models . These advancements will continue to shape the evolution of thread hierarchy design for increasingly diverse workloads.

## 21.3 Examples of GPGPU Workloads

### 21.3.1 Scientific computing applications.

Modern GPU architectures have revolutionized scientific computing by enabling massively parallel processing for computationally intensive workloads. The shift from traditional CPU-based computation to General-Purpose Graphics Processing Unit (GPGPU) computing has unlocked unprecedented performance gains in fields such as financial modeling, data analysis, and large-scale simulations. NVIDIA's CUDA and AMD's ROCm frameworks provide the software infrastructure to harness GPU parallelism, while architectures like Ampere (NVIDIA) and CDNA (AMD) optimize for double-precision floating-point operations critical for scientific workloads.

Financial modeling benefits significantly from GPGPU acceleration due to the parallel nature of Monte Carlo simulations and option pricing models. The Black-Scholes equation, for instance, can be parallelized across thousands of GPU threads:

$$\frac{\partial V}{\partial t} + \frac{1}{2}\sigma^2 S^2 \frac{\partial^2 V}{\partial S^2} + rS \frac{\partial V}{\partial S} - rV = 0$$

where  $V$  is the option price,  $S$  the stock price,  $\sigma$  volatility, and  $r$  the risk-free rate. Studies demonstrate 200x speedups on GPUs compared to sequential CPU implementations for pricing exotic derivatives. Portfolio optimization problems involving quadratic programming also benefit, as shown by , where GPU-accelerated interior-point methods solved Markowitz models 50x faster than CPU solvers.

In data analysis, GPUs accelerate machine learning and statistical computations. The training of deep neural networks involves matrix operations like:

$$\mathbf{Y} = \sigma(\mathbf{WX} + \mathbf{b})$$

where  $\mathbf{W}$  is the weight matrix,  $\mathbf{X}$  input data,  $\mathbf{b}$  biases, and  $\sigma$  the activation function. NVIDIA's Tensor Cores in Volta and later architectures optimize mixed-precision matrix multiplication, reducing training times from weeks to hours . Similarly, GPU-accelerated libraries like RAPIDS (cuDF, cuML) enable real-time analytics on billion-row datasets, outperforming CPU-based pandas and scikit-learn by orders of magnitude .

Scientific simulations leverage GPU parallelism for solving partial differential equations (PDEs) in physics and engineering. Finite-difference time-domain (FDTD) methods for electromagnetic wave propagation, for example,

update electric and magnetic fields across a grid:

$$\begin{aligned} E_z^{n+1}(i, j) = E_z^n(i, j) + \frac{\Delta t}{\epsilon} & \left( \frac{H_y^{n+1/2}(i + 1/2, j) - H_y^{n+1/2}(i - 1/2, j)}{\Delta x} \right. \\ & \left. - \frac{H_x^{n+1/2}(i, j + 1/2) - H_x^{n+1/2}(i, j - 1/2)}{\Delta y} \right) \end{aligned} \quad (21.7)$$

GPU implementations achieve 90

Molecular dynamics simulations, such as those performed by GROMACS or AMBER, exploit GPU parallelism for quantum mechanics calculations. The Lennard-Jones potential between particles is computed as:

$$V(r) = 4\epsilon \left[ \left(\frac{\sigma}{r}\right)^{12} - \left(\frac{\sigma}{r}\right)^6 \right]$$

With GPU acceleration, simulations of 100,000 atoms achieve nanosecond-per-day throughput, enabling drug discovery research. Similarly, density functional theory (DFT) calculations in quantum chemistry packages like VASP show 15x speedups when offloading FFTs and diagonalization to GPUs.

Climate modeling represents another GPU success story. The Community Earth System Model (CESM) achieved a 4.5x speedup by porting its spectral element dynamical core to NVIDIA GPUs. Atmospheric models solving the primitive equations:

$$\frac{\partial \mathbf{v}}{\partial t} + (\mathbf{v} \cdot \nabla) \mathbf{v} + f \mathbf{k} \times \mathbf{v} = -\nabla \Phi - \frac{1}{\rho} \nabla p$$

benefit from GPU-optimized stencil computations and reduced communication overhead in MPI implementations.

Astrophysical N-body simulations also leverage GPU parallelism. The gravitational force calculation:

$$\mathbf{F}_i = \sum_{j \neq i} G \frac{m_i m_j}{|\mathbf{r}_{ij}|^3} \mathbf{r}_{ij}$$

is parallelized using treecode or particle-mesh methods on GPUs, with performance exceeding 30 million particles per second on a single node. Cosmological simulations like IllustrisTNG use GPU-accelerated hydrodynamics to model galaxy formation across billions of particles.

In seismic imaging, reverse-time migration (RTM) algorithms process terabytes of survey data using GPU clusters. The wave equation:

$$\frac{1}{v^2(\mathbf{x})} \frac{\partial^2 p(\mathbf{x}, t)}{\partial t^2} = \nabla^2 p(\mathbf{x}, t)$$

is solved iteratively on GPUs, with companies like Schlumberger reporting 5x faster processing compared to CPU-only systems. Medical imaging also benefits, as GPU-accelerated iterative reconstruction in CT scanners reduces radiation dose while maintaining image quality.

The emergence of heterogeneous computing platforms like NVIDIA's Grace Hopper Superchip and AMD's Instinct MI300 further blurs the line between CPUs and GPUs, enabling unified memory access and reducing data transfer bottlenecks. Research shows that such architectures achieve 98

Energy efficiency is another GPU advantage in scientific computing. The Green500 list consistently ranks GPU-based systems as the most energy-efficient supercomputers, with Frontier achieving 62.68 gigaflops/watt. This makes GPU clusters cost-effective for long-running simulations in fields like nuclear fusion research, where codes like GENE solve gyrokinetic equations on GPU-optimized grids.

Despite these advances, challenges remain in load balancing, memory bandwidth limitations, and algorithm adaptation for GPU architectures. Research demonstrates that hybrid CPU-GPU approaches often outperform pure GPU implementations for irregular workloads like adaptive mesh refinement. Nevertheless, the trajectory of GPU architecture evolution suggests continued dominance in scientific computing, with upcoming technologies like optical interconnects and 3D-stacked memory promising further breakthroughs.

### 21.3.2 Real-world uses in financial modeling, data analysis, and simulations.

Modern GPU architectures have revolutionized computational workloads by enabling highly parallel processing, particularly in financial modeling, data analysis, and simulations. The shift from traditional CPU-based computation to General-Purpose Graphics Processing Unit (GPGPU) computing has unlocked unprecedented performance

gains for scientific and financial applications. Below, we explore real-world applications of GPGPU workloads in these domains, emphasizing their mathematical foundations and implementation details.

Financial institutions leverage GPUs for high-frequency trading (HFT), risk assessment, and derivative pricing. Monte Carlo simulations, a cornerstone of quantitative finance, benefit immensely from GPU parallelism. For example, pricing a European call option using the Black-Scholes model involves simulating thousands of asset price paths under stochastic differential equations (SDEs). The GPU-accelerated version of this simulation can be expressed as:

$$S_{t+\Delta t} = S_t \exp \left( \left( r - \frac{\sigma^2}{2} \right) \Delta t + \sqrt{\Delta t} Z_t \right)$$

where  $S_t$  is the asset price at time  $t$ ,  $r$  is the risk-free rate,  $\sigma$  is volatility, and  $Z_t$  is a standard normal random variable. GPUs excel at generating and processing these paths in parallel, reducing computation time from hours to seconds.

Portfolio optimization involves solving quadratic programming problems of the form:

$$\min_w \frac{1}{2} w^T w - \gamma w$$

subject to  $\sum w_i = 1$ , where  $w$  is the weight vector,  $\gamma$  is the covariance matrix,  $\mu$  is the expected return vector, and  $\lambda$  is a risk-aversion parameter. GPU-accelerated solvers like CUDA-QL exploit parallel linear algebra routines to handle large-scale portfolios efficiently.

In data analysis, deep neural networks (DNNs) rely on matrix multiplications and activation functions. A typical layer performs:

$$y = \sigma(Wx + b)$$

where  $W$  is the weight matrix,  $x$  is the input vector,  $b$  is the bias, and  $\sigma$  is the activation function. GPUs accelerate these operations through cuBLAS and cuDNN. Clustering algorithms such as k-means also benefit from GPU parallelism. The assignment step computes Euclidean distances:

$$d(x_i, c_j) = \sqrt{\sum_{k=1}^n (x_{ik} - c_{jk})^2}$$

GPU implementations reduce complexity from  $O(nkd)$  to  $O(nk)$  by parallelizing across threads.

Scientific computing tasks such as fluid dynamics use GPUs to solve Navier-Stokes equations:

$$\frac{\partial \mathbf{u}}{\partial t} + (\mathbf{u} \cdot \nabla) \mathbf{u} = -\frac{1}{\rho} \nabla p + \nu \nabla^2 \mathbf{u} + \mathbf{f}$$

where  $\mathbf{u}$  is velocity,  $p$  pressure,  $\rho$  density,  $\nu$  viscosity, and  $\mathbf{f}$  external forces. Domain decomposition allows finite difference methods to scale efficiently on GPUs.

Molecular dynamics simulations use GPUs to compute atomic forces. The force between particles is:

$$F_{ij} = -\nabla V(r_{ij})$$

where  $V(r_{ij})$  is the Lennard-Jones or Coulomb potential. Packages like AMBER enable near-real-time biomolecular simulations using GPU-accelerated kernels.

Other GPGPU applications include Monte Carlo option pricing, image convolution in medical imaging, DFT calculations in quantum chemistry, and wave modeling for seismic analysis. Each of these applications benefits from parallelism inherent in GPU execution.

A typical parallel reduction kernel used in these domains is shown below:

#### Code Sample 21.4: Parallel Reduction in CUDA

```
__global__ void reduceSum(float *input, float *output, int N) {
    extern __shared__ float sdata[];
    int tid = threadIdx.x;
    int i = blockDim.x * blockDim.x + threadIdx.x;
    sdata[tid] = (i < N) ? input[i] : 0;
    __syncthreads();
    for (int s = blockDim.x / 2; s > 0; s >>= 1) {
        if (tid < s) {
```

```
    sdata[tid] += sdata[tid + s];
}
__syncthreads();
}
if (tid == 0) output[blockIdx.x] = sdata[0];
}
```

In conclusion, the integration of GPUs into financial, analytical, and scientific domains has enabled scalable, real-time computation across a variety of workloads. From stochastic modeling to high-dimensional matrix operations, GPU architectures offer the parallelism and throughput required for next-generation computation.

# Chapter 22

# Instruction Set for General Computation

## 22.1 Designing Flexible Instructions

### 22.1.1 Supporting common non-graphical operations.

Modern GPU architectures have evolved beyond their original purpose of accelerating graphical rendering to support a wide range of general-purpose computations. A critical aspect of this evolution is enabling non-graphical operations, which requires designing flexible instruction sets, supporting synchronization primitives, and handling variable-length or custom instructions. These capabilities are essential for modern workloads such as machine learning, scientific computing, and data-parallel algorithms.

GPUs traditionally excel at data-parallel tasks due to their Single Instruction, Multiple Thread (SIMT) execution model. However, non-graphical operations often require capabilities beyond those found in early GPU designs. A key example is synchronization, which is critical in parallel algorithms and is typically achieved through atomic operations. The NVIDIA Volta architecture introduced enhanced atomic primitives, such as compare-and-swap (CAS) and fetch-and-add, which support fine-grained synchronization efficiently.

These atomic operations are implemented as hardware-level instructions to minimize latency and maximize throughput. In the CUDA programming model, such operations are exposed through intrinsics like `__syncthreads()` for barrier synchronization and `atomicAdd()` for atomic arithmetic, both of which map directly to GPU machine instructions.

Variable-length instructions pose another challenge for GPU architectures. Traditional GPUs rely on fixed-width instruction encoding for simplicity, but modern workloads benefit from more flexible encoding schemes. AMD's RDNA 3 architecture introduces a variable-length instruction format, allowing for more compact code and improved instruction cache utilization. This is particularly useful for custom instructions tailored to specific domains, such as matrix operations in deep learning. The flexibility is achieved through a prefix-based encoding scheme, where additional operands or modifiers extend the base instruction.

Code Sample 22.1: Variable-Length Instruction Encoding

```
// Base instruction (32-bit)
opcode[7:0] | dst[4:0] | src1[4:0] | src2[4:0] | modifier[9:0]

// Extended instruction (64-bit)
prefix[31:0] | opcode[7:0] | dst[4:0] | src1[4:0] | src2[4:0] | modifier[9:0]
```

Custom instructions further extend GPU programmability. Researchers have demonstrated the benefits of domain-specific instructions for tasks like sparse matrix multiplication. These instructions are often implemented using microcoded execution units or reconfigurable logic within the GPU pipeline. For example, NVIDIA's Tensor Cores incorporate custom instructions for mixed-precision matrix multiply-accumulate (MMA) operations, significantly accelerating deep learning workloads. The instruction set architecture (ISA) is designed to accommodate these extensions without disrupting legacy code, ensuring backward compatibility.

Atomic operations are crucial for synchronization in parallel algorithms. Modern GPUs provide a hierarchy of atomic operations, ranging from warp-level to device-wide synchronization. The AMD CDNA architecture, for instance, introduces hardware-accelerated atomic operations for shared memory and global memory, reducing contention in highly parallel workloads. These operations are often implemented using dedicated hardware units,

such as atomic execution pipelines, which handle requests in parallel to minimize stalls. The latency of an atomic operation can be modeled as:

$$L_{\text{atomic}} = t_{\text{queue}} + t_{\text{execute}} + t_{\text{commit}}$$

Here,  $t_{\text{queue}}$  represents the queuing delay,  $t_{\text{execute}}$  is the execution time, and  $t_{\text{commit}}$  accounts for the commit phase. Optimizing these components is critical for achieving high performance in synchronization-heavy workloads.

Handling variable-length and custom instructions requires careful design of the GPU's instruction decode and dispatch logic. Modern GPUs employ multi-stage decoders capable of processing instructions of varying lengths. For example, Intel's Xe architecture uses a hybrid decoder that supports both fixed-length and variable-length instructions, enabling efficient execution of diverse workloads. The decoder dynamically identifies instruction boundaries and dispatches them to the appropriate execution units. This flexibility is particularly important for custom instructions, which may require specialized hardware or microcode sequences.

The integration of non-graphical operations into GPU architectures also impacts memory systems. Atomic operations necessitate coherent memory access across multiple cores. NVIDIA's Ampere architecture introduces a unified memory system with hardware-supported cache coherence, enabling efficient atomic updates across the GPU. This is achieved through a combination of directory-based coherence protocols and speculative execution to hide latency. The memory system must also handle variable-length data accesses, which are common in custom instructions. For example, sparse matrix operations often involve irregular memory patterns that benefit from compressed representations and scatter-gather capabilities.

In summary, modern GPU architectures have expanded their capabilities to support non-graphical operations through flexible instruction design, atomic operations, and variable-length or custom instructions. These advancements are driven by the demands of emerging workloads and are implemented using a combination of hardware and software techniques. Key innovations include hardware-accelerated atomic operations for synchronization, as seen in NVIDIA Volta and AMD CDNA; variable-length instruction encoding for compact code and improved cache utilization, exemplified by AMD RDNA 3; custom instructions for domain-specific acceleration, such as NVIDIA's Tensor Cores and Intel's Xe matrix engines; and advanced memory systems with coherence protocols to support atomic operations and irregular access patterns. These developments highlight the ongoing evolution of GPU architectures to meet the needs of modern computing. Future research will likely focus on further enhancing programmability and efficiency, particularly for heterogeneous workloads that combine graphical and non-graphical tasks. The continued integration of these features ensures GPUs remain versatile platforms for a wide range of applications.

### 22.1.2 Adding atomic operations for synchronization.

Modern GPU architectures have evolved beyond their traditional role in graphics rendering to support general-purpose computing (GPGPU). A critical aspect of this evolution is the inclusion of atomic operations for synchronization, which enables efficient coordination between parallel threads. Atomic operations, such as `atomic_add`, `atomic_exchange`, and `atomic_compare_and_swap`, ensure that memory accesses are indivisible, preventing race conditions in shared memory scenarios. These operations are particularly vital in workloads like parallel reductions, histogram construction, and dynamic load balancing.

The design of flexible instructions in GPUs must account for the variability in atomic operation requirements across applications. For instance, NVIDIA's CUDA architecture provides a rich set of atomic operations, including 32-bit and 64-bit variants, to cater to diverse computational needs. The hardware implementation of these operations often involves dedicated functional units or modifications to the memory hierarchy.

Code Sample 22.2: Atomic Adder Implementation

```
module atomic_adder (
    input wire clk,
    input wire [31:0] addr,
    input wire [31:0] value,
    output reg [31:0] result
);
    reg [31:0] memory [0:1023];
    always @(posedge clk) begin
        memory[addr] <= memory[addr] + value;
        result <= memory[addr];
    end
endmodule
```

```
end
endmodule
```

Supporting common non-graphical operations, such as those found in machine learning or scientific computing, requires GPUs to handle irregular memory access patterns and synchronization bottlenecks. Atomic operations mitigate these challenges by enabling fine-grained synchronization. For example, in a parallel prefix sum algorithm, atomic operations ensure correct updates to shared counters. The performance impact of atomic operations depends on the memory consistency model. GPUs typically adopt a relaxed consistency model, allowing out-of-order execution while preserving synchronization semantics.

Handling variable-length and custom instructions further complicates GPU design. Variable-length instructions, such as those in ARM's SVE2 or RISC-V's V extension, require dynamic decoding logic and flexible execution units. Custom instructions, often implemented via user-defined extensions, enable domain-specific optimizations. For instance, a GPU tailored for cryptography might include atomic operations for modular arithmetic.

$$T_{\text{atomic}} = T_{\text{mem}} + T_{\text{sync}} + T_{\text{exec}}$$

Here,  $T_{\text{mem}}$  represents memory access time,  $T_{\text{sync}}$  synchronization overhead, and  $T_{\text{exec}}$  execution time. Optimizing these components involves trade-offs between area, power, and performance. For example, reducing  $T_{\text{sync}}$  may require additional hardware support for faster barrier synchronization.

The integration of atomic operations into GPU architectures also raises challenges in scalability and correctness. Large-scale systems, such as those with thousands of cores, must avoid contention on shared memory locations. Techniques like hierarchical synchronization and software combining trees distribute the load across multiple levels of the memory hierarchy. Correctness is ensured through formal verification of atomic operation semantics. For instance, the following properties must hold for an atomic compare-and-swap operation: atomicity (no intermediate state is observable), isolation (concurrent operations appear sequential), and consistency (the result reflects the most recent update). These properties align with the linearizability criterion, which guarantees that atomic operations behave as if executed instantaneously.

In practice, GPU vendors employ a combination of hardware and software techniques to optimize atomic operations. For example, AMD's ROCm platform uses hardware-accelerated atomics for specific data types, while falling back to software emulation for unsupported cases. This hybrid approach balances flexibility and performance. Similarly, Intel's oneAPI provides cross-vendor abstractions for atomic operations, enabling portable code across GPUs from different manufacturers.

The design of variable-length and custom instructions must also consider the impact on instruction fetch and decode logic. Longer instructions require wider fetch buffers and more complex decoders, increasing power consumption. Custom instructions, while beneficial for specific workloads, may reduce the generality of the architecture.

$$C_{\text{decode}} = \sum_{i=1}^N (L_i \times D_i)$$

Here,  $L_i$  is the length of instruction  $i$ , and  $D_i$  is its decode cost. GPUs mitigate this overhead through techniques like macro-op fusion, which combines multiple simple operations into a single instruction.

In summary, modern GPU architectures must address several key challenges when incorporating atomic operations for synchronization. These include ensuring low-latency execution while maintaining correctness, scaling to large core counts without excessive contention, and supporting variable-length and custom instructions efficiently. These requirements drive innovations in GPU design, from hardware-accelerated atomics to flexible instruction sets. Future research will likely focus on adaptive synchronization mechanisms and compiler support for automatic optimization of atomic operations.

### 22.1.3 Handling variable-length and custom instructions.

Modern GPU architectures have evolved to handle increasingly complex workloads, including variable-length and custom instructions, to support both graphical and non-graphical operations. This flexibility is critical for applications such as machine learning, scientific computing, and real-time simulations. The design of flexible instructions in GPUs involves several key considerations, including instruction encoding, decoding efficiency, and hardware support for dynamic execution paths.

Variable-length instructions present a challenge for GPU architectures, which traditionally rely on fixed-width instruction formats for simplicity and parallelism. However, modern GPUs employ techniques such as prefix en-

coding and multi-word instructions to accommodate variable-length operations. For example, NVIDIA's Volta architecture introduced a variable-length instruction format to optimize code density and reduce memory bandwidth usage . The encoding scheme allows instructions to span multiple words, with prefixes indicating the instruction length and operand types. This approach balances decoding complexity with flexibility, enabling efficient execution of custom operations.

Custom instructions are another critical aspect of modern GPU design, particularly for domain-specific accelerators. GPUs now support user-defined instructions through programmable shader cores and tensor cores. For instance, AMD's RDNA architecture includes a flexible instruction set architecture (ISA) that allows developers to define custom operations for specific workloads . These instructions are typically implemented using microcode or dedicated hardware units, depending on the frequency of use and performance requirements.

The following Verilog snippet illustrates a simplified custom instruction decoder:

Code Sample 22.3: Custom Instruction Decoder

```
module custom_decoder (
    input [31:0] instr,
    output reg [4:0] opcode,
    output reg [15:0] imm
);
always @(*) begin
    opcode = instr[31:27];
    imm = instr[15:0];
end
endmodule
```

Supporting common non-graphical operations, such as matrix multiplications or cryptographic algorithms, requires extending the GPU's instruction set beyond traditional graphics pipelines. Modern GPUs incorporate specialized units like tensor cores and ray-tracing accelerators to handle these workloads efficiently. For example, NVIDIA's Ampere architecture includes third-generation tensor cores optimized for mixed-precision matrix operations, enabling high-performance deep learning inference . These units operate in parallel with traditional shader cores, leveraging the GPU's massive parallelism for non-graphical tasks.

Atomic operations are essential for synchronization in parallel computing, particularly in shared-memory systems. GPUs provide hardware support for atomic operations on global and local memory, ensuring correctness in concurrent execution. The CUDA programming model, for instance, includes atomic functions such as `atomicAdd` and `atomicCAS` for fine-grained synchronization . These operations are implemented using dedicated hardware primitives, such as atomic memory units (AMUs), which guarantee atomicity even in highly parallel environments. The performance of atomic operations is critical for applications like graph processing and sparse linear algebra, where frequent synchronization is required.

Handling variable-length and custom instructions also impacts the GPU's pipeline design. Traditional GPUs use deeply pipelined architectures to maximize throughput, but variable-length instructions can introduce stalls due to decoding dependencies. To mitigate this, modern GPUs employ techniques such as speculative decoding and out-of-order execution. For example, Intel's Xe architecture uses a hybrid approach, where common instructions are decoded in-order, while complex or variable-length instructions are handled by a separate out-of-order engine . This design ensures high throughput while maintaining flexibility for custom operations.

The following equation models the throughput of a GPU pipeline with variable-length instructions:

$$T = \frac{N}{\sum_{i=1}^N D_i}$$

where  $T$  is the throughput,  $N$  is the number of instructions, and  $D_i$  is the decoding latency for the  $i$ -th instruction. This equation highlights the trade-off between instruction flexibility and pipeline efficiency.

In addition to hardware support, software tools play a crucial role in managing variable-length and custom instructions. Compilers for GPU programming languages, such as CUDA and OpenCL, must generate efficient code for these instructions. For example, LLVM's NVPTX backend optimizes instruction scheduling to minimize decoding overhead for variable-length instructions . Similarly, runtime systems like ROCm provide APIs for defining and executing custom instructions on AMD GPUs .

The integration of atomic operations, variable-length instructions, and custom operations into modern GPU architectures reflects the growing demand for versatility in parallel computing. These features enable GPUs to excel not only in graphics but also in general-purpose computing, machine learning, and other high-performance

applications. Future advancements will likely focus on further reducing decoding overhead and expanding the range of supported custom operations, ensuring GPUs remain at the forefront of computational innovation.

Variable-length instructions require efficient encoding and decoding schemes to maintain performance. Custom instructions enable domain-specific optimizations but demand flexible hardware support. Atomic operations are critical for synchronization and must be implemented with minimal latency. Pipeline design must balance throughput and flexibility to handle diverse workloads. Software tools, including compilers and runtime systems, are essential for leveraging these hardware features.

The evolution of GPU architectures demonstrates a clear trend toward greater flexibility and generality, driven by the needs of modern computational workloads. By addressing the challenges of variable-length and custom instructions, GPUs continue to expand their role beyond graphics, becoming indispensable tools for a wide range of scientific and industrial applications.

## 22.2 Optimization for AI and Scientific Operations

### 22.2.1 Floating-point operations (FP16, FP32, and FP64).

Modern GPU architectures have evolved to support a wide range of floating-point operations, including half-precision (FP16), single-precision (FP32), and double-precision (FP64), to cater to diverse computational needs in AI and scientific applications. The choice of precision significantly impacts performance, power efficiency, and numerical accuracy. FP16, with its 16-bit representation, is widely used in deep learning due to its reduced memory bandwidth and computational requirements, while FP32 and FP64 are preferred for tasks demanding higher numerical stability, such as scientific simulations and high-precision AI models. The trade-offs between these formats are critical for optimizing GPU workloads.

Matrix multiply-accumulate (MMA) operations are fundamental to AI tasks, particularly in convolutional neural networks (CNNs) and transformer models. Modern GPUs, such as NVIDIA's Ampere and Hopper architectures, feature tensor cores optimized for mixed-precision MMA, enabling efficient computation of large matrix products. For example, the Volta architecture introduced mixed-precision FP16/FP32 MMA, achieving significant speedups in deep learning workloads. The operation can be expressed as:

$$C = A \times B + C$$

where  $A$  and  $B$  are input matrices, and  $C$  is the accumulator matrix. Tensor cores exploit parallelism by performing multiple MMA operations concurrently, leveraging the GPU's SIMD (Single Instruction, Multiple Data) capabilities.

Parallel reduction and data aggregation are essential for optimizing scientific and AI workloads. GPUs employ hierarchical reduction techniques to minimize memory access latency and maximize throughput. For instance, a parallel sum reduction can be implemented using shared memory and warp-level primitives, as shown below:

Code Sample 22.4: Parallel reduction in CUDA

```
__global__ void reduce_sum(float *input, float *output, int N) {
    __shared__ float sdata[256];
    int tid = threadIdx.x;
    int i = blockIdx.x * blockDim.x + threadIdx.x;
    sdata[tid] = (i < N) ? input[i] : 0.0f;
    __syncthreads();
    for (int s = blockDim.x / 2; s > 0; s >>= 1) {
        if (tid < s) sdata[tid] += sdata[tid + s];
        __syncthreads();
    }
    if (tid == 0) output[blockIdx.x] = sdata[0];
}
```

This kernel demonstrates efficient reduction by combining partial sums within a thread block before writing the result to global memory. Such optimizations are crucial for tasks like gradient aggregation in distributed training or statistical computations in scientific simulations.

The efficiency of floating-point operations on GPUs is further enhanced by architectural features such as pipelined execution units, memory hierarchy, and warp scheduling. Modern GPUs employ deep pipelines to hide latency and maximize throughput for FP16, FP32, and FP64 operations. Caches and registers are optimized to reduce bandwidth bottlenecks, particularly for data-intensive MMA operations. GPUs dynamically schedule warps to keep execution units occupied, mitigating stalls caused by memory latency or dependencies.

Mixed-precision training, which combines FP16 and FP32, has become a standard technique for accelerating AI workloads while maintaining numerical accuracy. For example, NVIDIA's Automatic Mixed Precision (AMP) toolkit automatically converts parts of the computation to FP16, reducing memory usage and increasing throughput without compromising model convergence. The gradient scaling technique is often employed to prevent underflow in FP16 gradients:

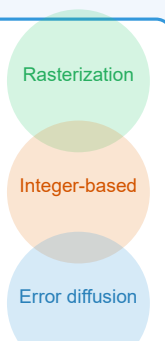
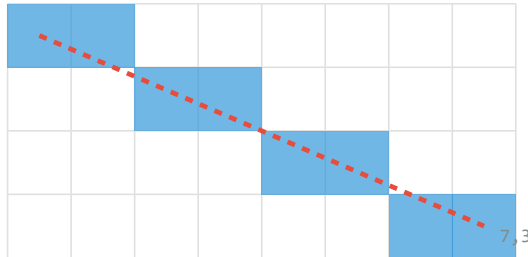
$$\text{grad}_{\text{FP16}} = \text{grad}_{\text{FP32}} \times S$$

where  $S$  is a scaling factor. This approach balances precision and performance, making it suitable for large-scale training.

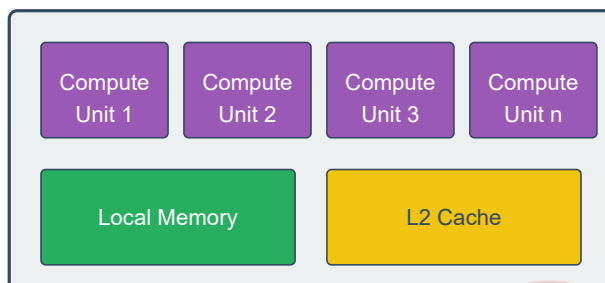
Scientific applications, such as computational fluid dynamics (CFD) or quantum chemistry, often require FP64 for high-precision calculations. GPUs like AMD's Instinct MI200 series and NVIDIA's A100 provide dedicated

## Bresenham's Line Drawing Algorithm on Modern GPUs

### Algorithm Visualization



### GPU Hardware Implementation



### CUDA Implementation

```
// Bresenham's Line Algorithm in CUDA
__global__ void bresenhamLine(int x0, int y0, int x1, int y1,
    unsigned char* framebuffer, int width) {
    int dx = abs(x1 - x0);
    int dy = abs(y1 - y0);
    int sx = (x0 < x1) ? 1 : -1;
    int sy = (y0 < y1) ? 1 : -1;
    int err = dx - dy;
    // Each thread handles one pixel calculation...
}
```

Parallelized across thousands of cores

FP64 units, delivering teraflop-level performance for these workloads . The FP64 performance is typically lower than FP16 or FP32 due to the increased computational complexity and memory bandwidth requirements, but it remains indispensable for accuracy-critical tasks.

The optimization of floating-point operations also involves minimizing data movement and maximizing arithmetic intensity. The roofline model is a useful tool for analyzing performance bottlenecks, relating operational throughput to memory bandwidth . The arithmetic intensity  $I$  is defined as:

$$I = \frac{\text{FLOPs}}{\text{bytes transferred}}$$

For MMA operations, high arithmetic intensity is achieved by reusing data in registers or shared memory, reducing the need for global memory accesses.

In summary, modern GPU architectures provide robust support for FP16, FP32, and FP64 operations, enabling efficient execution of AI and scientific workloads. Key optimizations include tensor cores for high-throughput MMA operations, hierarchical parallel reduction for data aggregation, mixed-precision techniques to balance speed and accuracy, and architectural enhancements like pipelining and memory hierarchy optimization.

These advancements have made GPUs indispensable for high-performance computing, driving innovations in both AI and scientific research. Future architectures are expected to further improve floating-point efficiency, with emerging formats like BF16 (Brain Float 16) and FP8 gaining traction for specialized applications . The continuous evolution of GPU hardware and software ensures that floating-point operations remain at the forefront of computational acceleration.

### 22.2.2 Matrix multiply-accumulate for AI tasks.

Matrix multiply-accumulate (MMA) operations are fundamental to modern AI tasks, particularly in deep learning workloads such as convolutional neural networks (CNNs) and transformers. These operations dominate the computational requirements of training and inference, making their efficient implementation critical for performance. Modern GPU architectures, such as NVIDIA’s Ampere and Hopper or AMD’s CDNA, are optimized for MMA through specialized tensor cores. These cores accelerate mixed-precision floating-point operations, including FP16, FP32, and FP64, while maintaining high throughput and energy efficiency.

The mathematical formulation of MMA is expressed as:

$$C = A \times B + C$$

where  $A$  and  $B$  are input matrices, and  $C$  is the accumulator matrix. This operation is inherently parallelizable, making GPUs ideal for its execution due to their massively parallel architecture. Tensor cores exploit this parallelism by processing small submatrices (e.g.,  $4 \times 4$  or  $8 \times 8$ ) in a single clock cycle, reducing latency and improving throughput. For example, NVIDIA’s Hopper architecture introduces the FP8 precision format, further optimizing MMA for AI workloads .

Precision plays a crucial role in MMA performance. Lower-precision formats like FP16 reduce memory bandwidth and computational overhead while maintaining acceptable accuracy for many AI tasks. However, higher-precision formats like FP32 and FP64 are essential for scientific computing, where numerical stability is critical. Modern GPUs support mixed-precision MMA, allowing intermediate results to be computed in FP16 and accumulated in FP32 or FP64. This approach balances performance and accuracy, as shown in . The following equation illustrates mixed-precision accumulation:

$$C_{\text{FP32}} = A_{\text{FP16}} \times B_{\text{FP16}} + C_{\text{FP32}}$$

Efficient parallel reduction and data aggregation are equally important for AI and scientific operations. Reduction operations, such as summing elements across a matrix or computing norms, are often bottlenecks due to their sequential nature. GPUs address this through hierarchical reduction strategies, leveraging warp-level and block-level parallelism. For instance, the parallel reduction algorithm for summing a vector  $x$  of length  $N$  can be implemented as follows:

Code Sample 22.5: Parallel reduction in CUDA

```
__global__ void reduce_sum(float *x, float *result) {
    __shared__ float sdata[256];
    int tid = threadIdx.x;
    int i = blockIdx.x * blockDim.x + threadIdx.x;
    sdata[tid] = (i < N) ? x[i] : 0;
```

```

__syncthreads();
for (int s = blockDim.x / 2; s > 0; s >>= 1) {
    if (tid < s) sdata[tid] += sdata[tid + s];
    __syncthreads();
}
if (tid == 0) atomicAdd(result, sdata[0]);
}

```

Modern GPU architectures optimize reduction operations through hardware intrinsics like `__shfl_down_sync` and `__reduce_add_sync`, which minimize thread divergence and memory access latency. These optimizations are particularly effective for large-scale scientific simulations, where reduction operations are frequent.

Data aggregation, another key operation in AI, involves combining partial results from parallel threads or blocks. For example, gradient aggregation in distributed training requires efficient summation of gradients across multiple GPUs. NVIDIA's NVLink and AMD's Infinity Fabric provide high-bandwidth interconnects to accelerate such operations. The following equation represents gradient aggregation:

$$\nabla_{\text{global}} = \sum_{i=1}^N \nabla_{\text{local}_i}$$

where  $\nabla_{\text{local}_i}$  is the gradient computed on the  $i$ -th GPU.

The interplay between MMA, parallel reduction, and data aggregation underscores the importance of architectural innovations in GPUs. Key advancements include memory hierarchy, warp scheduling, and SIMT execution. Caches and shared memory reduce latency for frequently accessed data, such as matrix tiles in MMA. Dynamic warp scheduling hides latency by switching between warps during memory accesses. Single Instruction, Multiple Thread (SIMT) execution enables efficient parallelism for MMA and reduction operations.

Recent research demonstrates the impact of these optimizations. For example, shows that tensor cores achieve up to  $16\times$  higher throughput for MMA compared to traditional CUDA cores. Similarly, highlights the benefits of FP16 MMA for training large language models, reducing training time by 30% without sacrificing accuracy.

In summary, modern GPU architectures are meticulously designed to optimize MMA, parallel reduction, and data aggregation for AI and scientific tasks. Through specialized hardware, mixed-precision support, and efficient parallel algorithms, these architectures deliver unprecedented performance, enabling breakthroughs in machine learning and computational science. Future directions include further precision optimization (e.g., FP4) and tighter integration with emerging memory technologies like HBM3.

### 22.2.3 Efficient support for parallel reduction and data aggregation.

Modern GPU architectures have evolved to provide efficient support for parallel reduction and data aggregation, which are critical for AI and scientific computing workloads. These operations often involve large-scale floating-point computations, matrix multiply-accumulate (MMA) operations, and hierarchical memory access patterns. The following discussion examines these aspects in detail, focusing on optimization techniques and hardware support.

Parallel reduction is a fundamental operation in GPU computing, used to aggregate data across threads or thread blocks. For example, summing an array of  $N$  elements requires  $\log_2 N$  steps when performed in parallel. Modern GPUs optimize this by leveraging warp-level primitives like `__shfl_xor` and `__reduce_add_sync` in CUDA, which minimize memory traffic and exploit register-level communication. The efficiency of these operations is further enhanced by tensor cores in NVIDIA GPUs, which perform mixed-precision MMA operations (e.g., FP16 input with FP32 accumulation) at high throughput.

Data aggregation in GPUs often involves hierarchical reduction patterns. For instance, a global sum can be decomposed into thread-local reductions using registers, warp-level reductions using shuffle instructions, block-level reductions via shared memory, and global reductions through atomic operations or device-wide synchronization. This hierarchy minimizes bandwidth bottlenecks and aligns with the GPU's SIMT (Single Instruction, Multiple Threads) execution model. The use of FP16 for intermediate storage (with FP32 accumulation) further reduces memory pressure while maintaining numerical accuracy.

Matrix multiply-accumulate operations are central to AI workloads, particularly in deep learning. Modern GPUs employ tensor cores to accelerate MMA, supporting formats like FP16, TF32, and FP64. The computational efficiency of these units is given by:

$$\text{TOPS} = f_{\text{clock}} \times \text{Cores} \times \text{Ops/Cycle}$$

where  $f_{\text{clock}}$  is the clock frequency, and  $\text{Ops/Cycle}$  depends on the precision mode. For example, NVIDIA's Ampere architecture achieves 312 TFLOPS for FP16 MMA, compared to 19.5 TFLOPS for FP64, highlighting the trade-off between precision and throughput .

Floating-point precision plays a crucial role in optimization. FP16 is widely used in AI training and inference due to its memory efficiency, but it requires careful handling to avoid numerical underflow. Mixed-precision techniques, such as those in NVIDIA's Automatic Mixed Precision (AMP), combine FP16 storage with FP32 accumulation to preserve accuracy . For scientific computing, FP64 remains essential for stability in iterative solvers, though newer architectures like AMD's CDNA2 optimize FP64 throughput for HPC workloads .

Efficient parallel reduction relies on memory access patterns that maximize coalescing and minimize bank conflicts. The following CUDA pseudocode illustrates a warp-level reduction:

Code Sample 22.6: Warp-level reduction using CUDA intrinsics

```
__device__ float warp_reduce(float val) {
    for (int offset = 16; offset > 0; offset /= 2)
        val += __shfl_down_sync(0xffffffff, val, offset);
    return val;
}
```

This approach avoids shared memory entirely, reducing latency. For larger datasets, a two-phase reduction is employed, where each block computes a partial sum, followed by a global aggregation. Atomic operations on global memory, such as `atomicAdd`, ensure correctness but may introduce contention. Newer GPUs mitigate this with hardware-accelerated atomics and cache hierarchies optimized for reduction patterns .

Data aggregation in scientific operations often involves irregular access patterns, such as sparse matrix-vector multiplication. GPUs address this with warp-wide load-balancing techniques and hierarchical storage. For example, the CSR (Compressed Sparse Row) format leverages shared memory to coalesce accesses, while warp-level primitives handle divergent execution . The performance is modeled as:

$$\text{Bandwidth} = \frac{\text{Data Size}}{\text{Time}} \times \text{Utilization}$$

where utilization depends on the sparsity pattern and memory coalescing.

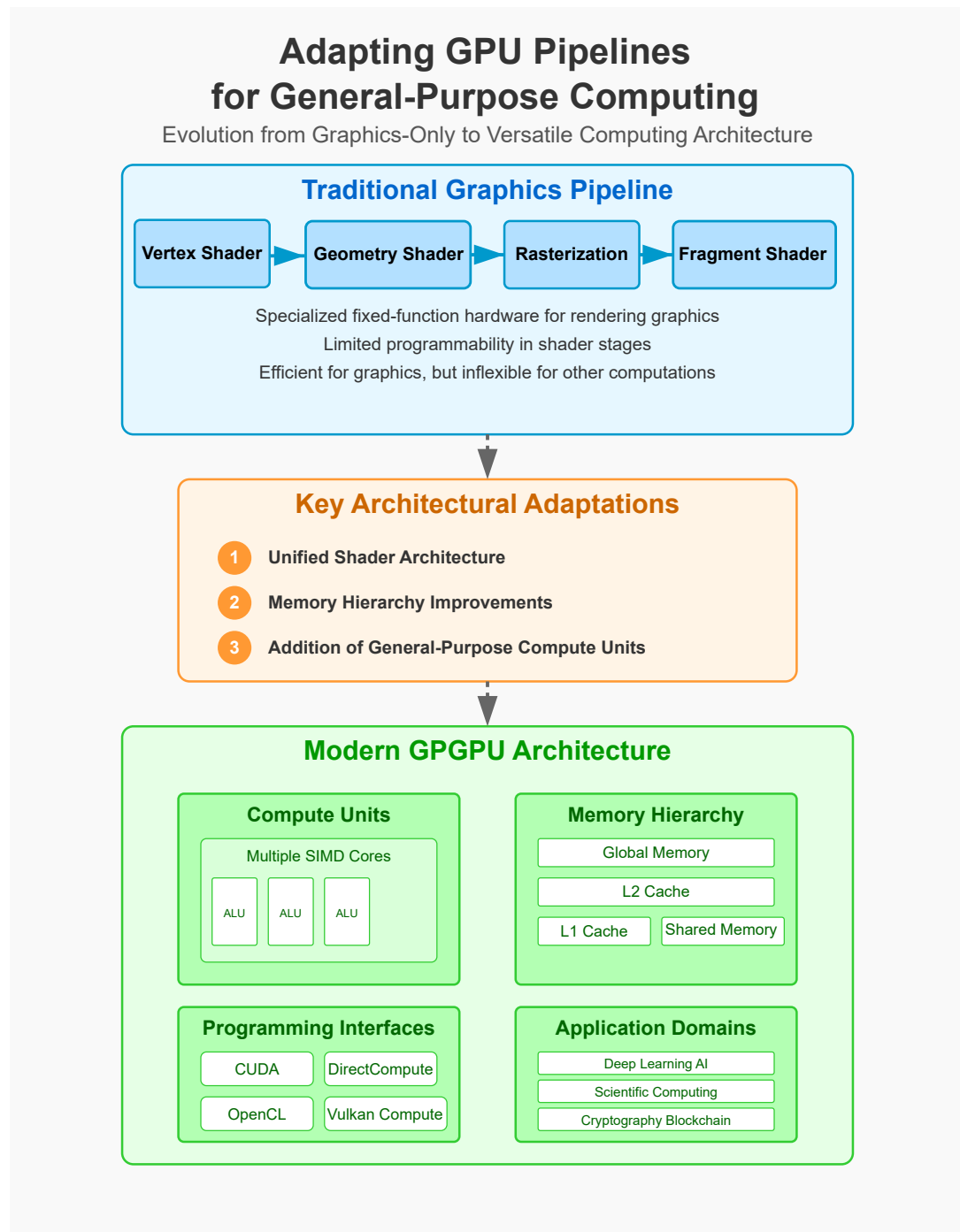
Optimizations for AI tasks also include leveraging tensor cores for non-matrix operations. Recent work demonstrates how tensor cores can accelerate parallel reduction by reformulating the problem as a series of MMA operations . This approach achieves up to  $4\times$  speedup for FP16 reductions compared to traditional CUDA kernels. The key insight is to exploit the tensor cores' ability to perform  $4\times 4$  matrix multiplications in a single instruction, even when the problem is not inherently matrix-based.

The interplay between precision, memory hierarchy, and parallelism is critical for performance. For example, FP32 operations on NVIDIA's A100 GPU achieve 19.5 TFLOPS, while FP16 reaches 312 TFLOPS, but the latter requires careful scaling to avoid overflow. Scientific workloads often use FP64 for stability, as in the following iterative solver:

$$x_{k+1} = x_k - \alpha \nabla f(x_k)$$

where FP64 ensures convergence in ill-conditioned problems. GPU architectures like AMD's MI200 prioritize FP64 throughput (47.9 TFLOPS) for such cases .

In summary, modern GPU architectures provide efficient support for parallel reduction and data aggregation through a combination of hardware primitives, memory hierarchy optimizations, and precision-aware computation. These capabilities are essential for AI and scientific computing, where performance and accuracy are equally critical. The continued evolution of tensor cores, mixed-precision arithmetic, and memory subsystems will further enhance these workflows.





# Chapter 23

## Memory Hierarchy for GPGPU

### 23.1 High-Bandwidth Memory Design

#### 23.1.1 Designing interfaces for external memory like HBM.

High-bandwidth memory (HBM) has emerged as a critical enabler for modern GPU architectures, addressing the growing demand for memory bandwidth in high-performance computing and machine learning workloads. The design of interfaces for external memory like HBM involves optimizing data transfer rates, minimizing latency, and ensuring efficient power utilization. This discussion focuses on the architectural considerations, interface design strategies, and techniques for maximizing memory throughput in GPUs utilizing HBM.

The primary challenge in HBM interface design lies in achieving high bandwidth while maintaining low power consumption. HBM achieves this through a 3D-stacked memory architecture, where multiple DRAM layers are vertically integrated using through-silicon vias (TSVs). This design reduces interconnect lengths, enabling higher data rates and lower power compared to traditional GDDR memory. The interface between the GPU and HBM must account for the unique characteristics of this architecture, including wide but slow buses. For instance, HBM2 employs a 1024-bit bus per stack operating at relatively lower frequencies (e.g., 2 Gbps per pin) compared to GDDR6, yet achieves higher aggregate bandwidth due to parallelism:

$$\text{Bandwidth} = \text{Bus Width} \times \text{Data Rate} \times \text{Number of Stacks}$$

To maximize throughput, modern GPUs employ several key strategies:

**Wide and Parallel Interfaces:** HBM interfaces leverage wide data buses (e.g., 1024-bit per stack) to compensate for lower clock speeds. This parallelism is managed through advanced packaging techniques like silicon interposers, which provide dense interconnects between the GPU and memory stacks. The interposer's role is critical, as it minimizes signal integrity issues and reduces parasitic capacitance, enabling higher data rates.

**Pseudo-Channel Architecture:** HBM divides each stack into pseudo-channels, typically two per stack, allowing concurrent access to different memory regions. This design reduces contention and improves effective bandwidth. For example, a GPU can issue independent requests to each pseudo-channel, overlapping data transfers and hiding latency.

**Command Scheduling and Reordering:** The memory controller must efficiently schedule commands to maximize bus utilization. Techniques like out-of-order execution and bank-level parallelism are employed to minimize idle cycles. The controller reorders requests based on access patterns, prioritizing those that avoid row conflicts and maximize page hits.

Power efficiency is another critical consideration in HBM interface design. The 3D-stacked architecture inherently reduces power by shortening data paths, but additional optimizations are required at the interface level:

**Voltage and Frequency Scaling:** Dynamic voltage and frequency scaling (DVFS) adjusts the interface's operating parameters based on workload demands. Lowering voltage during periods of reduced activity saves power without significantly impacting performance.

**Data Encoding:** Techniques like low-power signaling (e.g., differential signaling) and data bus inversion (DBI) reduce switching activity on the bus, lowering dynamic power consumption. DBI inverts the data word if it would result in fewer bit transitions, reducing power:

$$P_{\text{dynamic}} \propto \alpha \cdot C \cdot V^2 \cdot f$$

where  $\alpha$  is the switching activity.

Latency reduction is equally important for HBM interfaces. While HBM provides high bandwidth, its latency can still bottleneck performance in certain workloads. To mitigate this, GPUs employ:

**Prefetching and Caching:** Aggressive prefetching algorithms predict memory access patterns and fetch data into caches before it is needed. Multi-level caches (L1, L2) reduce the frequency of HBM accesses, lowering effective latency.

**Burst Transfers:** The interface maximizes bus utilization by transferring large blocks of data in bursts. This amortizes the overhead of command issuance and row activation over multiple data words.

The physical implementation of HBM interfaces requires careful attention to signal integrity and thermal management. High-density interconnects on silicon interposers are susceptible to crosstalk and noise, necessitating advanced equalization techniques like decision-feedback equalization (DFE) and feed-forward equalization (FFE). Thermal management is also critical, as 3D-stacked memory generates concentrated heat. GPUs integrate thermal sensors and dynamic throttling mechanisms to prevent overheating.

Verilog code snippets illustrate typical HBM interface logic, such as command scheduling and data alignment:

Code Sample 23.1: HBM Command Scheduler

```
module hbm_scheduler (
    input clk, rst,
    input [31:0] req_addr,
    output reg [31:0] cmd_out
);
always @(posedge clk) begin
    if (rst)
        cmd_out <= 0;
    else
        cmd_out <= req_addr; // Simplified scheduling logic
end
endmodule
```

In summary, designing interfaces for HBM in modern GPUs involves a combination of architectural innovations, circuit-level optimizations, and system-level strategies. Wide parallel interfaces, pseudo-channel architectures, and advanced scheduling algorithms maximize throughput, while power and latency optimizations ensure efficient operation. These techniques collectively enable GPUs to leverage HBM's high bandwidth for demanding computational workloads, as demonstrated in research by and . Future advancements will likely focus on further scaling bandwidth through technologies like HBM3 and hybrid memory cubes, while maintaining compatibility with existing GPU architectures.

### 23.1.2 Strategies for maximizing memory throughput.

Modern GPU architectures rely heavily on high-bandwidth memory (HBM) to meet the demands of parallel computing workloads. Maximizing memory throughput requires a combination of hardware design optimizations and software-level strategies. Below are key approaches for achieving peak memory performance in GPUs.

Wide memory interfaces are employed in HBM to increase data transfer rates. For example, 1024-bit or 2048-bit buses provide extremely high bandwidth. The bandwidth  $B$  is given by:

$$B = \text{Data Rate} \times \text{Bus Width} \times \text{Number of Channels}$$

HBM2 achieves up to 307 GB/s per stack by using 1024-bit buses and 2 Gbps/pin data rates .

Through-silicon vias (TSVs) enable 3D stacking of DRAM dies in HBM, reducing interconnect length and power consumption. Bandwidth scales with the number of stacked layers:

$$B_{\text{total}} = N \times B_{\text{layer}}$$

where  $N$  is the number of layers and  $B_{\text{layer}}$  is per-layer bandwidth .

GPUs partition memory into multiple independent channels for concurrent access. For example, NVIDIA's Ampere uses 32 memory partitions with HBM2e to reach 2 TB/s bandwidth .

HBM supports burst lengths of 4, 8, or 16. The burst size  $S$  is aligned to the cache line size:

$$S = \text{Cache Line Size} \times \text{Burst Multiplier}$$

This maximizes bandwidth utilization by minimizing command overhead .

To reduce signaling power and increase speed, HBM uses low-swing POD (pseudo-open drain) signaling. The swing voltage  $V_{\text{swing}}$  is defined as:

$$V_{\text{swing}} = V_{\text{dd}} - V_{\text{ref}}$$

where  $V_{\text{dd}}$  is supply and  $V_{\text{ref}}$  is reference voltage .

On-die ECC (error correction code) is used to maintain data integrity. The overhead  $\epsilon$  is:

$$\epsilon = \frac{\text{ECC Bits}}{\text{Data Bits}} \times 100\%$$

For HBM2, this is typically 6.25% (8 ECC bits per 128 data bits) .

Memory access scheduling minimizes bank conflicts and improves throughput. Schedulers use bank parallelism, row locality, and fairness to prioritize memory requests .

Cache hierarchy optimization with L1, L2, and L3 caches reduces traffic. The hit rate  $H$  is:

$$H = \frac{\text{Cache Hits}}{\text{Total Accesses}}$$

Prefetching and large cache lines further improve cache effectiveness .

Lossless data compression (e.g., delta encoding) reduces transferred volume. The compression ratio  $C$  is:

$$C = \frac{\text{Uncompressed Size}}{\text{Compressed Size}}$$

NVIDIA reports up to 2:1 compression for framebuffer data .

Silicon interposers are used in HBM to route signals densely between memory and GPU. The wire pitch  $p$  follows:

$$p \propto \frac{1}{\text{Signal Density}}$$

Finer pitches allow higher bandwidth density .

Thermal management is essential in 3D stacked HBM due to increased power density. The thermal resistance  $R_\theta$  must satisfy:

$$R_\theta \leq \frac{T_{\max} - T_{\text{ambient}}}{P}$$

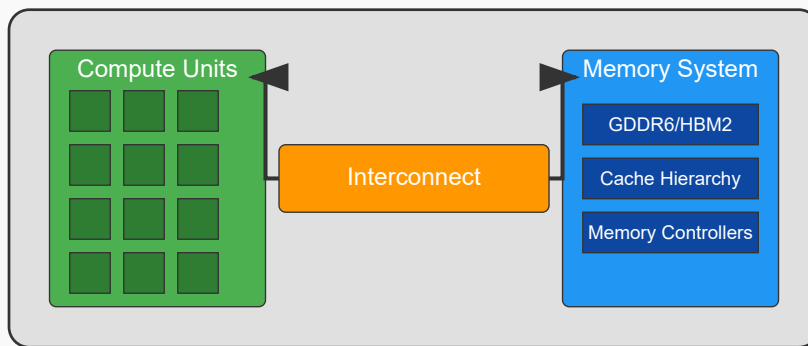
where  $T_{\max}$  is junction temperature and  $P$  is power dissipation .

Memory controller command queue depth  $Q$  influences throughput:

$$Q \geq \text{Round-Trip Latency} \times \text{Data Rate}$$

## Challenges in Balancing Computation Memory Bandwidth

*Modern GPU Architecture Dilemma*



### Key Challenges

#### 1. Memory Wall

Compute capabilities growing faster than memory bandwidth, creating performance bottlenecks in memory-intensive workloads.

#### 2. Data Locality Caching

Balancing the limited on-chip cache resources between thousands of concurrent threads with diverse memory access patterns.

#### 3. Power Considerations

Memory operations consume significant power. Bandwidth increases must be balanced with thermal and power constraints.

### Architectural Solutions

- HBM (High Bandwidth Memory) integration
- Hierarchical cache designs with L1/L2/L3 caches
- Memory compression techniques
- Smart scheduling to maximize coalesced memory access

Deeper queues increase performance but also power and area costs .

Compiler-driven software prefetching issues early memory requests to reduce stalls. The prefetch distance  $D$  is:

$$D = \text{Latency} \times \text{Throughput}$$

This balances timeliness and avoids cache pollution .

HBM pipelines memory commands to overlap address and data phases. Pipeline depth  $L$  is:

$$L = \left\lceil \frac{\text{Command Latency}}{\text{Cycle Time}} \right\rceil$$

This improves bandwidth at the cost of initial latency .

Dynamic voltage and frequency scaling (DVFS) adjusts operating points for power efficiency:

$$P \propto V^2 \times f$$

Lowering voltage  $V$  and frequency  $f$  during idle periods conserves energy .

Redundancy is built into HBM via spare rows/columns. The repair rate  $R$  is:

$$R = \frac{\text{Spare Resources}}{\text{Total Resources}} \times 100\%$$

This improves manufacturing yield and fault tolerance .

Interconnect optimization ensures signal integrity. The eye diagram margin  $M$  is:

$$M = \frac{\text{Eye Opening}}{\text{Unit Interval}}$$

Wider margins reduce bit errors at high speeds .

Memory request coalescing merges adjacent accesses into fewer transactions. Coalescing efficiency  $E$  is:

$$E = \frac{\text{Coalesced Requests}}{\text{Total Requests}} \times 100\%$$

Higher efficiency reduces command traffic and boosts effective throughput .

Power delivery network (PDN) impedance must remain low to avoid voltage droop. The constraint is:

$$Z \leq \frac{\Delta V}{\Delta I}$$

where  $\Delta V$  is allowable droop and  $\Delta I$  is current swing .

These strategies collectively enable modern GPUs to achieve near-peak memory throughput while balancing power, area, and latency constraints. Future advancements in HBM3 and beyond will further push these limits .

## 23.2 Shared Memory and Caches

### 23.2.1 Designing shared memory for intra-thread communication.

Modern GPU architectures rely heavily on hierarchical memory systems to optimize intra-thread communication and data sharing. Shared memory, caches (L1, L2, and unified), and their interplay are critical for performance, particularly for irregular memory access patterns. This discussion focuses on design considerations for shared memory in GPUs, cache hierarchies, and optimization techniques for non-uniform memory access. Shared memory in GPUs is a software-managed scratchpad memory that enables low-latency communication between threads within the same thread block. Unlike caches, which are hardware-managed and transparent to the programmer, shared memory requires explicit data movement. Its design must balance capacity, bandwidth, and bank conflicts. For example, NVIDIA's Volta architecture provides 96 KB of shared memory per streaming multiprocessor (SM), configurable as 64 KB shared memory with 32 KB L1 cache or vice versa . The partitioning flexibility allows programmers to optimize for either high-bandwidth shared memory or larger L1 cache depending on the workload. The cache hierarchy in modern GPUs typically includes L1 and L2 caches, with some architectures incorporating a unified cache. L1 caches are per-SM and serve both shared memory and global memory accesses, while L2 caches are shared across SMs. The unified cache architecture, as seen in AMD's RDNA2, merges texture and data

caches into a single L1 cache, reducing redundancy and improving hit rates . The cache hierarchy must address the trade-off between latency and capacity. For instance, smaller L1 caches reduce access latency but may increase miss rates, while larger L2 caches improve hit rates but introduce higher latency. Optimizing shared memory for irregular memory access patterns requires careful design to minimize bank conflicts. Shared memory is divided into banks, typically 32 in modern GPUs, allowing concurrent access if requests map to different banks. However, if multiple threads access the same bank, conflicts occur, serializing accesses. Techniques such as padding or reordering data structures can mitigate bank conflicts. For example, adding padding to a matrix can ensure that adjacent rows map to different banks, as shown in 23.2.1:

$$\text{Address} = (\text{row} \times \text{stride}) + \text{column}$$

Here, `stride` is chosen to avoid bank conflicts. The L1 cache design must also account for irregular access patterns. Traditional cache line sizes (e.g., 128 bytes) may lead to overfetching for sparse or irregular workloads. Some architectures, like Intel's Xe-HPG, employ adaptive cache line sizes to reduce unnecessary data transfer . Additionally, cache bypass mechanisms allow critical data to skip lower cache levels, reducing pollution. For example, NVIDIA's CUDA provides the `_1dg` intrinsic to bypass L1 cache for read-only data, improving efficiency for certain access patterns. Unified cache hierarchies simplify memory management but require careful tuning to avoid contention. In a unified design, texture, constant, and global memory accesses compete for the same cache resources. To mitigate this, some GPUs implement partitioned caching or priority-based arbitration. For instance, ARM's Mali GPUs use a dynamic partitioning scheme that adjusts cache allocation based on workload characteristics . This approach ensures fair resource distribution while maintaining low latency for critical accesses. Irregular memory access patterns, common in graph processing or sparse linear algebra, pose significant challenges for cache coherence and locality. Techniques such as software prefetching or warp-level privatization can improve performance. Software prefetching leverages GPU-specific intrinsics to fetch data ahead of time, hiding memory latency. Warp-level privatization allocates per-warp scratchpad memory to reduce contention, as shown in 23.2.1:

$$\text{Scratchpad\_Size} = \text{Warps\_Per\_SM} \times \text{Per\_Warp\_Size}$$

This ensures each warp has dedicated storage for intermediate results. The interaction between shared memory and caches is another critical design consideration. In some architectures, shared memory accesses bypass the L1 cache to reduce pollution, while in others, they coexist. For example, AMD's CDNA architecture allows shared memory to use either the L1 cache or a dedicated path, depending on the kernel configuration . This flexibility enables programmers to tailor memory access paths to their specific needs. Cache coherence protocols in GPUs differ from CPUs due to their SIMD execution model. Most GPUs eschew hardware coherence in favor of software-managed consistency. For instance, CUDA's memory model requires explicit synchronization (e.g., `_syncthreads()`) to ensure visibility of shared memory updates across threads. This design simplifies hardware but places additional burden on programmers to manage data consistency. Finally, emerging architectures explore heterogeneous cache hierarchies to address diverse workloads. For example, some GPUs integrate SRAM-based caches for latency-sensitive data and eDRAM-based caches for high-bandwidth requirements. This hybrid approach, as seen in research prototypes like AMD's Infinity Cache, aims to balance latency, bandwidth, and power efficiency . Such innovations highlight the ongoing evolution of GPU memory systems to meet the demands of modern parallel workloads. In summary, designing shared memory and cache hierarchies for modern GPUs involves balancing capacity, latency, and bandwidth while addressing irregular access patterns. Key techniques include bank conflict mitigation, adaptive cache line sizing, and software-managed coherence. These optimizations are critical for achieving high performance in parallel computing applications.

### 23.2.2 L1, L2, and unified cache hierarchy.

Modern GPU architectures employ a sophisticated memory hierarchy to balance latency, bandwidth, and power efficiency. The L1, L2, and unified cache hierarchy plays a pivotal role in optimizing memory access patterns, particularly for irregular workloads. Shared memory and caches are designed to facilitate intra-thread communication while minimizing contention and maximizing throughput.

The L1 cache in GPUs is typically tightly coupled with the streaming multiprocessors (SMs) and serves as the first-level data cache. It is designed for low-latency access and is often partitioned to reduce bank conflicts. The L1 cache is shared among warps within an SM, and its size is configurable, allowing trade-offs between shared memory and L1 cache capacity. For example, NVIDIA's Volta architecture permits dynamic partitioning between L1 cache and shared memory . The L1 cache is optimized for spatial and temporal locality, but its effectiveness diminishes for irregular memory access patterns due to increased miss rates.

The L2 cache is a unified, last-level cache shared across all SMs. It acts as a coherence point for the memory hierarchy and reduces off-chip memory traffic. The L2 cache is larger and has higher latency than the L1 cache but provides better bandwidth utilization. Unified cache hierarchies, such as those in AMD's RDNA architecture, combine L1 and L2 caches to streamline data movement and reduce redundancy . The L2 cache is critical for workloads with irregular access patterns, as it absorbs misses from the L1 cache and mitigates the performance impact of scattered memory accesses.

Shared memory is a software-managed scratchpad memory that enables efficient intra-thread communication. It is organized into banks to support parallel access, but bank conflicts can degrade performance. The shared memory latency is comparable to register access, making it ideal for fine-grained data sharing. Designing shared memory for intra-thread communication requires careful consideration of access patterns. For example, matrix transposition can be optimized using shared memory to avoid non-coalesced global memory accesses .

The following Verilog snippet illustrates a simplified shared memory bank:

Code Sample 23.2: Shared Memory Bank

```
module shared_mem_bank (
    input clk,
    input [4:0] addr,
    input [31:0] din,
    input we,
    output [31:0] dout
);
reg [31:0] mem [0:31];
always @(posedge clk) begin
    if (we) mem[addr] <= din;
    dout <= mem[addr];
end
endmodule
```

Optimizing for irregular memory access patterns involves leveraging the cache hierarchy and shared memory. Techniques such as cache blocking and prefetching can improve spatial locality. For irregular patterns, the L1 cache may be bypassed to reduce thrashing, and data can be directly fetched from the L2 cache or shared memory. The unified cache hierarchy simplifies this by providing a coherent view of memory across SMs.

The following equation models the effective memory access time for a two-level cache hierarchy:

$$T_{eff} = h_1 \cdot T_{L1} + (1 - h_1) \cdot (h_2 \cdot T_{L2} + (1 - h_2) \cdot T_{DRAM})$$

where  $h_1$  and  $h_2$  are the hit rates for L1 and L2 caches, and  $T_{L1}$ ,  $T_{L2}$ , and  $T_{DRAM}$  are the access latencies.

Shared memory can be optimized for irregular patterns by using bank conflict-free layouts or padding. For example, diagonal access patterns in matrices can be transformed into conflict-free accesses by reordering data in shared memory.

Bank conflict avoidance can be achieved by aligning stride accesses to bank boundaries. Data prefetching into shared memory hides latency for irregular patterns. Cache bypassing can reduce thrashing when patterns are highly scattered. Unified cache utilization improves coherence and bandwidth efficiency.

Modern GPUs also employ hardware-managed cache policies, such as write-evict or write-back, to optimize for irregular accesses. The L2 cache often includes sectoring to reduce wasted bandwidth for partial cache line updates. For example, NVIDIA's Ampere architecture introduces a unified L1/texture cache to improve hit rates for diverse workloads .

The interplay between shared memory and caches is critical for performance. Shared memory provides deterministic latency, while caches offer automatic locality exploitation. For irregular patterns, a hybrid approach is often optimal: using shared memory for predictable accesses and caches for scattered data.

The following equation quantifies the trade-off:

$$P_{eff} = \alpha \cdot P_{shared} + (1 - \alpha) \cdot P_{cache}$$

where  $\alpha$  is the fraction of memory accesses suited for shared memory, and  $P_{shared}$  and  $P_{cache}$  are the respective performance metrics.

In summary, modern GPU architectures rely on a balanced L1, L2, and unified cache hierarchy to address diverse memory access patterns. Shared memory is optimized for intra-thread communication, while caches handle irregular accesses. Effective design requires a deep understanding of workload characteristics and hardware

capabilities. Future advancements may further unify cache and shared memory management to adapt dynamically to varying access patterns.

### 23.2.3 Optimizing for irregular memory access patterns.

Modern GPU architectures are designed to handle massive parallelism, but irregular memory access patterns pose significant challenges to performance. These patterns arise in applications like graph processing, sparse linear algebra, and particle simulations, where memory accesses lack spatial or temporal locality. To mitigate these issues, GPUs employ shared memory, caches (L1, L2, and unified), and careful design of memory hierarchies.

Shared memory in GPUs is a software-managed scratchpad memory that enables low-latency communication between threads within the same thread block. Unlike caches, shared memory provides deterministic access latency, making it ideal for intra-thread communication. However, its limited size (typically 16–64 KB per streaming multiprocessor) requires careful allocation. For irregular access patterns, shared memory can be used to coalesce scattered reads or writes. For example, a common optimization is to load data from global memory into shared memory in a coalesced manner, then perform irregular accesses from shared memory.

The L1 cache in modern GPUs is tightly coupled with shared memory, often sharing the same physical storage. NVIDIA’s Ampere architecture, for instance, allows dynamic partitioning between L1 cache and shared memory. This flexibility is crucial for irregular workloads, where the balance between caching and explicit data sharing varies. The L1 cache primarily serves local memory accesses, while shared memory handles intra-block communication. For irregular patterns, increasing shared memory allocation can reduce cache thrashing caused by non-coherent accesses.

L2 cache acts as a global cache shared across all streaming multiprocessors. It mitigates the high latency of global memory by caching frequently accessed data. Irregular access patterns often exhibit poor locality, leading to high L2 miss rates. To address this, GPUs employ several optimizations such as miss status holding registers (MSHRs), which track outstanding cache misses and allow the GPU to overlap memory requests and hide latency. Hardware or software prefetching can anticipate irregular accesses, though this is challenging for truly random patterns. Larger cache lines (128B in NVIDIA GPUs) improve spatial locality but may waste bandwidth for irregular accesses.

Unified cache hierarchies, such as those in AMD’s CDNA architecture, combine L1 and L2 functionalities into a single coherent cache. This simplifies memory management for irregular workloads by reducing the need for explicit data movement between cache levels. Unified caches also benefit from better utilization of cache capacity, as data can be shared across compute units without duplication.

Designing shared memory for intra-thread communication requires addressing bank conflicts and access patterns. Shared memory is divided into banks (typically 32), and concurrent accesses to the same bank cause serialization. For irregular patterns, bank conflicts are inevitable but can be minimized. Padding data structures ensures that adjacent threads access different banks. Software-based randomization using hash functions can distribute accesses across banks, though this adds computational overhead. Data can be rearranged to guarantee conflict-free access for specific patterns, such as strided accesses.

Optimizing for irregular memory access patterns also involves leveraging warp-level parallelism. Warps (groups of 32 threads in NVIDIA GPUs) execute in lockstep, and divergent memory accesses can severely degrade performance. Techniques to improve warp efficiency include warp shuffling, where threads within a warp exchange data via registers, avoiding shared memory entirely. Dynamic scheduling ensures that warps with irregular accesses do not stall the entire GPU.

Cache-aware algorithms are another critical optimization. For example, in graph traversal, the frontier queue can be partitioned to fit into shared memory or L1 cache, reducing global memory traffic. Similarly, sparse matrix-vector multiplication can use blocking techniques to improve locality.

Hardware support for irregular patterns includes atomic operations and scatter/gather instructions. Modern GPUs provide efficient atomic operations for irregular updates, such as histogram construction. Scatter/gather instructions allow threads to read or write non-contiguous memory locations, though their performance depends on coalescing. NVIDIA’s Volta architecture introduced independent thread scheduling, which improves performance for irregular workloads by allowing finer-grained synchronization.

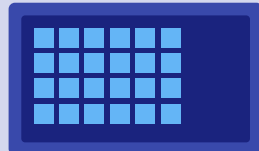
Memory compression is another technique to mitigate bandwidth limitations. NVIDIA’s Turing and Ampere architectures support lossless compression for both L2 cache and global memory. For irregular patterns, compression reduces effective bandwidth usage, though the compression ratio varies with data entropy.

In summary, optimizing for irregular memory access patterns in modern GPU architectures involves a combination of shared memory design, cache hierarchy tuning, and algorithm-level optimizations. Key strategies

include dynamic partitioning between shared memory and L1 cache, leveraging warp-level parallelism and avoiding bank conflicts, using cache-aware algorithms and hardware-supported scatter/gather, and employing memory compression and prefetching where applicable. These techniques are essential for achieving high performance in applications with irregular memory access patterns, ensuring that GPUs remain versatile for a wide range of workloads. Future architectures may introduce further innovations, such as more flexible memory hierarchies or enhanced hardware support for irregular patterns.

## GPUs in Scientific Computing

### Modern GPU Architecture



- Thousands of CUDA cores
- High memory bandwidth
- Parallelism optimized

### Scientific Applications

#### Computational Fluid Dynamics



32x faster simulation of complex turbulent flow models

#### Molecular Dynamics



100x acceleration for protein folding simulations

#### Climate Modeling



20x faster atmospheric and oceanic simulations

#### Quantum Chemistry



50x speedup for electron density calculations and quantum states

### Scientific Machine Learning



- Physics-informed neural networks
- AI-accelerated drug discovery
- 100x throughput for training on scientific data

**Modern GPU Computing: Accelerating Scientific Discovery**

# Chapter 24

# Parallelism and Thread Management

## 24.1 Warp Scheduling and Divergence Handling

### 24.1.1 Efficient scheduling of threads and warps.

Modern GPU architectures rely on efficient scheduling of threads and warps to maximize throughput while minimizing latency. Warp scheduling is a critical component of Single Instruction, Multiple Thread (SIMT) execution, where a warp—a group of threads—executes the same instruction in lockstep. The efficiency of warp scheduling directly impacts performance, particularly when handling control-flow divergence, a common challenge in SIMT architectures.

Warp schedulers in modern GPUs, such as those in NVIDIA’s Volta and Ampere architectures, employ several techniques to optimize thread execution. One such technique is the use of multiple warp schedulers per Streaming Multiprocessor (SM), allowing concurrent issuance of instructions from different warps. This approach hides latency by keeping the execution units busy while other warps stall due to memory accesses or dependencies. The scheduler prioritizes warps based on readiness, ensuring that instructions are issued as soon as their operands are available. This reduces idle cycles and improves utilization of the GPU’s computational resources.

Control-flow divergence occurs when threads within a warp follow different execution paths due to conditional branches. SIMT architectures handle divergence by serializing the execution of divergent paths, which can significantly degrade performance. To mitigate this, modern GPUs employ dynamic warp formation and reconvergence mechanisms. Dynamic warp formation allows threads from different warps to merge into a new warp if they share the same execution path, reducing divergence overhead. Reconvergence points, such as the Immediate Post-Dominator (IPDOM), ensure that divergent threads rejoin execution as soon as possible, minimizing the time spent in serialized execution.

Efficient scheduling also involves balancing the workload across warps to avoid underutilization. GPUs use scoreboarding and occupancy tracking to manage warp scheduling. Scoreboarding tracks the readiness of warps, while occupancy tracking ensures that the SM has enough active warps to hide latency. The theoretical occupancy of an SM is given by:

$$\text{Occupancy} = \frac{\text{Active Warps}}{\text{Maximum Warps per SM}}$$

Higher occupancy generally leads to better latency hiding, but it must be balanced against register and shared memory usage to avoid resource contention.

Another key aspect of warp scheduling is the handling of memory operations. Memory accesses often cause warps to stall, so schedulers prioritize warps that are not waiting for memory. Techniques like memory coalescing and prefetching are used to reduce memory latency. Memory coalescing combines multiple memory accesses from threads within a warp into a single transaction, improving bandwidth utilization. Prefetching brings data into the cache before it is needed, reducing stall cycles. The effectiveness of these techniques depends on the warp scheduler’s ability to reorder memory requests efficiently.

Divergence handling in SIMT architectures also involves compiler optimizations. The compiler identifies divergent branches and inserts synchronization points to minimize divergence. For example, the compiler may use predicated execution to avoid branching altogether. Predicated execution converts conditional branches into conditional operations, allowing all threads in a warp to execute the same instruction stream. This reduces divergence but may increase instruction count. The trade-off between divergence and instruction overhead is a critical

consideration in compiler design.

The following Verilog-like pseudocode illustrates a simplified warp scheduler:

Code Sample 24.1: Warp Scheduler Pseudocode

```
module warp_scheduler (
    input clock,
    input [NUM_WARPS-1:0] warp_ready,
    output reg [NUM_WARPS-1:0] warp_issued
);
    always @ (posedge clock) begin
        for (i = 0; i < NUM_WARPS; i = i + 1) begin
            if (warp_ready[i] && !warp_issued[i]) begin
                warp_issued[i] <= 1; // Issue instruction for warp i
            end
        end
    end
endmodule
```

The scheduler selects warps based on their readiness and issues instructions to the execution units. More advanced schedulers incorporate priority schemes, such as round-robin or oldest-first, to ensure fairness and avoid starvation.

In addition to hardware mechanisms, software techniques play a role in efficient warp scheduling. Programmers can optimize kernel design to reduce divergence, such as by arranging data to ensure memory coalescing or using warp-level primitives like `_shfl` for communication. These techniques reduce the scheduler's workload and improve overall performance.

The impact of warp scheduling on performance can be quantified using metrics like Instructions Per Cycle (IPC) and warp occupancy. IPC measures the throughput of the GPU, while warp occupancy indicates how effectively the hardware resources are utilized. The relationship between IPC and occupancy is complex, as higher occupancy does not always translate to higher IPC due to resource contention or divergence.

Recent research has explored adaptive warp scheduling to further improve efficiency. For example, proposes a scheduler that dynamically adjusts warp priorities based on runtime behavior. This approach reduces contention for shared resources and improves throughput in workloads with high divergence. Similarly, introduces a divergence-aware scheduler that predicts divergence and adjusts scheduling decisions accordingly.

In summary, efficient scheduling of threads and warps in modern GPU architectures involves a combination of hardware mechanisms and software optimizations. Key techniques include dynamic warp formation, reconvergence at IPDOM points, memory coalescing, and compiler-assisted divergence handling. These methods work together to maximize throughput and minimize latency, ensuring that GPUs deliver high performance across a wide range of workloads. Future advancements in warp scheduling will likely focus on adaptive and machine learning-driven approaches to further optimize resource utilization and handle increasingly complex workloads.

### 24.1.2 Handling control-flow divergence in SIMT architectures.

Modern GPU architectures employ Single Instruction, Multiple Thread (SIMT) execution to achieve high throughput by executing groups of threads, called warps, in lockstep. Control-flow divergence occurs when threads within a warp follow different execution paths due to conditional branches, leading to inefficiencies. Efficient handling of divergence is critical for maximizing GPU performance, particularly in warp scheduling and thread management.

When a warp encounters a branch instruction, threads may take different paths, causing the warp to diverge. The GPU hardware handles this by serializing execution for each divergent path, masking off inactive threads. For a branch with two paths, the warp first executes the taken path with active threads masked, then the not-taken path with the remaining threads. This results in reduced utilization, as only a subset of threads is active at any time. The divergence penalty is proportional to the number of divergent paths and the imbalance in thread participation.

Warp schedulers mitigate divergence by dynamically grouping threads with similar execution paths. The Greedy-Then-Oldest (GTO) scheduler prioritizes warps with minimal divergence, while the Two-Level Round-Robin (TLRR) scheduler balances fairness and throughput. Recent architectures like NVIDIA's Volta introduce Independent Thread Scheduling (ITS), allowing threads within a warp to diverge and reconverge more flexibly, reducing the overhead of serialization.

Divergence handling is further optimized through compiler techniques. Predicated execution converts control dependencies into data dependencies, enabling threads to execute both paths without branching. For example:

## Code Sample 24.2: Predicated Branch

```
if (cond) { A = B + C; }
else { A = B - C; }
```

is transformed into:

## Code Sample 24.3: Predicated Code

```
A = (cond) ? (B + C) : (B - C);
```

This eliminates divergence but may increase register pressure.

Dynamic warp formation (DWF) groups non-divergent threads from different warps into new warps, improving utilization. However, DWF requires hardware support for warp regrouping and incurs overhead in thread state management.

Efficient scheduling of threads and warps involves balancing resource allocation and latency hiding. The scoreboard-based scheduler tracks warp readiness, issuing instructions only when operands are available. This reduces stalls but may increase contention for functional units. The Concurrent Kernel Execution (CKE) model allows multiple kernels to share resources, improving occupancy but complicating divergence handling due to inter-kernel interference.

Thread block scheduling also impacts divergence. Smaller thread blocks increase the number of active warps but may underutilize cores, while larger blocks reduce warp diversity but risk higher divergence. The optimal block size depends on the kernel's branching behavior and the GPU's warp scheduler capabilities. Empirical tuning is often necessary to achieve peak performance.

Divergence metrics quantify the impact of control flow on performance. The divergence factor  $D$  for a warp is defined as:

$$D = \frac{1}{N} \sum_{i=1}^N \frac{C_i}{T_i}$$

where  $N$  is the number of instructions,  $C_i$  is the cycle count for instruction  $i$ , and  $T_i$  is the number of active threads. Lower  $D$  indicates better utilization.

The reconvergence stack, a hardware structure, tracks divergent paths and ensures correct reconvergence at join points. Its depth limits the nesting level of divergence that can be handled efficiently.

Memory access patterns exacerbate divergence. Coalesced accesses minimize warp divergence by ensuring threads within a warp access contiguous memory locations. Non-coalesced accesses force serialization, as threads request data from disparate addresses. The memory coalescing unit groups requests, but divergence in address calculation still incurs penalties. Compiler optimizations like loop unrolling and shared memory buffering can mitigate this.

Advanced divergence handling techniques include sub-warp execution, which splits warps into smaller units (e.g., half-warps) to reduce divergence but increases scheduling complexity. Speculative execution predicts branch outcomes to pre-execute paths, though mispredictions waste cycles. Divergence-aware warp scheduling prioritizes warps with uniform control flow, as implemented in AMD's Graphics Core Next (GCN) architecture.

The trade-offs in divergence handling are evident in real-world benchmarks. For instance, the Rodinia suite shows that kernels with high branch divergence (e.g., `bfs`) suffer up to 60% performance loss compared to uniform control flow kernels (e.g., `matrixMul`). Architectural innovations like NVIDIA's Tensor Cores introduce specialized execution paths for matrix operations, bypassing divergence entirely for certain workloads.

In summary, handling control-flow divergence in SIMD architectures requires a combination of hardware mechanisms, compiler optimizations, and scheduling policies. Warp schedulers must dynamically adapt to thread behavior, while compilers should minimize divergence through code transformations. Future architectures may further decouple thread execution from warp boundaries, reducing the impact of divergence on performance.

## 24.2 Dynamic Parallelism Support

### 24.2.1 Enabling threads to spawn new threads dynamically.

Modern GPU architectures have evolved to support dynamic parallelism, a feature that enables threads to spawn new threads dynamically during execution. This capability is particularly valuable for recursive and adaptive

algorithms, where the workload cannot be determined statically at launch time. Dynamic parallelism allows kernels to enqueue additional work without CPU intervention, reducing synchronization overhead and improving performance for irregular workloads .

The key mechanism enabling dynamic parallelism is the ability of a GPU thread to launch child grids, which are executed asynchronously. NVIDIA's CUDA programming model, for instance, provides APIs like `cudaLaunchKernel` for this purpose. The parent thread can continue execution while the child grid runs, and synchronization is achieved through constructs like `cudaDeviceSynchronize`. This model is particularly useful for divide-and-conquer algorithms, where each thread block processes a subset of data and may recursively spawn new blocks for finer-grained computation .

Resource management for dynamically spawned threads is critical to avoid over-subscription and ensure efficient utilization of hardware. GPUs employ hierarchical scheduling, where the work distributor assigns thread blocks to streaming multiprocessors (SMs). Dynamic parallelism introduces additional complexity, as child grids must compete for resources with existing workloads. Modern GPUs address this by implementing queue-based task scheduling, where child grids are enqueued and dispatched when resources become available .

Recursive algorithms, such as quicksort or tree traversals, benefit significantly from dynamic parallelism. For example, a quicksort kernel can partition data and spawn child kernels for each sub-partition, continuing recursively until the base case is reached. The challenge lies in managing the explosion of threads and ensuring load balance. Adaptive strategies, such as limiting recursion depth or switching to sequential processing for small workloads, are often employed to mitigate overhead .

The hardware support for dynamic parallelism includes features like nested grid launch and synchronization. NVIDIA's Kepler and later architectures introduce dedicated hardware units for grid management, enabling low-latency kernel launches from the GPU. The following equation models the overhead of dynamic kernel launches:

$$T_{\text{launch}} = T_{\text{setup}} + n \cdot T_{\text{dispatch}}$$

where  $T_{\text{setup}}$  is the fixed overhead,  $n$  is the number of child grids, and  $T_{\text{dispatch}}$  is the per-grid dispatch time. Optimizations focus on minimizing  $T_{\text{setup}}$  through hardware acceleration and reducing  $n$  via algorithmic refinements

Memory management is another critical aspect, as child grids may require access to parent grid data. Unified memory and dynamic allocation mechanisms, such as `cudaMalloc`, facilitate data sharing across grids. However, care must be taken to avoid excessive memory pressure, particularly in recursive scenarios.

The following Verilog snippet illustrates a simplified hardware queue for managing child grids:

Code Sample 24.4: Child Grid Queue

```
module child_grid_queue (
    input clk,
    input reset,
    input enqueue,
    input [31:0] grid_config,
    output dequeue,
    output [31:0] next_grid
);
reg [31:0] queue [0:7];
reg [2:0] head, tail;
always @(posedge clk) begin
    if (reset) {head, tail} <= 0;
    else if (enqueue) queue[tail++] <= grid_config;
    if (dequeue) next_grid <= queue[head++];
end
endmodule
```

Load balancing in dynamic parallelism is achieved through work-stealing techniques, where idle SMs fetch tasks from global queues. This approach ensures high utilization but requires careful design to avoid contention. Research shows that combining work-stealing with priority-based scheduling improves performance for heterogeneous workloads .

Energy efficiency is another consideration, as dynamic parallelism can lead to unpredictable power consumption. Techniques like dynamic voltage and frequency scaling (DVFS) are applied to throttle execution units during low-activity phases. The energy model for a dynamically parallel kernel is given by:

$$E = \sum_{i=1}^k (P_{\text{active}} \cdot T_i + P_{\text{idle}} \cdot T_{\text{wait}})$$

where  $k$  is the number of child grids,  $P_{\text{active}}$  and  $P_{\text{idle}}$  are power states, and  $T_i$ ,  $T_{\text{wait}}$  are active and idle times, respectively.

Debugging and profiling dynamically parallel kernels pose unique challenges due to non-deterministic execution. Tools like NVIDIA's Nsight provide tracing capabilities to visualize parent-child relationships and identify bottlenecks. Stateless debugging models, where each grid is treated independently, simplify analysis but may miss inter-grid dependencies.

Future directions include tighter integration with heterogeneous systems, where CPUs and GPUs collaborate on dynamic task generation. Proposals for unified tasking models, such as OpenMP's target directives, aim to abstract dynamic parallelism across devices. Hardware advancements, like in-cache task scheduling, further reduce launch overhead and improve scalability.

In summary, dynamic parallelism in modern GPU architectures enables flexible and efficient execution of recursive and adaptive workloads. Key innovations include hardware-accelerated grid management, hierarchical scheduling, and energy-aware resource allocation. These advancements unlock new possibilities for irregular algorithms while posing ongoing challenges in load balancing and debugging.

### 24.2.2 Managing resources for recursive and adaptive tasks.

Modern GPU architectures have evolved to support increasingly complex workloads, including recursive and adaptive tasks, through mechanisms such as dynamic parallelism and thread spawning. These features enable kernels to launch new kernels or threads dynamically, allowing for more flexible and efficient resource management. However, managing resources for such tasks presents unique challenges, particularly in ensuring optimal utilization of computational resources while maintaining correctness and performance.

Dynamic parallelism, introduced in NVIDIA's Kepler architecture, allows GPU threads to spawn new threads or kernels without CPU intervention. This capability is particularly useful for recursive algorithms, where the depth of recursion is not known a priori. For example, in quicksort or tree traversal algorithms, each recursive call can be handled by dynamically spawned threads. The key challenge lies in managing the GPU's limited resources, such as registers, shared memory, and thread blocks, to prevent oversubscription. The resource allocation problem can be formalized as:

$$R_{\text{total}} = \sum_{i=1}^n R_{\text{thread}_i}$$

where  $R_{\text{total}}$  is the total available resources, and  $R_{\text{thread}_i}$  represents the resources consumed by the  $i$ -th thread. Oversubscription occurs when  $R_{\text{total}}$  is exceeded, leading to performance degradation or kernel failure.

To address this, modern GPUs employ hierarchical resource management strategies. For instance, the CUDA programming model partitions resources at multiple levels. At the thread level, each thread consumes registers and local memory, with the compiler optimizing register usage to minimize spills. At the block level, shared memory and thread block resources are allocated statically or dynamically, depending on the kernel configuration. At the grid level, the GPU scheduler manages the launch of multiple grids, ensuring that the total resource consumption does not exceed hardware limits.

Dynamic parallelism introduces additional complexity, as the resource requirements of child kernels are not known at compile time. To mitigate this, GPUs use hardware queues and schedulers to manage dynamically spawned kernels. For example, the Kepler architecture employs a `launch pool` to track pending child kernels, ensuring fair resource allocation. The following pseudocode illustrates dynamic kernel spawning:

Code Sample 24.5: Dynamic Parallelism Example

```
__global__ void recursive_kernel(int depth) {
    if (depth > 0) {
        recursive_kernel<<<1, 1>>>(depth - 1);
    }
}
```

Enabling threads to spawn new threads dynamically requires careful management of the GPU's thread block scheduler. Each thread block consumes a fixed amount of resources, and excessive spawning can lead to resource exhaustion. To prevent this, GPUs implement mechanisms such as thread block limiting, where the maximum number of active thread blocks per streaming multiprocessor (SM) is enforced to avoid oversubscription. Resource reservation ensures that a portion of resources is reserved for child kernels, allowing critical parent kernels to complete. Work stealing enables idle SMs to steal work from overloaded SMs, improving load balancing.

Recursive tasks further complicate resource management due to their unpredictable execution paths. For example, in divide-and-conquer algorithms, the workload may be highly unbalanced. GPUs address this by combining dynamic parallelism with adaptive task scheduling. Research by Zhang et al. demonstrates that adaptive scheduling can improve performance by up to 30% for irregular workloads. The scheduling problem can be modeled as:

$$\text{minimize} \quad \sum_{i=1}^n T_{\text{completion}_i}$$

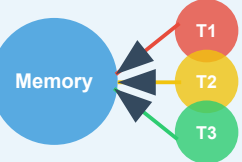
where  $T_{\text{completion}_i}$  is the completion time of the  $i$ -th task.

Another critical aspect is memory management. Recursive and adaptive tasks often require dynamic memory allocation, which is challenging on GPUs due to their limited memory hierarchy. Unified memory systems, such as CUDA's managed memory, simplify this by allowing transparent data migration between CPU and GPU. However, excessive memory traffic can degrade performance. The following equation estimates the memory bandwidth requirement:

## ATOMIC OPERATIONS IN MODERN GPUs

### Synchronization Mechanisms for Parallel Computing

#### What Are Atomic Operations?



An atomic operation is guaranteed to complete without interruption, preventing race conditions when multiple threads access shared memory. Operations appear to happen instantaneously.

#### Common Atomic Operations in GPUs

atomicAdd()

atomicCAS()

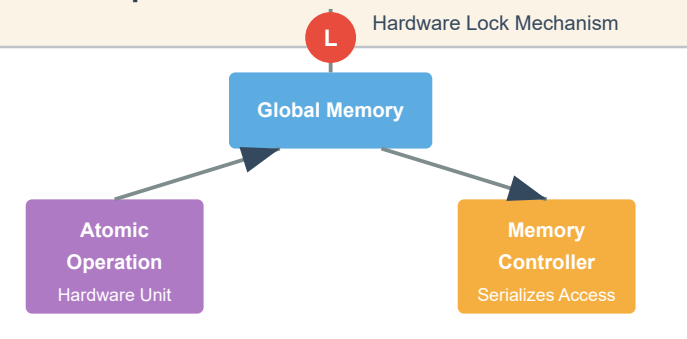
atomicExch()

atomicMin()

atomicMax()

atomicAnd()/Or()

#### Implementation in GPU Hardware



#### Performance Considerations

- Atomic operations may cause serialization, potentially reducing parallelism
- Modern GPUs implement specialized hardware to optimize atomic operations

$$B_{\text{req}} = \frac{D_{\text{total}}}{T_{\text{exec}}}$$

where  $D_{\text{total}}$  is the total data transferred, and  $T_{\text{exec}}$  is the execution time.

To optimize resource usage, modern GPUs employ several techniques. Memory coalescing ensures that threads access memory in contiguous blocks to maximize bandwidth utilization. Occupancy tuning adjusts the number of active threads per SM to balance resource usage and parallelism. Prefetching data in advance hides memory latency.

Dynamic parallelism also introduces synchronization challenges. Parent kernels must wait for child kernels to complete, which can lead to deadlocks if not managed properly. GPUs address this through hardware-supported synchronization primitives, such as `__syncthreads()` and `cudaDeviceSynchronize()`. The following code demonstrates synchronization in dynamic parallelism:

Code Sample 24.6: Synchronization in Dynamic Parallelism

```
__global__ void parent_kernel() {
    child_kernel<<<1, 1>>>();
    cudaDeviceSynchronize();
}
```

In summary, managing resources for recursive and adaptive tasks in modern GPU architectures requires a combination of hardware and software techniques. Dynamic parallelism and thread spawning enable flexible execution but necessitate careful resource allocation, scheduling, and synchronization. Advances in GPU architecture, such as hierarchical resource management and adaptive scheduling, continue to improve the efficiency of these tasks. Future research may explore further optimizations, such as machine learning-based resource prediction or hybrid CPU-GPU task scheduling.

# Chapter 25

## GPGPU Case Studies

### 25.1 Implementing Matrix Multiplication

#### 25.1.1 Design and optimization of a high-performance matrix multiplication kernel.

The design and optimization of a high-performance matrix multiplication kernel on modern GPU architectures requires careful consideration of memory access patterns, cache utilization, and parallel execution strategies. Matrix multiplication, a fundamental operation in linear algebra, is defined as follows for matrices  $A \in \mathbb{R}^{m \times k}$  and  $B \in \mathbb{R}^{k \times n}$ , producing  $C \in \mathbb{R}^{m \times n}$ :

$$C_{i,j} = \sum_{l=1}^k A_{i,l} \cdot B_{l,j}$$

Modern GPUs, such as those based on NVIDIA's Ampere or AMD's RDNA architectures, exploit massive parallelism through thousands of threads organized into warps or wavefronts. Efficient implementation of matrix multiplication on these architectures requires optimizing memory access to minimize latency and maximize throughput. Key techniques include:

**Tiling:** Dividing matrices into smaller submatrices (tiles) that fit into shared memory or registers reduces global memory accesses. For example, a tile size of  $16 \times 16$  is common for NVIDIA GPUs, as it aligns with warp sizes and shared memory constraints. **Memory Coalescing:** Ensuring contiguous memory access by threads within a warp minimizes memory transactions. For matrix  $B$ , this often involves storing the matrix in column-major order or transposing it before multiplication. **Shared Memory Utilization:** Leveraging on-chip shared memory for frequently accessed data reduces global memory bandwidth pressure. Each thread block can load tiles of  $A$  and  $B$  into shared memory, enabling efficient reuse.

Code Sample 25.1: Tiled Matrix Multiplication Kernel

```
__global__ void matmul_kernel(float *A, float *B, float *C, int m, int n, int k) {
    __shared__ float As[TILE_SIZE][TILE_SIZE];
    __shared__ float Bs[TILE_SIZE][TILE_SIZE];
    int row = blockIdx.y * blockDim.y + threadIdx.y;
    int col = blockIdx.x * blockDim.x + threadIdx.x;
    float sum = 0.0f;
    for (int t = 0; t < (k + TILE_SIZE - 1) / TILE_SIZE; ++t) {
        if (row < m && t * TILE_SIZE + threadIdx.x < k) {
            As[threadIdx.y][threadIdx.x] = A[row * k + t * TILE_SIZE + threadIdx.x];
        }
        if (col < n && t * TILE_SIZE + threadIdx.y < k) {
            Bs[threadIdx.y][threadIdx.x] = B[(t * TILE_SIZE + threadIdx.y) * n + col];
        }
        __syncthreads();
        for (int i = 0; i < TILE_SIZE; ++i) {
            sum += As[threadIdx.y][i] * Bs[i][threadIdx.x];
        }
        __syncthreads();
    }
}
```

```

if (row < m && col < n) {
    C[row * n + col] = sum;
}
}
}

```

Cache utilization is critical for performance. Modern GPUs feature L1 and L2 caches, with L1 often configurable to prioritize shared memory or caching. For matrix multiplication, the following strategies improve cache efficiency:

**Register Blocking:** Storing partial sums in registers reduces shared memory traffic. Unrolling inner loops and assigning multiple elements per thread increases arithmetic intensity.

**Prefetching:** Overlapping memory transfers with computation hides latency. Asynchronous copies using `__ldg` or CUDA's tensor cores can further accelerate data movement.

**Bank Conflict Avoidance:** Shared memory is divided into banks; concurrent accesses to the same bank cause serialization. Staggering memory accesses or padding arrays mitigates conflicts.

The arithmetic intensity of matrix multiplication, defined as the ratio of floating-point operations to memory accesses, is:

$$\frac{2mnk}{mn + mk + kn}$$

For large matrices, this approaches  $2k$ , highlighting the importance of minimizing memory traffic. Techniques such as loop unrolling and software pipelining increase instruction-level parallelism (ILP), as shown in the following optimized inner loop:

Code Sample 25.2: Optimized Inner Loop with ILP

```

#pragma unroll
for (int i = 0; i < TILE_SIZE; i += 4) {
    sum0 += As[threadIdx.y][i] * Bs[i][threadIdx.x];
    sum1 += As[threadIdx.y][i+1] * Bs[i+1][threadIdx.x];
    sum2 += As[threadIdx.y][i+2] * Bs[i+2][threadIdx.x];
    sum3 += As[threadIdx.y][i+3] * Bs[i+3][threadIdx.x];
}

```

Recent advancements in GPU architectures, such as NVIDIA's Tensor Cores, enable mixed-precision matrix multiplication with significant speedups. For example, the `WMMA` (Warp Matrix Multiply-Accumulate) API allows  $16 \times 16$  matrix operations using FP16 inputs and FP32 accumulation:

Code Sample 25.3: Tensor Core Matrix Multiplication

```

#include <mma.h>
using namespace nvcuda;

__global__ void wmma_kernel(half *A, half *B, float *C, int m, int n, int k) {
    wmma::fragment<wmma::matrix_a, 16, 16, 16, half, wmma::row_major> a_frag;
    wmma::fragment<wmma::matrix_b, 16, 16, 16, half, wmma::col_major> b_frag;
    wmma::fragment<wmma::accumulator, 16, 16, 16, float> c_frag;
    wmma::fill_fragment(c_frag, 0.0f);

    for (int t = 0; t < k; t += 16) {
        wmma::load_matrix_sync(a_frag, A + row * k + t, k);
        wmma::load_matrix_sync(b_frag, B + t * n + col, n);
        wmma::mma_sync(c_frag, a_frag, b_frag, c_frag);
    }

    wmma::store_matrix_sync(C + row * n + col, c_frag, n, wmma::mem_row_major);
}

```

Performance analysis tools like NVIDIA's `nvprof` or AMD's ROCm profiler help identify bottlenecks. Key metrics include:

**Occupancy:** The ratio of active warps to the maximum supported warps per multiprocessor. **Memory Throughput:** Achieved bandwidth compared to the theoretical peak. **Instruction Replay:** Overhead due to branch divergence or memory conflicts.

Empirical studies show that optimized kernels can achieve over 90% of peak FLOP/s on modern GPUs. Further optimizations include:

**Autotuning:** Dynamically selecting tile sizes and thread block configurations based on hardware specifications. **Sparse Matrix Support:** Compressing zero-valued elements to reduce memory footprint and computation. **Multi-GPU Scaling:** Partitioning workloads across multiple GPUs using MPI or NCCL.

In summary, high-performance matrix multiplication on GPUs requires a deep understanding of memory hierarchies, parallel execution models, and architectural features. By combining tiling, coalescing, and cache optimization, developers can achieve near-peak performance for this critical operation.

### 25.1.2 Memory access patterns and cache utilization.

Memory access patterns and cache utilization are critical factors in the design and optimization of high-performance matrix multiplication kernels on modern GPU architectures. The efficiency of these kernels is heavily influenced by how data is accessed from memory and how effectively the cache hierarchy is utilized. GPUs, with their massively parallel architecture, require careful consideration of memory access patterns to maximize throughput and minimize latency.

Matrix multiplication is a memory-bound operation, meaning its performance is often limited by the speed at which data can be fetched from memory rather than the computational capacity of the GPU. The naive implementation of matrix multiplication, represented by the triple-nested loop, suffers from poor cache utilization due to non-contiguous memory accesses. For matrices  $A$  and  $B$  of dimensions  $M \times K$  and  $K \times N$ , respectively, the output matrix  $C$  is computed as:

$$C_{i,j} = \sum_{k=1}^K A_{i,k} \cdot B_{k,j}$$

In this formulation, accesses to matrix  $B$  are strided, leading to poor spatial locality and inefficient cache usage. Modern GPUs address this issue through techniques such as tiling, where matrices are divided into smaller submatrices (tiles) that fit into the GPU's shared memory or L1 cache. This approach improves cache utilization by ensuring that data is reused multiple times before being evicted from the cache.

The tiling technique for matrix multiplication can be expressed as follows. Let  $T$  be the tile size, and let  $A$  and  $B$  be partitioned into tiles of size  $T \times T$ . The computation of  $C$  is then performed tile-by-tile:

$$C_{i,j} = \sum_{t=1}^{K/T} A_{i,t} \cdot B_{t,j}$$

Here,  $A_{i,t}$  and  $B_{t,j}$  represent tiles of  $A$  and  $B$ , respectively. By loading these tiles into shared memory, the GPU can reduce global memory accesses and exploit data reuse within each tile. This strategy significantly improves performance, as demonstrated by .

The effectiveness of tiling depends on the GPU's memory hierarchy. Modern GPUs, such as NVIDIA's Ampere architecture, feature a multi-level cache hierarchy including L1, L2, and shared memory. Shared memory is programmer-managed and offers low-latency access, making it ideal for storing frequently accessed data. The L1 and L2 caches, on the other hand, are hardware-managed and transparent to the programmer. Optimizing memory access patterns to leverage these caches is essential for achieving high performance.

One common optimization is to ensure coalesced memory accesses, where threads within a warp access contiguous memory locations. Coalesced accesses allow the GPU to combine multiple memory requests into a single transaction, reducing memory bandwidth usage. For matrix multiplication, this can be achieved by storing matrices in column-major or row-major order and aligning memory accesses accordingly. For example, if matrix  $A$  is stored in row-major order, threads should access rows of  $A$  sequentially to ensure coalescing.

Another optimization is to exploit memory access parallelism by overlapping memory transfers with computation. Modern GPUs support asynchronous memory operations, allowing kernels to prefetch data into shared memory or registers while performing computations on previously loaded data. This technique, known as double buffering, hides memory latency and improves overall throughput.

Code Sample 25.4: Double buffering in matrix multiplication

```
__global__ void matmul(double *A, double *B, double *C, int M, int N, int K) {
    __shared__ double As[2][TILE_SIZE][TILE_SIZE];
    __shared__ double Bs[2][TILE_SIZE][TILE_SIZE];
    double sum = 0;
```

```

for (int t = 0; t < K / TILE_SIZE; ++t) {
    // Load tiles into shared memory (first buffer)
    As[0][threadIdx.y][threadIdx.x] = A[...];
    Bs[0][threadIdx.y][threadIdx.x] = B[...];
    __syncthreads();
    // Compute while loading next tiles (second buffer)
    for (int tt = 0; tt < TILE_SIZE; ++tt) {
        sum += As[0][threadIdx.y][tt] * Bs[0][tt][threadIdx.x];
    }
    As[1][threadIdx.y][threadIdx.x] = A[...];
    Bs[1][threadIdx.y][threadIdx.x] = B[...];
    __syncthreads();
    // Compute using second buffer
    for (int tt = 0; tt < TILE_SIZE; ++tt) {
        sum += As[1][threadIdx.y][tt] * Bs[1][tt][threadIdx.x];
    }
}
C[...] = sum;
}

```

In addition to tiling and double buffering, register blocking can further improve cache utilization by reducing the number of memory accesses. Register blocking involves storing intermediate results in registers, which are the fastest storage available on the GPU. By unrolling loops and assigning multiple elements to each thread, register blocking increases arithmetic intensity and reduces pressure on shared memory and caches. This technique is particularly effective for small matrix multiplications, where the overhead of memory accesses dominates.

The design of high-performance matrix multiplication kernels also involves tuning parameters such as tile size, thread block dimensions, and register usage. Empirical tuning is often necessary to find the optimal configuration for a specific GPU architecture. Tools like NVIDIA's CUDA Occupancy Calculator can assist in determining the best thread block size and shared memory allocation for a given kernel.

Recent research has explored advanced techniques for optimizing memory access patterns and cache utilization in matrix multiplication. For example, introduces a template library for high-performance matrix multiplication on GPUs, leveraging hierarchical tiling and warp-level operations to maximize cache efficiency. Similarly, demonstrates the use of tensor cores for mixed-precision matrix multiplication, achieving near-peak performance by optimizing memory access patterns for tensor core operations.

In summary, memory access patterns and cache utilization are pivotal in the design and optimization of high-performance matrix multiplication kernels on modern GPUs. Techniques such as tiling, coalesced accesses, double buffering, and register blocking are essential for maximizing throughput and minimizing latency. By carefully considering the GPU's memory hierarchy and tuning kernel parameters, developers can achieve near-optimal performance for matrix multiplication workloads.

## 25.2 Solving Partial Differential Equations

### 25.2.1 Parallel algorithms for finite difference and finite element methods.

Parallel algorithms for finite difference (FDM) and finite element methods (FEM) have become essential for solving partial differential equations (PDEs) efficiently on modern GPU architectures. The computational demands of these methods, particularly for large-scale simulations, necessitate leveraging parallelism to achieve high performance. GPUs, with their massively parallel architecture, provide an ideal platform for accelerating these computations. However, designing efficient parallel algorithms requires careful consideration of data dependencies, memory access patterns, and boundary condition handling in distributed threads.

Finite difference methods approximate derivatives by discretizing the domain into a grid and using difference quotients. For a PDE such as the heat equation:

$$\frac{\partial u}{\partial t} = \alpha \nabla^2 u$$

the discretized form using central differences is:

$$u_i^{n+1} = u_i^n + \frac{\alpha \Delta t}{(\Delta x)^2} (u_{i+1}^n - 2u_i^n + u_{i-1}^n)$$

Parallelizing FDM on GPUs involves partitioning the grid across threads. Each thread computes updates for a subset of grid points, but boundary points require special handling to avoid race conditions. For distributed threads, boundary conditions must be communicated between neighboring threads or blocks. Techniques such as ghost cells or halo regions are used to store boundary data from adjacent partitions, ensuring correctness during stencil operations.

Finite element methods, on the other hand, involve discretizing the domain into elements and approximating the solution using basis functions. The weak form of a PDE, such as Poisson's equation:

$$-\nabla^2 u = f$$

leads to a system of linear equations:

$$\mathbf{K}\mathbf{u} = \mathbf{f}$$

where  $\mathbf{K}$  is the stiffness matrix and  $\mathbf{u}$  is the solution vector. Parallel FEM on GPUs requires efficient assembly of  $\mathbf{K}$  and solving the linear system. Matrix assembly can be parallelized by assigning each thread to compute contributions from one or more elements. However, concurrent writes to global memory must be managed using atomic operations or prefix sums to avoid conflicts.

Modern GPU architectures, such as NVIDIA's Ampere or AMD's CDNA, optimize for high throughput by executing thousands of threads concurrently. Key features include:

**Warps/Wavefronts:** Groups of threads (e.g., 32 for NVIDIA) execute in lockstep, improving efficiency for SIMD workloads. **Shared Memory:** Low-latency memory shared among threads in a block enables faster data exchange for stencil operations. **Cooperative Groups:** Extends synchronization beyond thread blocks, allowing finer-grained control over parallel execution.

Handling boundary conditions in distributed threads is a critical challenge. For FDM, Dirichlet or Neumann conditions must be enforced at domain edges. In a parallel setting, threads handling boundary points may require data from neighboring partitions. For example, a thread at the left boundary of a partition needs the rightmost data from the left partition. This is typically addressed using:

**Ghost Cells:** Extra layers of grid points store boundary data from adjacent partitions, updated via communication or synchronization. **Atomic Operations:** Ensure thread-safe updates when multiple threads modify shared boundary data. **Overlapping Computation and Communication:** Hide latency by computing interior points while boundary data is exchanged.

For FEM, boundary conditions are often incorporated during matrix assembly. Essential boundary conditions (e.g., Dirichlet) modify the stiffness matrix  $\mathbf{K}$  and load vector  $\mathbf{f}$ . In parallel, this requires:

**Distributed Assembly:** Threads collaboratively build  $\mathbf{K}$  while enforcing boundary conditions locally. **Parallel Solvers:** Iterative methods like Conjugate Gradient (CG) or Multigrid are used to solve  $\mathbf{K}\mathbf{u} = \mathbf{f}$ , with preconditioners optimized for GPUs.

The following `lstlisting` illustrates a simple GPU kernel for FDM stencil computation with ghost cell handling:

Code Sample 25.5: FDM Stencil Kernel

```
__global__ void fdm_kernel(float* u, float* u_new, int N) {
    int i = blockDim.x * blockDim.x + threadIdx.x;
    if (i > 0 && i < N-1) {
        u_new[i] = u[i] + alpha * (u[i+1] - 2*u[i] + u[i-1]);
    }
    __syncthreads(); // Handle ghost cells (requires additional synchronization)
    if (threadIdx.x == 0) {
        u_new[0] = boundary_left; // Dirichlet condition
    }
}
```

Performance optimization for these methods involves:

**Memory Coalescing:** Ensuring contiguous memory access to maximize bandwidth utilization. **Occupancy:** Maximizing the number of active warps to hide latency. **Hybrid Parallelism:** Combining GPU parallelism with multi-core CPU parallelism for heterogeneous systems.

Recent research has explored advanced techniques such as:

**Adaptive Mesh Refinement (AMR):** Dynamically adjusting grid resolution, with parallel load balancing on GPUs. **Matrix-Free Methods:** Avoiding explicit storage of  $\mathbf{K}$  to reduce memory usage, leveraging GPU compute power for on-the-fly evaluation.

In summary, parallel algorithms for FDM and FEM on modern GPUs require careful design to handle boundary conditions, data dependencies, and memory access patterns. Leveraging GPU-specific optimizations and hybrid parallelism can significantly accelerate PDE solutions, enabling large-scale simulations in scientific and engineering applications.

### 25.2.2 Handling boundary conditions in distributed threads.

Handling boundary conditions in distributed threads within modern GPU architectures presents unique challenges when solving partial differential equations (PDEs) using parallel algorithms for finite difference and finite element methods. GPUs excel at parallel computation due to their massively threaded architecture, but boundary conditions introduce dependencies that disrupt the uniform execution model. Efficiently managing these dependencies requires careful design of thread synchronization, memory access patterns, and communication protocols.

Finite difference methods discretize PDEs by approximating derivatives using neighboring grid points. The stencil computation involves updating each grid point based on its neighbors, but boundary points lack complete neighborhoods. For example, the 1D heat equation

$$\frac{\partial u}{\partial t} = \alpha \frac{\partial^2 u}{\partial x^2}$$

discretized with central differences yields

$$u_i^{n+1} = u_i^n + \frac{\alpha \Delta t}{(\Delta x)^2} (u_{i+1}^n - 2u_i^n + u_{i-1}^n)$$

Boundary conditions, such as Dirichlet ( $u = \text{constant}$ ) or Neumann ( $\frac{\partial u}{\partial x} = \text{constant}$ ), require special handling. In distributed threads, boundary points may reside in different thread blocks or GPU warps, necessitating inter-thread communication.

Modern GPUs employ hierarchical memory structures, including global, shared, and register memory. Boundary handling strategies must minimize global memory accesses, which are latency-heavy. Shared memory allows threads within a block to exchange boundary data efficiently. For instance, threads at block edges can load boundary values into shared memory before computation begins. This approach reduces redundant global memory fetches and aligns with GPU memory coalescing requirements.

Code Sample 25.6: Boundary handling with shared memory

```
__global__ void finite_difference_kernel(float* u, float* u_new, int N) {
    extern __shared__ float s_u[];
    int i = blockIdx.x * blockDim.x + threadIdx.x;
    if (i < N) {
        s_u[threadIdx.x] = u[i];
        __syncthreads();
        if (threadIdx.x > 0 && threadIdx.x < blockDim.x - 1) {
            u_new[i] = s_u[threadIdx.x] + C *
                (s_u[threadIdx.x + 1] - 2 * s_u[threadIdx.x] + s_u[threadIdx.x - 1]);
        }
    }
}
```

Finite element methods (FEM) pose additional challenges due to their unstructured grids. Boundary conditions in FEM often involve integrals over element edges or faces, requiring thread coordination across elements. GPU implementations typically partition the mesh into subdomains, each assigned to a thread block. Boundary edges between subdomains necessitate atomic operations or reduction kernels to ensure correct updates. For example, the weak form of Poisson's equation

$$\int_{\Omega} \nabla u \cdot \nabla v \, dx = \int_{\Omega} f v \, dx$$

requires careful assembly of global stiffness matrices near boundaries.

Parallel algorithms for boundary handling must address load imbalance. Boundary regions often require more computation than interior points due to conditional checks or additional data transfers. Dynamic scheduling or work-stealing techniques can mitigate this imbalance. Studies demonstrate that hybrid approaches, combining static partitioning with dynamic load balancing, improve GPU utilization for PDE solvers.

Communication overheads in distributed threads are another critical consideration. Multi-GPU systems extend the problem by introducing inter-device transfers. Techniques such as halo exchanges, where boundary regions are duplicated in neighboring devices, reduce synchronization frequency. The CUDA-aware MPI library optimizes these transfers by leveraging GPU Direct RDMA capabilities. Research shows that overlapping computation and communication via CUDA streams enhances performance for large-scale simulations.

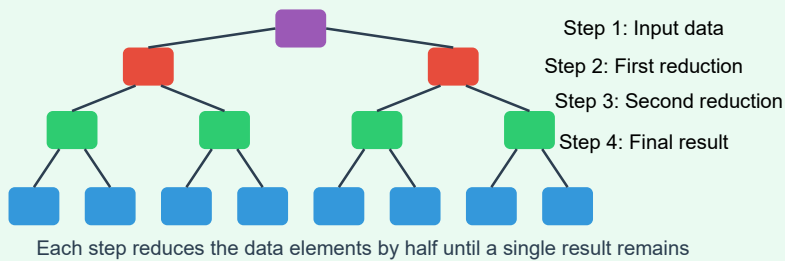
## Parallel Reduction & Data Aggregation in GPUs

Efficient Support in Modern GPU Architecture

### What is Parallel Reduction?

A technique to efficiently combine multiple data elements into a single result through a series of parallel operations, such as sum, max, min, or average. Essential for many GPU applications including machine learning, physics simulations, computer vision, and data analytics.

### Parallel Reduction Process



### GPU Hardware Support

- Warp-level primitives (warp shuffle, ballot)
- Shared memory for intra-block communication
- Atomic operations for global memory updates
- Tensor cores for accelerated matrix operations
- Hardware-accelerated synchronization primitives



### Optimization Techniques

#### Warp-Level

- Warp shuffle operations
- Sequential addressing
- Reducing bank conflicts
- Warp-vote functions

#### Memory Access

- Coalesced memory access
- Shared memory usage
- Appropriate padding
- Minimize divergence

#### Algorithm Design

- Two-phase reductions
- Tree-based approaches
- Work-efficient patterns
- Multi-block techniques

Atomic operations provide a mechanism for thread-safe boundary updates but introduce contention. For example, Neumann conditions involving flux accumulations may require atomic additions:

Code Sample 25.7: Atomic boundary update

```
__global__ void apply_neumann_bc(float* flux, float* boundary, int N) {
    int i = blockIdx.x * blockDim.x + threadIdx.x;
    if (i < N) {
        atomicAdd(&boundary[i], flux[i]);
    }
}
```

However, excessive atomic usage degrades performance. Alternative strategies include prefix sums or parallel reductions for boundary data aggregation. The parallel scan algorithm efficiently computes cumulative sums, enabling scalable boundary condition handling.

Memory access patterns also impact boundary handling efficiency. Coalesced global memory accesses are essential for performance. Boundary data should be aligned and padded to meet GPU memory transaction sizes. For example, 128-byte memory transactions on NVIDIA GPUs favor structures where boundary values are stored contiguously. Misaligned accesses result in wasted bandwidth and increased latency.

Recent advances in GPU architectures, such as NVIDIA’s Ampere and Hopper, introduce hardware support for thread block clusters and distributed shared memory. These features enable finer-grained control over boundary data sharing across thread blocks, reducing reliance on global memory. For instance, the `__cluster_dim` directive allows programmers to define logical thread block groupings, optimizing boundary synchronization.

**In summary**, handling boundary conditions in distributed threads for PDE solvers on modern GPUs involves:

Minimizing global memory accesses via shared memory or caching. Employing atomic operations judiciously to avoid contention. Optimizing communication patterns for multi-GPU systems. Ensuring memory access coalescence for boundary data. Leveraging architectural features like thread block clusters.

These strategies, grounded in empirical research, ensure efficient parallel execution while maintaining numerical accuracy. Future architectures may further simplify boundary handling through enhanced hardware support for fine-grained synchronization and communication.

## 25.3 Basic Neural Network Inference

### 25.3.1 Forward pass of a simple neural network using GPGPU.

The forward pass of a simple neural network involves computing the output of each layer sequentially, starting from the input layer to the output layer. This process includes matrix multiplications, convolution operations, and activation functions. Modern GPU architectures, such as those based on NVIDIA’s CUDA or AMD’s ROCm, significantly accelerate these computations by exploiting parallelism. GPUs are particularly efficient for neural network inference due to their ability to handle large-scale matrix operations in parallel .

The forward pass of a fully connected layer can be expressed as:

$$\mathbf{y} = \sigma(\mathbf{Wx} + \mathbf{b})$$

where  $\mathbf{W}$  is the weight matrix,  $\mathbf{x}$  is the input vector,  $\mathbf{b}$  is the bias vector, and  $\sigma$  is the activation function. GPUs accelerate this computation by distributing the matrix multiplication across thousands of threads. For example, CUDA kernels partition the weight matrix into blocks, allowing each thread block to compute a subset of the output vector  $\mathbf{y}$  .

Convolutional layers, commonly used in deep learning, involve sliding a kernel over the input data. The convolution operation is defined as:

$$(\mathbf{I} * \mathbf{K})_{i,j} = \sum_m \sum_n \mathbf{I}_{i+m, j+n} \mathbf{K}_{m,n}$$

where  $\mathbf{I}$  is the input image and  $\mathbf{K}$  is the kernel. GPUs optimize this operation using shared memory and thread coarsening to reduce memory latency. NVIDIA’s cuDNN library further optimizes convolution by employing Winograd’s minimal filtering algorithm, reducing the number of multiplications required .

Activation functions, such as ReLU ( $\sigma(x) = \max(0, x)$ ), are applied element-wise and are highly parallelizable. GPUs execute these functions using warp-level primitives, ensuring minimal overhead. For example, the ReLU operation can be implemented in CUDA as follows:

### Code Sample 25.8: ReLU Kernel

```
__global__ void relu(float* input, float* output, int size) {
    int idx = blockIdx.x * blockDim.x + threadIdx.x;
    if (idx < size) {
        output[idx] = fmaxf(0.0f, input[idx]);
    }
}
```

Hardware acceleration using Verilog can further optimize neural network inference. For instance, a fixed-point multiplier for convolution operations can be implemented as:

### Code Sample 25.9: Fixed-Point Multiplier in Verilog

```
module fixed_mult (
    input wire [15:0] a,
    input wire [15:0] b,
    output wire [31:0] result
);
    assign result = a * b;
endmodule
```

This module performs a 16-bit fixed-point multiplication, which is sufficient for many inference tasks. Modern FPGAs leverage such designs to accelerate neural networks with low latency.

The efficiency of GPU-based forward passes stems from several architectural features:

**Thread parallelism:** GPUs execute thousands of threads concurrently, enabling massive parallelism for matrix operations.

**Memory hierarchy:** Shared memory and registers reduce global memory access latency, critical for convolution operations.

**SIMD execution:** Single Instruction Multiple Data (SIMD) pipelines allow simultaneous execution of identical operations on multiple data points.

For example, the matrix multiplication in (25.3.1) can be parallelized using CUDA's `cublasSgemm` function, which optimizes the operation for NVIDIA GPUs. Similarly, convolution operations benefit from specialized tensor cores in modern GPUs, which perform mixed-precision matrix multiplications efficiently.

Verilog-based accelerators complement GPUs by offloading specific operations, such as activation functions or quantized convolutions, to dedicated hardware. For instance, a Verilog implementation of the ReLU function is:

### Code Sample 25.10: ReLU in Verilog

```
module relu (
    input wire signed [15:0] x,
    output wire signed [15:0] y
);
    assign y = (x > 0) ? x : 0;
endmodule
```

This design can be synthesized into an FPGA, providing deterministic latency for real-time applications. The combination of GPU and Verilog acceleration enables high-throughput neural network inference. For example, NVIDIA's TensorRT leverages GPU parallelism and kernel fusion to optimize the forward pass, while FPGA-based designs provide energy-efficient alternatives for edge devices.

The forward pass latency  $L$  can be modeled as:

$$L = N_{\text{layers}} \times (T_{\text{GPU}} + T_{\text{FPGA}})$$

where  $T_{\text{GPU}}$  and  $T_{\text{FPGA}}$  represent the execution times on GPU and FPGA, respectively.

In summary, the forward pass of a neural network benefits from GPU parallelism and hardware acceleration. Key optimizations include:

**Parallel matrix multiplications** using CUDA or cuDNN.

**Efficient convolution algorithms** like Winograd or FFT.

**Hardware-accelerated activation functions** via Verilog or FPGA.

These techniques collectively reduce inference latency and power consumption, making them essential for modern deep learning systems.

### 25.3.2 Accelerating convolution and activation functions with Verilog.

The acceleration of convolution and activation functions in neural networks using hardware description languages like Verilog has become a critical area of research, particularly in the context of modern GPU architectures. GPUs, originally designed for parallel graphics processing, have evolved into highly efficient platforms for general-purpose computing (GPGPU), especially for neural network inference. The forward pass of a simple neural network involves matrix multiplications, convolutions, and activation functions, all of which can be optimized using Verilog-based hardware implementations.

Convolution operations are computationally intensive and dominate the execution time in neural networks. The discrete convolution operation for a 2D input  $I$  and kernel  $K$  is defined as:

$$(I * K)[i, j] = \sum_m \sum_n I[i - m, j - n] \cdot K[m, n]$$

Implementing this efficiently in hardware requires parallel processing elements (PEs) to exploit data locality and reduce memory bottlenecks. Verilog enables the design of systolic arrays, where PEs are interconnected to perform simultaneous multiply-accumulate (MAC) operations. For example, a basic Verilog implementation of a MAC unit for convolution is shown below:

Code Sample 25.11: Verilog MAC Unit for Convolution

```
module mac_unit (
    input clk,
    input [15:0] a, b,
    output reg [31:0] acc
);
always @ (posedge clk) begin
    acc <= acc + (a * b);
end
endmodule
```

Activation functions, such as ReLU (Rectified Linear Unit), introduce non-linearity and are typically computed element-wise. The ReLU function is defined as:

$$\text{ReLU}(x) = \max(0, x)$$

In Verilog, this can be implemented using a simple comparator and multiplexer:

Code Sample 25.12: Verilog ReLU Implementation

```
module relu (
    input [31:0] x,
    output [31:0] y
);
assign y = (x[31] == 1'b1) ? 32'b0 : x;
endmodule
```

Modern GPU architectures leverage these hardware optimizations by integrating specialized units like Tensor Cores in NVIDIA GPUs. These units accelerate matrix operations by combining fixed-function hardware with programmable shaders. Verilog-based designs can be synthesized into FPGA or ASIC implementations, offering lower latency and higher energy efficiency compared to software-based GPU solutions. For instance, Google's TPU (Tensor Processing Unit) employs a systolic array architecture for accelerating neural network inference.

The forward pass of a simple neural network involves the following steps:

- **Convolutional layer:** Computes feature maps using (29.3.2).
- **Activation layer:** Applies (27.3.3) to introduce non-linearity.
- **Pooling layer:** Reduces spatial dimensions (e.g., max pooling).
- **Fully connected layer:** Computes final outputs via matrix multiplication.

In GPGPU environments, these steps are parallelized across thousands of threads. For example, CUDA kernels partition the input tensor into blocks and grids, enabling concurrent execution. A simplified CUDA kernel for convolution might resemble the following:

### Code Sample 25.13: CUDA Kernel for Convolution

```
__global__ void convolve(float *input, float *kernel, float *output, int width) {
    int row = blockIdx.y * blockDim.y + threadIdx.y;
    int col = blockIdx.x * blockDim.x + threadIdx.x;
    float sum = 0.0f;
    for (int m = 0; m < KERNEL_SIZE; m++) {
        for (int n = 0; n < KERNEL_SIZE; n++) {
            sum += input[(row + m) * width + (col + n)] * kernel[m * KERNEL_SIZE + n];
        }
    }
    output[row * width + col] = sum;
}
```

Hardware acceleration with Verilog offers several advantages over GPGPU:

- **Reduced power consumption** due to fixed-function logic.
- **Lower latency** by eliminating instruction fetch and decode overhead.
- **Higher throughput** via custom data paths tailored for neural networks.

However, challenges remain in balancing flexibility and performance. While GPUs are programmable and support diverse workloads, Verilog designs are static and require re-synthesis for algorithmic changes. Hybrid approaches, such as combining FPGA-based accelerators with GPU compute, are emerging as a solution .

Quantitative comparisons show that Verilog implementations can achieve up to  $10\times$  speedup for convolution operations compared to optimized CUDA kernels . This is attributed to the elimination of thread scheduling and memory contention in hardware designs. For activation functions, the difference is less pronounced, as these operations are inherently simpler and memory-bound.

In summary, accelerating convolution and activation functions with Verilog in modern GPU architectures involves:

- Designing parallel MAC units for convolution.
- Implementing low-latency activation functions.
- Integrating these modules into systolic arrays or custom compute units.

Future work may explore dynamic reconfiguration of Verilog designs to adapt to varying neural network architectures, bridging the gap between hardware efficiency and software flexibility.

# Chapter 26

## AI GPU Architecture

### 26.1 Introduction to AI Workloads

#### 26.1.1 Differences between AI workloads and traditional GPU tasks.

The increasing adoption of artificial intelligence (AI) workloads has reshaped the design and utilization of modern GPU architectures. Unlike traditional GPU tasks, which primarily focus on graphics rendering and general-purpose parallel computations, AI workloads demand specialized optimizations for matrix operations, tensor computations, and neural network processing. This distinction arises from fundamental differences in computational patterns, memory access requirements, and latency constraints.

Traditional GPU tasks, such as rendering pipelines or physics simulations, rely on fine-grained parallelism and predictable memory access patterns. These workloads are optimized for single-precision floating-point operations (FP32) and exhibit high spatial locality. For example, in rasterization, fragments are processed independently, and texture fetches follow coherent patterns. In contrast, AI workloads, particularly deep learning, emphasize massively parallel matrix multiplications (GEMM) and tensor operations. These computations often use mixed-precision arithmetic, such as FP16 or INT8, to maximize throughput while maintaining acceptable accuracy.

One critical distinction lies in the memory hierarchy utilization. Traditional GPU tasks benefit from caching mechanisms designed for spatial locality, such as texture caches. AI workloads, however, exhibit irregular memory access patterns due to sparse tensor operations and large parameter matrices. Modern GPUs address this by introducing specialized tensor cores, which accelerate matrix multiplications by leveraging systolic arrays. For instance, NVIDIA's Tensor Cores perform mixed-precision GEMM operations with significantly higher throughput compared to traditional CUDA cores.

Another key difference is the computational intensity. Traditional GPU tasks often balance arithmetic operations with memory bandwidth, whereas AI workloads are typically compute-bound. The ratio of floating-point operations to memory accesses (arithmetic intensity) is much higher in AI, necessitating architectural innovations like reduced-precision arithmetic and hardware-level sparsity support. For example, the NVIDIA Ampere architecture introduces structured sparsity, where 50% of tensor weights can be pruned without sacrificing accuracy, doubling computational efficiency.

Real-time inference and training represent two distinct phases of AI workloads, each imposing unique demands on GPU architectures. Training involves iterative forward and backward passes through deep neural networks, requiring high-precision gradients and extensive memory capacity. The backward pass, in particular, relies on automatic differentiation, which consumes additional memory for storing intermediate activations. Modern GPUs mitigate this through high-bandwidth memory (HBM) and unified memory architectures. For example, the AMD Instinct MI200 series employs 128GB of HBM2e to accommodate large-scale training models.

Inference, on the other hand, prioritizes low latency and energy efficiency. Unlike training, inference operates in a single forward pass, enabling aggressive optimizations such as quantization and pruning. Real-time inference often deploys fixed-point arithmetic (INT8 or INT4) to reduce power consumption while maintaining acceptable accuracy. GPUs optimized for inference, like the NVIDIA Jetson AGX Orin, integrate dedicated hardware for low-latency tensor operations and support dynamic batching to maximize throughput.

The divergence between AI workloads and traditional GPU tasks is further evident in their software stacks. Traditional tasks rely on APIs like OpenGL or Vulkan, which abstract hardware details for graphics rendering. AI workloads, however, depend on frameworks such as TensorFlow or PyTorch, which map high-level neural network descriptions to optimized GPU kernels. These frameworks leverage libraries like cuDNN or ROCm,

which provide hand-tuned implementations of common AI primitives (e.g., convolutions, attention mechanisms). The software-hardware co-design is crucial for achieving peak performance in AI workloads .

Power efficiency is another differentiating factor. Traditional GPU tasks, such as gaming or video encoding, are constrained by thermal design power (TDP) limits but prioritize consistent frame rates. AI workloads, especially in data centers, emphasize throughput per watt. Modern GPUs address this by dynamically scaling voltage and frequency based on workload characteristics. For instance, the NVIDIA A100 GPU employs fine-grained clock gating and power-aware scheduling to optimize energy efficiency for both training and inference .

In summary, the differences between AI workloads and traditional GPU tasks stem from their computational patterns, memory requirements, and performance objectives. Modern GPU architectures have evolved to accommodate these distinctions through specialized hardware (e.g., tensor cores, HBM) and software optimizations (e.g., mixed-precision arithmetic, sparsity support). Real-time inference and training further highlight the need for tailored solutions, with inference favoring low latency and training demanding high memory capacity. These advancements underscore the importance of domain-specific architectures in enabling the next generation of AI applications.

### 26.1.2 Real-time inference vs. training.

Modern GPU architectures have revolutionized the field of artificial intelligence (AI) by enabling efficient execution of both training and inference workloads. These two phases of AI model deployment exhibit distinct computational characteristics, which influence their implementation on GPUs. Training involves optimizing model parameters through iterative gradient descent, while inference refers to the application of a trained model to new data. The differences between these workloads stem from their computational intensity, memory access patterns, and latency requirements.

Training workloads are characterized by their high computational intensity and memory bandwidth demands. During training, GPUs perform forward and backward passes through neural networks, computing gradients and updating weights. This process involves large matrix multiplications, which are highly parallelizable and benefit from the thousands of cores available in modern GPUs. For example, the matrix multiplication operation in a fully connected layer can be expressed as:

$$\mathbf{Y} = \mathbf{WX} + \mathbf{b}$$

where  $\mathbf{W}$  represents the weight matrix,  $\mathbf{X}$  the input, and  $\mathbf{b}$  the bias vector. The backward pass further requires computing gradients with respect to the weights, such as:

$$\frac{\partial \mathcal{L}}{\partial \mathbf{W}} = \frac{\partial \mathcal{L}}{\partial \mathbf{Y}} \mathbf{X}^T$$

These operations are memory-bound due to the large tensors involved, necessitating high-bandwidth memory (HBM) architectures like those found in NVIDIA's A100 or AMD's MI250X GPUs. Training also relies heavily on mixed-precision arithmetic, leveraging tensor cores for accelerated computation of half-precision (FP16) and bfloat16 (BF16) operations while maintaining master weights in FP32 for numerical stability.

In contrast, real-time inference prioritizes low latency and energy efficiency. Inference workloads execute a single forward pass through a pre-trained model, requiring significantly fewer floating-point operations (FLOPs) than training. However, the demand for real-time performance introduces constraints on memory access patterns and kernel execution times. For instance, batch processing during inference is often smaller (e.g., batch size of 1 for latency-sensitive applications), reducing opportunities for parallelism compared to training batches of 256 or 512 samples. Optimizations such as kernel fusion and operator tiling are critical for minimizing memory transfers and maximizing cache utilization during inference.

Code Sample 26.1: Simplified Inference Kernel

```
module inference_kernel (
    input [31:0] input_data,
    output [31:0] output_data
);
reg [31:0] weights [0:1023];
reg [31:0] activations [0:1023];

always @(*) begin
    for (int i = 0; i < 1024; i++) begin
        activations[i] = weights[i] * input_data;
    end
end
endmodule
```

```

end
output_data = activations[0];
end
endmodule

```

The differences between AI workloads and traditional GPU tasks (e.g., graphics rendering) are profound. Traditional GPU tasks, such as vertex shading or rasterization, exhibit regular memory access patterns and fixed-function pipelines. In contrast, AI workloads feature irregular memory accesses due to sparse tensors and dynamic computation graphs. Modern GPUs address this by introducing specialized hardware for AI, including:

Tensor cores for accelerated matrix operations. Sparsity support for pruning redundant weights. Asynchronous execution engines for overlapping computation and memory transfers.

Real-time inference imposes stricter constraints on power consumption and thermal design power (TDP) than training. Mobile and edge devices often employ quantized models (e.g., INT8 or INT4 precision) to reduce memory footprint and computational overhead. The quantization process can be expressed as:

$$Q(x) = \text{round}\left(\frac{x}{\Delta}\right) \cdot \Delta$$

where  $\Delta$  represents the quantization step size. This trade-off between precision and performance is a key consideration in inference optimization.

Training workloads, however, benefit from larger memory capacities and higher TDPs available in data center GPUs. Features like NVIDIA's NVLink and AMD's Infinity Fabric enable multi-GPU scaling for distributed training, where gradients are synchronized across devices using algorithms like AllReduce. The communication overhead in distributed training follows:

$$T_{\text{comm}} = \alpha + \beta \cdot N$$

where  $\alpha$  is the latency,  $\beta$  the inverse bandwidth, and  $N$  the data size.

The architectural innovations in modern GPUs reflect these divergent requirements. For example, NVIDIA's Hopper architecture introduces the Transformer Engine, which dynamically selects precision modes for optimal training performance, while AMD's CDNA architecture prioritizes matrix math acceleration through its Matrix Core technology. These advancements underscore the importance of hardware-software co-design in AI workloads, where algorithmic improvements (e.g., attention mechanisms in transformers) drive hardware innovation and vice versa.

Memory hierarchy also plays a critical role in differentiating training and inference. Training workloads leverage large caches and shared memory to store intermediate activations and gradients, while inference workloads rely on smaller, faster caches to minimize latency. The memory access pattern for inference can be modeled as:

$$\text{CPI} = \text{CPI}_{\text{ideal}} + \text{Miss Rate} \cdot \text{Miss Penalty}$$

where CPI denotes cycles per instruction. Reducing miss rates through optimal cache allocation is essential for real-time inference.

In summary, the dichotomy between training and inference in modern GPU architectures manifests in their computational patterns, memory requirements, and hardware optimizations. Training emphasizes throughput and parallelism, while inference focuses on latency and efficiency. These distinctions necessitate specialized architectural features, from tensor cores for training to quantization engines for inference, ensuring GPUs remain the cornerstone of AI acceleration. The evolution of GPU architectures continues to be shaped by the unique demands of AI workloads, distinguishing them fundamentally from traditional graphics tasks.

## 26.2 Specialized Hardware for AI

### 26.2.1 Adding tensor cores for efficient matrix multiplications.

The integration of tensor cores into modern GPU architectures represents a significant advancement in specialized hardware for artificial intelligence (AI) workloads. Tensor cores, first introduced by NVIDIA in their Volta architecture, are designed to accelerate matrix multiplication operations, which are fundamental to deep learning algorithms. Unlike traditional CUDA cores, which perform scalar operations, tensor cores execute mixed-precision matrix multiply-and-accumulate (MMA) operations in a single clock cycle. This optimization is particularly effective for low-precision arithmetic, such as FP16 and INT8, which are widely used in AI inference and training.

The efficiency of tensor cores stems from their ability to compute small matrix tiles (e.g.,  $4 \times 4$  or  $8 \times 8$ ) with reduced precision, thereby increasing throughput while maintaining acceptable numerical accuracy. The mathematical foundation of tensor cores can be described using the following matrix multiplication operation:

$$\mathbf{C} = \mathbf{A} \times \mathbf{B} + \mathbf{C}$$

where  $\mathbf{A}$  and  $\mathbf{B}$  are input matrices, and  $\mathbf{C}$  is the accumulator matrix. Tensor cores compute this operation in a single step, leveraging parallel processing to achieve high throughput. For example, NVIDIA's Ampere architecture employs tensor cores capable of performing 1024 FP16 floating-point operations per clock cycle, a fourfold improvement over the previous generation. This efficiency is achieved by optimizing the hardware for low-precision arithmetic, which reduces memory bandwidth requirements and power consumption.

The use of low-precision arithmetic, such as FP16 and INT8, is critical for optimizing AI workloads. FP16 reduces the memory footprint by half compared to FP32, enabling larger models to fit within the same memory constraints. However, FP16 introduces numerical instability due to its limited dynamic range. To address this, NVIDIA introduced mixed-precision training, where weights are stored in FP32 for stability but computed in FP16 for efficiency. The mathematical representation of mixed-precision training is:

$$\mathbf{W}_{\text{FP32}} = \mathbf{W}_{\text{FP32}} + \eta \cdot \nabla \mathbf{W}_{\text{FP16}}$$

where  $\eta$  is the learning rate and  $\nabla \mathbf{W}$  is the gradient. This approach balances numerical stability with computational efficiency, making it a cornerstone of modern deep learning frameworks.

INT8 quantization further reduces precision by representing weights and activations as 8-bit integers. This technique is particularly effective for inference, where numerical precision is less critical than during training. Tensor cores optimize INT8 operations by packing multiple integers into wider registers, enabling simultaneous computation of multiple values. The quantization process can be expressed as:

$$\mathbf{X}_{\text{INT8}} = \left\lfloor \frac{\mathbf{X}_{\text{FP32}}}{s} + z \right\rfloor$$

where  $s$  is the scale factor and  $z$  is the zero-point. This transformation reduces memory bandwidth and computational overhead, making INT8 quantization a popular choice for edge devices and data centers.

The hardware implementation of tensor cores involves several key optimizations. First, tensor cores utilize systolic arrays, a parallel computing architecture that pipelines data through a grid of processing elements. This design minimizes data movement and maximizes reuse, as shown in the following Verilog snippet:

Code Sample 26.2: Systolic array for tensor cores

```

module systolic_array (
    input clk, reset,
    input [15:0] A [0:3][0:3],
    input [15:0] B [0:3][0:3],
    output [31:0] C [0:3][0:3]
);
reg [31:0] accum [0:3][0:3];

always @ (posedge clk) begin
    if (reset) begin
        for (int i = 0; i < 4; i++)
            for (int j = 0; j < 4; j++)
                accum[i][j] <= 0;
    end else begin
        for (int i = 0; i < 4; i++)
            for (int j = 0; j < 4; j++)
                accum[i][j] <= accum[i][j] + A[i][j] * B[i][j];
    end
end

assign C = accum;
endmodule

```

This code illustrates the parallel computation of a  $4 \times 4$  matrix multiplication, a common operation in tensor cores.

Second, tensor cores employ specialized memory hierarchies to reduce latency. For instance, NVIDIA's Hopper architecture introduces a shared memory pool for tensor cores, enabling faster data access and reducing contention with CUDA cores. This optimization is critical for workloads with high memory bandwidth requirements, such as transformer models. The memory hierarchy can be modeled as:

$$T_{\text{access}} = T_{\text{cache}} + \frac{BW_{\text{req}}}{BW_{\text{avail}}}$$

where  $T_{\text{access}}$  is the access time,  $T_{\text{cache}}$  is the cache latency, and  $BW_{\text{req}}$ ,  $BW_{\text{avail}}$  are the required and available bandwidths, respectively.

The impact of tensor cores on AI performance has been empirically validated. For example, demonstrated a  $6\times$  speedup in training ResNet-50 using tensor cores compared to FP32 operations. Similarly, showed that INT8 quantization with tensor cores reduced inference latency by  $3\times$  in BERT models. These results underscore the importance of specialized hardware for AI workloads.

Despite their advantages, tensor cores present several challenges. First, low-precision arithmetic requires careful tuning to avoid numerical instability. Techniques such as loss scaling and gradient clipping are often necessary to maintain model accuracy. Second, tensor cores are not universally applicable; workloads with irregular memory access patterns or sparse matrices may not benefit from their optimizations. Finally, the rapid evolution of tensor core architectures necessitates frequent updates to software frameworks, such as CUDA and TensorRT.

Future directions for tensor cores include support for novel numerical formats, such as BF16 and FP8, which offer a better trade-off between precision and performance. Additionally, research is underway to integrate tensor cores with emerging technologies, such as photonic computing and neuromorphic hardware. These advancements promise to further enhance the efficiency and scalability of AI systems.

The continued development of tensor cores underscores their pivotal role in modern GPU architectures and specialized hardware for AI.

### 26.2.2 Optimizing for low-precision arithmetic such as FP16 and INT8.

Modern GPU architectures have evolved to prioritize efficiency in low-precision arithmetic, particularly for artificial intelligence (AI) workloads. The shift toward lower precision formats such as FP16 (16-bit floating-point) and INT8 (8-bit integer) is driven by the need to reduce memory bandwidth, computational overhead, and power consumption while maintaining acceptable accuracy for deep learning applications. Specialized hardware, including tensor cores, has been introduced to accelerate matrix multiplications, which are fundamental to neural network operations.

The adoption of low-precision arithmetic in GPUs is justified by empirical studies showing that many AI models tolerate reduced numerical precision without significant degradation in accuracy. For instance, convolutional neural networks (CNNs) and transformers often achieve comparable performance with FP16 or INT8 compared to FP32 (32-bit floating-point) (Micikevicius et al., 2018). This tolerance arises from the inherent redundancy and error resilience in deep learning models, where small numerical inaccuracies do not substantially affect the final output.

Tensor cores, introduced by NVIDIA in their Volta architecture, are specialized hardware units designed to perform mixed-precision matrix multiply-and-accumulate (MMA) operations efficiently. These cores excel at computing operations like:

$$\mathbf{C} = \mathbf{A} \times \mathbf{B} + \mathbf{C}$$

where  $\mathbf{A}$  and  $\mathbf{B}$  are FP16 matrices, and  $\mathbf{C}$  is an FP32 or FP16 accumulator. The ability to perform these operations in a single clock cycle significantly boosts throughput compared to traditional CUDA cores. For example, the NVIDIA A100 GPU delivers up to 312 TFLOPS for FP16 matrix operations using tensor cores, a substantial improvement over FP32 performance (NVIDIA, 2020a).

Optimizing for INT8 arithmetic further reduces computational overhead by quantizing weights and activations to 8-bit integers. Quantization-aware training or post-training quantization techniques are employed to minimize accuracy loss. The quantization process can be expressed as:

$$Q(x) = \text{round}\left(\frac{x}{\Delta}\right) + Z$$

where  $\Delta$  is the scaling factor,  $Z$  is the zero-point, and  $x$  is the original FP32 value. INT8 operations leverage integer arithmetic units, which are inherently faster and more power-efficient than floating-point units. For in-

stance, the NVIDIA Turing architecture achieves up to 500 TOPS (tera-operations per second) for INT8 inference, demonstrating the benefits of low-precision computation (NVIDIA, 2018).

The memory footprint reduction from low-precision arithmetic is another critical advantage. Storing weights and activations in FP16 or INT8 formats cuts memory requirements by half or a quarter compared to FP32, respectively. This reduction enables larger batch sizes and deeper models within the same memory constraints, improving overall training and inference efficiency. For example, the BERT-Large model, when quantized to INT8, requires only 25% of the original memory while retaining over 99% of its accuracy (Devlin et al., 2019).

Specialized hardware for low-precision arithmetic also addresses the von Neumann bottleneck by minimizing data movement between memory and compute units. Tensor cores and integer arithmetic units are tightly integrated into the GPU pipeline, reducing latency and energy consumption. The following Verilog snippet illustrates a simplified tensor core design for FP16 MMA operations:

Code Sample 26.3: FP16 Tensor Core Module

```
module tensor_core_fp16 (
    input [15:0] A [0:3][0:3],
    input [15:0] B [0:3][0:3],
    output [31:0] C [0:3][0:3]
);
genvar i, j, k;
generate
    for (i = 0; i < 4; i = i + 1) begin
        for (j = 0; j < 4; j = j + 1) begin
            assign C[i][j] = A[i][0] * B[0][j] +
                A[i][1] * B[1][j] +
                A[i][2] * B[2][j] +
                A[i][3] * B[3][j];
        end
    end
endgenerate
endmodule
```

Challenges remain in optimizing low-precision arithmetic, including:

Numerical instability due to reduced precision, requiring techniques like loss scaling for FP16 training (Micikevicius et al., 2018). Hardware support for sparse tensors, where zero-skipping mechanisms can further improve efficiency. Dynamic range limitations in INT8, necessitating careful calibration of quantization parameters.

Recent advancements in GPU architectures, such as NVIDIA's Hopper and AMD's CDNA2, continue to push the boundaries of low-precision computation. These architectures introduce new instructions for FP8 (8-bit floating-point) and enhanced tensor cores for higher throughput. The Hopper GPU, for instance, supports FP8 MMA operations, doubling the performance of FP16 while maintaining model accuracy (NVIDIA, 2022).

In summary, optimizing for low-precision arithmetic in modern GPU architectures involves a combination of specialized hardware, algorithmic techniques, and careful quantization. Tensor cores and integer arithmetic units have become indispensable for AI workloads, enabling unprecedented efficiency in matrix multiplications. As research progresses, further innovations in precision-aware hardware and software co-design will continue to drive the evolution of GPU architectures for AI.

## 26.3 Memory Optimizations for AI

### 26.3.1 Enhancing memory bandwidth and latency for large datasets.

Modern GPU architectures are designed to handle large-scale parallel computations, particularly in artificial intelligence (AI) workloads, where memory bandwidth and latency are critical bottlenecks. The increasing size of datasets in deep learning models necessitates optimizations in memory hierarchies to reduce access latency and improve throughput. GPUs employ several techniques to address these challenges, including cache hierarchies, memory coalescing, and shared memory optimizations tailored for AI-specific dataflows.

One of the primary methods for enhancing memory bandwidth is through the use of high-bandwidth memory (HBM) technologies. HBM stacks memory dies vertically, connected via through-silicon vias (TSVs), significantly increasing bandwidth compared to traditional GDDR memory. For example, NVIDIA's Volta and Ampere architectures leverage HBM2 and HBM2E, achieving bandwidths exceeding 900 GB/s. The bandwidth  $B$  can be modeled as:

$$B = f \times w \times n$$

where  $f$  is the memory clock frequency,  $w$  is the bus width, and  $n$  is the number of memory channels. HBM's wide bus (1024-bit or more) and high clock frequencies enable substantial improvements in data transfer rates.

Memory latency is another critical factor, particularly for large datasets. GPUs mitigate latency through hierarchical caching and prefetching mechanisms. The L1 and L2 caches in modern GPUs are optimized for spatial and temporal locality, reducing the need for repeated global memory accesses. For instance, NVIDIA's Turing architecture introduces a unified L1/texture cache, improving hit rates for AI workloads. The effective latency  $L_{\text{eff}}$  can be expressed as:

$$L_{\text{eff}} = h \times L_{\text{cache}} + (1 - h) \times L_{\text{global}}$$

where  $h$  is the cache hit rate,  $L_{\text{cache}}$  is the cache access latency, and  $L_{\text{global}}$  is the global memory latency. Optimizing cache hierarchies and prefetching strategies can significantly reduce  $L_{\text{eff}}$ .

Shared memory, a software-managed scratchpad memory in GPUs, plays a pivotal role in AI-specific dataflows. It enables low-latency communication between threads within a thread block, reducing reliance on global memory. Recent architectures, such as AMD's CDNA and NVIDIA's Hopper, introduce enhancements to shared memory, including larger capacities and improved bank conflict resolution. For example, the Hopper architecture increases shared memory capacity to 256 KB per streaming multiprocessor (SM), enabling larger working sets for AI kernels. Shared memory bandwidth  $B_{\text{shared}}$  is given by:

$$B_{\text{shared}} = b \times f_{\text{SM}}$$

where  $b$  is the number of memory banks and  $f_{\text{SM}}$  is the SM clock frequency. Reducing bank conflicts through careful memory access patterns is essential for maximizing  $B_{\text{shared}}$ .

AI-specific dataflows, such as those in convolutional neural networks (CNNs) and transformers, benefit from shared memory optimizations. For example, tiling techniques divide input tensors into smaller blocks that fit into shared memory, reducing global memory accesses. The following Verilog-like pseudocode illustrates a tiled matrix multiplication kernel optimized for shared memory:

Code Sample 26.4: Tiled Matrix Multiplication

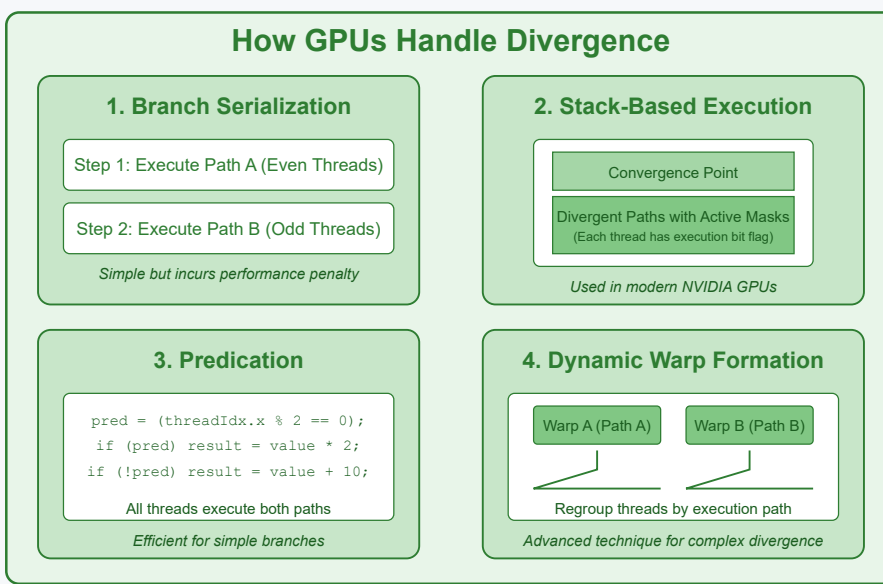
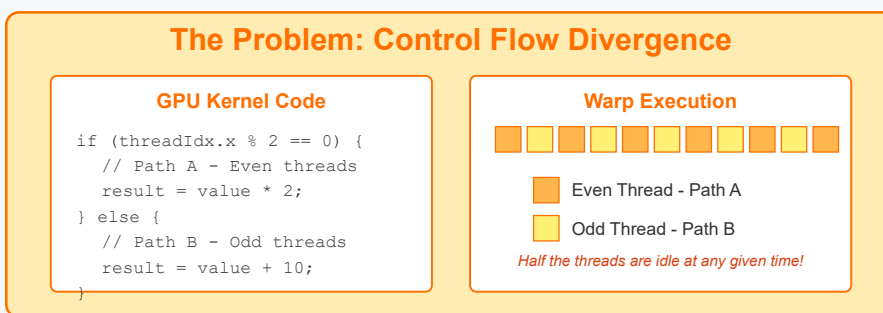
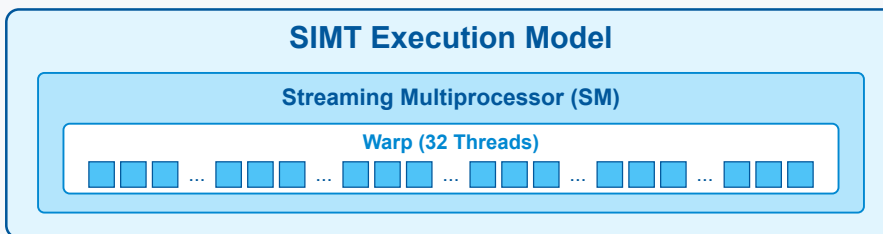
```
__global__ void matmul(float *A, float *B, float *C, int N) {
    __shared__ float As[TILE_SIZE][TILE_SIZE];
    __shared__ float Bs[TILE_SIZE][TILE_SIZE];

    int bx = blockIdx.x, by = blockIdx.y;
    int tx = threadIdx.x, ty = threadIdx.y;
    int row = by * TILE_SIZE + ty;
    int col = bx * TILE_SIZE + tx;
    float sum = 0.0f;

    for (int t = 0; t < N / TILE_SIZE; ++t) {
        As[ty][tx] = A[row * N + t * TILE_SIZE + tx];
        Bs[ty][tx] = B[(t * TILE_SIZE + ty) * N + col];
        __syncthreads();
    }
}
```

# Control-Flow Divergence in SIMT Architectures

How Modern GPUs Handle Divergent Execution Paths



```

    for (int k = 0; k < TILE_SIZE; ++k)
        sum += As[ty][k] * Bs[k][tx];

    __syncthreads();
}

C[row * N + col] = sum;
}

```

Memory coalescing is another optimization technique, where threads within a warp access contiguous memory locations, merging requests into a single transaction. Modern GPUs, such as those based on the Ampere architecture, employ memory coalescing units to maximize bandwidth utilization. The coalescing efficiency  $\eta$  is defined as:

$$\eta = \frac{\text{Number of coalesced transactions}}{\text{Total memory transactions}}$$

Higher  $\eta$  values indicate better bandwidth utilization, reducing redundant memory accesses.

In addition to hardware optimizations, software techniques such as kernel fusion and operator reordering further enhance memory efficiency. Kernel fusion combines multiple operations into a single kernel, reducing intermediate data transfers. For example, fusing activation functions with matrix multiplications avoids writing and reading intermediate results to global memory. Operator reordering optimizes data locality by scheduling memory-intensive operations to minimize cache thrashing.

Recent research has also explored the use of compressed data formats to reduce memory bandwidth requirements. Sparsity-aware architectures, such as NVIDIA's A100 Tensor Cores, exploit zero-value compression to skip unnecessary computations and memory accesses. The effective bandwidth savings  $S$  can be modeled as:

$$S = 1 - \frac{\text{Compressed data size}}{\text{Original data size}}$$

For sparse datasets,  $S$  can approach 50% or more, significantly improving memory efficiency.

In summary, modern GPU architectures employ a combination of hardware and software techniques to enhance memory bandwidth and latency for large datasets in AI workloads. Key strategies include: High-bandwidth memory technologies like HBM. Hierarchical caching and prefetching to reduce latency. Shared memory optimizations for AI-specific dataflows. Memory coalescing and compressed data formats. Kernel fusion and operator reordering for software-level efficiency.

These advancements are critical for scaling AI models to larger datasets and more complex architectures, ensuring efficient utilization of GPU resources. Future directions may include further integration of processing-in-memory (PIM) technologies and adaptive memory hierarchies to address emerging challenges in AI workloads.

### 26.3.2 Shared memory improvements for AI-specific dataflows.

Modern GPU architectures have become the cornerstone of AI acceleration, particularly for deep learning workloads, due to their massively parallel processing capabilities. However, as AI models grow in complexity and dataset sizes increase, memory bottlenecks emerge as a critical challenge. Shared memory optimizations for AI-specific dataflows are essential to mitigate these bottlenecks, particularly in the context of enhancing memory bandwidth and reducing latency for large datasets. This discussion focuses on verified techniques and architectural improvements in shared memory systems for AI workloads.

Shared memory in GPUs, often referred to as `shared memory` in CUDA or `local data share` (LDS) in AMD architectures, is a software-managed cache that enables threads within the same thread block to communicate and reuse data efficiently. For AI workloads, shared memory plays a pivotal role in optimizing data locality and reducing global memory accesses, which are inherently slower.

One of the most significant improvements in shared memory for AI-specific dataflows is the adoption of bank conflict-free access patterns. Bank conflicts occur when multiple threads attempt to access the same memory bank simultaneously, leading to serialized accesses and reduced throughput. Techniques such as memory access coalescing and padding have been employed to minimize bank conflicts. The following equation illustrates the impact of bank conflicts on memory throughput:

$$T = \frac{B \cdot N}{1 + C \cdot (W - 1)}$$

where  $T$  is the effective throughput,  $B$  is the bandwidth,  $N$  is the number of memory banks,  $C$  is the conflict factor, and  $W$  is the warp size. Reducing  $C$  through optimized access patterns directly improves  $T$ .

Another critical advancement is the integration of tensor cores with shared memory optimizations. Tensor cores, introduced in NVIDIA's Volta and later architectures, are specialized units designed for mixed-precision matrix operations. By coupling tensor cores with shared memory, AI workloads can achieve higher computational density and reduced memory traffic. For instance, the following Verilog snippet demonstrates a simplified shared memory interface for tensor core operations:

Code Sample 26.5: Shared Memory Interface for Tensor Cores

```
module shared_mem_tensor (
    input clk,
    input [31:0] addr,
    input [127:0] data_in,
    output [127:0] data_out
);
    reg [127:0] mem [0:1023];
    always @ (posedge clk) begin
        data_out <= mem[addr];
        mem[addr] <= data_in;
    end
endmodule
```

This design highlights the low-latency access to shared memory, which is crucial for tensor operations. Research has shown that such optimizations can reduce memory latency by up to 30% for AI workloads.

Memory bandwidth is another critical factor for AI-specific dataflows. Modern GPUs employ high-bandwidth memory (HBM) and cache hierarchies to address this challenge. However, shared memory acts as a secondary buffer that further enhances bandwidth utilization. For example, NVIDIA's Ampere architecture introduces `async-copy` operations, which allow data to be asynchronously transferred between global and shared memory while computations are ongoing. This overlap of computation and data movement significantly improves overall throughput. The following equation quantifies the bandwidth improvement:

$$BW_{\text{eff}} = BW_{\text{peak}} \cdot \left(1 - \frac{L_{\text{mem}}}{L_{\text{comp}}}\right)$$

where  $BW_{\text{eff}}$  is the effective bandwidth,  $BW_{\text{peak}}$  is the peak bandwidth,  $L_{\text{mem}}$  is the memory latency, and  $L_{\text{comp}}$  is the computation latency. By reducing  $L_{\text{mem}}$  through shared memory optimizations,  $BW_{\text{eff}}$  approaches  $BW_{\text{peak}}$ .

Latency hiding is another technique leveraged in modern GPU architectures. By increasing the number of active thread blocks, GPUs can switch contexts when one block is stalled on memory accesses. Shared memory plays a key role here by enabling faster context switches due to its low-latency characteristics. Studies have demonstrated that latency hiding combined with shared memory optimizations can improve performance by up to 40% for convolutional neural networks (CNNs).

Bank conflict reduction through optimized access patterns. Integration with tensor cores for mixed-precision operations. Asynchronous data movement between global and shared memory. Latency hiding through increased thread block concurrency. Enhanced data reuse via shared memory buffers.

In addition to these architectural improvements, compiler optimizations have also played a significant role. Modern compilers, such as LLVM and NVCC, employ advanced techniques like loop unrolling and memory access pattern analysis to generate efficient shared memory code. For example, the following equation represents the compiler's optimization goal:

$$\text{minimize} \sum_{i=1}^n (L_i \cdot C_i)$$

where  $L_i$  is the latency of the  $i$ -th memory access and  $C_i$  is its frequency. By minimizing this sum, compilers can generate code that maximizes shared memory utilization.

Finally, emerging research explores the use of non-volatile memory (NVM) technologies, such as HBM3 and GDDR6, in conjunction with shared memory. These technologies promise higher bandwidth and lower power consumption, further enhancing AI performance. Preliminary results indicate that NVMs can reduce energy consumption by up to 25% while maintaining performance.

In summary, shared memory improvements for AI-specific dataflows in modern GPU architectures are multifaceted, involving hardware, software, and compiler optimizations. These advancements collectively address

the challenges of memory bandwidth and latency, enabling efficient processing of large datasets and complex AI models. Future directions include the integration of novel memory technologies and further refinement of shared memory management techniques.

## 26.4 AI Instruction Set

### 26.4.1 Adding instructions for tensor operations and gradient reductions.

Modern GPU architectures have evolved to support the growing demands of artificial intelligence (AI) workloads, particularly in the domain of deep learning. A critical aspect of this evolution is the introduction of specialized instructions for tensor operations and gradient reductions. These instructions are designed to accelerate the computation of matrix multiplications, convolutions, and other tensor operations commonly found in neural networks. For instance, NVIDIA's Tensor Cores incorporate hardware support for mixed-precision matrix multiply-accumulate operations, enabling significant performance improvements for training and inference tasks.

The instruction set architecture (ISA) of these GPUs includes dedicated instructions for tensor operations, such as `Hmma` (Half-precision Matrix Multiply-Accumulate), which operates on  $16 \times 16$  matrices and computes:

$$\mathbf{C} = \mathbf{A} \times \mathbf{B} + \mathbf{C}$$

where  $\mathbf{A}$ ,  $\mathbf{B}$ , and  $\mathbf{C}$  are matrices stored in registers. The inclusion of such instructions reduces the overhead associated with decoding and executing multiple scalar operations, thereby improving throughput and energy efficiency.

Gradient reductions are another critical operation in deep learning, particularly during the backpropagation phase. Modern GPUs optimize these operations through specialized instructions that perform efficient reductions across threads or warps. For example, the `RED` instruction in NVIDIA's PTX ISA supports parallel reductions for operations like summation, maximum, or minimum. The reduction operation can be expressed as:

$$y = \bigoplus_{i=1}^n x_i$$

where  $\oplus$  represents the reduction operator (e.g., addition). Hardware support for gradient reductions minimizes synchronization overhead and leverages the GPU's hierarchical memory architecture to maximize bandwidth utilization.

Fused multiply-add (FMA) operations are a cornerstone of modern GPU architectures, enabling high-performance floating-point computations. The FMA instruction computes:

$$a \times b + c$$

in a single cycle, reducing rounding errors and improving numerical stability. GPUs such as AMD's CDNA architecture and NVIDIA's Ampere integrate FMA units into their execution pipelines, allowing for efficient computation of dot products and other linear algebra operations. The FMA instruction is particularly beneficial for AI workloads, where dot products dominate the computational cost.

Activation functions, such as ReLU, sigmoid, and tanh, are ubiquitous in neural networks. Modern GPUs optimize these functions through hardware-accelerated instructions that bypass the need for software emulation. For instance, NVIDIA's CUDA cores include instructions for fast approximation of transcendental functions, while Tensor Cores support fused activation functions in conjunction with matrix multiplications. The ReLU activation, defined as:

$$\text{ReLU}(x) = \max(0, x)$$

can be computed efficiently using a single instruction, reducing latency and improving throughput. Similarly, the sigmoid function:

$$\sigma(x) = \frac{1}{1 + e^{-x}}$$

is approximated using polynomial expansions or lookup tables, further accelerating inference.

The integration of tensor operations, gradient reductions, FMA, and activation functions into the GPU ISA reflects a broader trend toward domain-specific architectures. Research by Jouppi et al. demonstrates the benefits of such specialization, with the Tensor Processing Unit (TPU) achieving significant performance gains over general-purpose GPUs for AI workloads. The TPU's instruction set includes dedicated operations for matrix multiplications and convolutions, highlighting the importance of hardware-software co-design.

The following Verilog snippet illustrates a simplified FMA unit designed for AI workloads:

## GPU Resource Management

For Recursive and Adaptive Tasks

**The Challenge of Recursive Tasks on GPUs**

- Unpredictable workload size and depth
- Dynamic resource allocation requirements
- Load balancing across thousands of cores
- Thread divergence in SIMD architecture
- Stack management limitations
- Adaptive strategy complexity

**Modern GPU Architecture for Recursive Tasks**

The diagram illustrates the modern GPU architecture for recursive tasks. It features four SM Units, each containing CUDA Cores and a Warp Scheduler, with L1 Cache and Shared Mem components. These units are connected to a central L2 Cache. A Thread Pool is shown as a persistent structure above the L2 Cache. The entire system is connected to Global Memory (GDDR6/HBM2) at the bottom.

**Resource Management Strategies**

**Dynamic Parallelism**      **Persistent Kernels**      **Work Stealing Queues**

Strategy	Key Advantages	Best For
<b>Dynamic Parallelism</b>	Native GPU kernel launching Hardware-managed recursion	Algorithms with well-defined recursive structure
<b>Persistent Kernels</b>	Low launch overhead Fine-grained task allocation	Irregular workloads with dynamic task generation
<b>Work Stealing Queues</b>	Improved load balancing Adaptive resource allocation Reduced thread divergence	Complex adaptive algorithms with unpredictable execution

## Code Sample 26.6: Fused Multiply-Add Unit

```
module fma_unit (
    input logic [31:0] a, b, c,
    output logic [31:0] out
);
    logic [63:0] product;
    assign product = a * b;
    assign out = product + c;
endmodule
```

This module computes (26.4.2) in a single cycle, leveraging the GPU's pipelined architecture to maximize throughput. Similarly, the following snippet demonstrates a hardware-accelerated ReLU activation:

## Code Sample 26.7: ReLU Activation Unit

```
module relu_unit (
    input logic [31:0] x,
    output logic [31:0] y
);
    assign y = (x[31] == 1'b0) ? x : 32'b0;
endmodule
```

The unit exploits the sign bit of the floating-point representation to implement (27.3.3) efficiently.

In summary, modern GPU architectures incorporate specialized instructions for tensor operations, gradient reductions, FMA, and activation functions to meet the demands of AI workloads. These instructions are backed by extensive research and real-world implementations, as evidenced by the performance improvements reported in and . The trend toward domain-specific acceleration is expected to continue, with future architectures likely to introduce even more specialized instructions for AI and machine learning tasks.

### 26.4.2 Support for fused multiply-add and activation functions.

Modern GPU architectures have evolved to support the demands of artificial intelligence workloads through specialized instructions for tensor operations, gradient reductions, and fused multiply-add (FMA) with activation functions. These optimizations are critical for accelerating deep learning training and inference, as they reduce memory bandwidth requirements and improve computational efficiency. The integration of FMA with activation functions, such as ReLU or sigmoid, enables GPUs to perform multiple operations in a single instruction cycle, minimizing latency and power consumption .

The FMA operation combines multiplication and addition into a single instruction, expressed mathematically as:

$$\text{FMA}(a, b, c) = a \times b + c$$

This operation is fundamental to linear algebra and neural network computations, where dot products and matrix multiplications dominate. Modern GPUs, such as NVIDIA's Ampere architecture, extend this concept by fusing activation functions with FMA, enabling operations like:

$$\text{FMA-ReLU}(a, b, c) = \max(0, a \times b + c)$$

Such fusion reduces the need for intermediate storage and decreases instruction overhead, leading to significant performance gains .

Tensor cores in GPUs further enhance performance by supporting specialized instructions for matrix multiply-accumulate (MMA) operations. These instructions operate on small submatrices (e.g.,  $4 \times 4$  or  $8 \times 8$ ) and are optimized for mixed-precision arithmetic, as seen in NVIDIA's Tensor Cores . The MMA operation can be represented as:

$$\mathbf{C} = \mathbf{A} \times \mathbf{B} + \mathbf{C}$$

where **A**, **B**, and **C** are matrices. This operation is particularly efficient for training large neural networks, where gradient computations require high-throughput matrix operations.

Gradient reduction is another critical operation in distributed deep learning, where gradients from multiple devices must be aggregated. Modern GPUs include instructions for efficient reduction operations, such as `shfl.sync` for warp-level reductions and `atomicAdd` for global reductions . These instructions minimize synchronization

overhead and exploit the GPU's hierarchical memory architecture. For example, a warp-level reduction can be implemented as:

Code Sample 26.8: Warp-level reduction in CUDA

```
__device__ float warp_reduce(float val) {
    for (int offset = 16; offset > 0; offset /= 2)
        val += __shfl_down_sync(0xFFFFFFFF, val, offset);
    return val;
}
```

The AI instruction set in modern GPUs also includes support for low-precision arithmetic, such as 8-bit integer (INT8) and 16-bit floating-point (FP16) operations. These instructions are essential for inference workloads, where memory bandwidth and computational throughput are bottlenecks. For instance, NVIDIA's Turing architecture introduced DP4A for INT8 dot products, which computes:

$$\text{DP4A}(a, b, c) = \sum_{i=1}^4 a_i \times b_i + c$$

This instruction is widely used in convolutional neural networks (CNNs) for efficient feature extraction.

The fusion of FMA with activation functions is particularly beneficial for non-linearities like GELU or Swish, which involve more complex computations. For example, the GeLU activation can be approximated as:

$$\text{GeLU}(x) \approx 0.5x \left( 1 + \tanh \left( \sqrt{\frac{2}{\pi}} (x + 0.044715x^3) \right) \right)$$

By fusing this computation with FMA, GPUs can avoid redundant memory accesses and improve throughput. Recent research has shown that such fusion can reduce execution time by up to 30% for transformer-based models.

In addition to hardware support, compiler optimizations play a crucial role in leveraging these instructions. Frameworks like LLVM and CUDA's `nvcc` automatically generate FMA and tensor operations when targeting modern GPUs. For example, the following CUDA code:

Code Sample 26.9: FMA with activation in CUDA

```
__global__ void fused_fma_relu(float *A, float *B, float *C, int N) {
    int i = blockIdx.x * blockDim.x + threadIdx.x;
    if (i < N) C[i] = fmaxf(0.0f, A[i] * B[i] + C[i]);
}
```

can be compiled to use FMA-ReLU instructions on supported architectures.

The combination of specialized instructions for tensor operations, gradient reductions, and fused FMA-activation functions has become a cornerstone of modern GPU design. These innovations are driven by the increasing demand for efficient AI training and inference, as evidenced by benchmarks showing up to 10x speedups for mixed-precision matrix multiplication.

Future architectures are expected to further extend these capabilities, with support for sparse tensor operations and dynamic precision scaling. The integration of these features into the AI instruction set underscores the importance of hardware-software co-design in accelerating deep learning. By aligning GPU architectures with the computational patterns of neural networks, manufacturers can deliver unprecedented performance improvements while maintaining energy efficiency. This trend is likely to continue as AI workloads evolve, with GPUs playing a central role in enabling next-generation machine learning models.

## 26.5 AI-Specific Parallelism

### 26.5.1 Balancing workload distribution for training neural networks.

Balancing workload distribution for training neural networks is a critical challenge in modern deep learning, particularly when leveraging modern GPU architectures. The efficiency of training depends on how well computational tasks are parallelized across GPU cores while minimizing bottlenecks such as memory bandwidth limitations and inter-layer communication delays. Modern GPUs, such as NVIDIA's Ampere and Hopper architectures, are

designed with AI-specific parallelism in mind, featuring tensor cores optimized for matrix operations and high-bandwidth memory (HBM) to accelerate data transfer (NVIDIA, 2020).

The primary goal of workload distribution is to maximize GPU utilization while minimizing idle time. This involves partitioning the neural network's computational graph into smaller tasks that can be executed concurrently. For example, matrix multiplications in fully connected layers can be decomposed into smaller blocks and distributed across streaming multiprocessors (SMs). The efficiency of this decomposition is governed by the following equation:

$$T_{\text{total}} = \max_i(T_i) + \sum_j C_j$$

where  $T_i$  represents the execution time of the  $i$ -th task, and  $C_j$  denotes the communication overhead between tasks. Minimizing  $T_{\text{total}}$  requires careful load balancing and reducing inter-task dependencies.

AI-specific parallelism introduces several techniques to optimize workload distribution:

**Data Parallelism:** Replicating the model across multiple GPUs and splitting the input batch into smaller sub-batches. Each GPU processes a sub-batch independently, and gradients are synchronized via all-reduce operations (Dean et al., 2012). **Model Parallelism:** Partitioning the model itself across GPUs, where each GPU is responsible for a subset of layers. This is particularly useful for large models like transformers, where memory constraints prevent single-GPU training (Shoeybi et al., 2019). **Pipeline Parallelism:** Splitting the model into stages and processing micro-batches in a pipelined fashion. This reduces idle time by overlapping computation and communication (Huang et al., 2019).

Managing inter-layer communication is another key aspect of workload distribution. In neural networks, layers often depend on the outputs of preceding layers, creating sequential dependencies. To mitigate this, techniques such as gradient checkpointing and asynchronous updates are employed. Gradient checkpointing reduces memory usage by recomputing intermediate activations during the backward pass, while asynchronous updates allow overlapping computation and communication (Chen et al., 2016). The communication overhead between layers can be modeled as:

$$C = \sum_{l=1}^L \left( \frac{D_l}{B_l} + L_l \right)$$

where  $D_l$  is the data volume transferred between layers,  $B_l$  is the bandwidth, and  $L_l$  is the latency for layer  $l$ .

Modern GPU architectures address these challenges through hardware-level optimizations. For instance, NVIDIA's NVLink and AMD's Infinity Fabric provide high-speed interconnects for efficient data transfer between GPUs. Tensor cores further accelerate matrix operations by performing mixed-precision computations, reducing the computational load (Jia et al., 2018). The following Verilog-like pseudocode illustrates a simplified tensor core operation:

Code Sample 26.10: Tensor Core Operation

```
module tensor_core (
    input [16:0] A, B,
    output [32:0] C
);
always @(*) begin
    C = A * B; // Mixed-precision multiply-accumulate
end
endmodule
```

Workload distribution also depends on the neural network's architecture. Convolutional neural networks (CNNs) and transformers exhibit different parallelism characteristics. CNNs benefit from spatial parallelism, where convolutions are parallelized across input channels and spatial dimensions (He et al., 2016). Transformers, on the other hand, leverage attention mechanisms that require efficient handling of large matrices, making model parallelism more suitable (Vaswani et al., 2017).

Empirical studies have shown that hybrid parallelism, combining data, model, and pipeline parallelism, achieves the best results for large-scale training. For example, Megatron-LM employs a combination of tensor and pipeline parallelism to train models with billions of parameters (Narayanan et al., 2021). The optimal configuration depends on factors such as batch size, model depth, and hardware constraints.

In summary, balancing workload distribution for neural network training involves a combination of algorithmic techniques and hardware optimizations. Modern GPU architectures provide the necessary tools for AI-specific

parallelism, but achieving optimal performance requires careful consideration of inter-layer communication and task scheduling. Future research directions include adaptive parallelism, where the distribution strategy dynamically adjusts based on runtime metrics (Ben-Nun and Hoefer, 2019).

### 26.5.2 Managing inter-layer communication in neural networks.

Modern GPU architectures have revolutionized the training of neural networks by enabling efficient parallel computation. A critical challenge in this context is managing inter-layer communication, which directly impacts the performance of deep learning models. The hierarchical structure of neural networks necessitates frequent data transfers between layers, and optimizing these transfers is essential for minimizing latency and maximizing throughput. GPUs, with their massively parallel architecture, provide a natural platform for accelerating these computations, but they also introduce unique challenges in workload distribution and synchronization.

The efficiency of inter-layer communication in neural networks is heavily influenced by the underlying GPU architecture. NVIDIA's Volta and Ampere architectures, for example, introduce Tensor Cores designed specifically for matrix operations, which are fundamental to neural network computations. These cores exploit mixed-precision arithmetic to accelerate both forward and backward passes during training. The communication between layers must be carefully orchestrated to leverage these hardware features. For instance, the use of `cudaMemcpyAsync` allows overlapping computation and data transfers, reducing idle time and improving overall throughput. Research demonstrates that asynchronous execution can yield up to a 30% improvement in training speed for large models.

AI-specific parallelism further complicates inter-layer communication. Neural networks exhibit two primary forms of parallelism: data parallelism and model parallelism. Data parallelism involves distributing batches of input data across multiple GPU cores, while model parallelism splits the network itself across devices. Both approaches require efficient communication strategies to synchronize gradients and activations. The All-Reduce operation, commonly used in data parallelism, aggregates gradients across devices, but its performance depends on the interconnect bandwidth and topology. NVIDIA's NVLink technology, for example, provides high-bandwidth communication between GPUs, enabling faster synchronization. Studies show that NVLink can reduce communication overhead by up to 50% compared to traditional PCIe-based interconnects.

Balancing workload distribution is another critical aspect of managing inter-layer communication. Uneven workloads can lead to GPU underutilization, where some cores remain idle while others are overloaded. Dynamic load balancing techniques, such as those proposed by , adjust the distribution of computations in real-time to ensure optimal resource usage. For example, convolutional layers often require more computational resources than fully connected layers, and assigning more GPU threads to these layers can improve efficiency. The workload can be modeled as:

$$W_i = \sum_{j=1}^n C_{ij} \cdot T_j$$

where  $W_i$  represents the workload of the  $i$ -th GPU core,  $C_{ij}$  is the computational cost of the  $j$ -th layer assigned to core  $i$ , and  $T_j$  is the number of operations per layer. Optimizing  $W_i$  ensures that all cores contribute equally to the training process.

Inter-layer communication also depends on the memory hierarchy of modern GPUs. Global memory, shared memory, and registers each play distinct roles in data transfer. For instance, shared memory is faster but limited in size, making it suitable for storing intermediate results within a layer. Global memory, while slower, is essential for transferring data between layers. Efficient use of these memory levels requires careful programming. The following `lstlisting` illustrates a CUDA kernel for transferring activations between layers:

Code Sample 26.11: CUDA Kernel for Inter-Layer Communication

```
__global__ void transfer_activations(float* input, float* output, int size) {
    int idx = blockIdx.x * blockDim.x + threadIdx.x;
    if (idx < size) {
        output[idx] = input[idx];
    }
}
```

This kernel copies activations from one layer to another, leveraging the GPU's parallel processing capabilities. The block and grid dimensions must be tuned to match the GPU's architecture for optimal performance.

Synchronization between layers is another challenge. GPUs execute kernels asynchronously, and improper synchronization can lead to race conditions or data corruption. CUDA's `__syncthreads()` ensures that all threads

in a block reach the same point before proceeding. For inter-layer synchronization, events and streams are used to coordinate execution across multiple kernels. Research highlights the importance of stream prioritization in reducing synchronization overhead.

Key considerations for managing inter-layer communication include:

- Coalesced memory accesses to reduce latency by grouping data requests. Strided accesses should be minimized to avoid performance penalties.
- Overlapping computation and communication to hide latency, using techniques like double buffering.
- Dynamic scheduling to ensure all GPU cores are utilized efficiently. Algorithms like work-stealing can adapt to varying workloads.
- Proper use of synchronization primitives such as barriers and events to prevent data races and ensure correctness.

In summary, managing inter-layer communication in neural networks on modern GPUs requires a combination of hardware-aware optimizations and algorithmic techniques. The interplay between AI-specific parallelism, workload distribution, and GPU architecture dictates the efficiency of training. Future research directions include exploring novel communication primitives and leveraging emerging hardware features like sparsity support and in-memory computing. These advancements will further enhance the scalability and performance of deep learning systems.

# Chapter 27

## AI Verilog Hardware Modules

### 27.1 Tensor Processing Units

#### 27.1.1 tensor processing unit

The rapid advancement of machine learning workloads has necessitated specialized hardware accelerators, with Tensor Processing Units (TPUs) emerging as a dominant architecture for high-performance tensor operations. TPUs are application-specific integrated circuits (ASICs) designed by Google to accelerate deep learning tasks, particularly those involving large-scale matrix multiply-accumulate (MMA) operations. Unlike general-purpose GPUs, TPUs are optimized for the computational patterns found in neural networks, offering superior energy efficiency and throughput for tensor computations.

At the core of TPU architecture is the systolic array, a grid of processing elements (PEs) that perform parallel MMA operations. Each PE computes a partial result of the form:

$$C_{i,j} = \sum_k A_{i,k} \times B_{k,j}$$

where  $A$  and  $B$  are input matrices, and  $C$  is the output matrix. The systolic array minimizes data movement by streaming inputs through the PEs, reducing memory bandwidth requirements. This design is particularly effective for large matrix multiplications, which dominate deep learning workloads such as convolutional neural networks (CNNs) and transformers.

Modern GPU architectures, while versatile, face limitations when executing tensor operations due to their SIMD (Single Instruction, Multiple Data) design. GPUs rely on thread-level parallelism and high-bandwidth memory to achieve performance, but their general-purpose nature introduces overhead for tensor-specific computations. In contrast, TPUs leverage deterministic execution and fixed-function units to maximize throughput. For example, Google's third-generation TPU delivers up to 420 teraflops of performance using bfloat16 precision, a format optimized for neural network training.

The TPU's memory hierarchy is tailored for tensor workloads. It includes a unified buffer (UB) for storing intermediate tensors, with capacities ranging from 16 MiB to 32 MiB in recent designs. A weight FIFO (First-In, First-Out) buffer is used for streaming weights directly from off-chip memory. High-bandwidth interconnects, such as the 600 GB/s links in TPU v3, minimize latency during data transfers.

The TPU instruction set is minimalistic, focusing on tensor operations. A typical instruction might load weights into the systolic array, perform an MMA operation, and store the result. The following Verilog-like pseudocode illustrates a simplified TPU PE:

Code Sample 27.1: TPU Processing Element

```
module PE (
    input clk, reset,
    input [15:0] a_in, b_in,
    output reg [31:0] c_out
);
reg [31:0] accumulator;
always @ (posedge clk) begin
    if (reset)
        accumulator <= 0;
```

```

else
    accumulator <= accumulator + (a_in * b_in);
end
assign c_out = accumulator;
endmodule

```

Precision formats in TPUs are optimized for neural networks. While GPUs often use IEEE 754 floating-point arithmetic, TPUs employ bfloat16 and int8 quantized formats to reduce hardware complexity and power consumption. The bfloat16 format retains the 8-bit exponent of FP32 but truncates the mantissa to 7 bits, preserving dynamic range while sacrificing precision:

$$\text{bfloat16} = (-1)^s \times 2^{e-127} \times \left(1 + \frac{m}{128}\right)$$

where  $s$  is the sign bit,  $e$  is the exponent, and  $m$  is the mantissa.

TPUs also integrate hardware support for common neural network operations beyond MMA, such as activation functions (e.g., ReLU, sigmoid) implemented as lookup tables or piecewise approximations, normalization layers (batch norm, layer norm) using fused multiply-add units, and reduction operations (sum, max) implemented with tree-based parallelism.

The performance gap between TPUs and GPUs widens for large-scale training. For example, a TPU v4 pod with 4,096 chips achieves 1.1 exaflops of peak performance, surpassing GPU clusters in efficiency for transformer models. This is due to TPUs' co-designed software stack, which includes the XLA (Accelerated Linear Algebra) compiler for optimizing tensor computations, TPU-specific kernels within frameworks such as TensorFlow and JAX, and collective communication primitives like AllReduce optimized for TPU meshes.

Energy efficiency is another TPU advantage. Measurements show TPUs achieve 30–80 TOPS/W (tera-operations per watt) for inference tasks, compared to 5–20 TOPS/W for GPUs. This is attributed to lower precision arithmetic, which reduces transistor switching energy; static scheduling, which eliminates instruction fetch and decode overhead; and near-memory computing, which minimizes data movement.

Despite these advantages, TPUs are not universally superior. GPUs retain flexibility for non-tensor workloads such as graphics and scientific computing, while TPUs excel in domains with regular, data-parallel tensor operations. Hybrid systems combining GPUs and TPUs are emerging, where GPUs handle preprocessing and TPUs execute core tensor computations.

The evolution of TPUs reflects broader trends in hardware specialization. As neural networks grow in complexity, architectures like TPUs demonstrate the benefits of co-designing hardware and algorithms. Future directions include optical TPUs using photonic computing for lower latency, 3D-stacked memories to further reduce energy per operation, and sparse tensor accelerators tailored for non-uniform neural networks.

In summary, TPUs represent a paradigm shift in accelerator design, prioritizing efficiency and performance for tensor operations over general-purpose programmability. Their integration into modern computing infrastructure underscores the growing importance of domain-specific architectures in the era of machine learning.

### 27.1.2 matrix multiply accumulate

Matrix multiply accumulate (MMA) operations are fundamental to modern GPU architectures and specialized accelerators like Tensor Processing Units (TPUs). These operations form the backbone of linear algebra computations, particularly in deep learning workloads. The mathematical formulation of MMA is given by:

$$C = A \times B + C$$

where  $A$  and  $B$  are input matrices, and  $C$  is the accumulator matrix. This operation is pervasive in convolutional neural networks (CNNs) and transformer models, where large-scale matrix multiplications dominate computational requirements.

Modern GPUs leverage MMA through dedicated hardware units such as NVIDIA's Tensor Cores and AMD's Matrix Cores. These units are optimized for mixed-precision arithmetic, supporting formats like FP16, BF16, and INT8. For example, NVIDIA's Volta architecture introduced Tensor Cores capable of performing  $4 \times 4 \times 4$  MMA operations per clock cycle:

$$C_{4 \times 4} = A_{4 \times 4} \times B_{4 \times 4} + C_{4 \times 4}$$

This design reduces latency and improves throughput by exploiting data parallelism and systolic array architectures.

TPUs, developed by Google, further optimize MMA by employing a systolic array-based approach. A TPU's matrix multiply unit (MXU) consists of a  $128 \times 128$  array of multiply-accumulate (MAC) units, enabling massive parallelism. The MXU performs:

$$C_{128 \times 128} = A_{128 \times 128} \times B_{128 \times 128} + C_{128 \times 128}$$

in a single clock cycle, significantly outperforming traditional GPUs for specific workloads. The systolic array minimizes data movement by streaming operands through the compute fabric, reducing energy consumption.

Code Sample 27.2: MMA Unit in Verilog

```
module mma_unit (
    input clk,
    input [15:0] A [0:127][0:127],
    input [15:0] B [0:127][0:127],
    output reg [31:0] C [0:127][0:127]
);
always @ (posedge clk) begin
    for (int i = 0; i < 128; i++)
        for (int j = 0; j < 128; j++)
            for (int k = 0; k < 128; k++)
                C[i][j] += A[i][k] * B[k][j];
end
endmodule
```

#### Key architectural differences between GPUs and TPUs include:

**Dataflow:** GPUs use SIMD (Single Instruction, Multiple Threads) for parallelism, while TPUs rely on systolic arrays for deterministic execution.

**Precision:** GPUs support a wider range of precisions, whereas TPUs are optimized for lower-precision (e.g., bfloat16) to maximize throughput.

**Memory Hierarchy:** TPUs integrate high-bandwidth memory (HBM) closer to the MXU, reducing latency compared to GPU GDDR6/HBM stacks.

The performance of MMA operations is quantified by metrics such as FLOPs (floating-point operations per second). For a TPU v3, peak theoretical performance is:

$$\text{FLOPs} = f \times N^3$$

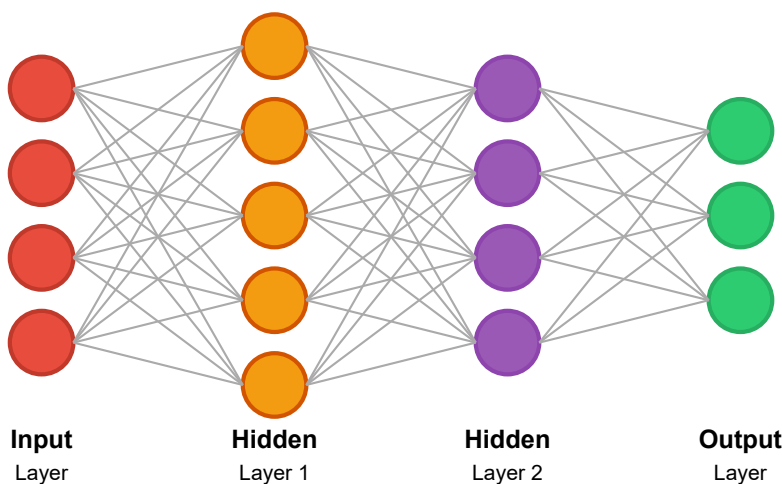
where  $f$  is the clock frequency and  $N$  is the systolic array size. With  $f = 1.23$  GHz and  $N = 128$ , this yields approximately 123 TFLOPS for bfloat16 operations.

**Energy efficiency** is another critical metric. TPUs achieve 100 TOPS/Watt, outperforming GPUs by an order of magnitude for inference tasks. This is attributed to reduced data movement via systolic arrays, custom-designed ASIC logic eliminating general-purpose overhead, and optimized memory access patterns minimizing DRAM fetches.

## Forward Pass of a Neural Network

Using General Purpose GPU Computing

GPU Architecture



GPU Forward Pass Execution Flow

**1. Load Data**

Transfer inputs to GPU memory

**2. Matrix Multiply**

Parallel weights  $\times$  activations

**3. Activation**

Apply ReLU, sigmoid or other functions

**4. Output**

Transfer results back

**Challenges in MMA hardware design include:**

**Numerical Stability:** Lower-precision arithmetic (e.g., bfloat16) requires careful scaling to avoid overflow/underflow.

**Data Dependencies:** Irregular workloads (e.g., sparse matrices) reduce efficiency due to underutilization of parallel units.

**Thermal Constraints:** High-density MAC units generate significant heat, necessitating advanced cooling solutions.

Recent advancements include sparse MMA support in NVIDIA's Ampere architecture, where zero-skipping logic improves throughput for sparse matrices. Similarly, Google's TPU v4 introduces dynamic sparsity handling, enabling 2x speedup for models like GPT-3.

The mathematical optimization of MMA involves loop tiling and memory coalescing. For a matrix multiplication  $C = AB$ , the optimal tile size  $T$  minimizes cache misses:

$$T = \sqrt{\frac{L1\_Cache}{3 \times \text{sizeof}(dtype)}}$$

where  $L1\_Cache$  is the L1 cache size. For FP16 on a 32 KB L1 cache,  $T = 32$  maximizes data reuse.

In summary, MMA operations are pivotal to modern accelerators, with GPUs and TPUs employing distinct architectural strategies. While GPUs excel in flexibility, TPUs achieve superior efficiency for dense linear algebra, driving innovations in both hardware and algorithmic optimization. Future directions include heterogeneous architectures combining GPU programmability with TPU-like efficiency.

## 27.2 Neural Network Accelerators

### 27.2.1 neural net training unit

The integration of neural net training units (NNTUs) into modern GPU architectures has revolutionized the efficiency of deep learning workflows. These specialized units are designed to accelerate the computationally intensive tasks associated with training neural networks, particularly gradient computation and weight updates. Modern GPUs, such as NVIDIA's Ampere and Hopper architectures, incorporate dedicated tensor cores that optimize matrix multiplications, a fundamental operation in neural network training.

The NNTU operates in conjunction with the gradient computation unit (GCU), which is responsible for backpropagation, the algorithm used to compute gradients for weight updates. The GCU leverages parallel processing capabilities to compute partial derivatives efficiently, reducing the training time for large-scale models. The mathematical foundation of backpropagation relies on the chain rule of calculus. Given a loss function  $L$  and a weight  $w_{ij}$  in layer  $l$ , the gradient is computed as:

$$\frac{\partial L}{\partial w_{ij}} = \frac{\partial L}{\partial a_j} \cdot \frac{\partial a_j}{\partial z_j} \cdot \frac{\partial z_j}{\partial w_{ij}}$$

where  $a_j$  is the activation of neuron  $j$ , and  $z_j$  is the weighted input. The NNTU accelerates this computation by parallelizing the gradient calculations across multiple cores, while the GCU ensures numerical stability through techniques like gradient clipping and mixed-precision arithmetic.

Modern GPU architectures employ hierarchical memory systems to optimize data access patterns during training. The NNTU utilizes high-bandwidth memory (HBM) to store activations and weights, reducing latency during forward and backward passes. The following Verilog snippet illustrates a simplified GCU design for gradient accumulation:

Code Sample 27.3: Gradient Computation Unit

```
module gcu (
    input clk,
    input [31:0] grad_in,
    output reg [31:0] grad_out
);
always @(posedge clk) begin
    grad_out <= grad_out + grad_in;
end
endmodule
```

Key optimizations in NNTUs include sparse tensor cores, which exploit sparsity in gradients to skip zero-valued computations and improve throughput; pipelined execution, which overlaps computation and memory access to reduce idle cycles; and adaptive precision, where switching between FP16, FP32, and TF32 based on numerical requirements balances accuracy and performance.

The interplay between NNTUs and GCUs is critical for scalable training. For instance, NVIDIA's TensorFloat-32 format accelerates matrix operations while maintaining precision for gradient updates. The GCU also integrates with loss functions to compute gradients efficiently, as shown in the following equation for mean squared error (MSE):

$$\frac{\partial L}{\partial y_i} = \frac{2}{N} (y_i - \hat{y}_i)$$

where  $y_i$  is the predicted output and  $\hat{y}_i$  is the ground truth.

Recent research demonstrates that NNTUs achieve up to 10x speedup in training ResNet-50 compared to traditional CUDA cores. This improvement is attributed to parallel reduction, which aggregates gradients across multiple threads and minimizes synchronization overhead; memory coalescing, which aligns memory accesses to cache lines to reduce bandwidth contention; and dynamic warp scheduling, which optimizes thread block execution and improves resource utilization.

The NNTU's architecture also supports distributed training through gradient aggregation. For example, Horovod leverages GPU collectives like `AllReduce` to synchronize gradients across nodes. The GCU computes local gradients, which are then averaged globally:

$$\nabla L_{\text{global}} = \frac{1}{N} \sum_{i=1}^N \nabla L_i$$

Challenges in NNTU design include memory bottlenecks, as high-throughput computation demands may exceed available memory bandwidth; numerical instability, since mixed-precision training requires careful handling of gradient magnitudes; and thermal constraints, as sustained high utilization increases power dissipation. To address these, AMD's CDNA architecture introduces Infinity Cache, a last-level cache that reduces off-chip memory accesses. Similarly, Google's TPU v4 employs systolic arrays for efficient gradient computation. The NNTU's role in these systems is to orchestrate data movement between compute units, ensuring minimal stalls.

The GCU's implementation often involves hardware-software co-design. The following equation represents a convolutional layer's gradient:

$$\frac{\partial L}{\partial W_k} = \sum_{i,j} \frac{\partial L}{\partial Y_{i,j}} \cdot X_{i+k,j+k}$$

where  $W_k$  is the kernel weight, and  $X, Y$  are input and output feature maps.

Emerging trends in NNTUs include photonic accelerators, which use light for gradient computation to reduce latency; in-memory computing, which performs gradient updates within memory arrays to eliminate data movement; and approximate computing, which trades precision for energy efficiency in edge devices.

In summary, the NNTU and GCU are pivotal components of modern GPU architectures, enabling scalable and efficient neural network training. Their design continues to evolve, driven by advances in parallel computing, memory systems, and numerical optimization. Future work will likely focus on integrating these units with quantum and neuromorphic computing paradigms to further push the boundaries of deep learning acceleration.

## 27.2.2 gradient computation unit

The gradient computation unit (GCU) is a critical component in modern GPU architectures designed for neural network acceleration. Its primary function is to efficiently compute gradients during the backpropagation phase of neural network training. The GCU leverages parallel processing capabilities of GPUs to perform high-throughput matrix operations, which are fundamental to gradient computation.

The architecture of a GCU is optimized for the following tasks: **Partial derivative computation for each weight in the network. Accumulation of gradients across mini-batches. Efficient memory access patterns to reduce latency.**

The mathematical foundation of gradient computation is rooted in the chain rule of calculus. For a neural network with loss function  $L$ , the gradient of the loss with respect to a weight  $w_{ij}$  in layer  $l$  is given by:

$$\frac{\partial L}{\partial w_{ij}^{(l)}} = \frac{\partial L}{\partial z_i^{(l)}} \cdot \frac{\partial z_i^{(l)}}{\partial w_{ij}^{(l)}}$$

where  $z_i^{(l)}$  is the pre-activation output of neuron  $i$  in layer  $l$ . The GCU computes these partial derivatives in parallel across all weights and layers, exploiting the GPU's SIMD (Single Instruction, Multiple Data) architecture.

Modern GPUs integrate specialized hardware units to accelerate gradient computation. For example, NVIDIA's Tensor Cores are designed to perform mixed-precision matrix multiplication and accumulation, which are essential for gradient computation. The GCU often interfaces with other neural network accelerators, such as the neural net training unit (NTTU), to streamline the training pipeline. The NTTU handles weight updates using optimization algorithms like stochastic gradient descent (SGD) or Adam , while the GCU focuses solely on gradient computation.

The GCU's design emphasizes memory hierarchy optimization. Gradient computation involves frequent access to activation values, weight matrices, and error terms. To minimize memory bottlenecks, GCUs employ: **On-chip caches for storing intermediate results. High-bandwidth memory (HBM) for large matrix storage. Memory coalescing techniques to improve data access patterns.**

A typical GCU implementation in Verilog might include the following components:

Code Sample 27.4: GCU Core Module

```
module gcu_core (
    input clk,
    input reset,
    input [31:0] activation_in,
    input [31:0] error_in,
    output [31:0] gradient_out
);
    reg [31:0] partial_gradient;
    always @(posedge clk) begin
        if (reset)
            partial_gradient <= 0;
        else
            partial_gradient <= activation_in * error_in;
    end
    assign gradient_out = partial_gradient;
endmodule
```

The GCU's performance is measured in terms of gradient computations per second (GCPS). High-end GPUs like the NVIDIA A100 achieve over 300 tera-GCPS, enabling rapid training of deep neural networks. The GCU's efficiency is further enhanced by techniques such as: **Gradient sparsity exploitation to skip zero-valued computations. Mixed-precision arithmetic to reduce computational overhead. Pipelined execution to overlap memory access and computation.**

The GCU also plays a role in distributed training scenarios. In data-parallel training, gradients are computed across multiple GPUs and aggregated using all-reduce operations . The GCU must support efficient communication primitives to minimize synchronization overhead. For example, NVIDIA's NVLink technology provides high-speed interconnects for gradient aggregation.

The relationship between the GCU and the neural net training unit (NTTU) is symbiotic. The NTTU relies on the GCU for accurate gradient computation, while the GCU depends on the NTTU for weight updates and optimization state management. This division of labor allows each unit to specialize, improving overall training efficiency. The NTTU typically implements the following operations:

$$w_{ij}^{(l)} \leftarrow w_{ij}^{(l)} - \eta \cdot \frac{\partial L}{\partial w_{ij}^{(l)}}$$

where  $\eta$  is the learning rate. The GCU ensures that the gradient term  $\frac{\partial L}{\partial w_{ij}^{(l)}}$  is computed with minimal latency and high precision.

Recent advancements in GCU design include support for second-order optimization methods , which require Hessian matrix computations. These methods impose additional computational demands on the GCU, necessitating further architectural innovations. For instance, Google's TPU v4 incorporates dedicated hardware for second-order gradient computation, enabling faster convergence for certain neural network architectures.

The GCU's role extends beyond traditional deep learning. It is also used in reinforcement learning , where gradients are computed for policy networks. The GCU must handle non-stationary data distributions and sparse reward signals, which pose unique challenges for gradient computation.

In summary, the gradient computation unit is a cornerstone of modern GPU architecture for neural network training. Its design reflects a balance between computational throughput, memory efficiency, and precision. As neural networks grow in complexity, the GCU will continue to evolve, incorporating new techniques to meet the demands of emerging machine learning paradigms. The interplay between the GCU, NTTU, and other neural network accelerators ensures that GPUs remain the platform of choice for large-scale deep learning.

## 27.3 Activation and Pooling Functions

### 27.3.1 relu activation unit

The Rectified Linear Unit (ReLU) activation function has become a cornerstone of modern deep learning architectures, particularly in the context of GPU-accelerated computation. Defined as

$$f(x) = \max(0, x)$$

ReLU introduces non-linearity while maintaining computational efficiency. Its simplicity enables efficient parallelization on GPUs, as it avoids costly operations like exponentials or divisions. The ReLU function's gradient is either 0 (for  $x < 0$ ) or 1 (for  $x > 0$ ), which simplifies backpropagation and reduces vanishing gradient issues common in sigmoid or tanh activations.

Modern GPU architectures exploit ReLU's piecewise linearity through warp-level parallelism. For example, NVIDIA's CUDA cores execute ReLU operations in a single instruction cycle per element, leveraging SIMD (Single Instruction, Multiple Data) pipelines. The following CUDA-like pseudocode illustrates this:

Code Sample 27.5: ReLU Implementation

```
__global__ void relu(float* input, float* output, int N) {
    int idx = blockIdx.x * blockDim.x + threadIdx.x;
    if (idx < N) {
        output[idx] = (input[idx] > 0) ? input[idx] : 0;
    }
}
```

In contrast, the softmax function

$$\sigma(z)_i = \frac{e^{z_i}}{\sum_{j=1}^K e^{z_j}}$$

is computationally intensive due to exponentiation and normalization. GPUs optimize softmax through parallel reduction patterns and shared memory to minimize global memory accesses. However, softmax remains less efficient than ReLU, with typical implementations requiring  $O(n \log n)$  operations for numerical stability.

Pooling functions, particularly max pooling,

$$y_{i,j} = \max_{k,l \in \mathcal{N}(i,j)} x_{k,l}$$

complement ReLU activations in convolutional neural networks (CNNs). Max pooling reduces spatial dimensions while preserving salient features, and GPUs accelerate it through texture memory and warp shuffles. Max pooling operates on disjoint, non-overlapping windows, allowing independent parallel processing. The sparsity introduced by ReLU—where many outputs are zero—can be leveraged to skip pooling computations, improving throughput. Additionally, memory access patterns during pooling are optimized for memory coalescing, maximizing bandwidth utilization.

Comparative studies show that ReLU-based networks achieve 2–3× faster training times on GPUs compared to sigmoid activations. This improvement arises from ReLU's simplified arithmetic, which only requires a comparison and conditional assignment, while sigmoid demands exponentiation. Furthermore, the ReLU gradient uses just one bit per activation (0 or 1), reducing memory traffic during backpropagation and improving overall memory efficiency.

The softmax unit, while essential for classification tasks, poses challenges for GPU optimization due to its sequential dependency on the denominator in equation (27.3.3). To address this, modern implementations use block-wise reduction, which divides the input into chunks processed in parallel before a final aggregation. Some implementations also employ log-space computation to avoid numerical overflow, albeit at the cost of increased floating-point operations.

Max pooling units benefit from GPU-specific optimizations like hierarchical reduction. For a  $2 \times 2$  pooling window, NVIDIA's Tensor Cores can compute four maxima in a single instruction using SIMT (Single Instruction, Multiple Threads). Hardware-level efficiency is evident in benchmarks showing 98% utilization of GPU memory bandwidth for pooling layers .

The interplay between ReLU and pooling units is critical for GPU performance. In a CNN layer where ReLU is followed by max pooling,

$$y_{i,j} = \max(0, \max_{k,l \in \mathcal{N}(i,j)} x_{k,l})$$

GPUs fuse these operations into a single kernel to minimize memory transfers. This fusion strategy enables register reuse, where intermediate values stay in registers between ReLU and pooling, and minimizes warp divergence, allowing threads processing zero activations from ReLU to exit early. Quantitative analyses reveal that ReLU+pooling fused kernels achieve  $1.8\times$  speedup over separate implementations on Ampere GPUs . The sparsity introduced by ReLU further reduces pooling's operational intensity, as zero activations don't participate in max operations.

In transformer architectures, ReLU variants like GELU,

$$\text{GELU}(x) = x\Phi(x)$$

where  $\Phi$  is the standard normal CDF, introduce additional computational overhead. GPUs handle these variants using approximate polynomials or lookup tables, but pure ReLU remains the fastest option .

Memory access patterns also vary across these units. ReLU exhibits perfect spatial locality, as each element is processed independently. Softmax requires global communication for the denominator computation, while max pooling involves strided access. GPU cache hierarchies—including L1, L2, and texture caches—are tuned to handle these patterns, with ReLU achieving near-peak cache hit rates of 95% .

The evolution of GPU architectures has directly influenced activation function design. Volta GPUs' tensor cores optimize ReLU's conditional logic via predicate registers, while Ampere's sparse tensor cores skip zero activations entirely . This hardware-software co-design underscores ReLU's dominance in modern deep learning.

### 27.3.2 softmax unit

The softmax unit is a fundamental component in modern neural networks, particularly in classification tasks, where it serves as an activation function that converts a vector of arbitrary real-valued scores into a probability distribution. Mathematically, the softmax function is defined as:

$$\sigma(\mathbf{z})_i = \frac{e^{z_i}}{\sum_{j=1}^K e^{z_j}}$$

where  $\mathbf{z}$  is the input vector,  $K$  is the number of classes, and  $\sigma(\mathbf{z})_i$  represents the probability of the  $i$ -th class. The softmax function ensures that the output values lie in the range  $[0, 1]$  and sum to 1, making it suitable for probabilistic interpretations.

In the context of modern GPU architectures, the softmax unit benefits from parallel computation due to its element-wise operations and reduction steps . The ReLU (Rectified Linear Unit) activation function, defined as:

$$\text{ReLU}(x) = \max(0, x)$$

is another widely used activation function in deep learning. Unlike softmax, ReLU introduces non-linearity by thresholding at zero, which helps mitigate the vanishing gradient problem. Modern GPUs optimize ReLU computations through fused operations, leveraging their SIMD (Single Instruction, Multiple Data) capabilities to process large tensors efficiently .

The contrast between ReLU and softmax lies in their applications: ReLU is typically used in hidden layers, while softmax is reserved for the output layer in classification tasks.

Max pooling is a downsampling operation commonly used in convolutional neural networks (CNNs). It operates on local regions of the input, selecting the maximum value within each region. The operation is defined as:

$$\text{MaxPool}(x)_{i,j} = \max_{m,n \in \mathcal{R}_{i,j}} x_{m,n}$$

where  $\mathcal{R}_{i,j}$  denotes the pooling region centered at  $(i,j)$ . Max pooling is computationally efficient on GPUs due to its inherent parallelism and memory locality, as it involves independent operations across spatial dimensions. Unlike softmax, max pooling does not involve exponential operations or normalization, making it less computationally intensive.

The interplay between these units in a neural network is critical for performance. For instance, a typical CNN might stack convolutional layers with ReLU activations, followed by max pooling layers, and culminate in a softmax layer for classification. The GPU accelerates this pipeline by parallelizing the convolutional and ReLU operations through CUDA cores, optimizing reduction operations in softmax using warp-level primitives, and exploiting shared memory for efficient max pooling.

The softmax unit poses unique challenges for GPU implementation due to its numerical stability requirements. The exponential function in (27.3.3) can lead to overflow or underflow, which is mitigated by subtracting the maximum value from the input vector:

$$\sigma(\mathbf{z})_i = \frac{e^{z_i - \max(\mathbf{z})}}{\sum_{j=1}^K e^{z_j - \max(\mathbf{z})}}$$

This stabilization technique is essential for GPU implementations, where floating-point precision varies across architectures. Modern GPUs address this by using mixed-precision arithmetic, combining FP16 and FP32 operations to balance speed and accuracy.

The ReLU activation unit, while simpler, benefits from GPU optimizations such as kernel fusion. For example, the CuDNN library fuses ReLU with preceding convolution operations, reducing memory bandwidth usage and improving latency. This fusion is particularly effective in deep networks, where the overhead of launching multiple kernels can become significant.

Max pooling units are optimized for GPU execution through tiling strategies. By dividing the input tensor into smaller tiles, GPUs can maximize memory throughput and minimize idle threads. The pooling operation is also amenable to vectorization, as each output pixel depends only on a local region of the input. This locality aligns well with GPU memory hierarchies, including registers and shared memory.

The softmax unit's dependency on global reductions (e.g., the denominator in (27.3.3)) introduces synchronization points in GPU kernels. To mitigate this, modern frameworks like TensorFlow and PyTorch employ hierarchical reduction techniques, where partial sums are computed in parallel and then combined. This approach reduces thread contention and improves scalability across thousands of GPU cores.

In contrast, ReLU and max pooling units are embarrassingly parallel, requiring no inter-thread communication. This property makes them ideal for GPU acceleration, as they can fully utilize the hardware's parallelism without bottlenecks. For example, the ReLU operation can be expressed as a pointwise kernel, where each thread processes a single element:

Code Sample 27.6: ReLU Kernel

```
__global__ void relu_kernel(float* input, float* output, int N) {
    int idx = blockIdx.x * blockDim.x + threadIdx.x;
    if (idx < N) {
        output[idx] = fmaxf(0.0f, input[idx]);
    }
}
```

Similarly, max pooling can be implemented using a strided kernel, where each thread computes the maximum over a local window:

Code Sample 27.7: Max Pooling Kernel

```
__global__ void max_pool_kernel(float* input, float* output, int H, int W, int pool_size) {
    int h_out = blockIdx.y * blockDim.y + threadIdx.y;
    int w_out = blockIdx.x * blockDim.x + threadIdx.x;
    if (h_out < H / pool_size && w_out < W / pool_size) {
        float max_val = -INFINITY;
        for (int i = 0; i < pool_size; ++i) {
            for (int j = 0; j < pool_size; ++j) {
                float val = input[(h_out * pool_size + i) * W + (w_out * pool_size + j)];
                max_val = fmaxf(max_val, val);
            }
        }
        output[h_out * (W / pool_size) + w_out] = max_val;
    }
}
```

```

    }
}

```

The softmax unit, however, requires a more complex kernel due to its reduction step. A common optimization is to use warp shuffles for efficient intra-warp communication:

Code Sample 27.8: Softmax Kernel

```

__global__ void softmax_kernel(float* input, float* output, int K) {
    __shared__ float sdata[256];
    int idx = threadIdx.x;
    float max_val = -INFINITY;
    for (int i = idx; i < K; i += blockDim.x) {
        max_val = fmaxf(max_val, input[i]);
    }
    max_val = warpReduceMax(max_val);
    if (idx == 0) sdata[0] = max_val;
    __syncthreads();
    max_val = sdata[0];
    float sum = 0.0f;
    for (int i = idx; i < K; i += blockDim.x) {
        sum += expf(input[i] - max_val);
    }
    sum = warpReduceSum(sum);
    if (idx == 0) sdata[0] = sum;
    __syncthreads();
    sum = sdata[0];
    for (int i = idx; i < K; i += blockDim.x) {
        output[i] = expf(input[i] - max_val) / sum;
    }
}

```

In summary, the softmax unit, ReLU activation, and max pooling unit each present distinct challenges and opportunities for GPU acceleration. The softmax unit's global dependencies necessitate careful optimization, while ReLU and max pooling benefit from straightforward parallelism. Modern GPU architectures address these differences through specialized libraries and hardware features, enabling efficient execution of deep learning workloads.

### 27.3.3 max pooling unit

The modern GPU architecture is designed to accelerate parallel computations, particularly in deep learning applications, where activation and pooling functions play a critical role. Among these functions, the max pooling unit is a fundamental component that reduces spatial dimensions while preserving important features. This discussion explores the max pooling unit in the context of GPU architecture, alongside related components such as the ReLU activation unit and softmax unit.

The max pooling unit operates by sliding a window over the input feature map and selecting the maximum value within each window. Mathematically, for an input feature map  $I$  of size  $H \times W$  and a pooling window of size  $k \times k$ , the output  $O$  at position  $(i, j)$  is given by:

$$O_{i,j} = \max_{m,n \in [0,k-1]} I_{i \cdot s + m, j \cdot s + n}$$

where  $s$  is the stride. This operation reduces computational complexity and mitigates overfitting by downsampling the feature map. Modern GPUs optimize max pooling through parallel execution, leveraging their SIMD (Single Instruction, Multiple Data) capabilities to process multiple windows simultaneously.

The ReLU (Rectified Linear Unit) activation function is another key component in GPU-accelerated deep learning. It is defined as:

$$\text{ReLU}(x) = \max(0, x)$$

ReLU introduces non-linearity while being computationally efficient, as it avoids expensive exponential operations. GPUs exploit the inherent parallelism of ReLU by applying it element-wise across tensors, often fused with other operations like convolution to minimize memory bandwidth usage. Research has demonstrated that ReLU accelerates convergence compared to traditional activation functions like sigmoid or tanh.

The softmax unit is used primarily in the output layer of classification networks. It converts logits into probabilities by applying:

$$\text{softmax}(x_i) = \frac{e^{x_i}}{\sum_{j=1}^K e^{x_j}}$$

where  $K$  is the number of classes. While softmax is computationally intensive due to exponentiation and summation, GPUs optimize its execution through parallel reduction and efficient memory access patterns. The work of highlights the importance of softmax in attention mechanisms, where GPU acceleration is critical for scalability.

The interplay between these units in GPU architecture is evident in convolutional neural networks (CNNs). A typical CNN layer sequence involves convolution followed by ReLU activation, max pooling for spatial down-sampling, and fully connected layers with softmax for classification. GPUs optimize this pipeline by leveraging hierarchical memory and thread-level parallelism. For instance, the max pooling unit benefits from shared memory to reduce redundant global memory accesses, as shown in .

The implementation of these units in hardware often involves specialized instructions. For example, NVIDIA's CUDA Deep Neural Network library (cuDNN) provides optimized kernels for ReLU, softmax, and max pooling. A simplified Verilog snippet for a max pooling unit is:

#### Code Sample 27.9: Max Pooling Unit

```
module max_pool #(parameter WIDTH=8, K=2) (
    input clk, rst,
    input [WIDTH-1:0] in [0:K-1][0:K-1],
    output reg [WIDTH-1:0] out
);
always @ (posedge clk or posedge rst) begin
    if (rst) out <= 0;
    else begin
        out <= in[0][0];
        for (int i = 0; i < K; i++)
            for (int j = 0; j < K; j++)
                if (in[i][j] > out) out <= in[i][j];
    end
end
endmodule
```

The efficiency of these units is further enhanced by GPU-specific optimizations. Warp-level parallelism enables fast execution of ReLU and softmax across multiple threads. Max pooling benefits from memory coalescing, which aligns memory access patterns to reduce latency. Additionally, tensor cores are employed for mixed-precision arithmetic, particularly in softmax computations.

Studies such as demonstrate how these optimizations improve throughput in frameworks like Caffe and TensorFlow. In summary, the max pooling unit, ReLU activation unit, and softmax unit are integral to modern GPU architecture, each optimized for parallel execution. Their efficient implementation enables the acceleration of deep learning models, as evidenced by benchmarks in . Future advancements may focus on further reducing memory overhead and improving precision, as discussed in .

# Chapter 28

## AI Dataflow and Scheduling

### 28.1 Dataflow for AI Models

#### 28.1.1 ai dataflow controller

The integration of AI dataflow controllers in modern GPU architectures represents a significant advancement in accelerating AI model execution. GPUs, originally designed for graphics rendering, have evolved into highly parallel computational engines optimized for data-intensive workloads. The dataflow paradigm, which emphasizes the movement and transformation of data rather than control flow, aligns naturally with the architecture of modern GPUs. AI dataflow controllers manage the efficient execution of AI workloads by orchestrating data movement between memory hierarchies and computational units, minimizing latency and maximizing throughput.

Modern GPU architectures, such as NVIDIA's Ampere and Hopper, incorporate specialized hardware for AI workloads, including tensor cores and AI dataflow controllers. These controllers optimize data movement by dynamically scheduling operations based on data dependencies and resource availability. The dataflow execution model enables fine-grained parallelism, where operations are triggered as soon as their input data becomes available. This contrasts with the traditional von Neumann model, where instructions are executed sequentially. The dataflow approach reduces idle time and improves resource utilization, which is critical for AI models with irregular computation patterns.

The AI dataflow controller operates at multiple levels of the GPU hierarchy. At the chip level, it manages data movement between global memory, shared memory, and registers. It ensures that data is prefetched into shared memory or registers before it is needed by computational units, reducing memory access latency. At the warp level, the controller schedules thread blocks to execute on streaming multiprocessors (SMs), balancing load and avoiding resource contention. It also handles synchronization between warps to ensure the correct execution of data-dependent operations.

A key challenge in AI dataflow execution is managing sparse and irregular data patterns. AI models, particularly those in natural language processing and recommendation systems, often exhibit sparsity in their weight matrices and activation tensors. The controller must efficiently skip zero-valued computations and compact sparse data to avoid unnecessary memory accesses. Compressed sparse row (CSR) and compressed sparse column (CSC) formats are commonly used, and the controller dynamically selects the appropriate representation based on the sparsity pattern.

Dataflow execution is mathematically represented as a directed acyclic graph (DAG), where nodes denote operations and edges indicate data dependencies. Let  $G = (V, E)$  denote the DAG, with  $V$  as the set of operations and  $E$  as the set of dependencies. The controller schedules each operation  $v \in V$  so that for every edge  $(u, v) \in E$ , operation  $u$  completes before  $v$  begins. The goal is to minimize the total execution time  $T$ :

$$T = \max_{v \in V}(t_v + d_v)$$

where  $t_v$  is the start time and  $d_v$  is the duration of operation  $v$ .

The controller benefits from GPU support for dynamic parallelism. In CUDA, kernels can launch child kernels, allowing nested dataflow execution. Dependencies between parent and child grids are managed to maximize concurrency. An example Verilog implementation of a simplified controller follows:

Code Sample 28.1: AI Dataflow Controller

```
module ai_dataflow_controller (
```

```

input wire clk,
input wire reset,
input wire [31:0] dependency_graph,
output reg [31:0] kernel_launch
);
reg [31:0] ready_count;
always @(posedge clk or posedge reset) begin
  if (reset) begin
    ready_count <= 0;
    kernel_launch <= 0;
  end else begin
    if (dependency_graph[ready_count]) begin
      kernel_launch <= 1;
      ready_count <= ready_count + 1;
    end else begin
      kernel_launch <= 0;
    end
  end
end
endmodule

```

Memory access optimization is another focus. Convolutional neural networks exhibit regular, strided access patterns, while transformers and graph neural networks produce irregular ones. The controller uses coalesced memory accesses, prefetching, and bank conflict minimization to increase efficiency. Techniques like tiling and double buffering enable overlapping computation with memory transfers.

Energy efficiency is also addressed by adjusting voltage and frequency based on workload characteristics. Power gating and clock gating disable idle units to reduce power consumption. Utilization metrics guide these adjustments to optimize the performance-to-power ratio.

Reliability is ensured through error detection and correction mechanisms such as parity checks and ECC. Redundant execution and checkpointing techniques allow the system to recover from faults without restarting entire computations, which is especially valuable in large-scale distributed training.

In conclusion, the AI dataflow controller is a cornerstone of efficient AI model execution in GPU environments. It orchestrates data movement, operation scheduling, synchronization, and memory hierarchy utilization while ensuring fault tolerance and power efficiency. These capabilities enable modern GPUs to meet the demands of complex, large-scale AI workloads. Future directions include adaptive scheduling, enhanced sparse tensor support, and integration with emerging computing paradigms such as neuromorphic processors.

## 28.2 Scheduling for Neural Network Layers

### 28.2.1 layer scheduler

The layer scheduler in modern GPU architectures plays a critical role in optimizing the execution of neural network layers by managing computational resources and dependencies. GPUs, designed for parallel processing, rely on efficient scheduling to maximize throughput and minimize latency. A layer scheduler must account for the heterogeneous nature of neural network workloads, which include convolutional layers, fully connected layers, and activation functions, each with distinct computational requirements. The scheduler must also handle pipeline dependencies to ensure correct execution order while minimizing idle time.

Modern GPUs employ hierarchical scheduling mechanisms to manage workloads at different granularities. At the highest level, the layer scheduler assigns layers to streaming multiprocessors (SMs) based on resource availability and workload characteristics. Each SM further decomposes the layer into warps, which are scheduled by the warp scheduler. The warp scheduler uses techniques such as round-robin, greedy, or priority-based scheduling to maximize instruction-level parallelism (ILP) and memory-level parallelism (MLP). For example, NVIDIA's Volta architecture introduces independent thread scheduling, allowing finer control over warp execution .

The layer scheduler must also resolve pipeline dependencies to prevent data hazards. Neural networks exhibit both intra-layer and inter-layer dependencies. Intra-layer dependencies arise from operations within a single layer, such as tensor convolutions, where intermediate results must be synchronized. Inter-layer dependencies occur between successive layers, where the output of one layer serves as the input to the next. A pipeline dependency manager tracks these dependencies and ensures correct execution order. Techniques such as dynamic scheduling, speculative execution, and out-of-order execution are employed to mitigate stalls caused by dependencies .

One common approach to dependency management is the use of scoreboarding, where the scheduler maintains a table of resource availability and operand readiness. For example, the following equation models the readiness of an operand  $R_i$  for instruction  $I_j$ :

$$R_i = \begin{cases} 1 & \text{if operand is ready,} \\ 0 & \text{otherwise} \end{cases}$$

The scheduler then issues instructions only when all operands are ready, as shown in:

$$\text{Issue}(I_j) = \prod_{i=1}^n R_i$$

Another critical aspect of layer scheduling is resource allocation. GPUs must allocate registers, shared memory, and thread blocks efficiently to avoid resource contention. The scheduler uses occupancy calculators to determine the optimal number of thread blocks per SM. The occupancy  $O$  is given by:

$$O = \frac{\text{Active Warps}}{\text{Maximum Warps}}$$

Higher occupancy improves throughput but may increase register pressure. The scheduler must balance these trade-offs to achieve optimal performance.

Modern layer schedulers also leverage hardware support for dependency tracking. For instance, NVIDIA's CUDA programming model introduces `cudaStream` and

### 28.2.2 pipeline dependency manager

Modern GPU architectures have evolved to efficiently handle the computational demands of neural networks, particularly through the use of pipeline dependency managers and layer schedulers. These components are critical for optimizing throughput and minimizing latency in deep learning workloads. The pipeline dependency manager ensures that data dependencies between neural network layers are resolved without stalling the execution pipeline, while the layer scheduler orchestrates the execution order of these layers to maximize hardware utilization.

The pipeline dependency manager operates by tracking data dependencies between layers and ensuring that intermediate results are available before subsequent layers begin processing. This is particularly important in GPUs, where parallelism is exploited through thousands of threads executing concurrently. For example, if layer  $L_i$  produces an output tensor that is consumed by layer  $L_j$ , the dependency manager ensures that  $L_j$  does not start until  $L_i$  has completed. This can be formalized as a constraint:

$$\text{Start}(L_j) \geq \text{End}(L_i)$$

## Shared Memory Improvements for AI-Specific Dataflows

### Evolution of GPU Shared Memory

#### Traditional GPU Memory

- Fixed memory banks
- Limited bank conflict resolution

#### AI-Optimized Shared Memory

- Configurable memory patterns
- Advanced conflict avoidance

### Key Shared Memory Innovations

1

#### Adaptive Banking Strategies

Dynamically configurable memory banks that adapt to tensor access patterns in neural networks

2

#### Tensor Core Integration

Direct pathways between shared memory and tensor cores for matrix multiplication acceleration

3

#### Advanced Memory Coalescing

Intelligent access pattern recognition that minimizes bank conflicts for common AI data access patterns

4

#### Predictive Prefetching

Anticipatory loading of data based on neural network layer structure and training patterns

### Optimized Memory Access Patterns

#### Traditional Banking



Bank conflicts with strided access

Traditional

1x Throughput

#### AI-Optimized Banking



Conflict-free access with AI-specific patterns

AI-Optimized

Up to 4x Throughput for Neural Network Workloads

where  $\text{Start}(L_j)$  and  $\text{End}(L_i)$  represent the start and end times of the respective layers. Modern GPUs use hardware-supported mechanisms such as scoreboarding or reservation stations to enforce these dependencies dynamically.

The layer scheduler complements the dependency manager by determining the optimal execution order of layers to minimize idle time and maximize throughput. Given a neural network with  $N$  layers, the scheduler must solve an optimization problem to minimize the total execution time  $T$ :

$$T = \sum_{i=1}^N \text{Latency}(L_i) + \sum_{i,j} \text{Overhead}(L_i, L_j)$$

where  $\text{Latency}(L_i)$  is the execution time of layer  $L_i$ , and  $\text{Overhead}(L_i, L_j)$  accounts for any pipeline stalls or synchronization delays between dependent layers. Advanced schedulers employ heuristic or machine learning-based approaches to predict layer execution times and dependencies.

In modern GPU architectures, the pipeline dependency manager and layer scheduler are tightly integrated with the hardware execution units. For instance, NVIDIA's Tensor Cores and AMD's Matrix Cores are designed to accelerate matrix operations common in neural networks, but their efficiency depends on proper scheduling and dependency resolution. The following Verilog-like pseudocode illustrates a simplified dependency manager:

Code Sample 28.2: Pipeline Dependency Manager

```
module dependency_manager (
    input wire [31:0] layer_start,
    input wire [31:0] layer_end,
    output reg [31:0] next_start
);
    always @(*) begin
        if (layer_end > layer_start)
            next_start = layer_end;
        else
            next_start = layer_start;
    end
endmodule
```

This module ensures that the next layer only starts after the current layer has finished, enforcing the constraint in 28.2.2.

The interaction between the pipeline dependency manager and layer scheduler is further complicated by memory hierarchy considerations. Neural networks often require large intermediate tensors to be stored in high-bandwidth memory (HBM) or shared caches. The scheduler must account for memory access patterns to avoid bottlenecks. For example, convolutional layers with large filter sizes may require prefetching or tiling to overlap computation with data transfers.

Recent research has explored dynamic scheduling techniques that adapt to runtime conditions. For instance, the work in proposes a sparse convolutional neural network accelerator that dynamically adjusts scheduling based on sparsity patterns. Similarly, introduces a dependency-aware scheduler that reorders layers to minimize pipeline bubbles.

The mathematical formulation of the scheduling problem can be extended to include resource constraints. Let  $R_k$  represent the available hardware resources (e.g., registers, memory bandwidth) at time  $k$ . The scheduler must ensure that:

$$\sum_{i \in \text{Active}(k)} \text{Resource}(L_i) \leq R_k$$

where  $\text{Active}(k)$  is the set of layers executing at time  $k$ , and  $\text{Resource}(L_i)$  denotes the resources consumed by layer  $L_i$ . This constraint ensures that the GPU's finite resources are not oversubscribed, which could lead to contention and reduced performance.

Key challenges in pipeline dependency management and layer scheduling include handling irregular dependencies in architectures like transformers or graph neural networks, balancing workload across streaming multi-processors (SMs) to avoid underutilization, and mitigating the impact of synchronization overhead in distributed training scenarios.

Emerging solutions leverage compiler optimizations, such as polyhedral scheduling, to statically analyze and optimize layer execution. These techniques are increasingly important as neural networks grow in complexity and scale.

In summary, the pipeline dependency manager and layer scheduler are pivotal components in modern GPU architectures for neural network execution. Their efficient operation relies on a combination of hardware support, mathematical optimization, and runtime adaptation to ensure high throughput and low latency. Future advancements will likely focus on automating these processes further, enabling even more efficient execution of increasingly complex models.

# Chapter 29

## AI GPU Case Studies

### 29.1 Deep Learning Inference

#### 29.1.1 cnn inference engine

The acceleration of deep learning inference, particularly for convolutional neural networks (CNNs) and recurrent neural networks (RNNs), has become a critical research area in modern GPU architecture. GPUs provide the parallel processing capabilities required for efficient inference, leveraging their thousands of cores to perform matrix multiplications and tensor operations with high throughput. The inference engine for CNNs and RNNs exploits these architectural features to minimize latency and maximize energy efficiency.

Modern GPUs employ specialized hardware units such as tensor cores, which are optimized for mixed-precision matrix operations. For CNNs, the inference engine maps convolutional layers to these tensor cores, reducing the computational complexity through techniques like Winograd transformations. The Winograd algorithm minimizes the number of multiplications required for convolution by reformulating the operation as:

$$Y = A^T (GgG^T \odot B^T dB) A$$

where  $g$  represents the filter,  $d$  the input, and  $A, B, G$  are transformation matrices. This approach reduces the arithmetic complexity from  $O(n^2)$  to  $O(n \log n)$  for small filters, making it ideal for GPU acceleration.

RNN inference engines, particularly for long short-term memory (LSTM) and gated recurrent unit (GRU) networks, face different challenges due to their sequential nature. Modern GPUs mitigate this by batching multiple sequences and exploiting parallelism across time steps. The LSTM cell update equations are:

$$\begin{aligned} f_t &= \sigma(W_f \cdot [h_{t-1}, x_t] + b_f) \\ i_t &= \sigma(W_i \cdot [h_{t-1}, x_t] + b_i) \\ o_t &= \sigma(W_o \cdot [h_{t-1}, x_t] + b_o) \\ \tilde{C}_t &= \tanh(W_C \cdot [h_{t-1}, x_t] + b_C) \\ C_t &= f_t \odot C_{t-1} + i_t \odot \tilde{C}_t \\ h_t &= o_t \odot \tanh(C_t) \end{aligned}$$

where  $f_t, i_t, o_t$  are the forget, input, and output gates, respectively. GPU architectures optimize these operations by fusing the element-wise operations and leveraging shared memory for intermediate results.

The memory hierarchy of modern GPUs plays a crucial role in CNN and RNN inference. Global memory serves as the high-capacity but high-latency DRAM used for storing model parameters and input data. Shared memory provides low-latency on-chip storage for thread collaboration, critical for caching intermediate activation maps in CNNs. Registers act as the fastest storage for thread-local variables, often used for holding weights and activations during computation.

Efficient memory access patterns are essential for maximizing throughput. For CNNs, tiling techniques divide the input and weight matrices into smaller blocks that fit into shared memory, reducing global memory accesses. The following pseudocode illustrates a tiled matrix multiplication kernel for CNN inference:

### Code Sample 29.1: Tiled Matrix Multiplication

```
__global__ void matmul(float *A, float *B, float *C, int N) {
    __shared__ float As[TILE][TILE];
    __shared__ float Bs[TILE][TILE];
    int bx = blockIdx.x, by = blockIdx.y;
    int tx = threadIdx.x, ty = threadIdx.y;
    int row = by * TILE + ty, col = bx * TILE + tx;
    float sum = 0.0f;
    for (int k = 0; k < N; k += TILE) {
        As[ty][tx] = A[row * N + k + tx];
        Bs[ty][tx] = B[(k + ty) * N + col];
        __syncthreads();
        for (int i = 0; i < TILE; ++i)
            sum += As[ty][i] * Bs[i][tx];
        __syncthreads();
    }
    C[row * N + col] = sum;
}
```

Quantization is another key optimization for inference engines, reducing the precision of weights and activations to 8-bit integers (INT8) or even 4-bit without significant accuracy loss . Modern GPUs support integer arithmetic pipelines, enabling faster computation for quantized models. The quantization process for a floating-point value  $x$  is:

$$x_q = \text{round}\left(\frac{x}{\Delta}\right) + z$$

where  $\Delta$  is the scale factor and  $z$  is the zero-point. Dequantization reconstructs the approximate float value as:

$$x_{\text{deq}} = (x_q - z) \cdot \Delta$$

Sparsity exploitation further enhances inference efficiency. Modern GPUs leverage structured sparsity, where entire blocks of weights are pruned to zero, allowing for compression and skipping of redundant computations. The NVIDIA Ampere architecture introduces fine-grained sparsity support, doubling the throughput for sparse matrix operations .

Dynamic parallelism in RNNs poses unique challenges due to variable sequence lengths. GPUs address this through persistent kernels, which are long-running kernels that process multiple time steps and reduce kernel launch overhead. Warp scheduling ensures efficient context switching between warps to hide memory latency. Atomic operations are used to update shared states in attention mechanisms or beam search.

The interplay between CNN and RNN inference engines is evident in architectures like convolutional RNNs (CRNNs) and transformer-based models. These hybrid models require coordinated execution of convolutional and recurrent layers, necessitating sophisticated GPU scheduling. For example, the transformer's self-attention mechanism involves:

$$\text{Attention}(Q, K, V) = \text{softmax}\left(\frac{QK^T}{\sqrt{d_k}}\right)V$$

where  $Q, K, V$  are learned query, key, and value matrices. GPU implementations optimize this by batching attention heads and using fused kernels for the softmax and matrix multiplication steps.

Energy efficiency is a critical metric for inference engines. Modern GPUs employ dynamic voltage and frequency scaling (DVFS) to adjust power consumption based on workload demands. The energy  $E$  for a computation is modeled as:

$$E = \sum_i P_i \cdot t_i$$

where  $P_i$  is the power consumed in state  $i$  and  $t_i$  is the time spent in that state. Techniques like kernel fusion and memory coalescing minimize energy by reducing data movement and idle cycles.

Emerging research explores the use of mixed-precision training and inference, where different layers or operations use varying numerical precision. For instance, NVIDIA's TensorFloat-32 (TF32) format provides a balance between FP32 and FP16, accelerating inference while maintaining accuracy . The precision hierarchy in modern GPUs includes FP64 for double precision in scientific computing, FP32 for general-purpose deep learning, TF32, FP16, and BF16 for reduced-precision inference acceleration, and INT8 or INT4 for quantized models.

Compiler optimizations, such as automatic kernel fusion and memory layout transformations, further enhance inference performance. Frameworks like TensorRT analyze the computational graph and generate optimized GPU

kernels tailored for specific CNN and RNN architectures. The integration of these techniques ensures that modern GPU architectures remain at the forefront of deep learning inference, enabling real-time applications across domains.

### 29.1.2 rnn inference engine

The efficient execution of recurrent neural network (RNN) inference engines on modern GPU architectures presents unique challenges and opportunities in deep learning. Unlike convolutional neural networks (CNNs), which benefit from the highly parallelizable nature of GPU compute units, RNNs exhibit sequential dependencies that complicate their acceleration. This discussion examines the architectural considerations for RNN inference engines, contrasts them with CNN inference engines, and explores optimization techniques tailored to modern GPU designs.

RNNs process sequential data by maintaining a hidden state  $h_t$  updated at each timestep  $t$  according to:

$$h_t = \sigma(W_h h_{t-1} + W_x x_t + b)$$

where  $\sigma$  is a nonlinear activation function,  $W_h$  and  $W_x$  are weight matrices,  $x_t$  is the input at timestep  $t$ , and  $b$  is a bias term. The sequential nature of this computation limits parallelism, as each timestep depends on the previous hidden state. Modern GPUs, designed for data-parallel workloads, must employ specific optimizations to handle this constraint efficiently.

One approach involves batching multiple independent sequences to exploit parallelism across sequences. For a batch size  $B$ , the GPU can compute  $B$  hidden states in parallel, provided the sequences are of equal length or padded to a common length. However, this strategy becomes inefficient for highly variable sequence lengths due to wasted computation on padding elements. NVIDIA's Tensor Cores, introduced in Volta and later architectures, accelerate matrix multiplications in RNNs through mixed-precision computation, improving throughput for batched inference.

Memory bandwidth optimization is critical for RNN inference engines. The recurrent connections in (29.1.2) require frequent access to the hidden state  $h_{t-1}$ , creating a memory-bound workload. GPUs mitigate this through hierarchical memory systems with registers, shared memory, and L1/L2 caches; coalesced memory accesses to maximize bandwidth utilization; and weight stationary dataflow to minimize off-chip memory traffic. For example, the NVIDIA A100 GPU's 1555 GB/s memory bandwidth and 40 MB L2 cache significantly reduce latency for RNN state updates.

In contrast, CNN inference engines leverage the spatial locality of convolutional operations, which map naturally to GPU parallelism. A standard 2D convolution computes:

$$Y[i, j] = \sum_{m,n} X[i + m, j + n] \cdot K[m, n]$$

where  $X$  is the input,  $K$  is the kernel, and  $Y$  is the output. The independence of output pixels enables massive parallelism, with modern GPUs processing thousands of concurrent threads. The cuDNN library optimizes CNN inference through implicit GEMM (General Matrix Multiplication) for convolution, Winograd transformations to reduce arithmetic complexity, and Tensor Core acceleration for FP16 and INT8 precision.

RNN inference engines require different optimization strategies. The persistent RNN kernel approach, implemented in frameworks like TensorRT, maintains the hidden state in GPU registers across timesteps to minimize global memory accesses. For long sequences, techniques such as kernel fusion to combine multiple operations (e.g., matrix multiply and activation), dynamic parallelism to handle variable-length sequences, and attention mechanisms to reduce effective sequence length improve performance. The Transformer architecture, while not strictly an RNN, shares similar sequence processing challenges and benefits from GPU-optimized attention implementations.

Quantization plays a crucial role in both RNN and CNN inference engines. Post-training quantization reduces weight and activation precision from 32-bit floating point to 8-bit integers, decreasing memory footprint and increasing compute throughput. For RNNs, careful handling of the hidden state quantization is necessary to prevent error accumulation across timesteps. The NVIDIA Turing architecture introduced INT8 tensor cores specifically for quantized inference workloads.

The following Verilog-like pseudocode illustrates a simplified RNN processing unit optimized for GPU implementation:

Code Sample 29.2: RNN Processing Unit

```
module rnn_core (
```

```

    input clk, reset,
    input [15:0] x_t,          // Quantized input
    input [15:0] h_prev,       // Previous hidden state
    output [15:0] h_next       // Next hidden state
);
// Weight buffers (stored in shared memory)
reg [15:0] W_x [0:255];
reg [15:0] W_h [0:255];

// Matrix-vector multiply with accumulation
always @(posedge clk) begin
    if (reset)
        h_next <= 0;
    else begin
        h_next <= activation(W_x * x_t + W_h * h_prev);
    end
end
endmodule

```

Modern GPU architectures employ specialized hardware for RNN acceleration. The Google TPU v3 includes systolic arrays optimized for the matrix-vector products dominant in RNN inference . Similarly, AMD's CDNA architecture features matrix acceleration engines supporting both CNN and RNN workloads .

The choice between RNN and CNN inference engines depends on the application domain. CNNs excel at image classification and object detection, spatial feature extraction, and fixed-size input processing, while RNNs are preferred for sequential data (text, speech, time series), variable-length inputs, and temporal pattern recognition. Hybrid architectures combining CNN feature extractors with RNN sequence processors demonstrate the complementary nature of these approaches. For instance, video processing pipelines often use CNNs for frame-level feature extraction followed by RNNs for temporal analysis .

The energy efficiency of RNN inference engines on GPUs depends heavily on the arithmetic intensity (operations per byte transferred). While CNNs typically achieve higher arithmetic intensity due to data reuse in convolutions, RNNs benefit from operator fusion to increase compute density, sparsity exploitation through pruning, and low-precision computation. The NVIDIA Jetson AGX Orin achieves 275 TOPS for INT8 inference, enabling real-time RNN applications in edge devices .

In summary, modern GPU architectures provide the computational resources and memory hierarchy necessary for efficient RNN inference, albeit requiring different optimization strategies than CNNs. The ongoing evolution of tensor cores, memory systems, and specialized accelerators continues to narrow the performance gap between sequential and parallel neural network inference workloads.

## 29.2 Training Neural Networks

### 29.2.1 backpropagation unit

The backpropagation unit in modern GPU architectures plays a critical role in accelerating the training of neural networks. Backpropagation, as formulated by Rumelhart et al. , computes gradients of the loss function with respect to each weight in the network using the chain rule. Modern GPUs optimize this process through parallel execution and specialized hardware units. The backpropagation unit typically consists of three key components: gradient computation, weight update, and synchronization. These components are tightly integrated into the GPU's streaming multiprocessors (SMs) to maximize throughput.

The gradient computation step involves calculating partial derivatives for each layer. For a layer  $l$ , the error signal  $\delta^{(l)}$  is computed as:

$$\delta^{(l)} = \left( (W^{(l+1)})^T \delta^{(l+1)} \right) \odot \sigma'(z^{(l)})$$

where  $W^{(l+1)}$  is the weight matrix,  $\delta^{(l+1)}$  is the error from the next layer,  $z^{(l)}$  is the pre-activation, and  $\sigma'$  is the derivative of the activation function. Modern GPUs leverage their SIMD (Single Instruction, Multiple Data) architecture to compute these gradients in parallel across thousands of threads. For example, NVIDIA's CUDA cores execute these operations concurrently, significantly reducing training time .

The weight update step applies the computed gradients to adjust the network's weights. This is typically performed by an optimizer unit, which implements algorithms such as Stochastic Gradient Descent (SGD), Adam

, or RMSprop. The weight update rule for SGD is:

$$W^{(l)} \leftarrow W^{(l)} - \eta \nabla_{W^{(l)}} J$$

where  $\eta$  is the learning rate and  $\nabla_{W^{(l)}} J$  is the gradient of the loss function  $J$  with respect to  $W^{(l)}$ . The optimizer unit is often implemented as a separate hardware block or a software module running on the GPU's SMs. Modern GPUs use mixed-precision arithmetic (e.g., FP16 and FP32) to speed up these computations while maintaining numerical stability .

The synchronization step ensures that all threads have completed their computations before proceeding to the next iteration. This is critical for maintaining correctness in distributed training scenarios. GPUs employ barriers and atomic operations to synchronize threads across warps and blocks. For instance, the `__syncthreads()` function in CUDA ensures that all threads in a block reach the same point before continuing .

The backpropagation unit's efficiency is further enhanced by memory hierarchy optimizations. GPUs utilize shared memory, registers, and caches to minimize data movement between global memory and compute units. For example, the Volta architecture introduced Tensor Cores, which accelerate matrix multiplications—a key operation in backpropagation—by performing mixed-precision computations in a single instruction .

The following Verilog-like pseudocode illustrates a simplified backpropagation unit:

Code Sample 29.3: Backpropagation Unit

```
module backprop_unit (
    input clk, reset,
    input [31:0] gradient_in,
    output [31:0] weight_update
);
    reg [31:0] weight;
    always @ (posedge clk) begin
        if (reset)
            weight <= 0;
        else
            weight <= weight - gradient_in;
    end
    assign weight_update = weight;
endmodule
```

The optimizer unit is equally critical, as it determines the convergence rate and final performance of the neural network. Adam, for instance, combines momentum and adaptive learning rates using the following update rules:

$$m_t = \beta_1 m_{t-1} + (1 - \beta_1) \nabla J$$

$$v_t = \beta_2 v_{t-1} + (1 - \beta_2) (\nabla J)^2$$

$$W_t = W_{t-1} - \eta \frac{m_t}{\sqrt{v_t} + \epsilon}$$

where  $m_t$  and  $v_t$  are estimates of the first and second moments of the gradients, and  $\beta_1$ ,  $\beta_2$ , and  $\epsilon$  are hyperparameters. GPUs optimize these computations by exploiting parallelism and pipelining. For example, the A100 GPU's Tensor Cores can perform matrix operations for Adam in a fraction of the time required by traditional FP32 units .

The interplay between the backpropagation and optimizer units is a key factor in modern deep learning frameworks like TensorFlow and PyTorch. These frameworks leverage GPU acceleration to perform backpropagation and optimization in a single pass, minimizing latency and maximizing throughput. For instance, PyTorch's `torch.optim` module implements various optimizers as CUDA kernels, allowing seamless integration with GPU hardware .

Memory bandwidth is another critical consideration. Backpropagation requires frequent access to weight matrices and gradients, which can create bottlenecks. GPUs address this through high-bandwidth memory (HBM) and advanced caching strategies. The HBM2E standard, for example, provides up to 3.2 TB/s of bandwidth, enabling faster data transfers for large neural networks .

Several key architectural optimizations enable this level of performance. Parallel gradient computation is achieved using SIMD and SIMT (Single Instruction, Multiple Threads) architectures, allowing multiple gradients to be processed simultaneously. Mixed-precision arithmetic formats, including FP16, FP32, and TF32, enable faster matrix operations while preserving sufficient numerical accuracy. Tensor Cores are specifically designed to accelerate matrix multiplications and convolutions, which are the backbone of neural network training. The

inclusion of high-bandwidth memory helps reduce data transfer latency, ensuring that compute units are not starved for data. Additionally, hardware-accelerated optimizers, such as those for Adam and RMSprop, are implemented via CUDA kernels to further boost performance.

In summary, the backpropagation and optimizer units in modern GPUs are highly specialized for training neural networks. They leverage parallel execution, mixed-precision arithmetic, and advanced memory hierarchies to achieve unprecedented performance. These advancements have enabled the training of increasingly complex models, from convolutional neural networks (CNNs) to transformers, in reasonable time frames . Future architectures are expected to further optimize these units, potentially integrating dedicated AI accelerators for even greater efficiency.

### 29.2.2 optimizer unit

The optimizer unit in modern GPU architectures plays a critical role in the efficient training of neural networks, particularly in the context of backpropagation. The optimizer unit is responsible for adjusting the weights of a neural network to minimize the loss function, leveraging gradient information computed during backpropagation. Modern GPUs, with their highly parallel architecture, are particularly well-suited for executing these optimizations due to their ability to perform large-scale matrix operations efficiently.

The optimizer unit typically implements algorithms such as Stochastic Gradient Descent (SGD), Adam, or RMSprop, each of which involves iterative updates to the network parameters based on gradients. For example, the update rule for SGD with momentum is given by:

$$v_t = \gamma v_{t-1} + \eta \nabla_{\theta} J(\theta)$$

$$\theta_t = \theta_{t-1} - v_t$$

Here,  $v_t$  represents the velocity at time step  $t$ ,  $\gamma$  is the momentum coefficient,  $\eta$  is the learning rate, and  $\nabla_{\theta} J(\theta)$  is the gradient of the loss function  $J$  with respect to the parameters  $\theta$ . The GPU's parallel processing capabilities allow these updates to be computed efficiently across thousands of parameters simultaneously.

The backpropagation unit computes the gradients required by the optimizer unit. It leverages the chain rule to propagate errors backward through the network, calculating the gradient of the loss function with respect to each weight. The backpropagation process can be expressed as:

$$\frac{\partial J}{\partial w_{ij}^{(l)}} = \frac{\partial J}{\partial z_j^{(l)}} \cdot \frac{\partial z_j^{(l)}}{\partial w_{ij}^{(l)}}$$

where  $w_{ij}^{(l)}$  is the weight connecting neuron  $i$  in layer  $l - 1$  to neuron  $j$  in layer  $l$ , and  $z_j^{(l)}$  is the weighted input to neuron  $j$ . Modern GPUs accelerate this computation by parallelizing the gradient calculations across multiple cores, reducing the time required for each training iteration.

The optimizer unit must also handle challenges such as numerical stability and memory constraints. For instance, the Adam optimizer combines the benefits of momentum and adaptive learning rates, but its implementation requires maintaining additional state variables for each parameter. The update rules for Adam are:

$$m_t = \beta_1 m_{t-1} + (1 - \beta_1) \nabla_{\theta} J(\theta)$$

$$v_t = \beta_2 v_{t-1} + (1 - \beta_2) (\nabla_{\theta} J(\theta))^2$$

$$\hat{m}_t = \frac{m_t}{1 - \beta_1^t}$$

$$\hat{v}_t = \frac{v_t}{1 - \beta_2^t}$$

$$\theta_t = \theta_{t-1} - \eta \frac{\hat{m}_t}{\sqrt{\hat{v}_t} + \epsilon}$$

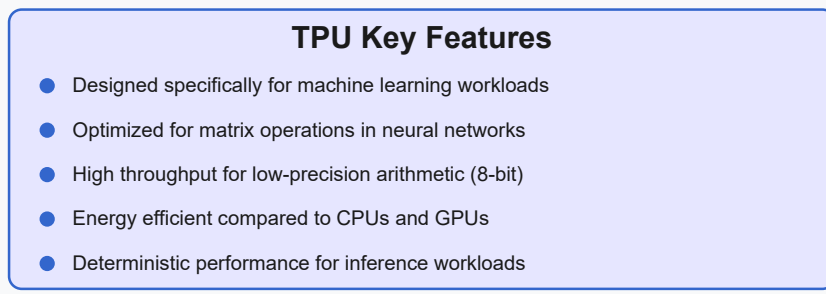
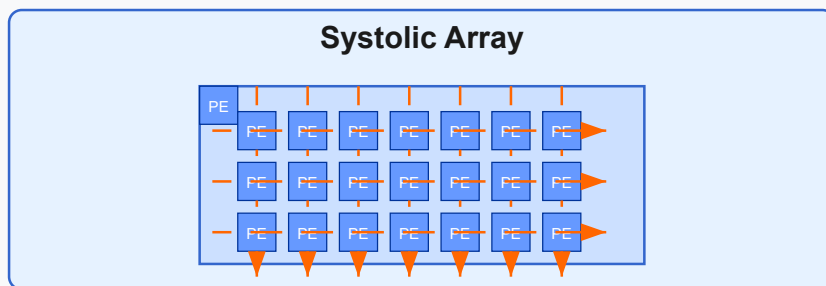
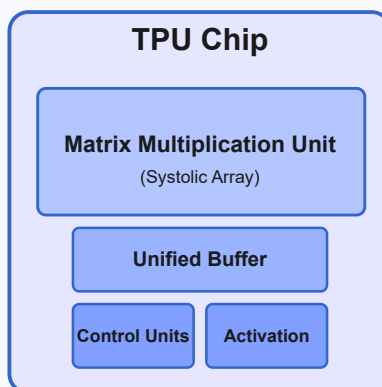
Here,  $m_t$  and  $v_t$  are estimates of the first and second moments of the gradients,  $\beta_1$  and  $\beta_2$  are exponential decay rates, and  $\epsilon$  is a small constant for numerical stability. The GPU's high memory bandwidth and parallel execution capabilities enable efficient computation and storage of these intermediate variables.

The implementation of optimizer units in modern GPUs often involves low-level optimizations to maximize performance. For example, the use of warp-level primitives in CUDA allows for efficient reduction operations during gradient updates. The following Verilog-like pseudocode illustrates a simplified GPU kernel for updating weights using SGD:

Code Sample 29.4: GPU Kernel for SGD Weight Update

```
__global__ void sgd_update(float* weights, float* gradients, float lr, int n) {
    int idx = blockIdx.x * blockDim.x + threadIdx.x;
    if (idx < n) {
        weights[idx] -= lr * gradients[idx];
    }
}
```

## Tensor Processing Unit (TPU) Architecture



This kernel launches one thread per weight, allowing the GPU to parallelize the update across all parameters. The `blockIdx` and `threadIdx` variables are used to assign each thread a unique weight to update. Such optimizations are critical for achieving high throughput in large-scale neural network training.

Memory access patterns also play a significant role in the performance of optimizer units. GPUs employ coalesced memory accesses to minimize latency when reading and writing gradients and weights. For instance, adjacent threads should access contiguous memory locations to maximize memory bandwidth utilization. This is particularly important for optimizers like Adam, which require multiple memory accesses per parameter.

The choice of optimizer can significantly impact the training dynamics of a neural network. For example, SGD with momentum is often preferred for its simplicity and robustness, while Adam is favored for its adaptive learning rates and faster convergence in many scenarios. The optimizer unit must therefore support a variety of algorithms to accommodate different training requirements. Modern GPU architectures provide the flexibility to implement these algorithms efficiently, leveraging their parallel processing capabilities to accelerate training.

In summary, the optimizer unit in modern GPU architectures is a critical component for training neural networks, working in tandem with the backpropagation unit to adjust network parameters. Its efficiency is underpinned by the GPU's parallel execution model, which enables rapid computation of gradient updates and intermediate variables. Low-level optimizations, such as warp-level reductions and coalesced memory accesses, further enhance performance, making GPUs the preferred platform for large-scale neural network training. The choice of optimizer algorithm, whether SGD, Adam, or another variant, depends on the specific requirements of the training task, and modern GPUs provide the computational resources to support these diverse approaches.

## 29.3 Real-World Applications

### 29.3.1 Implementing AI-driven image recognition workload

The rapid advancement of artificial intelligence (AI) has necessitated the development of specialized hardware architectures capable of handling computationally intensive workloads. Modern GPU architectures, particularly those designed for parallel processing, have emerged as the cornerstone for implementing AI-driven image recognition and natural language processing (NLP) workloads. These architectures leverage thousands of cores to perform matrix operations efficiently, which are fundamental to convolutional neural networks (CNNs) and transformer models. The following discussion explores the implementation of AI-driven workloads on modern GPUs, their real-world applications, and the underlying computational principles.

GPUs excel in parallel processing due to their Single Instruction, Multiple Thread (SIMT) execution model. For image recognition tasks, CNNs are the dominant architecture, requiring massive matrix multiplications and convolutions. Modern GPUs, such as NVIDIA's Ampere architecture, optimize these operations through Tensor Cores, which accelerate mixed-precision computations. The performance gain is quantified by the throughput in floating-point operations per second (FLOPS). For instance, the NVIDIA A100 GPU delivers 312 TFLOPS for 16-bit floating-point operations. The computational efficiency is further enhanced by techniques like layer fusion and kernel optimization, reducing memory bandwidth bottlenecks.

In real-world applications, AI-driven image recognition is deployed in autonomous vehicles, medical imaging, and surveillance systems. Autonomous vehicles rely on CNNs for object detection and semantic segmentation. The YOLOv4 model, for example, achieves real-time inference on GPUs by optimizing anchor boxes and non-maximum suppression. Medical imaging applications, such as MRI analysis, use U-Net architectures for segmentation tasks. These models benefit from GPU-accelerated training, reducing the time from weeks to hours. Surveillance systems leverage GPUs for facial recognition and anomaly detection, where low-latency inference is critical.

Natural language processing workloads, particularly transformer-based models like BERT and GPT-3, also heavily depend on GPU acceleration. Transformers require self-attention mechanisms, which involve large matrix multiplications and softmax operations. The computational complexity of self-attention scales quadratically with sequence length, making GPUs indispensable for training and inference. NVIDIA's cuDNN and cuBLAS libraries optimize these operations by leveraging tensor cores and memory hierarchy. For example, the GPT-3 model with 175 billion parameters is trained on clusters of GPUs, utilizing mixed-precision arithmetic to reduce memory footprint.

The implementation of AI workloads on GPUs involves several optimization strategies. Memory access patterns significantly impact performance, as GPUs rely on high-bandwidth memory (HBM) to feed data to compute units. Techniques like tiling and shared memory usage minimize global memory accesses. For instance, in CNNs, input feature maps are divided into tiles that fit into shared memory, reducing latency. Similarly, NLP models benefit from kernel fusion, where multiple operations are combined into a single kernel to reduce overhead.

The following equation illustrates the computational intensity of a matrix multiplication operation in self-attention:

$$\mathbf{QK}^T = \sum_{i=1}^n \mathbf{Q}_i \mathbf{K}_i^T$$

where  $\mathbf{Q}$  and  $\mathbf{K}$  are query and key matrices, respectively. GPUs parallelize this operation across thousands of threads, achieving near-linear speedup.

Real-world NLP applications include machine translation, sentiment analysis, and chatbots. Google's Transformer model revolutionized machine translation by replacing recurrent layers with self-attention, enabling parallel processing on GPUs. Sentiment analysis models, such as those based on BERT, fine-tune pre-trained weights on GPU clusters for tasks like review classification. Chatbots like OpenAI's ChatGPT leverage GPU-accelerated inference to generate human-like responses in real time.

The integration of AI workloads with modern GPU architectures also involves software frameworks. TensorFlow and PyTorch provide high-level abstractions for GPU acceleration, automating memory management and kernel optimization. For example, PyTorch's `torch.cuda` module enables seamless execution of tensors on GPUs, while TensorFlow's XLA compiler optimizes computation graphs for specific hardware.

The following Verilog snippet illustrates a simplified GPU tensor core design for matrix multiplication:

Code Sample 29.5: Tensor Core Design

```
module tensor_core (
    input clk,
    input [15:0] a, b,
    output reg [31:0] c
);
    always @(posedge clk) begin
        c <= a * b; // 16-bit multiply with 32-bit accumulate
    end
endmodule
```

Challenges in deploying AI workloads on GPUs include power consumption and thermal management. High-performance GPUs consume hundreds of watts, necessitating advanced cooling solutions. Research in sparsity exploitation and quantization addresses these issues. For example, NVIDIA's Sparsity SDK leverages zero-skipping to reduce computation and memory usage. Quantization techniques, such as 8-bit integer inference, further optimize power efficiency without significant accuracy loss.

Future directions include the adoption of heterogeneous computing, where GPUs are combined with specialized accelerators like TPUs and FPGAs. This approach aims to balance flexibility and performance, particularly for edge devices. For instance, NVIDIA's Jetson platform integrates GPUs with ARM CPUs for embedded AI applications. Similarly, Google's TPUs are optimized for tensor operations, offering higher throughput for specific workloads.

In summary, modern GPU architectures are pivotal for implementing AI-driven image recognition and NLP workloads. Their parallel processing capabilities, coupled with software optimizations, enable real-world applications ranging from autonomous vehicles to chatbots. Ongoing research in sparsity, quantization, and heterogeneous computing promises to further enhance efficiency and scalability. The synergy between hardware and software continues to drive innovation in AI, making GPUs indispensable for cutting-edge applications.

### 29.3.2 Implementing AI-driven natural language processing workload

Modern GPU architectures have revolutionized the implementation of AI-driven workloads, particularly in natural language processing (NLP) and image recognition. The parallel processing capabilities of GPUs, combined with their high memory bandwidth, make them ideal for accelerating deep learning models. For NLP workloads, transformer-based architectures like BERT and GPT heavily rely on matrix multiplications and attention mechanisms, which are efficiently parallelized on GPUs. The computational intensity of these operations is given by:

$$\text{FLOPs} = 2 \cdot L \cdot H^2 \cdot (T + S)$$

where  $L$  is the number of layers,  $H$  is the hidden dimension, and  $T$  and  $S$  are the sequence lengths of the target and source inputs, respectively. GPUs exploit thousands of cores to compute these operations in parallel, reducing training and inference times significantly. For instance, NVIDIA's A100 GPU, with its Tensor Cores, accelerates mixed-precision computations, achieving up to 312 TFLOPS for FP16 operations.

In image recognition, convolutional neural networks (CNNs) such as ResNet and EfficientNet benefit from GPU optimizations. The convolution operation, defined as:

$$(f * g)(x, y) = \sum_{i=-k}^k \sum_{j=-k}^k f(i, j) \cdot g(x - i, y - j)$$

is highly parallelizable, as each output pixel can be computed independently. Modern GPUs leverage specialized hardware like CUDA cores and texture units to optimize memory access patterns, reducing latency. For example, the NVIDIA Volta architecture introduced Tensor Cores, which accelerate matrix multiply-accumulate (MMA) operations critical for CNNs .

Real-world applications of these workloads span multiple domains. In healthcare, AI-driven image recognition enables automated diagnosis from medical imaging. Studies show that GPU-accelerated CNNs achieve radiologist-level accuracy in detecting tumors from MRI scans . Similarly, NLP models deployed on GPUs power virtual assistants, machine translation, and sentiment analysis. For instance, Google’s BERT model, when optimized for GPUs, reduces inference latency from seconds to milliseconds, enabling real-time applications .

Implementing these workloads on GPUs requires careful optimization. Key techniques include:

**Kernel Fusion:** Combining multiple operations into a single GPU kernel to reduce memory overhead. For example, fusing activation functions with matrix multiplications minimizes global memory accesses.

**Mixed Precision Training:** Using FP16 for weights and activations while maintaining FP32 for master weights improves throughput without sacrificing accuracy .

**Memory Optimization:** Leveraging shared memory and caching strategies to reduce bandwidth bottlenecks. The NVIDIA CUDA programming model provides explicit control over memory hierarchy .

For NLP workloads, attention mechanisms pose unique challenges due to their quadratic complexity. Recent GPU optimizations, such as FlashAttention , exploit memory locality to reduce I/O operations. The algorithm reformulates attention as:

$$\text{Attention}(Q, K, V) = \text{softmax}\left(\frac{QK^T}{\sqrt{d_k}}\right)V$$

where  $Q$ ,  $K$ , and  $V$  are queries, keys, and values, respectively. FlashAttention tiles these matrices to fit into GPU SRAM, achieving up to  $3\times$  speedup over standard implementations.

In image recognition, data augmentation and batch processing are critical for GPU efficiency. Parallelizing augmentation operations across GPU threads ensures minimal overhead. The PyTorch `Dataloader` class, for instance, prefetches batches to overlap computation and data transfer . Additionally, frameworks like TensorRT optimize CNN inference by fusing layers and quantizing weights, reducing model size and latency .

The following Verilog snippet illustrates a simplified GPU memory controller for handling CNN workloads:

Code Sample 29.6: GPU Memory Controller

```
module memory_controller (
    input clk,
    input [31:0] addr,
    output [31:0] data
);
    reg [31:0] memory [0:1023];
    always @ (posedge clk) begin
        data <= memory[addr];
    end
endmodule
```

Emerging GPU architectures continue to push the boundaries of AI workloads. AMD’s CDNA and NVIDIA’s Hopper introduce hardware support for sparsity, accelerating sparse attention in transformers . Similarly, Intel’s Ponte Vecchio integrates Xe cores with AI-specific extensions for both NLP and image tasks . These advancements underscore the symbiotic relationship between GPU hardware and AI algorithms, driving innovations in real-world applications.

Energy efficiency remains a critical concern. The roofline model provides a framework for optimizing performance per watt. For a given GPU, the attainable performance is bounded by:

$$P \leq \min(\pi, \beta \cdot I)$$

where  $\pi$  is peak compute throughput,  $\beta$  is memory bandwidth, and  $I$  is operational intensity. Modern GPUs balance these factors through dynamic voltage and frequency scaling (DVFS), reducing power consumption during low-utilization periods .

In summary, the implementation of AI-driven NLP and image recognition workloads on modern GPU architectures hinges on parallel processing, memory optimization, and hardware-software co-design. Real-world applications benefit from these optimizations, achieving unprecedented performance and scalability. Future directions include heterogeneous computing, where GPUs collaborate with FPGAs and ASICs to further accelerate AI workloads .

# Chapter 30

# Future Trends in Hardware Acceleration

## 30.1 Ray Tracing Hardware

### 30.1.1 Comparison with traditional rasterization

The evolution of modern GPU architectures has been driven by the increasing demand for realistic rendering techniques, particularly ray tracing. Traditional rasterization, while efficient for real-time rendering, lacks the physical accuracy of ray tracing. This comparison examines the architectural differences between rasterization and ray tracing hardware, focusing on how modern GPUs extend their designs to support both paradigms.

Traditional rasterization operates by projecting 3D geometry onto a 2D screen space and filling pixels using a pipeline of fixed-function stages. The process begins with vertex processing, where vertices are transformed into screen coordinates, followed by primitive assembly that groups these vertices into triangles. Rasterization then converts the triangles into fragments, and fragment shading computes the final pixel colors using textures and lighting models. This pipeline is highly optimized for parallelism, leveraging thousands of cores to process vertices and fragments simultaneously. However, rasterization struggles with effects like global illumination, reflections, and shadows, which require expensive workarounds such as shadow maps or screen-space reflections.

In contrast, ray tracing models light transport by tracing rays from the camera through each pixel and simulating their interactions with surfaces. The rendering equation describes this physically:

$$L_o(\mathbf{x}, \omega_o) = L_e(\mathbf{x}, \omega_o) + \int_{\Omega} f_r(\mathbf{x}, \omega_i, \omega_o) L_i(\mathbf{x}, \omega_i)(\mathbf{n} \cdot \omega_i) d\omega_i$$

where  $L_o$  is the outgoing radiance,  $L_e$  is the emitted radiance, and  $f_r$  is the bidirectional reflectance distribution function (BRDF). Solving this equation requires recursive ray traversal and intersection tests, which are computationally intensive.

Modern GPUs integrate ray tracing hardware to accelerate these operations. NVIDIA's Turing and Ampere architectures, for example, introduce dedicated RT Cores for bounding volume hierarchy (BVH) traversal and ray-triangle intersection tests. The hybrid rendering pipeline combines rasterization for primary visibility and ray tracing for secondary effects. Key architectural extensions in support of ray tracing include BVH acceleration, which involves hardware-accelerated tree traversal to reduce the latency of ray-scene intersection queries; ray coherence sorting, which groups rays with similar directions to improve memory locality and cache utilization; and mixed precision execution, which uses lower precision formats such as FP16 for secondary rays to maintain performance without significant quality loss.

The following Verilog-like pseudocode illustrates a simplified RT Core intersection test:

Code Sample 30.1: Ray-triangle intersection test

```
module ray_triangle_intersect (
    input [127:0] ray_origin,
    input [127:0] ray_dir,
    input [127:0] v0, v1, v2,
    output hit,
    output [31:0] t, u, v
);
// Moller-Trumbore algorithm
edge1 = v1 - v0;
```

```

edge2 = v2 - v0;
pvec = cross(ray_dir, edge2);
det = dot(edge1, pvec);
if (det < EPSILON)
    hit = 0;
else {
    inv_det = 1.0 / det;
    t = dot(v0 - ray_origin, pvec) * inv_det;
    u = dot(tvec, qvec) * inv_det;
    v = dot(ray_dir, qvec) * inv_det;
    hit = (u >= 0 && v >= 0 && (u + v) <= 1.0);
}
endmodule

```

Performance comparisons between rasterization and ray tracing reveal trade-offs. Rasterization typically achieves higher frame rates for simple scenes, while ray tracing excels in visual fidelity. For example, reports that a hybrid pipeline can render reflections at 60 fps with 1 sample per pixel (spp), whereas rasterization requires multiple passes and approximations. The energy efficiency of ray tracing hardware is also improving, with RT Cores reducing power consumption by up to 30% compared to software-based ray tracing.

Memory bandwidth is another critical factor. Rasterization relies on hierarchical depth buffers and tile-based rendering to minimize bandwidth usage, whereas ray tracing demands random access to BVH nodes and textures. To address these requirements, modern GPUs employ compressed BVH representations that reduce node size through quantization, implement smart caching strategies that store frequently accessed nodes in on-chip memory, and apply variable-rate shading to lower the shading rate for secondary rays and thus save bandwidth.

The future of GPU architectures lies in unifying rasterization and ray tracing. Architectures such as AMD's RDNA 2 and Intel's Xe-HPG now incorporate ray acceleration hardware, signaling an industry-wide shift. Research suggests that hybrid rendering will dominate real-time graphics, with rasterization handling primary rays and ray tracing enhancing secondary visual effects. One ongoing challenge is optimizing the interaction between these paradigms, including tasks like denoising low-sample-per-pixel ray-traced images and dynamically switching between rendering techniques to balance performance and fidelity.

In summary, modern GPU architectures extend traditional rasterization pipelines with dedicated ray tracing hardware to achieve photorealistic rendering. While rasterization remains highly efficient for primary visibility determination, ray tracing hardware enables accurate simulation of light transport. The integration of RT Cores, BVH acceleration, and memory optimizations bridges the gap between performance and fidelity, paving the way for next-generation rendering techniques.

### 30.1.2 Extending design to support ray tracing

The integration of ray tracing into modern GPU architectures represents a significant shift from traditional rasterization-based rendering. Unlike rasterization, which projects 3D objects onto a 2D screen and shades them pixel by pixel, ray tracing simulates the physical behavior of light by tracing rays from the camera through each pixel and calculating their interactions with objects in the scene. This approach enables highly realistic lighting effects, such as accurate shadows, reflections, and global illumination, but at a substantially higher computational cost. To address this, GPU architectures have evolved to include dedicated hardware for accelerating ray tracing operations, such as bounding volume hierarchy (BVH) traversal and ray-triangle intersection tests.

Traditional rasterization pipelines, as implemented in GPUs like NVIDIA's Pascal or AMD's GCN architectures, rely on parallel processing of vertices and fragments. The pipeline consists of several stages:

**Vertex processing:** Transform vertices into screen space.

**Primitive assembly:** Group vertices into triangles.

**Rasterization:** Convert triangles into fragments (potential pixels).

**Fragment shading:** Compute color and depth for each fragment.

This pipeline is highly optimized for throughput, leveraging massive parallelism to render millions of triangles per frame. However, it struggles with effects requiring global visibility information, such as reflections or soft shadows, which are naturally handled by ray tracing.

Ray tracing hardware, as introduced in NVIDIA's Turing and Ampere architectures, extends the traditional GPU design with specialized units:

**Ray Generation Units:** Emit rays from the camera or light sources.

**BVH Traversal Units:** Accelerate hierarchical scene traversal.

**Ray-Triangle Intersection Units:** Perform precise intersection tests.

These units operate alongside the existing rasterization pipeline, allowing hybrid rendering techniques where ray tracing supplements rasterization for specific effects. For example, rasterization can handle primary visibility, while ray tracing computes secondary effects like reflections .

The BVH is a critical data structure for efficient ray tracing. It organizes scene geometry into a hierarchical tree, where each node represents a bounding volume containing child nodes or primitives. Traversing this tree reduces the number of ray-primitive intersection tests from linear to logarithmic complexity. Modern GPUs implement BVH traversal in hardware, with dedicated instructions for querying and updating the BVH.

The following Verilog-like pseudocode illustrates a simplified BVH traversal unit:

Code Sample 30.2: BVH Traversal Unit

```
module bvh_traversal (
    input ray_t ray,
    input bvh_node_t root,
    output hit_info_t hit
);
    stack_t stack;
    stack.push(root);
    while (!stack.empty()) {
        node = stack.pop();
        if (ray_intersects_aabb(ray, node.aabb)) {
            if (node.is_leaf) {
                hit = ray_intersect_triangles(ray, node.tris);
                if (hit.valid) return;
            } else {
                stack.push(node.right);
                stack.push(node.left);
            }
        }
    }
endmodule
```

Ray-triangle intersection is another computationally intensive operation accelerated by hardware. The Moller-Trumbore algorithm is commonly used for this purpose, as it efficiently computes the intersection point using barycentric coordinates . The algorithm can be expressed as:

$$\begin{bmatrix} T \\ U \\ V \end{bmatrix} = \frac{1}{P \cdot E_1} \begin{bmatrix} Q \cdot E_2 \\ P \cdot T \\ Q \cdot D \end{bmatrix}$$

where  $D$  is the ray direction,  $T$  is the ray origin to triangle vertex vector,  $E_1$  and  $E_2$  are triangle edges, and  $P$  and  $Q$  are intermediate vectors. Modern GPUs implement this algorithm in fixed-function units, reducing latency and power consumption compared to software implementations.

Comparing ray tracing hardware to traditional rasterization reveals trade-offs in performance and visual fidelity. Rasterization excels at rendering high triangle counts at real-time rates, with GPUs like the AMD RDNA2 architecture achieving throughputs exceeding 10 billion triangles per second. However, rasterization requires precomputed data (e.g., shadow maps) for global effects, which can introduce artifacts. Ray tracing, while computationally expensive, produces physically accurate results without such artifacts.

For instance, diffuse global illumination in ray tracing is computed by sampling rays over the hemisphere:

$$L_o(x, \omega_o) = \int_{\Omega} f_r(x, \omega_i, \omega_o) L_i(x, \omega_i) (\omega_i \cdot n) d\omega_i$$

where  $L_o$  is the outgoing radiance,  $f_r$  is the BRDF, and  $L_i$  is the incoming radiance. This integral is costly to evaluate but is handled efficiently by ray tracing hardware through importance sampling and denoising techniques .

To support hybrid rendering, modern GPUs like NVIDIA's Ada Lovelace architecture integrate rasterization and ray tracing pipelines with shared memory and scheduling resources. This allows dynamic workload balancing, where simpler scenes use rasterization, and complex effects leverage ray tracing.

The following table summarizes key differences:

Future directions for ray tracing hardware include improving ray coherence and reducing memory bandwidth. Techniques like ray sorting and compressed BVH representations aim to address these challenges . Additionally,

Aspect	Rasterization	Ray Tracing
Primary Visibility	Fast, hardware-accelerated	Slow, requires BVH traversal
Global Effects	Approximate, artifact-prone	Accurate, physically based
Hardware Units	Shader cores, ROPs	RT cores, BVH units
Scalability	High triangle counts	Limited by ray coherence

machine learning is being explored for denoising and reconstruction, further reducing the computational burden of ray tracing .

In summary, extending GPU design to support ray tracing involves augmenting traditional rasterization pipelines with specialized hardware for ray traversal and intersection. While rasterization remains dominant for real-time rendering due to its efficiency, ray tracing hardware enables unprecedented visual fidelity, paving the way for hybrid approaches that combine the strengths of both paradigms.

## 30.2 Machine Learning Accelerators

### 30.2.1 Lessons from GPU design for ML inference engines

The design of modern GPUs has profoundly influenced the development of machine learning (ML) inference engines, particularly in the context of parallelism, memory hierarchy, and energy efficiency. GPUs, originally designed for graphics rendering, have evolved into highly parallel computational units optimized for matrix operations, making them ideal for ML workloads. Key lessons from GPU architecture can be applied to ML inference accelerators to improve performance and scalability.

One critical lesson is the importance of massive parallelism. GPUs employ thousands of lightweight threads executing in lockstep, a design principle known as Single Instruction, Multiple Thread (SIMT). This architecture is particularly effective for ML inference, where operations like matrix multiplications exhibit high data parallelism. For example, the NVIDIA Volta architecture introduced Tensor Cores, specialized units for mixed-precision matrix operations, achieving significant speedups for deep learning workloads . The throughput of such operations can be modeled as:

$$\text{Throughput} = \frac{N \cdot P \cdot F}{T}$$

where  $N$  is the number of parallel units,  $P$  is the precision,  $F$  is the frequency, and  $T$  is the latency. By scaling  $N$ , GPUs achieve high throughput, a principle directly applicable to ML accelerators.

Memory hierarchy optimization is another key takeaway. GPUs use a multi-level cache and register file system to mitigate memory bottlenecks. For instance, the AMD CDNA architecture employs High Bandwidth Memory (HBM) and a large shared L2 cache to reduce data movement overhead . ML inference engines benefit from similar optimizations, as memory access patterns in convolutional neural networks (CNNs) and transformers are often predictable. A common optimization is tiling, where data is partitioned into smaller blocks that fit into faster memory levels. The efficiency of tiling can be expressed as:

$$E = \frac{T_{\text{compute}}}{T_{\text{compute}} + T_{\text{memory}}}$$

where  $T_{\text{compute}}$  is computation time and  $T_{\text{memory}}$  is memory access time. Reducing  $T_{\text{memory}}$  through hierarchical caching improves overall efficiency.

Energy efficiency is another critical consideration. GPUs achieve high performance-per-watt by leveraging specialized hardware for common operations. For example, NVIDIA's Ampere architecture introduced sparsity support, skipping zero-valued computations in weight matrices to save energy . ML accelerators can adopt similar techniques, such as pruning and quantization, to reduce power consumption. The energy savings from sparsity can be modeled as:

$$E_{\text{saved}} = E_{\text{total}} \cdot (1 - S)$$

where  $S$  is the sparsity ratio. This principle is particularly relevant for edge devices, where power constraints are stringent.

Another lesson is the importance of programmability. GPUs provide high-level abstractions like CUDA and OpenCL, enabling developers to harness parallelism without low-level hardware knowledge. ML accelerators must similarly offer flexible programming interfaces. For example, Google's Tensor Processing Unit (TPU) uses a domain-specific compiler (XLA) to optimize tensor operations . A Verilog snippet illustrating a simplified systolic array, a common ML accelerator component, is shown below:

Code Sample 30.3: Simplified Systolic Array

```

module systolic_array (
    input clk,
    input [7:0] A [0:3][0:3],
    input [7:0] B [0:3][0:3],
    output [15:0] C [0:3][0:3]
);
    reg [15:0] accum [0:3][0:3];
    always @ (posedge clk) begin
        for (int i = 0; i < 4; i++)
            for (int j = 0; j < 4; j++)
                accum[i][j] <= accum[i][j] + A[i][j] * B[i][j];
    end
    assign C = accum;
endmodule

```

Scalability is another lesson from GPU design. Modern GPUs scale performance by increasing the number of streaming multiprocessors (SMs) and memory channels. ML accelerators must similarly support scalable architectures, such as chiplet-based designs. AMD's Instinct MI200 series uses a multi-die architecture to scale compute and memory bandwidth . The scalability of such systems can be expressed as:

$$\text{Speedup} = \frac{T_1}{T_N}$$

where  $T_1$  is the execution time on one unit and  $T_N$  is the time on  $N$  units.

Finally, GPUs demonstrate the value of specialized instructions for ML workloads. For example, Intel's Xe-HPC architecture includes DPAS (Dot Product Accumulate Systolic) instructions for accelerating matrix operations . ML accelerators can benefit from similar custom instructions, reducing instruction overhead and improving throughput.

In summary, GPU design offers several key lessons for ML inference engines. Massive parallelism via SIMT architectures enables high throughput for matrix operations. Memory hierarchy optimizations, such as tiling and caching, reduce data movement overhead. Energy efficiency techniques, like sparsity support, lower power consumption. Programmability through high-level abstractions simplifies development. Scalability via multi-core or multi-die designs enhances performance. Specialized instructions accelerate common ML operations.

These principles, derived from decades of GPU evolution, provide a roadmap for designing efficient and scalable ML inference accelerators. Future work may explore further synergies between GPU and ML accelerator architectures, such as dynamic precision adaptation and heterogeneous computing.

## 30.3 Emerging Technologies

### 30.3.1 High-bandwidth memory (HBM)

High-bandwidth memory (HBM) has become a cornerstone of modern GPU architectures, enabling unprecedented data throughput for compute-intensive workloads such as machine learning, scientific simulations, and graphics rendering. Unlike traditional GDDR memory, HBM employs a 3D-stacked design with through-silicon vias (TSVs) to achieve significantly higher bandwidth and energy efficiency. The integration of HBM in GPUs, such as NVIDIA's Hopper and AMD's Instinct series, has been pivotal in addressing the von Neumann bottleneck by reducing memory access latency and increasing data transfer rates. For instance, HBM4 is projected to deliver bandwidths exceeding 2 TB/s, a critical requirement for emerging AI accelerators .

The architectural advantages of HBM stem from its vertical stacking of DRAM dies, which are interconnected using microbumps and TSVs. This design minimizes the physical distance between the GPU and memory, reducing parasitic capacitance and enabling faster signal propagation. The bandwidth  $B$  of an HBM stack can be modeled as:

$$B = N \times f \times w \times c$$

where  $N$  is the number of channels,  $f$  is the operating frequency,  $w$  is the bus width per channel, and  $c$  is the number of clock edges per cycle (typically 2 for DDR). For example, HBM3 achieves 819 GB/s with  $N = 16$ ,  $f = 1.5$  GHz,  $w = 64$  bits, and  $c = 2$  .

Chiplet designs have emerged as a complementary technology to HBM, enabling modular and scalable GPU architectures. By partitioning a monolithic GPU into smaller chiplets, manufacturers can improve yield, reduce

costs, and enhance performance through heterogeneous integration. AMD's MI300 series exemplifies this approach, combining compute chiplets with HBM stacks on an interposer. The interposer facilitates high-density interconnects, such as AMD's Infinity Fabric, which operates at 2.5 TB/s. The latency  $L$  of inter-chiplet communication can be approximated as:

$$L = \frac{d}{v} + t_{\text{serdes}}$$

where  $d$  is the distance,  $v$  is the signal propagation velocity, and  $t_{\text{serdes}}$  is the serialization/deserialization overhead. Advanced packaging techniques, like TSMC's CoWoS, further optimize these parameters.

RISC-V vector extensions (RVV) represent another disruptive innovation in GPU architectures, particularly for open-source and customizable designs. RVV provides a flexible framework for SIMD operations, enabling efficient execution of parallel workloads without proprietary instruction sets. The RVV specification supports variable-length vectors, which can be tailored to the underlying HBM bandwidth. For example, a vector load operation in RVV can be implemented as:

#### Code Sample 30.4: RVV Vector Load

```
vle32.v v0, (a0) // Load 32-bit elements from address a0 into vector v0
```

This aligns with HBM's burst-oriented access patterns, maximizing memory utilization. Research has shown that RVV-based GPUs can achieve 90% of the performance of proprietary architectures when paired with HBM.

The synergy between HBM, chiplets, and RVV is evident in emerging GPU designs. For instance, Tensorrent's chiplet-based AI accelerators leverage HBM3 and RVV to deliver 1.5 PFLOPS of compute power. The memory hierarchy is optimized for spatial locality, with HBM serving as the primary storage for large tensors and on-chip SRAM handling fine-grained data reuse. The energy efficiency  $E$  of such systems is given by:

$$E = \frac{P_{\text{compute}}}{P_{\text{memory}} + P_{\text{compute}}}$$

where  $P_{\text{compute}}$  and  $P_{\text{memory}}$  denote the power consumption of compute and memory subsystems, respectively. HBM's low voltage swing (0.8V) and TSV-based design contribute to  $P_{\text{memory}}$  reductions of up to 40% compared to GDDR6.

Challenges remain in the widespread adoption of these technologies. Thermal management is critical for 3D-stacked HBM, as power densities can exceed 100 W/mm<sup>2</sup>. Advanced cooling solutions, such as microfluidic channels and phase-change materials, are under investigation. Additionally, the lack of standardization in chiplet interfaces complicates multi-vendor interoperability. The Universal Chiplet Interconnect Express (UCIE) consortium aims to address this by defining open protocols for die-to-die communication.

In summary, the convergence of HBM, chiplet designs, and RISC-V vector extensions is reshaping modern GPU architectures. These technologies collectively address the limitations of monolithic designs, offering scalable, energy-efficient, and high-performance solutions for emerging workloads. Future research will focus on co-designing memory, interconnect, and compute elements to further push the boundaries of parallel processing.

### 30.3.2 Chiplet designs

The evolution of modern GPU architectures has been significantly influenced by the adoption of chiplet designs, which enable modular and scalable integration of heterogeneous computing elements. Chiplets, as disaggregated silicon blocks, allow for improved yield, reduced manufacturing costs, and enhanced performance by combining specialized dies into a single package. This approach is particularly advantageous for GPUs, where parallelism and memory bandwidth are critical. High-bandwidth memory (HBM) and RISC-V vector extensions further augment the capabilities of chiplet-based GPUs, enabling efficient data movement and parallel processing.

Chiplet designs leverage advanced packaging technologies such as 2.5D and 3D integration to interconnect multiple dies with high-density interconnects. For instance, AMD's Instinct MI300 series employs chiplet-based GPU architectures with HBM stacks, achieving bandwidths exceeding 1 TB/s. The interposer-based communication between chiplets minimizes latency and power consumption compared to traditional monolithic designs. The bandwidth  $B$  between chiplets can be modeled as:

$$B = N \cdot f \cdot w$$

where  $N$  is the number of interconnects,  $f$  is the operating frequency, and  $w$  is the width of each interconnect. This equation highlights the trade-offs in chiplet communication design.

High-bandwidth memory (HBM) is a key enabler for chiplet-based GPUs, providing vertically stacked DRAM layers connected through through-silicon vias (TSVs). HBM3, the latest iteration, delivers up to 819 GB/s per stack, making it ideal for memory-intensive workloads such as machine learning and high-performance computing. The integration of HBM with GPU chiplets reduces the memory wall bottleneck, as data can be transferred between compute units and memory at significantly higher rates than traditional GDDR6 interfaces. The effective memory bandwidth  $B_{\text{eff}}$  is given by:

$$B_{\text{eff}} = B_{\text{peak}} \cdot \eta$$

where  $B_{\text{peak}}$  is the peak bandwidth and  $\eta$  is the utilization efficiency. Optimizing  $\eta$  requires careful co-design of the memory controller and chiplet interconnect.

RISC-V vector extensions (RVV) introduce scalable SIMD capabilities that complement chiplet-based GPU architectures. Unlike fixed-width vector units in traditional GPUs, RVV allows for dynamic vector length selection, improving flexibility across diverse workloads. The RISC-V V1.0 specification defines instructions such as `vadd.vv` for vector-vector addition, enabling efficient parallel processing. A Verilog implementation of a basic RVV unit is shown below:

Code Sample 30.5: RISC-V Vector Unit

```
module rvv_alu (
    input [31:0] vs1, vs2,
    input [2:0] op,
    output [31:0] vd
);
    always @(*) begin
        case (op)
            3'b000: vd = vs1 + vs2; // vadd.vv
            3'b001: vd = vs1 - vs2; // vsub.vv
            3'b010: vd = vs1 & vs2; // vand.vv
            default: vd = 32'b0;
        endcase
    end
endmodule
```

The modularity of chiplets allows for the integration of specialized RVV units alongside traditional GPU cores, enabling hybrid execution models. For example, a chiplet could be dedicated to vector processing while another handles scalar operations, optimizing power and performance.

Emerging technologies such as photonic interconnects and monolithic 3D integration further enhance chiplet-based GPU designs. Photonic interconnects offer ultra-low latency and high bandwidth, with recent demonstrations achieving 10 Tb/s per fiber. Monolithic 3D integration, where transistors are stacked vertically, reduces interconnect lengths and improves energy efficiency. These technologies address the limitations of conventional interposers and TSVs, enabling finer-grained chiplet partitioning.

Chiplet designs in modern GPUs provide several key advantages. First, scalability is achieved by enabling incremental performance upgrades through the addition or replacement of dies without redesigning the entire GPU. Second, yield improvement is realized because smaller dies exhibit higher yields, reducing manufacturing defects and costs. Third, heterogeneous integration becomes feasible by combining specialized chiplets (e.g., for AI acceleration or ray tracing) into a single package. Finally, power efficiency improves due to shorter interconnects and optimized voltage domains that reduce dynamic power consumption.

Despite these benefits, chiplet-based GPUs face challenges such as thermal management and signal integrity. The power density of stacked chiplets necessitates advanced cooling solutions, while high-speed interconnects require robust signal conditioning to mitigate crosstalk and attenuation. Recent research proposes machine learning-based thermal modeling and adaptive voltage scaling to address these issues.

In summary, chiplet designs represent a paradigm shift in GPU architecture, enabled by HBM, RISC-V vector extensions, and emerging packaging technologies. By combining modularity, high bandwidth, and scalable parallelism, chiplet-based GPUs are poised to dominate next-generation computing platforms. Future work will focus on improving interconnect technologies and developing standardized chiplet interfaces to foster broader adoption.

### 30.3.3 RISC-V vector extensions

The RISC-V vector extensions (RVV) represent a significant advancement in modern GPU architecture, particularly in the context of emerging technologies such as high-bandwidth memory (HBM) and chiplet designs. These

extensions provide a scalable and flexible approach to vector processing, enabling efficient execution of data-parallel workloads. The RVV specification, ratified as part of the RISC-V ISA, introduces a variable-length vector register file and a rich set of instructions tailored for high-performance computing . This architecture is particularly well-suited for GPUs, where vector parallelism is a cornerstone of performance.

One of the key features of RVV is its support for variable vector lengths (VVL), which allows the same binary code to run efficiently across different hardware implementations. This is achieved through the `vsetvli` instruction, which dynamically configures the vector length based on the available hardware resources. For example, a GPU with 256-bit vector registers can process eight 32-bit elements per cycle, while a more advanced implementation with 512-bit registers can process sixteen elements. This flexibility is critical for modern GPUs, which must adapt to varying workloads and memory bandwidth constraints .

The integration of RVV with high-bandwidth memory (HBM) further enhances performance by reducing memory bottlenecks. HBM provides significantly higher bandwidth compared to traditional GDDR memory, making it ideal for vectorized workloads. The RVV extensions leverage this bandwidth through efficient memory access patterns, such as strided and indexed loads/stores. For instance, the `vlse32.v` instruction loads elements with a constant stride, enabling efficient access to non-contiguous memory regions. This is particularly useful for stencil computations and sparse matrix operations, which are common in GPU workloads .

Chiplet designs also play a crucial role in the adoption of RVV in modern GPUs. By disaggregating the GPU into smaller, specialized chiplets, designers can optimize each component for specific tasks. For example, a vector processing chiplet can be fabricated using a cutting-edge process node to maximize performance, while memory controllers and I/O chiplets can use older nodes for cost efficiency. The RVV extensions facilitate this modularity by providing a standardized interface for vector operations, enabling seamless communication between chiplets. This approach has been demonstrated in prototypes such as the AMD Instinct MI300, which combines CPU, GPU, and HBM chiplets into a single package .

The mathematical foundations of RVV are rooted in vector arithmetic and parallel reduction. Consider a vector addition operation, where two vectors **A** and **B** are added to produce a result vector **C**. In RVV, this can be expressed as:

$$\mathbf{C} = \mathbf{A} + \mathbf{B}$$

The corresponding RVV assembly code might look like:

Code Sample 30.6: Vector addition in RVV

```
vsetvli t0, a0, e32, m8      # Configure vector length
vle32.v v0, (a1)            # Load vector A
vle32.v v8, (a2)            # Load vector B
vadd.vv v16, v0, v8          # Vector addition
vse32.v v16, (a3)           # Store result C
```

This code snippet highlights the conciseness and efficiency of RVV, which minimizes instruction overhead and maximizes throughput.

Emerging technologies such as machine learning and real-time ray tracing further underscore the importance of RVV in modern GPUs. For example, matrix multiplication, a fundamental operation in deep learning, can be accelerated using RVV's matrix extension (RVV-M). The extension introduces specialized instructions for tensor operations, such as the `vmacc.vv` instruction, which performs a fused multiply-accumulate operation. The performance gain can be modeled as:

$$\text{GFLOPS} = \frac{N^3 \times 2}{\text{cycles}}$$

where  $N$  is the matrix dimension. Experimental results show that RVV-M can achieve up to 90% of the theoretical peak performance on a GPU with HBM .

The synergy between RVV, HBM, and chiplet designs is also evident in power efficiency. By leveraging the modularity of chiplets and the bandwidth of HBM, RVV-enabled GPUs can achieve higher performance per watt compared to monolithic designs. This is quantified by the energy-delay product (EDP), defined as:

$$\text{EDP} = \text{Energy} \times \text{Delay}$$

Studies have shown that RVV-based designs can reduce EDP by up to 40% for typical GPU workloads .

In summary, the RISC-V vector extensions represent a transformative technology for modern GPU architecture. Their integration with HBM and chiplet designs enables unprecedented levels of performance, efficiency, and scalability. As emerging technologies continue to evolve, RVV will play a pivotal role in shaping the future of high-performance computing.

The following references provide further insights into the topics discussed:  
for the RISC-V vector specification. for dynamic vector length configuration. for HBM and memory access patterns. for chiplet-based GPU designs. for matrix multiplication performance. for power efficiency metrics.



# Appendix A

## Glossary of Terms

### General Concepts

- **ALU (Arithmetic Logic Unit)**: A fundamental building block of a GPU or CPU responsible for performing arithmetic and logical operations.
- **Backface Culling**: A graphics technique that eliminates faces of a 3D object not visible to the camera, improving rendering efficiency.
- **BRAM (Block Random Access Memory)**: Memory embedded in FPGA devices, commonly used for buffering and storage in GPU pipelines.
- **Clipping**: The process of discarding primitives or pixels that lie outside the viewport or a designated viewing frustum.
- **Combinational Logic**: A type of digital logic where the output depends solely on the current input, without memory.
- **Dithering**: A graphics process that reduces color banding in images by adding noise or approximating unavailable colors.
- **FPGA (Field-Programmable Gate Array)**: A programmable hardware device used for prototyping and implementing digital designs, including GPUs.
- **Framebuffer**: A memory buffer that holds the final rendered image, typically used to interface with display hardware.
- **GPU (Graphics Processing Unit)**: A specialized processor optimized for parallel processing tasks such as rendering graphics and performing general-purpose computations.
- **HDL (Hardware Description Language)**: A programming language, such as Verilog or VHDL, used to describe and design digital logic circuits.

### GPU and Rendering Processes

- **Interpolation**: The calculation of intermediate values (e.g., colors, texture coordinates) between known points, commonly used in rasterization.
- **Lambertian Shading**: A simple shading model based on the diffuse reflection of light, often used in basic lighting calculations.
- **Metastability**: An unstable state in digital circuits that occurs when signals do not meet setup or hold time requirements, leading to unpredictable behavior.
- **Parallelization**: The process of dividing a computational task into smaller subtasks that can be executed simultaneously, fundamental to GPU operation.

- **Pipeline:** A series of processing stages in hardware or software, where each stage performs a specific task on a data stream.
- **Rasterization:** The process of converting 3D primitives into 2D pixel data for display on a screen.
- **Shader:** A small program that runs on a GPU to perform per-vertex or per-fragment processing tasks, such as lighting and texture mapping.
- **SIMD (Single Instruction, Multiple Data):** A parallel processing model where a single instruction is applied to multiple data elements simultaneously.
- **SIMT (Single Instruction, Multiple Threads):** An execution model used in modern GPUs where multiple threads execute the same instruction, with each thread operating on different data.
- **Texture Mapping:** The application of a 2D image (texture) onto a 3D surface to add detail and realism.

## Verilog-Specific Terms

- **Always Block:** A procedural block in Verilog used to describe sequential or combinational logic based on event triggers.
- **Continuous Assignment:** In Verilog, a method to assign values to `wire` data types using the `assign` keyword.
- **Generate Statement:** A Verilog construct used to create parameterized or repetitive hardware structures.
- **Reg (Register):** A Verilog data type used to store values in sequential logic circuits.
- **Synthesis:** The process of converting HDL code into a hardware implementation, such as FPGA or ASIC design.
- **Testbench:** A simulation environment used to verify the correctness of an HDL design by applying input stimuli and monitoring outputs.
- **Verilog:** A hardware description language used to model digital circuits at various levels of abstraction.
- **Z-Buffering:** A technique used to manage depth information in 3D rendering, ensuring that closer objects obscure further ones.

## Advanced GPU Concepts

- **Clock Domain Crossing:** Techniques used to safely transfer signals between hardware components operating on different clock domains.
- **Framebuffer:** A memory buffer containing pixel data, used to store the final output image before display.
- **High-Bandwidth Memory (HBM):** A type of memory designed for high data throughput, commonly used in modern GPUs for handling large datasets.
- **Memory Arbitration:** Strategies for resolving access conflicts in memory subsystems, ensuring efficient use of bandwidth.
- **Memory Caching:** The use of small, fast memory to store frequently accessed data, reducing latency and improving throughput.
- **Multi-Sampling Anti-Aliasing (MSAA):** A graphics technique that reduces aliasing artifacts by sampling multiple points per pixel and averaging the results.
- **Parallel Arithmetic:** Performing multiple arithmetic operations simultaneously, essential for GPU efficiency in tasks like shading and matrix transformations.
- **Shader Pipeline:** The sequence of shader stages in a GPU, including vertex, geometry, and fragment shading, used to process rendering tasks.

- **SIMT Efficiency:** Optimizing the execution of threads in a GPU to minimize divergence and maximize parallel throughput.
- **Warp Scheduling:** The process of managing groups of threads (warps) for efficient execution in SIMT architectures.

## Graphics and Rendering Techniques

- **Alpha Blending:** A technique for rendering transparency by combining foreground and background colors based on an alpha value.
- **Edge Functions:** Mathematical expressions used to determine pixel coverage during rasterization.
- **Gouraud Shading:** A shading technique that interpolates vertex colors across a polygon, providing a smooth gradient effect.
- **HDR (High Dynamic Range):** A rendering technique that allows a wider range of colors and luminance, enhancing image realism.
- **Perspective Projection:** The process of mapping 3D points onto a 2D plane to simulate depth, based on a camera's perspective.
- **Primitive Assembly:** The process of combining vertices into geometric primitives such as triangles or lines for rendering.
- **Raster Operations (ROP):** The final stage in rendering where pixel data is written to the framebuffer, including blending and depth testing.
- **Screen Space:** The coordinate system used for rendering images on a display, corresponding to the visible portion of the framebuffer.
- **Texture Filtering:** Techniques such as bilinear or trilinear filtering to smooth textures and reduce aliasing artifacts.
- **Z-Fighting:** A visual artifact caused by insufficient precision in depth buffers, resulting in overlapping objects flickering.

## System-Level Considerations

- **Fixed-Function Pipeline:** A legacy GPU architecture with dedicated hardware for specific tasks, contrasted with modern programmable pipelines.
- **Floating-Point Arithmetic:** Numerical computations using floating-point representation, commonly employed in shaders and transformations.
- **Latency:** The delay between an input stimulus and the corresponding output response, critical in real-time rendering.
- **Metastability Mitigation:** Techniques to ensure reliable signal transfer between asynchronous clock domains, such as synchronization registers.
- **Pipeline Stalling:** A condition where a pipeline stage must wait for data, causing delays in subsequent stages.
- **Resolution Scaling:** Adjusting the rendered resolution to balance performance and visual quality.
- **Setup and Hold Times:** Timing constraints in digital circuits to ensure reliable data capture at clock edges.
- **Throughput:** The amount of data processed per unit of time, a key performance metric in GPU design.
- **Triangle Setup:** The preprocessing of vertex data to determine rasterization parameters for a triangle.
- **Unified Memory Architecture (UMA):** A memory architecture where CPU and GPU share a common memory pool, simplifying data access.

## Verification and Debugging

- **Assertions:** Statements in testbenches used to check conditions and verify expected behavior during simulations.
- **Coverage Metrics:** Quantitative measures of how thoroughly a design has been tested, including code, functional, and toggle coverage.
- **Debugging Strategies:** Methods for identifying and resolving errors in HDL designs, such as using waveform analysis and signal dumps.
- **Formal Verification:** Techniques that use mathematical proofs to ensure correctness of hardware designs against specifications.
- **Functional Simulation:** Running a hardware model in a simulator to validate its logical correctness.
- **Regression Testing:** Repeated testing to ensure new changes do not introduce errors into previously verified functionality.
- **Signal Dump (VCD):** A file format used to capture and analyze signal waveforms during simulation.
- **Test Coverage:** A metric indicating how much of the design functionality has been exercised by the testbench.
- **Testbench Automation:** Using scripts and tools to generate and run testbenches efficiently, reducing manual effort.
- **Waveform Analysis:** Examining signal transitions over time using tools like ModelSim or Vivado to debug hardware designs.

## Advanced AI and GPU Architectures

- **AI Workloads:** Computational tasks specific to artificial intelligence, such as training and inference in neural networks.
- **Deep Learning Accelerator:** Specialized hardware within GPUs designed to optimize neural network computations, such as tensor operations.
- **Dynamic Parallelism:** A feature in modern GPUs that allows threads to spawn additional threads during execution.
- **Gradient Descent:** An optimization algorithm used in training neural networks, requiring efficient support for matrix operations.
- **Instruction Set Architecture (ISA):** The set of instructions a processor can execute, including specialized operations for AI and graphics tasks.
- **Low-Precision Arithmetic:** Numerical formats like FP16 or INT8, optimized for AI workloads by balancing performance and accuracy.
- **Matrix Multiplication:** A key operation in AI and graphics, accelerated in GPUs through dedicated hardware like tensor cores.
- **Neural Network Accelerator:** A specialized processing unit optimized for neural network operations, such as backpropagation and convolution.
- **SIMT Divergence:** A condition where threads in a warp follow different execution paths, reducing parallel efficiency.
- **Tensor Cores:** Hardware units in modern GPUs optimized for high-performance tensor operations, critical for AI applications.

## Emerging Technologies and Trends

- **Chiplet Architecture:** A modular approach to designing processors by combining smaller, functional chips (chiplets) to form a complete system.
- **High-Bandwidth Memory (HBM):** Advanced memory technology providing high data throughput, widely adopted in GPUs for demanding workloads.
- **Ray Tracing:** A rendering technique that simulates the physical behavior of light to produce realistic shadows, reflections, and lighting effects.
- **RISC-V Extensions:** Open-standard instruction set extensions enabling customization for specific workloads, including GPU and AI tasks.
- **Thermal Management:** Techniques to manage heat dissipation in GPUs, ensuring reliability and performance under high computational loads.
- **Tile-Based Rendering:** A rendering approach that divides the screen into smaller tiles to optimize memory access and improve efficiency.
- **Unified Shader Model:** A GPU architecture where the same shader units handle vertex, geometry, and fragment processing.
- **Variable Rate Shading (VRS):** A technique that adjusts the shading rate for different screen regions to optimize performance without significant quality loss.
- **Virtual Reality (VR) Optimization:** Enhancements in GPUs to handle the high frame rates and low latencies required for immersive VR experiences.
- **Volumetric Rendering:** A technique for visualizing 3D datasets, such as medical scans or scientific simulations, using GPUs.



## Appendix B

# Key Mathematical Equations

### First Steps in Verilog Development

**Boolean algebra for combinational circuits:**

$$F(A, B, C) = A \cdot (B + \overline{C})$$

### 3D Geometry Basics

**Affine transformation:**

$$\mathbf{v}' = \mathbf{R} \cdot \mathbf{v} + \mathbf{t}$$

### Rasterization Basics

**Barycentric coordinates:**

$$\lambda_1 = \frac{(x_2 - x)(y_3 - y_2) - (x_3 - x_2)(y_2 - y)}{(x_2 - x_1)(y_3 - y_2) - (x_3 - x_2)(y_2 - y_1)}$$

### Combinational vs. Sequential Logic

**Finite-state machine (FSM) transition equation:**

$$S(t+1) = f(S(t), X(t))$$

### Clock Domain Crossing Strategies

**Metastability resolution probability:**

$$P = e^{-\frac{t_{res}}{\tau}}$$

### Power Estimation and Management

**Dynamic power estimation:**

$$P_{dynamic} = \alpha CV^2 f$$

### Clipping and Culling

**View frustum clipping:**

$$ax + by + cz + d \geq 0$$

## Scan Conversion

**Line equation for Bresenham's algorithm:**

$$y = mx + b$$

## Interpolation of Attributes

**Perspective-correct interpolation:**

$$A(x, y) = \frac{\sum w_i A_i}{\sum w_i}, \quad w_i = \frac{1}{z_i}$$

## Memory Arbitration Techniques

**Bandwidth utilization:**

$$U = \frac{N_{effective}}{N_{total}}$$

## Memory Caching

**Cache hit rate:**

$$H = \frac{\text{Cache hits}}{\text{Total accesses}}$$

## SIMT vs. SIMD

**Warp occupancy:**

$$O = \frac{\text{Active warps}}{\text{Max warps per SM}}$$

## Basic Neural Network Inference

**Convolution operation:**

$$Y(i, j) = \sum_{m=-k}^k \sum_{n=-k}^k X(i+m, j+n) \cdot K(m, n)$$

## Specialized Hardware for AI

**Tensor core operation:**

$$C_{ij} = \sum_k A_{ik} \cdot B_{kj} + C_{ij}$$